

**STRONG MOTION MODELLING OF RUPTURE
PLANE ALONG AN IDENTIFIED PROBABLE
CAUSATIVE FAULT**

A THESIS

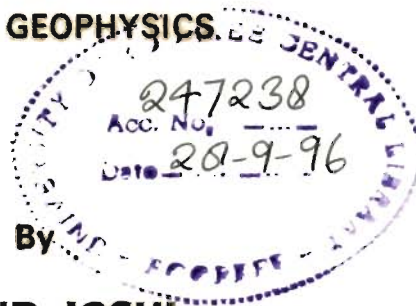
*submitted in fulfilment of the
requirements for the award of the degree*

of

DOCTOR OF PHILOSOPHY

in

APPLIED GEOPHYSICS.



ANAND JOSHI



**DEPARTMENT OF EARTH SCIENCES
UNIVERSITY OF ROORKEE
ROORKEE - 247 667 (INDIA)**

NOVEMBER, 1994

Smatis


1.

Candidate's Declaration

I hereby certify that the work, which is being presented in this thesis entitled "STRONG MOTION MODELLING OF RUPTURE PLANE ALONG AN IDENTIFIED PROBABLE CAUSATIVE FAULT" in fulfilment of the requirement for the award of the Degree of Doctor of Philosophy, submitted in the Department of Earth Sciences of the University, is an authentic record of my own work carried out during a period from January, 1991 to Nov, 1994 under the supervision of Prof. H.SINVHAL and Dr. (Mrs.) A. SINVHAL.

The matter embodied in this thesis has not been submitted by me for the award of any other degree.

DATE : 7/11/94


(ANAND JOSHI)

This is to certify that the above statement made by the candidate is correct to the best of our knowledge.



Signature of Supervisors

(H.SINVHAL)

Professor

Department of Earth Sciences

University of Roorkee,

Roorkee-247667, INDIA



(A.SINVHAL)

Lecturer

Department of Earthquake Engineering

University of Roorkee,

Roorkee-247667, INDIA

The PH.D. viva-voce examination of Mr. ANAND JOSHI, Research Scholar, was held on 20 May, 1995.

 
20.5.95

Signature of Guides


2/5

Signature of External Examiner

ACKNOWLEDGEMENTS

With a deep sense of gratitude I would like to thank my supervisors **Prof. H. Sinvhal** and **Dr. (Mrs.) A. Sinvhal** for their support, encouragement and guidance and for providing a healthy professional environment during the course of my stay as a research student. I am also thankful to the **(Late) Prof. R.K. Goel** ex Head and **Prof. A.K. Jain**, Head of the Department of Earth Sciences, University of Roorkee, for providing departmental facilities for carrying out my research work.

I owe special gratitude to many people for fruitful and encouraging discussions. Among them are **Prof. A.R. Chandrasekaran**, **Mr.A.D. Pandey**, **Dr. M.L. Sharma**, **Dr.(Mrs.) P.R. Bose** and **Mr.S.C. Gupta** at the Department of Earthquake Engineering, University of Roorkee; **Prof. D.M. Rosa** at the Institute of Geophysics, Zurich, Switzerland; **Prof. V.N.Singh** and **Dr. A.K.Saraf** at the Department of Earth Sciences, University of Roorkee, Roorkee; **Prof. V. Raiverman** at Wadia Institute of Himalayan Geology, Dehradun; **Mr.J.D. Das** at Department of Earthquake Engineering, University of Roorkee, Roorkee and **Prof. R.K. Gupta** at Department of Mathematics, University of Roorkee, Roorkee. **Dr. G.D. Gupta**, Director, Department of Science and Technology, New Delhi provided some of the data used in the present study. His cooperation and help is duly acknowledged.

I am thankful to my colleagues and friends who assisted in different ways during my stay at the department. I am thankful to **Mr. P.R. Pujari**, research scholar, Department of Earth Sciences for his generous help in proof reading the draft of the thesis and for all possible help from time to time. I am grateful to **Mr. S.K. Jain** of

Sardar Sarovar Narmada Nigam Ltd. for his help and stimulating discussions. Special thanks are due to **Mr. R.M. Sundaram**, research scholar at the Department of Earth Sciences for his involvement in the work related to the handling of computer software for word processing. Help received from **Mr. Sandeep Singh, Dr. R.C. Patel** and **Mr. Abhinandan Kumar** in the final stage of this thesis is thankfully acknowledged. **Mr. Anil Semwal, Ms. Anupama Rastogi, Mr. Nipun Kapur, Mr. Jayaram Sahoo, Mr. Jitender Kumar, Mr. V.K. Gahalaut, Mrs. Kalpana Gahalaut, Mr. Abid Hasan** and **Mr. Nepal Singh** research scholars at the Department of Earth Sciences, University of Roorkee and **Mr. B.B. Sahoo**, research scholar at the Department of Chemistry always came forward whenever I needed their help.

It would have been a difficult job for me to complete this task without support from my mother who always took keen interest in my research work. Equal support came from my father and brother. I am also thankful to **Mr. and Mrs. K.D. Dhariyal** who took keen interest in my work and helped me whenever I needed it.

I am specially thankful to **Prof. J.J. Wagner** of University of Geneva and the **United Nations University, Tokyo** for providing me funds for attending a course on Analysis and Management of Geological Risks, held in Geneva which gave me an exposure to the latest development in the field of earthquake risks. I am equally thankful to **Dr. R. Cola**, Assistant Professor, at the University of Philippines, Philippines and **Mr. Vassiliev**, Researcher, at the Russian Acadamey of Sciences, Moscow, Russia for making my stay in Geneva a memorable one.

I am thankful to **University Grants Commission, India** for providing me financial assistance in the form of Senior Research Fellowship for carrying out this

work. The funds made available by the Department of Science and Technology helped in providing computer facilities for the development of software.

Anand Joshi
(ANAND JOSHI)

ABSTRACT

Earthquakes are the most disastrous of all natural phenomenon. In this century alone, over five million lives have been lost due to earthquakes and they have been responsible for loss of property of over one hundred and thirty billion US dollars.

At the time of an earthquake the elastic energy travels from the focus in all direction. In the epicentral region (i.e., near the source) earthquake recording instruments (seismographs) go off scale or get saturated because of high amplitude of ground motion. In such cases accelerograms or strong motion records provide useful insight into the earthquake processes. Analysis and interpretation of observed and simulated strong ground motion records holds promise for an enhanced understanding of the earthquake process and about the nature, type and extent of the causative fault of an earthquake.

The main objectives of the present work are (i) to build a conceptual model of rupture plane along a causative fault identified on a map, (ii) to simulate accelerograms at selected observation points, and (iii) to compare the parameters extracted from simulated and field records for estimating the efficacy of the model.

The most probable causative fault for an earthquake is identified on the basis of the following data (i) Isoacceleration contours prepared from field strong motion data, (ii) Iseiseismal map, (iii) Tectonic map of the region, (iv) Location of aftershocks, (v) Geological cross sections and (vi) Fault plane solutions for the earthquake. It is not always possible to have all the above mentioned data for an earthquake, in which case, the available data is used to identify the causative fault. The fault thus identified is

marked on the tectonic map as the most probable causative fault. The location and strike (ϕ) of this fault is used for modelling.

The rupture on the causative fault is assumed to occur on a rectangular plane embedded in a homogeneous isotropic half space. The model is based on following parameters : rupture length (L), downward extension of the rupture plane (D), dip (δ), rupture velocity (V_r), velocity of the medium (V), geometry of rupture propagation, total number of elements within rupture plane and nucleation element. The length, downward extension of rupture plane and rupture velocity are computed from empirical relations. Dip and strike are obtained from fault plane solutions. Velocity of the medium is assigned according to local geological conditions and rock types.

The entire rupture plane is divided into equidimensional square elements of length (L_e). This is mapped in a three dimensional coordinate system. The element at which rupture initiates is called the nucleation element. Rupture propagates element by element in a radially outward direction till it covers the entire rupture plane.

The nucleation element and the successive elements which get effected as the rupture propagates, emit a source wavelet. The time lag between the activation of two successive elements depends upon the rupture geometry within the rupture plane.

From the nucleation element the rupture begins at time $T=t_0$, and energy starts travelling with velocity V and reaches the observation point at time $T=t$; which is the initial point (or starting point) on the synthetic record. The rupture spreads along the rupture plane. Total travel time between a particular element (other than nucleation element) and the observation point is the sum of :

- (a) The time taken by rupture to travel between nucleation element and that particular element with velocity V_r and
- (b) The travel time between that particular element and the observation point with the velocity of the medium (V).

The source wavelet from different elements reach an observation point at different times. The simulated record at the observation point takes into account the appropriate time lags due to geometry of rupture propagation and travel times of wavelet through the medium.

Various features have been extracted from both the field and simulated records, in time and frequency domains for quantitative comparison of the strong motion records. The parameters extracted are (i) Peak acceleration (P_a); (ii) Peak velocity (P_v); (iii) Peak displacement (P_d); (iv) Time of arrival of peak acceleration (T_a); (v) Duration of acceleration record (T_d); (vi) Ratio of area covered by acceleration record above and below the abscissa (R_a) and (vii) Sum of acceleration values on both side of abscissa (T_{area}). The parameters extracted from the autocorrelation function of the acceleration record are : (i) $ACF_1 = T_1$; (ii) $ACF_2 = T_2$; (iii) $ACF_3 = T_3$; (iv) $ACF_4 = T_m$; (v) $ACF_5 = A_1/A_0$; (vi) $ACF_6 = A_2/A_0$; (vii) $ACF_7 = A_3/A_0$; (viii) $ACF_8 = A_m/A_0$; (ix) $ACF_9 =$ Ratio of area under ACF from time $T = 0$ to $T = T_1$ with area under ACF from time $T = T_1$ to $T = T_2$ and (x) $ACF_{10} =$ area under ACF above the abscissa and area under ACF below the abscissa. Where $A_i =$ Autocorrelation function (ACF) at subscripted lag 'i'; $T_i =$ Time of i th zero crossing in ACF ($i = 1, 2, 3$); $T_m =$ Time of global minima in ACF and $A_m =$ Value of global minima of ACF. Parameters extracted from the power spectrum of acceleration records are : (i) F_p frequency at which maximum power occurs; (ii) F_i ($i = 1, 2, 3$) frequency at which 25th, 50th and 75th percentile of power occurs; (iii) F_i ($i =$

4,5,6) frequency at which 25th, 50th and 75th percentile of frequency weighted power occurs.

Three software packages were developed (i) to build a conceptual model of rupture plane along a causative fault identified on a map and to simulate strong motion records at selected observation points, (ii) to extract time domain parameters from simulated and field records and (iii) to extract frequency domain parameters from simulated and field records.

The most probable causative fault was identified for three recent earthquakes in India, for which strong motion data was available from networks operating in the vicinity of the earthquake epicenter. Synthetic strong motion records for these earthquakes was generated at selected observation points and twenty four features were extracted from field and simulated records. The data used and modelling parameters of earthquakes studied are listed in Tables 1 and 2, respectively.

A comparison of synthetic and field strong motion data was carried out for all twenty four extracted variables. Value of parameters R_{at} extracted from the synthetic record is atleast 80% of its value extracted from field record at all stations for the Dharamsala and the Uttarkashi earthquakes, while for the Meghalaya earthquake at eleven stations out of twelve. Value of parameter ACF_{10} extracted from the synthetic record is also atleast 80% of its value extracted from field record at all stations for the Dharamsala and the Uttarkashi earthquakes, while for the Meghalaya earthquake at eleven stations out of twelve. Value of parameter F_3 extracted from the synthetic record is again atleast 80% of its value extracted from field record at two stations for the Dharamsala and the Uttarkashi earthquakes, while for the Meghalaya earthquake at

eight stations out of twelve. The analysis brings out that three variables R_{nl} , ACF_{10} and F_3 are diagnostic parameters, i.e. the variable of synthetic record varies by a difference less than 20% that of the field record, at maximum numbers of stations for all three earthquakes.

Strong motion records were simulated for a hypothetical earthquake of magnitude 6.5 nucleating within the North Almora Thrust. Developed software packages were used to model the rupture plane for simulating strong motion records at Tehri. Five different positions of nucleation points were selected for simulating strong motion records. Peak acceleration obtained from the five simulated records vary between 273 to 446 cm/sec^2 . This strongly suggests that from the hypothetical situation the peak acceleration at Tehri will be atleast 273 cm/sec^2 and can go upto as much as 446 cm/sec^2 , depending upon the position of nucleation point within the rupture plane. If the strong motion records at or nearby Tehri are available, it will be of tremendous help in comparing parameters extracted from simulated records. This will add confidence in assigning design parameters to civil structures.

Since limited strong motion data is available in the Himalayan (MBT and MCT) region, therefore data from these networks can be used to give better estimates of modelling and simulation techniques and eventually to give better estimate of design parameters.

Table 1. Data used for identification of most probable causative fault for different earthquakes (From western to eastern Himalayas) studied in the present work.

S.N	DETAILS OF DATA	NAME OF THE EARTHQUAKE		
		DHARAMSALA	UTTARKASHI	MEGHALAYA
1.	Date	26.04.1986	19.10.1991	10.09.1986
2.	Epicenter in Degrees (USGS)	32.128, 76.37	30.78, 78.77	25.38, 92.0
3.	Origin Time (GMT)	07 hr 35m 16.1s	21hr 23m 14.3s	07 hr 50m 25.5s
4.	Magnitude (M_b)	5.5	6.5	5.2
5.	Recorded Maximum Peak Horizontal acceleration from strong Motion Network (cm/sec^2)	244.8	303.9	142.0
6.	(a) Station recording maximum horizontal acceleration	Shahpur	Uttarkashi	Saitsama
	(b) Instrument direction and	N15°W	N75°E	N32°E
	(c) Epicentral distance (km)	20.3	36	46.2
7.	No. of Stations having Strong Motion data	9 stations	13 stations	12 stations
8.	Isoseismal map	used	used	Not used
9.	Scale of Tectonic Map	1:250,000	1:250,000	1:1000,000
10.	Aftershock data	Not used	used	Not used
11.	Fault Plane Solution	used	used	Not used
12.	Geological Section in the epicentral region	used	used	Not used
13.	Name of Identified fault	Drini Thrust	MCT-1	Lincament 1 (Marked on tectonic Map)

Table 2. Modelling parameters of rupture along identified fault for different earthquakes.

S.NO.	MODELLING PARAMETERS	NAME OF THE EARTHQUAKE		
		DHARAMSALA	UTTARKASHI	MEGHALAYA
1.	(L) Length of rupture plane (km)	9	42	6
2.	(D) Downward extension of rupture plane (km)	9	29	6
3.	Total number of elements within Modelled Rupture Plane	81	1218	36
4.	Depth of nucleation point from surface of the earth (km)	8	17	31
5.	(ϕ) Strike of rupture plane (degree)	131	317	52
6.	(δ) Dip of rupture plane (degree)	69	14	90
7.	(V) Velocity of the medium (km/sec)	5.6	5.72	6.7
8.	V_r Rupture velocity (km/sec)	2.5	2.6	3.0

STRONG MOTION MODELLING OF RUPTURE PLANE ALONG AN IDENTIFIED PROBABLE CAUSATIVE FAULT

List of Contents

PREFACE

ACKNOWLEDGEMENT

ABSTRACT

CHAPTER 1 INTRODUCTION

- 1.1 Litreture review
- 1.2 Statement of the problem
- 1.3 Thesis layout

**CHAPTER 2 IDENTIFICATION OF MOST PROBABLE CAUSATIVE FAULT
ON MAP AND MODELLING PARAMETERS OF THE
RUPTURE PLANE**

- 2.1 Identification of most probable causative fault
- 2.2 Modelling parameters of the rupture plane
 - 2.2.1 Length of the rupture plane

- 2.2.2 Downward extension of the rupture plane
- 2.2.3 Elements within the rupture plane
- 2.2.4 Two dimensional coordinate system
- 2.2.5 Three dimensional coordinate system
- 2.2.6 Nucleation point
- 2.2.7 Source wavelet
- 2.2.8 Velocity of the medium
- 2.2.9 Geometry of the rupture propagation and rupture velocity
- 2.2.10 Travel time

2.3 Summary

CHAPTER 3 SIMULATION OF STRONG GROUND MOTION

- 3.1 Procedure of simulation of synthetic strong motion records for a model of the rupture plane
- 3.2 Simulation procedure of strong ground motion : an example
- 3.3 Summary

CHAPTER 4 FEATURE EXTRACTION FROM STRONG MOTION RECORD

- 4.1 Time domain parameters
 - 4.1.1 Parameters extracted from strong motion records
 - 4.1.2 Parameters extracted from autocorrelation function of acceleration record

- 4.2 Frequency domain parameters
- 4.3 Summary

CHAPTER 5 COMPUTER SOFTWARE

- 5.1 Subroutines used for simulating strong motion records
- 5.2 Subroutines used for generating source wavelet
- 5.3 Subroutines used for feature extraction from strong motion records
 - 5.3.1 Subroutines used for computing time dependent parameters
 - 5.3.2 Subroutines used for computing frequency dependent parameters
- 5.4 Summary

CHAPTER 6 DHARAMSALA EARTHQUAKE OF 26TH APRIL, 1986

- 6.1 Kangra strong motion array
- 6.2 Salient features of Dharamsala earthquake of 26th April, 1986
- 6.3 Identification of most probable causative fault for Dharamsala earthquake of 26th April, 1986
 - 6.3.1 Tectonic map (Kumar and Mahajan, 1990, 1991)
 - 6.3.2 Tectonic map (Raiverman et al., 1979)
 - 6.3.3 Isoacceleration map
 - 6.3.4 Composite isoseismal map (Kumar and Mahajan, 1990, 1991) and tectonic map (Raiverman et al., 1979)

- 6.3.5 Composite isoacceleration map (Section 6.3.3) and tectonic map (Raiverman et al., 1979)
- 6.4 Identification of most probable causative fault on map
- 6.5 Selection of observation points
- 6.6 Modelling parameters of rupture plane
 - 6.6.1 Length of rupture plane (L)
 - 6.6.2 Downward extension of rupture plane (D)
 - 6.6.3 Length of element (L_e)
 - 6.6.4 Three dimensional coordinate system
 - 6.6.5 Source wavelet
 - 6.6.6 Velocity of medium (V)
 - 6.6.7 Rupture geometry
 - 6.6.8 Rupture velocity (V_r)
 - 6.6.9 Selection of dip (δ) and (ϕ) of rupture plane
 - 6.6.10 Selection of location of rupture plane along identified causative fault
 - 6.6.11 Selection of starting point of rupture (or nucleation point) within the rupture plane
- 6.7 Simulation of strong motion records at selected observation points
- 6.8 Comparison of field and simulated records
- 6.9 Summary

CHAPTER 7 UTTARKASHI EARTHQUAKE OF 20TH, OCTOBER, 1991

- 7.1 Strong motion array
- 7.2 Salient features of the Uttarkashi earthquake of 20th October 1991
- 7.3 Identification of most probable causative fault
 - 7.3.1 Tectonic map of the region around Uttarkashi (Jain, 1987)
 - 7.3.2 Tectonic map (Purohit et al., 1990)
 - 7.3.3 Locations of aftershocks map
 - 7.3.4 Isoacceleration map
 - 7.3.5 Superimposed map of isoacceleration contours, aftershock locations, meizoseismal area and tectonics of the area
 - 7.3.6 Identification of most probable causative fault for the Uttarkashi earthquake
- 7.4 Selection of observation points
- 7.5 Modelling parameters of the rupture plane
 - 7.5.1 Length of rupture plane (L)
 - 7.5.2 Downward extension of rupture plane (D)
 - 7.5.3 Length of element (L_e)
 - 7.5.4 Three dimensional coordinate system
 - 7.5.5 Source wavelet
 - 7.5.6 Velocity of the medium (V)
 - 7.5.7 Geometry of rupture propagation within rupture plane and rupture velocity (V_r)
 - 7.5.8 Selection of dip (δ) and (ϕ) of the rupture plane,
 - 7.5.9 Selection of starting point of rupture (or nucleation point) within the

rupture plane

- 7.6 Simulation of strong motion records at selected observation points
- 7.7 Comparison of field and simulated records
- 7.8 Summary

CHAPTER 8 MEGHALAYA EARTHQUAKE OF 10TH SEPT, 1986

- 8.1 Strong motion array
- 8.2 Salient features of Meghalaya earthquake of 10th September, 1986
- 8.3 Identification of most probable causative fault for Meghalaya earthquake of 10th Sept, 1986
 - 8.3.1 Tectonic map of the region (Tilak et al., 1983)
 - 8.3.2 Isoacceleration map
 - 8.3.3 Composite isoacceleration and tectonic map of the region
 - 8.3.4 Identified most probable causative fault for Meghalaya earthquake of 10th Sept, 1986
- 8.4 Selection of observation points
- 8.5 Modelling parameters of rupture plane
 - 8.5.1 Length of rupture plane (L)
 - 8.5.2 Downward extension of rupture plane (D)
 - 8.5.3 Length of element (L_e)
 - 8.5.4 Three dimensional coordinate system
 - 8.5.5 Source wavelet
 - 8.5.6 Velocity of the medium (V)

8.5.7 Rupture velocity (V_p)

8.5.8 Selection of dip (δ) of the rupture plane

8.5.9 Selection of starting point of rupture (or nucleation point) within the rupture plane

8.6 Simulation of strong motion records at selected observation points

8.7 Comparison of field and simulated records

8.8 Summary

CHAPTER 9 APPLICATION OF MODELLING TECHNIQUE TO A HYPOTHETICAL EVENT

9.1 Modelling of rupture plane along the North Almora Thrust

9.1.1 Simulation of strong motion records at Tehri

9.2 Peak acceleration by attenuation relations

9.3 Peak acceleration by shifting isoacceleration contours

9.4 Summary

CHAPTER 10 CONCLUSIONS

10.1 Future work

REFERENCES

APPENDIX I

APPENDIX II

LIST OF FIGURES

APPENDIX III

LIST OF TABLES

APPENDIX IV

LIST OF SYMBOLS

APPENDIX V

LIST OF SYMBOLS USED IN FIGURES

CHAPTER 1

INTRODUCTION

A large part of Indian subcontinent lies in the Alpine Himalayan seismic belt which is seismically very active. In the past hundred years four great earthquakes above magnitude 8 on the Richter scale have occurred in this region (Assam 1897, 1950, Kangra 1905 and Bihar - Nepal 1934). In order to understand the earthquake process, it is important to determine the parameters that help in defining the size and the energy released in an earthquake. The source parameters of an earthquake can help in the assessment of the impact of the earthquake and can be deduced quantitatively by modelling the source for simulating strong motion records at any desired observation points. The efficacy of the model can be verified by comparing the simulated records with the data recorded by the strong motion instrument.

Strong motion recording instruments are used for recording acceleration data. The addition of accurate timing system through internal time code generator (T.C.G.) has increased the utility of this data and it can be used for both engineering applications as well as seismological research. In particular, deployment of strong motion arrays has shown that useful data can be obtained in a reasonably short time frame and better studies pertaining to the source dynamics in the near field region can be made. Another application pertains to the epicentral determination of earthquake (Srivastava, 1989).

This chapter presents a brief review of the various techniques used by researchers for simulation of strong motion records and their analysis.

1.1 LITERATURE REVIEW

An earthquake is a sudden, transient motion or series of motions of the ground originating in a limited region and spreading from their in all directions (Howell, 1959). Earthquakes can be caused by a variety of reasons like volcanic eruptions, landslides and tectonic movements, etc. However, the tectonic earthquakes surpass others both in size and frequency. Usually all tectonic earthquakes are a result of energy released by sudden shear movement (rupture) along fractures (faults) (DHA, 1993). "A fault is a slip surface in the earth, across which discontinuous land deformation takes place. It's configuration underground cannot be observed so we must construct a model of fault on the basis of the little surface evidence available (e.g. length of the fault and its offset during an earthquake). A rectangular shape for the fault plane with one pair of its sides parallel to the free surface is often assumed. The assumption may be accepted as a first approximation, because surface breakage is usually straight. In fact, the displacement field around a fault is explained reasonably well by this type of theoretical model .." (Kasahara, 1981, pp 54).

The rupture plane can be modelled for an earthquake and techniques are available for simulation of synthetic strong motion records due to this model. The simulation procedure provides a means of estimating the dependence of strong ground motion on specific fault parameters (Somerville et al., 1991). In the empirical data base, these dependencies are difficult to isolate as there are many factors that determine strong motion characteristics. The uncertainty (non uniqueness) in ground motion due

to a specific model can be reduced by comparison of field and simulated records by parametric studies (Abrahamson et al. 1990). If the simulation procedure is proved competent and the simulated records are in good agreement with the field records then it can play an important role in complimenting traditional empirical approaches of estimation of strong ground motions for seismic hazard analysis.

Statistical method of generating strong motion records was among the earliest methods of simulations. Using statistical approach synthetic records were generated by Housner and Jenning (1964) which had pertinent properties of recorded strong motion earthquake accelerograms. The model accelerogram in this case were sections of a stationary, Gaussian, random process with a power spectral density found from the average of undamped velocity spectra of recorded ground acceleration. Eight pseudo earthquake records of thirty seconds durations were generated on digital computer, and the velocities, displacements and velocity spectra were calculated. It was concluded in this study that synthetic earthquake records are satisfactory models of strong ground motion earthquake records for the purpose of structural analysis, and they can be used for calculating standard ground motions for the design of structures. The limitations of technique of modelling is that it does not include conceptual model of earthquake source and the passage of the energy released by the source through the medium.

These limitations are removed in the simulation procedure used by Hartzell (1978), Kamiyama (1988), Kanamori (1979), Hadely and Helmberger (1980), Irikura and Muramatsu (1982), Mendoza and Hartzell (1988), Hartzell and Helmberger (1982) and Kamiyama (1988). In these methods seismogram of aftershocks were treated as empirical Green's function. The advantage of this scheme is that there is no need to remove propagation effect (Fukuyama and Irikura, 1986). The major constraint in this

approach is availability of aftershock data. This is difficult for every earthquake recorded on strong motion array.

The method in which records of small event were used as Green's function for synthesising ground motions is the semi empirical approach. This has been used in many studies (eg. Hartzell, 1978; Tanaka et al., 1982; Irikura, 1983; 1986; Takemura and Ikeura, 1988 etc.) and successful results were obtained for synthesis of short period (high frequency) ground motion. However, number of small event record are not generally available at every site where this approach has to be applied (Midorikawa, 1993). Midorikawa (1993) proposed a method for calculating the peak ground acceleration in near field. In this method acceleration envelope waveform determined from empirical relation is used. To test the method peak acceleration were calculated for the 1985 Central Chile earthquake ($M_s = 7.8$), for which a considerable number of strong motion records at close distance were available. The calculated results are in good agreement with the observed data.

A simplified method of synthesising strong ground motion was used by Kamiyama (1988). In this approach strong motion accelerograms are synthesized. The parameters that are mainly needed in this method are earthquake magnitude, focal depth and source to station distance of mainshocks and its related small shocks (foreshocks or aftershocks). The method was employed for several representative earthquakes in Japan and it was seen that the synthesized accelerograms matched well with observed ones in terms of amplitude, duration and spectral characteristics.

The theoretical model calculates response of point source at the observation point by taking into account the rupture process within the rupture plane and

propagation of energy in the medium. Useful information about fault behaviour is contained in the seismic pulse shape (Kasahara, 1981). Based on different types of source pulse two different models are proposed, these are (1) Haskell model and (2) Brune model. Seismic pulse proposed by Haskell (Haskell, 1964 and Knopoff and Gilbert 1959) represent a process in which a uniform slip occurs over entire fault plane with a uniform velocity. Seismic pulse proposed by Brune (1970) neglects fault propagation effects. It assumes that the fault surface reflect elastic waves totally during rupture.

Ground motions due to quarry blast were simulated by Sinvhal and Srivastava (1986) which are comparable to an instrumentally observed record. The field ground motion was recorded on strong motion accelerograph. In this procedure effect of explosive quantity, blasting pattern, nature of source wavelet, travel times, wave propagation velocity and attenuation of ground motion in geological terrain was accounted in the simulated history of ground motions.

Brune (1970) describes source of an earthquake by considering effective stress available to accelerate the side of the fault. Model describe near and far field displacement time functions and spectra and includes the effect of fractional stress drop. The model explains near and far field spectra observed for earthquakes and indicates that the effective stress operating during earthquakes is of the order of 100 bars.

Rupture propagation on the fault plane plays a predominant role on the ground motion and several attempts have been made to take this into consideration in computing the expected peak accelerations at the site (Makarisis et al. 1992). Midorikawa

and Kobayashi (1980) proposed a method for estimating the response envelope of near field ground motion with regard to the rupture propagation. Another approach deals with the method of dividing the rupture plane into several small subfaults. Characteristics of the seismic wave from each subfault, such as waveform envelope and response spectrum are determined from various empirical relations. The method was applied for computing peak acceleration for Volos (Central Greece) earthquake of 9 July, 1980. Different modes of rupture propagation were considered for computing peak acceleration. The unilateral mode seems to be more realistic and shows consistency with the aftershock distribution Makaris et al. (1992).

In order to explain the model of the rupture plane one has to define the geometry of rupture propagation (rupture geometry) inside the rupture plane and the velocity of rupture propagation. According to Mikumo and Miyatake (1978) if static friction are homogeneous or weakly non uniform, the rupture propagation is nearly elliptical with a velocity equal to P wave (longitudinal wave) velocity along the direction of initial shear stress and with nearly S wave (transverse wave) velocity in the direction perpendicular to it.

Propagation of rupture on the fault plane plays an important role in modelling the source mechanism of an earthquake. The state of stress near the fault increases gradually as a long term process and the failure occurs when the static friction is insufficient to contain the high stresses stored in the rocks. The potential energy is then transferred into kinetic energy of wave propagation, followed by readjustment of stress in the vicinity of source (Oliveira, 1978).

The January 29, 1981 Taiwan earthquake ($M = 6.7$) was recorded digitally by triaxially force balanced accelerometers in SMART-1 strong motion array centered 30 km north northwest of epicenter (Abrahamson, 1985). The source of this event had a reverse mechanism with unilateral rupture from East to West. A method was used by Abrahamson (1985) to estimate time dependent rupture velocity. The rupture velocity varies from minimum of 2.1 km/sec to a maximum of 4.9 km/sec over a fault length of 14 km.

An approach for inverting teleseismic P waveform recorded by stations of Global Digital Seismograph Network is used by Mendoza and Hartzell (1988) for recovering slip distribution on fault plane. The earthquakes that are used for this study are 8 July, 1986 North Palm Springs Earthquake, California, the 28th October 1983 Borah Peak Earthquake, Idaho, and the 19th September 1985 Michiacan Earthquake, Mexico. In the inversion procedure a fault plane with fixed strike and dip is placed in the region of earthquake hypocenter and divided into several subfaults. Rupture is assumed to propagate with constant velocity away from hypocenter and synthetic ground motions are calculated at teleseismic stations for each subfault. The observed seismograms are then inverted to obtain the distribution of strike slip and dip slip displacement for the earthquake. The inversion results show that the global Digital Seismogram Network data are useful for deriving fault dislocation model for moderate to large events.

Strong motion records are recorded on accelerographs in the epicentral region. Such records are helpful in studying source mechanism, extent of rupture and rupture propagation. Strong motion records play an extremely important role in estimating various design parameters for engineering purposes. Strong ground motion recorded by digital array called SMART-1, capable of recording upto 0.24g horizontal

acceleration was used for such analysis (Bolt et al. 1982). One such digital array became operational in September 1980 in highly seismic region of Taiwan. The array had radius of 2 km and consisted of 37 accelerometers. During first year of recording it recorded 15 earthquakes with local magnitude ranging from 3.4 to 6.9. The preliminary engineering analysis included (1) transformations to principal axes, (2) development of generalized response spectrum, (3) ratios for characterizing multi support excitations, and (4) moving window analysis in the time and frequency domain for studying the spectral variations of recorded ground motions.

In Indian subcontinent four great earthquakes had occurred in a short span of 53 years (i.e., 1897 and 1950 Assam earthquakes, the 1905 Kangra earthquake and the 1934 Bihar Nepal earthquake). These event have occurred along the region where Indian plate collides against the Asian plate and been the locale of a large number of major earthquakes (Tandon, 1992).

In a study identifying the causative fault for Indian earthquakes which occurred in 1980s Rastogi (1992a) had studied nineteen earthquakes, with respect to fault plane solutions, isoseismal map, depth of earthquakes and geological data. For some earthquakes occurring in the Himalayan and Peninsular India, in the 1970s, the fault plane solutions have been worked out by a number of workers (Chandra, 1977, 1978, Das Gupta et al. 1987, Molnar and Tapponier, 1975, Ni and Barazangi, 1984). However, the identification of the causative fault for most of these earthquakes have been rather difficult, in the absence of hypocentral parameters to the desired accuracy and as such, the focal mechanisms could give only a general idea of seismotectonics. For several earthquakes which occurred in 1980s, it has been possible to correlate the

focal mechanism with the causative fault due to better location of hypocenters as well as macroseismic and aftershock studies (Rastogi, 1992a).

In the present work the causative fault for the three recent events viz., the Dharamsala earthquake of 26th April, 1986, Uttarkashi earthquake of 20th October, 1991 and Meghalaya earthquake of 10th September, 1986 have been identified with the help of the available data. Location of epicenters of these earthquakes are shown in Fig 1.1. The rupture plane has been modelled for these three events and synthetic strong motion records have been generated for various observation points. The simulated records at various stations are compared with the field records. The reason for choosing these earthquakes was the availability of field strong motion data which enables comparison of the synthetic and field data to verify the efficacy of the modelling process for generation of synthetic records.

Dharamsala earthquake of 26th April 1986 was among the first ever Indian earthquake for which recorded strong motion data in the epicentral region is available (Chandrasekaran, 1988b). Source parameters of this earthquake were studied by Srivastava (1989), Kumar and Mahajan (1990, 1991), Molnar (1990), Jain et al. (1992) and Das and Chandrasekaran (1993). Iseismal map for this earthquake was prepared by Kumar and Mahajan (1990) and Gupta et al. (1986). Damage report was presented by Arya et al. (1986). Causative fault for Dharamsala earthquake and its relation with isoseismals is studied by Narula and Shome (1992). Rastogi (1992a) had identified causative fault for this earthquake on the basis of fault plane solutions and isoseismals. Strong motion data was analysed by Chandrasekaran (1988a and 1988b) and Chandrasekaran and Das (1990b, 1992a, 1992b). Detailed tectonic study in the region is conducted by Kumar and Mahajan (1990, 1991) and Raiverman et al. (1979).

Velocity structure near the epicentral region is prepared by Srivastava and Chatterjee (1986).

Uttarkashi earthquake of 20th October, 1991 was recorded on a strong motion array operating in the epicentral area. Thirteen stations had recorded this earthquake (Chandrasekaran and Das, 1991, 1992c), Chandra et al. (1992) had performed study on the strong motion data obtained during Uttarkashi earthquake of 20th Oct, 1991. Singh and Prasad (1992) had studied the attenuation relation for Uttarkashi earthquake by using strong motion data from various regions. Source parameters for this earthquake were studied by Chadha (1992), Kamble (1992a and 1992b) and Dziewonski et al. (1992). Isoleismal map for this event has been prepared by Sinvhal et al. (1992), Kumar and Mahajan (1994) and Thakur and Kumar (1994). The damage pattern and isoseismals for this event were also studied by Narula et al. (1992). Detailed tectonic study of the region surrounding the epicenter has been published by Jain (1987) and Purohit et al. (1990). Velocity structure around the epicentral region was investigated by Kamble (1992b). Aftershock data was studied by Kayal et al. (1992). Study of a set of pre and post earthquake LISS-II sensor data was made by Gupta et al. (1994). LISS-II sensor is a CCD pushbroom line scanner aboard the Indian Remote Sensing Satellite and provides data in four spectral ranges ; blue, green, red and near infra red, with a ground resolution of 36.25 m. The study concluded that the MCT was activated during the earthquake.

Meghalaya earthquake of 10th Sept, 1986 was recorded on twelve stations of strong motion array operating in the area (Chandrasekaran et al., 1988). Parameters of this earthquake were computed by U.S.G.S. Epicenter of this earthquake using strong motion data was computed by Das and Chandrasekaran (1993). Strong motion

data for this earthquake was analysed by Chandrasekaran and Das (1990a, 1990b, 1992a and 1992b) and Chandrasekaran et al. (1988). Detailed tectonic map of the region has been published by Tilak et al. (1983). Velocity structure in the region is has been prepared by Saha et al. (1981).

Availability of good observational and instrumental data for these earthquakes has encouraged undertaking of the present work to model the source of these earthquakes along some identified causative faults. Attempt had been made by Joshi (1990) to model the rupture process for various magnitude earthquakes in the Dharamsala region. The rupture plane in this work was modelled in a two dimensional coordinate system. In this work seismotectonic setup in the region around Dharamsala was studied along with the case histories of the great Kangra earthquake of 4th April, 1905, Kinnaur earthquake of January 19, 1975 and Dharamsala earthquake of 26th April, 1986. Comparative study of simulated and field acceleration records for rupture process within a rupture plane in two dimensional coordinate system was done by Sinvhal et al. (1990, 1992 and 1993). Three dimensional modelling of the rupture plane for Uttarkashi earthquake of 20th Oct, 1991 has been done by Sinvhal et al. (1992). In this work most probable causative fault was also identified and rupture was modelled along this identified fault. Khattri (1994) had modelled the earthquake source to simulate acceleration records of Uttarkashi earthquake of 20th Oct, 1991.

1.2 STATEMENT OF THE PROBLEM

A need of heuristic approach for identification of causative fault on map and modelling rupture plane has been strongly felt for the earthquakes in the Himalayan region. In India three strong motion arrays have been installed in the states of

Himachal Pradesh, Uttar Pradesh, Assam and Meghalaya (Chandrasekaran and Das, 1992b). These arrays have recorded earthquakes in these region. Availability of observed strong motion records for the earthquakes hold promise for better modelling of the rupture plane as well as identification of the most probable causative fault for earthquakes in these region.

Use of recorded strong motion data has been made in the present work for three earthquakes viz., Dharamsala earthquake of 26th April, 1986, Uttarkashi earthquake of 20th October, 1991 and Meghalaya earthquake of 10th September, 1986. The entire work can be classified as : i) Collection of data of the earthquake to be studied, ii) Identification of most probable causative fault of the earthquake, iii) Specifying modelling parameters of the rupture plane along the identified fault, (iv) Simulation of the strong motion records due to the model of the rupture plane, (v) Selection of observation points for simulation of strong motion records and (vi) Comparison of various features of simulated record with that of the field record.

The rupture plane along the identified fault is modelled as a rectangular plane and is divided into numbers of square elements. The starting point of the rupture in these elements is termed as nucleation point and is the first element to be activated. The model of rupture plane along causative fault is shown in Fig 1.2 and has been discussed in Chapter 2.

1.3 THESIS LAYOUT

Three earthquakes from Indian subcontinent as stated above have been studied and presented in this dissertation. Most probable causative fault for these earthquakes

have been identified and rupture along identified fault is modelled to simulate strong ground motion records. Complete scheme of identification of most probable causative fault is given in Chapter 2. This chapter also defines various parameters required to model rupture process within the rupture plane. The method of modelling rupture plane to simulate strong motion record used in this dissertation is discussed in detail in Chapter 3. Various parameters which are extracted from the simulated and field records for comparison are discussed in Chapter 4. Chapter 5 discussed the algorithm of program developed for modelling of the rupture plane and computing parameters of simulated and field records for comparison. Chapters 6, 7 and 8 discuss the complete scheme for the identification of the most probable causative fault and modelling of the rupture plane for (i) Dharamsala earthquake of 26th April, 1986, (ii) Uttarkashi earthquake of 20th October, 1991 and (iii) Meghalaya earthquake of 10th Sept, 1986 respectively. Collected data, identified most probable causative fault, parameters required for modelling the rupture plane, simulated records and their comparison with field records for each earthquakes are presented in these chapters. The application of the complete scheme is given in the Chapter 9. The conclusions and directions of future work of the present study have been given in the Chapter 10.

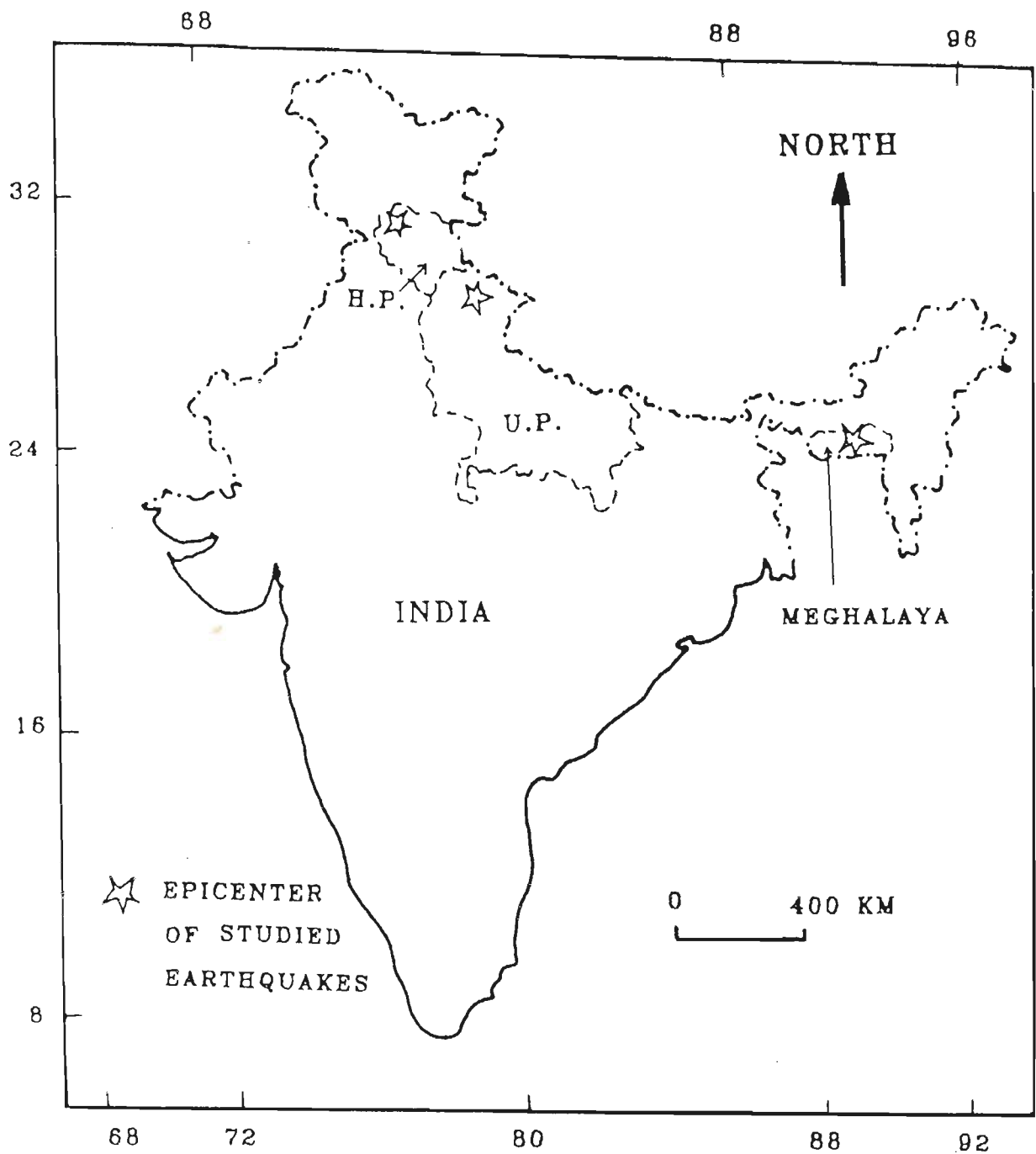


Fig 1.1 Location of epicenters of (i) Dharamsala earthquake of 26th April 1986, (ii) Uttarkashi earthquake of 20th October, 1991 and (iii) Meghalaya earthquake of 10th Sept 1986.

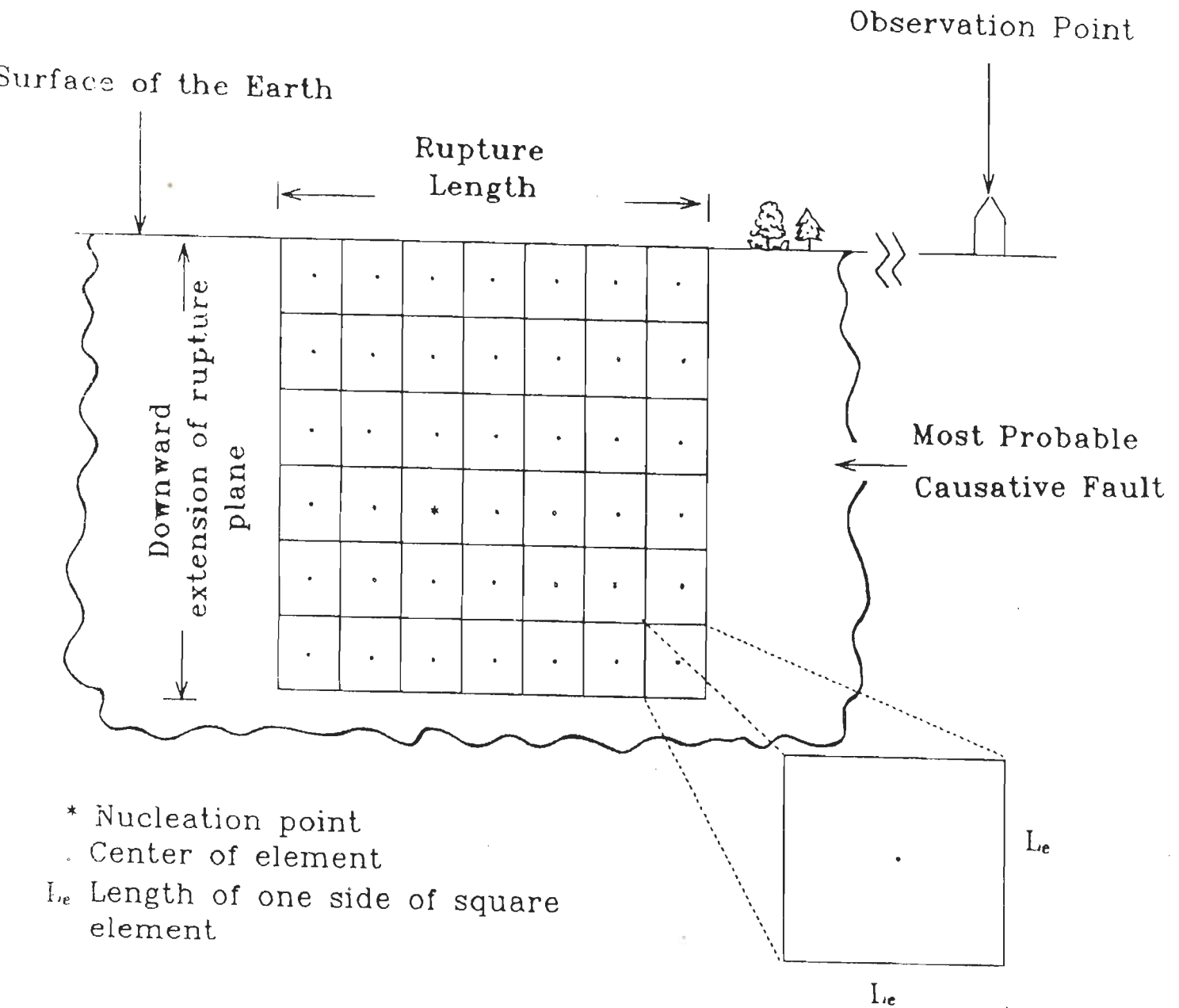


Fig 1.2 Model of a vertical rupture plane within an identified most probable causative fault.

CHAPTER 2

IDENTIFICATION OF MOST PROBABLE CAUSATIVE FAULT ON MAP AND MODELLING PARAMETERS OF THE RUPTURE PLANE

An earthquake is defined by specifying parameters such as the location of hypocenter and its magnitude. To simulate strong motion records an earthquake source can be defined in terms of the modelling parameters of the rupture plane within the identified most probable causative fault. A fault on the tectonic map has to be first identified as the most probable causative fault for the earthquake prior to the modelling of the rupture plane. A scheme to identify the most probable causative fault of an earthquake is presented in this chapter. Various modelling parameters which are required to define the rupture plane along the identified most probable causative fault have also been discussed.

2.1 IDENTIFICATION OF MOST PROBABLE CAUSATIVE FAULT

Identification of the most probable causative fault for an earthquake is important prior to the modelling of rupture plane along the identified causative fault for the earthquake. For identification of most probable causative fault following data can be used :

Isoacceleration map,
Isoseismal map of the earthquake,
Location of aftershocks,
Tectonic map of the region,
Geological cross section and
Fault plane solutions.

In practice isoacceleration, isoseismal, aftershock and tectonic maps on same scale (say 1:250,000) are superimposed on one another to get a composite map for identification of the most probable causative fault of an earthquake. It is generally observed that isoacceleration contours, isoseismals and aftershock zone have a close relationship with the strike of the most probable causative fault for an earthquake.

Isoacceleration map

"Peak acceleration near the fault region is expressed as a function of the fault parameters and relative collocation between the fault and the observation site " (Sato and Kiyono, 1986). From the study of Bihar Nepal earthquake of 21st Aug, 1988 it was observed by Fujiwara et al. (1989) that peak acceleration has a constant value for the range of distance that coincides with the length of the causative fault. This study indicates that the direction of isoacceleration contours follow the direction of the strike of the most probable causative fault for an earthquake.

Isoacceleration map of an earthquake, showing peak acceleration contours is used for the identification of most probable causative fault. For making isoacceleration contours, recorded peak value of acceleration at any station is used. The values of

peak accelerations at a number of stations are plotted on a map (say 1:250,000) for obtaining peak acceleration or isoacceleration contours. The isoacceleration and the tectonic map of the region are superimposed and the lineament nearest to the highest isoacceleration contour having strike in the direction of major axis of isoacceleration contours is considered as the most probable causative fault.

Isoseismal Map

Isoseismal map gives the idea of the damage due to an earthquake. The map can also be used for identification of the causative fault for an earthquake. Nineteen damaging earthquakes in India during 1980s were studied for establishing relationship of the isoseismals with the direction of faulting by Rastogi, (1992a). It is inferred that " Though isoseismal trend depends mainly upon the ground conditions, it is many times used to infer direction of faulting. If the ground can be assumed homogeneous, isoseismals are elongated along the fault direction and becomes wider in the direction of propagation of faulting. Though the latter characteristic has not been noticed for earthquakes during 1980s, isoseismals have been found to elongate in the fault direction for many of earthquakes during 1980s " (Rastogi, 1992a). Newmark and Rosenblueth (1971) inferred that "Isoseismals are often quite elongated in a direction parallel to the main geographic and geological (especially orographic and tectonic) features of region. This may be due to a greater transmissibility of waves in one direction than at right angle to it, or to a greater extent, it may reflect the manner in which earthquake originate".

The studies referred above indicate that the isoseismal map of the earthquake superimposed on the tectonic map of the region on same scale may be helpful in

revealing the orientation and location of the most probable causative fault for the earthquake. The isoseismal map and tectonic map, both on same scale (say 1:250,000) are superimposed on one another to get a composite map. The lineament nearest to the meizoseismal area having strike in the direction of the major axis of isoseismals is assumed to be the most probable causative fault for the earthquake.

Location of the Aftershocks

It is observed that the location of aftershocks (Aftershock zone map) can help in deciding the direction and the length of the causative fault. In some cases length of the elongated area of the aftershock zone is taken as length of causative fault. In case of Kinnaur earthquake of January 19, 1975, magnitude 6.8 (Singh et al., 1977), the length of ruptured fault is taken as that equal to length of aftershock zone which is about 120 km (Chaudhury and Srivastava, 1977).

Aftershock location map and the tectonic map are superimposed to get a composite map. The lineament or fault having cluster of epicenters of aftershocks can be assumed as the most probable causative fault for an earthquake.

In the present study all available maps are superimposed on one another to form a composite map to identify a lineament or fault as the most probable causative fault for an earthquake.

The identified most probable causative fault is further confirmed with the available depth section and the fault plane solutions for the event. In ideal conditions, all maps should be available for identification of the most probable causative fault.

However, it is not always possible to get all the mentioned data for identification of most probable causative fault. In cases where there is lack of sufficient information and only few of these maps are available, identification of probable causative fault is done on the basis of the available data.

2.2 MODELLING PARAMETERS OF THE RUPTURE PLANE

After identification of the most probable causative fault for an earthquake on map, the next task is to model the rupture plane along the identified causative fault. Rupture plane is assumed as a rectangular plane embedded in a homogeneous, isotropic half space and is defined by various modelling parameters. These parameters are required for the purpose of modelling of the rupture plane to simulate strong motion records at any observation points. Following sections discuss various modelling parameters required to model the rupture plane and their selection criteria.

2.2.1 LENGTH OF THE RUPTURE PLANE

Empirical relations between rupture length and the magnitude of the earthquake are discussed by various workers e.g., Araya and Kiureghian (1988), Dan et al. (1990), Housner (1970), Naeim (1989), Otsuka (1965), Sato (1979), Tocher (1958) etc. However, using the relations given by different workers between the rupture length and the magnitude, value of the rupture length may vary considerably from one relation to another for an earthquake of a given magnitude. This is due to the fact that empirical relations are computed considering the parameters of earthquakes for a specific region, and for different regions these relations may differ significantly.

The relation between rupture fault length and the magnitude of an earthquake using data for faulting due to ten earthquakes in California and Nevada, given by Tocher (1958) is as follows:

$$\text{Log } L = 1.02M - 5.77 \quad (2.1)$$

Where, L is ruptured fault length in km for an earthquake of magnitude M .

By applying the least squares method to the source parameters for 18 events, consisting of foreshocks, aftershocks and main event of 1980 Izo-Hanto-Toho-Oki Japan earthquake following relations among M , $\text{Log } M_0$ and L were obtained by Dan et al. (1990):

$$\text{Log } L = .319 \text{ Log } M_0 - 6.91 \quad (2.2)$$

$$\text{Log } M_0 = 1.22M + 17.43 \quad (2.3)$$

Where,

L = Ruptured fault length in km,

M_0 = Seismic moment of the earthquake and

M = Richter magnitude of the earthquake.

Sato (1979) proposed the following relations between rupture length and earthquake magnitude for shallow and large earthquakes for magnitudes above 5:

$$\text{Log } L = 1/3 \text{ log } M_0 - 7.28 \quad (2.4)$$

$$\text{Log } M_0 = 1.5M + 16.2 \quad (2.5)$$

Where,

L = Ruptured fault length in km,

M_0 = Seismic moment of the earthquake and

M = Richter magnitude of the earthquake.

Relation derived using surface rupture lengths data available for all types of faults worldwide by Araya and Kiureghian (1988) is given by the following expression :

$$\text{Log}_{10} L = -2.77 + .619 M_s \quad (2.6)$$

Where,

L = rupture length in km and

M_s = surface wave magnitude.

Relationship between magnitude of the earthquake and length of ruptured fault is calculated by Otsuka (1965) for 44 events which occurred in Japan and other parts of the world in between 1847 - 1955. The formula evolved on the basis of this study gives the upper limit of rupture length for an earthquake as :

$$\text{Log } L_m = 3.2 + .5 M \quad (2.7)$$

Where,

L_m = Maximum length of rupture in cm and

M = Magnitude of the earthquake.

Housner (1970) has provided following table between length of the rupture plane and the magnitude M of the earthquake.

Magnitude	Rupture length (km)	Magnitude	Rupture length (km)
8.8	1609	5.0	3
8.5	852	4.5	2
8.0	305	4.0	1
7.5	112	3.0	0.50
7.0	2	2.0	0.22
6.5	14	1.0	0.08
6.0	8	0.0	0.02
5.5	5		

A table between the rupture length and the magnitude of the earthquake as given by Naeim (1989) is:

Magnitude Richter	Rupture length km	Magnitude Richter	Rupture Length km
5.5	5 - 10	7.5	60 - 100
6.0	10 - 15	8.0	100 - 200
6.5	15 - 30	8.5	200 - 400
7.0	30 - 60		

The expressions discussed above clearly indicate that for an earthquake of a given magnitude the rupture length as derived from different relations may differ significantly. Table 2.1 shows rupture length obtained from different relations for Dharamsala earthquake of 26th April, 1986 having $M_b = 5.5$ and $M_s = 5.3$ and $M_o = 2.3 \times 10^{19}$ Nm (U.S.G.S.). Rupture length varies from 1 km to 9 km for this earthquake as derived from different relations. Data used for computing these relations by different workers is major source of dissimilarity. However it is seen that relation provided by Otsuka (1965) gives maximum limit of ruptured fault and its applicability is worldwide. This relation together with the relation by Araya and Kiureghian (1988) can be used for

calculating the rupture length for earthquake of given magnitude. The calculated rupture length can be checked with the table by Naiem (1989) which gives lower and upper limit of ruptured fault length for an earthquake of given magnitude.

2.2.2 DOWNWARD EXTENSION OF THE RUPTURE PLANE

Downward extension (D) of rupture plane is shown in Fig 1.2. For smaller earthquakes ($M < 6.0$) the vertical and horizontal dimensions of slipped rupture are presumed approximately the same but for the large earthquakes the length of slipped rupture may be measured in hundreds of kilometers whereas the perpendicular dimension is thought to be at most some 15-30 km in extent (Housner, 1970).

Area of ruptured fault during an earthquake can also be used for calculating downward extension of rupture plane. Area of ruptured fault plane (A) can be derived by relation given by Kanamori and Anderson (1975) :

$$\text{Log}(A) = M_s - 4 \quad (2.8)$$

Where,

A = Area of ruptured fault and

M_s = Surface wave magnitude of the earthquake.

This relation is derived for earthquake having surface wave magnitude greater than or equal to 6. The area (A) of a rectangular rupture plane can be expressed as :

$$A = L \times D \quad (2.9)$$

Where,

L = Length of the rupture plane and

D = Downward extension of the rupture plane

Hence,

$$D = A/L \quad (2.10)$$

Earthquakes of magnitude less than 6 can be assumed to have a square rupture plane so that D is equal to L, while for earthquakes of magnitude greater than 6, D can be calculated using expression 2.9 and 2.10.

Geological depth section, if available, can also be used for having an idea about the downward extension of rupture plane.

The hypocenter can be defined as a point where rupture begins (Kasahara, 1981). Therefore, according to the definition of downward extension of the rupture plane, the hypocenter of an earthquake must lie within the rupture plane. The hypocentral depth of an earthquake thus plays an important role in deciding the downward extension of the rupture plane.

2.2.3 ELEMENTS WITHIN THE RUPTURE PLANE

Rupture plane is assumed to be rectangular plane divided into several square elements or subfaults. The length of element is kept equal for entire simulation procedure. On this basis the entire rectangular rupture plane is divided into several

elements (Fig 1.2). Length of element (L_e) remains same for two dimensional and three dimensional coordinate systems.

For modelling of the rupture plane for the earthquakes studied in the present work, the length of element is assumed as 1 km. On the basis of calculated rupture length (L) and downward extension (D) of rupture plane, total number of elements within the rupture plane are calculated as :

$$N = \frac{L \times D}{L_e^2}$$

The rectangular rupture plane which is divided into numbers of square elements contains:

Total number of elements along length = L/L_e

Total number of elements along downward extension = D/L_e

Total number of elements within the entire rupture plane = $\frac{L \times D}{L_e^2}$

2.2.4 TWO DIMENSIONAL COORDINATE SYSTEM

For modelling of a rupture plane one can either use two dimensional or three dimensional coordinate systems. For two dimensional coordinate system the X axis is assumed along the strike of the modelled rupture plane, while the Z axis is positive vertically downward. The origin of the coordinate system is assumed to be a point lying at the center of one of the topmost element at the extreme corners of the rupture plane, thus the depth of the origin from the upper extension of the rupture plane is equal to

$L_c/2$. Fig 2.1 shows the two dimensional coordinate system. This coordinate system can only be used for modelling of the vertical rupture plane.

2.2.5 THREE DIMENSIONAL COORDINATE SYSTEM

For mapping the dipping rupture plane a third axis is required. In this system the X axis is assumed along the strike of the rupture plane, the Y axis is perpendicular to the X axis and is positive in the direction of its dip and the Z axis is positive vertically downward. For the purpose of three dimensional modelling of the rupture plane coordinate system assumed is shown in Fig 2.2. In the present work three dimensional coordinate system has been used for the purpose of modelling of the rupture plane for all three earthquakes mentioned in Chapter 1.

2.2.6 NUCLEATION POINT

Once the rupture plane is divided into several square elements, one element is decided from which rupture initiates. This point is termed as initial point, nucleation point or starting point of the rupture. The nucleation point within the rupture plane can be calculated by following methods:

METHOD I

The focus or the hypocenter of the earthquake is the point where rupture begins (Kasahara, 1981). Thus the nucleation point within the rupture plane can be the point which coincides with the hypocenter of the earthquake. For computing the location of the nucleation point the rupture plane is divided into several elements and the element

coinciding with the hypocenter of the earthquake is assumed as nucleation point. Dip of rupture plane (δ) is taken from the fault plane solutions. The distance of the nucleation point from the surface of the earth for an earthquake with hypocentral depth 'h', epicenter 'E' and the dip ' δ ' (Shown in Fig 2.3) can be calculated using following expression.

$$= h/\sin \delta \quad (2.11)$$

METHOD II

The nucleation point on the rupture plane can be other than the hypocenter. In such a case various elements within the rupture plane are assumed as the nucleation point and records are simulated at selected observation points. The element which when assumed as nucleation point gives maximum number of comparable parameters of simulated records with that of field records is assumed as nucleation point.

Method I provides an initial guess of the nucleation point within the rupture plane, however Method II gives quantitative support to the selected location of the nucleation point. For each of three earthquakes modelled in the present work the initial guess of the nucleation point is made by Method I and later this has been refined using Method II.

2.2.7 SOURCE WAVELET

Energy released at the center of an element when rupture approaches its center is expressed in the form of a source wavelet. Source wavelet is defined as the

disturbance which moves outward through the earth as changing wave form (Ricker, 1977). The source pulse is defined as movement of earth at the source (shot) (Ricker, 1977). At the observation point energy is received in the form of a source wavelet. Source wavelet assumed in the present work is formulated by Ricker (1940, 1977) for homogeneous and isotropic earth, at a considerable distance from source (shot). This form of source wavelet has been used by many investigators for generating synthetic seismogram which include Daut et al. (1989), Kawase and Aki (1989), Papageorgiou and Kim (1991), Li et al. (1992), Minami and Ohori (1992), Takemiya and Tomono (1992) and Abe et al. (1992).

On the basis of recorded as well as computed observations, Ricker (1940, 1977) gave the source wavelet, velocity type of which can be given by following expression (Ricker, 1977) :

$$u(t) = (2\pi^2 f_c^2 t^2 - 1) \exp(-\pi^2 f_c^2 t^2) \quad (2.12)$$

Where,

f_c = Frequency of source wavelet

Velocity form of the source wavelet of desired frequency can be generated using this expression. One such source wavelet of 5 Hz frequency is shown in Fig 2.4b. This source wavelet has two crossings and is symmetrical. The displacement and acceleration forms of the source wavelet can be obtained by its integration and differentiation, respectively and are shown in Fig 2.4a and 2.4c. The data used in these figures is given in Table 2.2. Source wavelet of different frequencies are shown in Fig 2.5 and their digitized values at 4 msec sampling interval is given in Table 2.3. The

frequency of source wavelet assumed for the present study is 5 Hz for the Dharamsala and the Meghalaya earthquakes and 2.5 Hz for the Uttarkashi earthquake.

2.2.8 VELOCITY OF THE MEDIUM

The emitted source wavelet travels with the velocity of the medium by the shortest route. The velocity of medium in the region is taken from the seismic section available for the region. Velocity of the medium in any region depends on the rock type in the region, hence different regions having different rock type will have different velocity of the medium.

2.2.9 GEOMETRY OF THE RUPTURE PROPAGATION AND RUPTURE VELOCITY

Rupture within the rupture plane propagates according to the geometry of rupture propagation from the nucleation point towards surrounding elements. In the present work radial geometry of rupture propagation has been assumed in the study of all three earthquakes.

Radial Rupture Geometry : In this type of geometry, the rupture propagates from the nucleation element simultaneously to all elements whose center are equidistant from the center of the nucleation element. The rupture thus progressively propagates to elements with center at distances $L_e, \sqrt{2} L_e, 2 L_e, \sqrt{5} L_e, 2\sqrt{2} L_e \dots$ etc. and so on till the entire rupture plane is covered with constant rupture velocity V_r . This type of rupture geometry is shown in Fig 2.6.

Rupture velocity within the rupture plane can be computed by expression given by Bath (1974) as

$$\text{Log}(L/V_r) = .5M - 1.9 \quad (2.13)$$

where,

L = length of rupture plane in km

V_r = rupture velocity in km/s

M = Richter magnitude of the earthquake

Rupture velocity can also be assumed as 80% of S wave velocity in region surrounding the earthquake source (Mendoza and Hartzell, 1988, Reiter, 1990). This dependency of rupture velocity on shear wave velocity incorporates the property of the medium in which rupture plane is assumed to be lying.

For the Dharamsala earthquake of magnitude 5.5 and rupture length (L) as 9 km, the rupture velocity of 1.27 km/sec is calculated from empirical relation given in expression 2.13. However in the Dharamsala region having shear wave velocity as 3.23 km/sec the rupture velocity is calculated as 2.58 km/sec. As the rupture propagates along the fault in many case with an average rupture velocity of 3 -3.5 km/sec (Menahem and Singh, 1981 and Kasahara, 1981). The rupture velocity of 2.58 km/sec calculated using 80% of shear wave velocity is close to the average rupture velocity of 3 - 3.5 km/sec (Menahem and Singh, 1981 and Kasahara, 1981).

For the purpose of modelling of the rupture plane along identified causative fault rupture velocity is assumed as 80% of shear wave velocity.

2.2.10 TRAVEL TIME

The source wavelet from each element reaches the observation point with different time lags. This depends on the time taken by rupture to reach a particular element from the nucleation point and the time taken by the source wavelet to reach the observation point with the velocity of the medium. If D_r is the distance travelled by rupture from the starting point of rupture to the particular element and R is the distance travelled by source wavelet to reach the observation point with the velocity of the medium by shortest route, then the source wavelet will arrive at the observation point after a time which can be calculated by the following expression (Fig 2.7 gives more details).

$$T = D_r/V_r + R/V \quad (2.14)$$

Where,

T = Total time taken by source wavelet to reach the observation point,

V_r = Rupture velocity,

V = Velocity of the medium,

D_r = Distance between starting point of rupture and center of the element and

R = Distance between center of an element and observation point.

2.3 SUMMARY

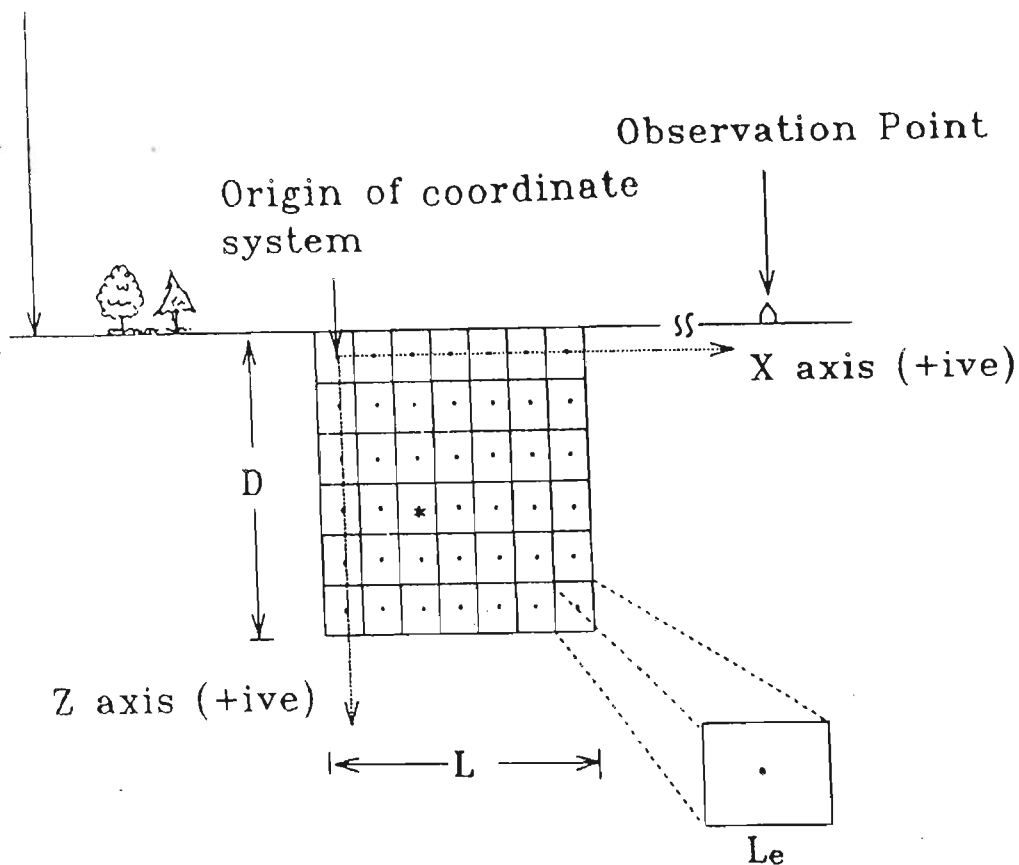
The identification of fault on a map which could be most probable causative fault for the earthquake is an important task prior to the modelling of the rupture plane along the fault. Various observational and instrumental data are used for this purpose. Once

the most probable causative fault is identified, rupture plane is modelled within the fault. The rupture plane along the identified fault is defined by the following modelling parameters :

S.No	Parameter	S.No	Parameter
1.	Length of rupture plane (L)	6.	Dip of rupture plane (ϕ)
2.	Downward extension of rupture plane (D)	7.	Rupture Velocity (V_r)
3.	Length of element (L_e)	8.	Velocity of medium (V)
4.	Nucleation point	9.	Rupture Geometry
5.	Strike of rupture plane (ϕ)		

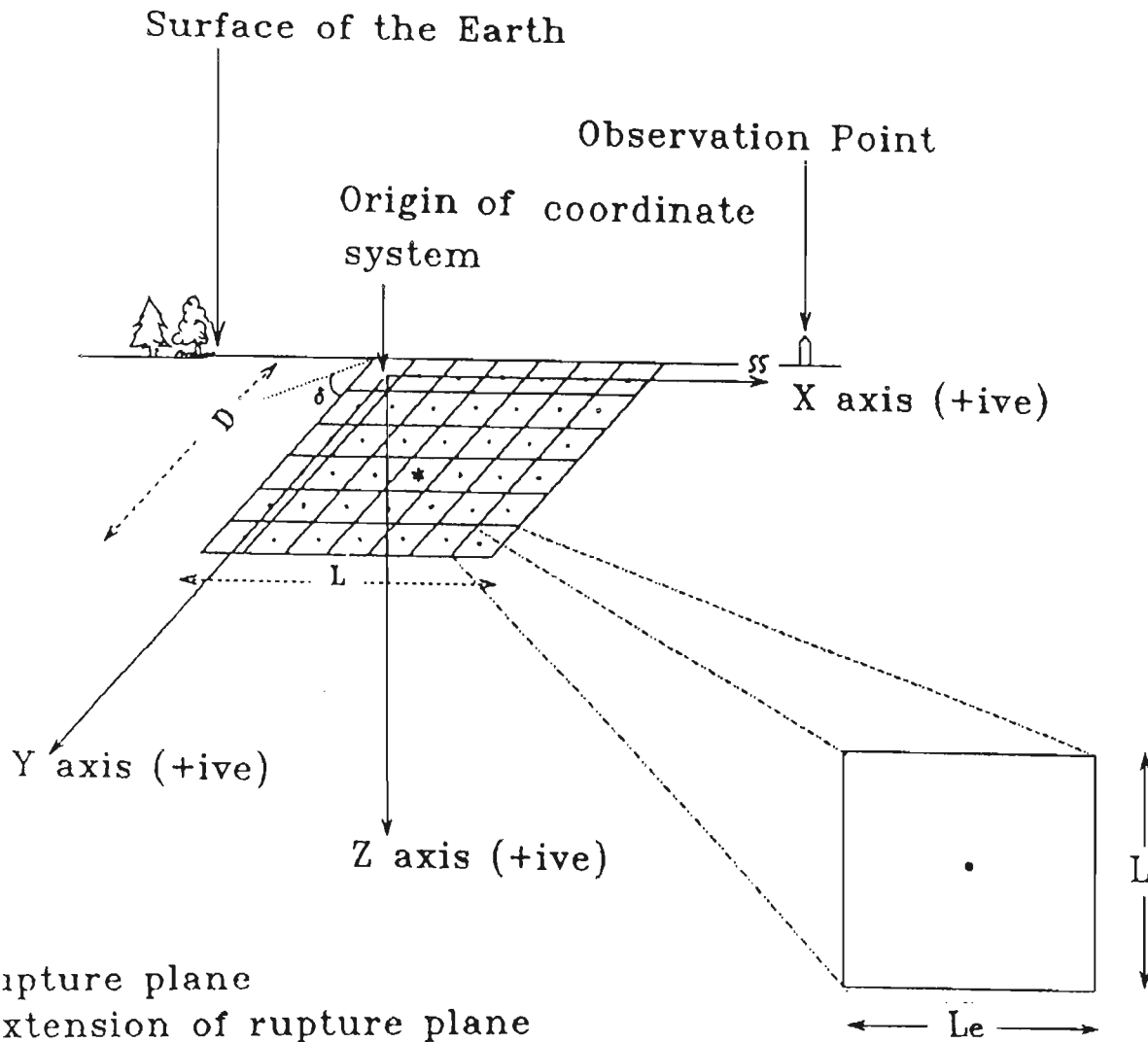
Fig 2.2 shows model of rupture plane with various parameters. The rupture plane is modelled to simulate strong motion records at the selected observation points. The procedure for modelling of the rupture plane is discussed in detail in the next chapter.

Surface of the earth



- L Length of rupture plane
- D Downward extension of rupture plane
- * Denotes nucleation point
- . Denotes center of element
- L_e Length of one side of square element

Fig 2.1 Two dimensional coordinate system used for modelling the rupture plane. Origin of coordinate system is at the center of (topmost element) extreme corner of the rupture plane. In this case origin lies at the topmost element at extreme left corner of rupture plane.



- Length of rupture plane
- Downward extension of rupture plane
- Dip of rupture plane
- Denotes nucleation point
- Denotes center of element
- Length of one side of square element

Fig 2.2 Three dimensional coordinate system used for modelling the rupture plane. Origin of coordinate system is at the center of (topmost element) extreme corner of the rupture plane. In this case origin lies at the topmost element at extreme left corner of rupture plane.

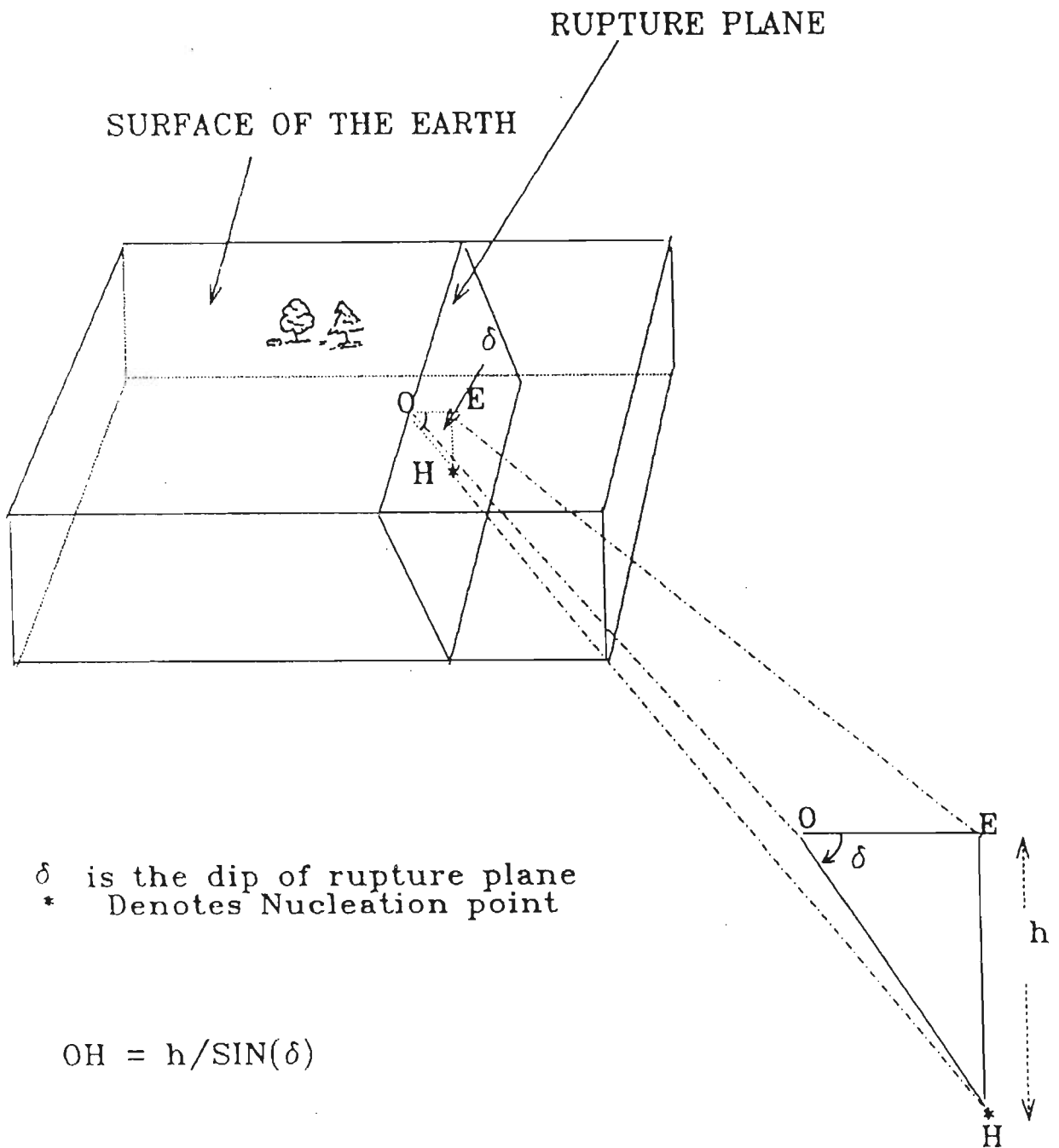


Fig 2.3 Method of computing the location of the nucleation point within the rupture plane. 'E' is the epicenter and 'h' is the hypocentral depth of the earthquake and ' δ ' is dip of the rupture plane. The distance OH gives the location of nucleation point within the rupture plane.

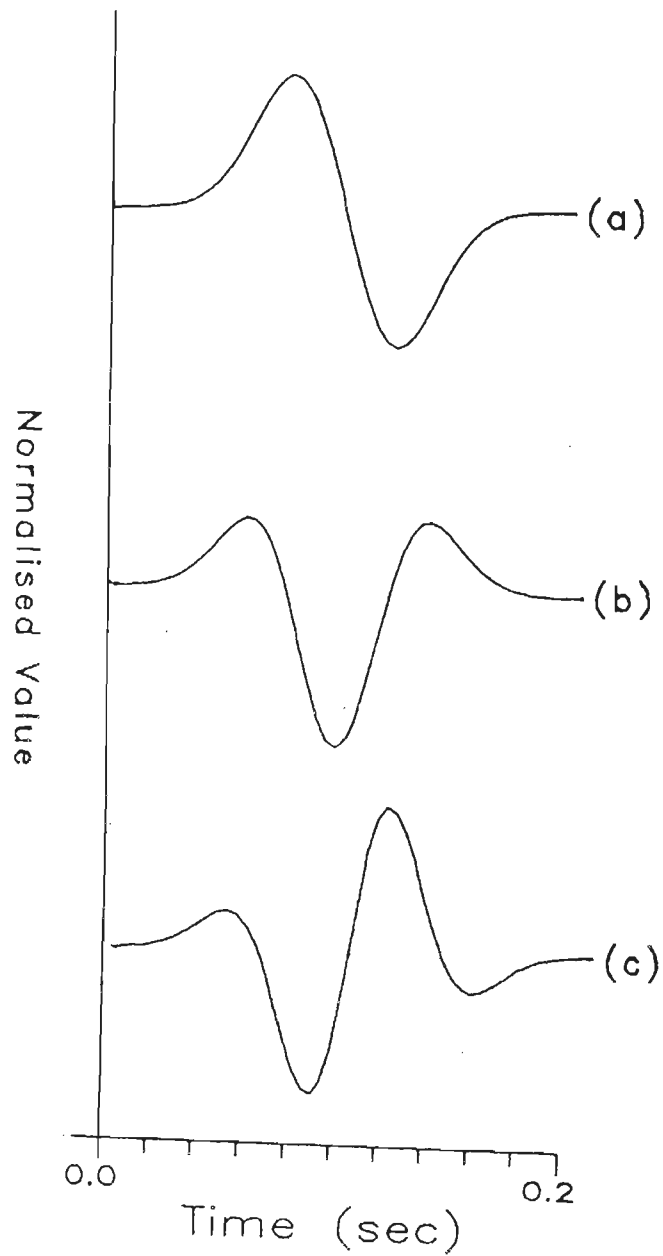


Fig 2.4 Normalised (a) Displacement form, (b) Velocity form and (c) Acceleration form of source wavelet of frequency 5 Hz at sampling interval of 4 ms. Acceleration and displacement form of source wavelet is computed by differentiation and integration of velocity form, respectively. The data is given in Table 2.2.

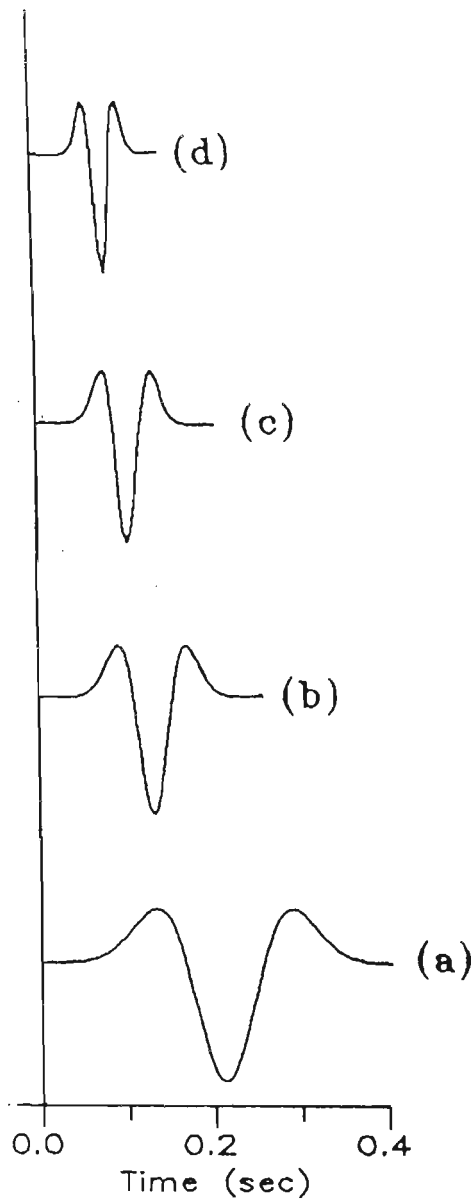


Fig 2.5 Velocity type source wavelet of frequencies (a) 2.5 Hz, (b) 5.0 Hz, (c) 7.5 Hz and (d) 10.0 Hz. The normalised values of source wavelets at sampling interval of 4 ms is given in Table 2.3.


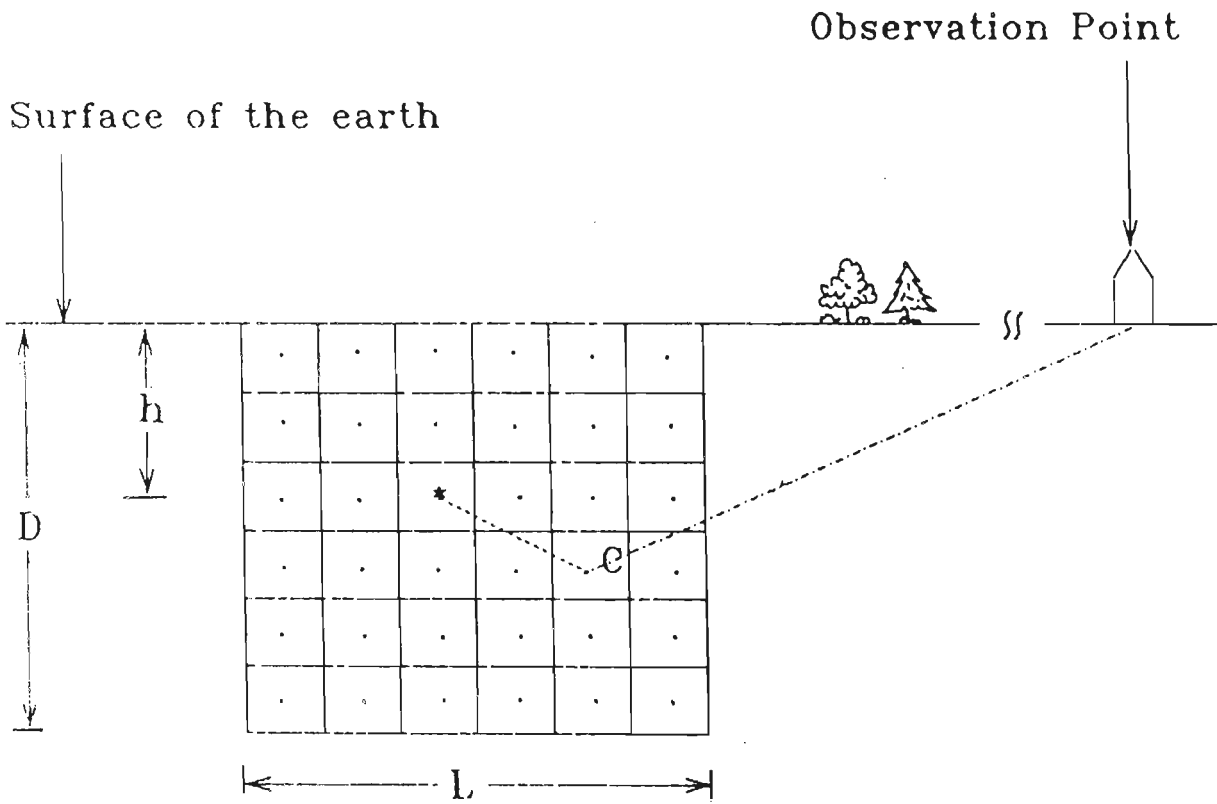
5	4	3	4	5	8
4	2	1	2	4	7
3	1		1	3	6
4	2	1	2	4	7
5	4	3	4	5	8
8	7	6	7	8	9

Fig 2.6 Radial type of rupture propagation from nucleation element, within rupture plane. Number 1,2,3,4,... represent 1st, 2nd, 3rd, 4th etc. group of elements within rupture plane effected by the propagation of rupture from nucleation point.



.....	Distance between center C of the element and nucleation point
.....	Distance between center C of the element and observation point
*	Nucleation point
·	Center of element
L	Length of rupture plane
D	Downward extension of rupture plane

Fig 2.7 Time of arrival of released source wavelet from the center of element 'C' within the rupture plane to the observation point. This time is the sum of (a) time taken by rupture to reach the center of the element 'C' within the rupture plane from the nucleation point and the time taken by released wavelet from the center 'C' of the element to reach the observation point.

S.N	REF. OF FORMULA	RUPTURE LENGTH IN KM	FORMULA	REGION FROM WHICH DATA HAS BEEN USED FOR DEVELOPING RELATION
1.	Tocher (1958)	1	$\text{Log } L = 1.02 - 5.77$	U.S.
2.	Dan et al. (1990)	7	$\text{Log } L = .319 \text{ Log } M_o - 6.91$ $\text{Log } M_o = 1.22M + 17.43$	Japan
3.	Sato (1979)	9	$\text{Log } L = 1/3 \text{ Log } M_o - 7.28$ $\text{Log } M_o = 1.5M + 16.2$	Japan
4.	Araya and Kiureghian (1988)	3	$\text{Log } L = -2.77 + .619M_s$	Worldwide
5.	Otsuka (1965)	9	$\text{Log } L_m = 3.2 + .5M$	Worldwide
6.	Housner (1970)	6	Table	Worldwide
7.	Naeim (1989)	5 to 10	Table	Worldwide

Table 2.1 Rupture length for the Dharamsala earthquake of 26th April, 1986 calculated from different empirical relations. The rupture length calculated by relation of Otsuka (1965) and Naeim (1989) gives the maximum rupture length and the upper and lower limits of rupture length, respectively.

DIS. VALUE	VEL. VALUE	ACC. VALUE
.0000	.0019	.2709
.0000	.0037	.6151
.0001	.0068	1.0652
.0002	.0122	1.7704
.0003	.0210	2.8197
.0005	.0348	4.2954
.0008	.0554	6.2420
.0013	.0847	8.6231
.0020	.1244	11.2682
.0029	.1749	13.8254
.0041	.2350	15.7373
.0056	.3008	16.2667
.0072	.3651	14.5920
.0091	.4175	9.9799
.0109	.4449	2.0166
.0125	.4336	-9.1500
.0136	.3717	-22.6324
.0140	.2526	-36.7690
.0135	.0776	-49.2954
.0121	-.1418	-57.7265
.0096	-.3842	-59.8918
.0062	-.6209	-54.4950
.0023	-.8202	-41.5395
-.0019	-.9532	-22.4762
-.0059	-1.0000	.0000
-.0094	-.9532	22.4762
-.0120	-.8202	41.5395
-.0136	-.6209	54.4950
-.0142	-.3842	59.8918
-.0138	-.1418	57.7265
-.0127	.0776	49.2954
-.0111	.2526	36.7690
-.0093	.3717	22.6324
-.0074	.4336	9.1500
-.0056	.4449	-2.0166
-.0041	.4175	-9.9799
-.0029	.3651	-14.5920

Continued in the next page...

Continued from previous page...

DIS. VALUE	VEL. VALUE	ACC. VALUE
-.0020	.3008	-16.2667
-.0013	.2350	-15.7373
-.0008	.1749	-13.8254
-.0005	.1244	-11.2682
-.0003	.0847	-8.6231
-.0002	.0554	-6.2420
-.0001	.0348	-4.2954
.0000	.0210	-2.8197
.0000	.0122	-1.7704
.0000	.0068	-1.0652
.0000	.0037	-.8561
.0000	.0000	-.4625

DIS. = Displacement

VEL. = Velocity

ACC. = Acceleration

Table 2.2 Sampled values of (a) displacement, (b) velocity and (c) acceleration form of source wavelet of 5 Hz frequency at sampling interval of 4 ms. Displacement and acceleration form of source wavelet is obtained after the integration and the differentiation of velocity form of source wavelet, respectively. Fig 2.4 shows plot of displacement, velocity and acceleration form of source wavelet using data from this table.

S.N.	FREQUENCY			
	2.5Hz	5.0Hz	7.5Hz	10.0Hz
1	.001	.000	.000	.000
2	.002	.000	.000	.000
3	.003	.000	.000	.000
4	.004	.000	.000	.000
5	.005	.000	.000	.000
6	.007	.000	.000	.000
7	.009	.000	.000	.000
8	.012	.000	.000	.000
9	.016	.000	.000	.000
10	.021	.000	.000	.000
11	.027	.000	.000	.000
12	.035	.000	.000	.000
13	.044	.000	.000	.000
14	.055	.000	.000	.000
15	.069	.000	.000	.000
16	.085	.000	.000	.000
17	.103	.000	.000	.000
18	.124	.000	.000	.000
19	.148	.000	.000	.000
20	.175	.000	.000	.000
21	.204	.000	.000	.000
22	.235	.000	.000	.000
23	.268	.000	.000	.000
24	.301	.000	.000	.000
25	.334	.001	.000	.000
26	.365	.002	.000	.000
27	.394	.004	.000	.000
28	.417	.007	.000	.000
29	.435	.012	.000	.000
30	.445	.021	.000	.000
31	.445	.035	.000	.000
32	.434	.055	.001	.000
33	.410	.085	.002	.000
34	.372	.124	.006	.000
35	.319	.175	.013	.000
36	.253	.235	.028	.000
37	.172	.301	.054	.000
38	.078	.365	.097	.001
39	-.028	.417	.160	.004

Continued on the next page...

Continued from previous page...

S.N.	FREQUENCY			
	2.5Hz	5.0Hz	7.5Hz	10.0Hz
40	-.142	.445	.242	.013
41	-.262	.434	.334	.039
42	-.384	.372	.413	.097
43	-.505	.253	.446	.199
44	-.621	.078	.399	.334
45	-.727	-.142	.244	.437
46	-.820	-.384	-.015	.399
47	-.897	-.621	-.343	.126
48	-.953	-.820	-.670	-.343
49	-.988	-.953	-.911	-.806
50	-1.000	-1.000	-1.000	-1.000

Table 2.3 Normalised value of velocity form of source wavelet of 2.5, 5.0, 7.5 and 10.0 Hz frequency. This data has been used in Fig. 2.5.

CHAPTER 3

SIMULATION OF STRONG GROUND MOTION

Once a fault has been identified as the most probable causative fault on the map, the next step for generation of synthetic strong motion records is to model the rupture plane along a fault. The scheme of identification of most probable causative fault on a map is discussed in Chapter 2 and the parameters required for modelling of rupture plane within the identified most probable causative fault have also been defined therein. This chapter deals with the procedure adopted for modelling of the rupture plane to simulate the strong motion records. The synthetic strong motion records are simulated at selected observation points, taking into account the various modelling parameters of rupture plane discussed in the previous chapter. An example of a model of vertical rupture plane used for simulating strong motion records for the Meghalaya earthquake of 10th Sept, 1986 is presented in this chapter to explain the methodology.

3.1 PROCEDURE OF SIMULATION OF SYNTHETIC STRONG MOTION RECORDS FOR A MODEL OF RUPTURE PLANE

The rupture plane is modelled as a rectangular plane embedded in a homogeneous isotropic half space with its geometry defined by length (L) and downward extension (D) of the rectangular plane. The length of the rupture plane and its downward extension is calculated using empirical relations as discussed in detail in Chapter 2. Dip (δ) of the rupture plane is taken from the fault plane solutions of the earthquake (if available). In case the fault plane solution is not available, the dip (δ) can be selected

from value of 90° (vertical), 0° (horizontal) or 45° (dipping) for simplicity in the rupture model.

The rectangular rupture plane is divided into several equidimensional square elements mapped on a three dimensional coordinate system. The X-axis of the coordinate system is parallel to the strike of rupture plane and the origin of the system is at the center of topmost element on extreme corner. For vertical rupture model the depth of origin lies at a distance of $L_e/2$ from the upper extension of the rupture plane. The Y-axis is perpendicular to the X-axis and is positive in the direction of the dip of rupture plane. The Z-axis is positive vertically downwards. The coordinates of the observation points in the assumed system can be calculated using a suitably scaled map of the area containing the observation points at which field records are available and where the synthetic records are desired to be generated. The location of the rupture plane is also be marked on the same map.

An element within the rupture plane is assumed as starting point of rupture and is called the nucleation point. Rupture starts from the nucleation point in the rupture plane (as discussed in Chapter 2) and propagates radially to the center of surrounding elements with the assumed rupture velocity. The geometry of the rupture propagation is radial. As soon as the rupture reaches the center of the surrounding elements it emits energy in the form of assumed source wavelet ($V_s(t)$) of amplitude A_{vr} .

For simulation of strong ground motion records, energy released by an element is scaled with the amplitude of source wavelet released by the same element. The method of scaling of the released energy with the amplitude of source wavelet released by the element is presented in the form of a flow chart shown in Fig 3.1.

STEP 1. Energy released in an earthquake (E) is computed from the Magnitude Energy relation (Gutenberg and Richter, 1956, Kasahara, 1981)

$$\text{Log } E = 11.8 + 1.5 M \quad (3.1)$$

Where,

E = Energy released during earthquake in ergs

M = Richter local Magnitude of the earthquake

The value of M used in expression (3.1) can be computed from body wave magnitude M_b by the expression (Gutenberg and Richter, 1956, Kasahara, 1981)

$$M = 1.59 M_b - 3.97 \quad (3.2)$$

Where,

M_b = Body wave magnitude of the earthquake

The expression (3.1) can hence be expressed as :

$$\text{Log } E = 5.8 + 2.4 M_b \quad (3.3)$$

STEP 2. The energy is assumed to be divided equally among all elements. Let N be the total number of elements within the rupture plane, then the energy released by an element is given by the expression :

After page no. 48, page numbering is one less than that typed on page

$$E_e = E/N \quad (3.4)$$

STEP 3. It is assumed that the energy is released by the point source in the form of a radiated sinusoidal wave of period T_o and amplitude A_d and can be expressed as (Gutenberg and Richter, 1956, Kasahara, 1981):

$$E = 3.\pi^3.h^2.V.t_{no}.\rho (A_d/T_o)^2 \quad (3.5)$$

where,

- T_o = Period of wave released by point source,
- t_{no} = Total duration of wave train radiated by point source
= nT_o (n is number of wave radiated by point source),
- h = Hypocentral depth,
- ρ = Density of the medium,
- V = Velocity of propagation of wave and,
- E = Energy released during an earthquake.

The expression (3.5) can also be expressed as :

$$A_d^2 = E.T_o^2/(3.\pi^3.h^2.V.t_{no}.\rho) \quad (3.6)$$

Expression (3.5) shows that energy is proportional to the second power of the frequency and amplitude of the wave. Derivation of this expression (After Kasahara, 1981) is given in Appendix I. The amplitude of the wave calculated by this expression is meant for a recording station lying exactly at the epicenter



of the earthquake shown in Fig 3.2. As strong motion records are recorded close to the epicenter, the expression (3.6) is applied for scaling of the energy with the amplitude of source wavelet in the present approach.

The sinusoidal wave of period T_0 and amplitude A_d reaching at the epicenter can be expressed in terms of ground displacement $X(t)$ (Kasahara, 1981) as :

$$X(t) = A_d \cos(2\pi t/T_0) \quad (3.7)$$

Where,

A_d = Amplitude of sinusoidal wave radiated by point source and

T_0 = Period of wave.

(the observation point is assumed to be at epicenter as shown in Fig 3.2).

From expression (3.7) it is seen that the ground displacement varies from $-A_d$ to $+A_d$. Since the displacement varies with time, each particles of the medium has a velocity $v(t)$ (Telford et al., 1976). The ground motion velocity $v(t)$ at the epicenter for displacement expressed in (3.7) is given as (Kasahara, 1981):

$$v(t) = (-2\pi A_d/T_0) \sin(2\pi t/T_0)$$

$$v(t) = A_v \sin(2\pi t/T_0)$$

Where,

$$A_v = (2\pi A_d/T_0)$$

Substituting value of A_d from (3.6) the following expression is obtained :

$$A_v = [4E/(3\pi \cdot h^2 \cdot V \cdot t_{no} \cdot \rho)]^{1/2} \quad (3.8)$$

where,

T_0 = Period of wave released by point source,

t_{no} = Total duration of wave train radiated by point source

= nT_0 (n is number of wave radiated by point source),

h = Hypocentral depth,

ρ = Density of the medium,

V = Velocity of propagation of wave and

E = Energy released during an earthquake.

A_v gives the amplitude of velocity wavelet radiated by a point source for an earthquake releasing energy E.

STEP 4. A_v obtained from expression (3.8) is for a velocity form of sinusoidal wave radiated by point source, shown in Fig 3.3 and is mathematically expressed in expression (3.7). The amplitude of assumed source wavelet of known frequency (period) can be computed by following two methods :

METHOD I (GRAPHICAL)

Maximum amplitude (A_{vr}) of the source wavelet of the form shown in Fig 3.4 can be related with the maximum amplitude A_v of the sinusoidal wave shown in Fig 3.3 by the expression :

$$2A_v = 1.446 A_{vr} \quad (3.9)$$

This expression is derived on the basis of ratio of A_v and A_{vr} as shown in Fig 3.3 and 3.4, respectively, and hence can also be written as:

$$A_{vr} = 1.383 A_v \quad (3.10)$$

METHOD II (ANALYTICAL)

Velocity form of wavelet ($v(t)$) radiated by point source is related with the energy released (E) during an earthquake by following relation (Gutenberg and Richter, 1956, Kasahara, 1981) :

$$E = 4\pi h^2 V t_{no} \rho / 2T_o \int_0^{T_o} v^2(t) dt \quad (3.11)$$

Where,

T_o = Period of wave released by an element,

h = Hypocentral depth,

ρ = Density of the medium,

V = Velocity of propagation of wave,

E = Energy released by an element and

t_{no} = Total duration of wave train radiated by point source.

For a point source radiating sinusoidal wave $(v(t))$ of period T_o and given by expression (3.7), following expression is obtained :

$$\int_0^{T_o} v^2(t) dt = T_o/2$$

For a sinusoidal wave of period .2 sec (frequency =5 Hz) and amplitude A_v , following expression is obtained :

$$\int_0^{T_o} v^2(t) dt = .1A_v^2$$

Substituting this value in expression (3.11), the following expression is obtained:

$$E = K_1 (.1)A_v^2 \quad (3.12)$$

Where,

$$K_1 = 4\pi rh^2 V_{t_{no}}^2 \rho / 2T_o$$

For point source radiating velocity type wavelet $v_s(t)$ of the form shown in Fig 3.4 having the same frequency as that of the sinusoidal wavelet (i.e. 5 Hz) and amplitude A_{vr} , the following expression is obtained:

2.9312

$$\int_0^{T_o} v_s^2(t) dt = A_{vr}^2 (.05)$$

The value of definite integral is obtained from Trapezoidal rule for integration explained in detail in Chapter 5 using the digitised value of source wavelet at a sampling interval of 4 ms as given in Table 2.3.

Substituting this value in expression 3.11, the following relation between energy released and amplitude of source wavelet is obtained :

$$E = K_1 A_{vr}^2 (.05) \quad (3.13)$$

As the energy released by an element will remain the same, therefore E obtained by expressions (3.12) and (3.13) are similar and hence,

$$(.1) A_v^2 = (.05) A_{vr}^2$$

$$A_{vr} = 1.41 A_v \quad (3.14)$$

Amplitude A_v of velocity form of sinusoidal wave, obtained from expression (3.8) can be related with the amplitude of assumed source wavelet of form shown in Fig 3.4 by the expressions (3.10) or (3.14). The expression 3.14 is derived taking into consideration of the total energy within the source wavelet and is used in the present work.

STEP 5. For the velocity type source wavelet of form shown in Fig 3.4, A_{vr} can be computed by expression (3.10) or (3.14). Following table gives the values of amplitude of the velocity type source wavelet (A_{vr}) for three different earthquakes studied in the present work.

S.N.	Magnitude M_b	V km/s	h km	N	T_o sec	A_{vr} cm/sec
1.	5.5	5.6	6	81	.2	.98
2.	6.5	5.7	12	1218	.4	1.40
3.	5.2	6.7	28	49	.2	.13

Where,

M_b = Body wave magnitude,

h = Hypocentral depth,

N = Total Number of elements within rupture plane,

T_o = Time period of source wavelet,

A_{vr} = Amplitude of velocity form of source wavelet released by an element and

V = Velocity of the medium.

Density of the medium (ρ) in all cases is kept as 2.7 gm/cm^3 (Kasahara, 1981). The term A_{vr} gives the amplitude of the velocity type source wavelet released by an element and has been used in the present study. The value of A_{vr} calculated above is assumed to be same for all wavelets released by different elements within the rupture plane.

Nucleation element is the first element within the rupture plane to emit source wavelet. The time taken by the source wavelet, released by the nucleation element to reach the observation point is equal to the time taken by the wavelet to travel the distance between nucleation point and the observation point with the velocity of the medium.

The time taken by source wavelet to reach the observation point, which start from a particular element within rupture plane other than nucleation point is equal to the sum of :

- (a) The time taken by rupture to reach the particular element from the nucleation point with velocity V_r and
- (b) The time taken by the wavelet to travel the distance between that particular element and the observation point with the velocity of the medium.

The wavelets from different elements reach the observation point at different times. The total record at the observation point takes into account the appropriate time lags due to the geometry of rupture propagation and travel times of energy released in the form of source wavelet through the homogeneous medium. As the wavelet released is velocity type source wavelet, the simulated record at the observation point represent

velocity record. Differentiation and integration of this record yield acceleration and displacement records, respectively.

3.2 SIMULATION PROCEDURE OF STRONG GROUND MOTION: AN EXAMPLE

The method of simulation of strong ground motion explained in detail in above sections is applied for a model of vertical rupture plane for Meghalaya earthquake of 10th Sept, 1986. The most probable causative fault for this earthquake is identified and discussed in detail in Chapter 8. Various modelling parameters for this rupture plane are :

Length of the rupture plane = 6 km,

Downward extension of the rupture plane = 6 km,

Dip = 90° ,

Strike = $N52^\circ E$,

Length of the element = 1 km,

Total number of elements within rupture plane = 36,

Coordinate of starting point of rupture = (2,0,2),

Velocity of the medium = 6.7 km/s and

Rupture velocity = 3.0 km/s.

The model for rupture plane is shown in Fig 8.22. Strong motion records are simulated at station Saitsama using this model. Coordinates of Saitsama station in the rectangular coordinate system shown in Fig 8.23 are (23.5,9.25,-28.4). Arrival time of the energy released by different elements, at Saitsama station is calculated as explained in earlier sections. This gives the net time shift required for energy released

by different elements in the form of source wavelets to reach the station at Saitsama. The value of scaling factor which takes into account the total energy released by an element is computed as .13 cm/sec for model of rupture plane. This value is multiplied with normalised value of source wavelet released by different elements. Table 2.3 gives the digitised value of source wavelet of 5 hz frequency at a sampling interval of 4 ms. Various elements within the rupture plane are denoted by different numbers as shown in Fig 3.5a. The impulse response due to the rupture model is shown in Fig 3.5b and Fig 3.5c shows source wavelet at Saitsama station, released by different elements with appropriate arrival time at the station. Addition of these shifted source wavelet gives velocity record due to model of rupture plane, at Saitsama station and is shown in Fig 3.5d.

The simulated velocity record shown in Fig 3.5d and 3.6a is obtained at a sampling interval of 4 ms. Differentiation of this velocity record gives acceleration record. As field acceleration records are available at 20 ms (.02 sec) therefore the sampling interval of simulated acceleration record is converted into 20 ms. From the integration of the velocity record, displacement records are produced at a sampling interval of 100 ms (.1 sec) as this is the sampling interval of available field displacement records. Fig 3.6a and 3.6b shows velocity and acceleration records at Saitsama at sampling interval of 4 ms, respectively. Fig 3.6c shows the acceleration record at sampling interval of 20 ms (.02 sec) and Fig 3.6d shows the displacement record at sampling interval of 100 ms (.1 sec).

3.3 SUMMARY

Simulation provides a potential tool for modelling the propagation of rupture within the rupture plane and propagation of energy in a homogeneous medium. Records can be simulated at any observation point for a radial rupture geometry within the rupture plane. As an example, strong motion records for Meghalaya earthquake of 10th Sept, 1986 have been simulated at Saitsama station for a model of rupture plane. Acceleration, velocity and displacement records have also been simulated at Saitsama station for this model.

Efficacy of this approach can be checked by comparison of the parameters of the synthetic and field records. Various parameters which are used for comparison of simulated records with field records at the selected observation points are discussed in the following chapter (Chapter 4). Algorithms of programs for the purpose of simulation of strong ground motion record at the selected observation points and that for extraction of parameters used for comparison of field and simulated records are discussed in detail in Chapter 5.

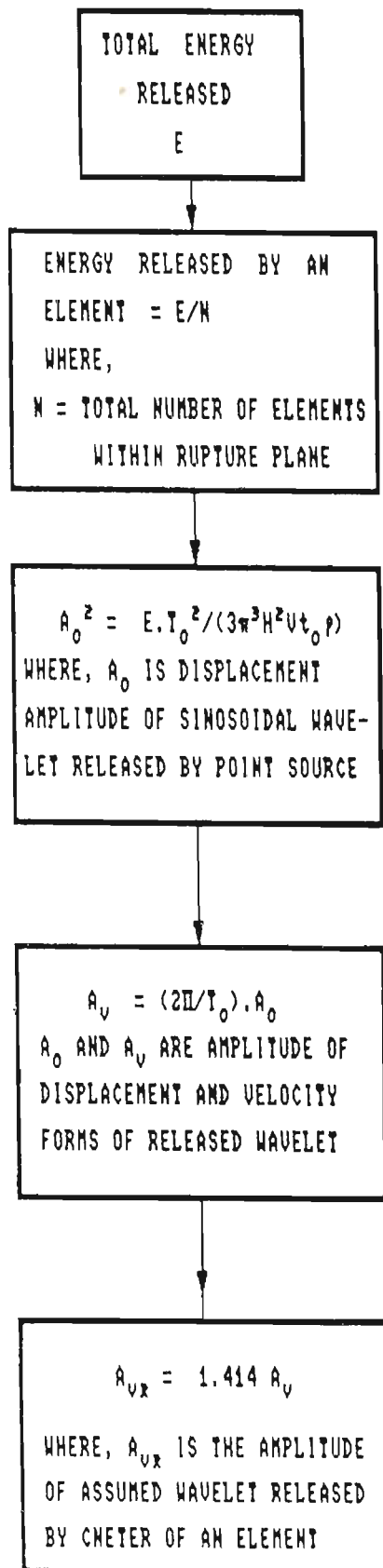
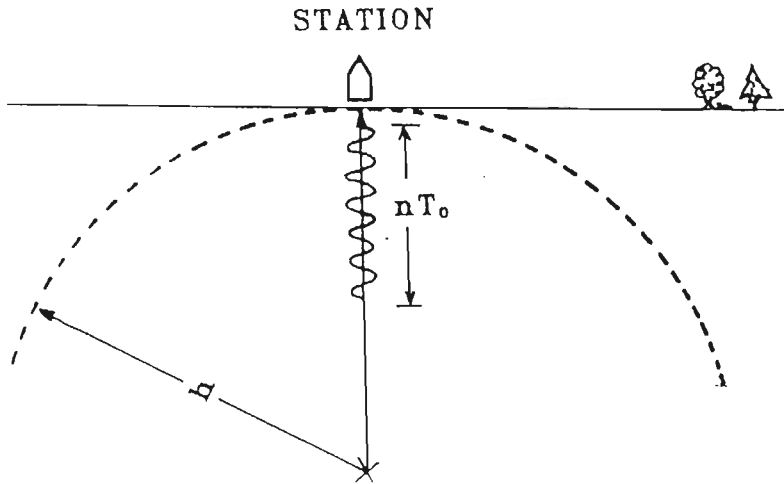


Fig 3.1 Block diagram showing various steps involved for scaling the amplitude of the source wavelet released by an element.

SURFACE OF THE EARTH



- n = Number of released waves
- T = Period of wave
- h = Hypocentral depth
- X = Hypocenter of the earthquake

Fig 3.2 Schematic diagram of part of a wave train from point source approaching a station at the epicenter (After Kasahara, 1981).

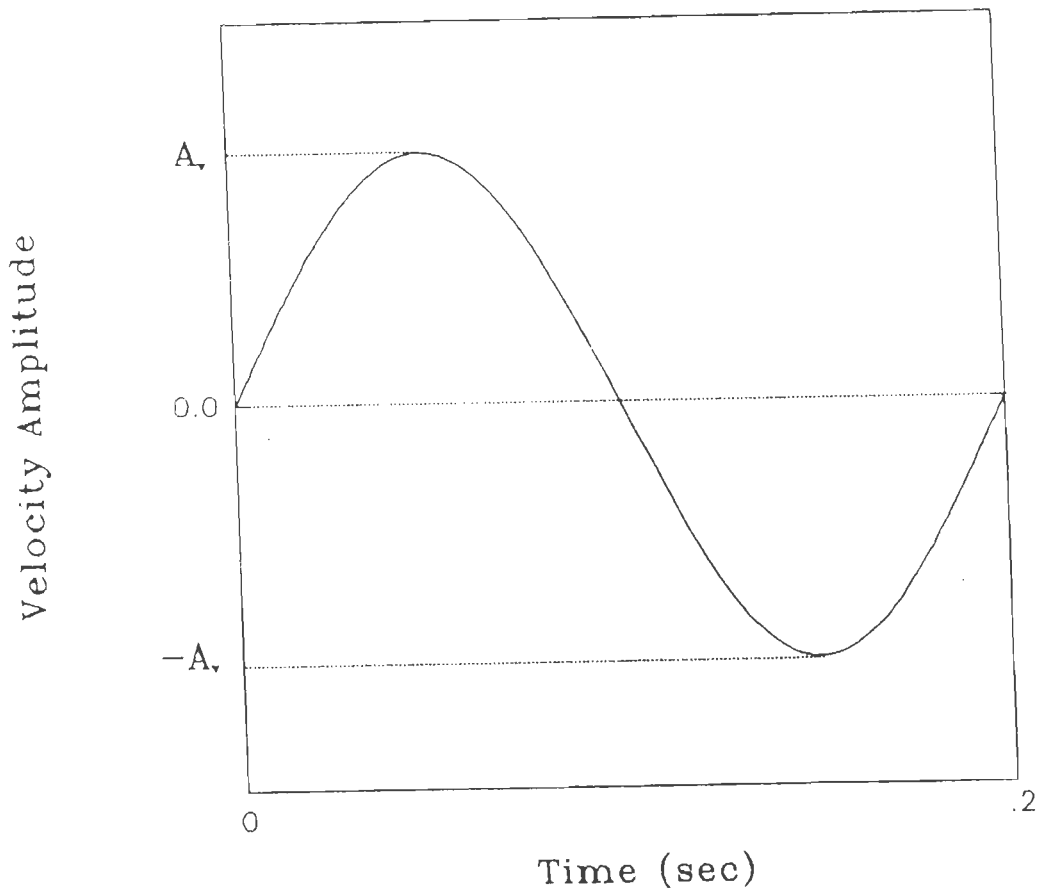


Fig 3.3 Normalised form of velocity type sinusoidal wavelet with peak amplitude A_v .

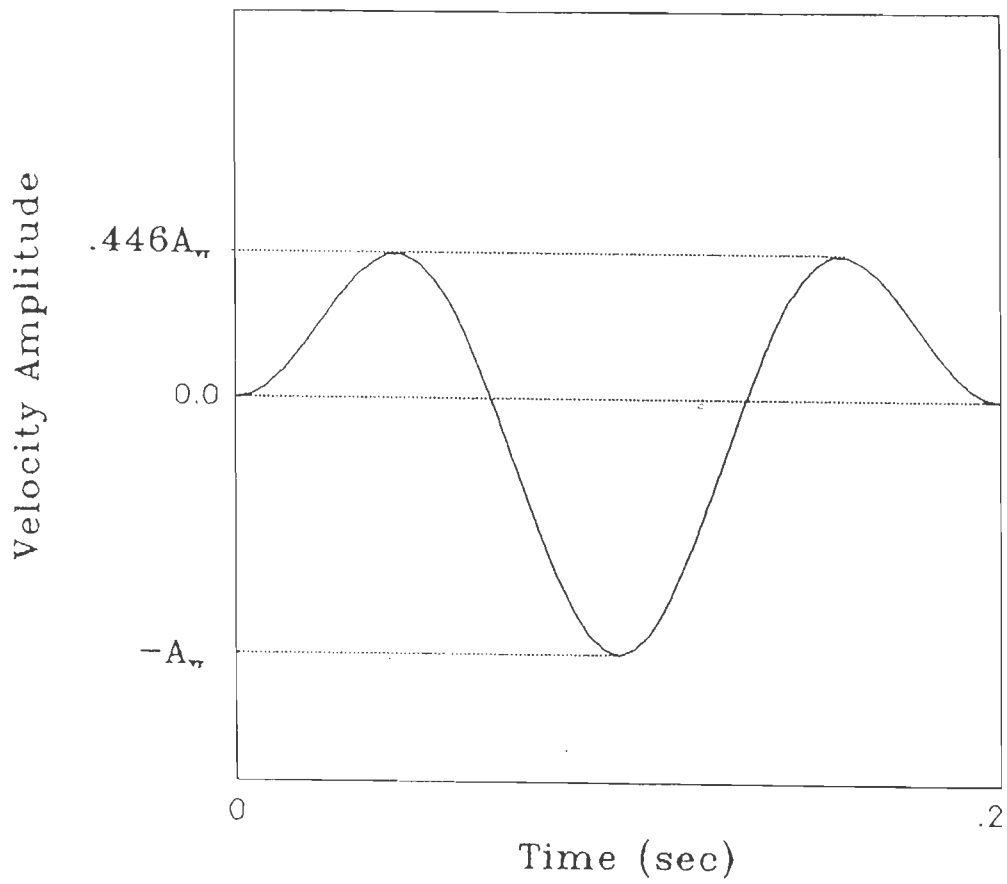


Fig 3.4 Normalised form of velocity type wavelet with peak amplitude A_v , assumed for present study.

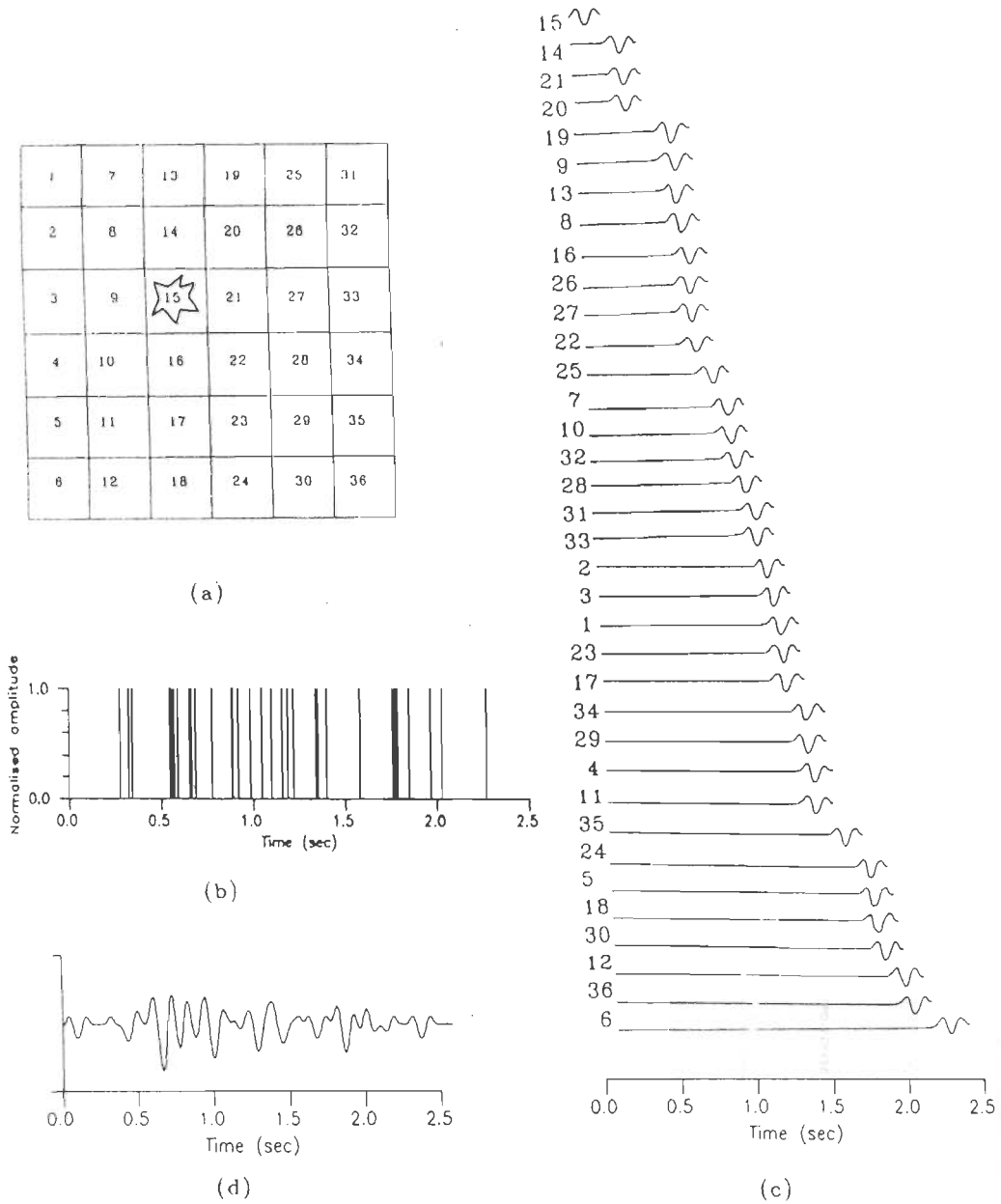


Fig 3.5 (a) Model of rupture plane with various elements represented by different numbers. Element numbered as 15 is the starting point of rupture in the assumed model. This model is same as used for the Meghalaya earthquake of 10th Sept, 1986. (b) Impulse response due to the rupture model shown in Fig 3.5(a) at Saitsama station. Time of arrival of spikes at station is arrival time of source wavelet from the center of the element to reach the observation point. Time of arrival of spikes at station is shown in Fig 2.7. (c) Source wavelets released by different element with appropriate arrival time at Saitsama. Arrival time at the station takes into consideration time taken by rupture to reach a particular element and the time taken by source wavelet from same element to reach observation point. The number in this figure corresponds to the element number shown in (a). and (d) addition of delayed source wavelets shown in Fig 3.5(b) to obtain velocity record at the observation point.

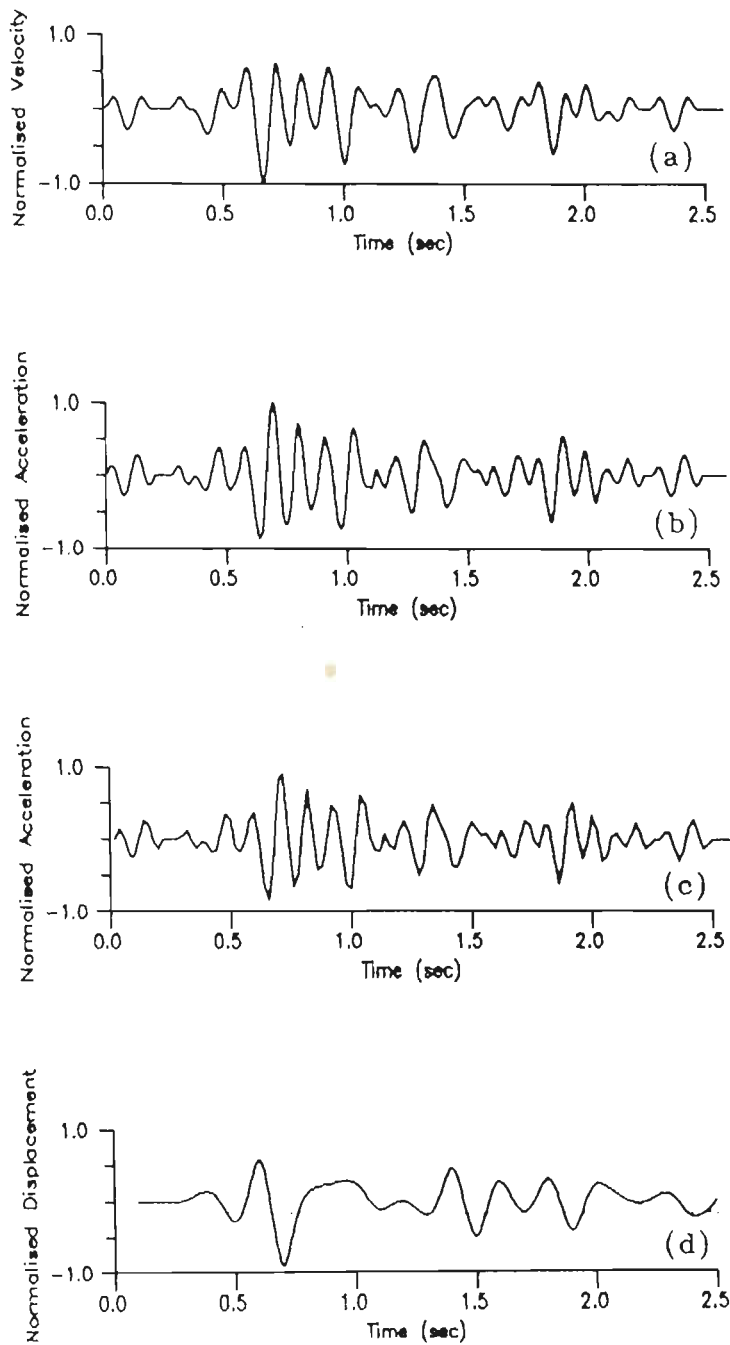


Fig 3.6 Normalised value of (a) Simulated velocity record at 4 msec (.004 sec) sampling interval, at Saitsama station due to the rupture model shown in Fig 3.5 (a), (b) acceleration record at 4 msec sampling interval obtained after differentiation of simulated velocity record, (c) acceleration record at 20 msec (.02 sec) sampling interval and (d) displacement record obtained from integration of simulated velocity record at sampling interval of 100 ms (.1 sec).

CHAPTER 4

FEATURE EXTRACTION FROM STRONG MOTION RECORD

Synthetic strong motion records for any selected observation point can be simulated by the procedure given in the previous chapter (Chapter 3). The selected observation points are generally taken as those at which actual field records are available so that the synthetic and field records can be compared. Feature extraction or parameter selection is of key importance in comparison of field and simulated for a defined model. The parameters extracted for comparison between the field and simulated records can be classified into two categories (i) Time domain parameters and (ii) Frequency domain parameters. The parameters selected for comparative study are defined and discussed in this chapter. As an example, features extracted from the simulated records at Saitsama station for Meghalaya earthquake of 10th Sept, 1986 are discussed.

4.1 TIME DOMAIN PARAMETERS

Various parameters which have been extracted from time series of field and simulated records are classified under this category and are given as :

Parameters extracted from strong motion record are :

- (i) P_a = Value of peak acceleration in the acceleration record (cm/sec^2),
- (ii) P_v = Value of peak velocity in the velocity record (cm/sec),
- (iii) P_d = Value of peak displacement in the displacement record (cm),
- (iv) T_D = Duration of the acceleration record (sec),
- (v) T_{at} = Arrival time of peak in the acceleration record (sec),
- (vi) R_{at} = Ratio of area covered by the acceleration record above and below the abscissa and
- (vii) T_{area} = Sum of the acceleration values on both side of abscissa.

Symbols used for parameters obtained from autocorrelation function (ACF) of acceleration record are:

- A_i = Value of autocorrelation function at subscripted lag 'i',
- T_i = Time of i th zero crossing in ACF,
- T_m = Time of arrival of global minima and
- A_m = Global minimum value of ACF.

Parameters extracted from autocorrelation function of acceleration record are:

- (viii) $ACF_1 = T_1$ = Time of first zero crossing,
- (ix) $ACF_2 = T_2$ = Time of second zero crossing,
- (x) $ACF_3 = T_3$ = Time of third zero crossing,
- (xi) $ACF_4 = T_m$ = Time of arrival of global minima,
- (xii) $ACF_5 = A_1/A_0$,

- (xiii) $ACF_6 = A_2/A_0$,
- (xiv) $ACF_7 = A_3/A_0$,
- (xv) $ACF_8 = A_m/A_0$,
- (xvi) $ACF_9 =$ Ratio of area under ACF between time $T=0$ to $T=T_1$ and area under ACF between time $T=T_1$ to $T=T_2$ and
- (xvii) $ACF_{10} =$ Ratio of area under ACF above and below the abscissa.

$A_0, A_1, A_2, A_3, A_m, T_1, T_2, T_3, T_m$, are computed directly from the autocorrelation function of acceleration record. Parameters mentioned in (viii) to (xv) have also been identified by Sinvhal (1976 and 1979) and Sinvhal and Sinvhal (1992), for comparison between the simulated and field records for seismic prospecting.

4.1.1 PARAMETERS EXTRACTED FROM STRONG MOTION RECORDS

Various parameters that have been extracted from the strong motion records are $P_a, P_v, P_d, T_{at}, T_D, R_{at}$ and T_{area} . Parameters P_a, P_v and P_d represent the amplitude of ground motion at a particular site. All of these parameters are discussed in detail in following section:

(i) **Peak acceleration (P_a):** Peak acceleration is the maximum value of acceleration observed in the accelerogram. For comparison of peak acceleration of simulated record with field record, accelerograms are simulated at the observation point for which field accelerograms are available. Fig 4.1 shows method of computing P_a from the acceleration record. Acceleration record shown in this figure is a simulated record at Saitsama station for Meghalaya earthquake of 10th Sept, 1986.

(ii) **Peak velocity (P_v):** Peak velocity is maximum value of velocity observed in the velocity record. For comparison of peak velocity of simulated record with field record, velocity records are simulated at the same observation point for which field velocity records are available. Fig 4.2 shows method of computing P_v from velocity record. Velocity record shown in this figure is simulated record at Saitsama station for Meghalaya earthquake of 10th Sept, 1986.

(iii) **Peak Displacement (P_d):** Peak displacement is maximum value of displacement in the displacement record. For comparison of peak displacement of the simulated record with the field record, displacement record are simulated at the same observation point for which field displacement records are available. Fig 4.3 shows method of computing P_d from displacement record. Displacement record shown in this figure is simulated record at Saitsama station for Meghalaya earthquake of 10th Sept, 1986.

(iv) **Duration of record (T_p):** For calculating the duration of the strong motion record in the present work, a function $AI(t)$ representing cumulative addition of the square of acceleration values is computed. This criteria has been already defined by Trifunac and Brady (1975). The function $AI(t)$ can be given as :

$$AI(t) = \sum_0^T a^2(t) dt \quad (4.1)$$

Where,

$a(t)$ = Acceleration record and

T = Total time length of record.

The difference between the arrival time of 5% and 95% of maximum value of function $AI(t)$ is defined as the duration of the record. Parameters T_{dl} and T_{dh} are defined as the arrival time of 5% and 95% of maximum value of function $AI(t)$, respectively. The duration of acceleration record (T_D) can thus be defined as:

$$T_D = T_{dh} - T_{dl} \quad (4.2)$$

where,

T_D = Duration of acceleration record,

T_{dh} = Time of arrival of 95% of peak value of function $AI(t)$ and

T_{dl} = Time of arrival of 5% of peak value of function $AI(t)$.

Fig 4.4 shows the method of computing duration of strong motion record by using function $AI(t)$. The acceleration record used for example purpose is the simulated acceleration record at Saitsama station for the Meghalaya earthquake. Computed values of parameters T_{dl} , T_{dh} and T_D in this case are .48, 2.02 and 1.54 sec, respectively.

(v) Arrival time of peak acceleration in acceleration record (T_{at}): This parameter is defined as the time difference of T_{dl} and the arrival time of peak acceleration (T_a) in the acceleration record. Arrival time in acceleration record is defined by parameter T_{dl} , which is the arrival time of 5% of peak value of function $AI(t)$. Let T_a be the time at which peak acceleration in acceleration record occurs then the parameter T_{at} can be defined as:

$$T_{at} = T_a - T_{dl} \quad (4.3)$$

Fig 4.5 shows the method of computing parameter T_{at} from the acceleration record. The acceleration record used in this case is simulated record at Saitsama station for the Meghalaya earthquake. In this case $T_{dl} = .48$ sec, $T_a = .68$ sec and $T_{at} = .22$ sec.

(vi) **Ratio of area covered by the acceleration record above and below the abscissa (R_{at})** : For computing the parameter R_{at} , acceleration record is divided into several rectangles of width equal to its sampling interval and height equal to the acceleration value at that time. The sum of area covered by acceleration record on one side of the abscissa can be calculated by calculating sum of the area of rectangles on that side. Parameter R_{at} can be obtained by computing the ratio of the sum of area of rectangles above the abscissa with the sum of area of rectangles below the abscissa. As the sampling interval of the record is uniform therefore the parameter R_{at} is equal to the ratio of the sum of acceleration values above the abscissa with the sum of acceleration values below the abscissa.

(vii) **Sum of the acceleration values on both sides of abscissa (T_{area})**: This parameters is computed from the acceleration record and is the sum of the acceleration values on both sides of axis. This parameter represent the total area covered by the acceleration record on both side of abscissa.

The parameters P_a , P_v , P_d , T_D , T_{at} , R_{at} and T_{area} were extracted from the simulated acceleration, velocity and displacement record for Meghalaya earthquake of 10th Sept, at Saitsama station. These parameters are shown in Fig 4.1, 4.2, 4.3, 4.4 and 4.5. Value of these parameters is given as :

S.N.	Parameter	Value	S.N	Parameter	Value
1	P_a	100 cm/sec ²	5	T_D	1.5 sec
2	P_v	2.3 cm/sec	6	T_{at}	.2 sec
3	P_d	.2 cm	7	R_{at}	.93
4	T_{area}	2612			

4.1.2 PARAMETER EXTRACTED FROM AUTOCORRELATION FUNCTION OF ACCELERATION RECORD

Various parameters which have been already mentioned earlier (Section 4.1) are selected from the autocorrelation function of acceleration record for comparison studies. Autocorrelation is the process of correlation of data set with itself (Telford et al., 1976). Autocorrelation function (ACF) A_i of a data set X_i , where $i = 1, 2, \dots, N$ is defined as

$$A_i = \frac{\sum_{k=1}^{k=N} X_{k+i} X_k}{N} \quad (4.4)$$

Where $k = 1, \dots, N$

N = Total number of samples in the data set

Autocorrelation function is symmetrical because a time shift to the right is the same as a shift to the left. From eq. 4.4, following expression is obtained :

$$A_i = A_{-i} \quad (4.5)$$

"..The autocorrelation function has its peak value at zero time shift (that is, a data set is most like itself before it is time shifted). If the autocorrelation has a large value at some time shift $\Delta t \neq 0$, it indicates that the set tends to be periodic with the period Δt . Hence the autocorrelation function may be thought of as a measure of the repetitiveness of a function... (Telford et al., 1976, p 383)."

Parameters selected from autocorrelation function provide an important tool in process of feature extraction. Parameters A_0, A_1, A_2 and A_3 are defined as amplitude of autocorrelation function at 0,1,2 or 3 time lags, respectively. These can be expressed mathematically using expression 4.4 as :

$$A_0 = \sum_{k=1}^{k=N} X_k X_k \quad (4.6)$$

$$A_1 = \sum_{k=1}^{k=N} X_{k+1} X_k \quad (4.7)$$

$$A_2 = \sum_{k=1}^{k=N} X_{k+2} X_k \quad (4.8)$$

$$A_3 = \sum_{k=1}^{k=N} X_{k+3} X_k \quad (4.9)$$

Parameter A_m is defined as the global minimum value of the autocorrelation function and the parameter T_m is the time of global minima in the autocorrelation function. Time of first, second and third zero crossings of the autocorrelation function are defined as T_1, T_2 and T_3 , respectively. Autocorrelation function of the simulated acceleration record at the Saitsama station for Meghalaya earthquake of 10th Sept, 1986 is shown in Fig 4.6. Parameters $A_0, A_1, A_2, A_3, A_m, T_m, T_1, T_2$ and T_3 are shown in Fig 4.7. Parameters named as $ACF_1, ACF_2, ACF_3, ACF_4, ACF_5, ACF_6, ACF_7$ and

ACF₈ are calculated using the computed values of A₀, A₁, A₂, A₃, A_m, T_m, T₁, T₂ and T₃ by following expressions :

- (i) $ACF_1 = T_1,$
- (ii) $ACF_2 = T_2,$
- (iii) $ACF_3 = T_3,$
- (iv) $ACF_4 = T_m,$
- (v) $ACF_5 = A_1/A_0,$
- (vi) $ACF_6 = A_2/A_0,$
- (vii) $ACF_7 = A_3/A_0$ and
- (viii) $ACF_8 = A_m/A_0.$

Parameters ACF₁, ACF₂ and ACF₃ are the time of first, second and third zero crossing in the autocorrelation function of acceleration record. As the location of zero crossing in the sampled autocorrelation function is governed by its sampling interval, therefore interpolation is done for obtaining zero crossing in autocorrelation function. For the autocorrelation function of simulated acceleration record of Meghalaya earthquake at Saitsama station shown in Fig 4.6 and 4.7, time of first zero crossing T₁ (ACF₁) lies in between .02 to .04 sec. In this case A₁ = 47339 and A₂ = -50663. The method of interpolation used can be explained by this example. Let t₁ be the distance of zero crossing from the time at which A₁ occurs as shown in Fig 4.8, by simple geometry t₁ can be given as

$$t_1 = A_1 \cot \theta_1 \quad (4.10)$$

where,

$$\theta_1 = 90^\circ - \tan^{-1} si/(A_1 + A_2)$$

Angle θ_1 is shown in Fig 4.8. Using $A_1 = 47339$, $A_2 = -50663$ and $si = .02$ sec t_1 is obtained as .066 sec and therefore,

$$T_1 = .02 + .066 = .0266 \text{ sec} \approx .03 \text{ sec}$$

The example shown in Fig 4.8 is for simulated record at Saitsama station for Meghalaya earthquake of 10th Sept, 1986 and it does not imply that in all autocorrelation functions T_1 will lie in between the arrival times of A_1 and A_2 .

Using same approach of interpolation T_2 and T_3 can be calculated from autocorrelation function of the acceleration record.

Parameter ACF_0 defines the ratio of the area under ACF between time $T=0$ to $T=T_1$ and the area under ACF between time $T=T_1$ to $T=T_2$. This parameter is computed by dividing autocorrelation function of the acceleration record into number of rectangles of width equal to the sampling interval of the autocorrelation function and height equal to the value of the autocorrelation function. As the autocorrelation function is at a uniform sampling interval, therefore parameter ACF_0 can be defined as the ratio of the sum of values of ACF between time $T=0$ to $T=T_1$ with the sum of values of ACF between time $T=T_1$ to $T=T_2$.

For autocorrelation function of simulated acceleration record at Saitsama station for Meghalaya earthquake of 10th Sept, 1986 shown in Fig 4.1 parameter ACF_0 can be

computed using Fig 4.7. In this figure sum of autocorrelation values at time $T = 0$ to $T = T_1$ is equal to the sum of A_0 and A_1 and the sum of the autocorrelation values at time $T = T_1$ to $T = T_2$ is equal to $(A_2 + A_3 + A_4)$, hence in this case ACF_9 can be given as:

$$ACF_9 = \frac{|A_0| + |A_1|}{|A_2| + |A_3| + |A_4|} \quad (4.11)$$

The values of A_i should always be kept positive while computing this parameter. As in this case $A_0 = 104037$, $A_1 = 47339$, $A_2 = -50667$, $A_3 = -79525$ and $A_4 = -23802$, the value of parameter ACF_9 is obtained as .983.

Parameter ACF_{10} is defined as ratio of area under ACF above the abscissa and the area under ACF below the abscissa. Like ACF_9 , ACF_{10} can be obtained as a ratio of the sum of all values of ACF above the abscissa with the sum of values of the ACF below the abscissa.

Calculated values of parameters $ACF_1, ACF_2, ACF_3, ACF_4, ACF_5, ACF_6, ACF_7, ACF_8, ACF_9$ and ACF_{10} are given in the following table :

S.N.	Parameter	Value	S.N	Parameter	Value
1	ACF_1	.03 sec	6	ACF_6	-.487
2	ACF_2	.088 sec	7	ACF_7	-.764
3	ACF_3	.139 sec	8	ACF_8	-.764
4	ACF_4	.06 sec	9	ACF_9	.983
5	ACF_5	.455	10	ACF_{10}	1.098

4.2 FREQUENCY DOMAIN PARAMETERS

In strong ground motions frequency content present in the record is an important parameter. "Frequency content is a critical factor because structures, and in some cases surface deposits, may respond in a resonant manner depending upon the frequency content of ground motion. Relatively large deformations and stresses can occur in a structures on unconsolidated surface deposits if the shaking includes significant amount of energy at frequencies close to the natural frequencies of the system (UNDRO, 1990)". Frequency dependent parameters can be extracted from the acceleration records by using fourier transform. This powerful tool serves as a bridge between time and frequency domains. Discrete Fourier transform (DFT) of a signal f_n can be written as :

$$F_k = \sum_{n=0}^{N-1} f_n w_N^{nk}, \quad k = 0, 1, 2, \dots, N-1 \quad (4.12)$$

Inverse discrete Fourier transform (IDFT) is given as :

$$f_n = 1/N \sum_{k=0}^{N-1} F_k w_N^{-nk}, \quad n = 0, 1, 2, \dots, N-1 \quad (4.13)$$

Where N are total number of samples, and $w_N = e^{-2\pi i/N}$

From the Discreta Fourier transform of signal f_n , F_k is obtained in which both f_n and F_k are complex number. Amplitude, phase and power spectrum of signal f_n ($n = 0, 1, \dots, N-1$) can be obtained as:

$$F_k = A_k + iB_k$$

$$\text{Amp}_k = [A_k^2 + B_k^2]^{1/2} \quad (4.14)$$

$$\text{Phase}_k = \tan^{-1} (B_k/A_k) \quad (4.15)$$

$$\text{Power}_k = [\text{Amp}_k]^2 \quad (4.16)$$

Where,

Amp_k = Amplitude spectrum,

Phase_k = Phase spectrum and

Power_k = Power spectrum.

For extracting parameters in frequency domain acceleration records have been used. Using fourier transform, the power spectrum of the acceleration record can be computed using expression 4.16. Following parameters are computed from the power spectrum of acceleration record:

- (i) F_p , Predominant frequency from power spectrum of acceleration record,
- (ii) F_1 , Frequency at which 25th percentile of power occurs,
- (iii) F_2 , Frequency at which 50th percentile of power occurs,
- (iv) F_3 , Frequency at which 75th percentile of power occurs,
- (v) F_4 , Frequency at which 25th percentile value of frequency weighted power occurs,
- (vi) F_5 , Frequency at which 50th percentile value of frequency weighted power occurs and
- (vii) F_6 , Frequency at which 75th percentile value of frequency weighted power occurs.

Amplitude spectrum of acceleration record can be obtained using expression 4.14. Amplitude spectrum obtained from acceleration record vary rapidly and may show large variations which could be due to small near surface effects. For this reason their extensive study would appear to be of limited importance. However, this limitation can be reduced in the power spectrum calculated using expression 4.16. The power spectrum accentuates the effects of higher amplitudes. From the power spectrum of acceleration record parameter F_p is extracted. This is the frequency at which maximum power is obtained in the power spectrum. Fig 4.9 shows the method of computing parameter F_p from the power spectrum of acceleration record. The acceleration record used for this purpose is the simulated record at Saitsama station for the Meghalaya earthquake.

F_1 , F_2 and F_3 represent frequency at which 25th, 50th and 75th percentile of power occurs. Fig 4.10 shows method of computing parameters F_1 , F_2 and F_3 from the cumulative power spectrum of acceleration record. The acceleration record used for this purpose is the simulated record at Saitsama station for the Meghalaya earthquake. Because of the definition of these variables, F_1 will be lowest and F_3 highest frequency amongst these three, with F_2 somewhere in between.

F_4 , F_5 and F_6 represent frequency at which 25th, 50th and 75th percentile value of frequency weighted power occurs. Fig 4.11 shows method of computing parameters F_4 , F_5 and F_6 from the frequency weighted cumulative power spectrum of acceleration record. The acceleration record used for this purpose is the simulated record at Saitsama station for the Meghalaya earthquake. Because of the definition of these variables, F_4 will be the lowest and F_6 the highest frequency amongst these three, with F_5 somewhere in between.

Following table gives the calculated values of frequency domain parameters extracted from simulated acceleration records for the above referred station and earthquake :

S.N.	Parameter	Value	S.N.	Parameter	Value
1.	F_p	9.2 Hz	5.	F_4	7.6 Hz
2.	F_1	8.2 Hz	6.	F_5	8.9 Hz
3.	F_2	9.1 Hz	7.	F_6	9.6 Hz
4.	F_3	10.1 Hz			

Features are identified with the aim that they will aid in selection of the best record among various simulated records at same station by using different models of rupture planes. This it would provide a reasonable criteria for selection of model of the rupture plane.

4.3 SUMMARY

Various parameters which are extracted from simulated and field records and which can be used as a basis for extracting features for comparison of simulated records with the field records have been discussed. The parameters are extracted from field and simulated records in both time and frequency domain, respectively.

The synthetic records for Saitsama station for Meghalaya earthquake of 10th Sept, 1986 have been used as an example to discuss the various features which have been extracted from the strong motion records.

The total number of parameters which have been selected for feature extraction are :

S.No.	PARAMETERS		S.No.	PARAMETERS	
	Time Domain	Frequency Domain		Time Domain	Frequency Domain
1.	P_a	F_p	10.	ACF_3	-
2.	P_v	F_1	11.	ACF_4	-
3.	P_d	F_2	12.	ACF_5	-
4.	T_D	F_3	13.	ACF_6	-
5.	T_{at}	F_4	14.	ACF_7	-
6.	R_{at}	F_5	15.	ACF_8	-
7.	T_{area}	F_6	16.	ACF_9	
8.	ACF_1		17.	ACF_{10}	-
9.	ACF_2				

The next chapter (Chapter 5) deals with the software development programs and their algorithms which are used to calculate various parameters used for feature extraction defined in this Chapter (Chapter 4). Chapter 5 also discusses the algorithms of programs used for the simulation of strong ground motion due to a modelled rupture plane. The packages prepared were used to simulate synthetic records for three earthquakes in Indian subcontinent for which field strong motion data was available.

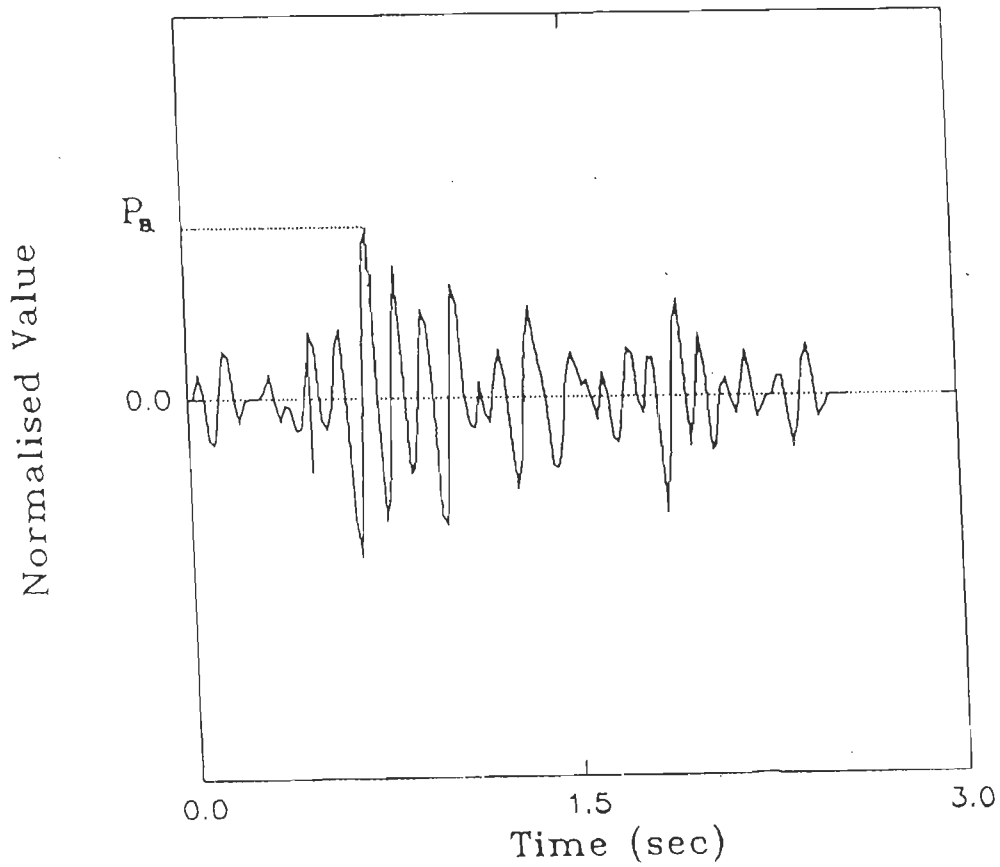


Fig 4.1 Method of extraction of parameter P_a from acceleration record. Acceleration record shown in this figure is a simulated record at Saitsama station for Meghalaya earthquake of 10th Sept, 1986.

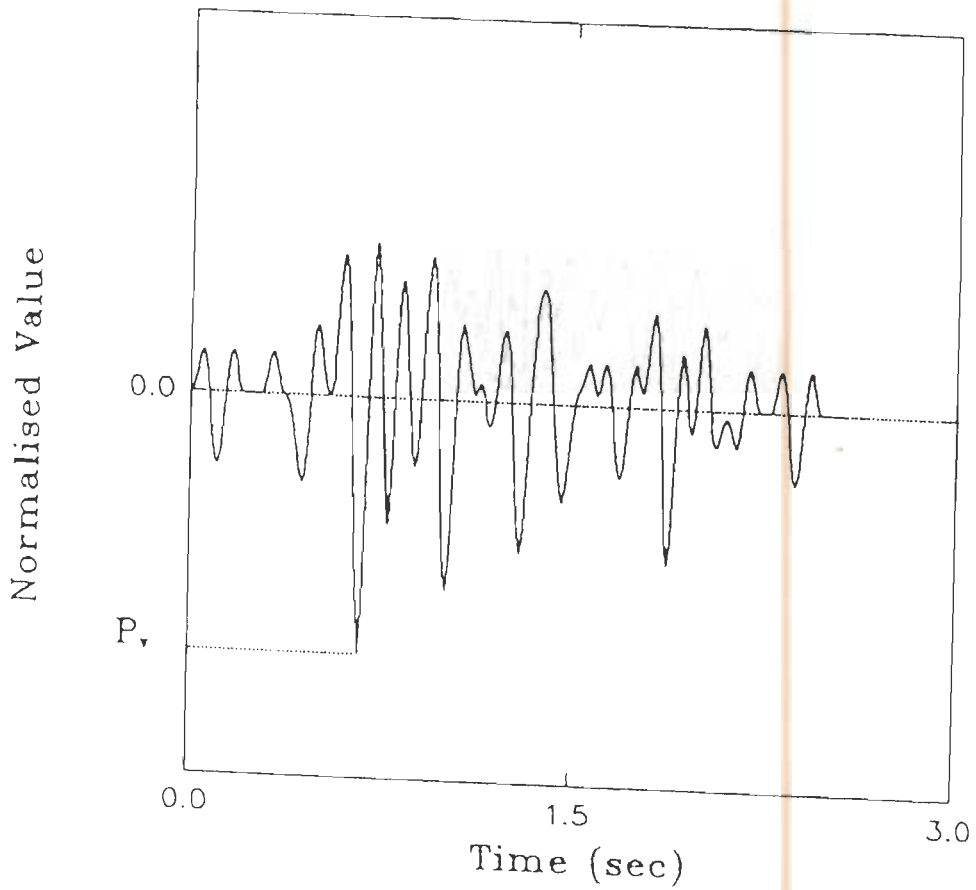


Fig 4.2 Method of extraction of parameter P_v from velocity record. Velocity record shown in this figure is a simulated record at Saitsama station for Meghalaya earthquake of 10th Sept, 1986.

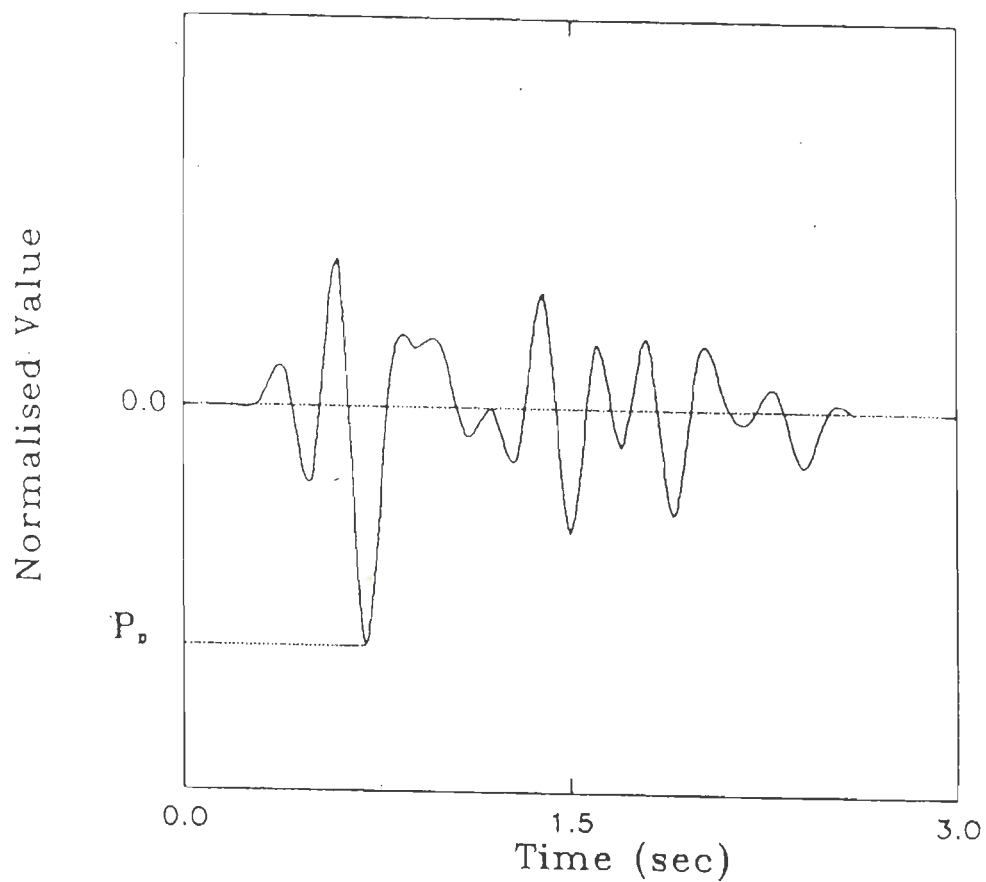


Fig 4.3 Method of extraction of parameter P_d from displacement record. Displacement record shown in this figure is a simulated record at Saitsama station for Meghalaya earthquake of 10th Sept, 1986.

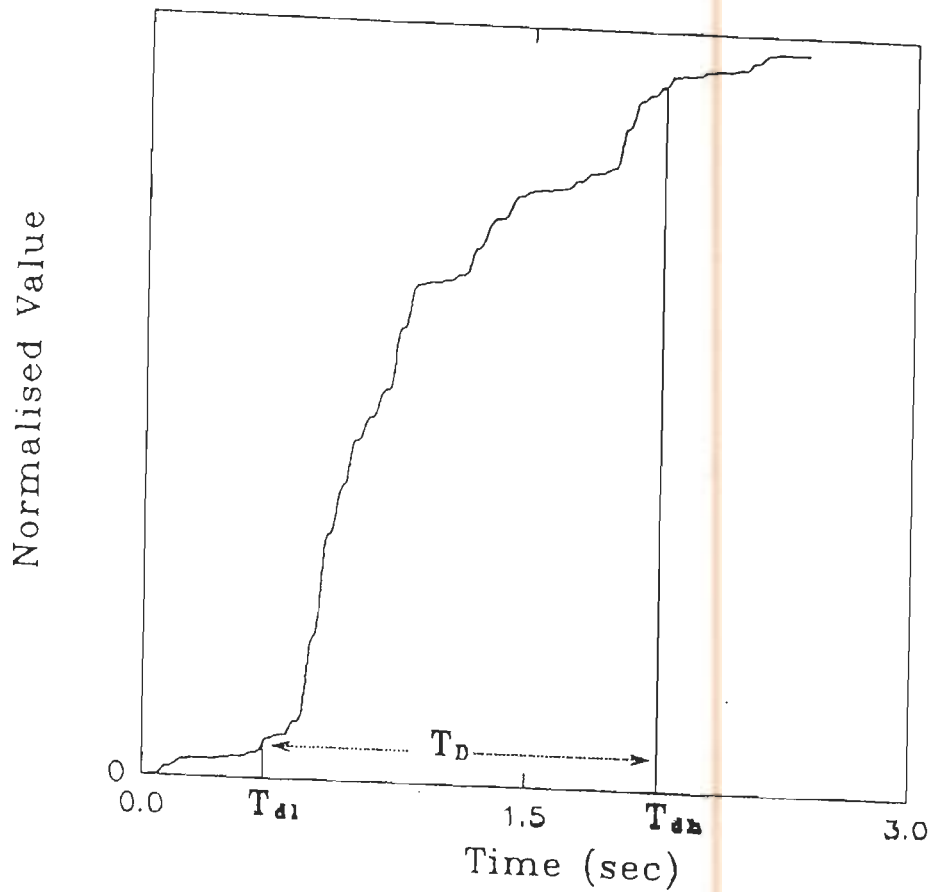


Fig 4.4 Extraction of variable T_D , duration of record as per Trifunac and Brady criteria (1975). This is computed from the cumulative addition of the square of the acceleration values shown in this figure. T_{d1} and T_{d95} are defined as the time at which the value becomes 5% and 95% of maximum value, respectively. The acceleration record used for this purpose is the simulated acceleration record at Saitsama station for Meghalaya earthquake of 10th Sept, 1986.

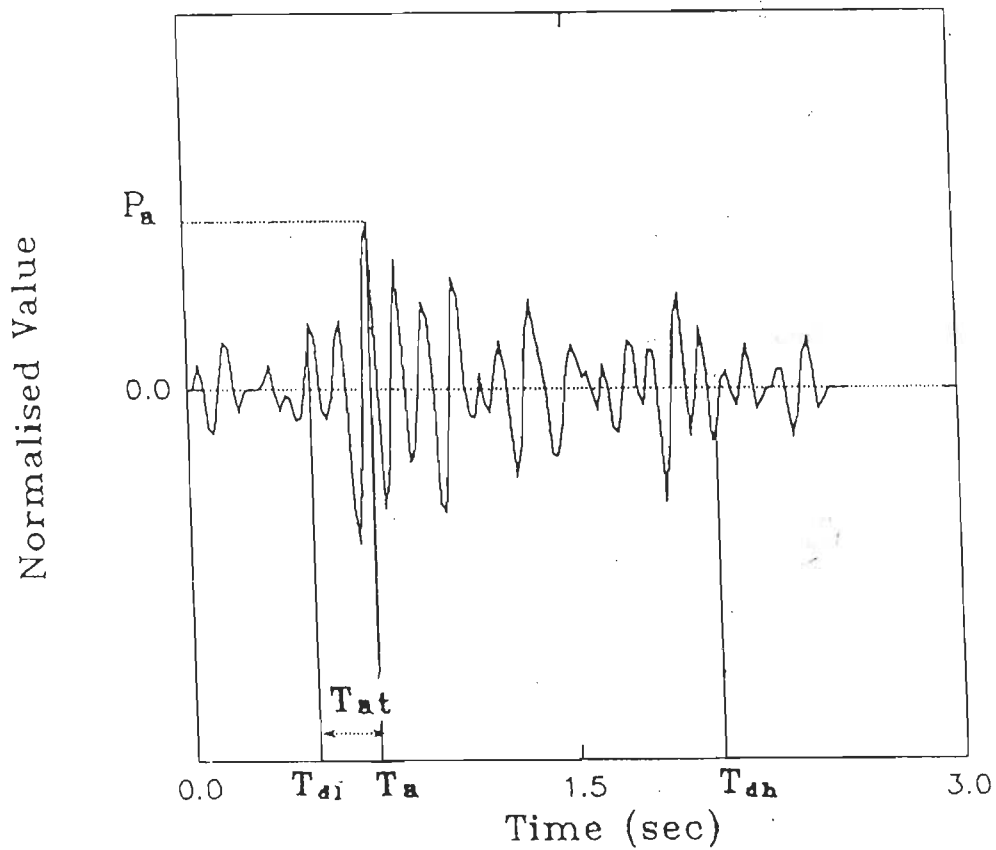


Fig 4.5 Method of extraction of variable T_a from the acceleration record. Acceleration record shown in this figure is a simulated record at Saitsama station for the Meghalaya earthquake of 10th Sept, 1986.

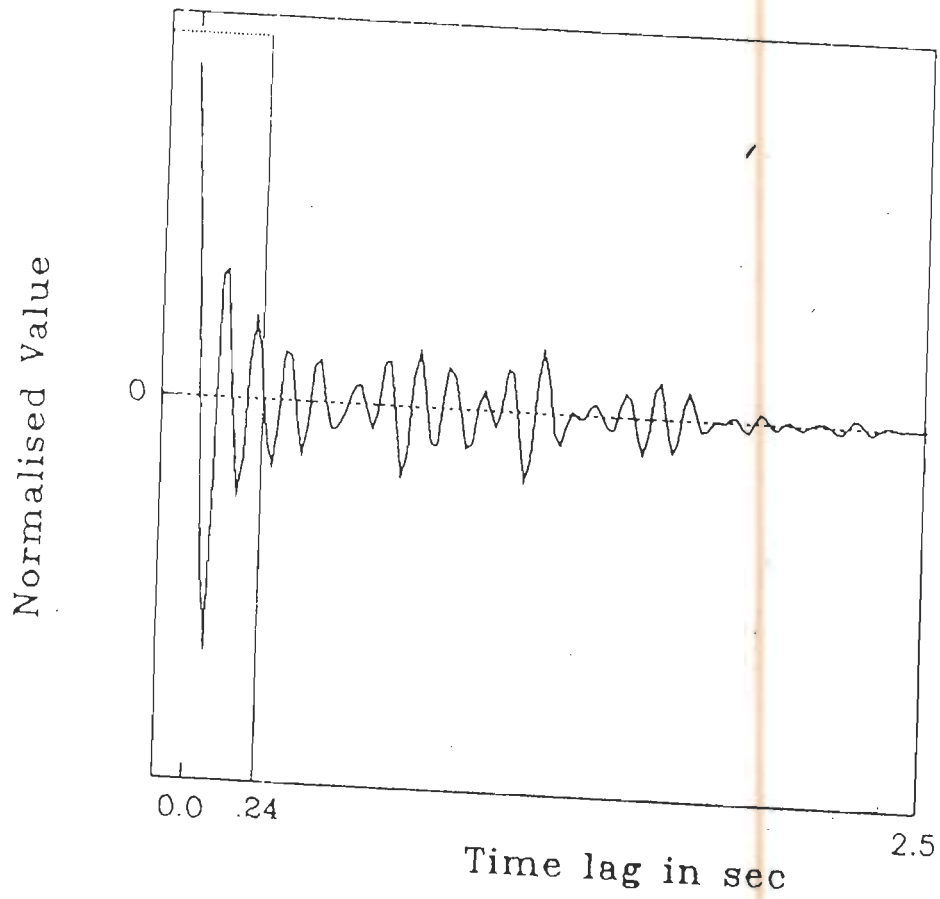


Fig 4.6 Normalised value of autocorrelation function of simulated acceleration record at Saitsama station for Meghalaya earthquake of 10th Sept, 1986. Autocorrelation function till .24 sec is shown in detail in Fig 4.7 from which various parameters of autocorrelation function are taken.

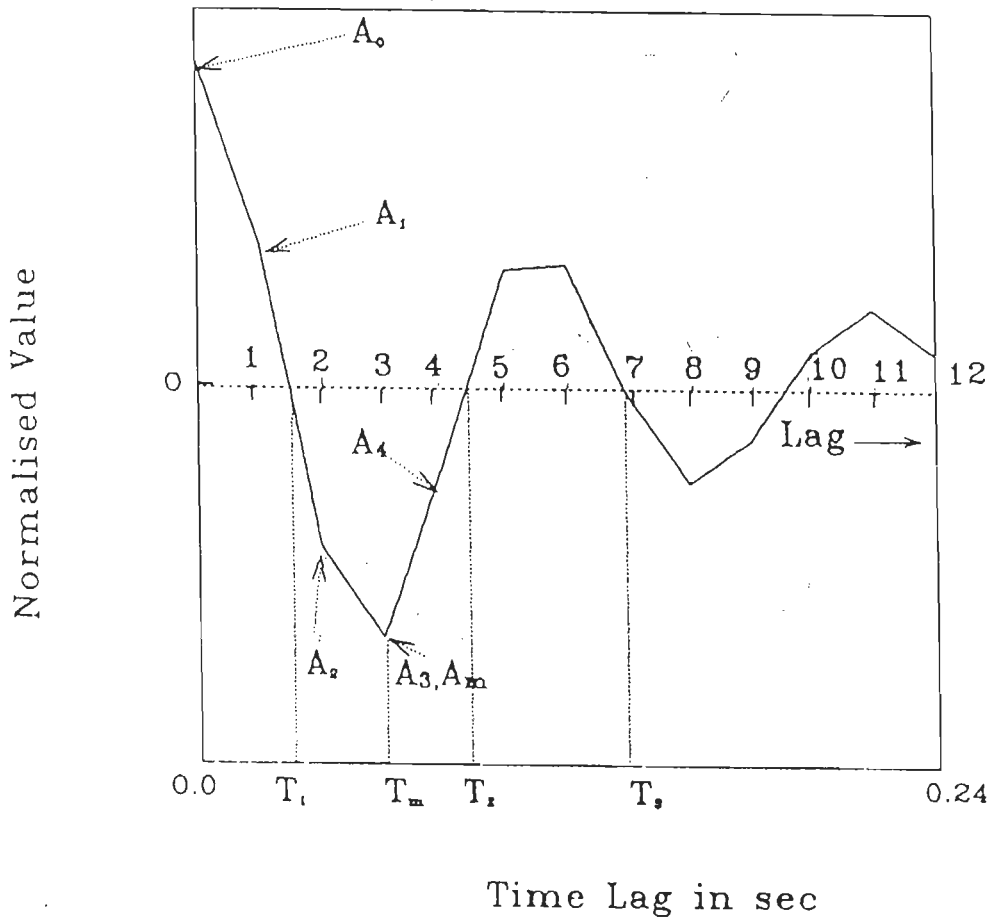
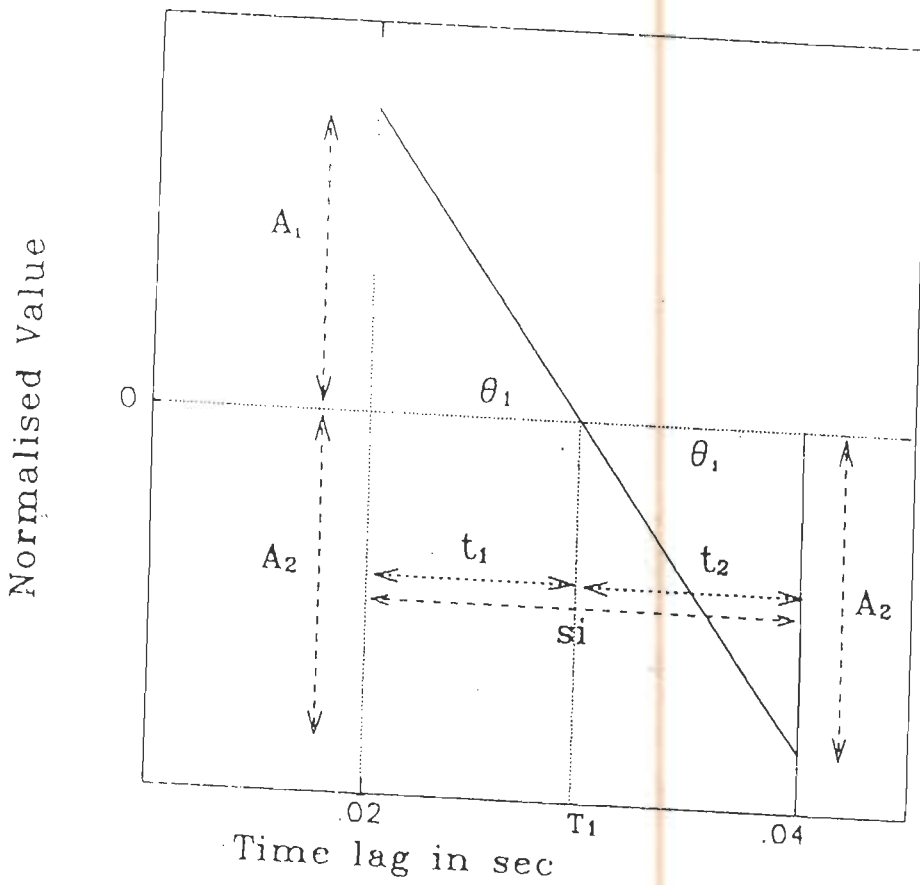


Fig 4.7 Normalised value of a portion of autocorrelation function (ACF) for acceleration record at Saitsama station for Meghalaya earthquake of 10th Sept, 1986, shown in Fig 4.6, showing variables $A_0, A_1, A_2, A_3, A_4, A_m, T_1, T_2, T_3$ and T_m . A_i ($i=1,4$) is the value of ACF at subscripted lag, A_m is value of global minima in ACF, T_i ($i=1,2,3$) represent i th zero crossing in the ACF and T_m is the time of arrival of global minima in ACF.



$$A_1 = 47339, \quad A_2 = 50664 \quad \text{and} \quad s_1 = .02$$

$$\tan \theta_1 = \frac{A_1 + A_2}{t_1 + t_2} = \frac{47339 + 50664}{.02}$$

$$\theta_1 = 89.99; \quad \tan \theta_1 = A_1/t_1; \quad t_1 = \frac{A_1}{\tan \theta_1}$$

$$t_1 = .0096$$

Hence,

$$T_1 = .02 + t_1 = .0296 \quad .03 \text{ sec}$$

Fig 4.8 Method of computing T_1 (i.e. first zero crossing) in the autocorrelation function (ACF) of the simulated acceleration record at Saitsama station for Meghalaya earthquake of 10th Sept, 1986. A_1 and A_2 are value of the ACF at lag 1 and 2, respectively and also shown in Fig 4.7. The time between first zero crossing and time of ACF at 1 lag is shown by t_1 . This method has also been used for computing parameter T_2 and T_3 , respectively.

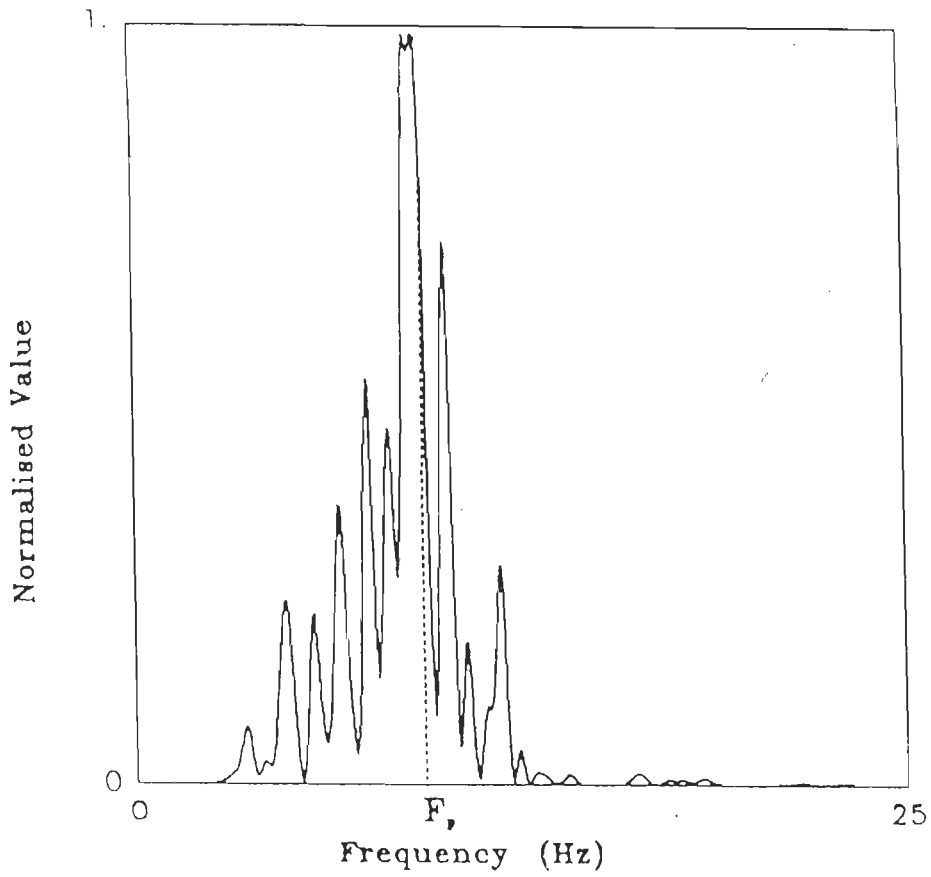


Fig 4.9 Method of computing parameter F_p from the power spectrum of the acceleration record. Acceleration record used here is the simulated record at Saitsama station for Meghalaya earthquake of 10th Sept, 1986.

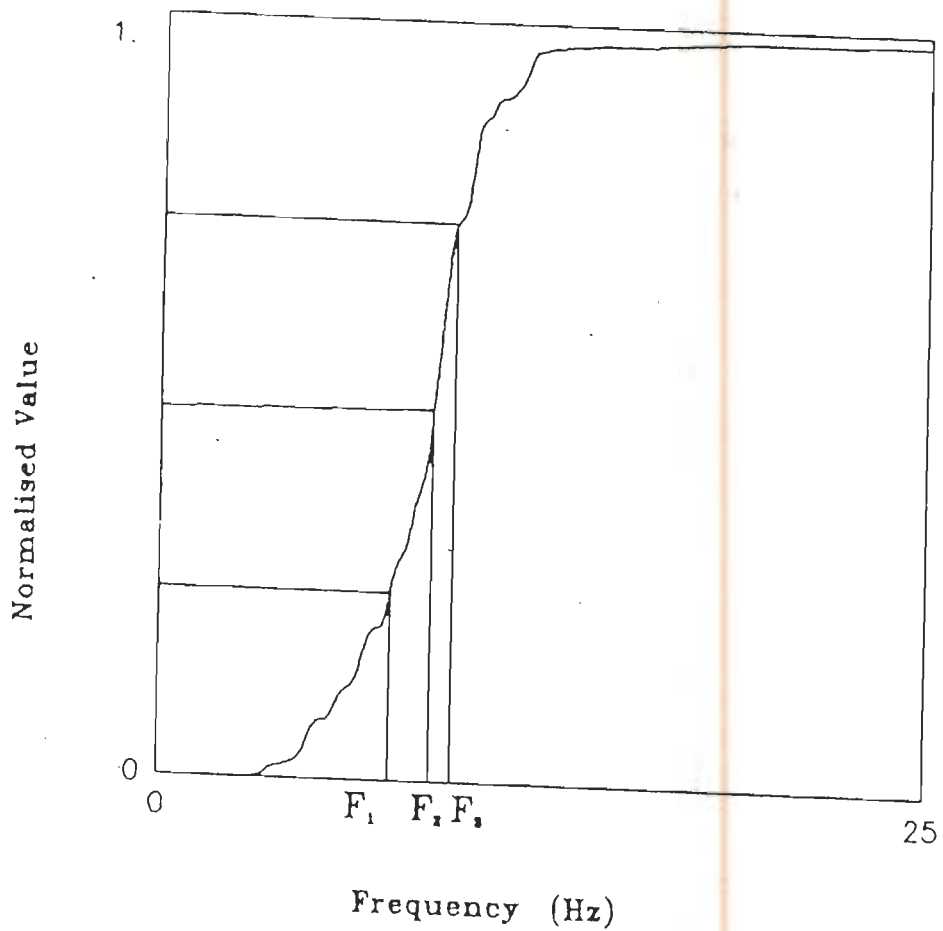


Fig 4.10 Method of computing parameters F_1 , F_2 and F_3 from the cumulative power spectrum of acceleration record. Acceleration record used here is the simulated record at Saitama station for Meghalaya earthquake of 10th Sept, 1986. For this case $F_1 = 8.3$ Hz, $F_2 = 9.9$ Hz and $F_3 = 10.9$ Hz.

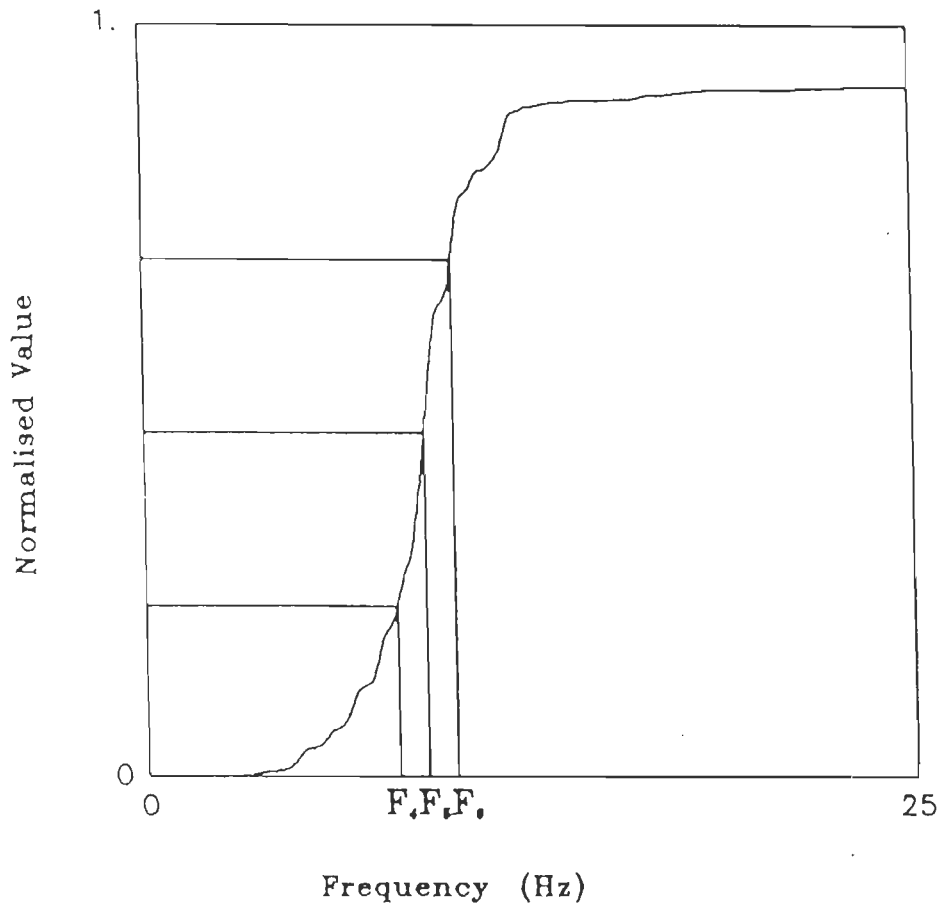


Fig 4.11 Method of computing parameters F_4 , F_5 and F_6 from the frequency weighted power spectrum of acceleration record. Acceleration record used here is the simulated record at Saitsama station for Meghalaya earthquake of 10th Sept, 1986. For this case $F_4 = 7.9$ Hz, $F_5 = 9.5$ Hz and $F_6 = 10.5$ Hz.

CHAPTER 5

COMPUTER SOFTWARE

Modelling of rupture process within the identified fault and the procedure of extraction of features from strong motion records require a large amount of mathematical calculations which can only be performed on a computer. In the present study computer programs for the modelling of the rupture plane within the identified causative fault to simulate strong motion records at observation points are developed in FORTRAN IV language. Program for computing various features of strong motion records explained in Chapter 4 are also developed in FORTRAN IV language. These can be executed on any IBM compatible PC under DOS environment. Graphical representation of program are given in the form of flow charts. Flow chart is a graphical representation of an algorithm, i.e. it is a visual picture which gives the steps of an algorithm and also the flow of control between the various steps (Lipschutz and Poe, 1982). Different types of operations in FORTRAN language are represented by different types of symbols which are shown in Fig 5.1.

Strong motion record at any observation point can be simulated using a special package named STRMR (Strong Motion Record) which has been developed. The package is made for radial type of geometry of rupture propagation with the rupture plane as explained in detail in Chapter 2 (Section 2.2.9). For extracting various features of strong motion records explained in Chapter 4 packages named TIMEP and FREQP have been developed. These packages use various subroutine programs during

execution. The programs and subroutines developed for these packages are given as:

PACKAGE NAME	SUBROUTINE NAME	INPUT PARAMETERS	OUTPUT
STRMR	DELAY TIME SHIFT RRG SCALE VEL DIF INTEG	(i) Coordinates of observation point (ii) $L, D, \delta, V, V_r, M, N, H$ and ρ and (iii) Coordinate of starting point of rupture	(i) Velocity record (ii) Displacement record (iii) Acceleration record
TIMEP	ACAM AREA AREAT AUTO AUTOC DATA DURA INTERPL PICK PTD RATIO START	(i) Acceleration record (ii) Velocity record (iii) Displacement record	(i) Autocorrelation function of acceleration record (ii) Accelerogram intensity function and (iv) Parameters $P_a, P_v, P_d, T_D, T_{at}, R_{at}, ACF_1, ACF_2, ACF_3, ACF_4, ACF_5, ACF_6, ACF_7, ACF_8, ACF_9, ACF_{10}$
FREQP	COMPLEX FFT PICF PICK POLAR VPOW POWER	(i) Acceleration record at uniform sampling interval	(i) Power spectrum (ii) Cumulative power spectrum (iii) Frequency weighted power spectrum and (iv) Parameters $F_p, F_1, F_2, F_3, F_4, F_5, F_6$
SWLT	SWAVE VELR DIF INTEG	(i) Desired frequency and sampling interval of source wavelet	Displacement, velocity and acceleration form of source wavelet

The above mentioned subroutines are tested with input parameters for the rupture model of the Meghalaya earthquake of 10th Sept, 1986. Records are simulated at Saitsama station for this model by using various subroutines discussed in this chapter. The input parameters required for executing each program or subroutine are defined and the output obtained from is given in the respective sections in which the subroutines are discussed.

5.1 SUBROUTINES USED FOR SIMULATING STRONG MOTION RECORDS

Name of package used for simulating strong motion records at selected observation point is **STRMR** (**Strong Motion Record**). This package simulates acceleration, velocity and displacement record due to the radial geometry of rupture propagation within the rupture plane. This package consist of various subroutines. The package takes into consideration:

- (i) Modelling parameters of rupture plane, (Section 2.2),
- (ii) Geometry of rupture propagation inside rupture plane, (Section 2.2) and
- (iii) Propagation of energy in the form of source wavelet within the homogeneous medium (Section 2.2).

The package **STRMR** consists of following subroutines :

- 1) **RRG** (Radial Rupture Geometry),
- 2) **VEL** (Velocity Record),
- 3) **DIF** (Differentiation program) and
- 4) **INTEG** (Integration program).

RRG (Radial Rupture Geometry)

Input for this subroutine consists of :

- (i) Length of rupture plane,
- (ii) Downward extension of rupture plane,
- (iii) Dip of rupture plane,
- (iv) Starting point of rupture,
- (v) Coordinates of observation point in rectangular coordinate system,
- (vi) Rupture velocity,
- (vii) Velocity of the medium,
- (viii) Sampling interval of source wavelet and
- (ix) Length of unit element.

Output of this subroutine consists of:

- (i) Total time taken by source wavelet to travel the distance between the center of the element and the observation point,
- (ii) Coordinates of the center of each element within the rupture plane and
- (iii) Total distance from center of element to the observation point.

Output from this subroutine is used as input for the subroutines VEL, DIF and INTEG. Flow chart for this subroutine is shown in Fig 5.2. Subroutine RRG includes one subroutine named as TIME. Following table gives the output of this subroutine for a given input. The input parameters defined in this case are used for the model of rupture plane.

EXAMPLE:

INPUT FOR THE SUBROUTINE RRG	OUTPUT OF THE SUBROUTINE					
Length of rupture plane = 6km	(i)	R km	X	Y	Z	M
Downward extension of rupture plane = 6 km		38.00	0	0	0	1653
		38.75	0	0	1	1632
		39.52	0	0	2	1641
Dip of rupture plane = 90°		40.29	0	0	3	1689
		41.08	0	0	4	1789
		:	:	:	:	:
Starting point of rupture = (2,0,2)		:	:	:	:	:
		35.13	5	0	1	1604
		35.94	5	0	2	1621
Coordinate of observation point = (23.5,9.25,-28.4)		36.76	5	0	3	1666
		38.43	5	0	4	1734
		39.28	5	0	5	1819
Rupture velocity = 3.0 km/sec	Where,					
Velocity of the medium = 6.7 km/sec	R is the distance between center of the element having coordinate X,Y and Z and the observation point					
Sampling interval of source wavelet = .004 sec	AT is the arrival time of the energy at the observation point (AT = M x .004 = sec)					
Length of unit element = 1 km						

(i) **TIME:** This subroutine calculates the distance travelled by the rupture front from the starting point of rupture to the center of element and distance travelled by the source wavelet from center of element to the observation point and their respective times as explained in Section 2.2.10. Input for this subroutine are :

- (i) Dip of the rupture plane,
- (ii) Length of the unit element within rupture plane,
- (iii) Total number of elements along length of the rupture plane,
- (iv) Total number of elements along downward extension of rupture plane,
- (v) Coordinates of the observation point in the rectangular three dimensional coordinate system explained in Section 2.2,
- (vi) Coordinates of the center of the elements and
- (vii) Coordinates of nucleation element.

Values of these parameters is given in free format. Output of this subroutine is :

- (i) Net arrival times of energy released in the form of source wavelet from center of different elements at the observation point. This already has been given in the previous table.

Fig 5.3 shows for flow chart of this subroutine.

SCALE

This subroutine is used for scaling the total energy released in an earthquake with the amplitude of velocity form of source wavelet released by each elements. The subroutine is based on formulation explained in detail in (Section 3.1). Input for this subroutine are:

- (i) Body wave magnitude of the earthquake (M_b),
- (ii) Hypocentral depth in cm,
- (iii) Frequency of the released wavelet,
- (iv) Velocity of the medium in cm/sec,

- (v) Total number of elements and
- (vi) Density of the medium in gm/cm^3 .

Output of this subroutine is the amplitude of the released velocity type source wavelet. Flow chart of this subroutine is given in Fig 5.4

EXAMPLE:

Example of the input and output of this subroutine is given as :

INPUT FOR THE SUBROUTINE SCALE	OUTPUT OF THE SUBROUTINE
(i) Body wave magnitude (M_b) = 5.2	Scaling factor = .13 cm/sec
(ii) Hypocentral depth = 28×10^5 cm	
(iii) Frequency of released wavelet = 5 Hz	
(iv) Velocity of the medium = 6.7×10^5 cm/sec	
(v) Total number of elements = 36	
(vi) Density of the medium = 2.7 gm/cm^3	

VEL

This subroutine calculates the velocity record at the observation point due to the modelled rupture plane. Input for this subroutine consists of:

- (i) Sampled value of velocity form of source wavelet of assumed frequency,
- (ii) Sum of the time taken by rupture to reach the center of element from starting point of the rupture and time taken by source wavelet to travel

from the center of element to the observation point. This is the output of subroutine RRG,

- (iii) Scaling factor for calculating amplitude of velocity form of source wavelet released by each element. This is the output of subroutine SCALE and
- (iv) Desired Sampling interval of the velocity record.

Output consist of velocity record at the selected observation point whose coordinates are specified in input of the subroutine RRG. This subroutine calls subroutine DELAY and SHIFT. Flow chart of this subroutine is shown in Fig 5.5.

(i) **DELAY:** This subroutine gives shift to the source wavelet delayed due to its arrival time at the observation point. Given subroutine gives sampled value of delayed source wavelet. Input for this subroutine consists of:

- (i) Sampled value of the source wavelet,
- (ii) Total number of samples of source wavelet,
- (iii) Sampling interval of source wavelet and
- (iv) Amount of time shift given to the source wavelet to reach the observation point.

The output consists of a shifted source wavelet. Flow chart of this subroutine is shown in Fig 5.6.

EXAMPLE:

Example of the input and output of this subroutine is given in a tabular form in the next page as:

INPUT FOR THE SUBROUTINE DELAY		OUTPUT OF THE SUBROUTINE	
(i)	Digitised Value of source wavelet	S.No.	Shifted Source wavelet (Sampling interval = 4 ms)
	.0019		
	.0037		
	.0068		
	.0122	1	0.0000
	.0210	2	0.0000
	:	3	0.0000
	:	:	:
	:	:	:
	.0210	50	0.0000
	.0122	51	0.0019
	.0068	52	0.0037
	.0037	53	0.0068
	.0019	54	0.0122
		55	0.0210
(ii)	Number of samples = 50	:	:
		:	:
(iii)	Sampling interval = .004 sec	96	0.0210
		97	0.0122
(iv)	Amount of shift = .2 sec	98	0.0068
	= 50 x .004 sec	99	0.0037
		100	0.0019

Shifted source wavelets emitted by different elements is also shown in Fig 3.5.

(ii) **SHIFT** :This subroutine computes the total sum of delayed source wavelets from each element multiplied by their corresponding scaling factor which reaches the observation point. Input for this subroutine are as follows:

- (i) Total shift required for source wavelet emitted by an element to reach the observation point (output AT of subroutine RRG),
- (ii) Scaling factor calculated from subroutine SCALE,
- (iii) Sampled value of source wavelet and
- (iv) Sampling interval of source wavelet.

Output is the velocity record at the observation point.

EXAMPLE:

INPUT FOR THE SUBROUTINE SHIFT	OUTPUT OF THE SUBROUTINE																								
(i) M 1653 1632 1641 1689 1789 : 1604 1621 1666 1734 1819 AT = M x .004 =sec	Velocity record at sampling interval of .004 sec. <table border="0"> <thead> <tr> <th>S.No.</th> <th>Velocity (cm/sec)</th> </tr> </thead> <tbody> <tr><td>1.</td><td>.00</td></tr> <tr><td>2.</td><td>.01</td></tr> <tr><td>3.</td><td>.03</td></tr> <tr><td>4.</td><td>.04</td></tr> <tr><td>5.</td><td>.07</td></tr> <tr><td>6.</td><td>.09</td></tr> <tr><td>7.</td><td>.11</td></tr> <tr><td>:</td><td>:</td></tr> <tr><td>:</td><td>:</td></tr> <tr><td>610</td><td>.13</td></tr> <tr><td>611</td><td>.11</td></tr> </tbody> </table>	S.No.	Velocity (cm/sec)	1.	.00	2.	.01	3.	.03	4.	.04	5.	.07	6.	.09	7.	.11	:	:	:	:	610	.13	611	.11
S.No.	Velocity (cm/sec)																								
1.	.00																								
2.	.01																								
3.	.03																								
4.	.04																								
5.	.07																								
6.	.09																								
7.	.11																								
:	:																								
:	:																								
610	.13																								
611	.11																								
(ii) Scaling factor calculated from subroutine SCALE. =.13 cm/sec	<table border="0"> <tbody> <tr><td>612</td><td>.09</td></tr> <tr><td>613</td><td>.07</td></tr> <tr><td>614</td><td>.04</td></tr> <tr><td>615</td><td>.03</td></tr> </tbody> </table>	612	.09	613	.07	614	.04	615	.03																
612	.09																								
613	.07																								
614	.04																								
615	.03																								
(iv) Sampling interval of source wavelet =.004 sec	<table border="0"> <tbody> <tr><td>616</td><td>.01</td></tr> <tr><td>617</td><td>.00</td></tr> <tr><td>618</td><td>.00</td></tr> </tbody> </table>	616	.01	617	.00	618	.00																		
616	.01																								
617	.00																								
618	.00																								
(iii) Sampled value of source wavelet at 4 ms sampling interval .0019 .0037 .0068 .0122 .0210 : : .0210 .0122 .0068 .0037 .0019																									

Fig 5.7 shows flow chart of this subroutine. Simulated Velocity record at Saitsama station for model of rupture plane for Meghalaya earthquake of 10th Sept, 1986 is shown in Fig 3.5.

DIF

This subroutine is used for obtaining acceleration record at an observation point by the differentiation of velocity record. The differentiation $f'(x)$ of function $f(x)$ can be given as:

$$f'(x) = [f(x + \delta h) - f(x - \delta h)] / 2 \cdot \delta h \quad (5.1)$$

This can be derived by Taylor expansion of function $f(x)$

$$f(x + \delta h) = f(x) + \delta h f'(x) + \delta h^2 f''(x) / 2! + \delta h^3 / 3! f'''(x) + \dots \quad (5.2)$$

$$f(x - \delta h) = f(x) - \delta h f'(x) + \delta h^2 f''(x) / 2! - \delta h^3 / 3! f'''(x) + \dots \quad (5.3)$$

Subtracting expression 5.3 from 5.2 and dividing by $2\delta h$, following expression is obtained:

$$f'(x) = [f(x + \delta h) - f(x - \delta h)] / 2 \cdot \delta h \quad (5.4)$$

Using this formula acceleration record can be obtained from uniformly sampled velocity record. Let $V_1(1), V_1(2), V_1(3), \dots, V_1(M-1)$ and $V_1(M)$ be M samples of velocity records at a uniform sampling interval 'si' then acceleration value $(a(1))$ can be computed by expression 5.4 as :

$$a(I) = [V_I(I+1) - V_I(I-1)]/2s_i ,$$

Where $I = 1, 2, 3, \dots, M$

Input and output for this subroutine are as follows:

- (i) Sampling interval of velocity record and
- (ii) Sampled value of velocity record.

Output consist of acceleration record. The flow chart of this subroutine is shown in Fig 5.8.

EXAMPLE:

INPUT FOR THE SUBROUTINE DIF		OUTPUT OF THE SUBROUTINE	
(i) Sampling interval of velocity record = .004 sec		Sampled value of acceleration	
(ii) S.No.	Velocity (cm/sec)	S.No.	Acceleration (cm/sec ²)
1.	.00	1.	.07
2.	.01	2.	3.83
3.	.03	3.	7.36
4.	.04	4.	10.31
5.	.07	5.	12.43
6.	.09	6.	13.49
7.	.11	:	:
:	:	612	-13.40
610	.13	613	-13.58
611	.11	614	-12.40
612	.09	615	-10.31
613	.07	616	-07.36
614	.04	617	-03.08
615	.03	618	00.99
616	.01		
617	.00		
618	.00		

DATA

This subroutine is prepared for obtaining acceleration record in any desired sampling interval. Input for this subroutine are:

- (i) Sampled values of acceleration record obtained from subroutine DIF,
- (ii) Sampling interval of acceleration record and
- (iii) Desired sampling interval.

Output to this subroutine consists of same acceleration record at desired sampling interval. Flow chart of this subroutine is shown in Fig 5.9.

EXAMPLE

INPUT FOR THE SUBROUTINE DATA	OUTPUT OF THE SUBROUTINE
(ii) Sampling interval = .004 sec	(i) Sampling interval of obtained acceleration record
(iii) Desired sampling interval = .02 sec	(ii) Total number of samples in obtained acceleration record
(i) Sampled value of acceleration record at 4 ms	S.No. Acceleration at .02 sec sampling interval (cm/sec ²)
S.No. Acceleration (cm/sec ²)	
1. .07	1. .07
2. 3.83	2. 13.75
3. 7.36	3. 2.24
4. 10.31	4. -22.00
5. 12.43	5. -25.78
6. 13.75	6. 00.00
:	:

INPUT FOR THE SUBROUTINE DATA		OUTPUT OF THE SUBROUTINE	
S.No.	Acceleration (cm/sec ²)	S.No.	Acceleration at .02 sec sampling interval (cm/sec ²)
:	:	:	:
612	-13.40	36.	100.30
613	-13.50	:	:
614	-12.40	119	-12.50
615	-10.31	120	17.98
616	-07.36	121	27.50
617	-03.80	122	7.80
618	.99	123	-12.20
619	00.00	124	-07.30
		125	00.00

Simulated acceleration at sampling interval of .02 sec is shown in Fig 3.6c.

INTEG

This subroutine is used for integration of simulated velocity record to compute displacement record at the observation point. The integration approach is based trapezoidal rule. This rule can be given as (Vygodsky,1975) :

$$\int_a^b f(x)dx = (b-a/2)[(y_0 + y_n)/2 + y_1 + y_2 + \dots + y_{n-1}] \quad 5.5$$

Where,

$$x_0 = a ; x_n = b \text{ and } f(x_i) = y_i, \quad i=1,2,3,\dots,n-1,n$$

This yields total area of trapezoids shown in Fig 5.10a.

Using this formulation subroutine INTEG is developed for computing displacement record from the velocity record. Input for this subroutine are:

- (i) Sampled values of velocity record,
- (ii) Total number of samples,
- (ii) Sampling interval and
- (iii) Desired sampling interval of displacement record.

Output consists of the displacement record at the same observation point. Flow chart of this subroutine is shown in Fig 5.10b.

EXAMPLE :

INPUT FOR THE SUBROUTINE INTEG	OUTPUT OF THE SUBROUTINE
(i) Total number of samples in velocity record = 618	(i) The Sampling interval of displacement record is .1 sec.
(ii) Sampling interval of velocity record = .004 sec	(ii) Total number of samples in displacement record = 25
(iii) Sampled value of simulated velocity record	S.No. Displacement (cm)
S.No. Velocity (cm/sec)	1. .00
1. .00	2. .00
2. .01	3. .02
3. .03	4. .12
4. .04	5. -.28
5. .07	6. -.56
6. .09	: :
7. .11	
: :	

INPUT FOR THE SUBROUTINE INTEG		OUTPUT OF THE SUBROUTINE	
S.No.	Velocity (cm/sec)	S.No.	Displacement (cm)
610	.13	:	:
611	.11	:	:
612	.09	21	-.05
613	.07	22	-.03
614	.04	23	.08
615	.03	24	-.22
616	.01	25	.00
617	.00		
618	.00		
(iv) Desired sampling interval of displacement record = .1 sec			

Displacement record simulated at Saitsama station for Meghalaya earthquake of 10th Sept, 1986 is shown in Fig 3.6d.

5.2 SUBROUTINES USED FOR GENERATING SOURCE WAVELET

Source wavelet used for complete simulation process is generated using subroutine SWAVE. Input parameters for this subroutine consist of :

- (i) Frequency of assumed source wavelet and
- (ii) Sampling interval of source wavelet.

Output consists of the source wavelet in time domain with the desired sampling interval. This subroutine calls subroutines VELR, DIF and INTEG. Flow chart for this subroutine is given in Fig 5.11.

VELR: This subroutine is used for generating velocity type source wavelet. Formulation for generation of velocity type source wavelet is given in Section 2.2.7. Input for this subroutine are :

- (i) Frequency of assumed source wavelet and
- (ii) Sampling interval of source wavelet.

Output consist of velocity type source wavelet in time domain. Flow chart for this subroutine is shown in Fig 5.12. Velocity type source wavelet generated using this subroutine is shown in Fig 2.4.

EXAMPLE:

INPUT FOR THE SUBROUTINE VELR	OUTPUT OF THE SUBROUTINE
(i) Frequency of source wavelet = 5 Hz, (ii) Sampling interval = .004 sec	Digitised values of the velocity form of source wavelet at sampling interval of .004 sec) .0019 .0037 .0068 .0122 .0210 : : : .0210 .0122 .0068 .0037 .0019

The displacement and acceleration form of this source wavelet can be obtained by using the subroutines for integration and differentiation, respectively.

5.3 SUBROUTINES USED FOR FEATURE EXTRACTION FROM STRONG MOTION RECORDS

Various features which have been identified from strong motion records have been discussed in detail in Chapter 4. These are classified into time and frequency domain parameters. Two different packages **TIMEP** (Time Parameters) and **FREQP** (Frequency Parameters) have been developed for computing time domain and frequency domain parameters.

5.3.1 SUBROUTINES USED FOR COMPUTING TIMEDEPENDENT PARAMETERS

The time domain parameters that are extracted from strong motion records are:

- (i) Peak acceleration of the acceleration record (P_a),
- (ii) Peak velocity of the velocity record (P_v),
- (iii) Peak displacement of the displacement record (P_d),
- (iv) Duration of the acceleration record (T_D),
- (v) Arrival time of peak in the acceleration record (T_{at}) and
- (vi) Ratio of the area covered by the acceleration record above and below the abscissa (R_{at}).

Other time domain parameters are computed from autocorrelation function (ACF) of strong motion records. Parameters $A_0, A_1, A_2, A_3, A_m, T_1, T_2, T_3$ and T_m are computed directly from the autocorrelation function of the acceleration record. The parameters extracted from autocorrelation function are:

- (i) $ACF_1 = T_1$ Time of first zero crossing,
- (ii) $ACF_2 = T_2$ Time of second zero crossing,
- (iii) $ACF_3 = T_3$ Time of third zero crossing,
- (iv) $ACF_4 = T_m$ Time of global minimum,
- (v) $ACF_5 = A_1/A_0$,
- (vi) $ACF_6 = A_2/A_0$,
- (vii) $ACF_7 = A_3/A_0$,
- (viii) $ACF_8 = A_m/A_0$,
- (ix) $ACF_9 =$ Ratio of area under ACF between time $T=0$ to $T=T_1$ with the area under ACF between time $T=T_1$ to $T=T_2$ and
- (x) $ACF_{10} =$ Ratio of area under ACF above the abscissa and area under ACF below the abscissa.

All of these parameters mentioned above are computed using package named as **TIMEP**. This package consist of subroutines **PTD** (Parameters in Time Domain) and **AUTO** (Autocorrelation).

PTD (Parameters computed from Time Series)

This subroutine is used to compute $P_a, P_v, P_d, T_D, T_{at}$ and R_{at} from the strong motion record. Input for this subroutine consist of following parameters :

- (i) Total number of samples in the record,
- (ii) Sampled value and
- (iii) Sampling interval.

Output of this subroutine consist of value of parameters P_a , P_v , P_d , T_D , T_{at} and R_{at} . Flow chart of this subroutine is shown in Fig 5.13. This subroutine calls three subroutines (i) PICK, (ii) DURA and (iii) AREAT.

PICK

This subroutine is used for picking maximum amplitude from a given record and its corresponding time. Input parameters for this subroutine consist of:

- (i) Total number of samples in the record,
- (ii) Sampled value and
- (iii) Sampling interval.

Output consists of the maximum value of amplitude and the time at which it occurs. Flow chart for this subroutine is given in Fig 5.14.

EXAMPLE:

INPUT FOR THE SUBROUTINE PICK		OUTPUT OF THE SUBROUTINE
(i) Total number of samples in the acceleration record = 125		Peak acceleration (P_a) = 100.3 cm/sec ²
(ii)		Time of arrival of peak acceleration (T_a) = .68 sec
S.No.	Acceleration (cm/sec ²)	
1.	.07	
2.	13.75	
3.	2.24	
4.	-22.00	
5.	-25.78	
6.	00.00	
:	:	
36.	100.30	

INPUT FOR THE SUBROUTINE PICK	
:	:
119	-12.50
120	17.98
121	27.50
122	7.80
123	-12.20
124	-07.30
125	00.00
(iii) Sampling interval = .02 sec	

Parameter P_a and T_a are shown in Fig 4.5.

DURA

This subroutine is used for computing duration of strong motion record. The duration is computed using the approach explained in Chapter 4. For computing duration of the acceleration record $a(t)$, a function $AI(t)$ is calculated by using the following expression :

$$AI(t) = \sum_0^t a^2(t)dt$$

Duration (T_D) is defined as the difference of arrival time of 5% of maximum value of function $AI(t)$ (T_{dl}) and that of 95% of the maximum value of function $AI(T)$ (T_{dh}). Therefore T_D is :

$$T_D = T_{dh} - T_{dl}$$

Where,

T_{dh} = Time of arrival of 95% of the maximum value of function $AI(t)$

T_{dl} = Time of arrival of 5% of the maximum value of function $AI(t)$

Input for this subroutine are :

- (i) Sampling interval of the acceleration record,
- (ii) Sampled value of the acceleration record and
- (iii) Total number of sampled value.

Output consist of :

- (i) Function $AI(t)$,
- (ii) Time of arrival of 5% of the maximum value of the function $AI(t)$ (T_{dl}),
- (iii) Time of arrival of 95% of the maximum value of the function $AI(t)$ (T_{dh}) and
- (iv) Duration of the record (T_D).

Flow chart of this subroutine is shown in Fig 5.15.

EXAMPLE:

INPUT FOR THE SUBROUTINE DURA		OUTPUT OF THE SUBROUTINE	
(i) Sampling interval of acceleration record = .02 sec		(i) Function $AI(t)$ at a sampling interval of .02 sec.	
(ii) Sampled value of acceleration		S.No.	Cumulative addition of square of acceleration $AI(t)$
S.No.	Acceleration (cm/sec ²)		
1	.07	1	.00
2	13.75	2	.04
3	2.24	3	.67
4	-22.00	4	.98
5	-25.78	5	2.11
6	00.00	6	4.31
:	:	:	:
36	100.30		
:	:		

INPUT FOR THE SUBROUTINE DURA	OUTPUT OF THE SUBROUTINE
: 119 -12.50 120 17.98 121 27.50 122 7.80 123 -12.20 124 -07.30 125 00.00	: : 120 225.00 121 225.20 122 225.70 123 226.10 124 226.20 125 226.26
(iii) Total numbers of samples = 125	(ii) $T_{dl} = .48$ sec
	(iii) $T_{dh} = 2.02$ sec
	(iv) $T_D = 1.22$ sec

Fig 4.4 shows the plot of function $AI(t)$ computed from the simulated acceleration record at Saitsama station for the Meghalaya earthquake.

AREAT

This subroutine computes parameter R_{at} , which is defined as the ratio of area under acceleration record on positive and negative sides of time axis. Method of calculation of R_{at} is explained in detail in Chapter 4. Input for this subroutine consist of

- (i) Total number of sampled values of acceleration record,
- (ii) Sampled values of acceleration record at uniform sampling interval and
- (iii) Sampling interval.

Output to this subroutine consist of parameter R_{at} . Flow chart of this subroutine is shown in Fig 5.16.

EXAMPLE:

INPUT FOR THE SUBROUTINE AREAT	OUTPUT OF THE SUBROUTINE																																					
(i) Total number of samples of acceleration record = 125	$R_{at} = .999$																																					
(ii) Sampled value																																						
<table style="width: 100%; border-collapse: collapse;"> <thead> <tr> <th style="text-align: left;">S.No.</th> <th style="text-align: left;">Acceleration (cm/sec²)</th> </tr> </thead> <tbody> <tr><td>1.</td><td>.07</td></tr> <tr><td>2.</td><td>13.75</td></tr> <tr><td>3.</td><td>2.24</td></tr> <tr><td>4.</td><td>-22.00</td></tr> <tr><td>5.</td><td>-25.78</td></tr> <tr><td>6.</td><td>00.00</td></tr> <tr><td>:</td><td>:</td></tr> <tr><td>:</td><td>:</td></tr> <tr><td>36.</td><td>100.30</td></tr> <tr><td>:</td><td>:</td></tr> <tr><td>:</td><td>:</td></tr> <tr><td>119</td><td>-12.50</td></tr> <tr><td>120</td><td>17.98</td></tr> <tr><td>121</td><td>27.50</td></tr> <tr><td>122</td><td>7.80</td></tr> <tr><td>123</td><td>-12.20</td></tr> <tr><td>124</td><td>-07.30</td></tr> <tr><td>125</td><td>00.00</td></tr> </tbody> </table>		S.No.	Acceleration (cm/sec ²)	1.	.07	2.	13.75	3.	2.24	4.	-22.00	5.	-25.78	6.	00.00	:	:	:	:	36.	100.30	:	:	:	:	119	-12.50	120	17.98	121	27.50	122	7.80	123	-12.20	124	-07.30	125
S.No.	Acceleration (cm/sec ²)																																					
1.	.07																																					
2.	13.75																																					
3.	2.24																																					
4.	-22.00																																					
5.	-25.78																																					
6.	00.00																																					
:	:																																					
:	:																																					
36.	100.30																																					
:	:																																					
:	:																																					
119	-12.50																																					
120	17.98																																					
121	27.50																																					
122	7.80																																					
123	-12.20																																					
124	-07.30																																					
125	00.00																																					
(iii) Sampling interval = .02 sec																																						

Autocorrelation of a record can be computed by method explained in Section 4.1.2. Various parameters that are extracted from autocorrelation function are also explained in this section. The subroutines that are used for this purpose are (i) **DATA**, (ii) **AUTO**C (iii) **ACAM**, (iv) **RATIO** and (v) **INTERPL**.

DATA

This subroutine is prepared for obtaining acceleration record in any desired sampling interval and has already been discussed earlier.

AUTO C

Autocorrelation of a acceleration record is computed using the expression explained in Section 4.1.2. The subroutine AUTO C computes autocorrelation function of acceleration record sampled at a uniform sampling intervals. This subroutine has been prepared by Sinvhal et al. (1992). Input for this subroutine consist of:

- (i) Sampled values of acceleration record,
- (ii) Total number of samples and
- (iii) Sampling interval.

Output of this subroutine is the autocorrelation function of acceleration record. Flow chart of this subroutine is shown in Fig 5.17.

EXAMPLE:

INPUT FOR THE SUBROUTINE AUTO C	OUTPUT OF THE SUBROUTINE
(i) Total number of samples = 125	(i) Total number of samples in obtained autocorrelation function = 125
(ii) Sampling interval of acceleration record = .02 sec	(ii) Sampling interval of autocorrelation function = .02 sec

INPUT FOR THE SUBROUTINE AUTOC		OUTPUT OF THE SUBROUTINE	
(iii) Sampled values		(i) Autocorrelation function of acceleration record at uniform sampling interval of .02 sec.	
S.No.	Acceleration (cm/sec ²)	Time	Autocorrelation function of acceleration record
1.	.07	1	104037
2.	13.75	2	47339
3.	2.24	3	-50667
4.	-22.00	4	-79525
5.	-25.78	5	-23802
:	:	6	38738
:	:	7	40399
36.	100.30	:	:
:	:	:	:
:	:	:	:
119	-12.50	:	:
120	17.98	120	852
121	27.50	121	242
122	7.80	122	-182
123	-12.20	123	-100
124	-07.30	124	000
125	00.00	125	000

ACAM

This subroutine is used for computing parameters A_0, A_1, A_2, A_3, A_m and T_m . Input for this subroutine consist of:

- (i) Sampled values of autocorrelation function,
- (ii) Total number of samples of autocorrelation function and
- (iii) Sampling interval.

Output consist of parameters A_0, A_1, A_2, A_3, A_m and T_m . Flow chart of this subroutine is given in Fig 5.18.

EXAMPLE :

INPUT FOR THE SUBROUTINE ACAM		OUTPUT OF THE SUBROUTINE
(i) Autocorrelation function of acceleration record at .02 sec sampling interval		(i) $A_0 = 104037$
Time	Autocorrelation function of acceleration record	(ii) $A_1 = 47339$
1	104037	(iii) $A_2 = -50667$
2	47339	(iv) $A_3 = -79525$
3	-50667	(v) $A_m = -79525$
4	-79525	(vi) $T_m = ACF_4 = .06 \text{ sec}$
5	-23802	
6	38738	
7	40399	
:	:	
:	:	
:	:	
120	852	
121	242	
122	-182	
123	-100	
124	000	
125	000	
(ii) Total number of samples = 125		

RATIO

This subroutine is used for computing parameters ACF_5 , ACF_6 , ACF_7 and ACF_8 from the autocorrelation function. Input for this subroutine consist of:

- (i) Sampled values of autocorrelation function,
- (ii) Total number of samples of autocorrelation function,
- (iii) Sampling interval and
- (iv) A_m .

Output consists of parameters ACF_5 , ACF_6 , ACF_7 and ACF_8 . Flow chart of this subroutine is given in Fig 5.19.

EXAMPLE:

INPUT FOR THE SUBROUTINE RATIO		OUTPUT OF THE SUBROUTINE
(i) Autocorrelation function of acceleration record at .02 sec sampling interval		(i) $ACF_5 = .455$
Time	Autocorrelation function of acceleration record	(ii) $ACF_6 = -.487$
1	104037	(iii) $ACF_7 = -.764$
2	47339	(iv) $ACF_8 = -.764$
3	-50667	
4	-79525	
5	-23802	
6	38738	
7	40399	
:	:	
:	:	
120	852	
121	242	
122	-182	
123	-100	
124	000	
125	000	
(ii) Total number of samples = 125		
(iii) $A_m = -79525$		

INTERPL

This subroutine is used for computing the parameters ACF_1 , ACF_2 and ACF_3 which are the time of first, second and third zero crossing in the autocorelation function.

Zero crossing in the autocorrelation function is computed by interpolation formula explained in detail in Chapter 4. Input for this subroutine consists of :

- (i) Sampled values of autocorrelation function,
- (ii) Total number of samples of autocorrelation function and
- (iii) Sampling interval.

Output consists of parameters ACF_1 , ACF_2 and ACF_3 . Flow chart of this subroutine is given in Fig. 5.20.

EXAMPLE :

INPUT FOR THE SUBROUTINE INTERPL		OUTPUT OF THE SUBROUTINE
(i) Autocorrelation function of acceleration record at .02 sec sampling interval		(i) $ACF_1 = .03$ sec
		(ii) $ACF_2 = .088$ sec
Time	Autocorrelation function of acceleration record	(iii) $ACF_3 = .139$ sec
1	104037	
2	47339	
3	-50667	
4	-79525	
5	-23802	
6	38738	
7	40399	
:	:	
:	:	
120	852	
121	242	
122	-182	
123	-100	
124	000	
125	000	
(ii) Total number of samples = 125		

AREA

This subroutine together with subroutine AREAT computes parameters ACF_9 and ACF_{10} . Parameter ACF_9 and ACF_{10} are determined by computing area under the autocorrelation function of acceleration record as explained in detail in the Section 4.1.2. Input parameters for this subroutine are :

- (i) Sampled value of autocorrelation function,
- (ii) Total number of samples and
- (iii) Sampling interval.

Output consist of values of parameters ACF_9 and ACF_{10} . Flow chart of this subroutine is shown in Fig 5.21.

EXAMPLE:

INPUT FOR THE SUBROUTINE AREA		OUTPUT OF THE SUBROUTINE																		
(ii)	Total number of samples = 125	(i) $ACF_9 = .983$																		
(iii)	Sampling interval = .02 sec	(ii) $ACF_{10} = 1.098$																		
(i)	<table border="0" style="width: 100%;"> <tr> <td style="text-align: left;">Time</td> <td style="text-align: left;">Autocorrelation function of acceleration record</td> </tr> <tr> <td>1</td> <td>104037</td> </tr> <tr> <td>2</td> <td>47339</td> </tr> <tr> <td>3</td> <td>-50667</td> </tr> <tr> <td>4</td> <td>-79525</td> </tr> <tr> <td>5</td> <td>-23802</td> </tr> <tr> <td>6</td> <td>38738</td> </tr> <tr> <td>7</td> <td>40399</td> </tr> <tr> <td>:</td> <td>:</td> </tr> </table>	Time	Autocorrelation function of acceleration record	1	104037	2	47339	3	-50667	4	-79525	5	-23802	6	38738	7	40399	:	:	
Time	Autocorrelation function of acceleration record																			
1	104037																			
2	47339																			
3	-50667																			
4	-79525																			
5	-23802																			
6	38738																			
7	40399																			
:	:																			

INPUT FOR THE SUBROUTINE AREA	OUTPUT OF THE SUBROUTINE
:	:
:	:
120	852
121	242
122	-182
123	-100
124	000
125	000

5.3.2 SUBROUTINES USED FOR COMPUTING FREQUENCY DEPENDENT PARAMETERS

For computing various features of strong motion records in frequency domain, Fourier transform $F(\omega)$ of a signal $f(t)$ is computed. The expression for obtaining fourier transform has already been explained in Section 4.2. From the Fourier transform of acceleration record power spectrum can be obtained.

Various features that are identified from strong motion records in frequency domain are :

- (i) F_p frequency at which maximum power occurs,
- (ii) F_1 Frequency at which 25th percentile of power occurs,
- (iii) F_2 Frequency at which 50th percentile of power occurs,
- (iv) F_3 Frequency at which 75th percentile of power occurs,
- (v) F_4 Frequency at which 25th percentile value of frequency weighted power occur,
- (vi) F_5 Frequency at which 50th percentile value of frequency weighted power

occur and

- (vii) F_6 Frequency at which 75th percentile value of frequency weighted power occur.

These parameters are discussed in detail in the Section 4.2. Parameters defined in (i) to (vii) are computed using package **FREQP**. The subroutines used for the purpose are **FFT** and **POWER**.

Parameters extracted from the power spectrum of acceleration records are explained in Chapter 4. Subroutines used for this purpose are **COMPLEX**, **FFT**, **POLAR** and **PICK**.

COMPLEX

This subroutine is used for computing input data for FFT. The requirement for input data in subroutine of FFT is that it should always be in form of complex number and total number of samples should be 2^m , where m is a positive integer. This subroutine transforms real array into complex one by making imaginary part of complex number as zero and also convert total number of samples equal to 2^m . Input for this subroutine consist of:

- (i) Sampled value of acceleration record,
- (ii) Total number of samples in the record,
- (iii) Desired number of samples in the record (2^m) and
- (iv) Sampling interval of record.

Output of this subroutine consists of sampled values of the acceleration record in the form of imaginary number. Flow chart for this subroutine is shown in Fig 5.22.

EXAMPLE:

INPUT FOR THE SUBROUTINE COMPLEX		OUTPUT OF THE SUBROUTINE		
(ii) Total number of samples = 125		(i) Total number of samples in the complex form of acceleration data = 1024		
(iii) Desired number of samples = 1024 = 2 ¹⁰		Complex form of acceleration data		
(iv) Sampling interval of record = .02 sec		S.No. Acceleration (cm/sec ²)		
S.No. Acceleration (cm/sec ²)		Real Imaginary		
1.	.07	1.	.07	0.0
2.	13.75	2.	13.7	0.0
3.	2.24	3.	2.24	0.0
4.	-22.00	4.	-22.0	0.0
5.	-25.78	5.	-25.78	0.0
6.	00.00	6.	00.00	0.0
:	:	:	:	:
:	:	:	:	:
:	:	:	:	:
:	:	:	:	:
119	-12.50	119	-12.50	0.0
120	17.98	120	17.98	0.0
121	27.50	121	27.50	0.0
122	7.80	122	7.80	0.0
123	-12.20	123	-12.20	0.0
124	-07.30	124	-07.30	0.0
125	00.00	125	00.00	0.0
		:	:	:
		2	00.00	0.0
		1023	00.00	0.0
		1024	00.00	0.0

FFT

Fourier transform of a discrete value function can be computed by expression 4.12 explained in Section 4.2. Fourier transform can be obtained by using FFT (Fast Fourier Transform) algorithms. The term FFT has been widely used to define algorithms for DFT which require fewer operations, particularly multiplications, than the direct implementation of DFT given by expression 4.12. Subroutine FFT used in the present work has been taken from Clarebout (1976), and flow chart of algorithm is given in Fig 5.23.

Input for this subroutine consists of :

- (i) Sampled value of acceleration record,
- (ii) Total number of samples and
- (iii) Sampling interval.

Major requirements for executing FFT are :

- (i) Total number of samples in the input data should always equal 2^m , where m is an integer. In case data is not equal to 2^m , zeros are added at the end to make number of samples equal to 2^m ,
- (ii) The data should be uniformly sampled and
- (iii) Data should be in the form of complex number.

Output to this subroutine is the fourier transform of input data in terms of complex number.

EXAMPLE

The example for this subroutine is shown below in the tabular form where input requirements of the subroutine together with the obtained output is shown in same table.

INPUT FOR THE SUBROUTINE FFT			OUTPUT OF THE SUBROUTINE		
(ii) Total number of samples = 1024 = 2^{10}			Fourier transform of acceleration record.		
(iii) Sampling interval = .02 sec			S.No.	Fourier Transform	
(i) Sampled values of acceleration record in terms of complex number (i.e. Output of subroutine COMPLEX)				Real	Imaginary
S.No.	Acceleration (cm/sec ²)				
	Real	Imaginary			
1.	.07	0.0	1	-0.90	.00
2.	13.75	0.0	2	-0.87	.01
3.	2.24	0.0	3	-0.85	.10
4.	-22.00	0.0	4	-0.93	.24
5.	-25.78	0.0	5	-1.18	.31
6.	00.00	0.0	6	-1.51	.14
:	:	:	:	:	:
:	:	:	:	:	:
119	-12.50	0.0	509	-.63	-1.41
120	17.98	0.0	510	-.74	-0.96
121	27.50	0.0	511	-.83	-0.60
122	7.80	0.0	512	-.88	-0.29
123	-12.20	0.0			
124	-07.30	0.0			
125	00.00	0.0			
:	:	:			
:	:	:			
1022	00.00	0.0			
1023	00.00	0.0			
1024	00.00	0.0			

POLAR

Output of FFT is a complex series in the form of $P + iR$. Where P and R are real and imaginary part of complex number. This quantity can be represented as:

$$P + iR = \text{Amp } e^{i\text{Phase}}$$

where Amp is amplitude part and phase is phase part of the fourier transform.

$$\text{Amp} = [P^2 + R^2]^{1/2} \text{ and}$$

$$\text{Phase} = \tan^{-1} R/P.$$

From the amplitude spectrum, the power spectrum (Pow) can be given as:

$$\text{Pow} = (\text{Amp})^2$$

The subroutine POLAR computes phase and amplitude part from the output of FFT for each frequency. Input for this subroutine consists of :

- (i) Real and imaginary part of fourier transform (output of subroutine FFT),
- (ii) Total number of samples and
- (iii) Sampling interval of acceleration record.

Output consists of amplitude, phase and power spectrum. Flow chart of this subroutine is shown in Fig 5.24.

EXAMPLE :

INPUT FOR THE SUBROUTINE POLAR			OUTPUT OF THE SUBROUTINE			
(i) Real and imaginary part of fourier transform (output of subroutine FFT)			(i) Amplitude, phase and power spectrum			
S.No.	Fourier Transform		S.No.	Amplitude	Phase	Power
	Real	Imaginary				
1	-0.90	.00	1	.90	-3.14	.81
2	-0.87	.01	2	.87	3.12	.76
3	-0.85	.10	3	.85	3.02	.73
4	-0.93	.24	4	.96	2.88	.93
5	-1.18	.31	5	1.22	2.88	1.49
6	-1.51	.14	6	1.52	3.04	2.32
:	:	:	:	:	:	:
:	:	:	:	:	:	:
:	:	:	:	:	:	:
509	-.63	-1.41	509	1.55	-1.99	2.41
510	-.74	-0.96	510	1.22	-2.22	1.49
511	-.83	-0.60	511	1.03	-2.51	1.06
512	-.88	-0.29	512	.93	-2.82	.86

PICK

This subroutine is used for picking maximum power from a power spectrum and its corresponding frequency (F_p). Input parameters for this subroutine consist of:

- (i) Number of samples in power spectrum,
- (ii) Digitised value of power spectrum and
- (iii) Sampling frequency.

Output is the value of F_p at which maximum power occurs. Flow chart for this subroutine is given in Fig 5.14.

EXAMPLE:

INPUT FOR THE SUBROUTINE PICK		OUTPUT OF THE SUBROUTINE
(i) Number of samples in power spectrum = 512		Maximum value of power = 1139139 $F_p = 9.22$ Hz
(ii) Digitised value of power spectrum		
S.No.	Power	
1	.81	
2	.76	
3	.73	
4	.93	
5	1.49	
:	:	
:	:	
:	:	
509	2.41	
510	1.49	
511	1.06	
512	.86	

POWER

For computing parameters F_1, F_2, F_3, F_4, F_5 and F_6 from the power spectrum of the acceleration record, subroutine POWER is developed. This subroutine consists of subroutines **VPOW** and **PICKF**. Flow chart of this subroutine is given in Fig 5.25.

VPOW

This subroutine is used for computing cumulative power spectrum and cumulative frequency weighted power spectrum. This subroutine has been developed by Sinvhal et al. (1992). Flow chart of this subroutine is shown in Fig 5.26. The input for this subroutine are:

- (i) Power spectrum of acceleration record (i.e. output of subroutine POLAR),
- (ii) Sampling frequency and
- (iii) Total number of samples in the power spectrum.

Output of this subroutine consists of :

- (i) Sampled value of cumulative power spectrum,
- (ii) Number of samples,
- (iii) Sampled value of frequency weighted cumulative power spectrum,
- (iv) Number of samples,
- (v) 25th Percentile value of power,
- (vi) 50th Percentile value of power,
- (vii) 75th Percentile value of power,
- (viii) 25th Percentile value of frequency weighted cumulative power,
- (ix) 50th Percentile value of frequency weighted cumulative power and
- (x) 75th Percentile value of frequency weighted cumulative power.

EXAMPLE:

INPUT FOR THE SUBROUTINE VPOW		OUTPUT OF THE SUBROUTINE			
(i) Power spectrum of acceleration record		Frequency weighted cumulative power spectrum and cumulative power spectrum			
S.No.	Power	S.No.	Frequency cumulative spectrum	Weighted power	Cumulative power spectrum
1	.81				
2	.76				
3	.73	1	.030		.81
4	.93	2	.110		1.58
5	1.49	3	.220		2.31
:	:	4	.400		3.25
:	:	:	:		:
:	:	:	:		:
509	2.41	509	4.6×10^8		53267420
510	1.49	510	4.6×10^8		53267440
511	1.06	511	4.6×10^8		53267450
512	.86	512	4.6×10^8		53267450
(ii) Total number of samples in the power spectrum = 512		(ii) 25th Percentile value of power = 13316860			
(iii) Sampling Interval = .02 sec		(iii) 50th Percentile value of power = 26633730			
		(iv) 75th Percentile value of power = 39950590			
		(v) 25th Percentile value of frequency weighted cumulative power = 1.1×10^8			
		(vi) 50th Percentile value of frequency weighted cumulative power = 2.3×10^8			
		(vii) 75th Percentile value frequency weighted cumulative power = 3.4×10^8			

PICKF

This subroutine is used for computing F_1, F_2, F_3, F_4, F_5 and F_6 from the cumulative power spectrum and frequency weighted cumulative power spectrum. Input for this subroutine consists of :

- (i) Sampled value of cumulative power spectrum,
- (ii) Number of samples,
- (iii) Sampled value of frequency weighted cumulative power spectrum,
- (iv) Number of samples,
- (v) 25th Percentile value of power,
- (vi) 50th Percentile value of power,
- (vii) 75th Percentile value of power,
- (viii) 25th Percentile value of frequency weighted cumulative power,
- (ix) 50th Percentile value of frequency weighted cumulative power and
- (x) 75th Percentile value of frequency weighted cumulative power.

Output of this subroutine are the values of F_1, F_2, F_3, F_4, F_5 and F_6 . Flow chart of this subroutine is shown in Fig 5.27.

EXAMPLE:

INPUT FOR THE SUBROUTINE PICKF				OUTPUT OF THE SUBROUTINE
S.No.	Frequency cumulative spectrum	Weighted power	Cumulative power spectrum	$F_1 = 8.2$ Hz, $F_2 = 9.1$ Hz, $F_3 = 10.1$ Hz, $F_4 = 7.6$ Hz, $F_5 = 8.9$ Hz and $F_6 = 9.6$ Hz
1	.030		.81	
2	.110		1.58	
3	.220		2.31	
4	.400		3.25	
:	:		:	

INPUT FOR THE SUBROUTINE PICKF		
:	:	:
:	:	:
509	4.6×10^8	53267420
510	4.6×10^8	53267440
511	4.6×10^8	53267450
512	4.6×10^8	53267450
(ii) 25th Percentile value of power = 13316860		
(iii) 50th Percentile value of power = 26633730		
(iv) 75th Percentile value of power = 39950590		
(v) 25th Percentile value of cumulative frequency weighted power = 1.1×10^8		
(vi) 50th Percentile value of cumulative frequency weighted power = 2.3×10^8		
(vii) 75th Percentile value of cumulative frequency weighted power = 3.4×10^8		

Fig 4.10 and Fig 4.11 shows cumulative power spectrum and frequency weighted cumulative power spectrum respectively, computed from the simulated acceleration record at Saitsama station for the Meghalaya earthquake of 10th Sept, 1986.

5.4 SUMMARY

For simulation of strong ground motion record due to a modelled rupture plane package **STRMR** has been developed in FORTRAN IV language. The procedure of modelling of rupture plane is discussed in detail in Chapter 3. Various features that can

be extracted from strong motion record are explained in Chapter 4. Packages named as **TIMEP** and **FREQP** are developed for extracting time and frequency dependent parameters of strong motion records.

To illustrate the use of these packages the Meghalaya earthquake of 10th Sept, 1986 with vertical rupture plane has been modelled and strong motion records at Saitsama station due to this model were simulated. Developed package **STRMR** is used for modelling of the rupture plane within the identified fault. The results obtained after modelling of rupture process and comparison of simulated and field records for Dharamsala earthquake of 26th April, 1986, Uttarkashi earthquake of 20th Oct, 1991 and Meghalaya earthquake of 10th Sept, 1986 are discussed in detail in Chapter 6, 7 and 8, respectively.



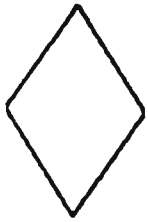
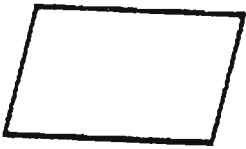
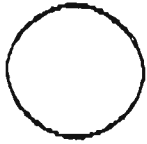
FIGURE	SHAPE	DESCRIPTION
	OVAL	FOR START OR STOP
	RECTANGLE	FOR CALCULATION OR PROCESS OTHER THAN DECISION
	DIAMOND	FOR A DECISION
	PARALLELOGRAM	FOR INPUT OR OUTPUT
	SMALL CIRCLE	FOR A CONNECTION

Fig 5.1 Various symbols used for preparation of flow charts.

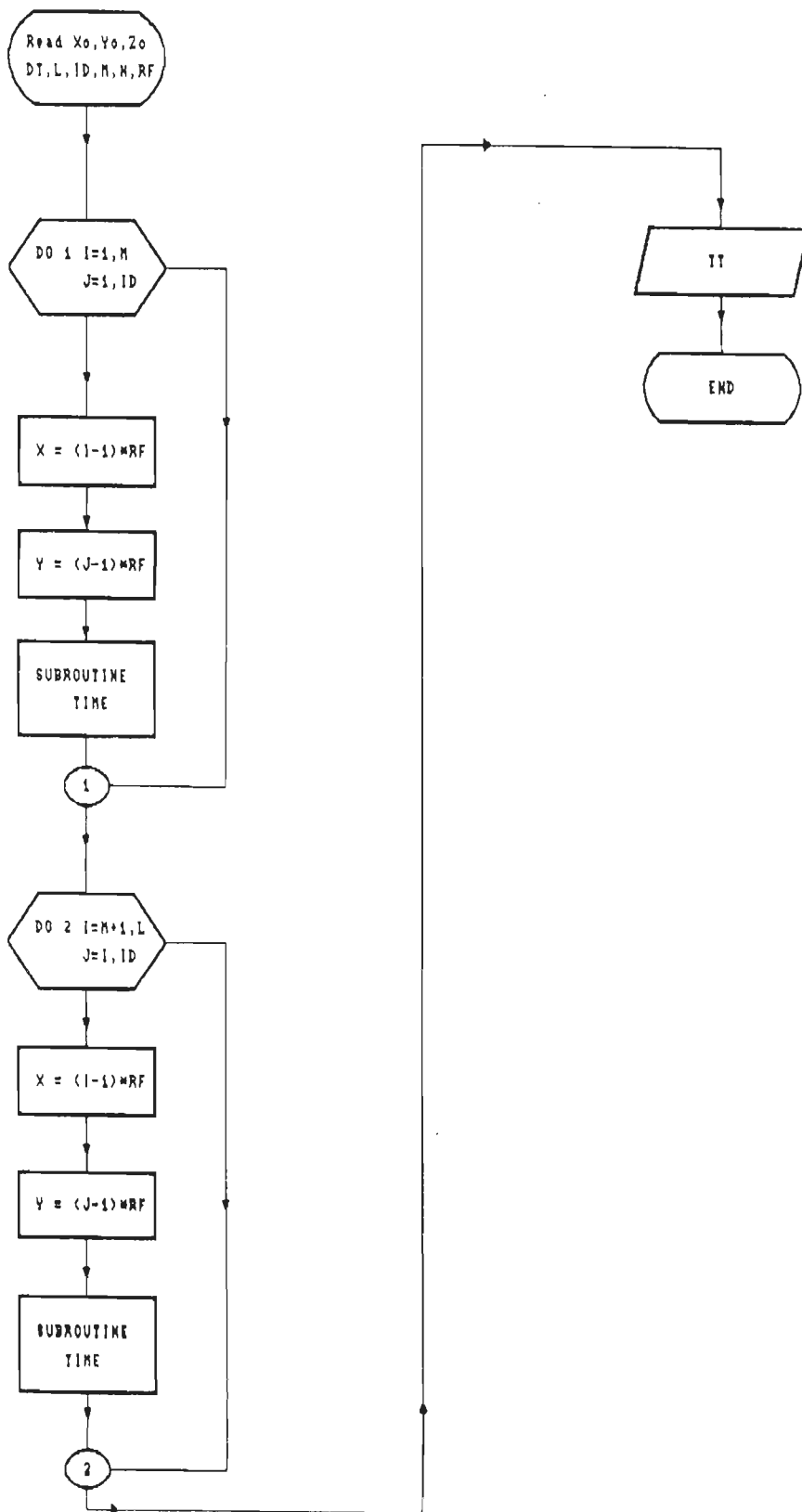


Fig 5.2 Flow chart of subroutine **RRG**.

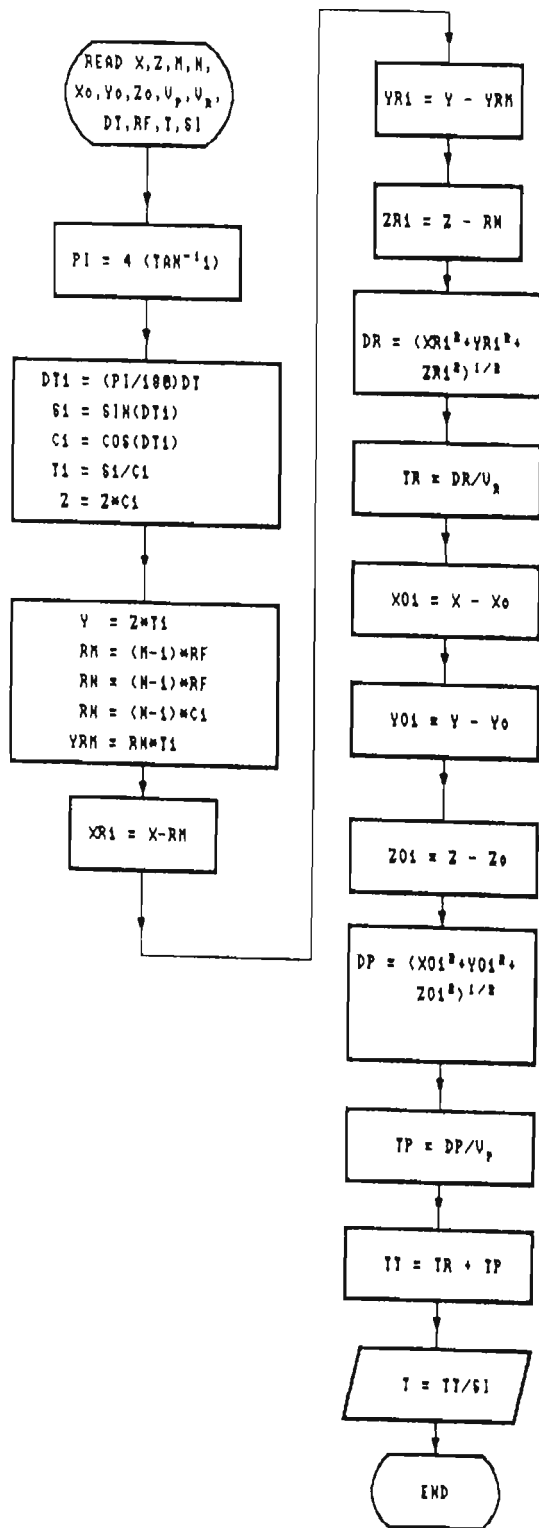


Fig 5.3 Flow chart of subroutine TIME.

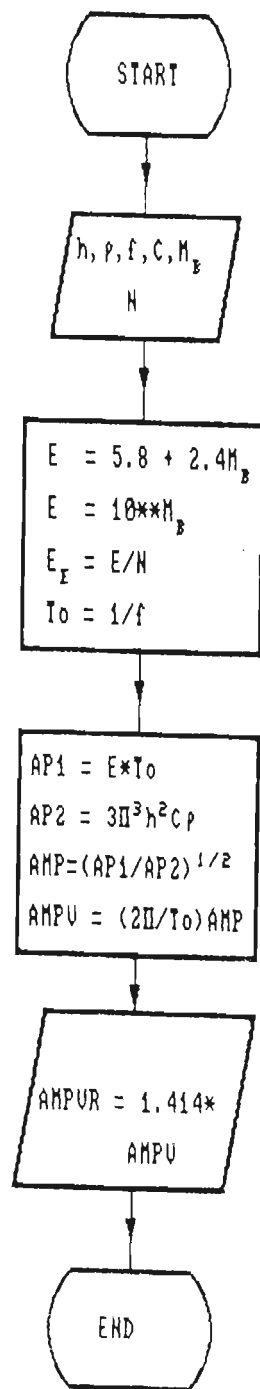


Fig 5.4 Flow chart of subroutine SCALE.

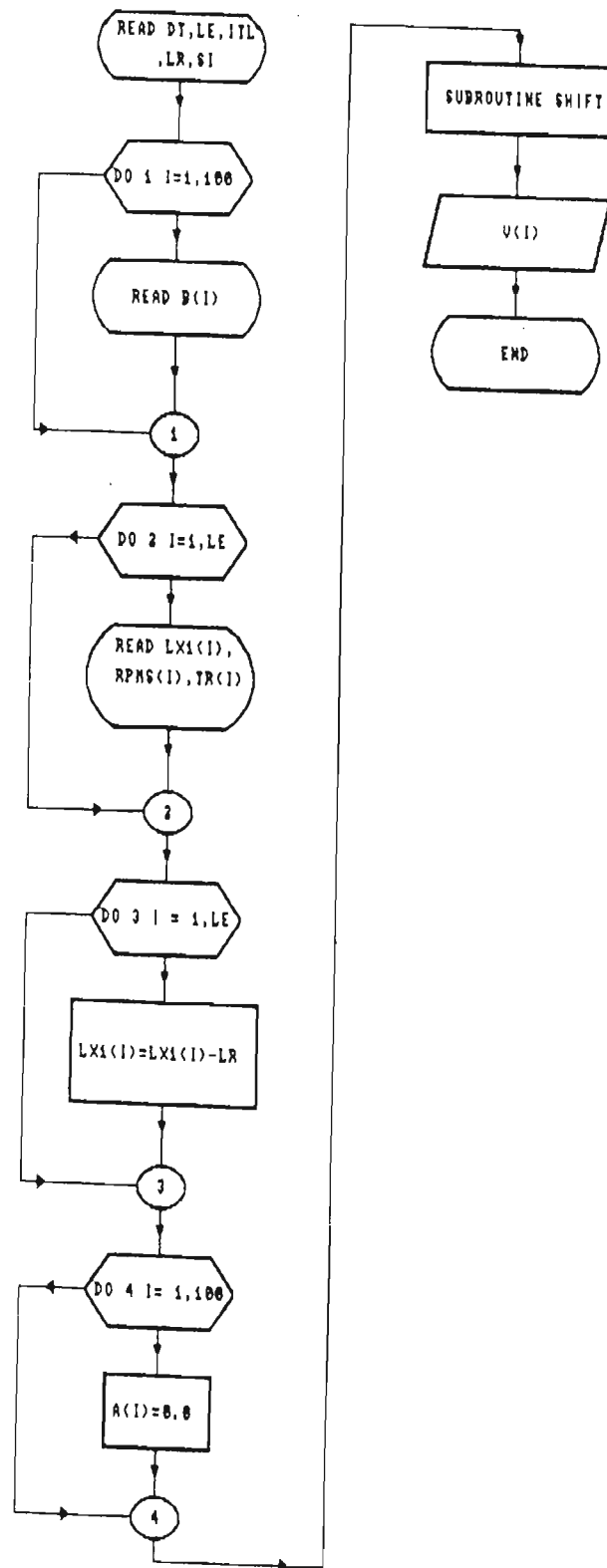


Fig 5.5 Flow chart of subroutine VEL.

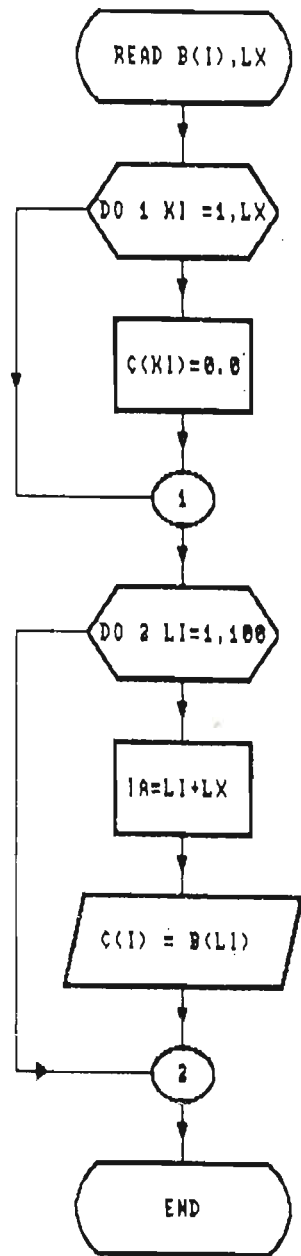


Fig 5.6 Flow chart of subroutine DELAY.

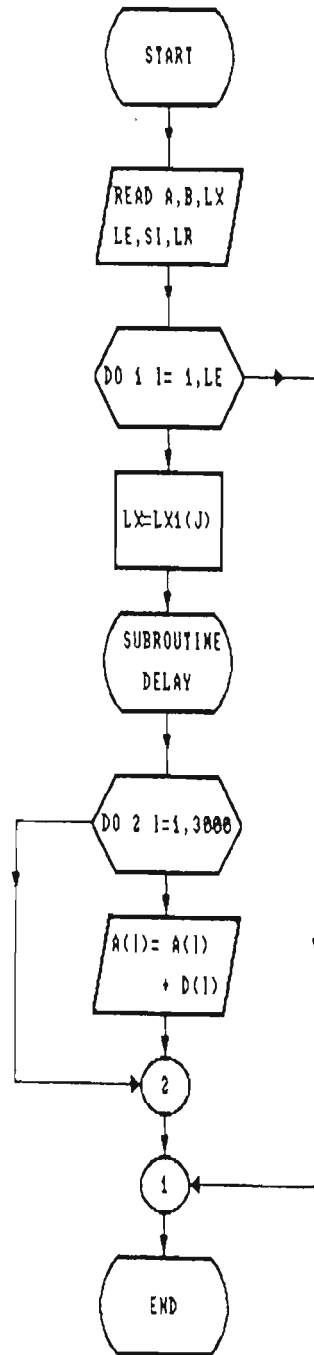


Fig 5.7 Flow chart of subroutine **SHIFT**

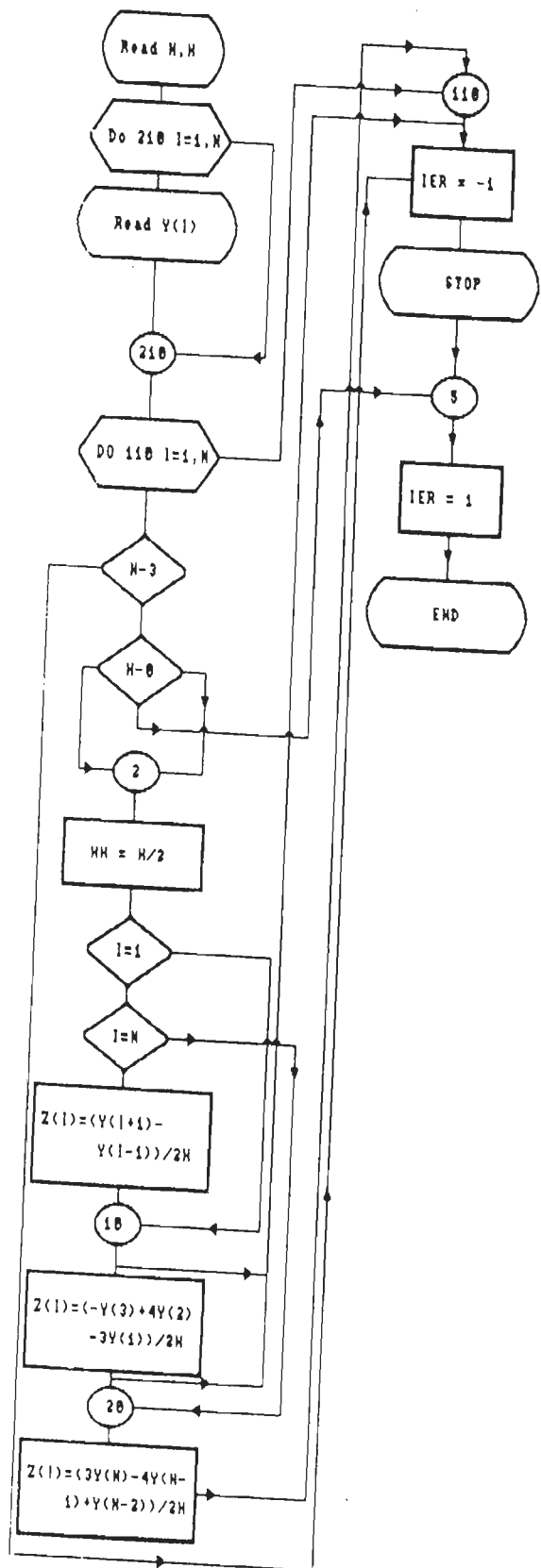


Fig 5.8 Flow chart of subroutine DIF.

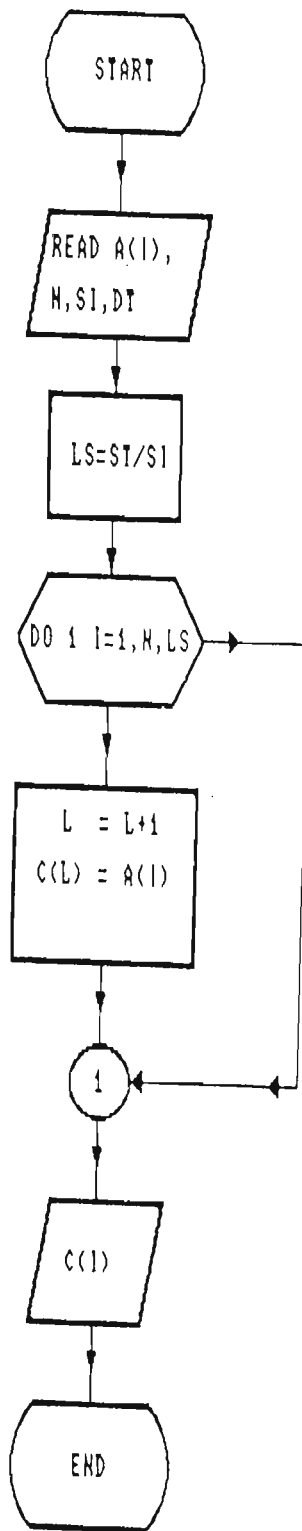


Fig 5.9 Flow chart of subroutine **DATA**.

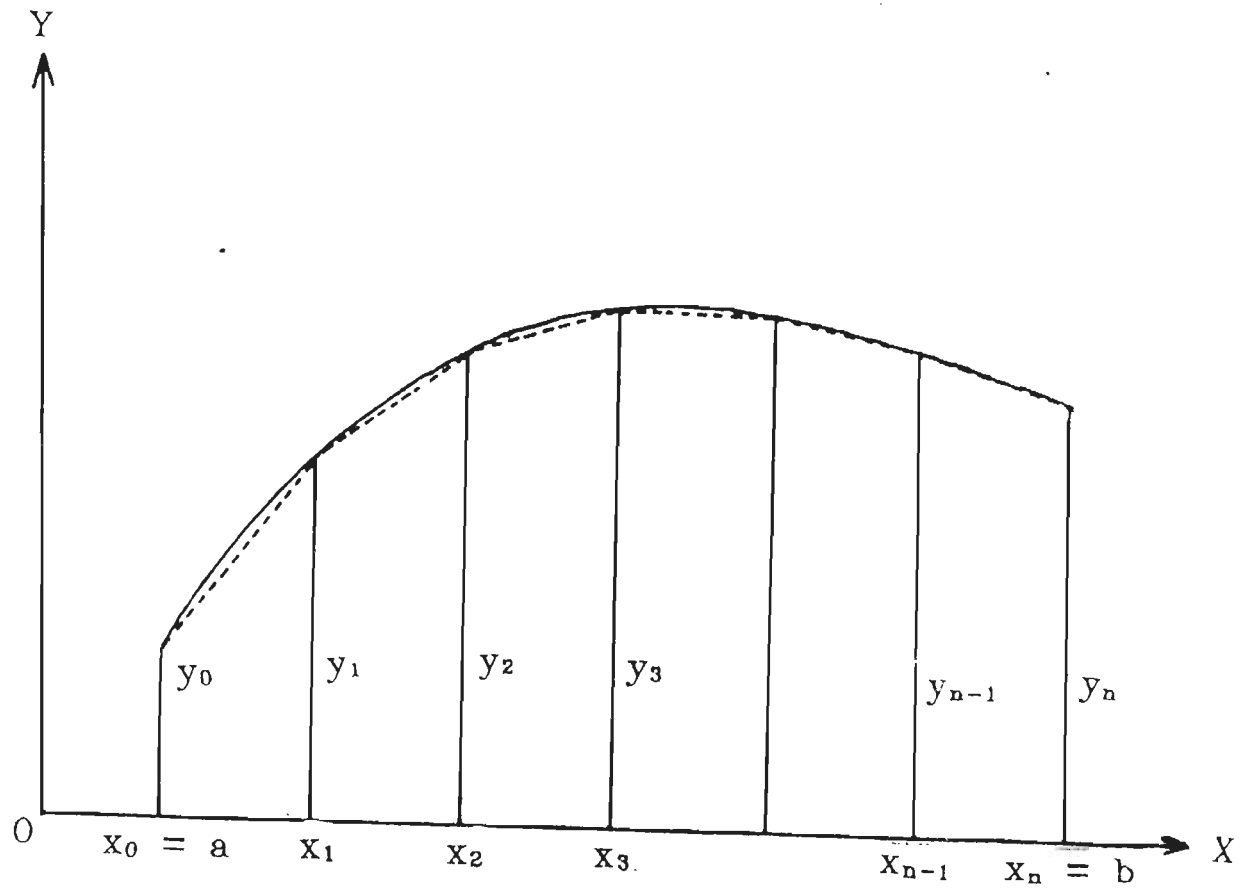


Fig 5.10a Function divided into numbers of trapezoids. This rule has been used for integration of a given function.

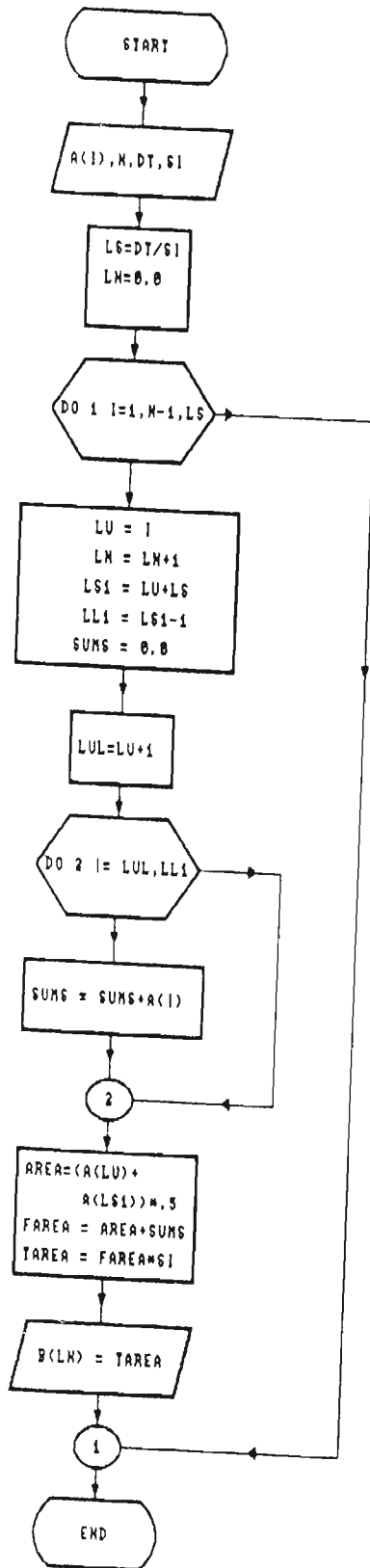


Fig 5.10b Flow chart of subroutine INTEG.

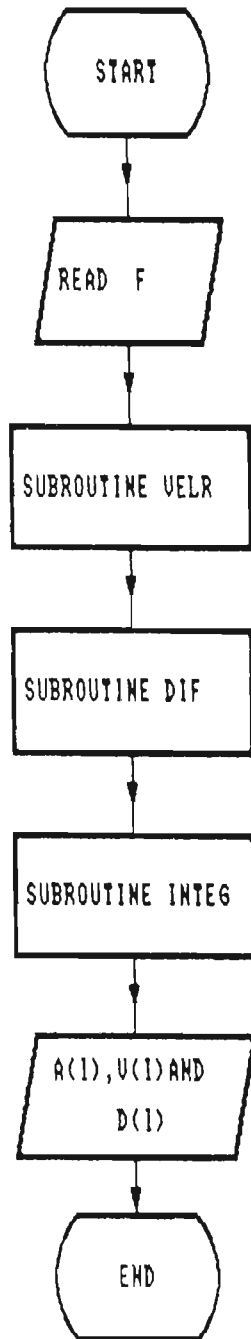


Fig 5.11 Flow chart of subroutine SWAVE.

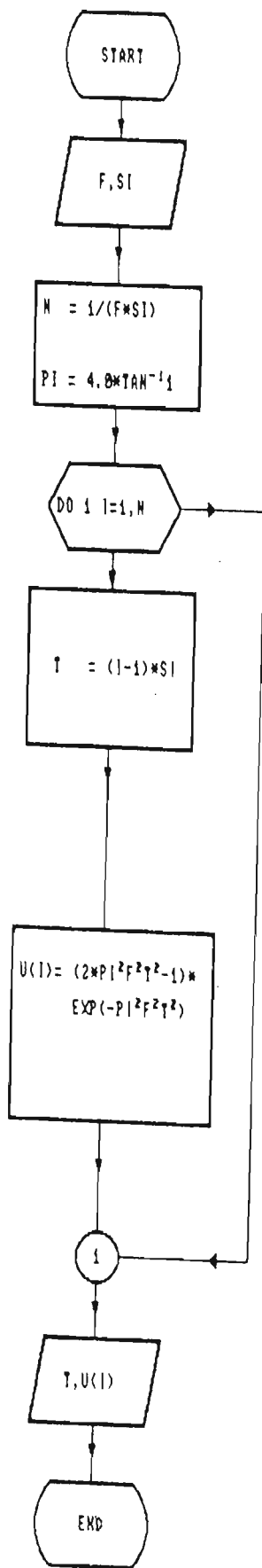


Fig 5.12 Flow chart of subroutine **VELR**.

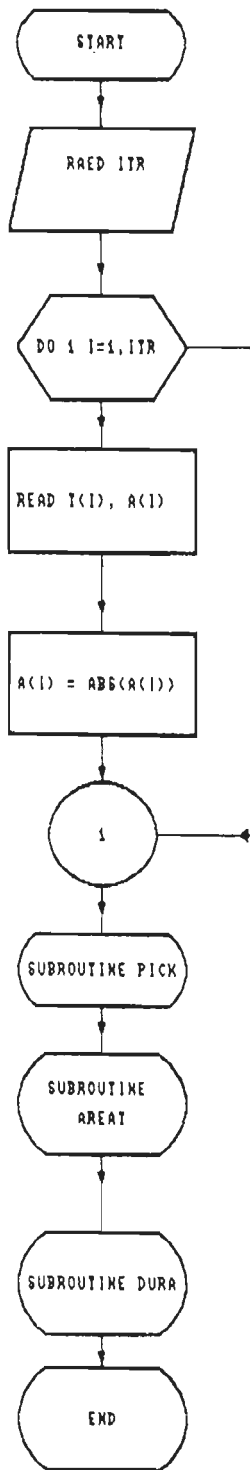


Fig 5.13 Flow chart of subroutine PTD.

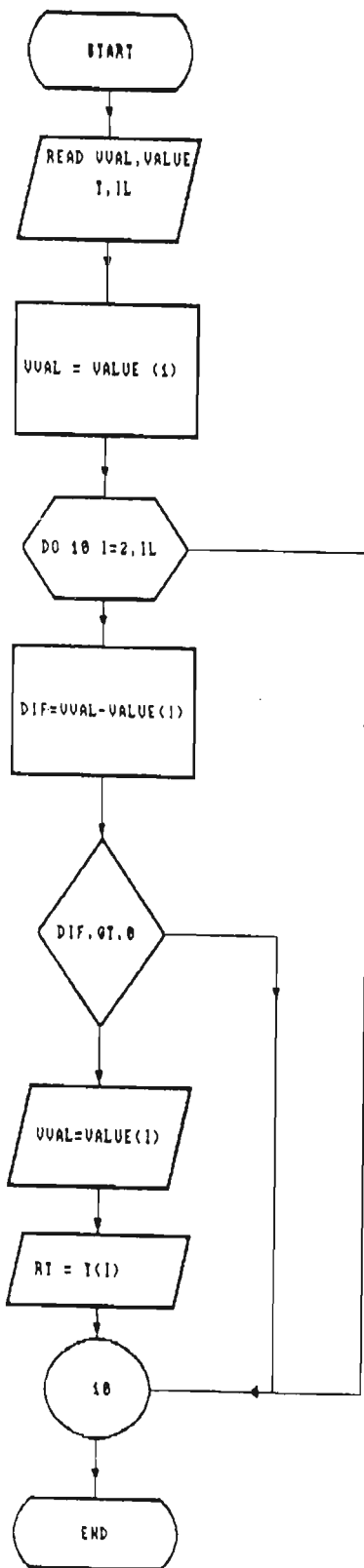


Fig 5.14 Flow chart of subroutine **PICK**.

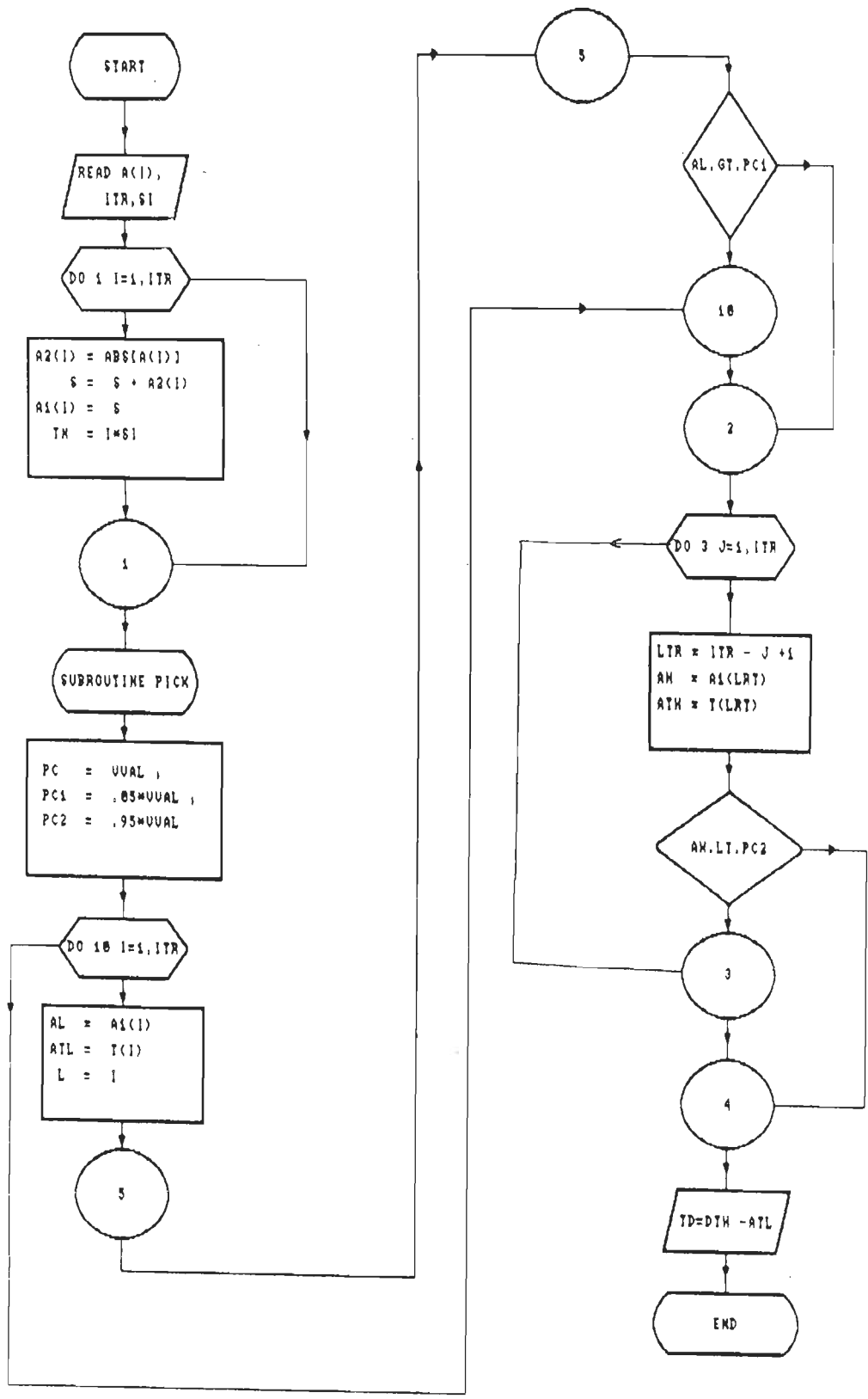


Fig 5.15 Flow chart of subroutine DURA.

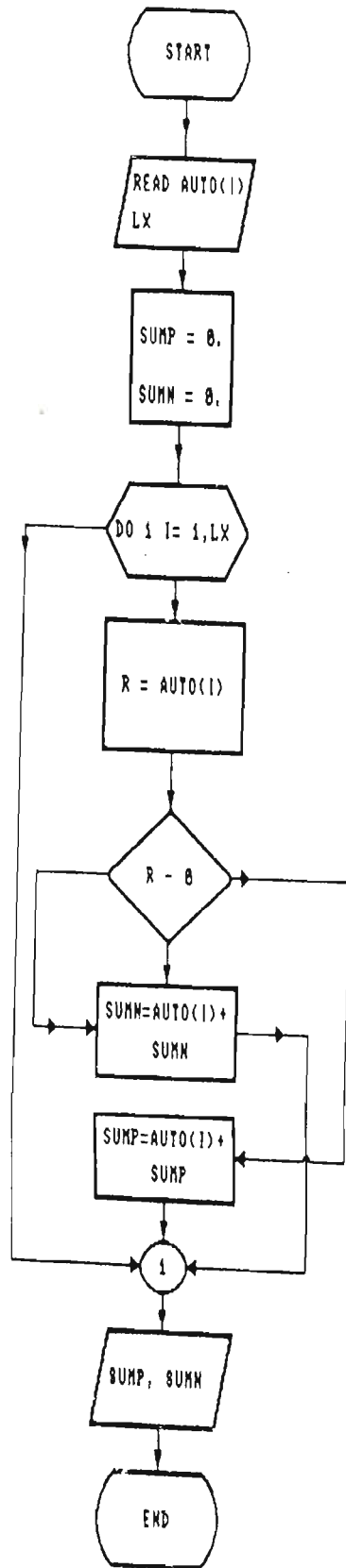


Fig 5.16 Flow chart of subroutine AREAT.

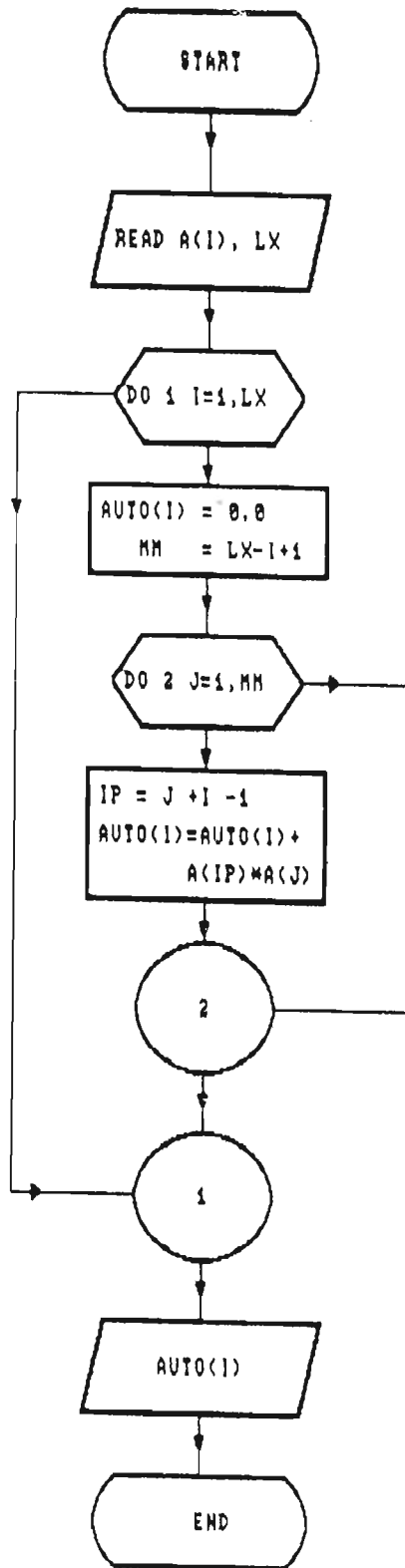


Fig 5.17 Flow chart of subroutine AUTOC.

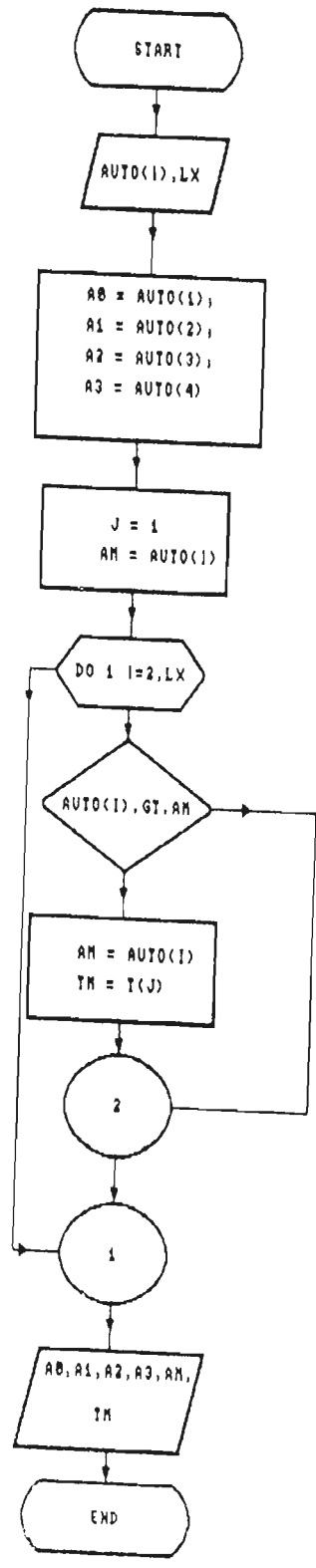


Fig 5.18 Flow chart of subroutine ACAM.

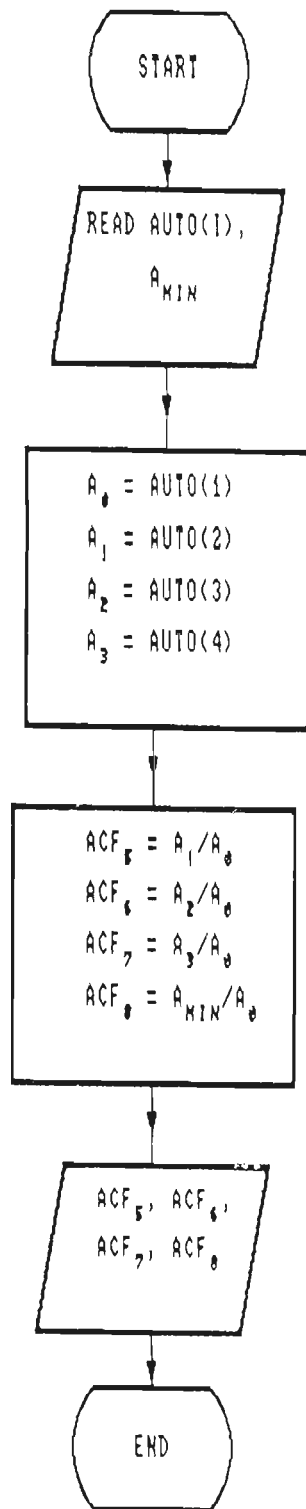


Fig 5.19 Flow chart of subroutine **RATIO**.

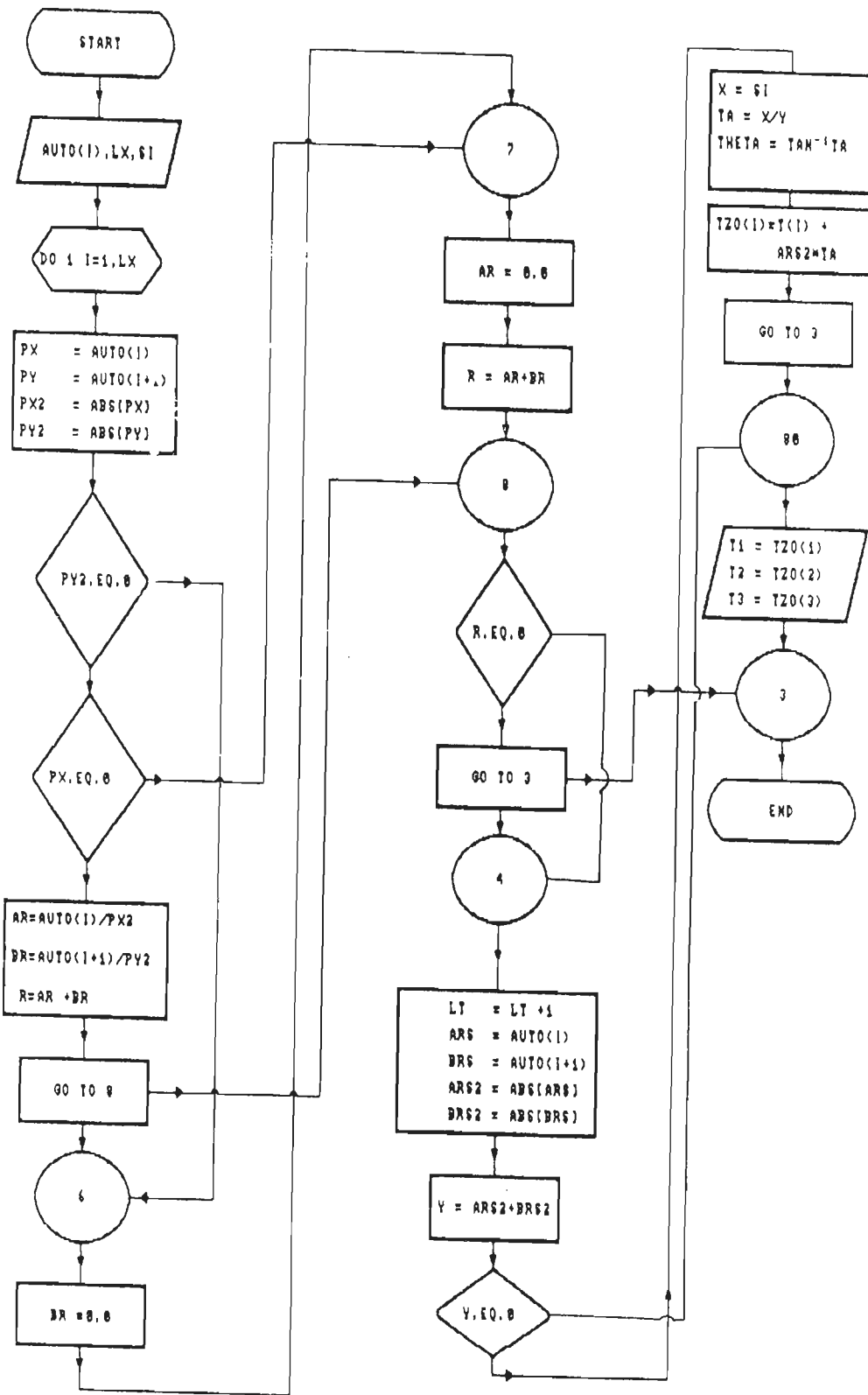


Fig 5.20 Flow chart of subroutine **INTERPL**.

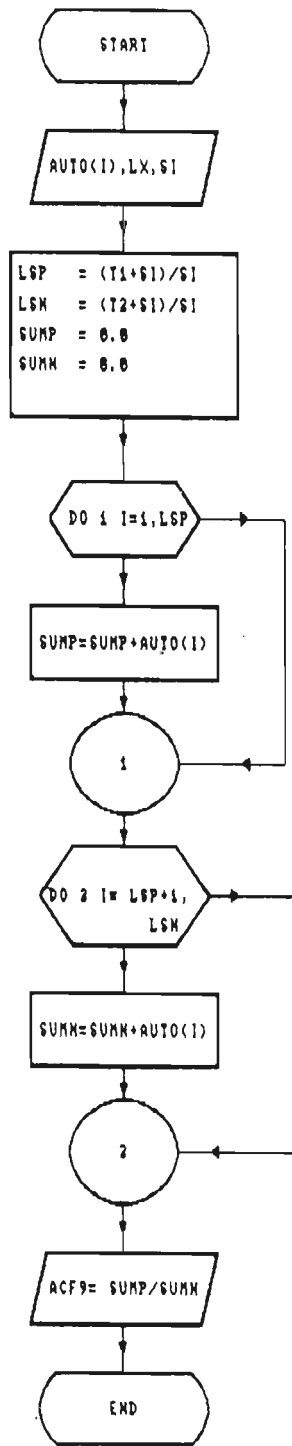


Fig 5.21 Flow chart of program AREA.

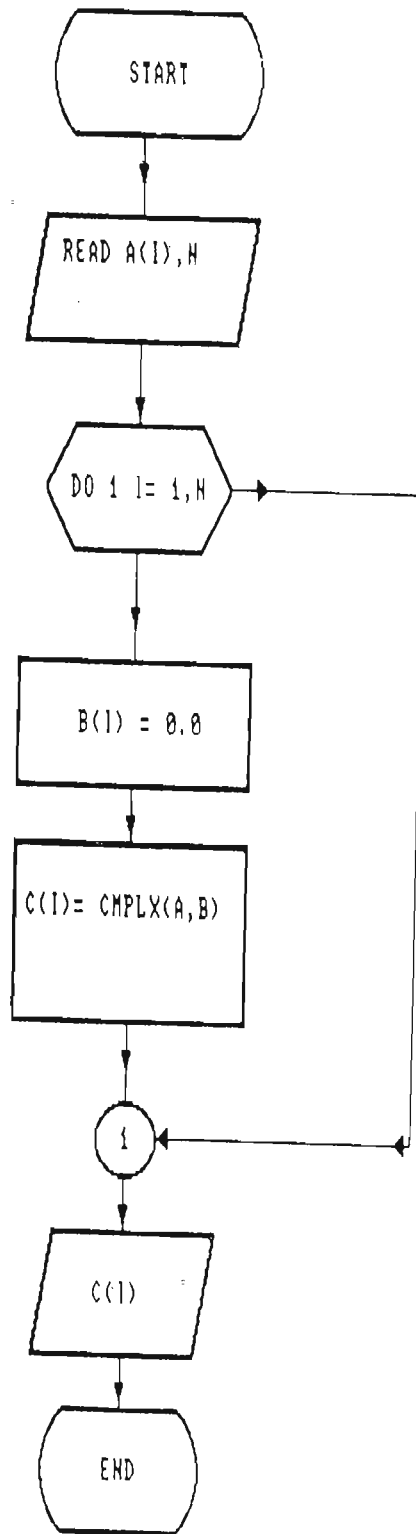


Fig 5.22 Flow chart of subroutine **COMPLEX**.

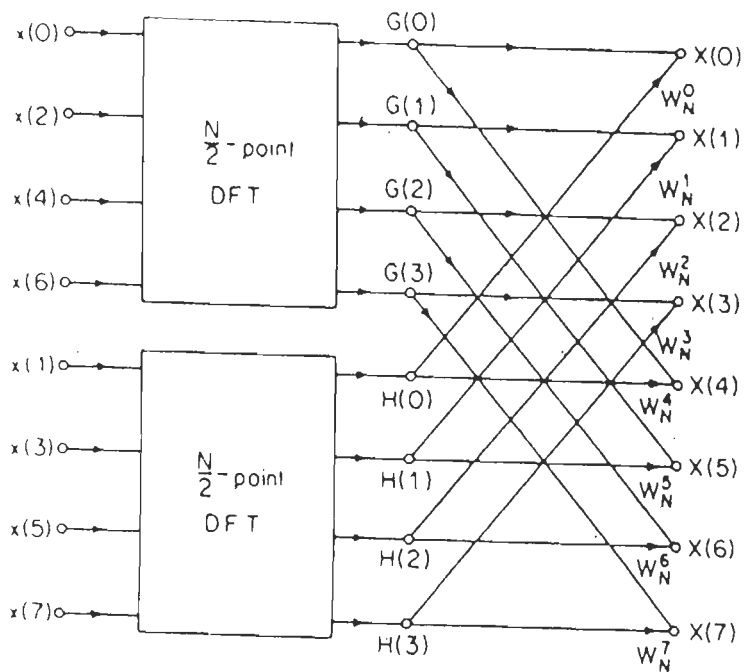


Fig 5.23 Flow chart of the decimation in time decomposition of N point DFT computations into $N/2$ point DFT computations ($N=8$) (Oppenheim and Schaffer, 1988).

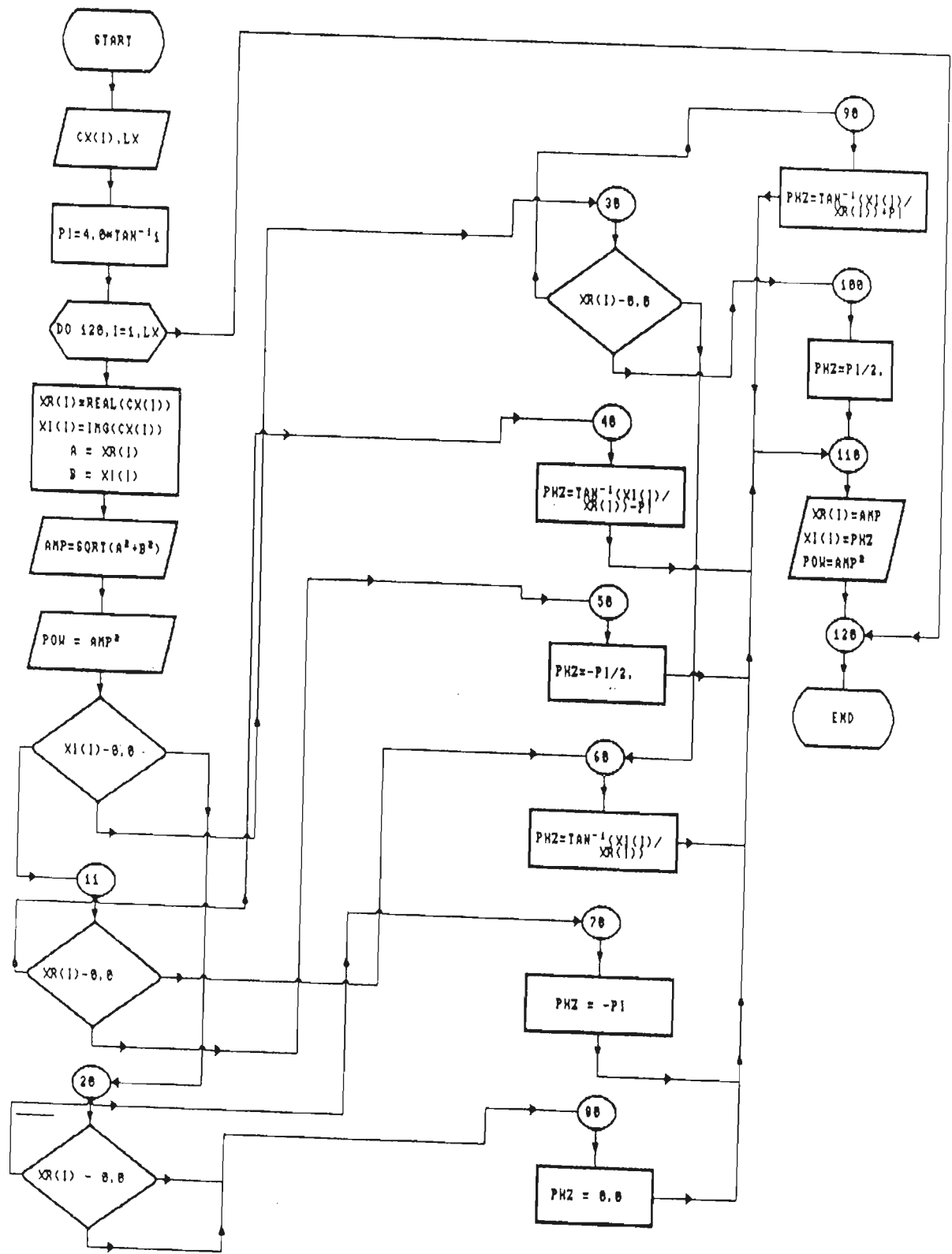


Fig 5.24 Flow chart of subroutine POLAR.

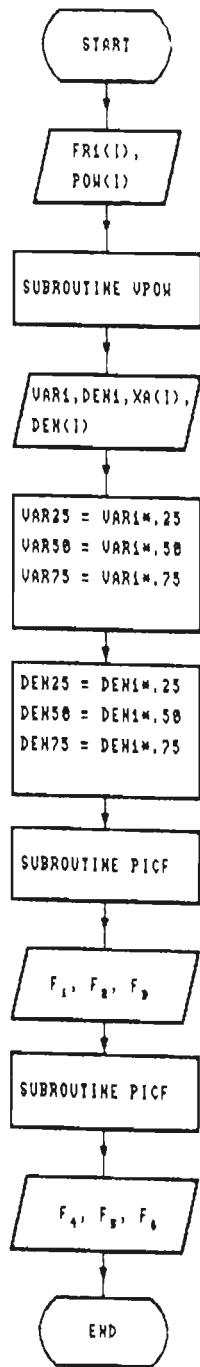


Fig 5.25 Flow chart of subroutine **POWER**.

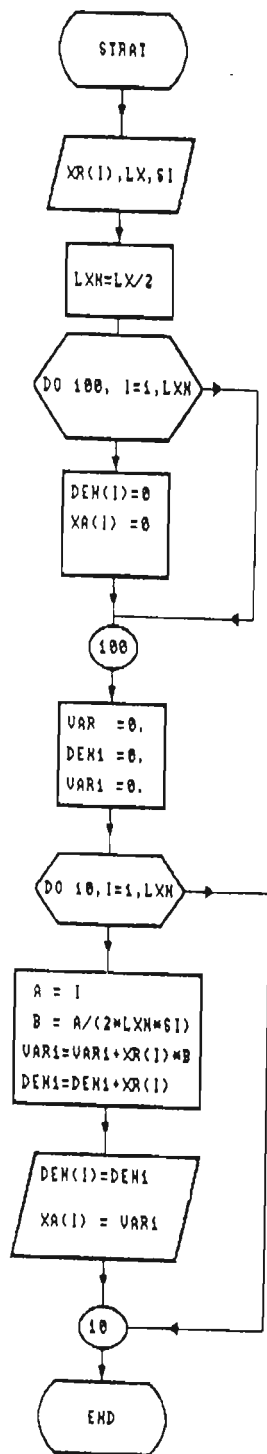


Fig 5.26 Flow chart of subroutine VPOW.

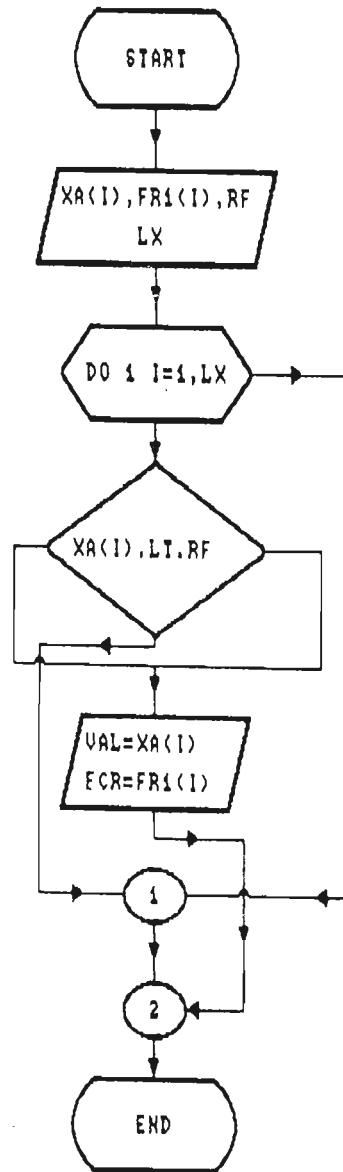


Fig 5.27 Flow chart of subroutine **PICKF**.

CHAPTER 6

DHARAMSALA EARTHQUAKE OF 26TH APRIL, 1986

Himachal Pradesh has experienced many damaging earthquakes in the recent past as is evident from Table 6.1 and Fig 6.1. The most damaging earthquake in the area was the great Kangra earthquake of 1905. Salient features of the 1905 earthquake (After Middlemiss, 1910) are:

Date	04.04.1905
Time	6 Hr 10 Min 43 Sec (IST)
Epicenter	32.00°E, 77.00° N
Magnitude	8 +
Depth of Focus	Between 20 and 33 km
Maximum intensity	X on Rossi Forel Scale

Middlemiss (1910, pp 34-35) had theoretically computed acceleration due to Kangra earthquake of 1905 for various places. These are given in Table 6.2. An earthquake of magnitude (M_b) 5.5 occurred on 26th April, 1986 in the Dharamsala region of Himachal Pradesh, which has been studied in detail in the present work and herein after this earthquake has been referred to as the Dharamsala earthquake.

6.1 KANGRA STRONG MOTION ARRAY

The region around Kangra is very prone to earthquakes, therefore a dense array of strong motion recorders is operated in this area by the Department of Earthquake

Engineering University of Roorkee. The array encompasses three major river valleys Sutlej, Beas and Ravi. The entire area has an undulating topography with hills and valleys.

Fifty analogue strong motion accelerographs (SMA-1 with Time Code Generator made by Kinometrics Pasadena, USA) constitute the array elements. The array trends northwest to southeast and has a linear dimension of about 240 km and runs parallel to the regional strike of tectonic features. The width of the array in a direction transverse to the geological features varies from about 40 to 80 km. This array covers an area of about 60 X 240 km. The interstation spacing varies between 7 to 21 km. Table 6.3 and Fig 6.2 provide complete detail of station location and elevation of instruments above the mean sea level (MSL). The elevation of the stations ranges between 470m for Nadaun to 2870m for Bagi.

The Dharamsala earthquake of 26th April, 1986 was recorded on the Kangra strong motion array. Instruments at nine stations (Fig 6.2) were triggered by this event. The epicenter was within the network. At each stations two horizontal and one vertical component of ground acceleration were recorded. This is computationally converted into velocity and displacement records.

6.2 SALIENT FEATURES OF DHARAMSALA EARTHQUAKE OF 26TH APRIL, 1986

An earthquake of body wave magnitude 5.5 on Richter scale was felt at Dharamsala in Kangra district. Damage due to this earthquake was investigated by Gupta et. al. (1986) and Arya et al. (1986). Causative fault for this earthquake was

identified by Kumar and Mahajan (1990, 1992), Narula and Shome (1992) and Rastogi (1992a). Source parameters for this earthquake were computed by Srivastava and Chatterjee (1986), Srivastava (1989), Molnar (1990), Srivastava (1992), Jain et al. (1992) and Das and Chandrasekaran (1993). Rupture plane for this earthquake was modelled by Sinval et al. (1990, 1993). Strong motion data was analysed by Chandrasekaran (1988a and 1988b) and Chandrasekaran and Das (1990b, 1992a, 1992b). Seismic studies related to the velocity structure in the region are given by Srivastava and Chatterjee (1986), Chaudhury and Srivastava (1977) and Balakrishnan and Choudhury (1976). Various parameters for this earthquake as reported by different authors/agencies are given in Table 6.4.

The earthquake was felt upto Amritsar, Srinagar and Simla which are at distances of 140, 240 and 160 km, respectively, from the epicenter of the earthquake. The earthquake was felt in entire Kangra valley, in Mandi, Chamba and Kullu areas of Himachal Pradesh (Kumar and Mahajan, 1990, 1991). The shock was felt in upper storeys of multistoreyed buildings at Delhi, 400 km away from the epicentral region.

Damage to property, in the form of cracks along mortar joints and fall of plaster, etc. was confined to Dharamsala town. Collapse of walls of mud houses and Govt. buildings were reported from Naddi village, Dharamsala Cantonment, Nargota, Sudher, Chari and Chilgari villages. The villages of Nargota and Naddi were completely destroyed. Newly constructed Tibetan school which is located just near village Naddi suffered damage. Old mud houses in village Naddi and stone houses using mud mortar in Nargota village collapsed. At Naddi, along fracture developed on land close to the temple.

Residents of Naddi, Macleodganj, Sudher, Chari, Nargota, Chillgari, Dharamsala, Kaned and Yol villages testified during field investigations, that they felt earthquake waves with motion which was up and down and not lateral (Kumar and Mahajan, 1990).

The isoseismal map for the Dharamsala earthquake of 26th April, 1986 (Kumar and Mahajan, 1990) shows intensities from IV to VII on the Modified Mercalli intensity scale. This map is shown in Fig 6.3. The isoseismals are elliptical and the larger axis trends about N30°W. This map is used for the purpose of identification of most probable causative fault for the Dharamsala earthquake.

Fault plane solutions for this earthquake have been given by Kumar and Mahajan (1991), USGS (Table 6.5) and it reveals that mechanism of this earthquake is strike slip faulting (Kumar and Mahajan, 1991).

6.3 IDENTIFICATION OF MOST PROBABLE CAUSATIVE FAULT FOR THE DHARAMSALA EARTHQUAKE OF 26TH APRIL, 1986

Most probable causative fault for this earthquake is identified on the tectonic map on the basis of available isoseismal, tectonic and isoacceleration maps. The specific maps considered are:

- (i) Isoseismal map of Dharamsala earthquake of 26th April, 1986 earthquake (Kumar and Mahajan, 1990, 1991)
- (ii) Tectonic map of the region (Kumar and Mahajan, 1991 and Raiverman et al., 1979), and
- (iii) Isoacceleration map

6.3.1 TECTONIC MAP (KUMAR AND MAHAJAN, 1990, 1991)

Lineaments in the epicentral tracts of the Dharamsala earthquake identified on a map of 1:250,000 scale prepared by Kumar and Mahajan (1990, 1991) is shown in Fig 6.4a. Main lineaments are parallel to Himalayan trend, such as Drini thrust and Main Boundary Thrust. Strike of Drini thrust is N45W and strike of Main boundary thrust is N47W (Kumar and Mahajan, 1990, 1991). The geological section along a section line shown in the tectonic map shown in Fig 6.4a is given in Fig 6.4b. This map has been used for nomenclature of the identified most probable causative fault for the Dharamsala earthquake.

6.3.2 TECTONIC MAP (RAIVERMAN ET AL., 1979)

Tectonic map in the region shows several tectonic lineaments, mostly of thrust type (Raiverman et al. 1979) with Main Boundary fault separating the pre Tertiary sequences of rocks juxtaposed against the Tertiary rocks about 4 km north of the epicenter of the earthquake and Jawalamukhi thrust. Fig 6.5 shows main lineaments in the area which are :

- (i) Main Boundary Thrust (MBT),
- (ii) Palampur thrust and
- (iii) Jawalamukhi thrust.

6.3.3 ISOACCELERATION MAP

The earthquake was well recorded on the Strong Motion Array in this region. Digitised values of acceleration, velocity and displacement records are taken from the

report of Earthquake Engineering Department, University of Roorkee (Chandrasekaran, 1988b). Resultant peak acceleration calculated from the two horizontal components, namely the longitudinal and the transverse has been used for drawing isoacceleration contours. Value of resultant peak acceleration at different stations is given in Table 6.6 (Chandrasekaran, 1988b). Isoacceleration contour map shown in Fig 6.6 has been prepared from the peak acceleration values.

6.3.4 COMPOSITE ISOSEISMAL MAP (KUMAR AND MAHAJAN, 1990, 1991) AND TECTONIC MAP (RAIVERMAN ET AL., 1979)

The isoseismal map (Kumar and Mahajan, 1990, 1991) and tectonic map (Raiverman et al., 1979) are superimposed to form a composite map. It is seen that MBT and lineament identified as lineament D1 passes through isoseismal VII. The epicenters marked as E_{D3} and E_{D4} are along lineament D1 within isoseismal V and E_{D3} lies within isoseismal IV as shown in Fig 6.7. These two epicenters are close to the lineament D1 as compared to epicenters named as E_{D1} and E_{D2} .

6.3.5 COMPOSITE ISOACCELERATION MAP (SECTION 6.3.3) AND TECTONIC MAP (RAIVERMAN ET AL., 1979)

Isoacceleration and tectonic map were superimposed to give a single composite map, given in Fig 6.8. and it is seen that northern part of lineament D1 passes almost parallel to peak acceleration contour of 150 cm/sec^2 while its southern part intersects with the isoacceleration contours of value 150 and 200 cm/sec^2 , respectively. Contour map does not cover area on eastern side of lineament 1 due to lack of strong motion data for this region.

6.4 IDENTIFICATION OF MOST PROBABLE CAUSATIVE FAULT ON MAP

All these maps are superimposed on a single composite map shown in Fig 6.9 and following points emerge :

- (i) The direction of major axis of isoseismals (Kumar and Mahajan, 1990, 1991) follows the trend of lineaments in the region.
- (ii) Direction of elongated axis follows the strike of lineament D1 and Main Boundary thrust [From composite isoseismal (Kumar and Mahajan, 1990, 1991) and tectonic map (Kumar and Mahajan, 1990, 1991)]. Epicenter E_{D_3} and E_{D_4} of this earthquake are close to Drini thrust.
- (iii) Lineament D1 of Raiverman et al. (1979) coincides with the Drini thrust of Kumar and Mahajan (1990, 1991) shown in Fig 6.4a.
- (iv) Maximum peak acceleration is at Shahpur station which lies at a perpendicular distance of 6 km from Drini thrust [Composite isoacceleration and tectonic map (Kumar and Mahajan, 1990, 1991)].
- (v) Highest isoacceleration contours from field strong motion data are concentrated along Drini Thrust and follows its strike. The portion of the region close to the maximum isoacceleration contour and meizoseismal area is enlarged and shown in Fig 6.10. From Fig 6.10 a lineament D1 is identified as most probable causative fault.

(vi) Three points along the Drini thrust are marked at which rupture might have occurred. These points are selected so as to cover the length of Drini thrust which follows the elongated axis of isoseismals. The total length of Drini thrust which is calculated from map is 22 km. The considered points named as O_1 , O_2 and O_3 lies within this length and are shown in Fig 6.10. Coordinates of O_1 , O_2 and O_3 and their elevation calculated from the toposheet are :

Name of point on map	Geographical coordinates		Elevation (m)
	Latitude	Longitude	
O_1	32.27° N	76.19°E	750
O_2	32.24°N	76.27°E	1902
O_3	32.18°N	76.31°E	765

The corner of rupture plane which could have generated this earthquake is assumed to lie at points O_1 , O_2 and O_3 and are used for simulating strong ground motion records at observation point.

From the study of different maps following information can be summarised:

- (i) Trend of isoseismal = N30°W (Kumar and Mahajan, 1990,1991)
- (ii) Trend of major axes of
isoacceleration contours = N51°W
- (iii) Strike of lineaments in the region
Drini thrust = N45°W
MBT = N47°W

This information suggests that NW striking fault is the most probable causative fault for the Dharamsala earthquake. Drini thrusts is the tectonic feature in area which follows the strike in NW direction. Moreover epicenter E_{D_4} lies exactly on its western side at a perpendicular distance of 2 km. From field study also this fault has been identified as probable causative fault by Kumar and Mahajan (1991). Rastogi (1992a) has suggested NW trending fault as a causative fault for Dharamsala earthquake on the basis of fault plane solutions for this earthquake. Depth of this fault below epicenter by assuming dip of 69° in SW direction (Kumar and Mahajan, 1991) is estimated as 6 km. The hypocentral depth of this earthquake as calculated by Das and Chandrasekharan (1993) is 7 km. The depth section along the Drini thrust shown in Fig 6.4b also confirm the amount of dip calculated from fault plane solution. On the basis of these results Drini thrust is identified as most probable causative fault for Dharamsala earthquake of 26th April, 1986.

6.5 SELECTION OF OBSERVATION POINTS

Strong motion records are available for the Dharamsala earthquake from nine stations of the strong motion array installed in this region. Maximum horizontal acceleration of 244.8 cm/sec^2 in $N15^\circ W$ was recorded at Shahpur station. Maximum vertical acceleration of 83.3 cm/sec^2 was recorded at Dharamsala station.

Fig 6.11 to 6.19 shows the acceleration record, its autocorrelation function, its power spectrum, its cumulative power spectrum and its frequency weighted power spectrum for all records (i.e. two horizontal and one vertical) at nine stations. Features extracted from these records are given in Table 6.7 to 6.11. Values of these extracted

features are used for comparison with the extracted features of simulated record for the selected model of rupture plane.

From these tables (6.7 to 6.11) the component of acceleration record at a station which gives maximum value of parameter T_{area} has been used for comparison with the simulated record at the same station. Parameter T_{area} gives the total area within the acceleration record and it represent the energy content of the record. The simulated record at any station is representative of the ground motion due to the total release of the energy. For this reason the component of field record which contains maximum energy is selected for comparison with the simulated record. On this basis following table is prepared which gives the component of acceleration record selected for the comparison with the simulated record at the same station for all subsequent comparisons.

Station	Component of acceleration record selected for comparison
Dharamsala	Transverse
Shahpur	Transverse
Kangra	Transverse
Nagrota Bagwan	Longitudinal
Baroh	Longitudinal
Sihunta	Longitudinal
Jawali	Longitudinal
Bandlakhas	Longitudinal
Bhawarana	Transverse

6.6 MODELLING PARAMETERS OF RUPTURE PLANE

Rupture along the identified most probable causative fault is modelled by specifying parameters like rupture length (L), downward extension of rupture plane (D), rupture geometry, rupture velocity (V_r), velocity of the medium (V), length of square element (L_s), starting point of rupture, dip of rupture plane (δ), strike of rupture plane (ϕ) and location of rupture plane on the map.

6.6.1 LENGTH OF RUPTURE PLANE (L)

Various empirical relations which give rupture length are explained in detail in Section 2.2.1. For calculating rupture length for the Dharamsala earthquake, relations by Otsuka (1965), Araya and Kiureghian (1988) and Naeim (1989) have been used. For this earthquake the rupture length by these relations have been calculated as :

S.No.	Rupture Length (L)	Rupture length calculated using empirical relations given by
1.	3 km	Otsuka (1965)
2.	9 km	Araya and Kiureghian (1988)
3.	Lower limit = 5 km Upper limit = 10 km	Naeim (1989)

It is seen that the rupture length calculated by relation provided by Araya and Kiureghian (1988) gives value which lies within the lower and upper limit of rupture

length provided by Naiem (1989). For this reason rupture length of 9 km is assumed for the Dharamsala earthquake.

6.6.2 DOWNWARD EXTENSION OF RUPTURE PLANE (D)

Downward extension of rupture plane can be assumed to be equal to the length of rupture plane for magnitude 5.5 earthquake and hence for rupture length of 9 km, downward extension of rupture plane is assumed as 9 km.

6.6.3 LENGTH OF ELEMENT (L_e)

Length (L_e) of the element is assumed as 1 km, and remains constant for entire simulation scheme. Number of elements along length and downward extension of rupture plane form a 9 x 9 square. Total number of elements within the rupture plane are hence 81.

6.6.4 THREE DIMENSIONAL COORDINATE SYSTEM

For modelling the rupture plane, it is necessary that the rupture along the identified most probable causative fault located in the geographical coordinate system must be transferred into rectangular coordinate system suitable for the simulation purpose. The origin of this system lies at the center of the element on extreme corner of the rupture plane.

Three dimensional rectangular coordinate system has been defined in detail in Chapter 2. The X axis of this coordinate system follows the strike of rupture plane and

the Y axis is positive in the direction of dip of the rupture plane while the Z axis is positive vertically downward.

For calculating the three dimensional coordinates of stations, information regarding the elevation of each stations with respect to mean sea level has been taken from Chandrasekaran (1988a and 1988b). Elevation of each recording stations is given in Table 6.3 and this data has been used for computing coordinates of the recording stations in three dimensional coordinate system.

6.6.5 SOURCE WAVELET

Energy is released from the element in the form of assumed source wavelet which is explained in detail in Chapter 2 and shown in Fig 2.4. For modelling of the rupture plane along the identified causative fault for the Dharamsala earthquake, source wavelet of 5 Hz frequency is used. Digitised value of source wavelet is given in Table 2.3. Normalised value of this wavelet is scaled by a factor of .98 cm/sec which is already explained in detail in Section 3.1.

6.6.6 VELOCITY OF THE MEDIUM (V)

Velocity of medium plays an important role in simulation scheme. This is the velocity by which source wavelet released by an element reaches the observation point.

In order to study the seismicity close to and around Thein Dam, microearthquake survey was conducted around area by opening seven temporary stations initially and then six stations during March-April 1983 (Srivastava and Chatterjee, 1986).

Observations at the above stations were supplemented by data from two stations at Udhampur(UDP) and Jyotipurum (JTP) under Salal project and three at Nurpur (NUR), Dalhousie (DAL) and Dharamsala (DHM) (Fig 6.20). The crustal structure was based on minimisation of error of root mean squares, epicentral location and depth of focus. The model adopted with $V_p/V_s = 1.70$ was as follows :

Layer Number	Depth from the surface of exrth (km)	P wave Velocity (km)/sec
1	0.0	3.46
2	2.8	5.59
3	24.0	6.61
4	45.0	8.22

Proposed velocity structure shows that the velocity in the second layer is equal to 5.59 km/sec and the modelled rupture plane lies in this layer. The velocity of the medium is assumed as 5.6 km/sec for the simulation of records. Chaudhury and Srivastava (1977) also have given the velocity of first layer as 5.6 km/sec for this region.

6.6.7 RUPTURE GEOMETRY

Geometry of rupture propagation inside rupture plane is assumed as radial type as explained in detail in Section 2.2.9. Records at selected observation points were simulated using this geometry of the rupture propagation within the rupture plane.

6.6.8 RUPTURE VELOCITY (V_r)

Rupture velocity is assumed as 80 % of shear wave velocity. Taking S wave velocity as 3.23 km/sec, rupture velocity is computed as 2.6 km/sec.

The rupture model prepared for Dharamsala earthquake is shown in Fig 6.21 and the various modelling parameters of rupture plane which are studied in Sections 6.6.1 to 6.6.8 are assumed as the modelling parameters of the rupture plane along the identified most probable causative fault. These modelling parameters of the rupture plane are given in a tabular form which is shown as :

S.N	Parameter	Value	S.N	Parameter	Value
1.	Rupture Length (L)	9 km	4.	Total numbers of elements (N)	81
2.	Downward extension of rupture plane (D)	9 km	5.	Velocity of the medium (V)	5.6 km/s
3.	Length of the element (L_e)	1 km	6.	Rupture velocity (V_r)	2.6 km/s

Dip (δ) of rupture plane, strike of rupture plane (ϕ), location of the rupture plane on map and coordinates of nucleation point are assumed for final model by iteratively modelling different possibilities of these parameters. The final values of modelling parameters are selected on the basis of comparison of features extracted from simulated records with that of the field records by modelling the rupture plane after changing one parameter at a time.

6.6.9 SELECTION OF DIP (δ) AND STRIKE (ϕ) OF RUPTURE PLANE

Dip and strike of rupture plane are taken from two existing fault plane solutions for the Dharamsala earthquake. These nodal planes are given as :

S.No.	Strike (ϕ)	Dip (δ)	Reference
1.	153°	74°	U.S.G.S. (EDR)
2.	131°	69°	Kumar and Mahajan (1991)

On the basis of these two fault plane solutions, two different models of rupture plane named as MD_U and MD_K are prepared. Starting point of rupture is assumed as that element which coincides with the hypocenter of the earthquake, which is taken as E_{D3} with hypocentral depth of 7 km (Das and Chandrasekaran, 1993). One end of rupture plane is located at O₃ and it lies at a distance of 4 km from the epicenter E_{D3}. The modelling parameters of these two rupture models are:

PARAMETER	VALUE FOR MODEL MD _U	VALUE FOR MODEL MD _K
Rupture length in km	9	9
Downward extension of rupture plane in km	9	9
Dip of rupture plane	74°	69°
Strike of rupture plane	153°	131°
Length of element in km	1.0	1.0
Nucleation point	(0,1.3,4.8)	(1.0,1.7,4.6)
Velocity of the medium in km/sec	5.6	5.6
Rupture velocity in km/sec	2.6	2.6

Direction of strike and dip is different for these two models, therefore the assumed rectangular coordinate system will be different for these two models. Coordinates of Dharamsala and Shahpur stations as calculated for these two different models of rupture plane are given below :

Station	Model	
	MD _U	MD _K
Dharamsala	(1.9,-2.2,-.7)	(1.5,3.1,-.7)
Shahpur	(7.7,6.7,0.0)	(10,4.6,0.0)

The model of rupture plane and simulated records are shown in Fig 6.22 and 6.23. Table 6.12 shows the features extracted from the simulated strong motion records for these two models. Table 6.13 shows that at both Dharamsala and Shahpur station model MD_K gives least difference between the extracted parameters of field and simulated records. For this reason model MD_K is selected as the final model. The dip and strike of the selected models are 69° and 131°, respectively.

6.6.10 SELECTION OF LOCATION OF RUPTURE PLANE ALONG IDENTIFIED FAULT ON MAP

Three different portions O₁A, O₂B and O₃C along the Drini thrust shown in Fig 6.10 are selected and the model of the rupture plane is placed at these portions. Models of rupture plane at O₁, O₂ and O₃ are called as MD₁, MD₂ and MD₃, respectively. The parameters of model are given as :

PARAMETER	VALUE
Rupture length in km	9
Downward extension of rupture plane in km	9
Dip of rupture plane	69°
Strike of rupture plane	131°
Length of element in km	1.0
Velocity of the medium in km/sec	5.6
Rupture velocity in km/sec	2.6

The starting point within the rupture plane is assumed as that element which coincides with the hypocenter of earthquake. The direction of X and Y axis are 131° and 221°, respectively. Placing this rectangular coordinate system at O₁, O₂ and O₃, the coordinates of Dharamsala and Shahpur were obtained as :

STATION	COORDINATES		
	MD ₁	MD ₂	MD ₃
Dharamsala	(10.9,-3.2,-.7)	(5.2,-1.6,.5)	(1.5, -3.1,-.7)
Shahpur	(4.8,1.9,0.0)	(-3.2,6.4,1.2)	(10.0,4.6,0.0)

Coordinates of the nucleation point within the rupture plane for model MD₁, MD₂ and MD₃ are (8.0,1.7,4.6), (4.0,1.7,4.6) and (1.0,1.7,4.6), respectively. Records are simulated at Dharamsala and Shahpur stations for models MD₁, MD₂ and MD₃. These records are shown in Fig 6.24. Table 6.14 shows feature extracted from the strong motion record simulated from these three models. Table 6.15 shows that at both Dharamsala and Shahpur stations model MD₃ gives least difference between the extracted parameters of field and simulated records. For this reason MD₃ is selected

as the final model and this shows that the rupture plane along the identified causative fault should be placed at O_3 .

6.6.11 SELECTION OF STARTING POINT OF RUPTURE (OR NUCLEATION POINT) WITHIN THE RUPTURE PLANE

For models MD_K and MD_3 , starting point of rupture within rupture plane is assumed as that element which coincides with the hypocenter of the earthquake. However there is possibility that starting point of rupture can be any other elements within rupture plane. This possibility is checked by modelling different elements within rupture plane as starting point of rupture. Modelling parameters of rupture plane are :

PARAMETER	VALUE
Rupture length in km	9
Downward extension of rupture plane in km	9
Dip of rupture plane	69°
Strike of rupture plane	131°
Length of element in km	1.0
Velocity of the medium in km/sec	5.6
Rupture velocity in km/sec	2.6
Position of rupture plane on map	O_3

Six different elements within rupture plane are assumed as the nucleation point giving rise to six different models identified as MD_{n1} to MD_{n6} . X, Y and Z coordinates of nucleation point in rectangular coordinate system and the model name is given in the following table :

Coordinates of nucleation point and number given to the element (Fig 6.25)	Model Name
(1.0,1.7,4.6) 15	MD _{n1}
(0.0,0.0,0.0) 1	MD _{n2}
(0.0,2.8,7.4) 9	MD _{n3}
(8.0,0.0,0.0) 73	MD _{n4}
(8.0,2.8,7.4) 81	MD _{n5}
(4.0,1.4,3.7) 41	MD _{n6}

In the model MD_{n1} the starting point of rupture coincides with the hypocenter of earthquake. Coordinate of Dharamsala and Shahpur obtained by placing rectangular coordinate system at O₃ are given as:

STATION	(X,Y,Z) COORDINATES
Dharamsala	(1.5, -3.1, -.7)
Shahpur	(10.0,4.6,0.0)

Records are simulated at these two stations for models MD_{n1}, MD_{n2}, MD_{n3}, MD_{n4}, MD_{n5} and MD_{n6} and are shown in Fig 6.25. Table 6.16 and 6.17 show feature extracted from the strong motion record simulated at Dharamsala and Shahpur stations for these six models which are compared with the extracted parameters of field records. Table 6.18 shows that for both Dharamsala and Shahpur stations model MD_{n3} gives least difference between the extracted parameters of field and simulated records. For this reason MD_{n3} is selected as the final model. For model MD_{n3} the depth of nucleation point or starting point of rupture is 8 km from surface of the earth. The depth of hypocenter for Dharamsala earthquake as computed by Das and Chandrasekaran (1993) is 7 km.

6.7 SIMULATION OF STRONG MOTION RECORDS AT SELECTED OBSERVATION POINTS

The final modelling parameters of the rupture plane are :

S.N.	Parameter	Value	S.N.	Parameter	Value
1	Rupture Length (L)	9 km	7.	Location of rupture on map	O ₃ (on map)
2	Downward extension of the rupture plane (D)	9 km	8.	Velocity of the medium (V)	5.6 km/s
3	Length of the element (L _e)	1 km	9.	Rupture velocity (V _r)	2.6 km/s
4	Total number of elements (N)	81	10.	Coordinates of the nucleation point	(0,2.8,7.4)
5.	Dip (δ)	69°	11.	Depth of nucleation point	8 km
6.	Strike (ϕ)	131°			

Table 6.19 shows coordinates of selected stations on the assumed rectangular coordinate system. Fig 6.26 shows the location of recording stations with respect to rectangular coordinate system. Table 6.20 and 6.21 shows value of extracted parameters from simulated records at these stations. Plots of simulated acceleration records, their autocorrelation function, its power spectrum, its cumulative power spectrum and its frequency weighted cumulative power spectrum at different stations are shown in Fig 6.27, 6.28 and 6.29, respectively.

6.8 COMPARISON OF FIELD AND SIMULATED RECORDS

Table 6.20 and 6.21 shows that at Dharamsala, Shahpur, Kangra and Nagrota Bagwan stations which lie at a hypocentral distance of 8.5, 10, 10.5 and 15 km respectively, peak acceleration of simulated record matches with the observed peak acceleration in the field records as shown in table below.

Station	Hypocentral Distance	Peak acceleration from simulated record (cm/sec ²)	Peak acceleration from field record (cm/sec ²)
Dharamsala	8.5	166	188
Kangra	10.5	153	148
Shahpur	10.0	202	244

This table shows that the peak acceleration observed in field records is more at Shahpur although it is at a greater distance from nucleation point (hypocenter) as compared to Dharamsala. This trend is also observed in the simulated records. This may be due to the source directivity effect, that is, the acceleration in the direction of rupture propagation is higher than in opposite direction (Midorikawa, 1993). The location of Shahpur station is in the direction of the dip of the rupture plane while Dharamsala lies in a direction just opposite to that of dip of the rupture plane. The direction of rupture within the rupture plane from nucleation point is also towards Shahpur.

The difference in the peak acceleration at Kangra and Shahpur station can also be explained on the basis of this directivity effect. The coordinate of starting point of

rupture is (0,2.8,7.4) and stations at Shahpur and Kangra lie at a distance of 10 and 10.5 km, respectively. The coordinate of Shahpur and Kangra are (10.0,4.6,0.0) and (-3.9,9.6,-.2), respectively. This shows that the direction of rupture propagation within rupture plane from starting point of rupture having coordinate (0,2.8,7.4) is towards the Shahpur station, and at Kangra station it is just opposite. Thus directivity effects which is observed in the field records can be explained by this model.

In the field records at stations Baroh, Jawali and Bhawarana which lie at hypocentral distances greater than 20 km, peak acceleration starts decreasing considerably. At Bandlakhas station which lies at a hypocentral distance of 26 km peak acceleration from field records is 141 cm/sec². This value is quite high for a station at this hypocentral distance. The station is located at the foothill of a hill stream. Thus rise in peak acceleration can be due to local geological conditions (Chandrasekaran, 1988b) which has not been included in the modelling procedure.

From Table 6.7 to 6.11 and 6.20 and 6.21 following table is prepared which gives the maximum and minimum values of parameters extracted from simulated and field strong motion records.

PARAMETER	FIELD RECORD		SIMULATED RECORD	
	MAXIMUM VALUE AND STATION	MINIMUM VALUE AND STATION	MAXIMUM VALUE AND STATION	MINIMUM VALUE AND STATION
P_a (cm/sec ²)	244 Shahpur	15 Jawali	202 Shahpur	100 Baroh
T_{at} (sec)	1.6 Kangra	.2 Nagrota Bagwan, Bhawarana	3.4 Kangra	1.00 Dharamsala

PARAMETERS	FIELD	RECORD	SIMULATED	RECORDS
	MAXIMUM VALUE AND STATION	MINIMUM VALUE AND STATION	MAXIMUM VALUE AND STATION	MINIMUM VALUE AND STATION
T_D (sec)	8.0 Bhawarana	2.0 Shahpur	4.51 Baroh	2.2 Shahpur
P_v (cm/sec)	15.8 Shahpur	3.2 Bhawarana	3.76 Shahpur	2.12 Bhawarana
P_d cm	4.0 Dharamsala	1.1 Baroh	.144 Jawali	.053 Bhawarana
R_{at}	1.118 Jawali	.949 Bandlakhas	.999 Shahpur, Baroh	.990 Bhawarana, Bandlakhas
T_{area}	10158 Shahpur	1306 Jawali	9293 Kangra	6462 Shahpur

This table shows that both the maximum and minimum value of the parameter P_v extracted from field and simulated records occur at the same station. Maximum value of parameters P_a and T_{at} and minimum value of parameters T_D and R_{at} from simulated as well as field records occur at same stations.

From Table 6.7 to 6.11 and 6.20 and 6.21 following table is prepared which gives the maximum and minimum values of the parameters extracted from the autocorrelation function of field acceleration records.

PARAMETER	FIELD RECORD		SIMULATED RECORD	
	MAXIMUM VALUE AND STATION	MINIMUM VALUE AND STATION	MAXIMUM VALUE AND STATION	MINIMUM VALUE AND STATION
ACF ₁	.103 Sihunta	.051 Baroh	.03 Baroh, Sihunta , Dharamsala	.028 Bhawarana
ACF ₂	.414 Nagrota Bagwan	.131 Baroh	.093 Baroh	.08 Bhawarana
ACF ₃	.511 Sihunta	.218 Bhawarana	.203 Baroh	.132 Bhawarana and Sihunta
ACF ₄	.200 Sihunta	.108 Baroh	.08 Same at all stations	.08 Same at all stations
ACF ₅	.890 Sihunta	.775 Baroh	.456 Dharamsala	.375 Bhawarana
ACF ₆	.670 Sihunta	.265 Baroh	-.455 Baroh	-.623 Bhawarana
ACF ₇	.430 Sihunta	-.234 Baroh	-.660 Sihunta	-.729 Bhawarana
ACF ₈	-.105 Shahpur	-.664 Bandlakhas	-.660 Sihunta	-.776 Kangra
ACF ₉	3.58 Bhawarana	.88 Shahpur	1.088 Nagrota Bagwan	.963 Kangra
ACF ₁₀	1.15 Jawali	1.01 Dharamsala	1.09 Shahpur	1.056 Bandlakhas

It is seen from this table that maximum value of parameters ACF₁, ACF₇, and minimum value of the parameter ACF₃ occur at the same station for both simulated and field records.

Following table presents the maximum and minimum values of the extracted parameters of power spectrum of field acceleration records and the stations at which it occurs.

PARAMETERS	FIELD RECORDS		SIMULATED RECORDS	
	MAXIMUM VALUE AND STATION	MINIMUM VALUE AND STATION	MAXIMUM VALUE AND STATION	MINIMUM VALUE AND STATION
F_p Station	5.2 Bandlakhass	2.1 Sihunta	11.0 Nagrota Bagwan	6.1 Sihunta
F_1 Station	11.2 Sihunta	2.8 Shahpur	8.5 Bhawarana	7.3 Baroh
F_2 Station	7.1 Sihunta	4.9 Shahpur	10.0 Bhawarana	8.9 Kangra
F_3 Station	21.4 Sihunta	6.2 Bandlakhass	11.1 Nagrota Bagwan	10.3 Dharamsala
F_4 Station	4.0 Bandlakhass	2.1 Kangra	9.7 Jawali	6.3 Sihunta
F_5 Station	9.0 Sihunta	2.9 Shahpur, Kangra	9.4 Bhawarana	8.4 Baroh
F_6 Station	16.9 Sihunta	3.9 Kangra	10.9 Nagrota Bagwan	9.7 Bandlakhass, B aroh and Bhawarana

The comparison shows that minimum value of the parameter F_p extracted from simulated and field records occur at the same station.

Comparison of extracted features from simulated and field records is given in the following table for those parameters which show a difference of less than 20% in its value extracted from field and simulated records.

PARAMETER	NUMBER OF STATIONS HAVING A DIFFERENCE OF LESS THAN 20 IN ITS EXTRACTED PARAMETER FROM SIMULATED AND FIELD RECORD
P_a	4
T_{at}	1
T_D	4
R_{at}	9
ACF_3	1
ACF_8	1
ACF_9	5
ACF_{10}	9
F_3	2

The difference in the value of extracted parameters between simulated and field records can be due to factors which are not taken into account in the simulation scheme. These factors are discussed in detail in Chapter 10. Some of these factors are:

(i) Topographic effect : Stations Jawali, Shahpur, Kangra, Nagrota Bagwan and Baroh lie in valley while stations Dharamsala and Bandlakhass are on hills. The location of stations and surrounding topography of the region is shown in Fig 6.30. In the simulation scheme elevation has been is considered in calculating the arrival time of

energy at a station while the effect of topography on the amount of energy has not been considered. This consideration may play an important role in the simulated strong motion records at these stations.

(ii) Transmission path : The travel path of energy in the medium may not be simple and would be effected by various geological features which are encountered in the path. In the simulation scheme the transmission path is assumed as a straight line.

(iii) Geology of the region : The geology of region can also play an important role in the modelling of earthquake source which is not taken into account in present scheme.

(iv) The location of the hypocenter of the earthquake is important for modelling of the rupture plane. The hypocenter computed by different agencies/authors differ considerably. A minor differences in the location of hypocenters may result in significant difference in the simulated strong motion records.

(v) Attenuation effects : Simulated records at Baroh, Jawali, Bhawarana and Bandlakhas do not decrease in peak acceleration. This is because attenuation effects have not been taken into consideration in the simulation scheme. Attenuation effects play an important role in decreasing peak acceleration of strong ground motion at any point of observation with respect to the distance from the source of the earthquake.

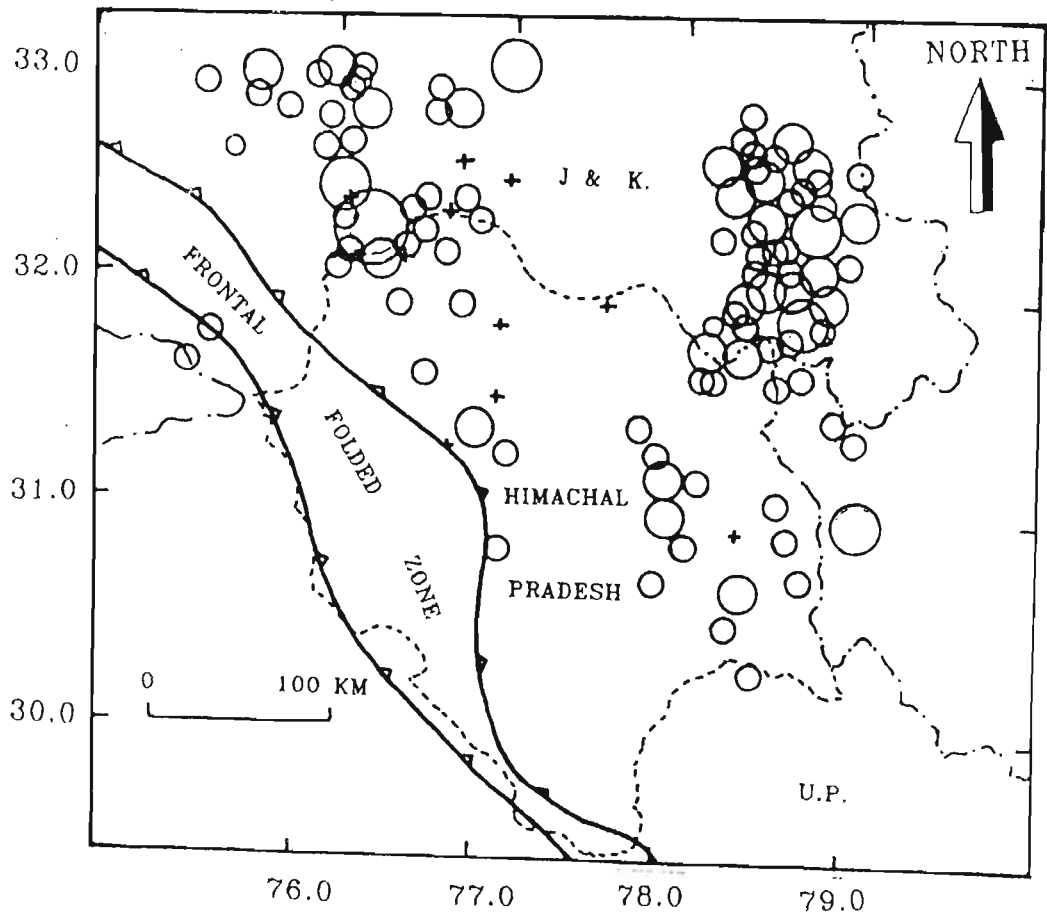
6.9 SUMMARY

In this chapter the scheme of identification of most probable causative fault is applied for the Dharamsala earthquake. On the basis of the available data Drini thrust

is identified as the most probable causative fault for this earthquake. The rupture plane along the identified portion of most probable causative fault is defined by following final modelling parameters :

S.N.	Parameter	Value	S.N.	Parameter	Value
1	Rupture Length (L)	9 km	7.	Location of rupture on map	O ₃ (on map)
2	Downward extension of the rupture plane (D)	9 km	8.	Velocity of the medium (V)	5.6 km/s
3	Length of the element (L _e)	1 km	9.	Rupture velocity (V _r)	2.38 km/s
4	Total number of elements (N)	81	10.	Coordinates of nucleation point	(0.0,2.8,7.4)
5.	Dip (δ)	69°	11.	Depth of nucleation point	8 km
6.	Strike (ϕ)	131°			

Using these parameters the strong motion records are simulated at nine selected observation points and 24 features were extracted from the simulated records at these stations. The comparison of extracted parameters of field and simulated records shows that parameters P_a , T_{at} , T_D , R_{at} , ACF_3 , ACF_8 , ACF_9 , ACF_{10} and F_3 give a difference of less than 20% at various stations establishing that the model selected for the Dharamsala earthquake is acceptable.



LEGEND

- 3 < M < 4
- 4 < M < 5
- 5 < M < 6
- 6 < M < 7
- 8 < M
- + MAGNITUDE NOT KNOWN

Fig 6.1 Location of epicenters in H.P. and surrounding region. Epicentral data is taken from Singh et al. (1975) and USGS - NEIC (1990) and reproduced in Table 6.1. The tectonics of the region is taken from Eremenko and Negi (1968).

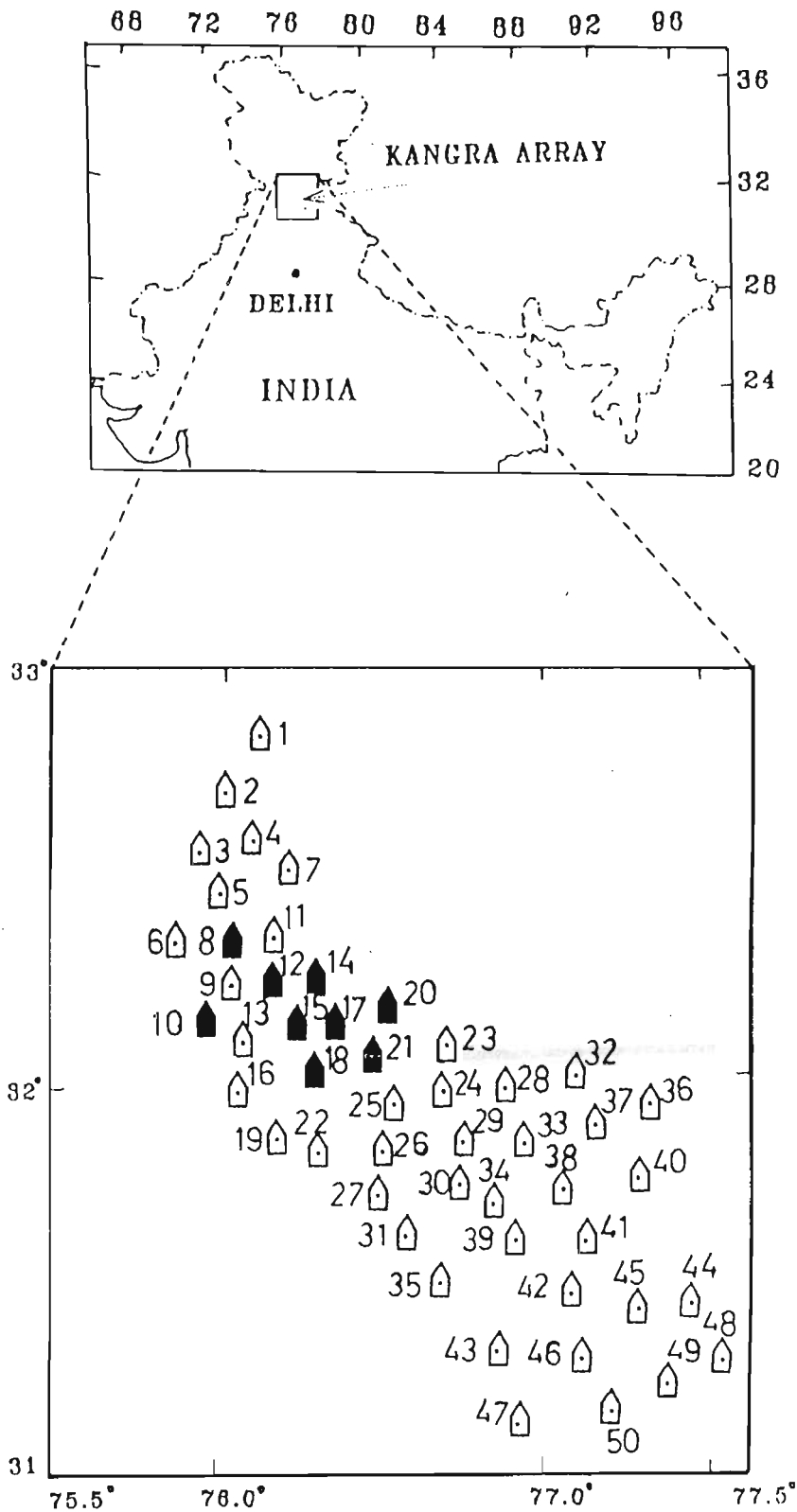


Fig 6.2 Location of elements of strong motion Kangra array. Geographical coordinates of recording stations is taken from Chandrasekaran and Das (1992b) and reproduced in Table 6.3. Station is represented by a number given in Table 6.3. The station marked by black colour represent those which had recorded the Dharamsala earthquake of 26th April, 1986.

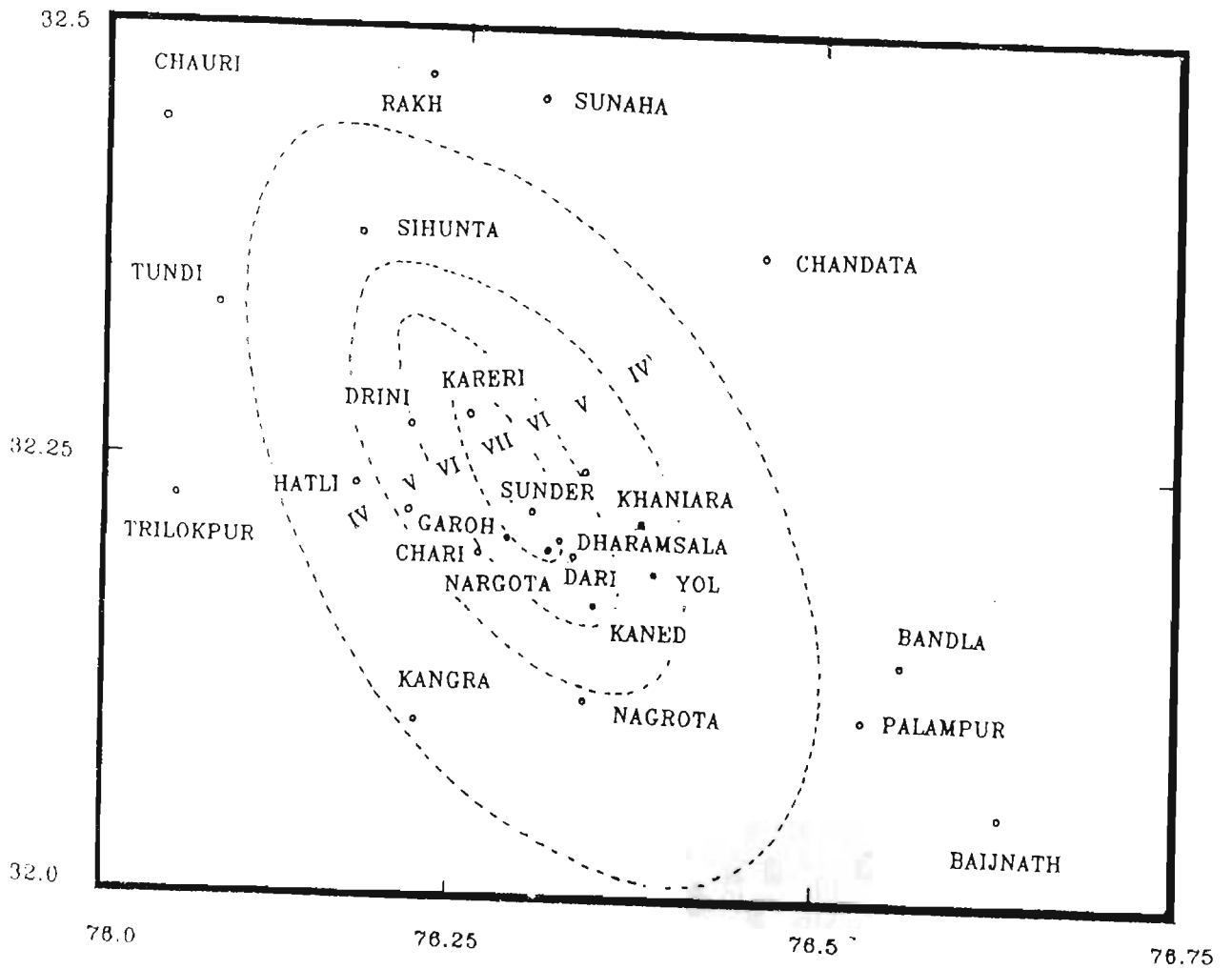


Fig 6.3 Isoseismal map of Dharamsala earthquake of 26th April, 1986 (After Kumar and Mahajan, 1990, 1991).

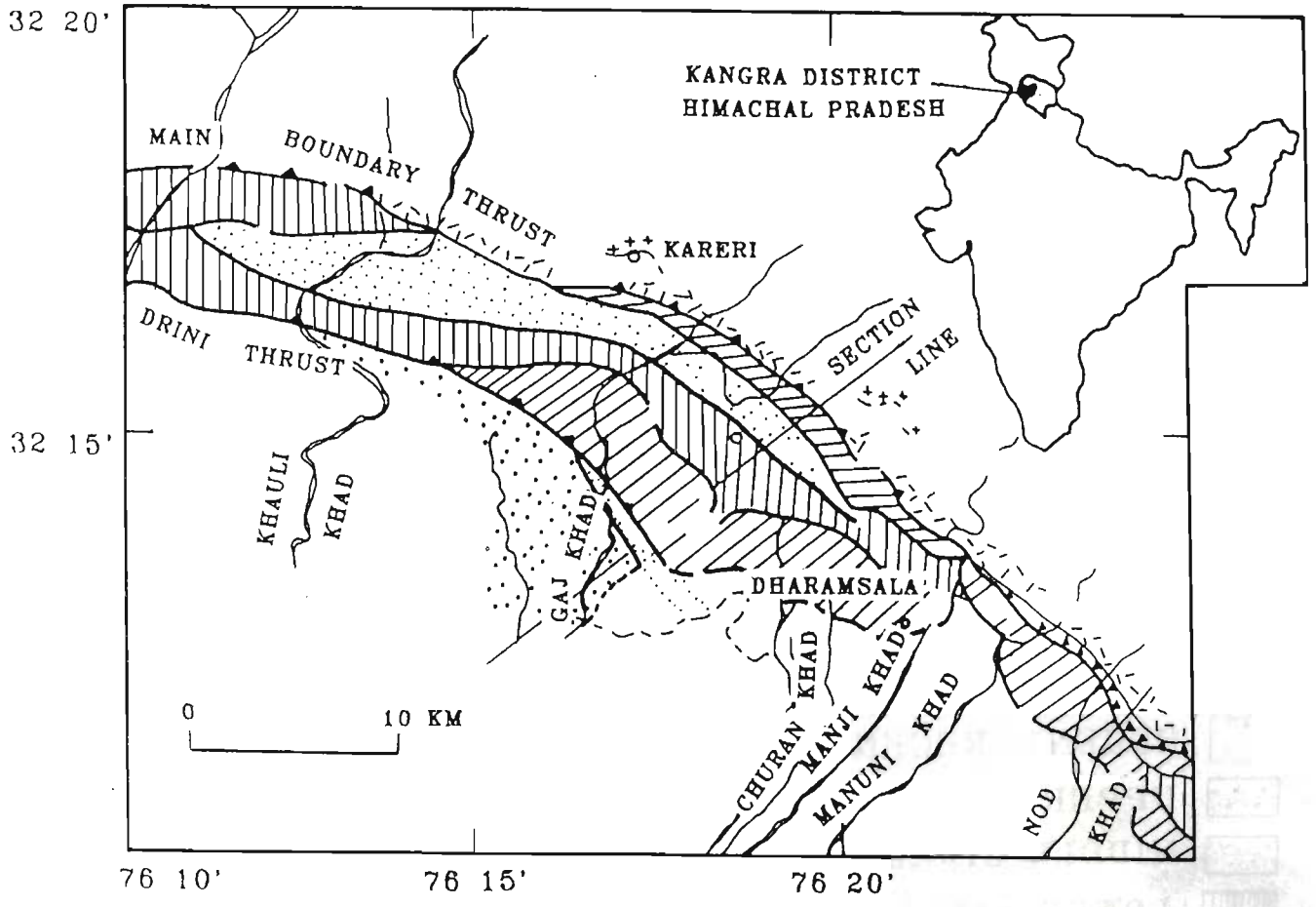


Fig 6.4a Tectonic map of region around Dharamsala (After Kumar and Mahajan, 1991) showing location of Drini thrust. Legend given in Fig 6.4b.

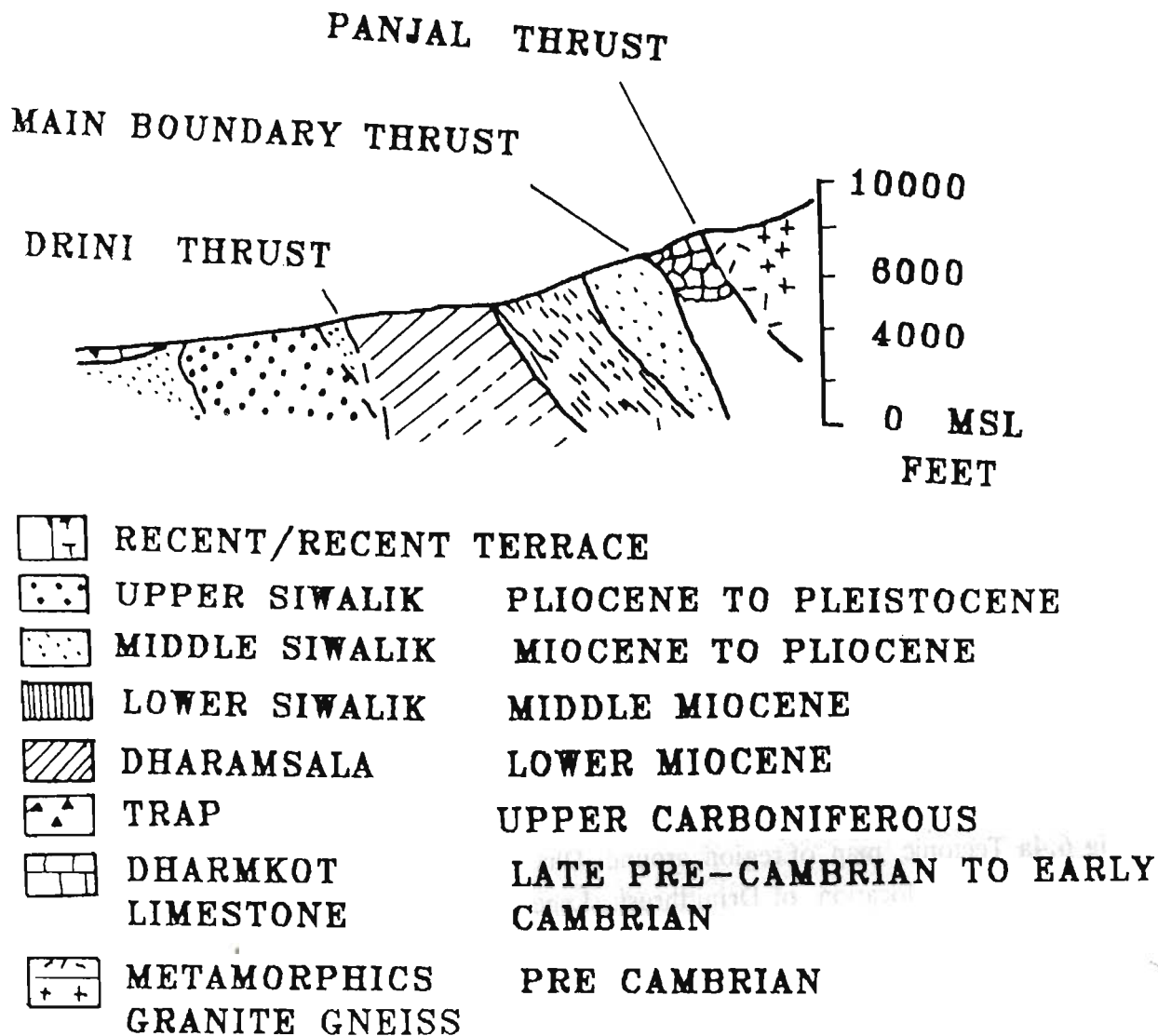


Fig 6.4b Geological section showing Drini thrust. (After Kumar and Mahajan, 1990, 1991) along the section line shown in Fig 6.4a.

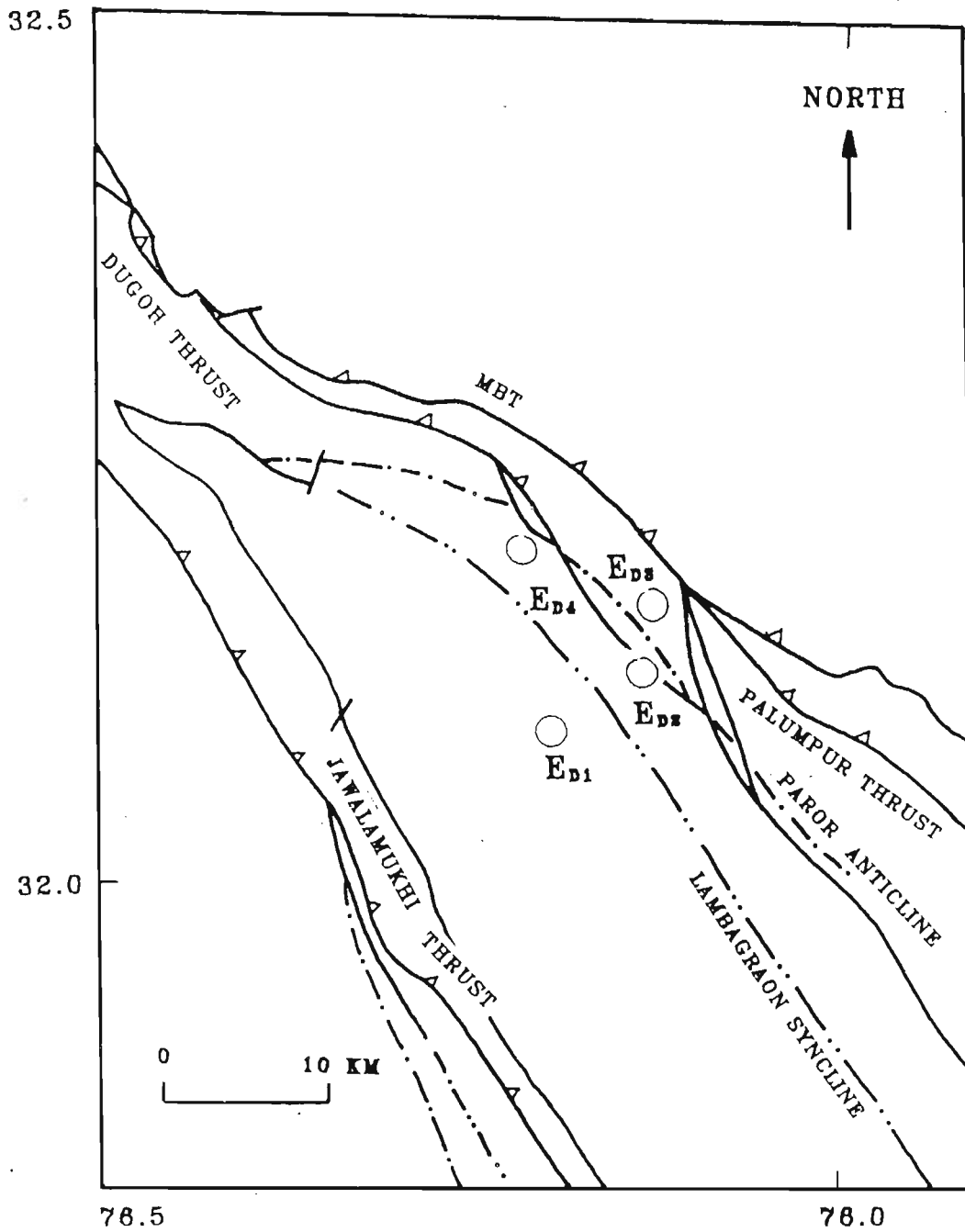


Fig 6.5 Tectonic map of region around Dharamsala (Raiverman et al. 1979). Epicentral coordinates for the epicenter E_{D1} , E_{D2} , E_{D3} and E_{D4} are shown in Table 6.4.

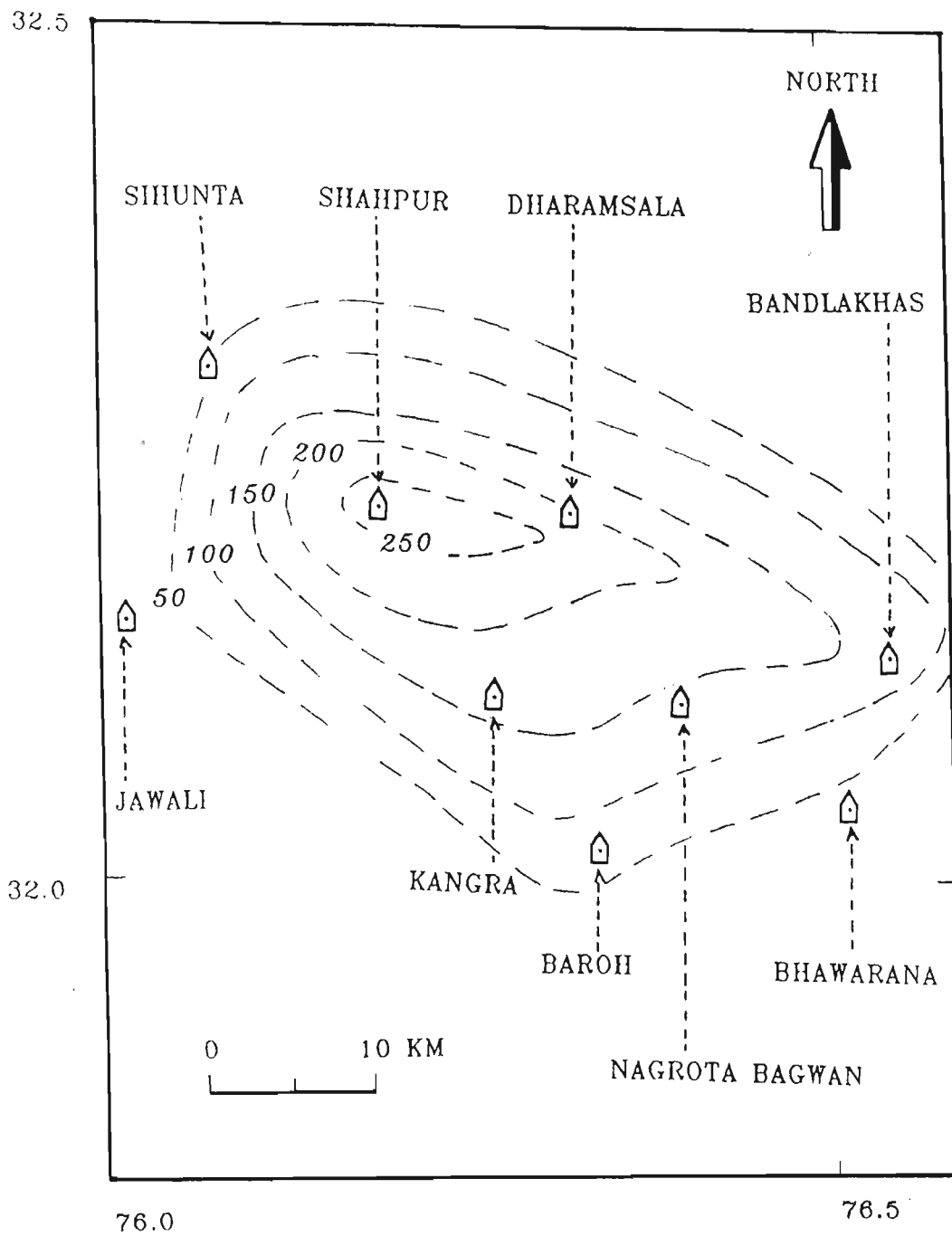


Fig 6.6 Isoacceleration contours of resultant horizontal peak acceleration for the Dharamsala earthquake of 26th April, 1986. Data for resultant peak acceleration is taken from Chandrasekaran (1988b) and reproduced in Table 6.6.

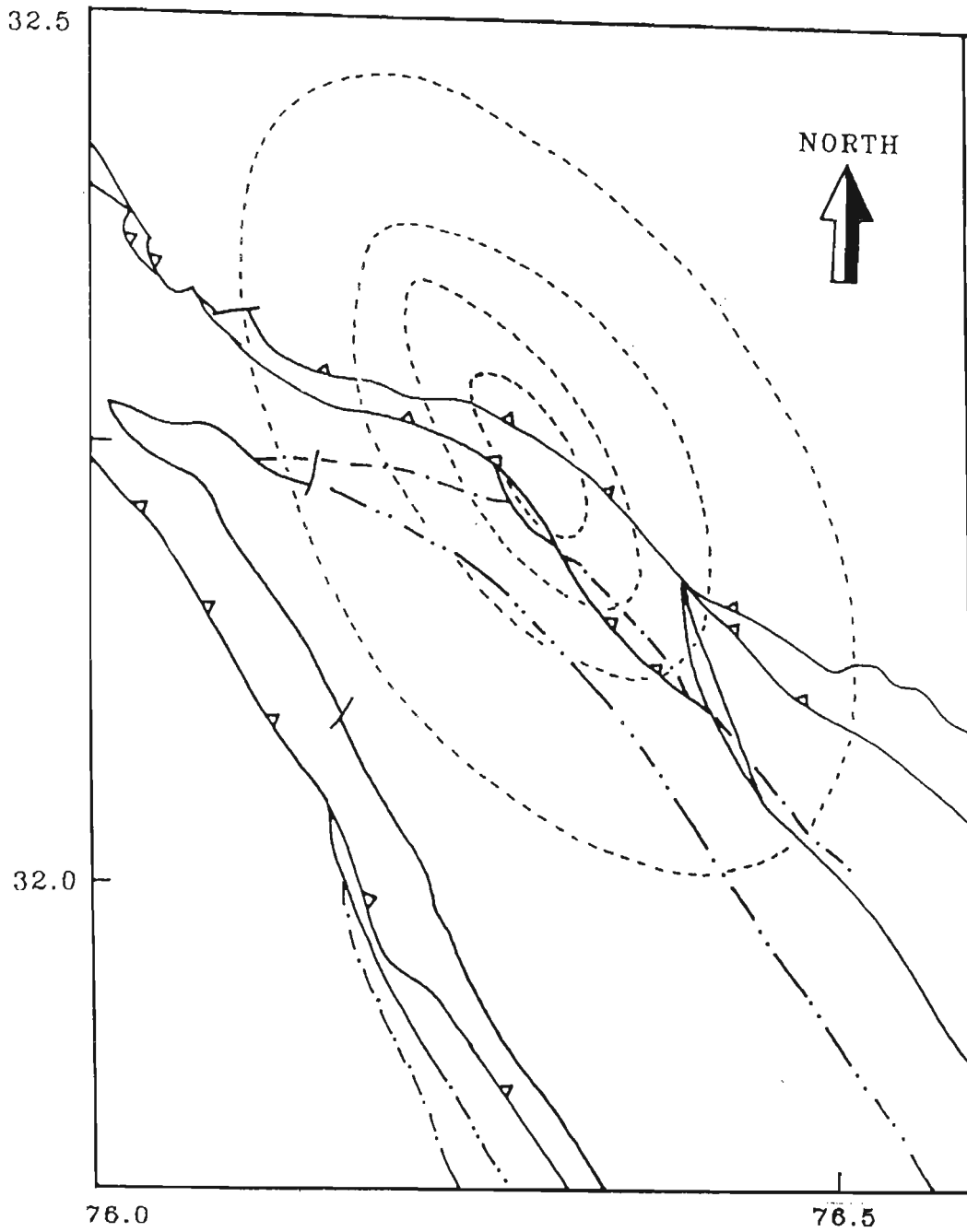


Fig 6.7 Composite tectonic map (Raiverman et al. 1979) and isoseismal map (Kumar and Mahajan, 1990, 1991) for the Dharamsala earthquake of 26th April, 1986.

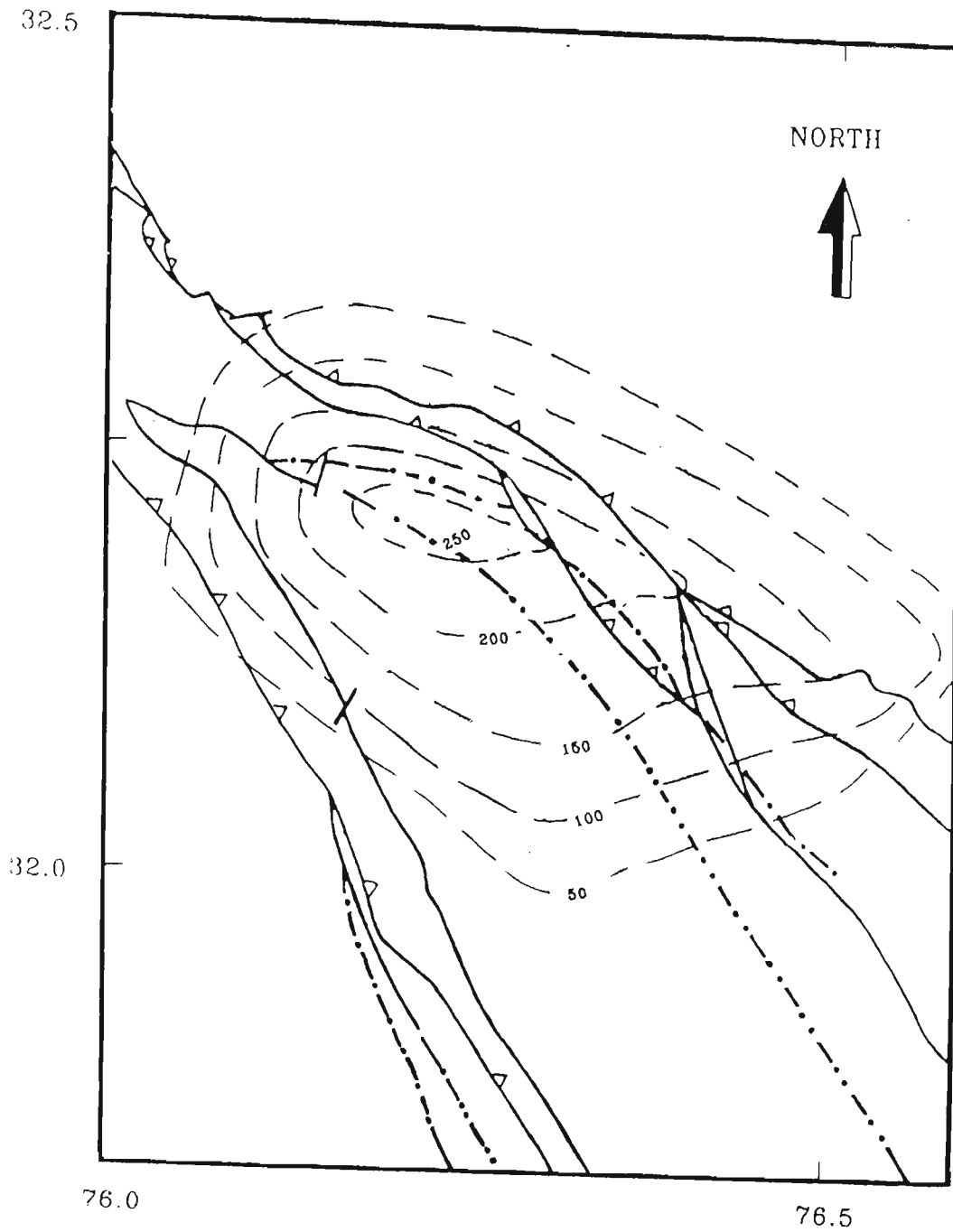


Fig 6.8 Composite Tectonic (Raiverman et al., 1979) and isoacceleration map for Dharamsala earthquake of 26th April, 1986.

32.5

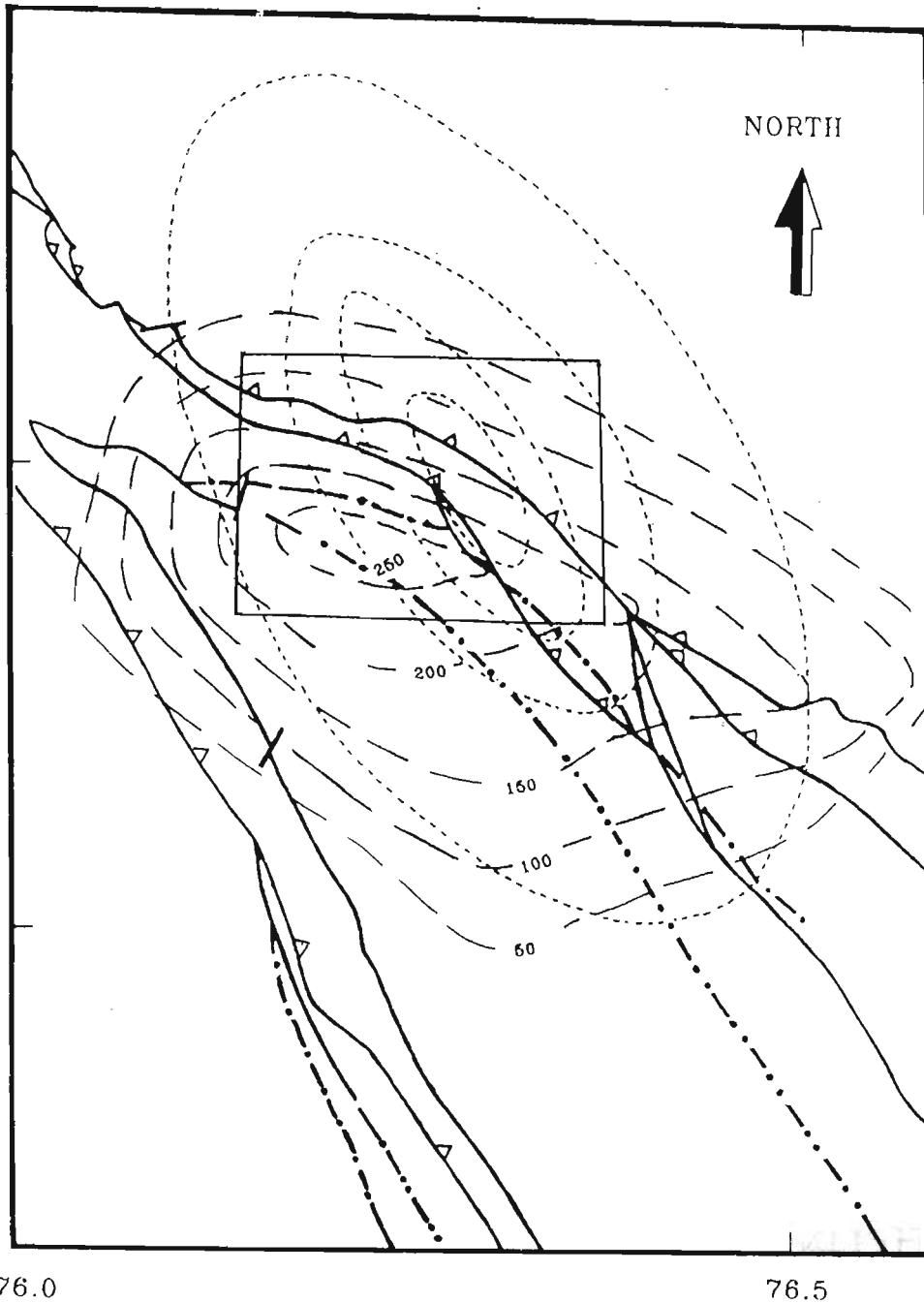
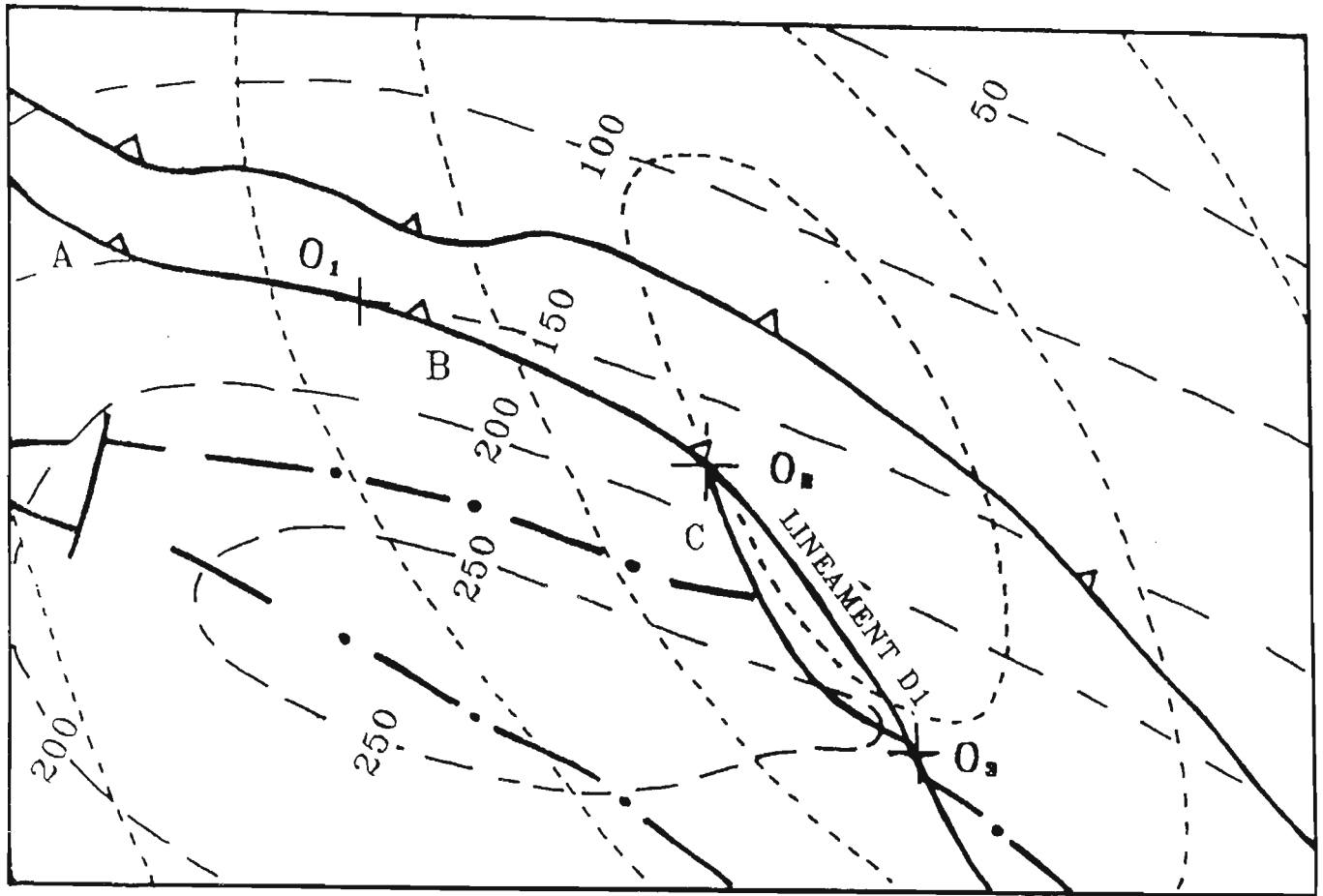


Fig 6.9 Superimposed composite map of tectonics (After Raiverman et al., 1979), isoseismal (After Kumar and Mahajan, 1990, 1991) and isoacceleration contour for Dharamsala earthquake of 26th April, 1986. Details of rectangle is shown in Fig 6.10.



LEGEND

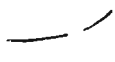


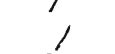

-  ISO ACCELERATION CONTOUR
-  ISOSEISMAL LINES
-  THRUST
-  LINEAMENT
-  ANTICLINE

Fig 6.10 Detailed portion of the rectangular block shown in Fig 6.9 giving the Location of identified causative fault for the Dharamsala earthquake of 26th April, 1986.

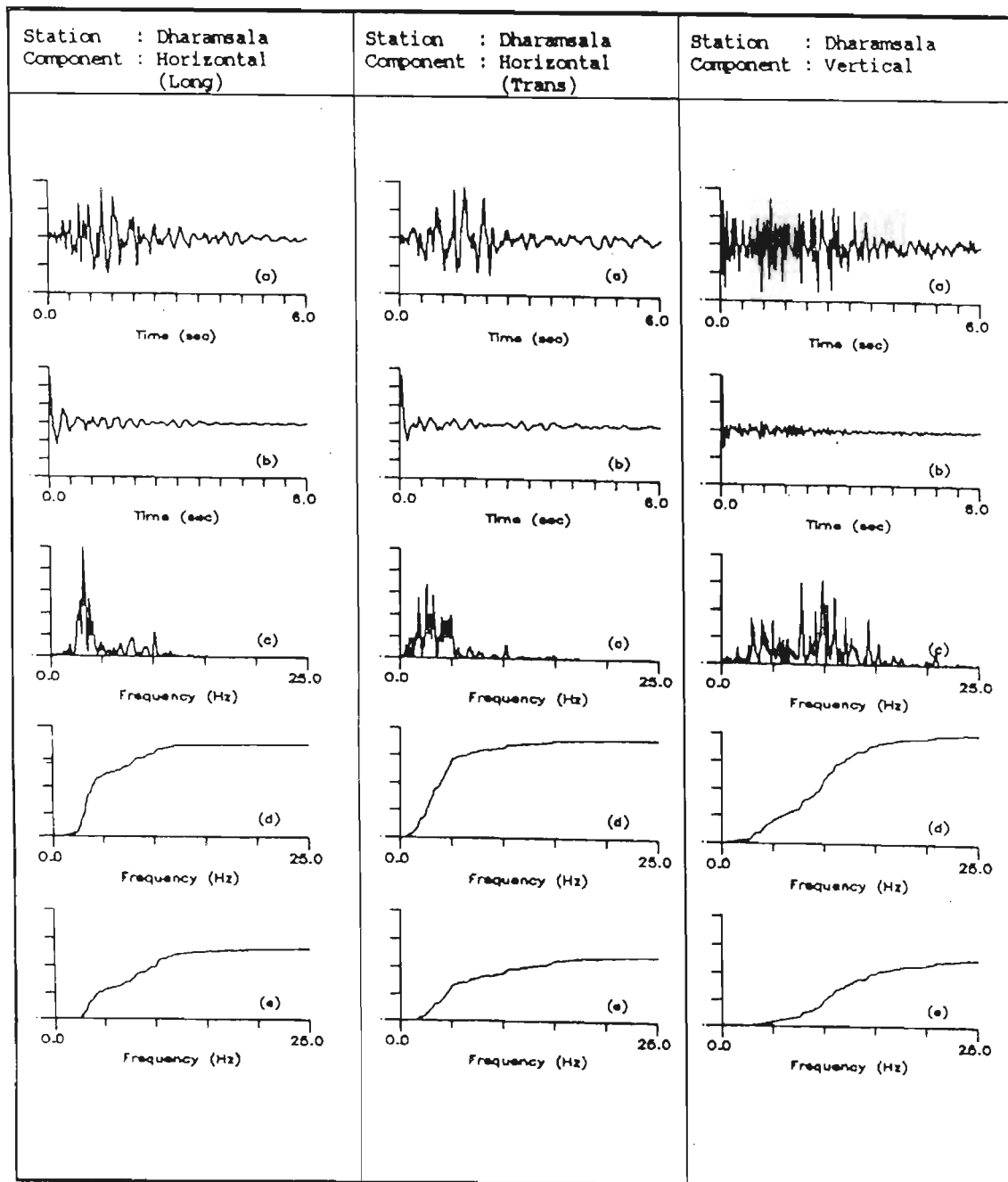


Fig 6.11 Dharamsala earthquake of 26th April, 1986, longitudinal, transverse and vertical components recorded at Dharamsala station. Y axis shows normalised value of (a) acceleration record, (b) its autocorrelation function, (c) its power spectrum, (d) its cumulative power spectrum and (e) its frequency weighted cumulative power spectrum. X axis for (a) and (b) shows time and for (c), (d) and (e) shows frequency. Features extracted from these records are given in Table 6.7.

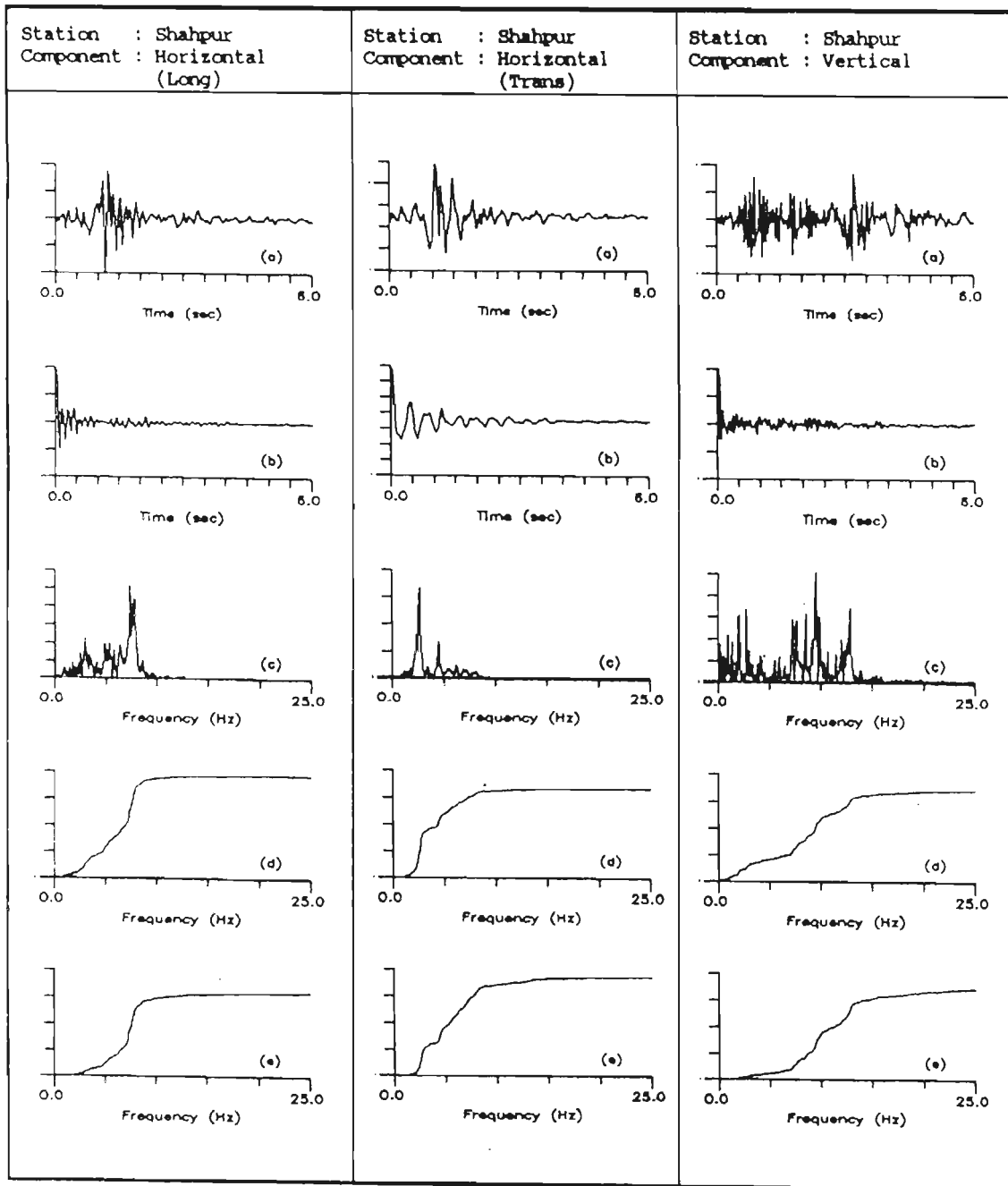


Fig 6.12 Dharamsala earthquake of 26th April, 1986, longitudinal, transverse and vertical components recorded at Shahpur station. Y axis shows normalised value of (a) acceleration record, (b) its autocorrelation function, (c) its power spectrum, (d) its cumulative power spectrum and (e) its frequency weighted cumulative power spectrum. X axis for (a) and (b) shows time and for (c), (d) and (e) shows frequency. Feature extracted from these records are given in Table 6.7.

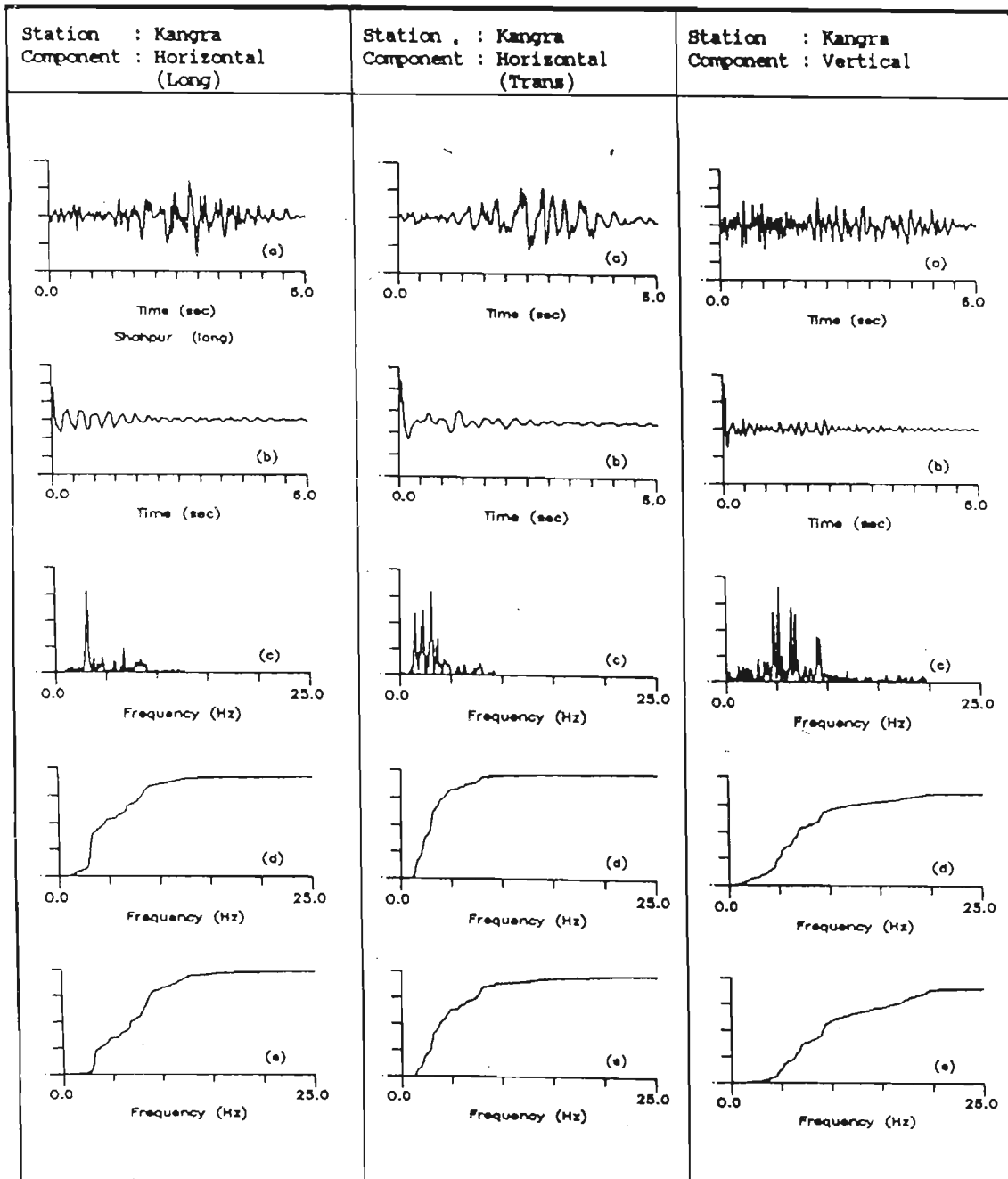


Fig 6.13 Dharamsala earthquake of 26th April, 1986, longitudinal, transverse and vertical components recorded at Kangra station. Y axis shows normalised value of (a) acceleration record, (b) its autocorrelation function, (c) its power spectrum, (d) its cumulative power spectrum and (e) its frequency weighted cumulative power spectrum. X axis for (a) and (b) shows time and for (c), (d) and (e) shows frequency. Feature extracted from these records are given in Table 6.8.

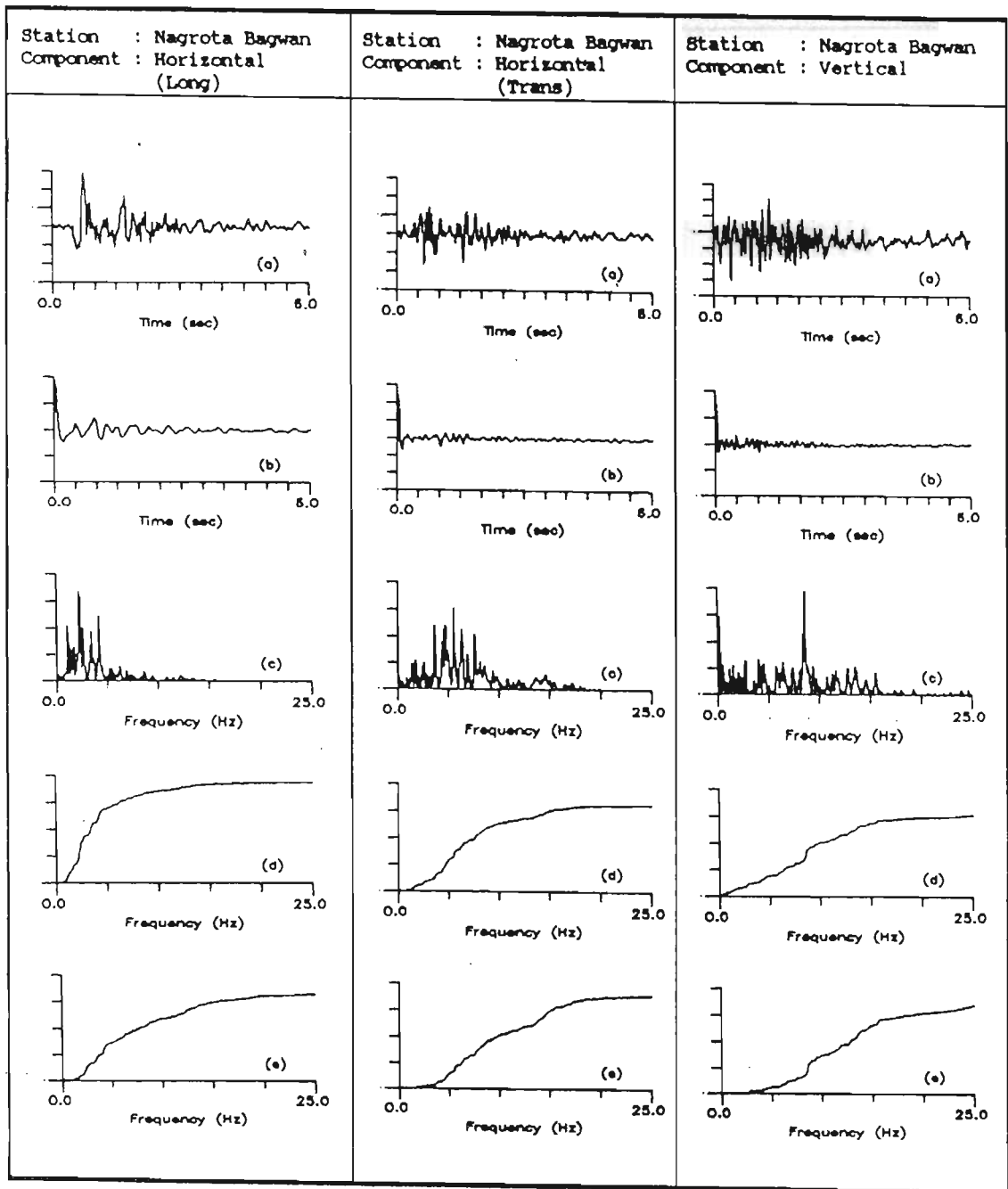


Fig 6.14 Dharamsala earthquake of 26th April, 1986, longitudinal, transverse and vertical components recorded at Nagrota Bagwan station. Y axis shows normalised value of (a) acceleration record, (b) its autocorrelation function, (c) its power spectrum, (d) its cumulative power spectrum and (e) its frequency weighted cumulative power spectrum. X axis for (a) and (b) shows time and for (c), (d) and (e) shows frequency. Feature extracted from these records are given in Table 6.8.

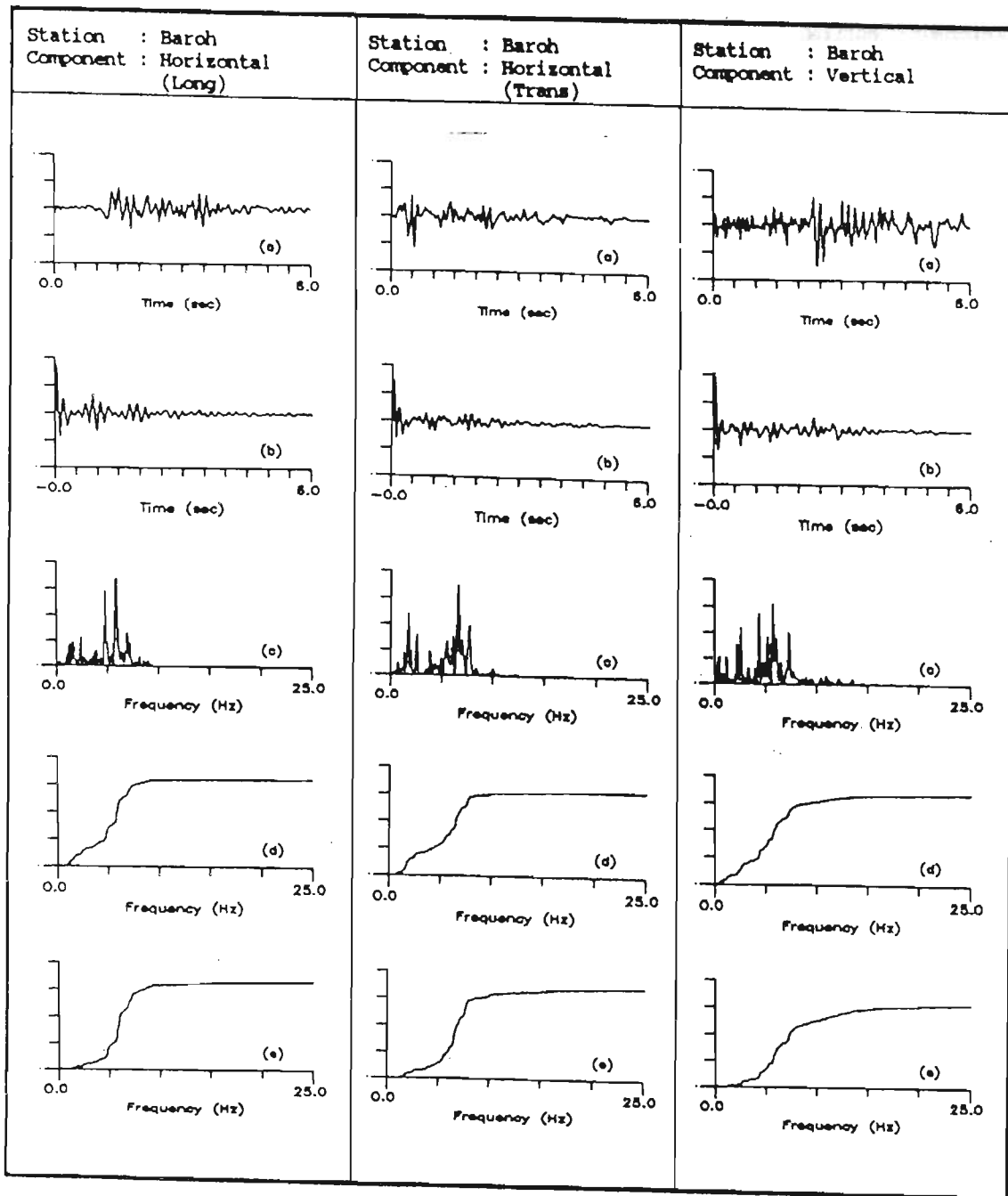


Fig 6.15 Dharamsala earthquake of 26th April, 1986, longitudinal, transverse and vertical components recorded at Baroh station. Y axis shows normalised value of (a) acceleration record, (b) its autocorrelation function, (c) its power spectrum, (d) its cumulative power spectrum and (e) its frequency weighted cumulative power spectrum. X axis for (a) and (b) shows time and for (c), (d) and (e) shows frequency. Feature extracted from these records are given in Table 6.9.

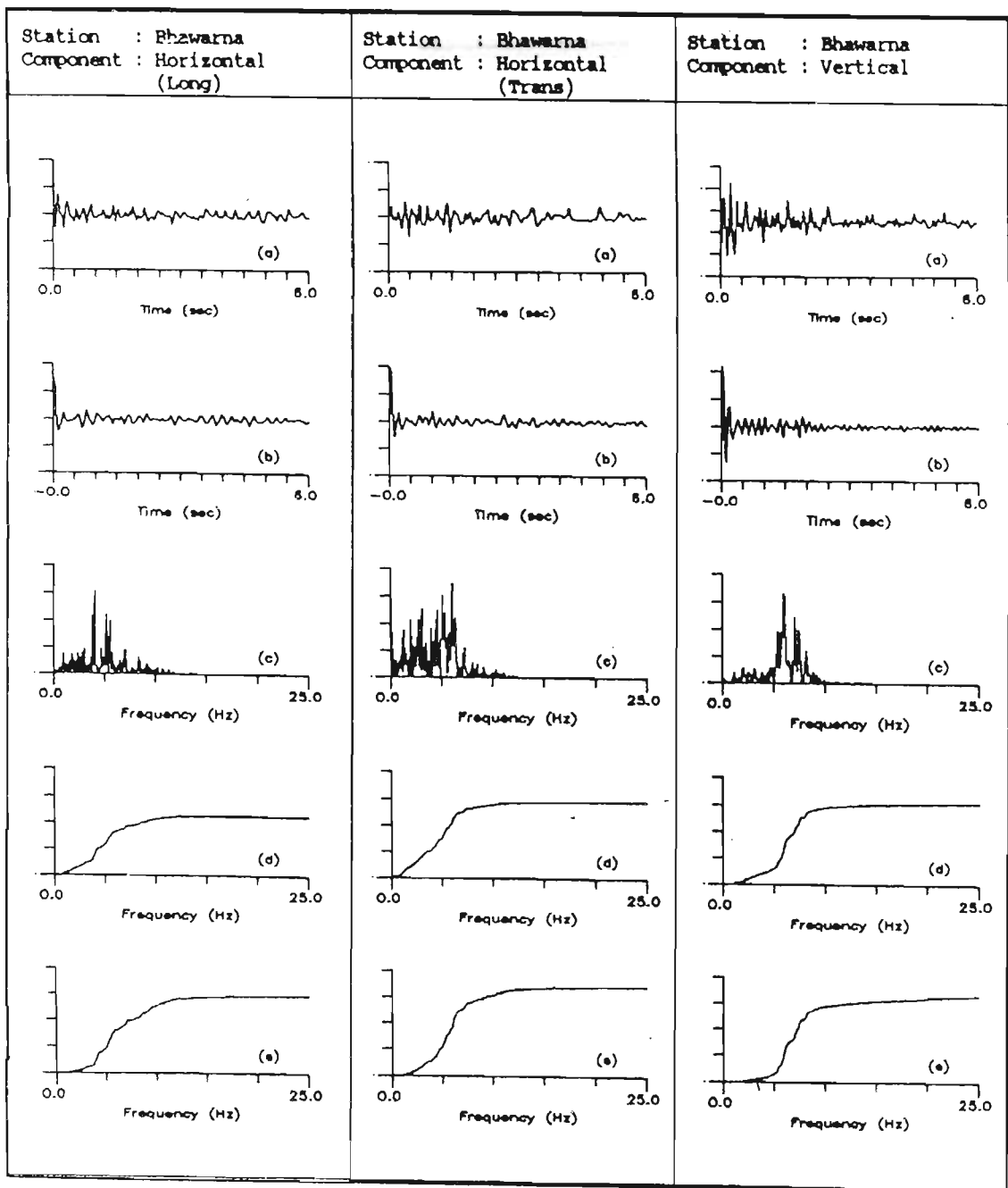


Fig 6.16 Dharamsala earthquake of 26th April, 1986, longitudinal, transverse and vertical components recorded at Bhawarana station. Y axis shows normalised value of (a) acceleration record, (b) its autocorrelation function, (c) its power spectrum, (d) its cumulative power spectrum and (e) its frequency weighted cumulative power spectrum. X axis for (a) and (b) shows time and for (c), (d) and (e) shows frequency. Feature extracted from these records are given in Table 6.9.

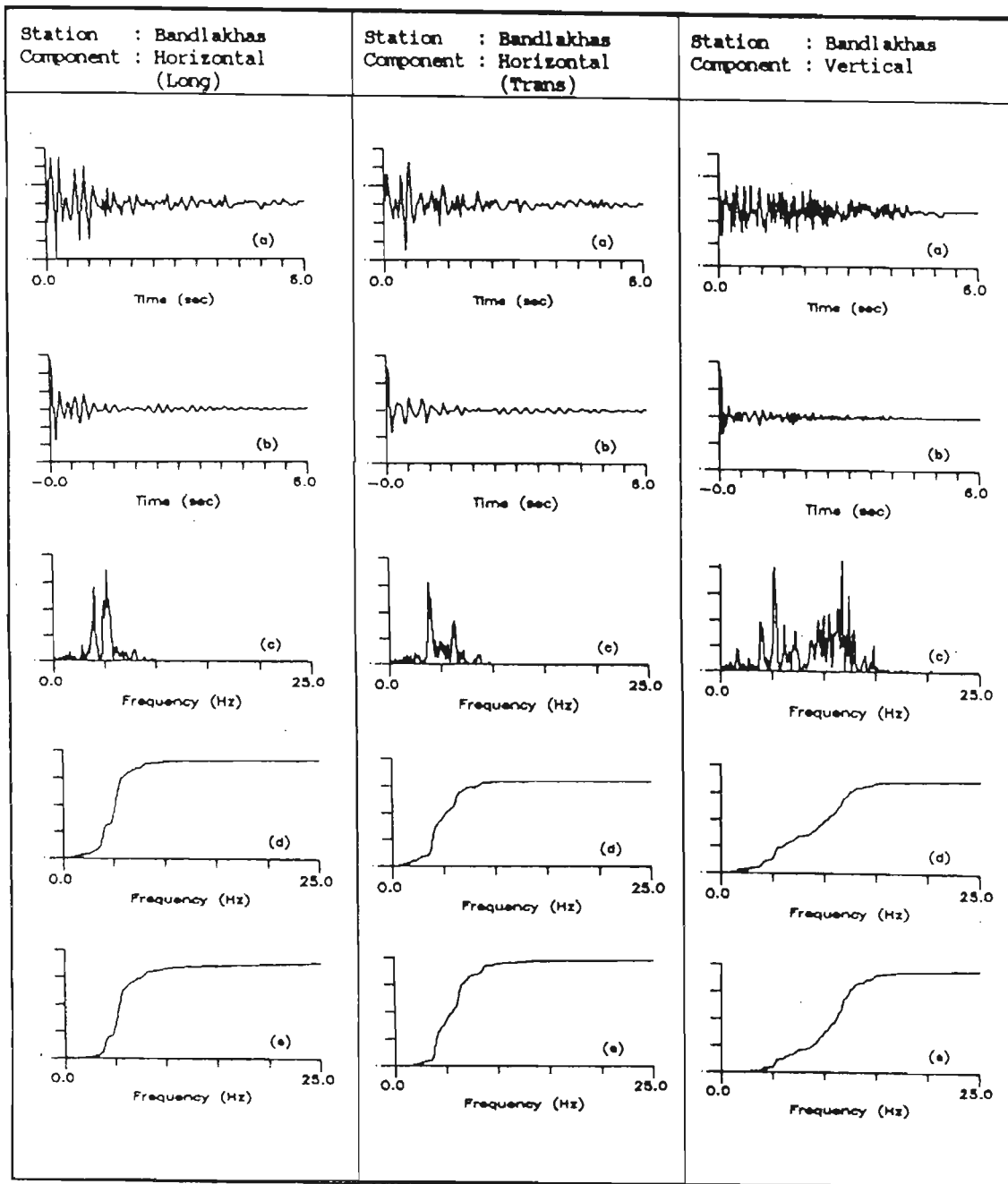


Fig 6.17 Dharamsala earthquake of 26th April, 1986, longitudinal, transverse and vertical components recorded at Bandlakhias station. Y axis shows normalised value of (a) acceleration record, (b) its autocorrelation function, (c) its power spectrum, (d) its cumulative power spectrum and (e) its frequency weighted cumulative power spectrum. X axis for (a) and (b) shows time and for (c), (d) and (e) shows frequency. Feature extracted from these records are given in Table 6.10.

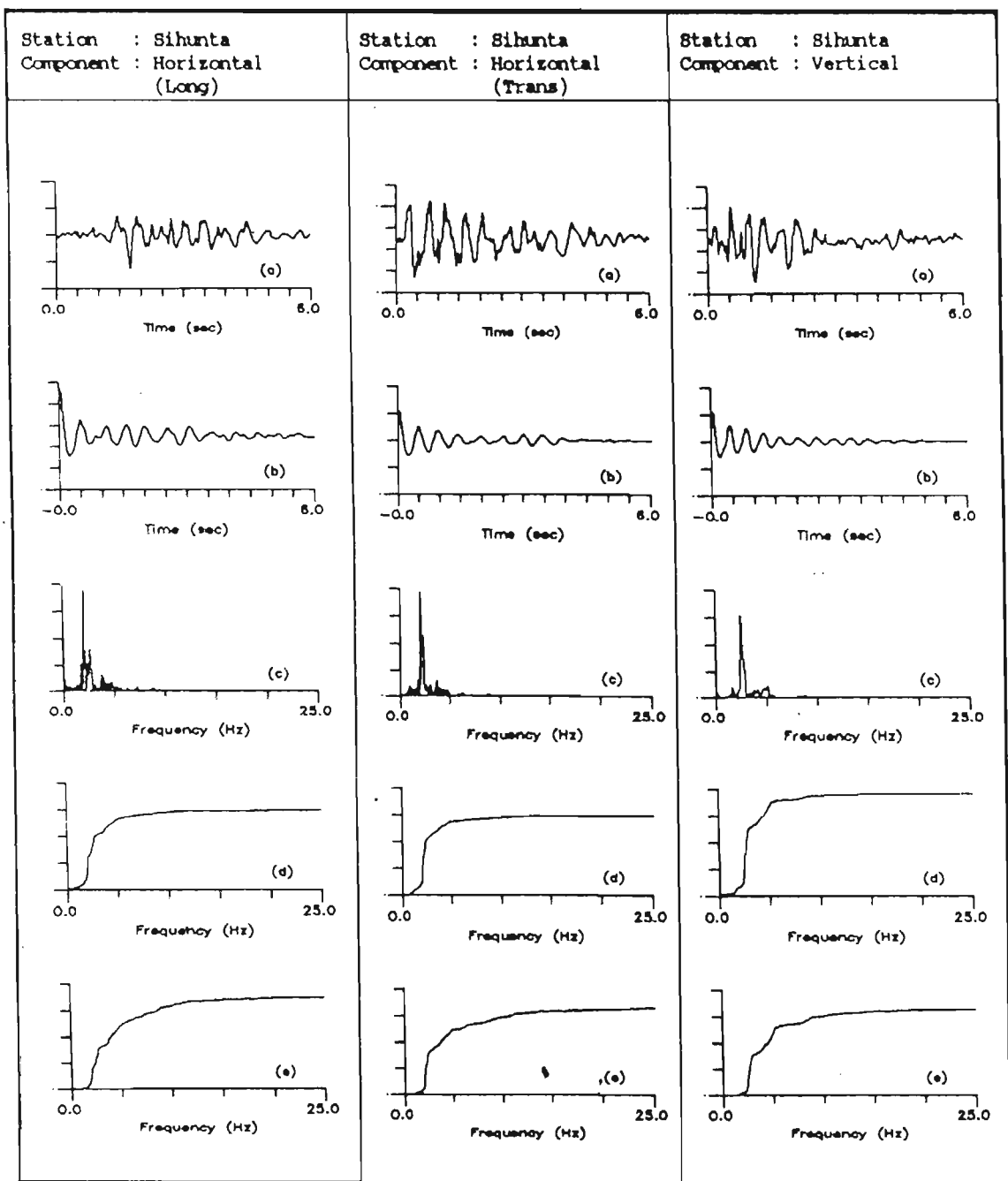


Fig 6.18 Dharamsala earthquake of 26th April, 1986, longitudinal, transverse and vertical components recorded at Sihunta station. Y axis shows normalised value of (a) acceleration record, (b) its autocorrelation function, (c) its power spectrum, (d) its cumulative power spectrum and (e) its frequency weighted cumulative power spectrum. X axis for (a) and (b) shows time and for (c), (d) and (e) shows frequency. Feature extracted from these records are given in Table 6.10.

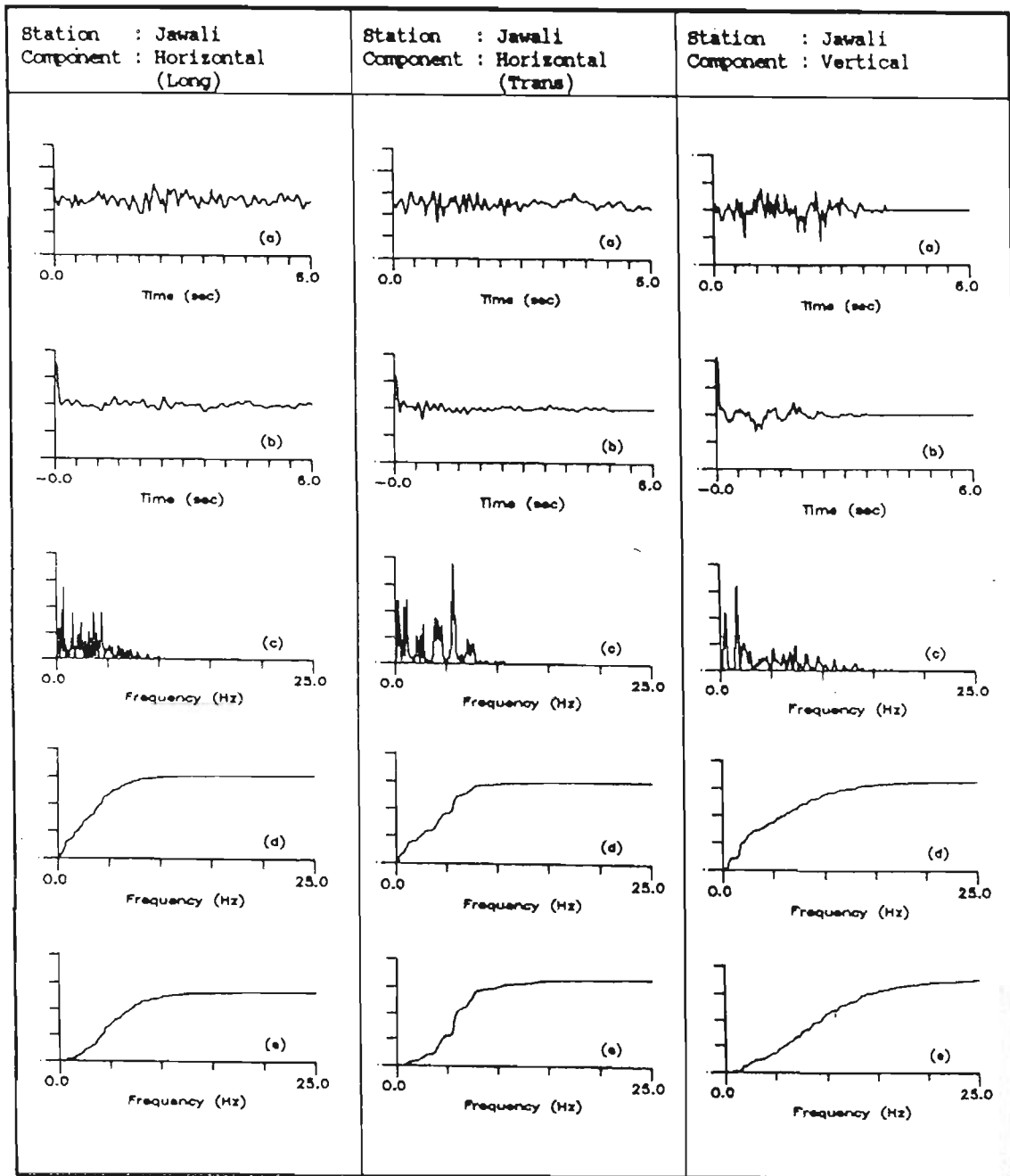


Fig 6.19 Dharamsala earthquake of 26th April, 1986, longitudinal, transverse and vertical components recorded at Jawali station. Y axis shows normalised value of (a) acceleration record, (b) its autocorrelation function, (c) its power spectrum, (d) its cumulative power spectrum and (e) its frequency weighted cumulative power spectrum. X axis for (a) and (b) shows time and for (c), (d) and (e) shows frequency. Feature extracted from these records are given in Table 6.11.

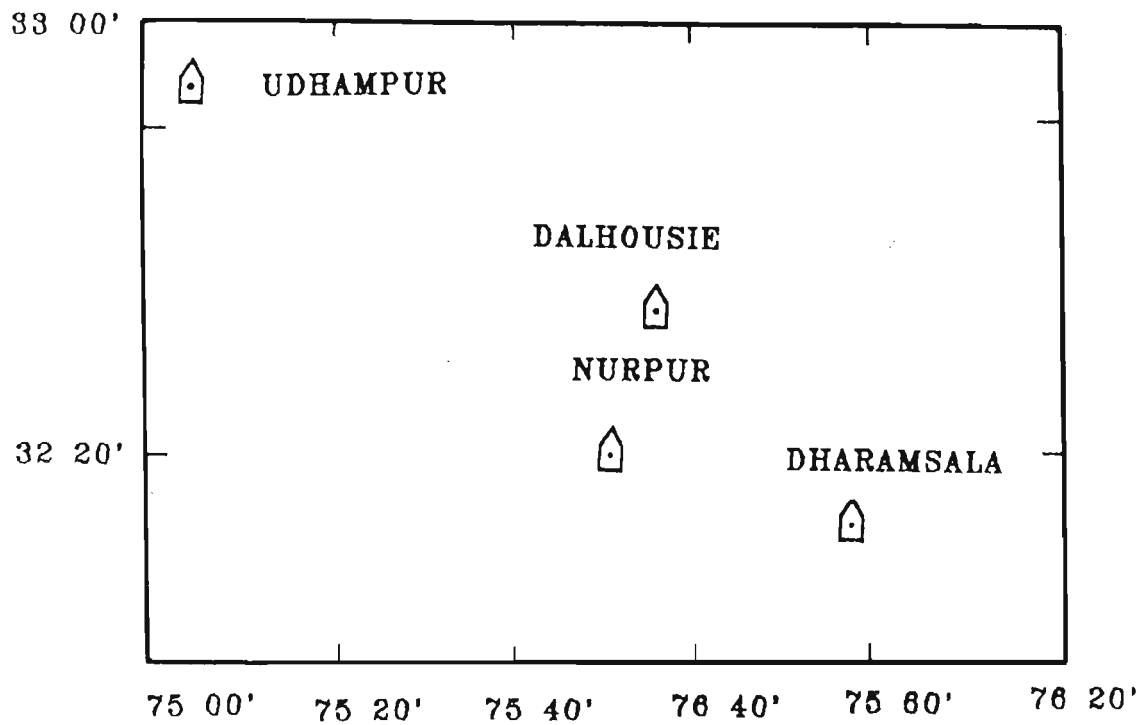


Fig 6.20 Locations at which micro earthquake studies were carried out for estimating velocity structure (After Srivastava and Chatterjee, 1986).

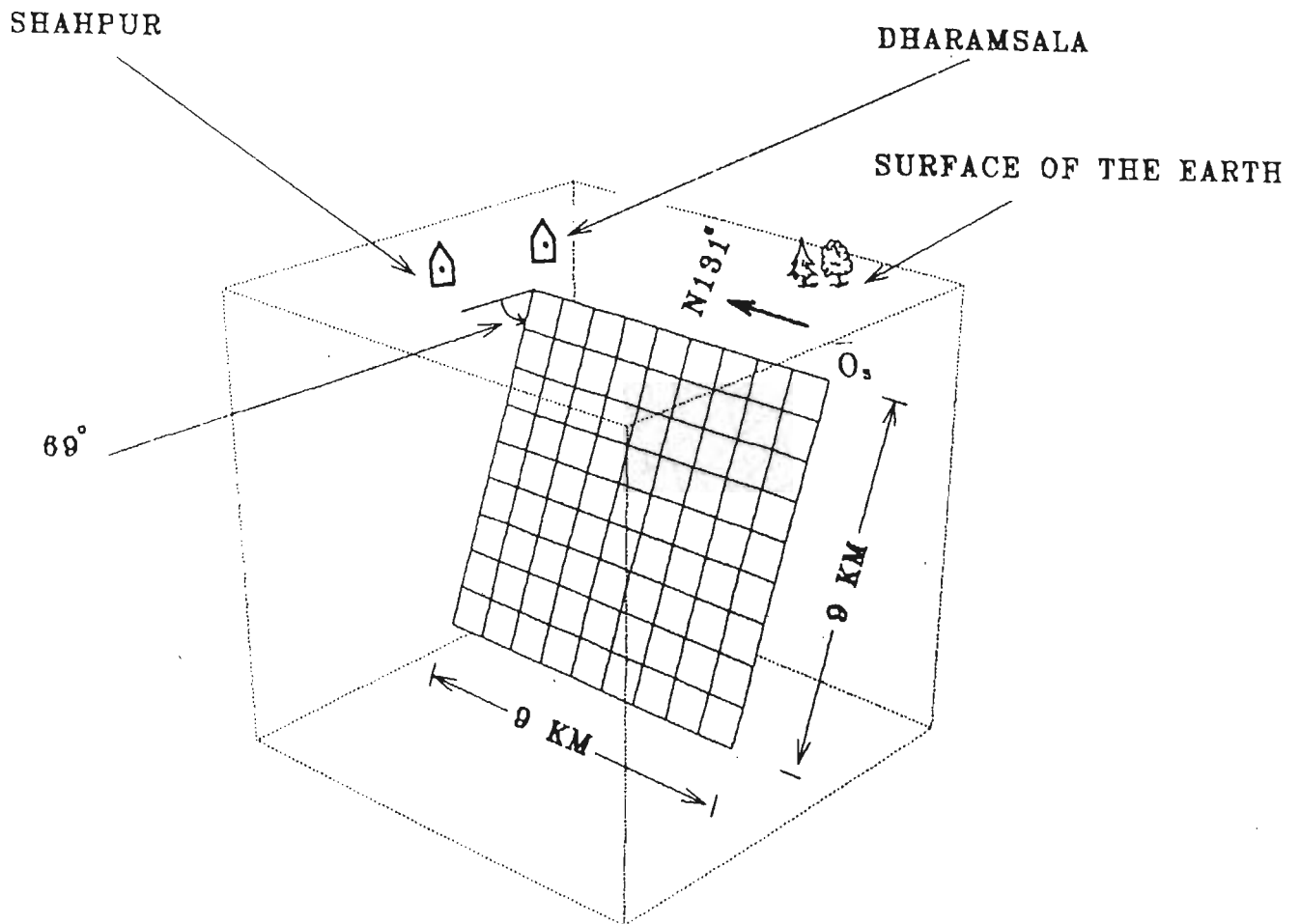


Fig 6.21 Model of the rupture plane for Dharamsala earthquake of 26th April, 1986. Minimum distance between the fault and Dharamsala station is 2 km and Shahpur is 7 km from the edge of the modelled fault.

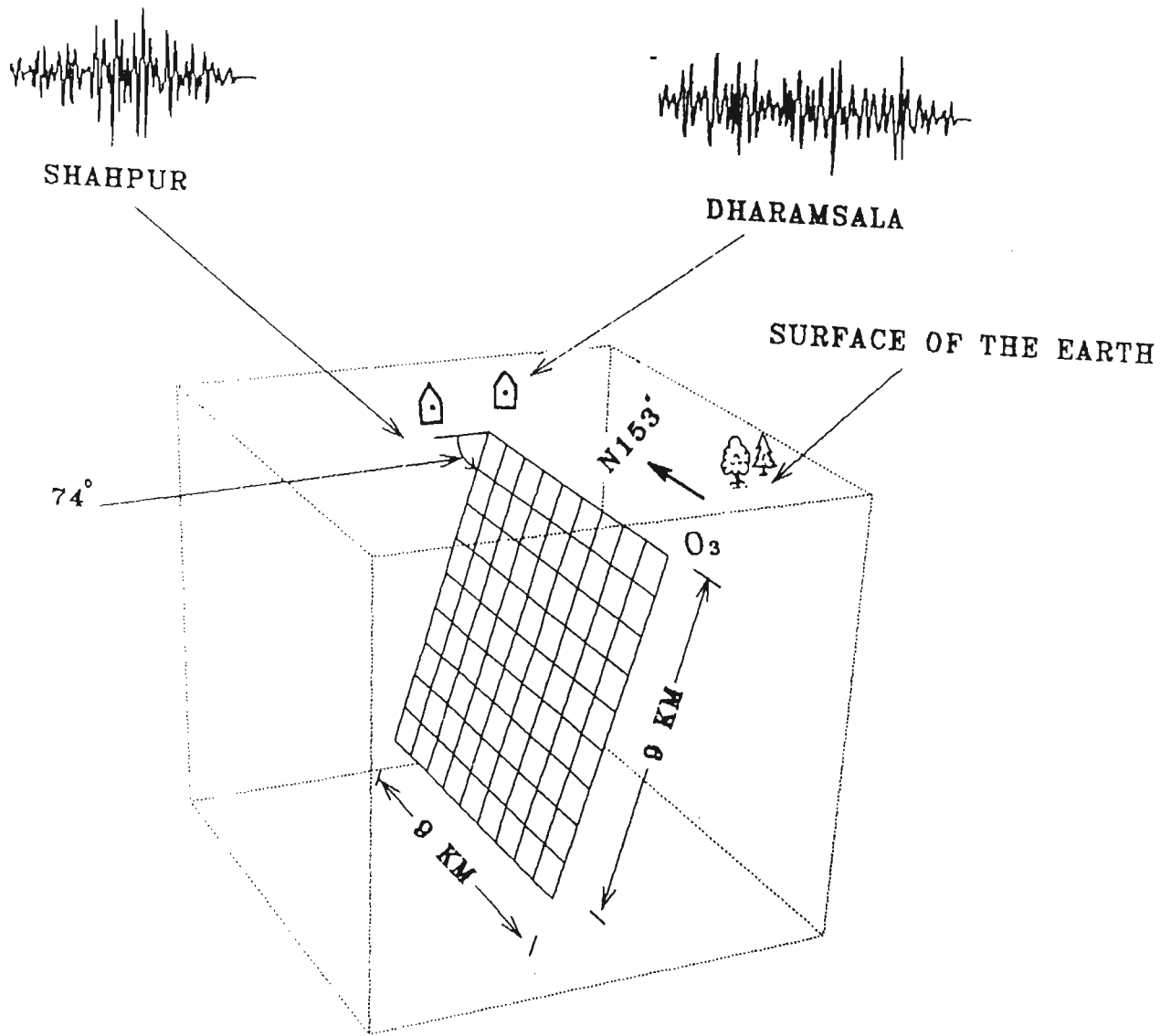


Fig 6.22 Model MD_u of rupture plane for Dharamsala earthquake of 26th April, 1986. Dip and strike of this model are 74° and 153° , respectively. Simulated acceleration records at Dharamsala and Sharpur stations are shown with the model of rupture plane. The parameters extracted from these records are given in Table 6.12.

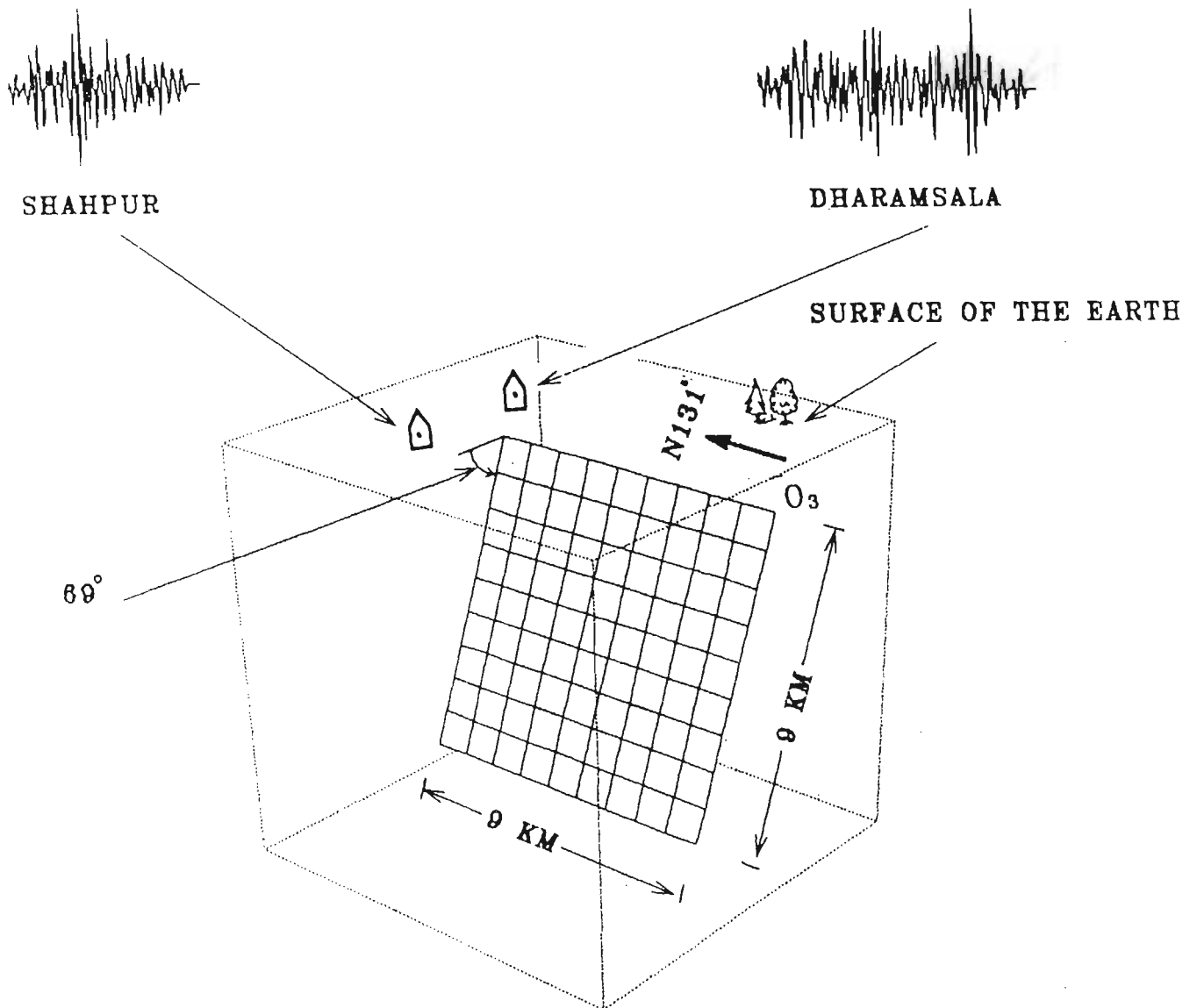


Fig 6.23 Model MD_k of rupture plane for Dharamsala earthquake of 26th April, 1986. Dip and strike of this model are 69° and 131° , respectively. Simulated acceleration records at Dharamsala and Shahpur stations are shown with the model of rupture plane. The parameters extracted from these records are given in Table 6.12.

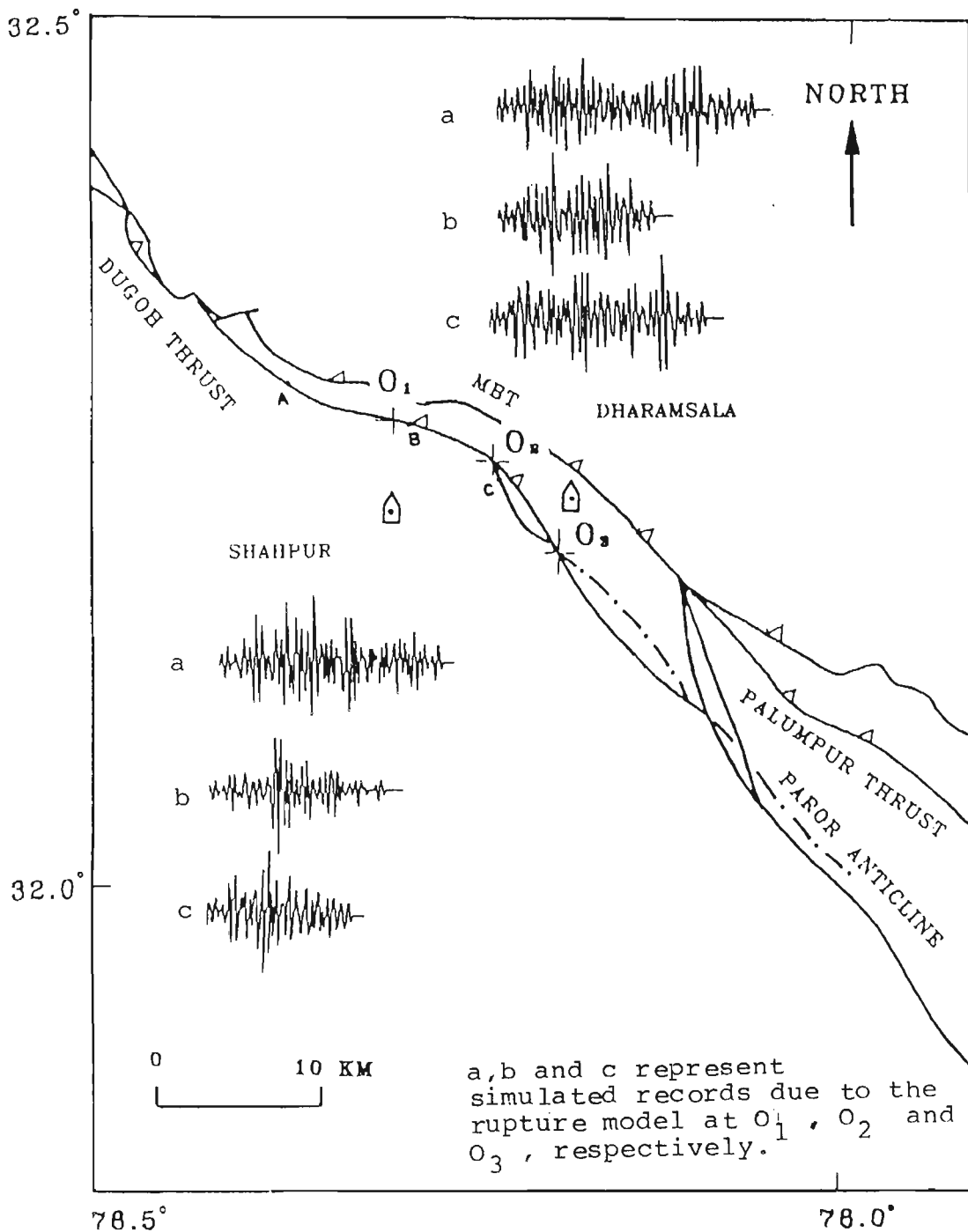


Fig 6.24 Drini thrust has been identified as the causative fault at which rupture could have possibly started. O₁A, O₂B and O₃C are three portions along this fault which have been modelled for simulation. Feature extracted from the simulated acceleration records shown in this figure are given in Table 6.14.

SHAHPUR

DHARAMSALA

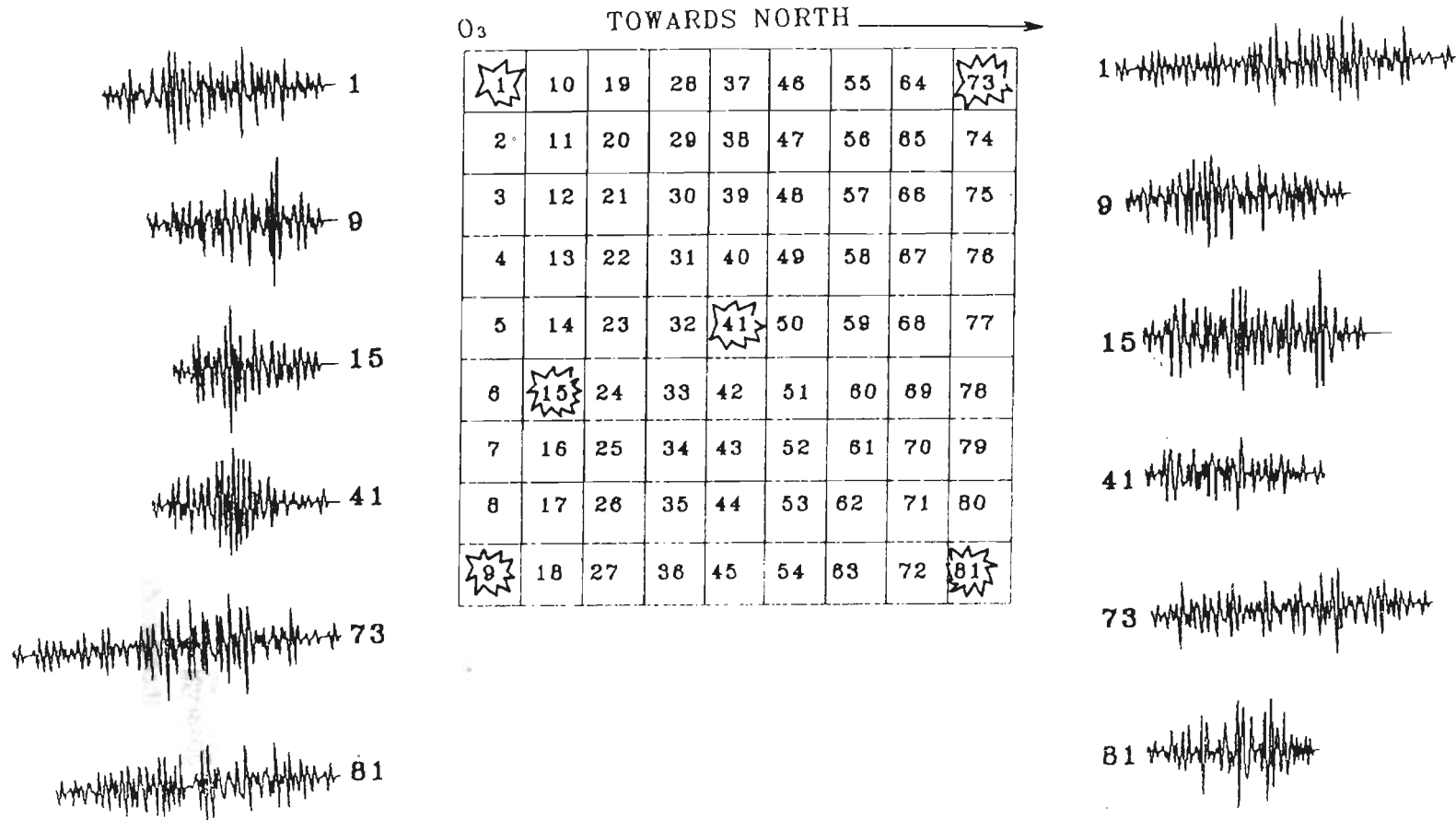


Fig 6.25 Model of rupture plane showing method of numbering elements within the rupture plane. Acceleration records are simulated at Dharamsala and Shahpur stations by assuming different elements within rupture plane as starting point of rupture. Number corresponding to each simulated record shows the element number which is assumed as nucleation point. Feature extracted from these simulated records are given in Table 6.16 and 6.17. The center of the element numbered as '1' is the origin of three dimensional rectangular coordinate system.

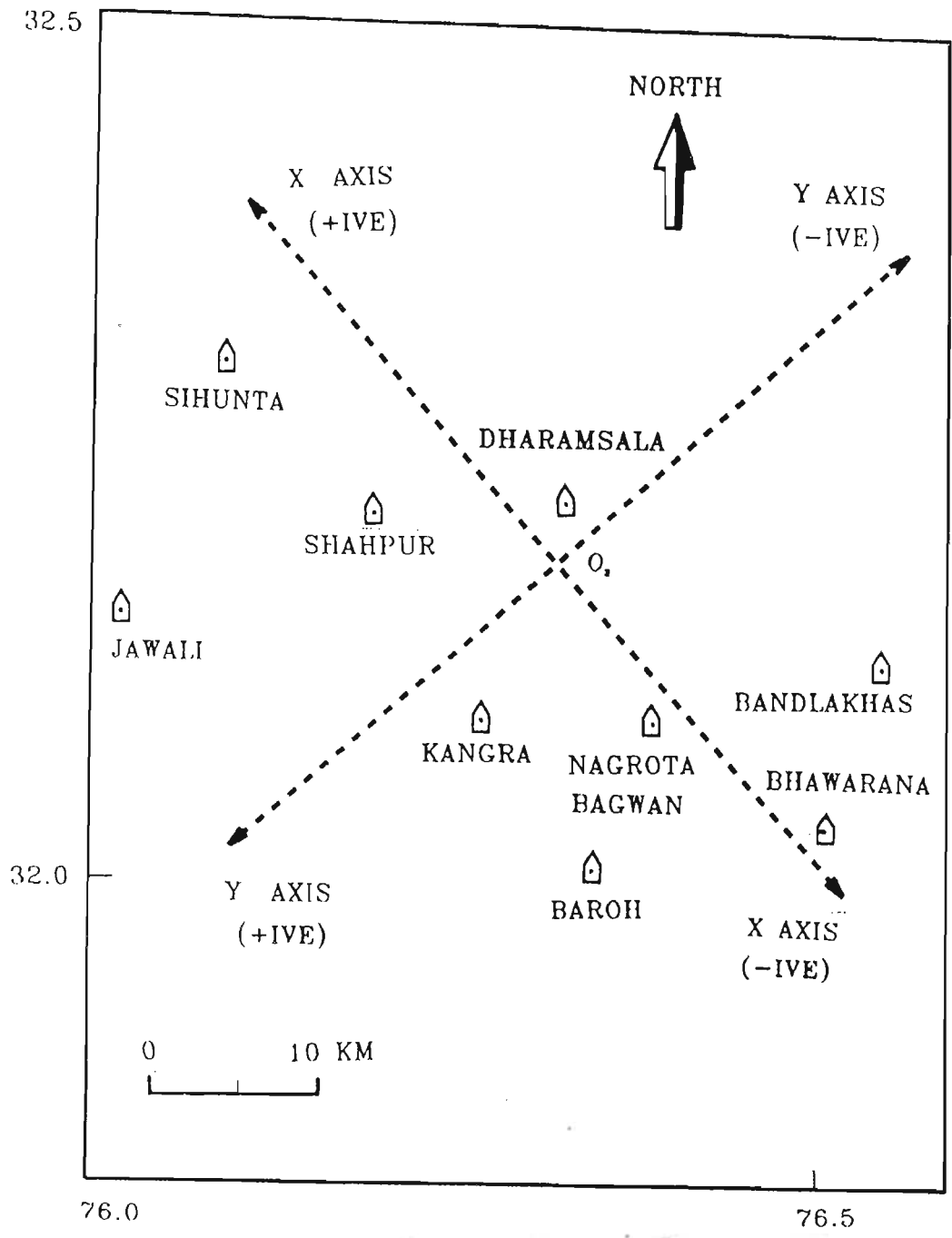


Fig 6.26 Location of observation points at which acceleration records are synthesised. The origin point of the coordinate system is placed at O_3 also shown in Fig 6.10. The coordinates of observation points in rectangular coordinate system are given in Table 6.19.

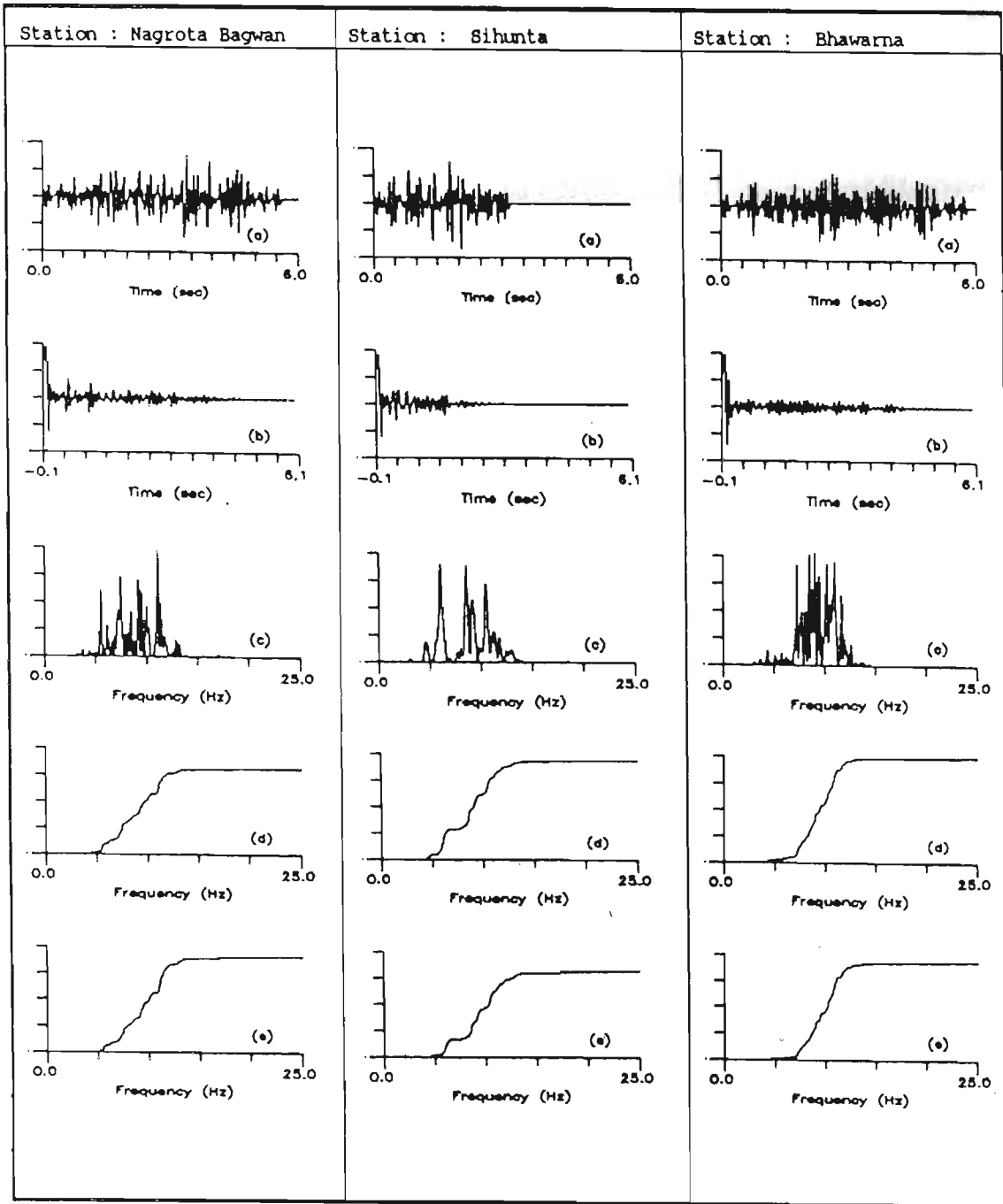


Fig 6.27 Dharamsala earthquake of 26th April, 1986, simulated records at Shahpur, Dharamsala, and Kangra stations. Y axis shows normalised value of (a) acceleration record, (b) its autocorrelation function, (c) its power spectrum, (d) its cumulative power spectrum and (e) its frequency weighted cumulative power spectrum. X axis for (a) and (b) shows time and for (c), (d) and (e) shows frequency. Feature extracted from simulated records at these stations are given in Table 6.20.

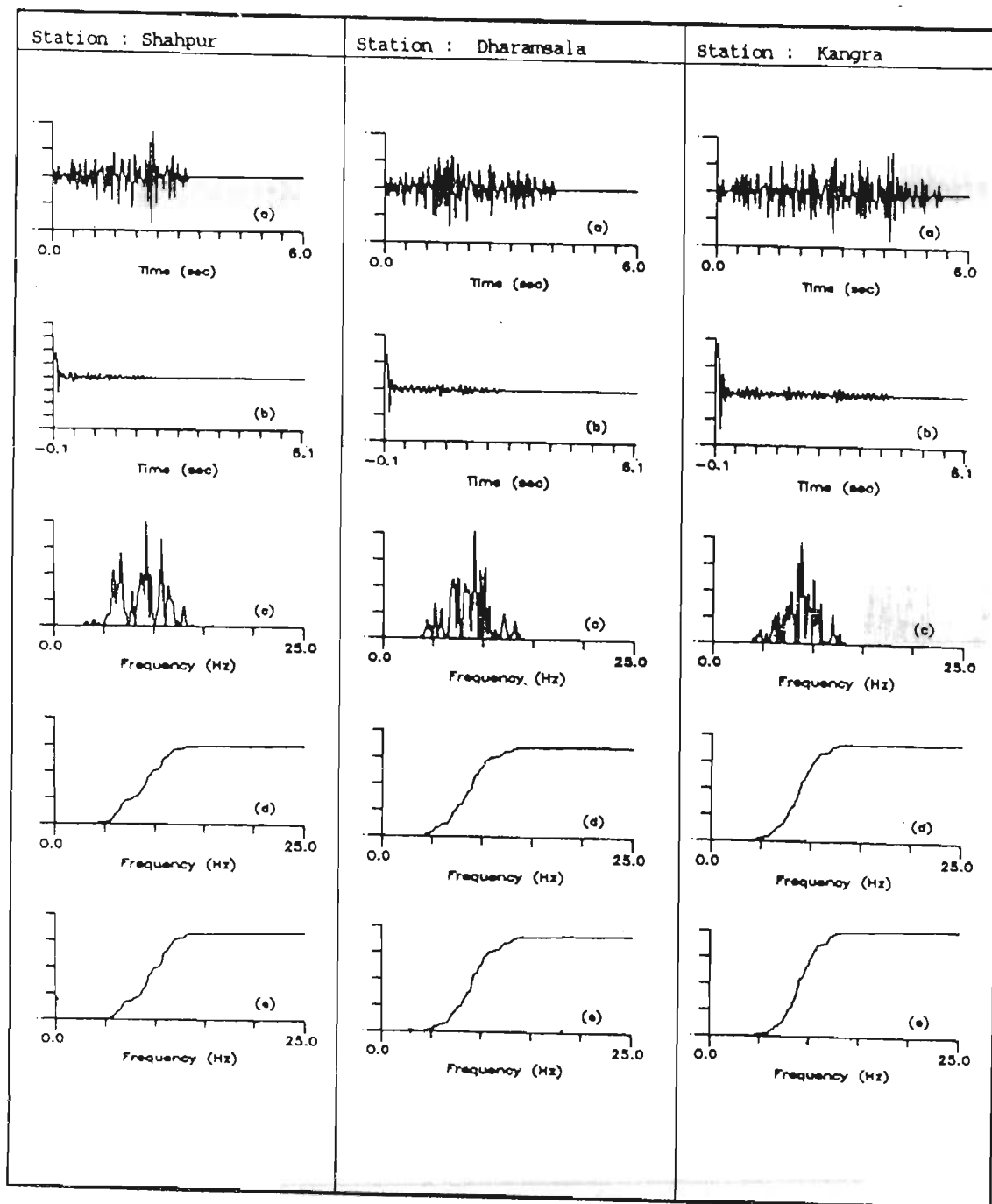


Fig 6.28 Dharamsala earthquake of 26th April, 1986, simulated records at Nagrota Bagwan, Sihunta and Bhawarna stations. Y axis shows normalised value of (a) acceleration record, (b) its autocorrelation function, (c) its power spectrum, (d) its cumulative power spectrum and (e) its frequency weighted cumulative power spectrum. X axis for (a) and (b) shows time and for (c), (d) and (e) shows frequency. Feature extracted from simulated records at these stations are given in Table 6.20 and 6.21.

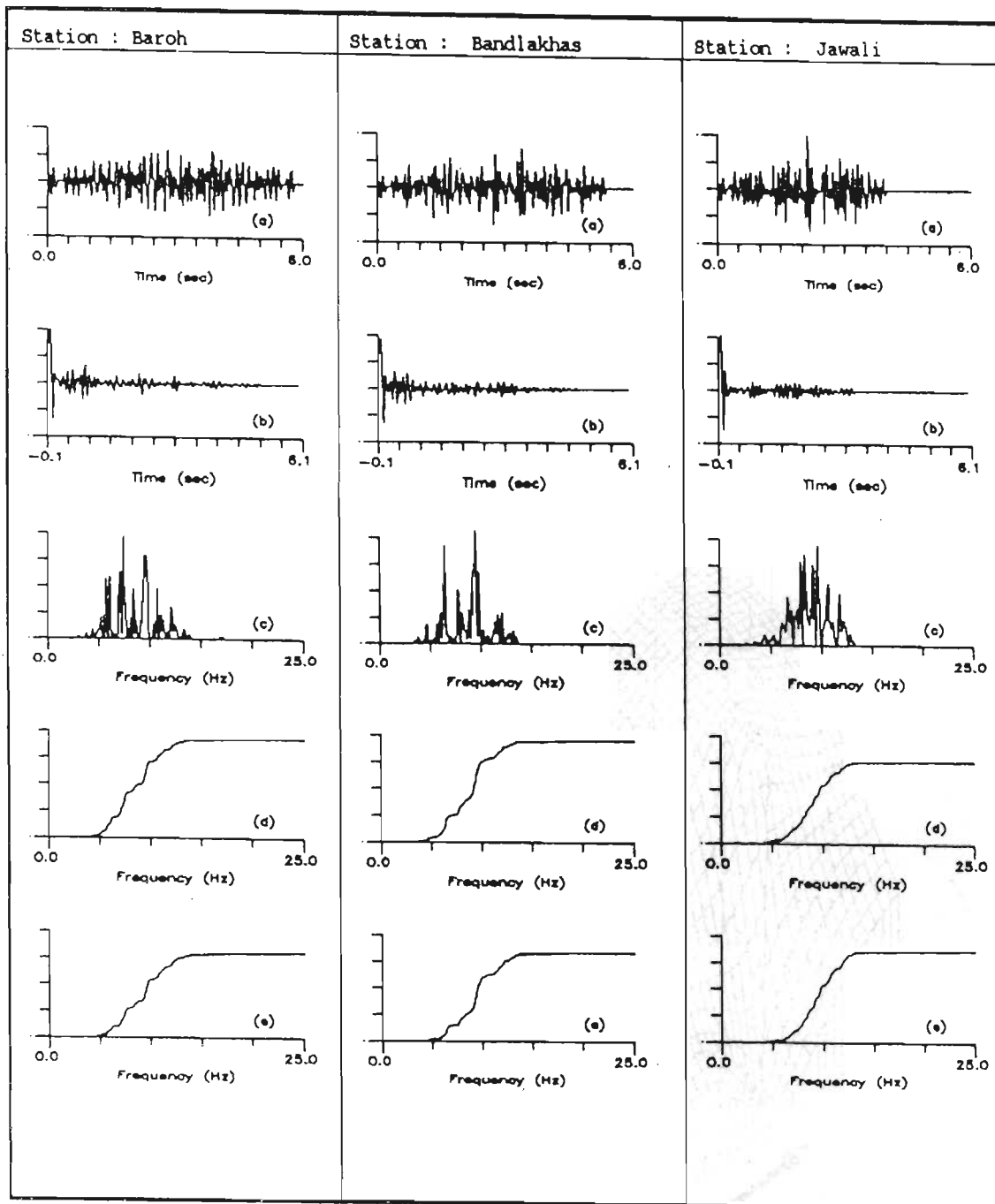


Fig 6.29 Dharamsala earthquake of 26th April, 1986, simulated records at Baroh, Bandlakhas and Jawali stations. Y axis shows normalised value of (a) acceleration record, (b) its autocorrelation function, (c) its power spectrum, (d) its cumulative power spectrum and (e) its frequency weighted cumulative power spectrum. X axis for (a) and (b) shows time and for (c), (d) and (e) shows frequency. Feature extracted from simulated records at these stations are given in Table 6.20 and 6.21.

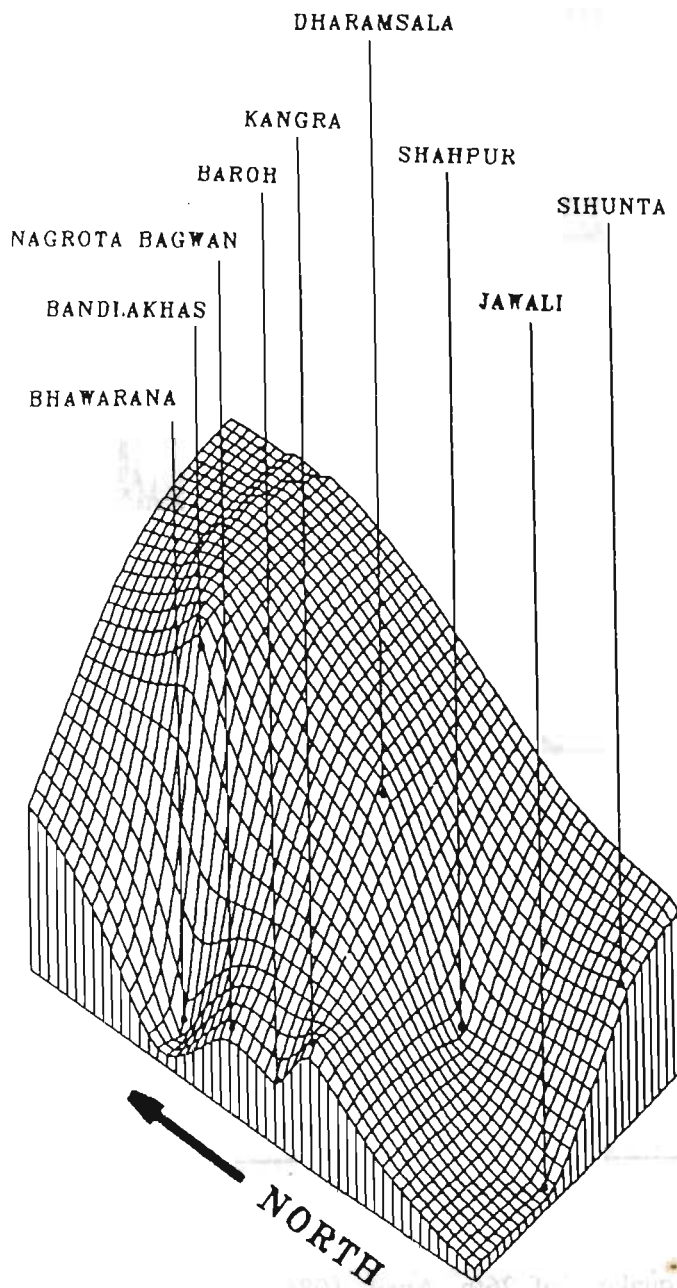


Fig 6.30 Elevations of different recording stations with respect to Mean Sea Level (MSL) that have recorded Dharamsala earthquake of 26th April, 1986. Elevation data for each station is taken from Chandrasekaran and Das (1988) and reproduced in Table 6.19. The diagram shows the relative height of the stations with respect to each other. The maximum elevation of the recording station is at 1800 m at Bandlakhas and the minimum elevation of recording station is 500 m at Bhawarana.

S.No	Date			Origin Time			Epicenter		Depth of focus km	Magnitude
	Year	M	D	H	M	S	°N Lat	°E Long		
1	1842	3	05	-	-	-	Near	Mussoorie	-	5.5
2	1842	3	05	-	-	-	Near	Mussoorie		
3	1856	4	07	-	-	-	Near	Kotgur	-	5.0
4							Simla	Hills		
5	1858	8	11	-	-	-	-	-	-	-
6	1860	7	09	-	-	-	-	-	-	-
7	1865	4	11	-	-	-	-	-	-	-
8	1869	10	05	-	-	-	-	-	-	-
9	1902	6	16	-	-	-	31.0	79.0	-	6.0
10	1905	4	04	-	-	-	32.25	76.25	-	8.0
11	1906	2	28	-	-	-	31.0	79.0	-	5.5
12	1908	12	11	-	-	-	31.0	79.0	-	5.0
13	1929	1	14	9	45	-	31.70	77.00	-	0.00
14	1930	5	11	11	30	-	31.70	77.00	-	0.00
15	1937	10	20	1	23	-	31.00	78.00	-	5.50
16	1940	4	7	14	28	-	31.50	77.00	-	0.00
17	1945	6	22	18	00	-	32.50	76.00	60	6.50
18	1947	7	10	10	19	-	33.00	77.00	60	6.00
19	1950	8	12	3	59	-	32.60	75.90	-	0.00
20	1950	9	25	17	58	-	32.60	75.90	-	0.00
21	1951	9	20	23	19	-	32.60	75.90	-	0.00
22	1955	3	10	21	16	-	32.50	77.00	-	0.00
23	1955	4	14	1	00	-	32.40	76.10	-	0.00
24	1955	6	27	10	14	-	32.00	78.50	-	5.80
25	1955	6	27	13	46	-	31.50	78.50	-	0.00
26	1959	5	12	00	35	-	32.40	78.66	-	6.30
27	1962	8	29	11	30	-	30.90	78.40	36	0.00
28	1963	4	12	00	41	-	32.00	78.80	28	5.10
29	1963	7	14	14	48	-	30.30	78.50	-	4.80
30	1963	11	12	15	28	-	31.70	78.50	-	4.60
31	1964	10	19	2	15	-	31.40	79.00	-	4.80
32	1965	2	21	3	25	-	32.40	76.90	-	4.50
33	1965	5	31	2	4	-	32.60	78.20	-	5.30
34	1967	9	20	20	25	-	32.60	76.10	59	0.00
35	1968	11	5	2	2	-	32.38	76.38	-	4.90
36	1968	11	5	3	7	-	32.38	76.57	-	0.00
37	1969	1	23	20	1	-	32.24	76.06	-	4.00
38	1969	1	23	23	46	-	32.17	76.03	-	0.00
39	1970	3	5	18	34	-	32.42	76.50	-	4.90
40	1972	1	29	6	49	-	32.86	75.96	58	4.70
41	1972	9	6	2	51	-	32.50	78.31	44	5.30
42	1973	1	14	11	39	-	32.95	75.34	90	4.00
43	1973	10	25	2	52	-	32.86	75.55	105	4.10
44	1973	12	16	9	16	-	32.28	76.03	-	4.90
45	1974	2	24	21	32	-	30.94	78.05	45	4.70
46	1974	7	7	20	56	-	30.63	78.69	33	4.90
47	1974	11	16	16	18	-	32.84	76.13	63	4.80

Continued on next page ...

Continued from previous page...

S.No	Date		Origin Time				Epicenter		Depth Magnitude	
	Year	M	D	H	M	S	°N Lat	°E Long	of focus km	
48	1975	1	19	8	0	-	32.43	78.59	60	5.30
49	1975	1	19	8	2	-	32.45	78.43	33	6.80
50	1975	1	19	8	12	-	31.95	78.52	33	6.00
51	1975	1	19	8	18	-	32.11	78.50	33	4.80
52	1975	1	19	9	12	-	32.41	78.53	33	4.70
53	1975	1	19	10	39	-	32.20	78.62	33	3.80
54	1975	1	19	13	4	-	32.13	78.64	33	5.00
55	1975	1	19	17	41	-	32.60	78.72	33	4.10
56	1975	1	20	11	6	-	32.50	78.56	48	4.80
57	1975	1	20	13	24	-	32.12	78.54	33	4.60
58	1975	1	22	17	26	-	31.89	78.50	51	4.70
59	1975	1	27	8	10	-	32.46	78.72	33	5.00
60	1975	1	27	9	23	-	32.02	78.63	33	4.90
61	1975	1	27	13	41	-	32.31	78.49	33	4.80
62	1975	1	27	15	58	-	32.71	78.47	33	4.50
63	1975	1	29	15	49	-	31.87	78.48	33	4.90
64	1975	1	31	14	4	-	32.41	78.47	45	4.60
65	1975	2	2	19	14	-	32.59	78.52	21	5.10
66	1975	2	11	6	41	-	32.15	78.47	33	4.70
67	1975	3	10	3	7	-	32.21	78.78	49	4.90
68	1975	4	1	16	18	-	31.87	78.47	33	4.70
69	1975	4	9	21	45	-	31.58	78.51	33	4.50
70	1975	5	8	11	56	-	32.38	78.50	33	4.80
71	1975	5	11	6	48	-	31.96	78.58	26	4.80
72	1975	6	10	9	44	-	32.55	78.62	28	4.90
73	1975	7	2	11	6	-	32.53	78.59	33	4.90
74	1975	7	19	6	10	-	31.92	78.60	40	5.30
75	1975	7	19	7	26	-	32.33	78.62	33	4.40
76	1975	7	21	7	26	-	32.12	78.53	33	4.70
77	1975	7	29	2	40	-	32.55	78.45	51	5.50
78	1975	8	14	15	16	-	31.85	78.38	61	3.90
79	1975	9	16	4	20	-	32.37	76.45	44	4.60
80	1975	9	19	17	53	-	32.22	78.93	33	4.30
81	1975	9	19	17	59	-	31.97	78.47	33	5.10
82	1975	10	30	14	20	-	32.70	75.38	112	4.90
83	1975	10	30	14	36	-	32.90	75.99	34	5.20
84	1975	11	5	0	35	-	32.03	78.80	28	5.20
85	1975	12	10	5	3	-	32.82	76.19	33	5.00
86	1975	12	11	10	9	-	32.84	75.98	59	5.10
87	1976	1	7	0	24	-	32.85	75.96	50	5.40
88	1976	1	9	23	50	-	32.98	76.02	22	4.70
89	1976	2	5	12	4	-	31.32	76.95	37	5.00
90	1976	3	4	18	45	-	32.55	75.42	121	3.70
91	1976	4	10	7	9	-	32.72	76.51	50	4.50
92	1976	4	16	20	15	-	32.87	76.01	92	4.00
93	1976	5	6	8	21	-	31.78	78.66	51	4.50

Continued on next page...

Continued from previous page...

S.No	Date		Origin Time					Epicenter		Depth of focus km	Magnitude
	Year	M	D	H	M	S	°N Lat	°E Long			
94	1976	5	22	18	32	-	32.73	75.69	89	4.30	
95	1976	7	6	2	55	-	32.28	78.27	56	4.80	
96	1976	9	8	20	13	-	32.04	78.68	18	5.40	
97	1976	9	29	7	47	-	31.77	78.34	29	5.00	
98	1976	10	3	15	3	-	31.90	78.76	16	4.70	
99	1977	1	21	14	57	-	32.83	75.79	51	4.60	
100	1977	1	28	3	48	-	31.53	78.27	55	4.70	
101	1977	2	19	6	15	-	31.78	78.41	40	5.40	
102	1977	2	19	6	39	-	31.58	78.22	33	4.70	
103	1977	3	27	5	36	-	32.70	78.54	26	5.00	
104	1977	4	14	18	26	-	32.02	78.54	33	4.30	
105	1977	10	19	7	14	-	32.73	78.41	33	4.80	
106	1977	12	21	2	8	-	32.83	76.63	33	5.10	
107	1978	1	15	1	10	-	31.94	77.57	33	0.00	
108	1978	1	15	2	30	-	31.91	78.30	60	4.50	
109	1978	2	19	18	56	-	31.68	75.25	59	4.00	
110	1978	3	30	23	44	-	32.84	78.30	50	4.20	
111	1978	4	11	7	55	-	32.63	78.61	33	4.50	
112	1978	6	14	16	12	-	32.31	76.52	18	5.00	
113	1978	10	17	20	10	-	32.19	76.35	69	0.00	
114	1979	3	27	5	27	-	32.05	78.61	33	4.30	
115	1979	5	11	21	56	-	32.08	78.80	33	4.40	
116	1979	12	28	1	59	-	30.62	78.44	33	5.00	
117	1980	5	29	22	40	-	31.56	76.57	33	4.20	
118	1980	8	23	21	36	-	32.91	75.63	25	5.20	
119	1980	8	23	21	50	-	32.83	75.62	33	5.20	
120	1980	9	22	20	37	-	32.45	78.51	65	4.70	
121	1981	5	28	23	14	-	31.85	78.41	33	5.10	
122	1981	6	13	0	56	-	31.70	78.33	33	5.00	
123	1981	7	12	8	45	-	32.73	76.00	50	4.50	
124	1981	8	10	10	58	-	31.26	77.93	33	4.60	
125	1982	5	7	7	44	-	32.61	75.88	33	4.80	
126	1982	7	16	4	15	-	30.71	77.03	103	4.20	
127	1982	12	14	23	57	-	31.45	78.91	33	4.60	
128	1983	2	27	20	33	-	32.61	78.55	33	5.30	
129	1984	5	3	13	17	-	30.50	78.40	33	4.50	
130	1984	5	23	3	14	-	32.94	75.91	58	4.80	
131	1984	12	15	10	54	-	31.28	77.80	33	4.70	
132	1985	3	11	14	36	-	31.25	77.04	33	4.80	
133	1985	3	22	0	48	-	31.38	76.71	33	0.00	
134	1985	12	29	21	31	-	32.62	76.10	33	4.90	
135	1986	4	22	9	29	-	31.85	76.78	33	4.70	
136	1986	4	26	7	35	-	32.12	76.37	33	5.50	
137	1986	7	16	22	3	-	31.04	77.99	33	5.60	
138	1986	9	11	4	22	-	32.66	78.55	33	4.80	

Continued on next page...

Continued from previous page..

S.No	Date		Origin Time				Epicenter		Depth of focus km	Magnitude
	Year	M	D	H	M	S	°N Lat	°E Long		
139	1987	7	18	16	29	-	31.14	78.04	54	4.70
140	1987	10	6	16	33	-	31.92	76.44	33	4.70
141	1987	12	26	1	3	-	32.12	76.69	33	4.30
142	1988	7	27	7	7	-	31.60	78.63	33	4.40
143	1988	12	26	11	11	-	30.61	77.98	33	4.20
144	1989	1	27	11	3	-	30.98	78.65	33	3.70
145	1990	4	3	1	8	-	31.73	78.73	51	3.90
146	1990	10	3	18	20	-	31.09	78.55	33	4.40

Table 6.1 Epicenters of important earthquakes in H.P. and surrounding regions. Data taken from Singh et al. (1975) and USGS - NEIC (1990). This epicentral data is plotted in Fig 6.1.

Name of Town	Distt	Lat	Long	Measured Acceleration in cm/sec ²
Dehradun	Dehradun	30°43'	77°54'	> 280
Kangra	Kangra	32°06'	76°19'	400
Landour	Landour	30°27'	78°07'	< 340
Rajpur	Rajpur	30°24'	78°05'	210

Table 6.2 Estimated acceleration at various places for Kangra earthquake of 4th April, 1905 (After Middlemiss, 1910, reprint 1981).

S.No.	Station	Latitude		Longitude		Elevation (in meter)
		D	M	D	M	
1.(31)	Aghar	31	36	76	34	880
2.(41)	Bagsiad	31	33	77	07	1850
3.(48)	Bagi	31	14	77	33	2870
4.(37)	Bajaura	31	50	77	09	1120
5.(40)	Bali	31	41	77	16	1120
6.(20)	Bandlakhas	32	07	76	32	1800
7.(18)	Baroh	31	59	76	18	720
8.(1)	Bhajradu	32	50	76	09	1720
9.(21)	Bhawarna	32	02	76	29	500
10.(23)	Bir	32	02	76	43	1560
11.(4)	Chamba	32	33	76	07	1000
12.(45)	Choridhar	31	21	77	18	1580
13.(5)	Chuwarikhas	32	25	76	01	1600
14.(16)	Dadasiba	31	55	76	05	470
15.(44)	Dalash	31	23	77	25	1870
16.(3)	Dalhousie	32	32	75	58	1900
17.(29)	Dharampur	31	48	76	45	760
18.(14)	Dharamsala	32	12	76	19	1400
19.(33)	Drang	31	48	76	56	980
20.(35)	Ghumarwin	31	26	76	42	740
21.(27)	Hamirpur	31	41	76	31	760
22.(10)	Jawali	32	08	76	00	550
23.(28)	Jhatingri	31	56	76	53	1960
24.(42)	Jhungi	31	25	77	05	1830
25.(15)	Kangra	32	05	76	15	950
26.(9)	Kotla	32	14	76	03	800
27.(32)	Kulu	31	57	77	06	1260

S.No.	Station	Latitude		Longitude		Elevation in meters
		D	M	D	M	
28.(47)	Kunihar	31	04	76	56	960
29.(24)	Ladbharol	31	56	76	42	740
30.(25)	Lambagaon	31	53	76	33	560
31.(22)	Nadaun	31	46	76	20	470
32.(17)	Nagrota Bhagwan	32	06	76	22	800
33.(13)	Nagrota Suryan	32	03	76	05	500
34.(43)	Namhol	31	15	76	52	1170
35.(6)	Nurpur	32	18	75	53	600
36.(38)	Pandoh	31	40	77	03	880
37.(26)	Patlander	31	46	76	32	800
38.(19)	Pragpur	31	49	76	12	560
39.(7)	Rakh	32	28	76	14	2200
40.(34)	Rewalsar	31	37	76	50	1200
41.(11)	Rirkmar	32	18	76	11	1200
42.(49)	Sandhu	31	09	77	22	2410
43.(30)	Sarkaghat	31	42	76	44	900
44.(12)	Shahpur	32	12	76	11	700
45.(50)	Shimla	31	06	77	13	2200
46.(8)	Sihunta	32	18	76	05	1000
47.(39)	Sunder Nagar	31	33	76	54	840
48.(2)	Sundla	32	40	76	02	800
49.(46)	Sunni	31	14	77	07	680
50.(36)	Surani	31	53	76	20	900

Table 6.3 List of stations of Kangra array. Geographical coordinates and elevation of station is taken from Chandrasekaran and Das (1992b). Location of stations of array is shown in Fig 6.2. Station name in the Fig 6.2 is represented by a number given in the bracket for each station.

MAGNITUDE	DATE	ORIGIN TIME (H:M:S)	EPICENTER	FOCAL DEPTH (KM)	REF.	NAME GIVEN TO THE EPICENTER
$M_L = 5.7$	24.6.86	7:35:17	32.10°N 76.30°E	10	IMD	E_{D1}
$M_b = 5.5$ $M_s = 5.3$	24.6.86	7:35:16.1	32.128°N 76.374°E	33	USGS	E_{D2}
-	24.6.86	7:35:16.4	32.175°N 76.287°E	7	D,C	E_{D3}
-	24.6.86	-	32.193°N 76.29°E	-	IMD (Revised)	E_{D4}

D,C Das and Chandrasekaran (1993)

Table 6.4 Epicentral parameters of Dharamsala earthquake of 26th April, 1986 reported by different agencies. The epicenters E_{D1} , E_{D2} , E_{D3} and E_{D4} given in this table are plotted in Fig 6.5.

DATE	NP1		NP2		REF
	STRIKE	DIP	STRIKE	DIP	
26.06.86	232°	60°	131°	69°	K,M
26.06.86	299°	19°	153°	74°	USGS

K,M Kumar and Mahajan (1990)

Table 6.5 Dip and strike of two nodal planes of fault plane solutions for the Dharamsala earthquake of 26th April, 1986 given by different agencies.

STATION	PEAK ACCELERATION FROM LONGITUDINAL COMPONENT IN CM/SEC ²	PEAK ACCELERATION FROM TRANSVERSE COMPONENT IN CM/SEC ²	RESULTANT PEAK ACCELERATION IN CM/SEC ²
Bandlakhas	141.6	122.8	142.9
Baroh	58.8	57.1	61.8
Bhawarana	37.4	36.3	39.3
Dharamsala	176.3	188.1	244.3
Jawali	15.9	16.7	19.7
Kangra	148.5	112.6	160.4
Nagrota Bagwan	147.0	80.6	147.1
Shahpur	204.5	244.8	265.0
Sihunta	50.9	35.9	57.2

Table 6.6 Resultant peak ground acceleration of two horizontal components recorded at different stations for Dharamsala earthquake of 26th April, 1986 (After Chandrasekaran, 1988b). Isoacceleration contour map of resultant peak acceleration for this earthquake is shown in Fig 6.6.

PARAMETERS	DHAR LONG	DHAR TRANS	DHAR VERT	SHAH LONG	SHAH TRANS	SHAH VERT
P_s	176	188	83	204	244	67
T_{st}	.7	.9	1.1	1.1	.5	2.5
T_D	2.5	3.9	4.3	2.8	2.0	6.4
P_v	7.1	9.4	3.0	6.9	15.8	4.1
P_d	1.6	3.3	2.46	1.6	2.7	3.5
T_{ARAF}	7612	7734	6576	7919	10158	54657
R_{st}	.977	1.01	.98	1.01	1.01	1.00
ACF_1	.058	.075	.031	.042	.070	.032
ACF_2	.231	.372	.084	.112	.322	.072
ACF_3	.402	.477	.108	.167	.500	.140
ACF_4	.160	.140	.06	.08	.20	.06
ACF_5	.752	.795	.303	.689	.834	.435
ACF_6	.288	.455	-.265	.041	.476	-.263
ACF_7	-.038	.193	-.266	-.455	.126	-.272
ACF_8	-.512	-.358	-.266	-.519	-.367	-.272
ACF_9	.830	1.36	2.46	1.46	.88	2.68
ACF_{10}	1.062	1.06	1.09	1.07	1.05	1.05
F_p	3.2	2.6	9.8	7.3	2.6	9.4
F_1	3.5	3.3	9.0	6.0	2.8	8.4
F_2	6.8	4.9	11.1	7.3	4.9	9.9
F_3	9.5	10.2	15.2	7.9	7.1	12.7
F_4	3.2	2.6	5.7	4.7	2.5	5.5
F_5	3.9	3.5	9.6	6.8	2.9	8.9
F_6	7.1	4.9	12.2	7.7	5.4	11.3

Table 6.7 Extracted features from three components of field records of Dharamsala earthquake of 26th April, 1986 recorded at Dharamsala and Shahpur stations. Field records at Dharamsala and Shahpur stations are shown in Fig 6.11 and 6.12, respectively.

PARAMETER	KANGRA LONG	KANGRA TRANS	KANGRA VERT	NAGR -OTA LONG	NAGR- OTA TRANS	NAGR -OTA VERT
P_s	148	112	73	146	81	52
T_m	2.8	1.6	1.8	.2	.1	2.5
T_D	4.7	3.2	5.3	4.1	5.0	15.0
P_v	4.9	9.6	3.4	8.2	4.0	3.1
P_d	.31	2.0	2.5	3.2	3.0	2.9
T_{ARAF}	9701	9985	7228	6204	5523	5229
R_m	1.00	.989	.972	1.048	.994	1.01
ACF_1	.054	.091	.059	.092	.040	.053
ACF_2	.235	.348	.165	.414	.137	.101
ACF_3	.393	.411	.258	.551	.248	.177
ACF_4	.180	.180	.100	.180	.100	1.02
ACF_5	.74	.877	.545	.789	.546	.388
ACF_6	.241	.611	-.021	.473	-.008	-.194
ACF_7	-.103	.330	-.285	.259	.167	-.195
ACF_8	-.412	-.449	-.403	-.269	-.297	-.207
ACF_9	.985	1.065	1.560	1.218	4.909	3.55
ACF_{10}	1.035	1.044	1.054	1.050	1.072	1.06
F_p	3.2	3.0	5.2	2.2	5.5	8.6
F_1	3.7	2.9	6.3	3.4	5.8	8.4
F_2	6.8	3.7	8.9	5.9	8.6	11.3
F_3	8.7	6.9	13.4	11.2	14.1	14.6
F_4	3.1	2.1	4.7	2.2	4.5	5.1
F_5	4.2	2.9	6.4	3.3	6.2	8.5
F_6	7.6	3.9	9.1	5.2	9.3	12.0

Table 6.8 Extracted features from three components of field records of Dharamsala earthquake of 26th April, 1986 recorded at Kangra and Nagrota Bagwan (Nagrota) stations. Field records at Kangra and Nagrota Bagwan stations are shown in Fig 6.13 and 6.14, respectively.

PARAMETER	BAROH LONG	BAROH TRANS	BAROH VERT	BHAW-AR LONG	BHAW-AR TRANS	BHAW-AR VERT
P_s	59	57	23	37	36	35
T_{st}	.3	.3	1.8	.6	.2	.2
T_D	4.3	3.2	4.5	8.5	8.0	4.0
P_v	3.3	3.1	1.5	1.5	3.2	1.7
P_d	1.1	1.1	1.0	.73	2.1	1.0
T_{ARAF}	4344	1916	1119	2435	2800	1310
R_{st}	.972	8.47	1.07	1.025	1.00	1.018
ACF_1	.051	.049	.050	.053	.057	.041
ACF_2	.131	.114	.132	.171	.147	.119
ACF_3	.212	.185	.206	.259	.218	.194
ACF_4	.08	.08	.080	.100	.100	.08
ACF_5	.775	.733	.717	.756	.793	.662
ACF_6	.265	.194	.198	.258	.340	.036
ACF_7	-.234	-.259	-.190	-.143	-.062	-.478
ACF_8	-.496	-.406	-.346	-.325	-.324	-.611
ACF_9	1.531	1.733	1.992	1.87	3.58	1.17
ACF_{10}	1.048	2.518	1.080	1.04	1.05	1.065
F_p	5.9	6.6	5.8	4.1	6.0	6.0
F_1	4.9	5.6	5.2	4.1	4.5	5.9
F_2	5.9	6.6	6.4	5.7	5.8	6.9
F_3	6.9	7.6	8.5	8.5	7.1	8.1
F_4	3.9	2.7	3.4	3.8	2.7	5.3
F_5	5.7	6.1	5.7	4.9	4.8	6.1
F_6	6.1	7.0	7.2	6.5	6.0	7.4

Table 6.9 Extracted features from three components of field records of Dharamsala earthquake of 26th April, 1986 recorded at Baroh and Bhawarna (Bhawar) stations. Field records at Baroh and Bhawarna stations are shown in Fig 6.15 and 6.16, respectively.

PARAMETER	SIHUN LONG	SIHUN TRANS	SIHUN VERT	BANDL LONG	BANDL TRANS	BANDL VERT
P_s	51	36	40	142	123	23
T_{st}	.5	.1	.7	1.2	.4	.1
T_D	6.8	3.8	3.1	2.8	3.1	3.5
P_v	4.2	4.8	3.8	6.6	3.9	2.5
P_d	2.9	3.1	3.9	2.0	1.8	1.7
T_{ARAF}	3724	2611	1901	5648	4516	1531
R_{st}	1.03	.902	.737	.949	1.01	.99
ACF_1	.103	.108	.086	.072	.073	.030
ACF_2	.35	.355	.310	.175	.188	.077
ACF_3	.59	.576	.492	.278	.350	.103
ACF_4	.20	.22	.160	.120	.120	.040
ACF_5	.890	.906	.886	.783	.796	.408
ACF_6	.670	.716	.633	.385	.324	-.383
ACF_7	.43	.501	.342	-.221	.407	-.383
ACF_8	-.42	-.538	-.520	-.664	-.166	-.383
ACF_9	.876	.792	.825	1.09	1.35	1.952
ACF_{10}	1.03	1.046	1.147	1.06	1.05	1.088
F_p	2.0	2.1	2.5	5.2	3.9	11.7
F_1	2.2	2.1	2.6	4.8	4.1	8.6
F_2	3.7	2.6	3.7	5.3	5.5	11.0
F_3	5.7	5.1	5.1	6.2	6.4	12.2
F_4	2.0	2.1	2.5	4.0	3.0	5.4
F_5	2.4	2.2	2.7	5.1	4.4	9.4
F_6	3.7	3.0	4.1	5.6	6.2	11.6

Table 6.10 Extracted features from three components of field records of Dharamsala earthquake of 26th April, 1986 recorded at Sihunta and Bandlakhas (Bandl) stations. Field records at Bandlakhas and Sihunta stations are shown in Fig 6.17 and 6.18, respectively.

PARAMETER	JAWALI LONG	JAWALI TRANS	JAWALI VERT
P_s	15.9	16.7	11.1
T_{st}	.6	.7	1.82
T_D	4.1	4.5	1.82
P_v	3.3	2.0	3.7
P_d	3.1	1.5	2.7
T_{ARAF}	1306	1024	387
R_{st}	1.118	1.13	1.15
ACF_1	.095	.068	.171
ACF_2	.153	.124	.382
ACF_3	.317	.403	.631
ACF_4	3.5	.620	.88
ACF_5	.86	.822	.690
ACF_6	.57	.439	.265
ACF_7	.27	.081	.096
ACF_8	-.19	-.364	-.284
ACF_9	32.3	7.7	2.8
ACF_{10}	1.15	1.1	1.1
F_p	.73	5.7	9.7
F_1	3.6	4.2	5.5
F_2	4.8	5.7	8.4
F_3	7.1	7.2	12.1
F_4	1.5	1.4	1.8
F_5	3.2	4.2	4.4
F_6	4.8	5.8	7.9

Table 6.11 Extracted features from three components of field records of Dharamsala earthquake of 26th April, 1986 recorded at Jawali station. Field record at Jawali is shown in Fig 6.19.

MODEL NAME	MD _k	MD _u	MD _k	MD _u
STATION	DHARM	DHARM	SHAH	SHAH
P _z	154	148	189	175
T _u	2.7	2.1	.64	1.4
T _D	2.9	3.1	1.9	2.1
P _v	3.0	3.1	.08	.10
P _d	.106	.091	.077	.106
T _{ARAF}	6948	7879	5813	6224
R _u	.99	.99	.99	.99
ACF ₁	.032	.030	.029	.028
ACF ₂	.093	.090	.086	.084
ACF ₃	.156	.156	.138	.136
ACF ₄	.06	.06	.06	.06
ACF ₅	.477	.451	.420	.398
ACF ₆	-.427	-.485	-.538	-.561
ACF ₇	-.726	-.744	-.737	-.695
ACF ₈	-.726	-.744	-.737	-.695
ACF ₉	1.03	.98	.99	1.044
ACF ₁₀	1.06	1.07	1.08	1.09
F _p	8.0	8.1	9.6	10.8
F ₁	7.9	8.0	7.8	8.3
F ₂	8.5	9.0	9.6	9.9
F ₃	10.2	10.5	10.5	10.8
F ₄	6.8	7.2	7.5	7.6
F ₅	8.1	8.5	9.4	9.1
F ₆	9.5	10.0	10.0	10.8

Table 6.12 Extracted features from simulated records at Dharamsala and Shahpur station for two different models MD_u and MD_k of rupture planes. The model of these two rupture planes and the simulated records are shown in Fig 6.22 and 6.23.

PARAMETERS	MODEL GIVING LEAST DIFFERENCE IN THE VALUE OF EXTRACTED PARAMETER FROM SIMULATED AND FIELD RECORDS AT DHARAMSALA	MODEL GIVING LEAST DIFFERENCE IN THE VALUE OF EXTRACTED PARAMETERS FROM SIMULATED AND FIELD RECORDS AT SHAHPUR
P_s	MD_k	MD_k
T_w	MD_{II}	MD_k
T_D	MD_k	MD_{II}
P_v	MD_k	MD_k
P_d	MD_k	MD_{II}
T_{ARAF}	MD_{II}	MD_{II}
R_{st}	MD_k, MD_{II}	MD_k, MD_{II}
ACF_1	MD_k	MD_k
ACF_2	MD_k	MD_k
ACF_3	MD_{II}, MD_k	MD_k
ACF_4	MD_k, MD_{II}	MD_k, MD_{II}
ACF_5	MD_k	MD_k
ACF_6	MD_k	MD_k
ACF_7	MD_k	MD_{II}
ACF_8	MD_k	MD_{II}
ACF_9	MD_k	MD_k
ACF_{10}	MD_{II}	MD_k
F_p	MD_k	MD_k
F_1	MD_{II}, MD_k	MD_k
F_2	MD_k	MD_k
F_3	MD_k	MD_k
F_4	MD_k	MD_{II}
F_5	MD_k	MD_k
F_6	MD_k	MD_k

Table 6.13 Selection of dip and strike of rupture plane by comparing extracted parameter of simulated records at Dharamsala and Shahpur stations due to different models MD_u and MD_k of rupture planes shown in Fig 6.22 and 6.23, respectively.

MODEL NAME	MD ₁	MD ₂	MD ₃	MD ₁	MD ₂	MD ₃
STATION	DHARM	DHARM	DHARM	SHAH	SHAH	SHAH
P _s	124	159	154	147	221	189
T _s	3.1	.5	2.7	1.1	.8	.6
T _D	3.5	1.9	2.9	3.0	1.8	1.9
P _v	2.3	3.56	3.00	2.96	3.78	3.8
P _d	.07	.08	.106	.08	.03	.08
T _{ARAF}	7165	6080	6948	6822	6005	5813
R _s	.99	.99	.99	.99	.99	.99
ACF ₁	.029	.031	.032	.028	.027	.029
ACF ₂	.087	.094	.093	.082	.079	.086
ACF ₃	.134	.156	.156	.134	.130	.138
ACF ₄	.06	.06	.06	.06	.06	.06
ACF ₅	.424	.487	.477	.398	.368	.420
ACF ₆	-.498	-.428	-.427	-.575	-.666	-.538
ACF ₇	-.672	-.783	-.726	-.717	-.767	-.737
ACF ₈	-.672	-.783	-.726	-.712	-.767	-.737
ACF ₉	1.08	.92	1.00	1.03	.92	.99
ACF ₁₀	1.07	1.08	1.06	1.07	1.09	1.08
F _p	7.2	8.0	8.0	8.6	9.7	9.6
F ₁	7.7	8.0	7.9	8.5	8.9	7.8
F ₂	9.9	8.6	8.5	9.4	9.5	9.6
F ₃	11.0	9.2	10.2	10.9	10.5	10.5
F ₄	7.0	7.1	6.8	8.3	8.7	7.5
F ₅	8.4	8.1	8.1	8.1	9.7	9.4
F ₆	9.9	9.1	9.5	9.1	9.7	10.0

Table 6.14 Feature Extracted from simulated records at Shahpur and Dharamsala stations for three different models MD₁, MD₂ and MD₃ of rupture planes along Drini Thrust shown in Fig 6.24.

PARAMETERS	MODEL GIVING LEAST DIFFERENCE IN THE VALUE OF EXTRACTED PARAMETERS FROM SIMULATED AND FIELD RECORDS AT DHARAMSALA	MODEL GIVING LEAST DIFFERENCE IN THE VALUE OF EXTRACTED PARAMETERS FROM SIMULATED AND FIELD RECORDS AT SHAHPUR
P_s	MD ₂	MD ₂
T_u	MD ₂	MD ₃
T_D	MD ₃	MD ₃
P_v	MD ₂	MD ₂
P_d	MD ₃	MD ₁ , MD ₃
T_{ARAF}	MD ₁	MD ₁
R_u	MD ₁ , MD ₂ , MD ₃	MD ₁ , MD ₂ , MD ₃
ACF ₁	MD ₃	MD ₃
ACF ₂	MD ₂	MD ₃
ACF ₃	MD ₂ , MD ₃	MD ₃
ACF ₄	MD ₁ , MD ₂ , MD ₃	MD ₁ , MD ₂ , MD ₃
ACF ₅	MD ₁	MD ₃
ACF ₆	MD ₃	MD ₃
ACF ₇	MD ₁	MD ₁
ACF ₈	MD ₁	MD ₁
ACF ₉	MD ₁	MD ₂
ACF ₁₀	MD ₂	MD ₁
F_p	MD ₂ , MD ₃	MD ₁
F_1	MD ₃	MD ₃
F_2	MD ₃	MD ₁
F_3	MD ₃	MD ₂ , MD ₃
F_4	MD ₃	MD ₃
F_5	MD ₃	MD ₁
F_6	MD ₂	MD ₁

Table 6.15 Selection of possible location of rupture plane along identified causative fault on map, by comparing the extracted parameters of field records at Dharamsala and Shahpur stations with that of simulated records at these stations due to models MD₁, MD₂ and MD₃. Rupture plane is located at three different locations shown in Fig 6.24.

MODEL NAME	MD _{n1}	MD _{n2}	MD _{n3}	MD _{n4}	MD _{n5}	MD _{n6}
P _s	154	144	161	151	194	120
T _{st}	2.7	3.3	1.0	2.8	1.0	1.3
T _D	2.9	4.4	2.9	3.9	1.9	1.4
P _v	3.9	3.0	3.2	2.7	3.7	2.8
P _d	.106	.100	.101	.108	.105	.102
T _{ARAF}	6948	9021	7036	7999	6033	4698
R _{st}	.99	.99	.99	.99	.99	.99
ACF ₁	.031	.020	.033	.030	.030	.030
ACF ₂	.093	.089	.09	.09	.09	.09
ACF ₃	.156	.166	.140	.150	.150	.159
ACF ₄	.060	.06	.06	.06	.06	.06
ACF ₅	.477	.435	.45	.456	.474	.44
ACF ₆	-.427	-.495	-.45	-.466	-.439	-.430
ACF ₇	-.726	-.700	-.700	-.730	-.769	-.608
ACF ₈	-.726	-.700	-.700	-.730	-.769	-.608
ACF ₉	1.00	1.03	1.09	.99	.93	1.12
ACF ₁₀	1.05	1.069	1.08	1.06	1.08	1.07
F _p	8.0	9.8	9.1	8.7	8.0	7.0
F ₁	7.9	7.8	7.6	7.8	7.8	7.1
F ₂	8.5	9.1	9.0	8.9	8.5	9.3
F ₃	10.2	11.1	10.1	10.5	9.6	11.5
F ₄	6.8	7.3	7.1	7.2	7.5	6.9
F ₅	8.1	8.4	8.6	8.6	8.1	8.1
F ₆	9.5	10.3	9.8	9.8	9.8	10.9

Table 6.16 Feature extracted from simulated records at Dharamsala station for six different location of nucleation point or starting point of rupture within the rupture plane. The rupture models differ from each other only in the location of nucleation point. These models are named as MD_{n1}, MD_{n2}, MD_{n3}, MD_{n4}, MD_{n5} and MD_{n6}. Location of nucleation points and simulated acceleration records at Dharamsala station are shown in Fig 6.25.

MODEL NAME	MD _{n1}	MD _{n2}	MD _{n3}	MD _{n4}	MD _{n5}	MD _{n6}
P _a	189	154	202	160	126	175
T _u	.6	.8	1.8	1.9	2.0	1.1
T _D	1.9	2.9	2.3	4.3	3.7	1.8
P _v	3.8	3.1	3.8	3.4	2.6	2.9
P _d	.08	.10	.11	.11	.086	.075
T _{ARAF}	5813	7799	6462	10006	8395	6526
R _u	.99	.99	.99	.99	.99	.99
ACF ₁	.029	.030	.020	.029	.029	.027
ACF ₂	.096	.093	.088	.089	.088	.079
ACF ₃	.138	.173	.136	.156	.140	.128
ACF ₄	.06	.06	.06	.06	.06	.06
ACF ₅	.420	.429	.43	.436	.442	.372
ACF ₆	-.538	-.452	-.499	-.496	-.499	-.637
ACF ₇	-.737	-.715	-.690	-.715	-.734	-.736
ACF ₈	-.737	-.715	-.690	-.715	-.734	-.736
ACF ₉	.99	.99	1.06	1.00	1.00	.99
ACF ₁₀	1.08	1.08	1.08	1.07	1.05	1.07
F _p	9.6	7.6	9.2	8.1	9.4	10.4
F ₁	7.8	7.5	7.9	7.9	7.8	9.4
F ₂	9.6	8.6	9.3	9.0	9.4	10.1
F ₃	10.5	10.9	10.8	11.2	10.3	10.5
F ₄	7.5	7.1	6.7	7.4	7.3	7.7
F ₅	9.4	8.0	9.0	8.6	8.9	9.8
F ₆	10.0	10.1	10.6	10.1	9.9	10.5

Table 6.17 Feature extracted from simulated records at **Shahpur** station for six different location of nucleation point or starting point of rupture within the rupture plane. The rupture models differ from each other only in the location of nucleation point. These models are named as MD_{n1}, MD_{n2}, MD_{n3}, MD_{n4}, MD_{n5} and MD_{n6}. Location of nucleation points and simulated acceleration records at Shahpur station are shown in Fig 6.25.

PARAMETERS	MODEL GIVING LEAST DIFFERENCE IN VALUE OF EXTRACTED PARAMETER FROM SIMULATED AND FIELD RECORDS AT DHARAMSALA	MODEL GIVING LEAST DIFFERENCE IN THE VALUE OF EXTRACTED PARAMETER FROM SIMULATED AND FIELD RECORDS AT SHAHPUR
P_s	MD_{n5}	MD_{n3}
T_{s1}	MD_{n3}, MD_{n5}	MD_{n5}
T_D	MD_{n4}	MD_{n3}
P_v	MD_{n5}	MD_{n3}
P_d	MD_{n4}	MD_{n3}, MD_{n4}
T_{ARAF}	MD_{n4}	MD_{n4}
R_{at}	$MD_{n1}, MD_{n2}, MD_{n3}, MD_{n4}, MD_{n5}, MD_{n6}$	$MD_{n1}, MD_{n2}, MD_{n3}, MD_{n4}, MD_{n5}, MD_{n6}$
ACF_1	MD_{n3}	MD_{n2}
ACF_2	MD_{n1}	MD_{n2}
ACF_3	MD_{n2}	MD_{n2}
ACF_4	$MD_{n1}, MD_{n2}, MD_{n3}, MD_{n4}, MD_{n5}, MD_{n6}$	$MD_{n1}, MD_{n2}, MD_{n3}, MD_{n4}, MD_{n5}, MD_{n6}$
ACF_5	MD_{n1}	MD_{n5}
ACF_6	MD_{n1}	MD_{n2}
ACF_7	MD_{n6}	MD_{n3}
ACF_8	MD_{n6}	MD_{n3}
ACF_9	MD_{n3}	MD_{n3}
ACF_{10}	MD_{n3}	MD_{n3}
F_p	MD_{n5}	MD_{n4}
F_1	MD_{n6}	MD_{n2}
F_2	MD_{n5}	MD_{n2}
F_3	MD_{n3}	MD_{n4}
F_4	MD_{n1}	MD_{n3}
F_5	MD_{n6}	MD_{n2}
F_6	MD_{n1}	MD_{n4}

Table 6.18 Selection of possible location of nucleation point by comparing extracted parameter of simulated records at Dharamsala and Shahpur stations, for six different models of rupture plane having different positions of nucleation point within the rupture plane.

STATION	GEOGRAPHICAL COORDINATES				ELEVATION (M)	COORDINATE IN RECTANGULAR COORDINATE SYSTEM IN KM
	LATITUDE D	LATITUDE M	LONGITUDE D	LONGITUDE M		
Bandlakhas	32	08	76	32	1800	(-18.0,-9.3,-1.1)
Baroh	32	00	76	19	720	(-14.3,12.1,0.0)
Bhawarana	32	03	76	30	500	(-23.4,-1.0,0.3)
Dharamsala	32	13	76	19	1400	(1.5,-3.1,-0.6)
Jawali	32	09	76	01	550	(16.2,19.6,0.2)
Kangra	32	06	76	16	950	(-3.97,9.6,-0.2)
Nagrota Bagwan	32	06	76	23	800	(-11.2,1.8,0.0)
Shahpur	32	13	76	11	700	(10.0,4.6,0.0)
Sihunta	32	18	76	05	1000	(22.1,5.3,-0.2)

Table 6.19 Selected observation points with geographical coordinates, elevation and coordinate in rectangular three dimensional coordinate system. Geographical coordinates and elevation of stations had been taken from Chandrasekaran and Das (1992b). The origin of the coordinate system is defined by O_3 on map. Fig 6.26 shows location of these selected observation points and assumed three dimensional coordinate system on map.

PARAMETER	SHAH	DHARM	KANGR	SIHUN	NAG BAG	BAROH
P_s	202	166	153	157	140	101
T_{s1}	1.8	1.0	3.4	1.6	2.6	2.1
T_D	2.3	2.9	3.8	2.3	4.0	4.5
P_v	3.8	3.5	2.8	3.3	3.0	2.6
P_d	.11	.09	.09	.08	.09	.08
T_{ARAF}	6462	7868	9293	5856	8638	8238
R_{s1}	.99	.99	.99	.99	.99	.99
ACF_1	.029	.03	.029	.03	.029	.03
ACF_2	.088	.09	.088	.089	.086	.093
ACF_3	.136	.148	.144	.132	.134	.203
ACF_4	.06	.06	.06	.06	.06	.06
ACF_5	.433	.456	.442	.438	.415	.455
ACF_6	-.499	-.458	-.507	-.467	-.514	-.455
ACF_7	-.69	-.717	-.766	-.660	-.666	-.674
ACF_8	-.69	-.717	-.766	-.660	-.666	-.674
ACF_9	1.06	1.01	.963	1.108	1.088	1.065
ACF_{10}	1.09	1.082	1.069	1.078	1.059	1.061
F_p	9.2	9.1	8.7	6.1	11.1	7.4
F_1	7.9	7.6	7.9	8.4	7.5	7.3
F_2	9.3	9.0	8.9	9.3	9.5	9.4
F_3	10.8	10.2	10.3	10.7	11.1	10.8
F_4	6.7	7.1	7.6	6.3	7.3	6.9
F_5	9.0	8.6	8.7	8.7	9.1	8.4
F_6	10.6	9.8	10.0	10.4	10.9	9.8

Table 6.20 Feature extracted from simulated records at different stations for Dharamsala earthquake of 26th April, 1986. Simulated records are shown in Fig 6.27, 6.28 and 6.29.

PARAMETERS	BHAWAR	BANDLA	JAWALI
P_a	117	132	177
T_{at}	1.9	2.1	1.5
T_D	4.2	4.1	2.9
P_v	2.1	2.8	3.5
P_d	.06	.09	.144
T_{ARAE}	9166	8593	7385
R_{at}	.99	.99	.99
ACF_1	.028	.029	.029
ACF_2	.080	.098	.095
ACF_3	.132	.143	.139
ACF_4	.06	.06	.06
ACF_5	.375	.435	.417
ACF_6	-.623	-.492	-.544
ACF_7	-.729	-.692	-.726
ACF_8	-.729	-.692	-.726
ACF_9	1.018	1.049	1.014
ACF_{10}	1.063	1.056	1.086
F_P	8.9	9.5	9.6
F_1	8.5	7.9	8.2
F_2	10.1	9.4	9.5
F_3	10.9	10.8	10.7
F_4	8.2	6.7	9.7
F_5	9.4	9.2	9.0
F_6	10.7	9.8	10.5

Table 6.21 Feature extracted from simulated records at different stations for Dharamsala earthquake of 26th April, 1986. Simulated records are shown in Fig 6.27, 6.28 and 6.29.

CHAPTER 7

UTTARKASHI EARTHQUAKE OF 20TH OCTOBER, 1991

The Himalayan region is known not only for its lofty peaks and beautiful valleys but also for devastating earthquakes that the region experiences from time to time. Fig 7.1 shows the recent seismic events that have occurred in the Uttarakhand and surrounding regions of Uttar Pradesh. The epicenter of these events are give Table 7.1 (USGS-NEIS, 1990). Several rivers originate in this region and hence the area has vast potential for generation of hydroelectricity. This area has attracted not only seismologist but also planners and engineers, because of this reason it is utmost important that the seismicity of this region is well studied to enable engineers to design structures which will be able to withstand any future events.

The Uttarkashi region was rocked by a moderately strong earthquake ($M_b = 6.5$) in the early hours of October, 20, 1991. Herein after referred to as the Uttarkashi earthquake. It is one of the few Indian earthquakes for which strong motion data is available. In the present work the most probable causative fault for this earthquake has been identified with the help of available data and rupture plane along this identified fault has been modelled to simulate strong motion records.

7.1 STRONG MOTION ARRAY

Under a project entitled "Strong Motion Array" of The Himalayan Seismicity project, the Department of Earthquake Engineering, University of Roorkee, Roorkee has installed and operated a Strong motion array in the Uttarkashi and adjoining region. Upto October 1991, 28 out of planned 40 station in the array had been installed. Locations of these stations is shown in Fig 7.2. Each station consists of a three component strong motion analog accelerograph, SMA-1 of M/S Kinemetrics, U.S.A. (Chandrasekaran and Das, 1991).

Of the 28 stations where strong motion recorders have been installed in the region, 13 recorded the Uttarkashi earthquake of 20th October, 1991. At 13 other stations, the instruments were found to be functional but the instruments were not triggered as the intensity of ground shaking was lower than threshold level of starter at those sites (Starting level is 1% of g, Chandrasekaran and Das, 1991). At other two stations, the power supply had malfunctioned. The available strong motion data from these stations is used to compare the simulated strong motion records with the field records.

7.2 SALIENT FEATURES OF THE UTTARKASHI EARTHQUAKE OF 20TH OCTOBER, 1991

At 02:53 hrs (IST) on October 20, 1991 a moderately strong earthquake of body wave magnitude 6.5 occurred in Uttarkashi region in the state of Uttar Pradesh, India. Parameters of this earthquake as reported by United State Geological Survey (PDE, 1991) are as follows:

Origin Time : Oct 20, 1991	02 Hr 30 Min 15.1 Sec (IST)
Epicenter	30.73°N, 78.77°E
Focal Depth	19 km
M_b	6.5
M_s	7.1

Parameters of this earthquake as given by other agencies are given in Table 7.2. Fault plane solutions for this earthquake as reported by different agencies are given in Table 7.3. The source parameters of this earthquake are given by Dziewonski et al. (1992), Kamble (1992a and 1992b), PDE (1991) and Rastogi (1992b). Destruction due to Uttarkashi earthquake and the causative fault responsible for it was investigated by Saklani (1992), Chadha (1992), Narula et al. (1992), Sinvhal et al. (1992), Kumar and Mahajan (1994), Gupta et al. (1994) and Thakur and Kumar (1994). Study of strong motion data for the Uttarkashi earthquake has been done by Chandra et al. (1992), Chandrasekaran and Das (1991, 1992c) and Singh and Prasad (1992). Aftershocks sequence of the Uttarkashi earthquake had been studied by Kayal et al. (1992) and Kamble (1992b). The isoseismal map for this earthquake has been prepared by Sinvhal et al. (1992), Kumar and Mahajan (1994) and Thakur and Kumar (1994). Tectonics of the region around Uttarkashi has been studied by Jain (1987), Purohit et al. (1990) and Agarwal and Kumar (1973).

Isoseismal map for this earthquake prepared on the basis of field survey (Sinvhal et al., 1992) is shown in Fig 7.3.

7.3 IDENTIFICATION OF MOST PROBABLE CAUSATIVE FAULT

Most probable causative fault for the Uttarkashi earthquake is identified on the basis of :

- (i) Isoseismal map of Uttarkashi earthquake of 20th October, 1991
- (ii) Tectonic maps of region (After Jain, 1987 and Purohit et al. 1990)
- (iii) Aftershock location map
- (iv) Isoacceleration map for Uttarkashi earthquake of 20th October 1991 (Data taken from Chandrasekaran and Das (1991, 1992c).

7.3.1 TECTONIC MAP OF THE REGION AROUND UTTARKASHI (JAIN, 1987)

Tectonic map of the region around Uttarkashi prepared by Jain (1987) (Fig 7.4 and 7.5) have been used for the identification of most probable causative fault on map. The region contains number of lineaments and prominent feature in this region is the Main Central Thrust (MCT) and its intersection with other lineaments nearby Bhatwari.

7.3.2. TECTONIC MAP (PUROHIT ET AL., 1990)

The area has also been mapped by Purohit et al., (1990) and is shown in Fig 7.6. In order to correlate the identified most probable causative fault with the mapped fault in the region, the map prepared by Purohit et al., (1990) and Jain (1987) have been used as complementary to each other. Major lineaments in the region are MCT-I (Chail thrust), MCT-II (Jutogh thrust) and MCT-III (Vaikrita thrust). It is seen that all major lineaments strike NW and dip towards northeast.

7.3.3. LOCATION OF AFTERSHOCKS MAP

Aftershock location map (Fig 7.7) is prepared using data (Kayal et al., 1992) given in Table 7.4. It is seen from this map that the cluster of aftershocks lie almost at the eastern side of Bhatwari and Uttarkashi, where maximum damage has taken place. This cluster is observed at a point where MCT intersects with other lineaments or faults in this area. There is some discrepancy in the location of the epicenter of main shock as reported by various agencies. However, all reported epicenters for main shocks of Uttarkashi earthquake lie within the region of aftershocks of this earthquake.

7.3.4 ISOACCELERATION MAP

The observed resultant value of horizontal peak acceleration for Uttarkashi earthquake at each of the thirteen stations where the accelerographs were triggered (Chandrasekaran and Das, 1991, 1992c) are given in Table 7.5. These values are plotted in map on a scale 1:250,000. From these plotted values of peak horizontal acceleration, isoacceleration contours are drawn with a contour interval of 100 cm/sec^2 . The maximum and minimum peak acceleration contour value are 300 cm/sec^2 and 100 cm/sec^2 . Irregular pattern of isoacceleration contour is seen from isoacceleration map in Fig 7.8. This may be due to inadequate coverage as discussed in detail in Chapter 10. The direction of major axis of isoacceleration contour is $N50^\circ W$. Epicenter E_{u1} , E_{u2} and E_{u3} lie within the isoacceleration contour of 200 cm/sec^2 .

7.3.5 SUPERIMPOSED MAP OF ISOACCELERATION CONTOURS, AFTERSHOCK LOCATION, MEIZOSEISMAL AREA AND TECTONICS OF THE AREA

Composite map containing resultant horizontal peak isoacceleration contours, aftershock region, meizoseismal area and the tectonics of the region (Fig 7.9) shows that contours of peak acceleration having value 300 cm/sec is close to the cluster of aftershocks. While peak acceleration contours of value 200 cm/sec² covers entire aftershock region. Southern part of meizoseismal area lie inside aftershock region. The map indicates that most lineaments inside aftershock zone strikes NW, and there is a cluster of aftershocks at the intersection of lineaments marked as a point O on the map.

7.3.6 IDENTIFICATION OF MOST PROBABLE CAUSATIVE FAULT FOR THE UTTARKASHI EARTHQUAKE

A perusal of composite map indicates that :

- (i) Area containing aftershock zone also cover area of maximum isoacceleration contours. Southern part of meizoseismal area lies inside the aftershocks zone. It is hence logical to suppose that causative fault for Uttarkashi earthquake should also lie inside this aftershocks zone.
- (ii) Major faults and lineaments inside aftershock zone dip in the northeastern side. Epicenter of this earthquake given by different agencies lie at the eastern side of these faults and lineaments. This suggests that the hypocenter of this

earthquake could lie in the downward extension of one of these faults or lineaments.

- (iii) Cluster of aftershocks at point O is seen. At this point two faults intersect, as shown in Fig 7.7. Point O can hence be assumed as one of the corner of rupture plane along the identified causative fault.
- (iv) The identified probable causative fault marked as Lineament-U1 on the tectonic map of Jain (1987) is shown in Fig 7.10. This identified fault corresponds to the MCT-1 of Purohit et al., (1990) shown in Fig 7.11.
- (v) Trend of isoseismals is nearly 320° and it follows the strike of MCT-1 in this area. The meizoseismal area lies at a distance of 5 km from point O.
- (vi) The fault identified as MCT -1 (Shown in Fig 7.10 and 7.11) passes in southern direction from point O. Fault plane solutions for the Uttarkashi earthquake reveal that thrust movement along shallow plane dipping towards northeast is responsible for this earthquake (Rastogi, 1992b). MCT -1 also intersects with the two other faults at point O shown in Fig 7.5. The point of intersection can be assumed as point from where the rupture could initiate. The strike of MCT-1 calculated from Fig 7.11 is $N15^\circ W$.
- (vii) Table 7.2 shows that the hypocentral depth given by Kamble (1992a) as 12 km coincides approximately with the estimated depth of MCT from the depth section (Kayal, 1994) below the epicenter of this earthquake.

(viii) The depth section in this region (Seeber, 1981 and modified after Kayal, 1994) is shown in Fig 7.12. This model indicates that the main shock of the Uttarkashi earthquake occurred at the juncture of MCT and Basement thrust (Kayal, 1994). The estimated hypocenter depth for this earthquake by Kamble is 12 km and fault plane solution for this earthquake indicates that the causative fault could be nearly horizontal fault.

The above observations suggest that the rupture plane within the identified causative fault for the Uttarkashi earthquake could lie at a depth of 12 km below the point O shown in Fig 7.10. The model of the rupture plane in the depth section is shown in Fig 7.12.

7.4 SELECTION OF OBSERVATION POINTS

The Uttarkashi earthquake was recorded at thirteen strong motion recording stations. Maximum peak acceleration of 303 cm/sec^2 is recorded on horizontal component in $N75^\circ W$ direction at station Uttarkashi which lies at an epicentral (Epicenter E_{U1}) distance of 31 km. Maximum vertical acceleration of 288 cm/sec^2 is recorded at Bhatwari which lies at an epicentral distance of 22 km.

Twenty four features (as explained in Chapter 4) given in Table 7.6 to 7.12 were extracted from the acceleration records at these thirteen stations. The field acceleration records, their autocorrelation function, power spectrum, cumulative power spectrum and frequency weighted power spectrum are shown in Fig 7.13 to 7.51.

From these tables, the component of acceleration record at a station which gives maximum value parameter T_{area} has been used for comparison with the simulated acceleration record at the same station. The following table gives the component of acceleration record selected for comparison with the simulated record at the same station.

STATION	COMPONENT OF ACCELERATION RECORD SELECTED FOR COMPARISON
Almora	Transverse
Barkot	Longitudinal
Bhatwari	Transverse
Ghansiali	Longitudinal
Karnprayag	Longitudinal
Kosani	Transverse
Koteshwar	Longitudinal
Koti	Transverse
Purola	Transverse
Rudrprayag	Longitudinal
Srinagar	Longitudinal
Tehri	Transverse
Uttarkashi	Transverse

7.5 MODELLING PARAMETERS OF THE RUPTURE PLANE

After identification of the most probable causative fault for the Uttarkashi earthquake rupture along the portion of identified fault is modelled to simulate synthetic records at selected observation points which contain field records. The position of

rupture plane along this identified fault is shown in Fig 7.12. Various modelling parameters of rupture plane used in modelling are discussed in the following sections.

7.5.1 LENGTH OF RUPTURE PLANE (L)

Several relations are available to calculate the rupture length from the magnitude for a given earthquake. Assuming the body wave magnitude of the Uttarkashi earthquake as 6.5 (USGS), the rupture lengths as calculated using different empirical relations, is given in the following table.

S.NO.	RUPTURE LENGTH (KM)	RUPTURE LENGTH CALCULATED USING EMPIRICAL RELATIONS GIVEN BY
1.	42	Araya and Kiureghian (1988)
2.	32	Otsuka (1965)
3.	Lower limit = 30 Higher limit = 60	Naeim (1989)

A rupture length of 42 km obtained by (1) has been used for modelling the rupture plane. This length lies within the lower and upper limit of rupture length specified by Naeim (1989).

7.5.2 DOWNWARD EXTENSION OF RUPTURE PLANE (D)

Downward extension of rupture plane is calculated using expression 2.8 given in Chapter 2. For a surface wave magnitude of 7.1 (PDE, 1991) downward extension (D) is calculated as 29 km.

7.5.3 LENGTH OF ELEMENT (L)

Length of element for simulation procedure is assumed to be 1 km. The length of the rupture plane is 42 km hence total number of elements along the length are 42. and the total number of elements within the entire rupture plane are 29×42 i.e. 1218.

7.5.4 THREE DIMENSIONAL COORDINATE SYSTEM

The assumed rectangular system is defined in Section 2.2.5. For the Uttarkashi earthquake the rupture plane is located at a vertical depth of 12 km below the point O. The geographical coordinates of point O are 30.75°N , 78.63°E and this point is at a distance of 6 km from Bhatwari station. The X and Y coordinates of recording stations are calculated from the point O shown in Fig 7.10. X and Y axes follows the strike and dip direction of rupture plane, respectively.

The entire rupture plane is mapped on three dimensional rectangular system by taking elevation of the recording stations into consideration. In this case Z axis is assumed to be positive downwards. The depth of origin of this system is 12.5 km from surface of the earth.

7.5.5 SOURCE WAVELET

The form of source wavelet used for generating synthetic records is shown in Fig 2.4 and 2.5 and is same as used for modelling the Dharamsala earthquake. Frequency of emitted source wavelet for this earthquake has been taken as 2.5 Hz. Normalised

value of the source wavelet is scaled by a factor of 1.4 cm/sec which is explained in detail in Section 3.1.

7.5.6 VELOCITY OF THE MEDIUM (V)

Velocity model for the Uttarkashi region used for the present work is given in the following table (Kamble, 1992a and 1992b) :

VELOCITY (KM/SEC)	THICKNESS OF LAYER (KM)
5.72	Surface - 24
6.61	24 - 45
8.22	>45

The rupture plane lies at a depth of 12 km and hence 5.72 km/sec has been used as the velocity of the medium.

7.5.7 GEOMETRY OF RUPTURE PROPAGATION WITHIN RUPTURE PLANE AND RUPTURE VELOCITY (V_r)

Radial type of geometry of rupture propagation is used in the simulation procedure and is discussed in detail in Section 2.2.9. The rupture velocity is assumed as 80% of velocity of S wave in the medium. The velocity of P wave is 5.72 km/sec in the region (Kamble, 1992a). The S wave velocity in the medium is 3.30 km/sec, hence rupture velocity is assumed as 2.64 km/sec.

The modelling parameters of rupture plane along the identified causative fault for the Uttarkashi earthquake which are assumed as initial parameters are given as :

SN	Parameter	Value	SN	Parameter	Value
1	L (Length of rupture plane)	42.0 km	6	Rupture Velocity	2.64 km/sec
2	D (Downward extension of rupture plane)	29.0 km	7	Velocity of the medium	5.72 km/sec
3	L_e (Length of element)	1.0 km	8	δ (Dip of the rupture plane)	14°
4	N (Total number of elements)	1218	9	ϕ (Strike of the rupture plane)	317°
5	Depth of Rupture plane	12 km			

These are initial modelling parameters of rupture plane. Other parameters have been selected by iteratively modelling the rupture plane and comparing extracted parameters from simulated records with those from field records. The parameters that have been selected by iteratively modelling the rupture plane are (i) Dip (δ) and strike (ϕ) of rupture plane and (ii) Starting point or nucleation point within the rupture plane. The procedure of selection of these parameters is discussed in detail in following sections.

7.5.8 SELECTION OF DIP (δ) AND STRIKE (ϕ) OF THE RUPTURE PLANE

The dip and strike of the modelled rupture plane is based on the fault plane solutions available for the Uttarkashi earthquake. The dip and strike of the two available

fault plane solutions are given as below :

S.No.	Strike (ϕ)	Dip (δ)	Reference
1.	317°	14°	Dziewonski et al. 1992
2.	296	5°	(USGS)

Two different models of rupture plane viz., MU_{d1} and MU_{d2} are based on the dip and strike given in above table. Starting point of rupture for these models is assumed as that element which coincides with the hypocenter of this earthquake (E_{U3}) given by Kamble (1992a). Rupture plane is placed at a depth of 12 km from point O. The modelling parameters of the two models of the rupture plane are computed on the basis of procedures explained in Section 7.5. These parameters are given in tabular form as:

Model Name → /Parameter	MU_{d1}	MU_{d2}
L (km)	42	42
D (km)	29	29
δ (degree)	14°	5°
ϕ (degree)	317°	296°
L_e (km)	1	1
Coordinates of nucleation point	(14.0,16.5,4.1)	(19.0,9.9,0.8)
V (km/sec)	5.72	5.72
V_r (km/sec)	2.64	2.64

Direction of strike and dip of rupture plane is different for model MU_{d1} and MU_{d2} , therefore the X and Y axes of assumed coordinates system will follow different directions. Coordinates of stations computed for assumed rectangular coordinate system will also be different for these two different models. Records are simulated at Bhatwari and Uttarkashi stations. These are the two nearest stations in the strong motion network from epicenter E_{U3} . The coordinate of Uttarkashi and Bhatwari for two different models are given as:

Model Name	Coordinates of Uttarkashi	Coordinates of Bhatwari
MU_{d1}	(-11.2,-14.0,-11.9)	(-5.5,2.7,-11.5)
MU_{d2}	(-16.0,-9.0,-11.9)	(-4.2,3.0,-11.5)

The extracted features from simulated records at these two different stations for models MU_{d1} and MU_{d2} are given in Table 7.13 and shown in Fig 5.52 and 7.53. Extracted parameters from simulated records due to models MU_{d1} and MU_{d2} at Bhatwari and Uttarkashi stations are compared with the field records at these two stations. Table 7.14 shows that for both Bhatwari and Uttarkashi stations model MU_{d1} shows least difference between the extracted parameters from simulated and field records. It is for this reason model MU_{d1} is selected for final modelling purposes. The amount of dip (δ) and strike (ϕ) of this rupture plane are 14° and 317° , respectively.

7.5.9 SELECTION OF STARTING POINT OF RUPTURE (OR NUCLEATION POINT) WITHIN THE RUPTURE PLANE

The starting point of rupture within the rupture plane for models MU_{d1} and MU_{d2} is assumed as that element which coincides with the hypocenter of the earthquake.

However, there is a possibility that starting point of rupture can be any other element within the rupture plane. This possibility is checked by assuming different elements within rupture plane as starting point of rupture. The modelling parameters of rupture plane are :

Parameter	Value	Parameter	Value
L (km)	42	L_c (km)	42
D (km)	29	V (km/sec)	5.72
δ	14°	V_r (km/sec)	2.64
ϕ	317°		

Six different elements within the rupture plane are assumed as the nucleation point giving rise to six different models identified as MU_{n1} to MU_{n6} . For first five models (MU_{n1} and MU_{n5}) assumed nucleation point lies at the center and different corners of the rupture plane and for sixth model it coincides with the hypocenter given by IMD. X, Y and Z coordinates of nucleation elements and the name of models are given below:

Coordinates of nucleation point within the rupture plane	Model Name
(0.0,0.0,0.0)	MU_{n1}
(0.0,27.1,6.7)	MU_{n2}
(41.0,0.0,0.0)	MU_{n3}
(41.0,27.0,6.7)	MU_{n4}
(20.0,12.6,3.1)	MU_{n5}
(14.0,16.5,4.1)	MU_{n6}

Coordinates of Uttarkashi and Bhatwari stations obtained by placing rectangular coordinate system at point O are given as:

Station Name	Coordinates in assumed rectangular coordinate system
Uttarkashi	(-11.2,-14.0,-11.9)
Bhatwari	(-5.5,2.7,-11.5)

Six records at both stations are simulated for models MU_{n1} , MU_{n2} , MU_{n3} , MU_{n4} , MU_{n5} and MU_{n6} . These records are shown in Fig 7.54. The features extracted from the simulated records for these six models at Bhatwari and Uttarkashi stations are given in Table 7.15 and 7.16. As the simulated records due to models MU_{n3} and MU_{n5} give values of peak acceleration at Uttarkashi less than that at Bhatwari, these models are rejected, since the observed value of peak acceleration at Uttarkashi is higher than that at Bhatwari. Table 7.17 shows the model which gives minimum difference in the value of the parameters extracted from field and simulated records at Uttarkashi and Bhatwari stations for models MU_{n1} , MU_{n2} , MU_{n4} and MU_{n6} . This table (Table 7.17) shows that for both Bhatwari and Uttarkashi stations model MU_{n4} shows least difference between the extracted parameters from simulated and field records. It is for this reason model MU_{n4} is selected for final modelling purposes. The depth of nucleation point or starting point of rupture for this model is 19 km from surface of the earth which coincides with the hypocentral depth of 19 km given by USGS (PDE).

7.6 SIMULATION OF STRONG MOTION RECORDS AT SELECTED OBSERVATION POINTS

The modelling parameters of the rupture plane along the identified probable causative fault are taken as :

SN	Parameter	Value	SN	Parameter	Value
1.	L (Length of rupture plane)	42.0 km	7.	Depth of Nucleation point	19 km
2.	D (Downward extension of rupture plane)	29.0 km	8.	Velocity of medium	5.72 km/sec
3.	L_e (Length of element)	1.0 km	9.	Rupture Velocity	2.64 km/sec
4.	N (Total number of elements)	1218	10.	δ (Dip of rupture plane)	14°
5.	Depth of Rupture plane	12 km	11.	ϕ (Strike of rupture plane)	317°
6.	X, Y and Z coordinates of nucleation point	(41.0, 27.1, 6.1)	12.	Location of origin of assumed system in map	O (on map)

The coordinates and locations of selected stations on the assumed rectangular coordinate system are shown in Table 7.18 and Fig 7.55, respectively. The extracted parameters from the simulated and field records are given in Table 7.6 to 7.12 and 7.19 to 7.21, respectively.

Simulated acceleration records, their autocorrelation function, power spectrum, cumulative power spectrum and frequency weighted cumulative power spectrum at different stations are shown in Fig 7.56 to 7.68.

7.7 COMPARISON OF FIELD AND SIMULATED RECORDS

At Bhatwari and Uttarkashi stations the trend of peak acceleration of simulated record matches with the peak acceleration observed in the field records as seen in the table below.

Station	Hypocentral Distance	Peak acceleration from simulated record (cm/sec ²)	Peak acceleration from field record (cm/sec ²)
Bhatwari	33	430	241
Uttarkashi	47	455	303

This table shows that the peak acceleration in the field record is more at Uttarkashi although it is at a greater distance from the starting point of rupture (hypocenter) as compared to Bhatwari. This trend is also observed in the simulated record. This can be due to the source directivity effect which has been earlier discussed in Chapter 6. The direction of the propagation of rupture from nucleation point is towards Uttarkashi.

The minimum and maximum value of parameters extracted from field and simulated strong motion records and the corresponding stations are given in the following table :

PARAMETER	FIELD RECORDS		SIMULATED RECORDS	
	MAXIMUM VALUE AND STATION	MINIMUM VALUE AND STATION	MAXIMUM VALUE AND STATION	MINIMUM VALUE AND STATION
P_a	303 cm/sec ² Uttarkashi	21.6 cm/sec ² Almora	469 cm/sec ² Purola	273 cm/sec ² Kosani
T_{at}	11 sec Kosani	.16 sec Koti	13.9 sec Karnprayag	2.1 sec Koti
T_d	25 sec Srinagar	5.4 sec Bhatwari	19.3 sec Kosani	7.3 sec Barkot
P_v	29.7 cm/sec Bhatwari	1.26 cm/sec Almora	14.0 Purola	8.2 Srinagar
P_d	5.3 cm Bhatwari	.45 cm Almora	.417 Uttarkashi	.222 Koteshwar
T_{area}	36945 Bhatwari	3562 Almora	52489 Kosani	31605 Bhatwari
R_{at}	1.029 Kosani	.98 Barkot	1.09 Srinagar	.980 Ghansiali

This table shows that in field as well as simulated records minimum value of extracted parameter T_{at} is observed at the same station.

The maximum and minimum values of the parameters extracted from autocorrelation function of field and simulated acceleration records and the corresponding station at which it is observed are given in following table :

PARAMETERS	FIELD RECORDS		SIMULATED RECORDS	
	MAXIMUM VALUE AND STATION	MINIMUM VALUE AND STATION	MAXIMUM VALUE AND STATION	MINIMUM VALUE AND STATION
ACF ₁	.325 Tehri	.027 Srinagar	.032 Bhatwari, Uttarkashi, Barkot, Ghansiali, Kosani, Almora, Tehri and Koti	.030 Srinagar
ACF ₂	.796 Tehri	.071 Srinagar	.095 Tehri, Ghansiali	.090 Uttarkashi
ACF ₃	1.298 Tehri	.114 Srinagar	.204 Rudraprayag	.104 Koti
ACF ₄	.36 Bhatwari	.04 Srinagar	.048 All	.048 All
ACF ₅	.93 Koti	.325 Srinagar	.295 Almora, Kosani	.225 Srinagar
ACF ₆	.753 Koti	-.527 Srinagar	-.570 Koti	-.699 Srinagar
ACF ₇	.654 Karnprayag	-.728 Rudrprayag	-.382 Koti	-.516 Kosani
ACF ₈	-.351 Almora	-.728 Rudrprayag	-.570 Koti	-.699 Srinagar
ACF ₉	2.75 Barkot	.798 Tehri	1.175 Tehri	1.028 Purola
ACF ₁₀	1.038 Bhatwari	1.016 Karnprayag	1.058 Bhatwari	1.020 Kosani

The table shows that the maximum and minimum value of parameters ACF₁ and ACF₆ are observed at same stations for both simulated and field records. Maximum value of parameters ACF₂ and ACF₁₀ is obtained at same station for both field and simulated records. Minimum value of parameter ACF₅ is observed also at same station

for both field and simulated records.

The maximum and minimum values of the extracted parameters from the power spectrum of field acceleration records and the stations at which it occurs are given in the following table.

PARAMETERS	FIELD RECORDS		SIMULATED RECORDS	
	MAXIMUM VALUE AND STATION	MINIMUM VALUE AND STATION	MAXIMUM VALUE AND STATION	MINIMUM VALUE AND STATION
F_p	1.4 Srinagar	1.0 Tehri	13.2 Rudraprayag	7.7 Tehri
F_1	9.6 Srinagar	2.3 Bhatwari	10.2 Purola	7.0 Koti
F_2	11.1 Srinagar	3.0 Karnprayag	11.2 Koti	8.8 Bhatwari
F_3	12.0 Srinagar	3.1 Koti	13.2 Rudraprayag	10.4 Uttarkashi
F_4	8.2 Srinagar	1.0 Tehri	8.5 Karnprayag	5.4 Uttarkashi
F_5	10.3 Srinagar	2.0 Tehri	10.9 Purola, Koti	8.7 Bhatwari and Srinagar
F_6	11.7 Srinagar	3.0 Koti	12.8 Rudraprayag	9.8 Bhatwari

The comparison shows that minimum value of parameter F_p occur at same station for both simulated and field records.

Following table shows the parameters and number of stations at which difference is less than 20% :

PARAMETER	NUMBER OF STATIONS HAVING DIFFERENCE LESS THAN 20%	PARAMETER	NUMBER OF STATIONS HAVING DIFFERENCE LESS THAN 20%
P_v	1	ACF_{10}	12
P_d	2	F_p	1
T_D	5	F_2	1
R_{at}	13	F_3	2
T_{area}	2	F_4	1
ACF_1	3	F_5	2
ACF_2	3	F_6	1
ACF_3	2		
ACF_4	2		
ACF_7	3		
ACF_8	4		
ACF_9	4		

The difference in the value of extracted parameters from simulated and field records can be due to those factors which have not been taken into accounts and have been discussed in detail in Chapter 10.

7.8 SUMMARY

In this chapter most probable causative fault for Uttarkashi is identified using the scheme discussed in Chapter 2. On the basis of available data as given in this chapter, MCT-1 is identified as the most probable causative fault for this earthquake. This fault

has been marked on the tectonic map of the region. By using depth section and location of hypocenter this fault is placed at a vertical depth of 12 km from surface of the earth. The rupture plane along the identified portion of the most probable causative fault is modelled to simulate strong motion records at thirteen observation points for which field records were available and 24 features have been extracted for comparison with field records. Final modelling parameters of rupture plane for the Uttarkashi earthquake of 20 Oct, 1991 are :

SN	PARAMETER	VALUE	SN	PARAMETER	VALUE
1.	L (Length of rupture plane)	42.0 km	7.	Depth of Nucleation point from surface of earth	19 km
2.	D (Downward extension of rupture plane)	29.0 km	8.	Velocity of medium	5.72 km/sec
3.	L_e (Length of element)	1.0 km	9.	Rupture Velocity	2.64 km/sec
4.	N (Total number of elements)	1218	10.	δ (Dip of rupture plane)	14°
5.	Depth of Rupture plane	12 km	11.	ϕ (Strike of rupture plane)	317°
6.	X,Y and Z coordinates of nucleation point in km	(41.0,27.1,6.7)	12.	Location of origin of assumed system in map	O (on map)

The strong motion records are simulated at all selected observation points and 24 features are extracted from the simulated records at these stations. The comparison of extracted parameters of field and simulated records shows that parameters P_v , P_d , T_D , R_{at} , T_{area} , ACF_1 , ACF_2 , ACF_3 , ACF_4 , ACF_7 , ACF_8 , ACF_9 , ACF_{10} , F_p , F_2 , F_3 , F_4 , F_5 and F_6 , differ less than twenty percent at various stations.

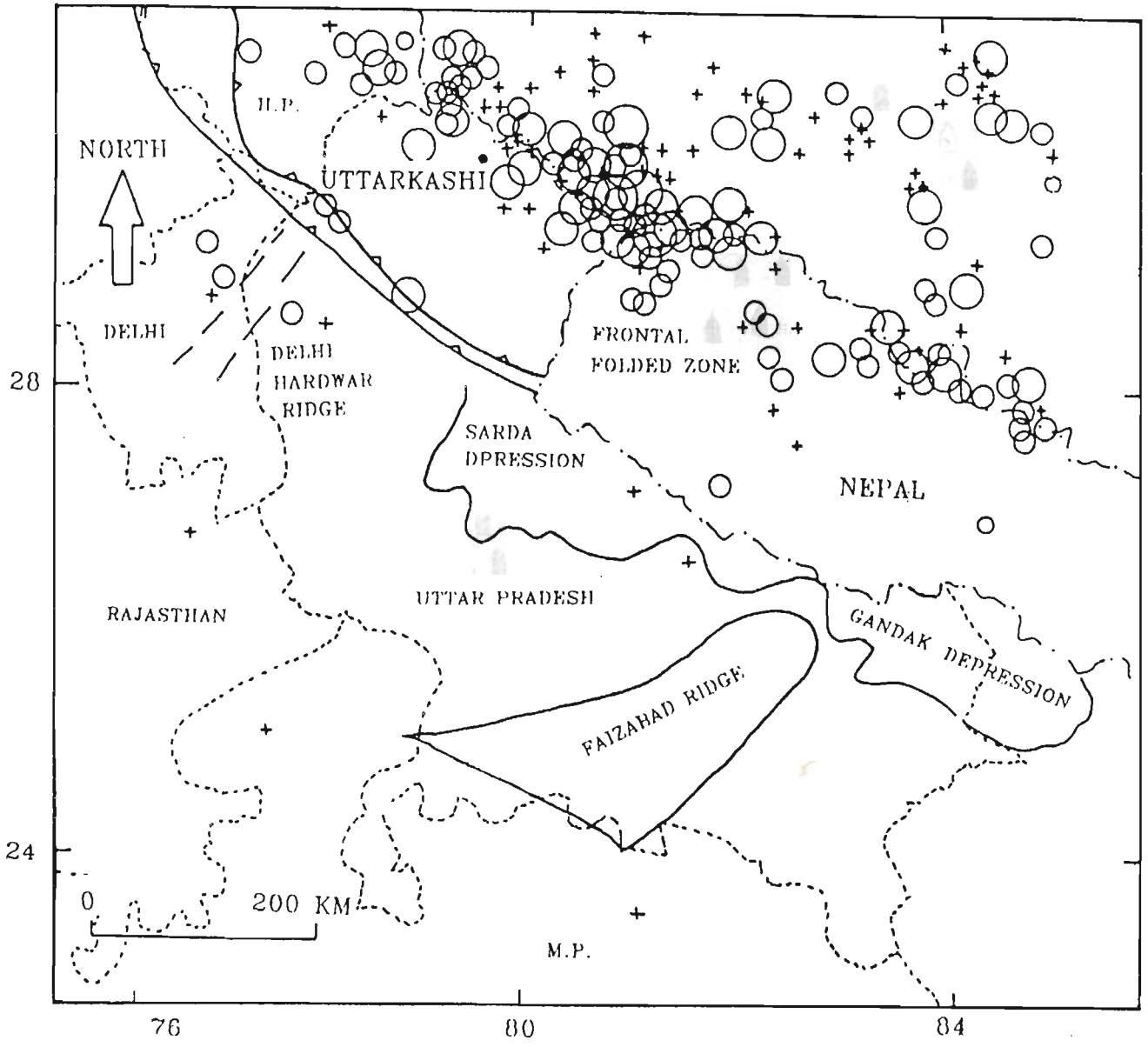


Fig 7.1 Location of epicenters in Uttarkashi and surrounding region. Epicentral data is taken from USGS-NEIC (1990) and reproduced in Table 7.1. The tectonics of the region is taken from Eremenko and Negi (1968).

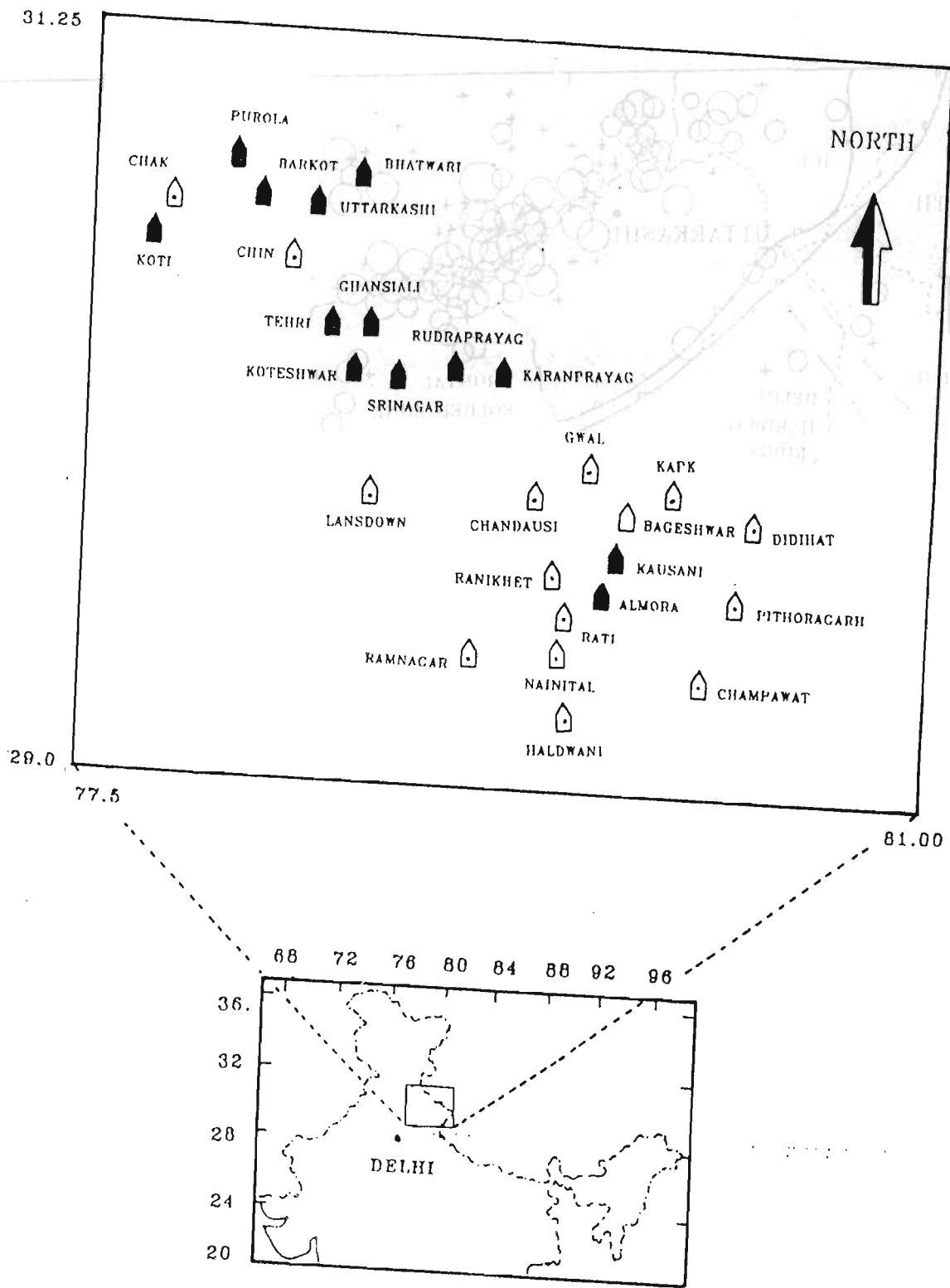


Fig 7.2 Location of recording stations of strong motion array in Uttarkashi region. The stations marked with black colour represent those which had recorded the Uttarkashi earthquake of 20th Oct, 1991.

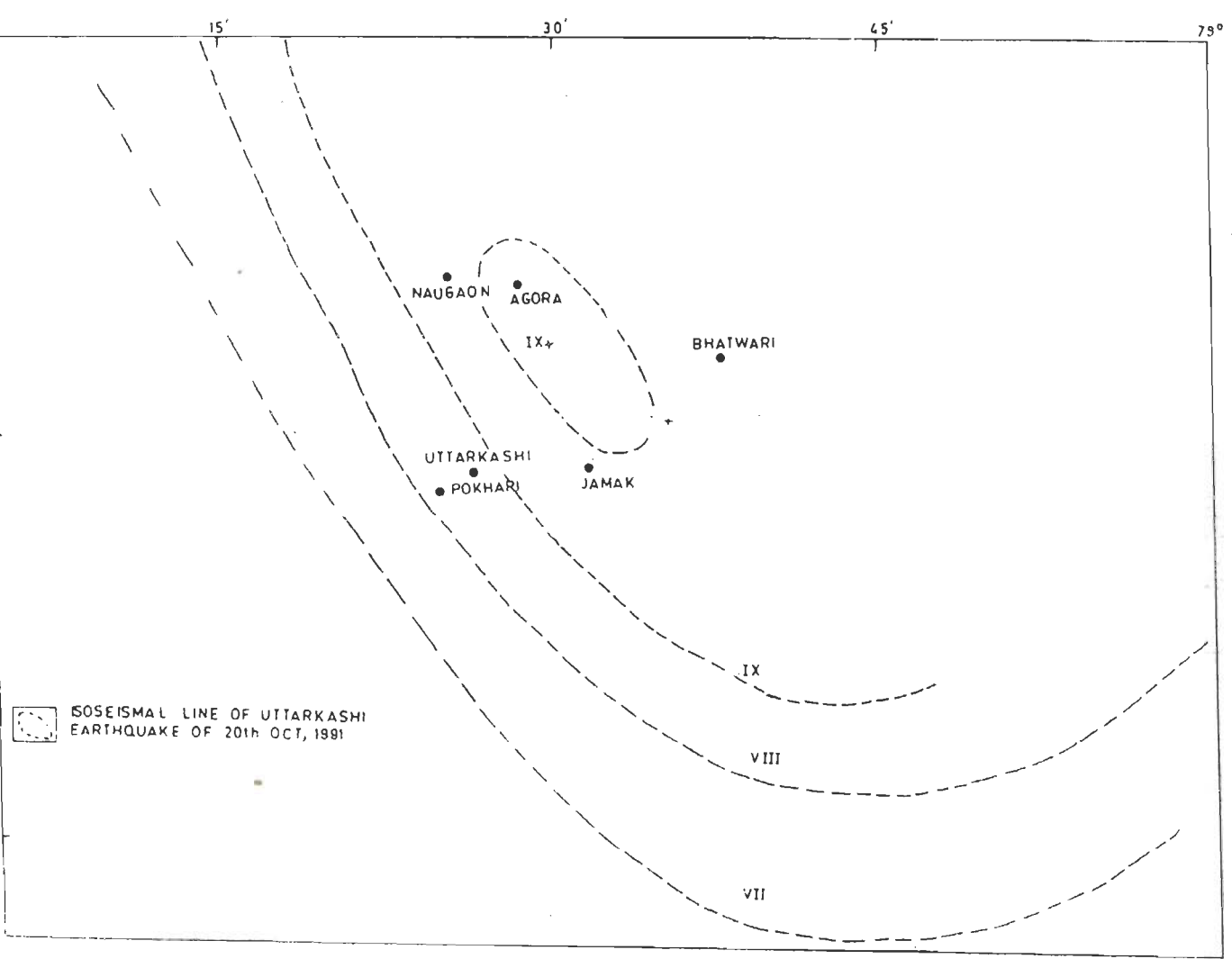


Fig 7.3 Isoseismal map of Uttarkashi earthquake of 20th October, 1991 (Sinvhal et al. 1992).

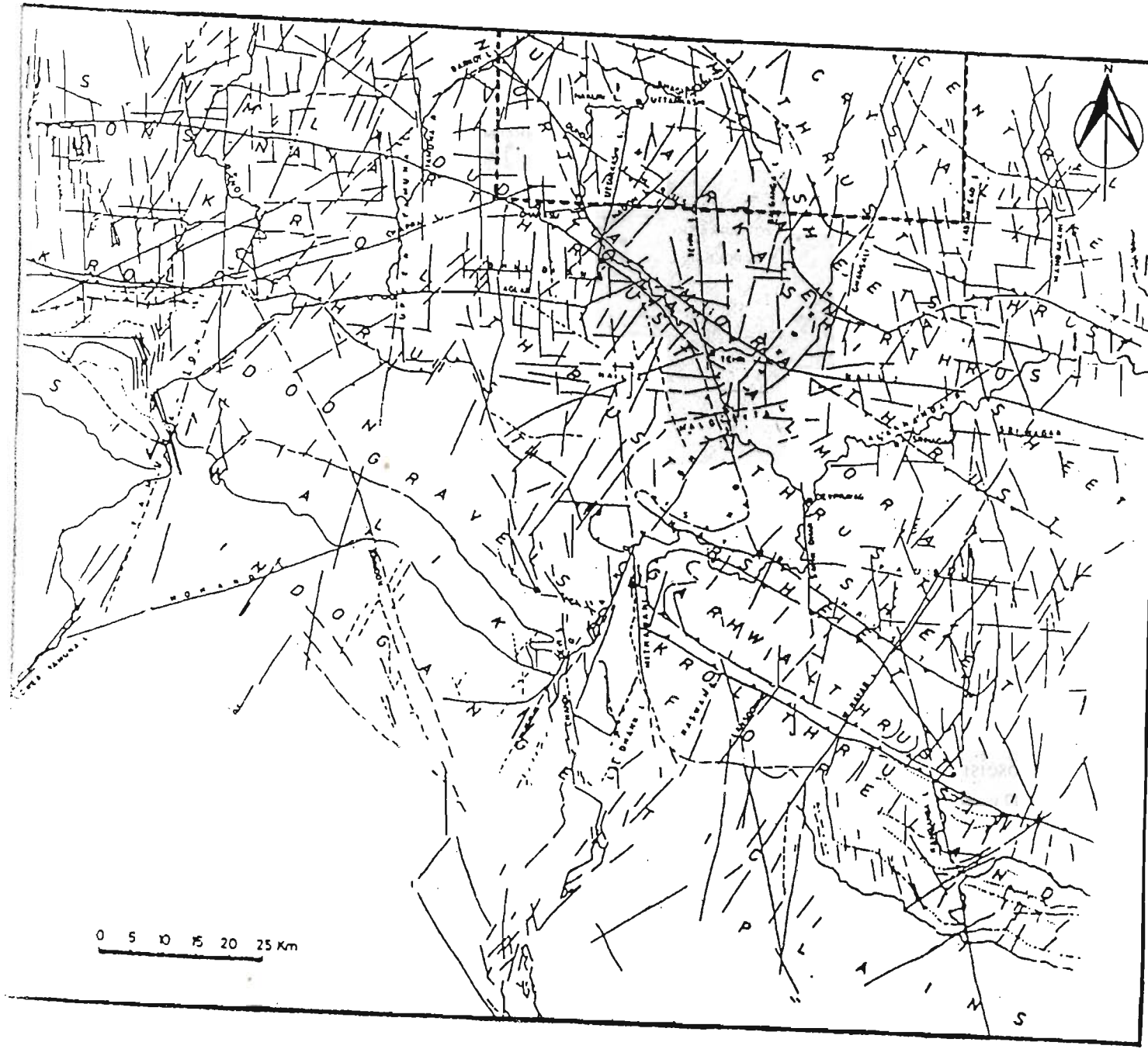
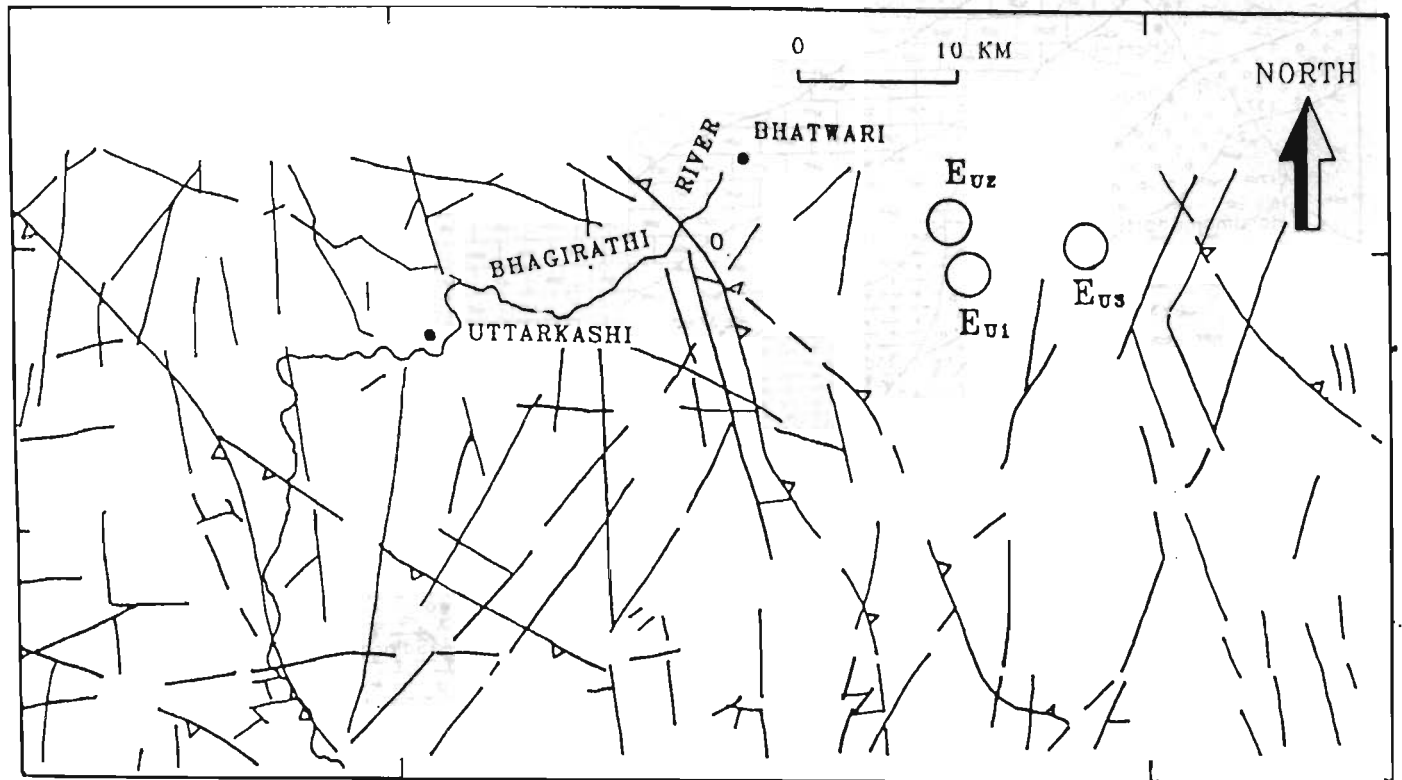


Fig 7.4 Lineament map from satellite imagery of Garhwal Himalaya (After Jain, 1987). Study area shown by dashed rectangle is enlarged in Fig 7.5.



LEGEND

78.5

79.0

- OBSERVATION POINT
- ~ RIVER
- / LINEAMENT
- ^ THRUST
- EPICENTER OF UTTARKASHI EARTHQUAKE OF 20TH OCT, 1991

Fig 7.5 Tectonics of the region around Uttarkashi taken from map shown in Fig 7.4. E_{U1} , E_{U2} and E_{U3} are the epicenter of Uttarkashi earthquake of 20th October, 1991 given by different agencies and this data is given in Table 7.2.

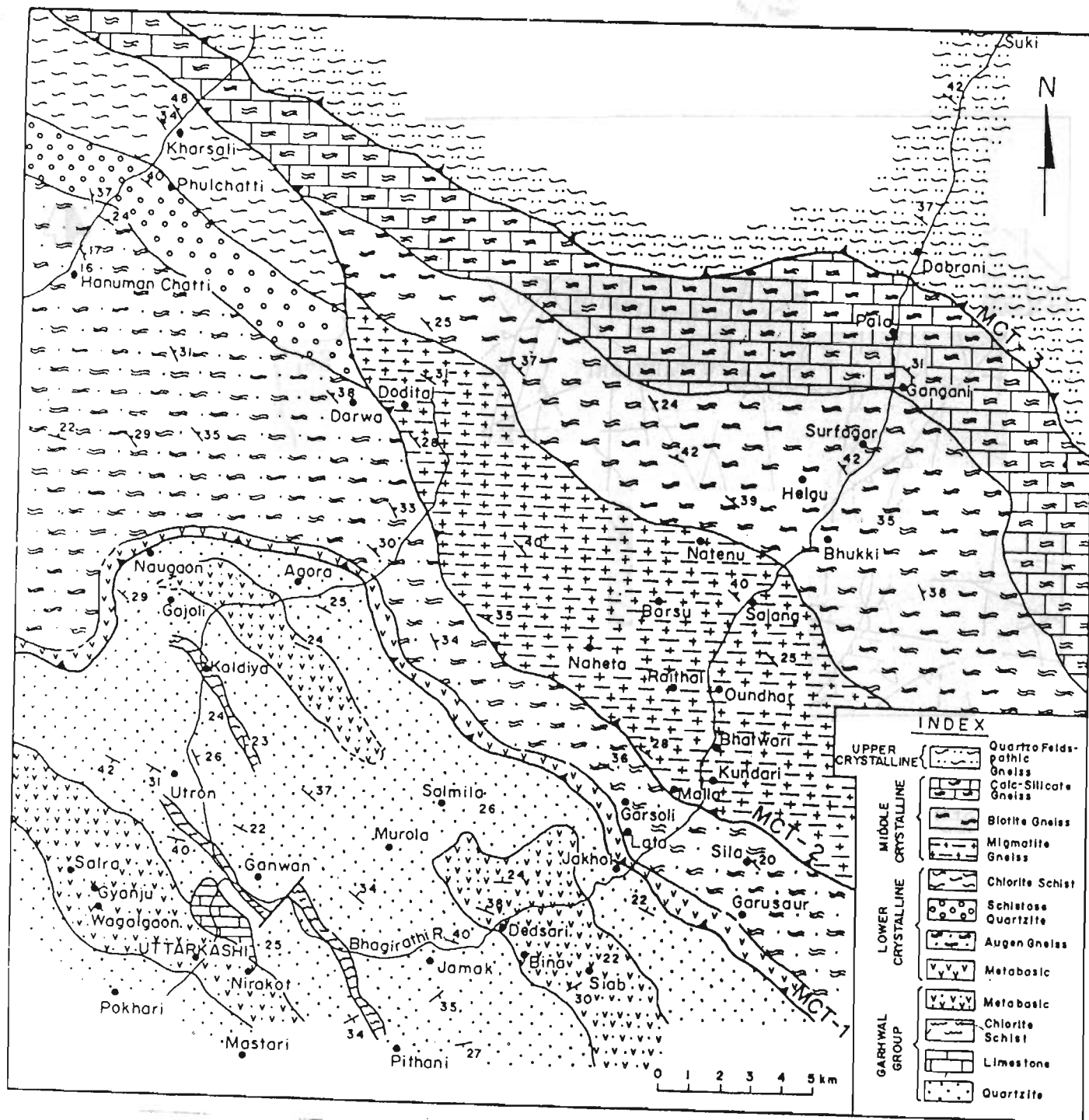


Fig 7.6 Tectonic map of Uttarkashi region (After Purohit et al., 1990).

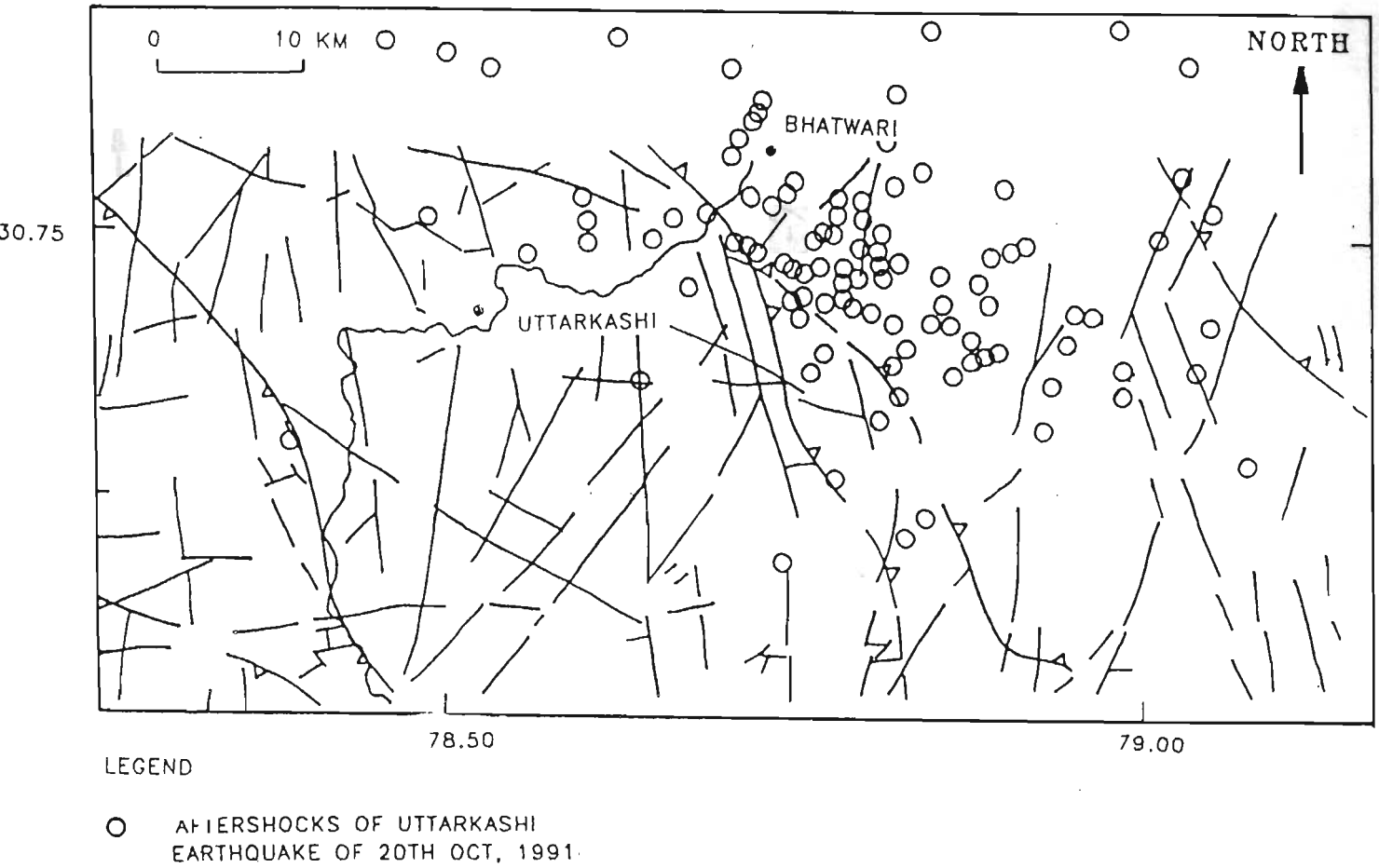


Fig 7.7 Location of aftershocks of Uttarkashi earthquake of 20th October, 1991. Data plotted in this figure is reproduced in Table 7.4 and the tectonics of the region is taken after Jain (1987). Epicentral parameter of main shock is reproduced in Table 7.4.

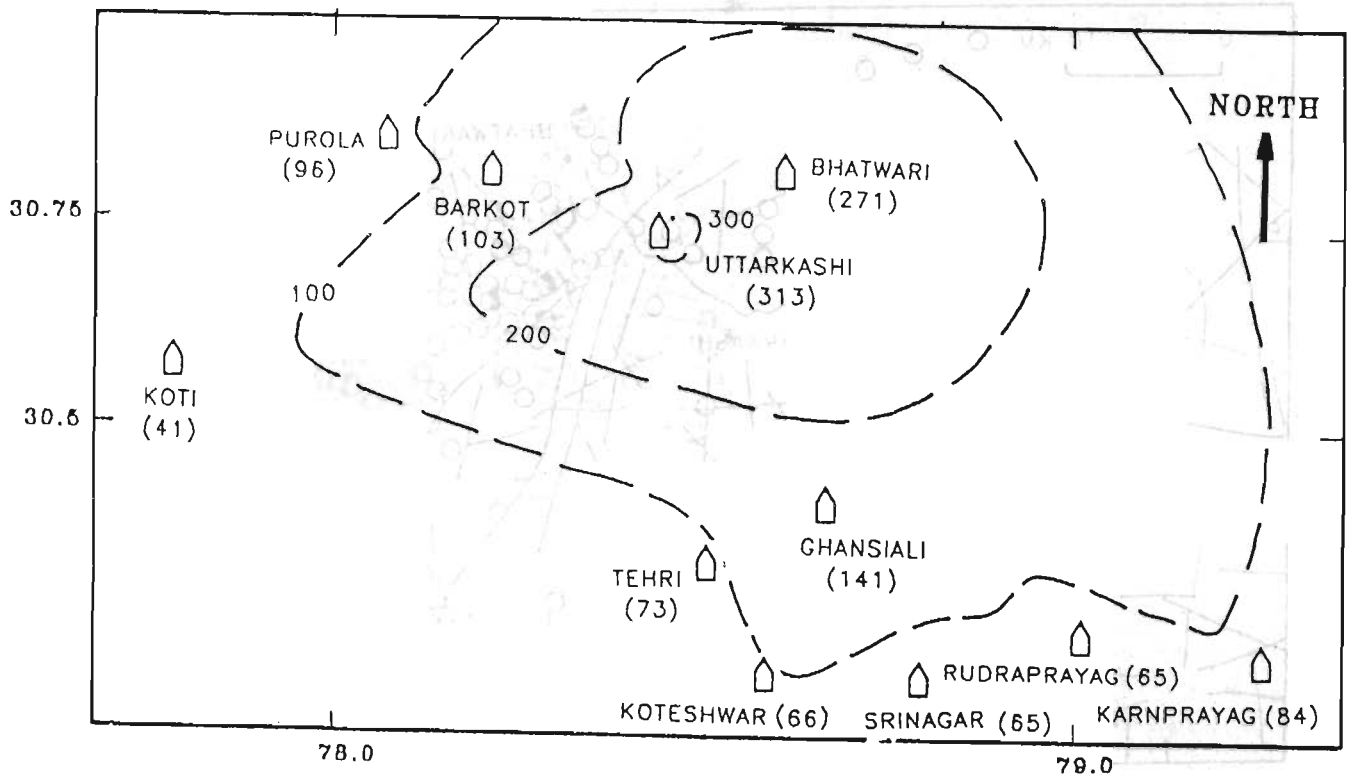


Fig 7.8 Isoacceleration contour map for Uttarkashi earthquake of 20th October, 1991. Acceleration data is taken from Chandrasekaran and Das (1991, 1992c) and reproduced in Table 7.5.

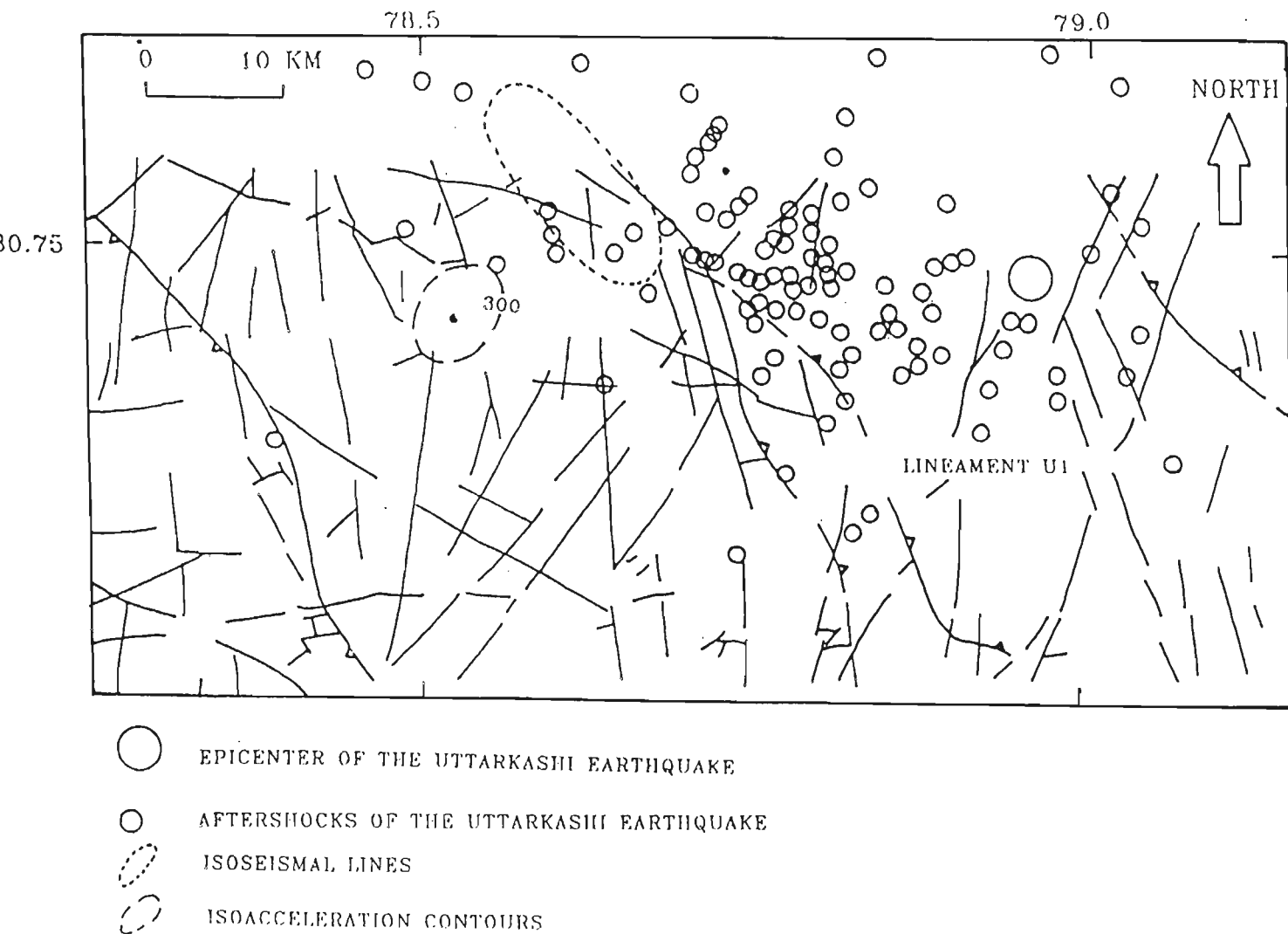


Fig 7.9 Composite map of isoacceleration contours, aftershock location, meizoseismal area of Uttarkashi earthquake of 20th October, 1991 and tectonics of the region. (Data taken from Chandrasekaran and Das, 1991, 1992c, Kayal et al. 1992 and Jain, 1987).

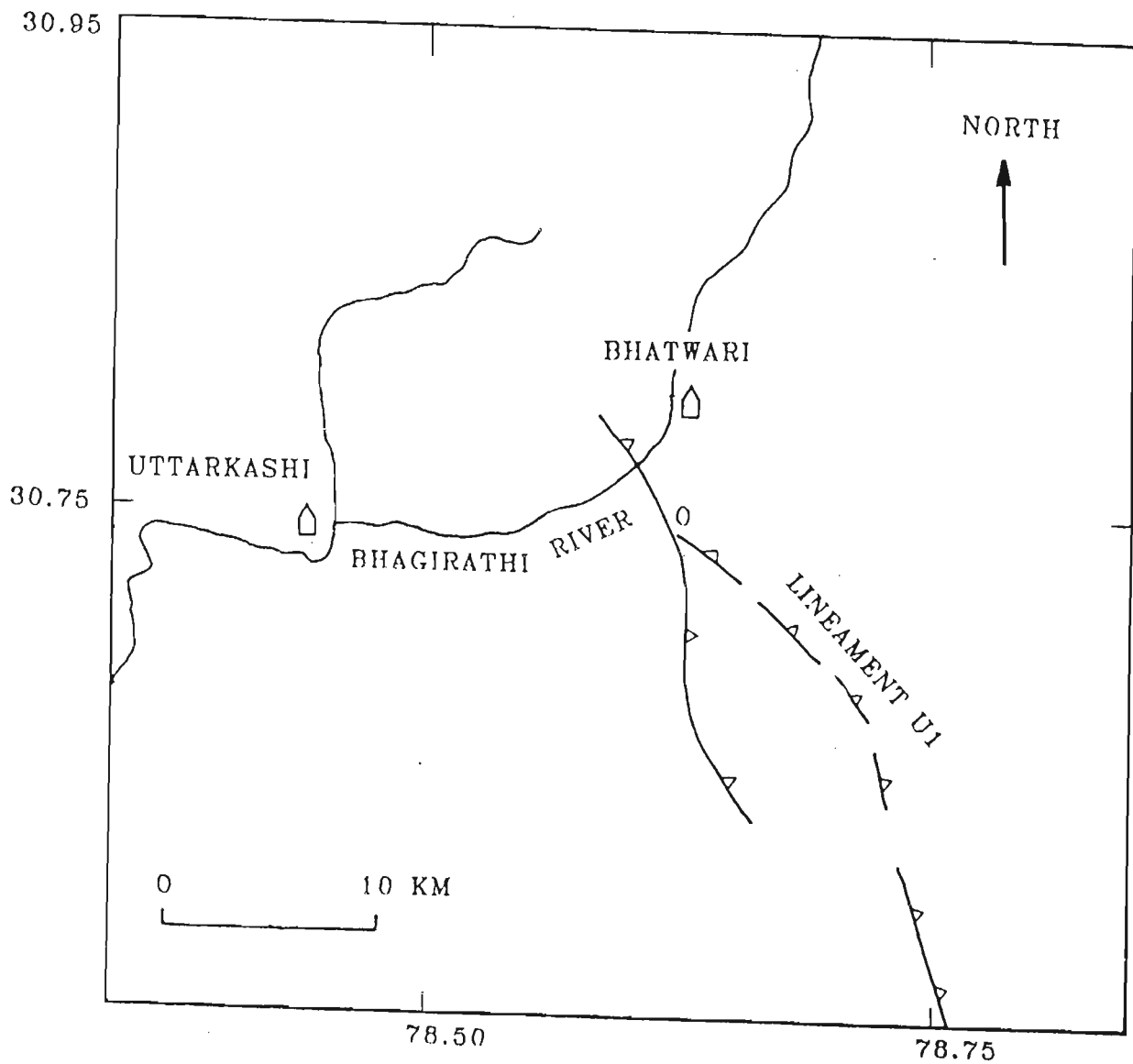


Fig 7.10 Location of identified most probable causative fault from the composite map shown in Fig 7.9. Tectonics of the region is after Jain (1987).

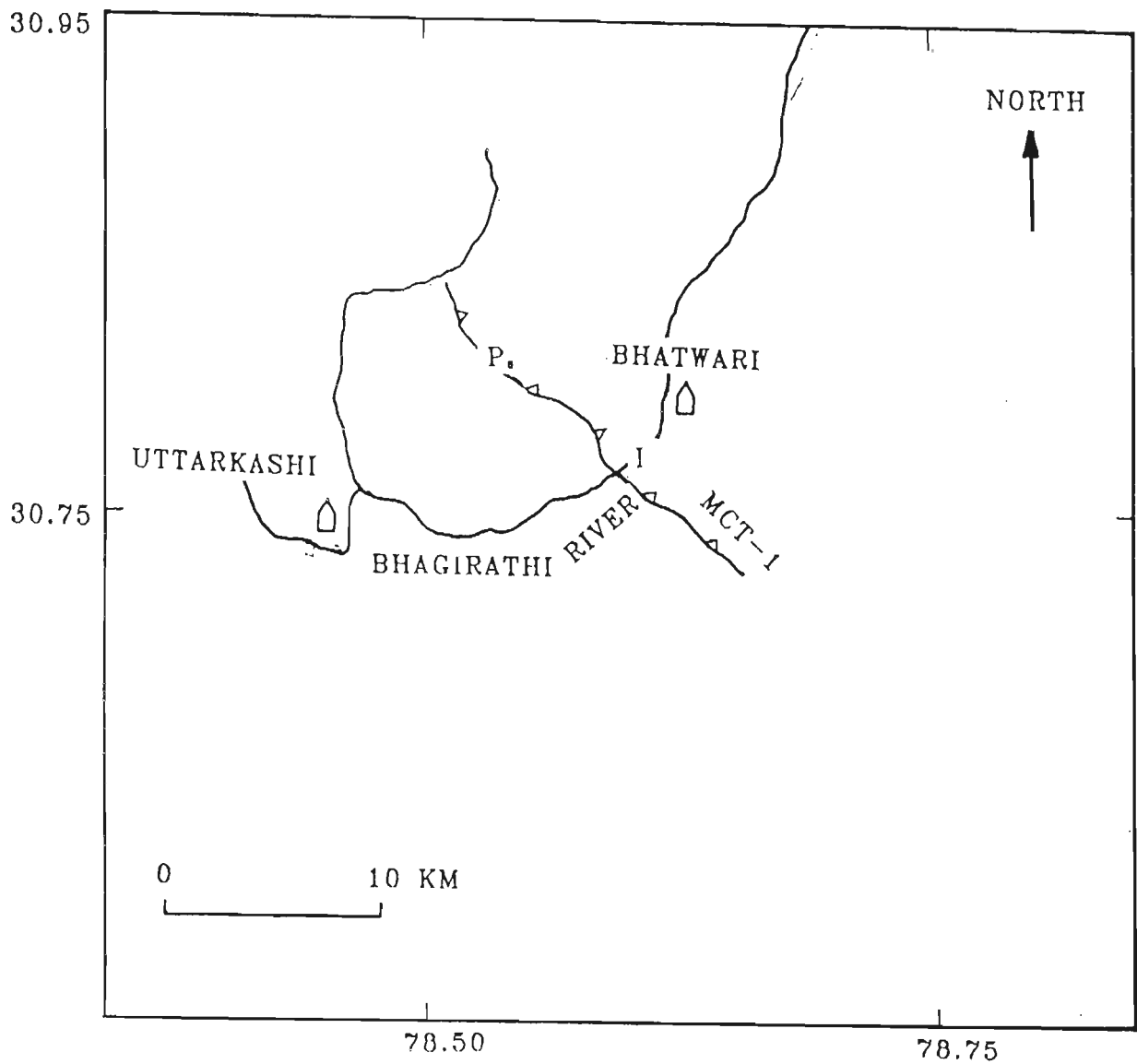
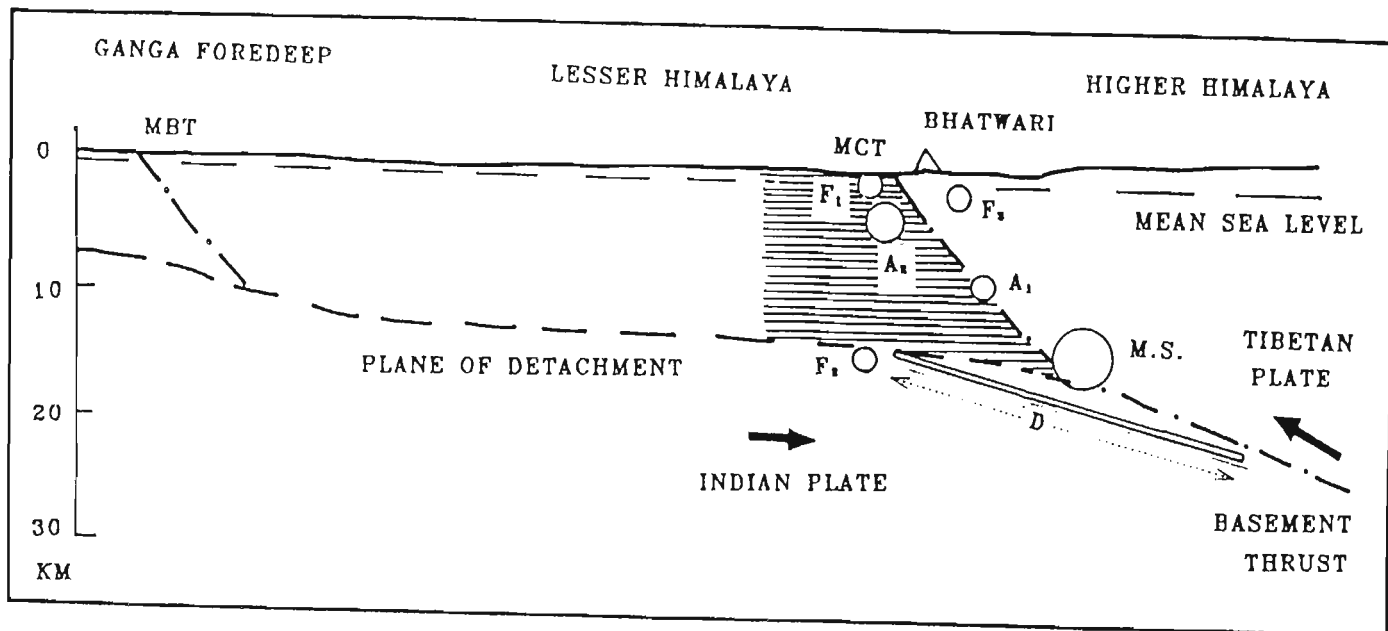


Fig 7.11 Location of MCT-1 from the tectonic map of Purohit et al. (1990).



- $4 < M < 5$
- $5 < M < 6$
- $6 < M < 7$

Fig 7.12 Geological section in the dip direction of the MCT showing the downward extension D of the rupture plane (Modified after Kayal, 1994). Shaded zone indicates the MEQ aftershocks area (After Kayal et al., 1993). The plane of detachment and Basement thrust are taken from Seeber et al. (1981). Solid arrows indicate relative movement of the plates. F_1 , F_2 and F_3 represent foreshocks of the Uttarkashi earthquake of 20th October, 1991 that occurred 49 hours before the main shocks (M.S.). Largest foreshock F_2 has magnitude 4.7 (M_D). A_1 and A_2 represent aftershocks that occurred 24 hours of main shock. Largest aftershock A_2 has magnitude 5.2 (M_D). Point O marked in this figure is also shown in Fig 7.11.

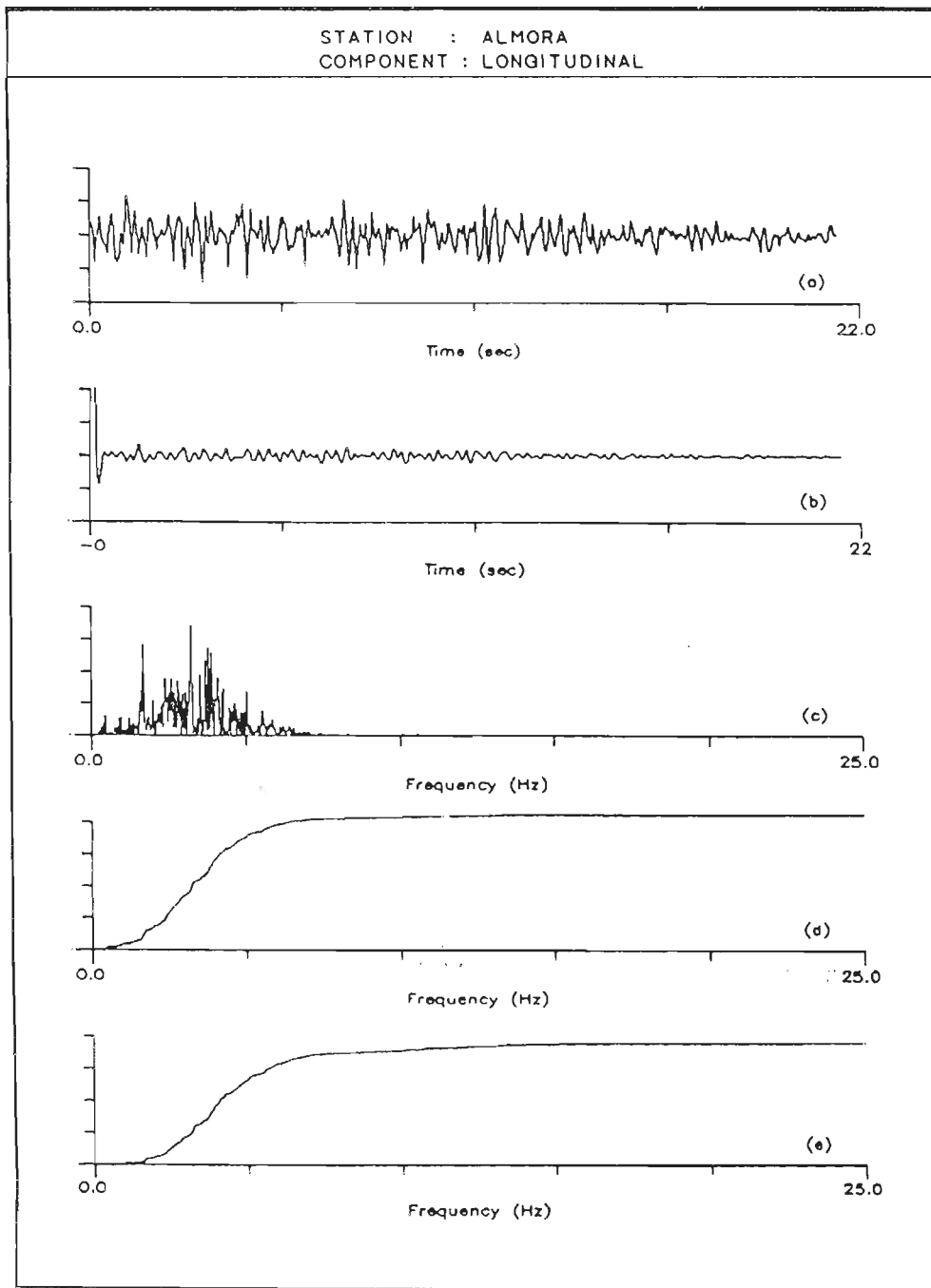


Fig 7.13 Uttarkashi earthquake of 20th Oct, 1991 longitudinal component recorded at Almora station. Y axis shows normalised value of (a) acceleration record, (b) its autocorrelation function, (c) its power spectrum, (d) its cumulative power spectrum and (e) its frequency weighted cumulative power spectrum. X axis for (a) and (b) shows time and for (c), (d) and (e) shows frequency. Feature extracted from field records at this station is given in Table 7.6.

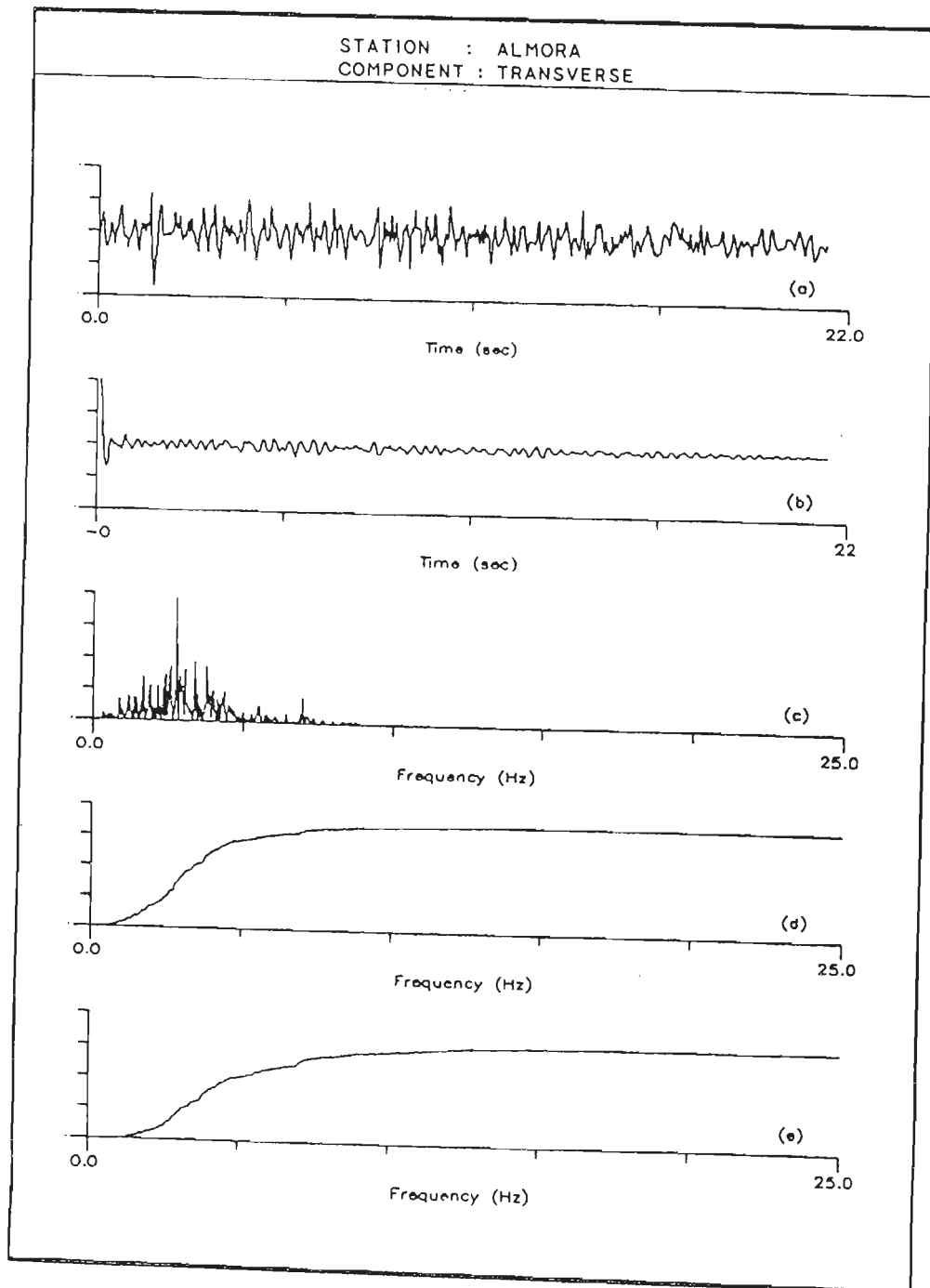


Fig 7.14 Uttarkashi earthquake of 20th Oct, 1991 transverse component recorded at Almora station. Y axis shows normalised value of (a) acceleration record, (b) its autocorrelation function, (c) its power spectrum, (d) its cumulative power spectrum and (e) its frequency weighted cumulative power spectrum. X axis for (a) and (b) shows time and for (c), (d) and (e) shows frequency. Feature extracted from field records at this station is given in Table 7.6.

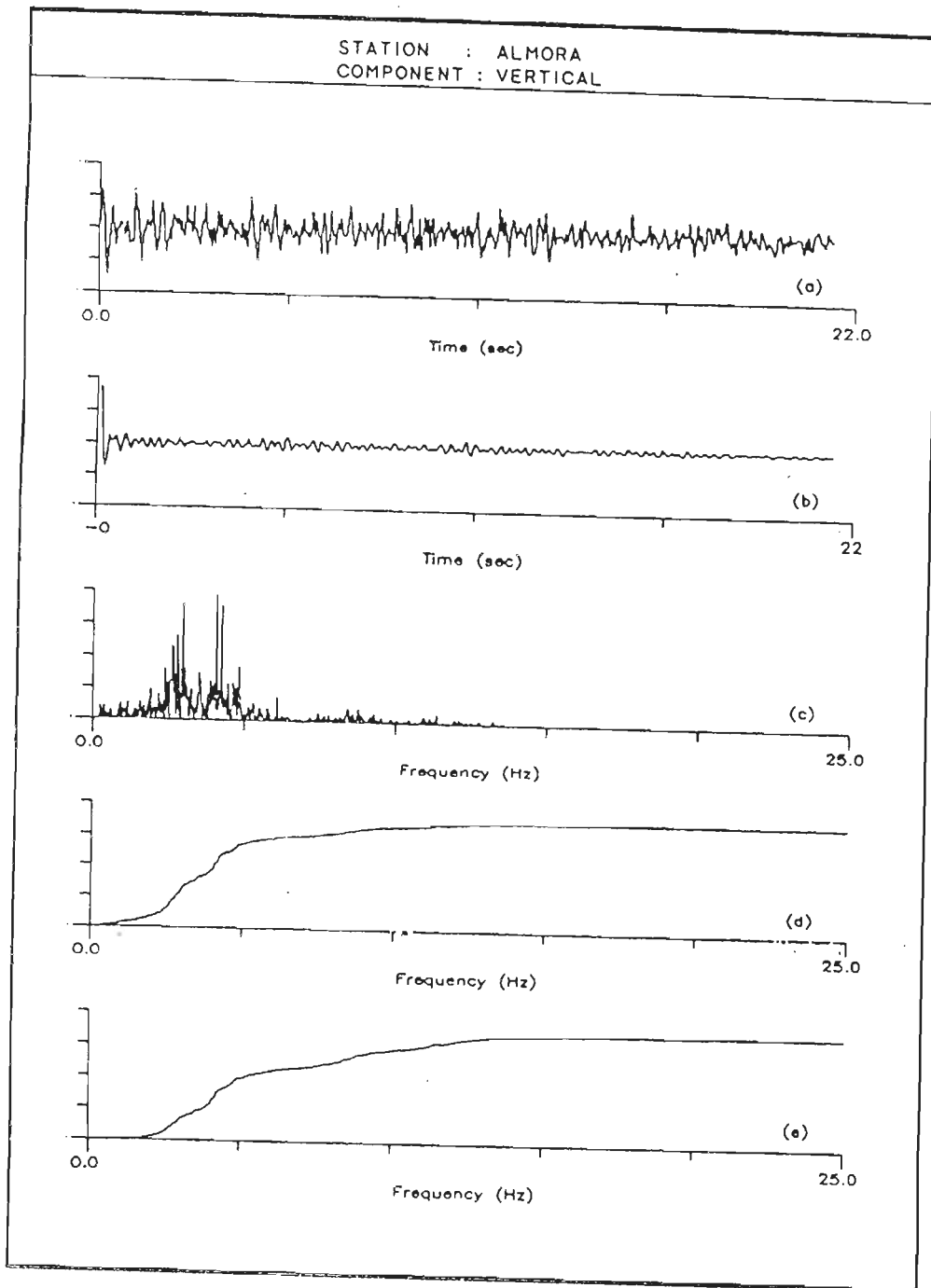


Fig 7.15 Uttarkashi earthquake of 20th Oct, 1991 vertical component recorded at Almora station. Y axis shows normalised value of (a) acceleration record, (b) its autocorrelation function, (c) its power spectrum, (d) its cumulative power spectrum and (e) its frequency weighted cumulative power spectrum. X axis for (a) and (b) shows time and for (c), (d) and (e) shows frequency. Feature extracted from field records at this station is given in Table 7.6.

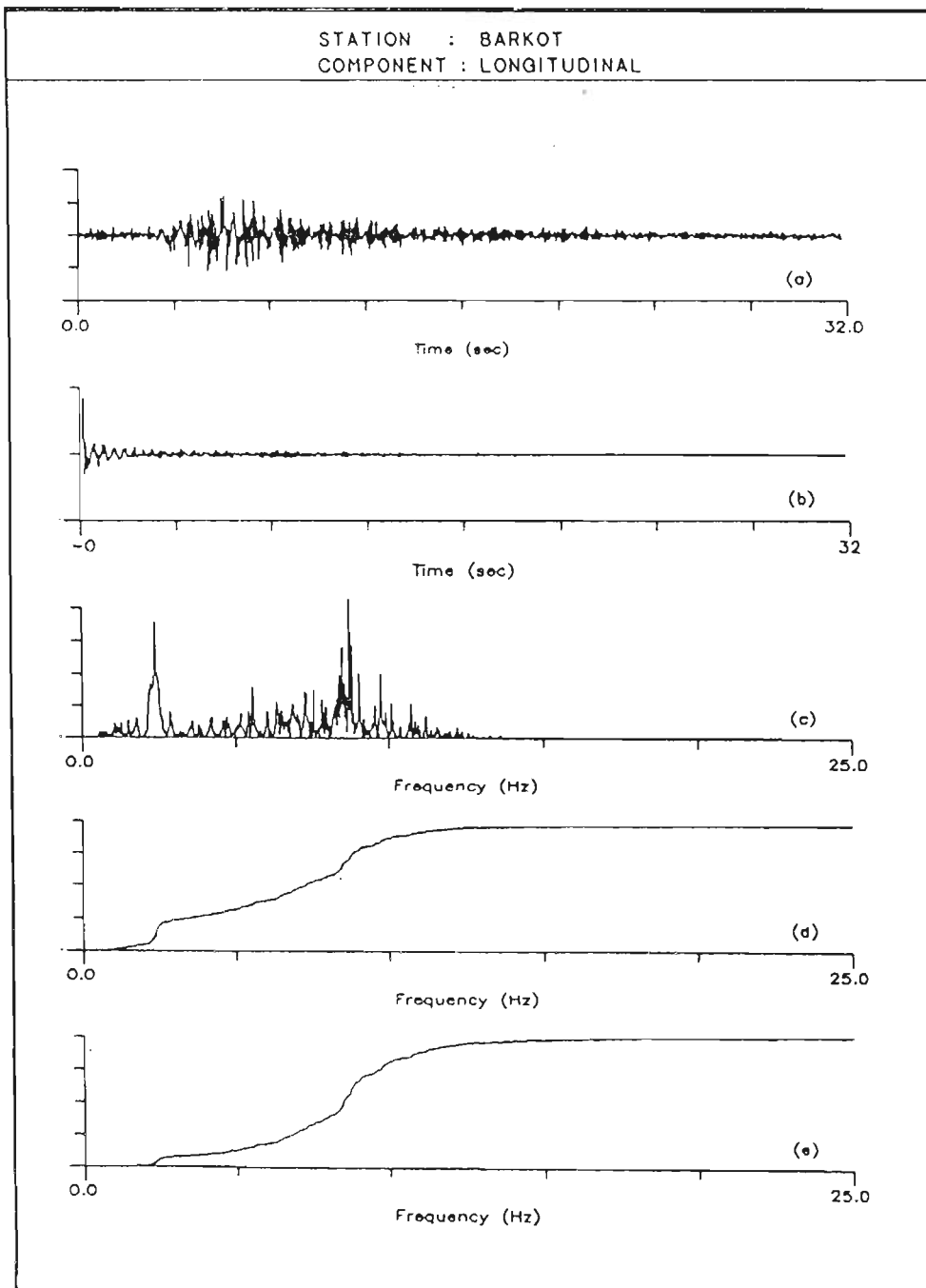


Fig 7.16 Uttarkashi earthquake of 20th Oct, 1991, longitudinal component recorded at Barkot station. Y axis shows normalised value of (a) acceleration record, (b) its autocorrelation function, (c) its power spectrum, (d) its cumulative power spectrum and (e) its frequency weighted cumulative power spectrum. X axis for (a) and (b) shows time and for (c), (d) and (e) shows frequency. Feature extracted from field records at this station is given in Table 7.6.

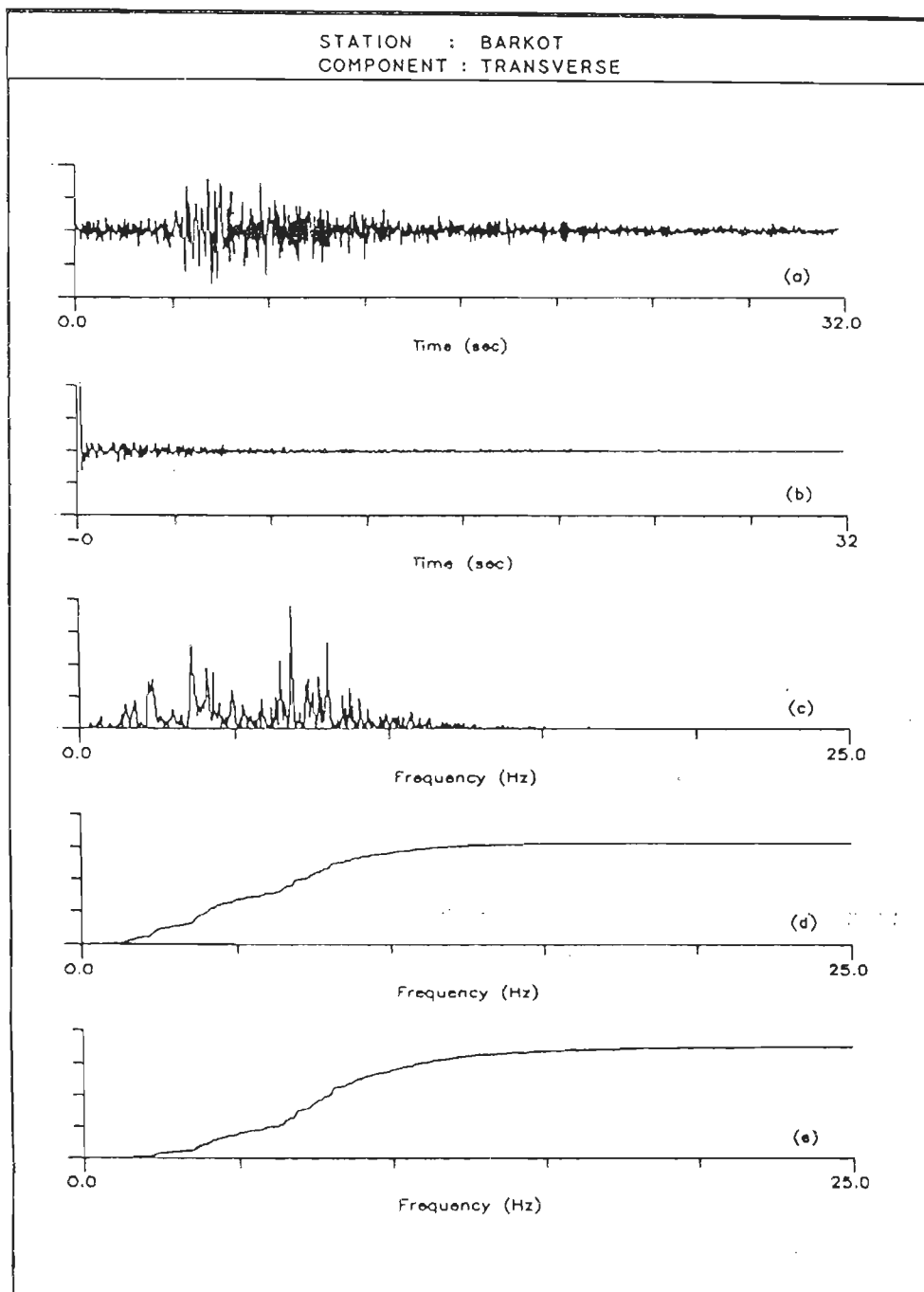


Fig 7.17 Uttarkashi earthquake of 20th Oct, 1991, transverse component recorded at Barkot station. Y axis shows normalised value of (a) acceleration record, (b) its autocorrelation function, (c) its power spectrum, (d) its cumulative power spectrum and (e) its frequency weighted cumulative power spectrum. X axis for (a) and (b) shows time and for (c), (d) and (e) shows frequency. Feature extracted from field records at this station is given in Table 7.6.

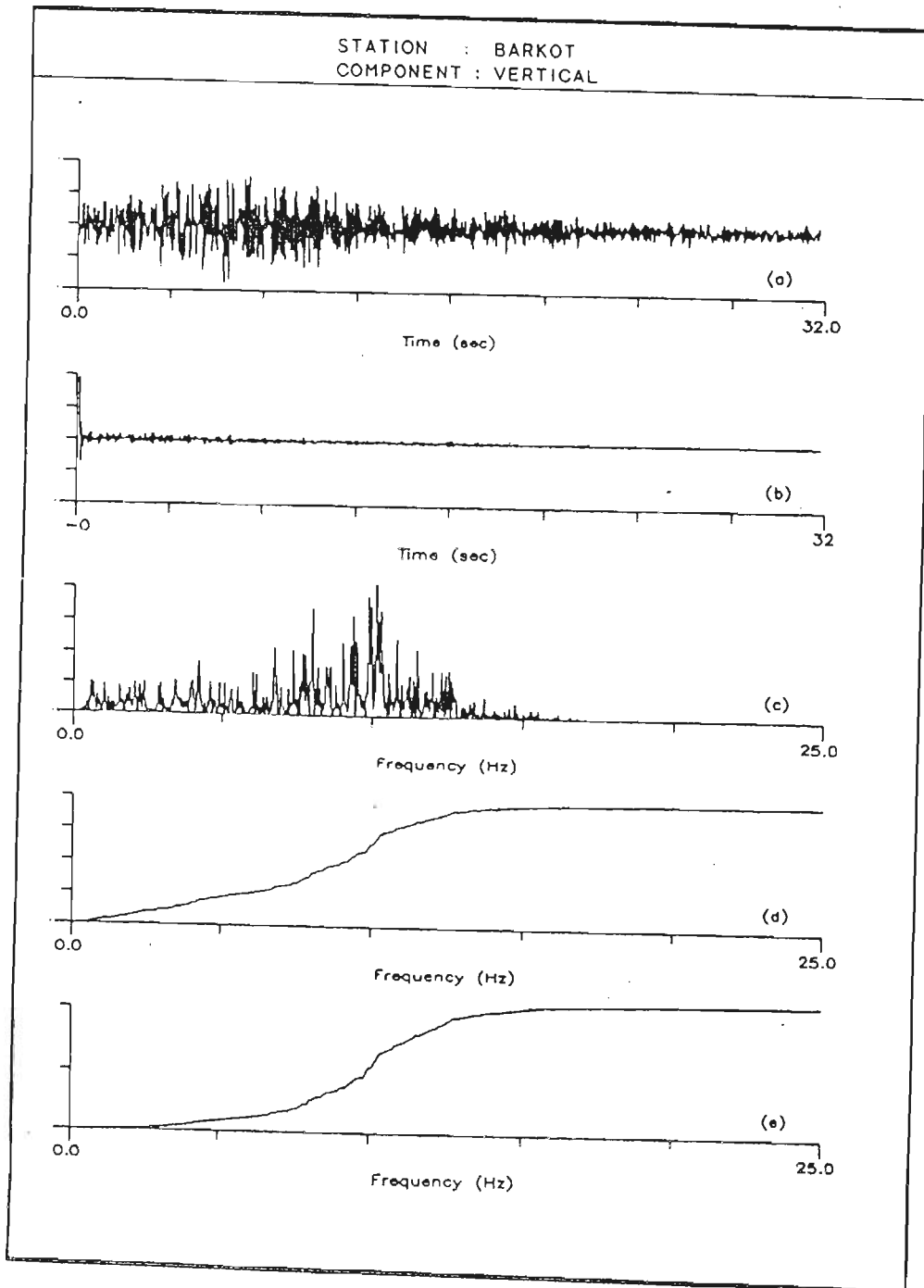


Fig 7.18 Uttarkashi earthquake of 20th Oct, 1991, vertical component recorded at Barkot station. Y axis shows normalised value of (a) acceleration record, (b) its autocorrelation function, (c) its power spectrum, (d) its cumulative power spectrum and (e) its frequency weighted cumulative power spectrum. X axis for (a) and (b) shows time and for (c), (d) and (e) shows frequency. Feature extracted from field records at this station is given in Table 7.6.

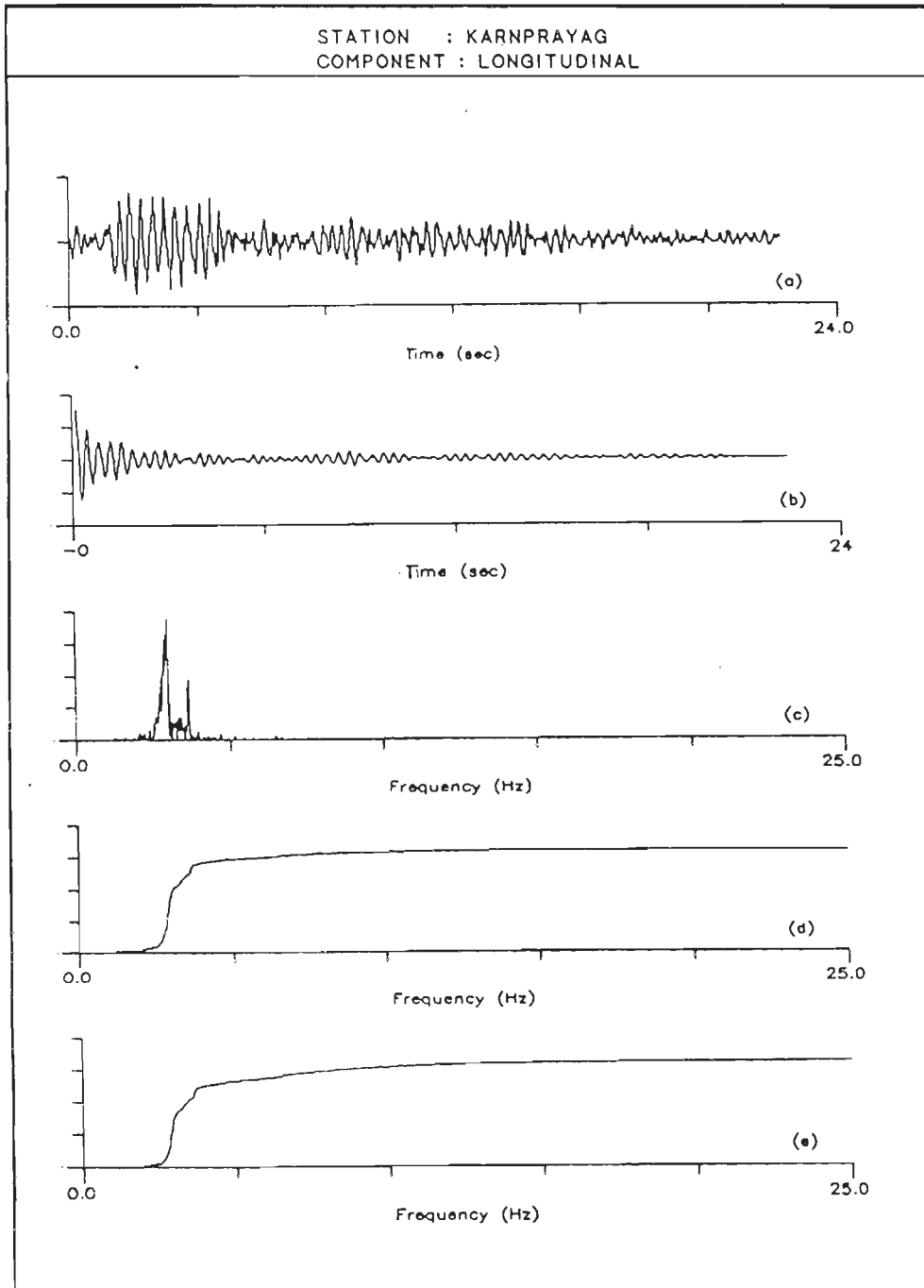


Fig 7.19 Uttarkashi earthquake of 20th Oct, 1991, longitudinal component recorded at Karnprayag station. Y axis shows normalised value of (a) acceleration record, (b) its autocorrelation function, (c) its power spectrum, (d) its cumulative power spectrum and (e) its frequency weighted cumulative power spectrum. X axis for (a) and (b) shows time and for (c), (d) and (e) shows frequency. Feature extracted from field records at this station is given in Table 7.7.

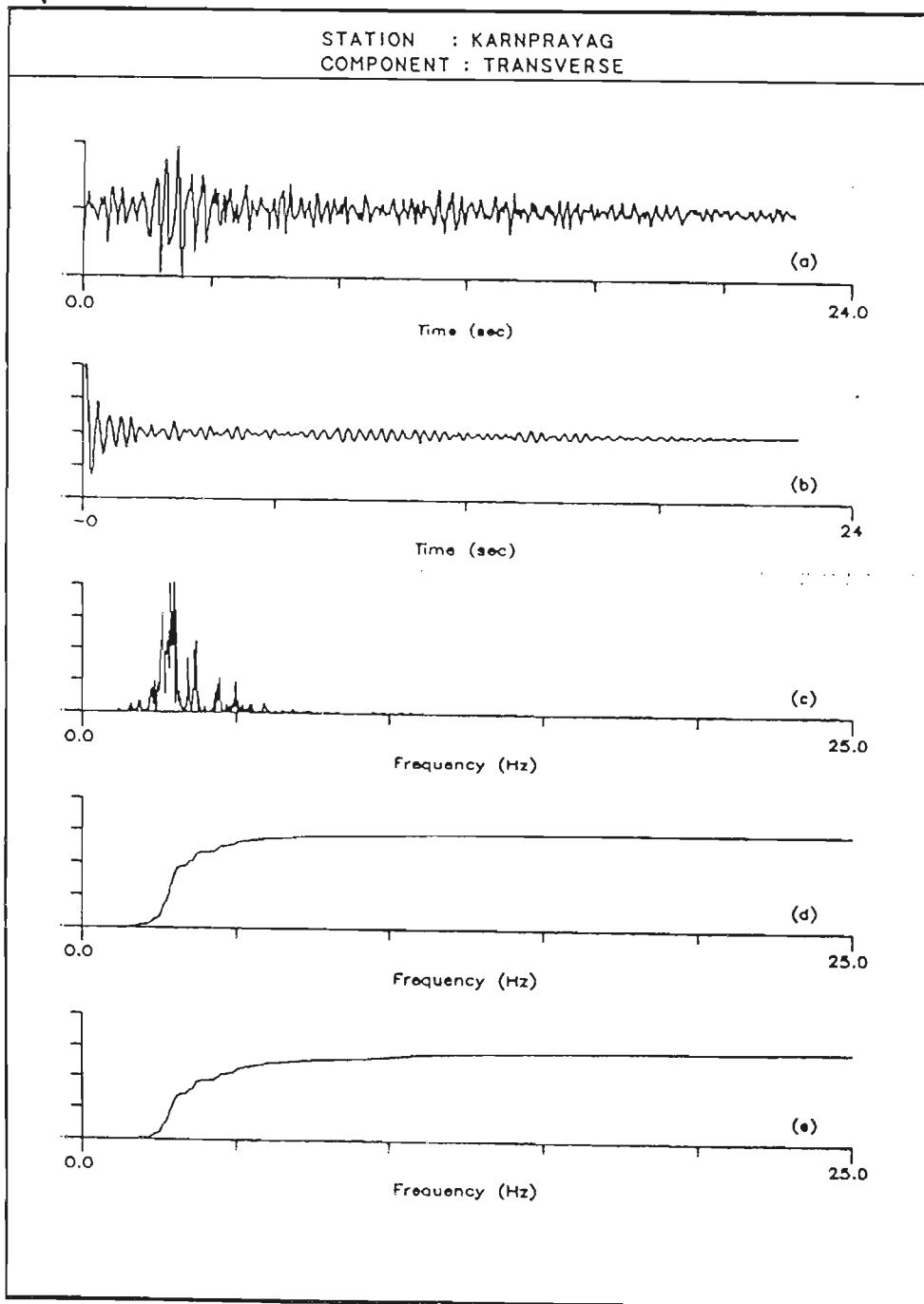


Fig 7.20 Uttarkashi earthquake of 20th Oct, 1991, transverse component recorded at Karnprayag station. Y axis shows normalised value of (a) acceleration record, (b) its autocorrelation function, (c) its power spectrum, (d) its cumulative power spectrum and (e) its frequency weighted cumulative power spectrum. X axis for (a) and (b) shows time and for (c), (d) and (e) shows frequency. Feature extracted from field records at this station is given in Table 7.7.

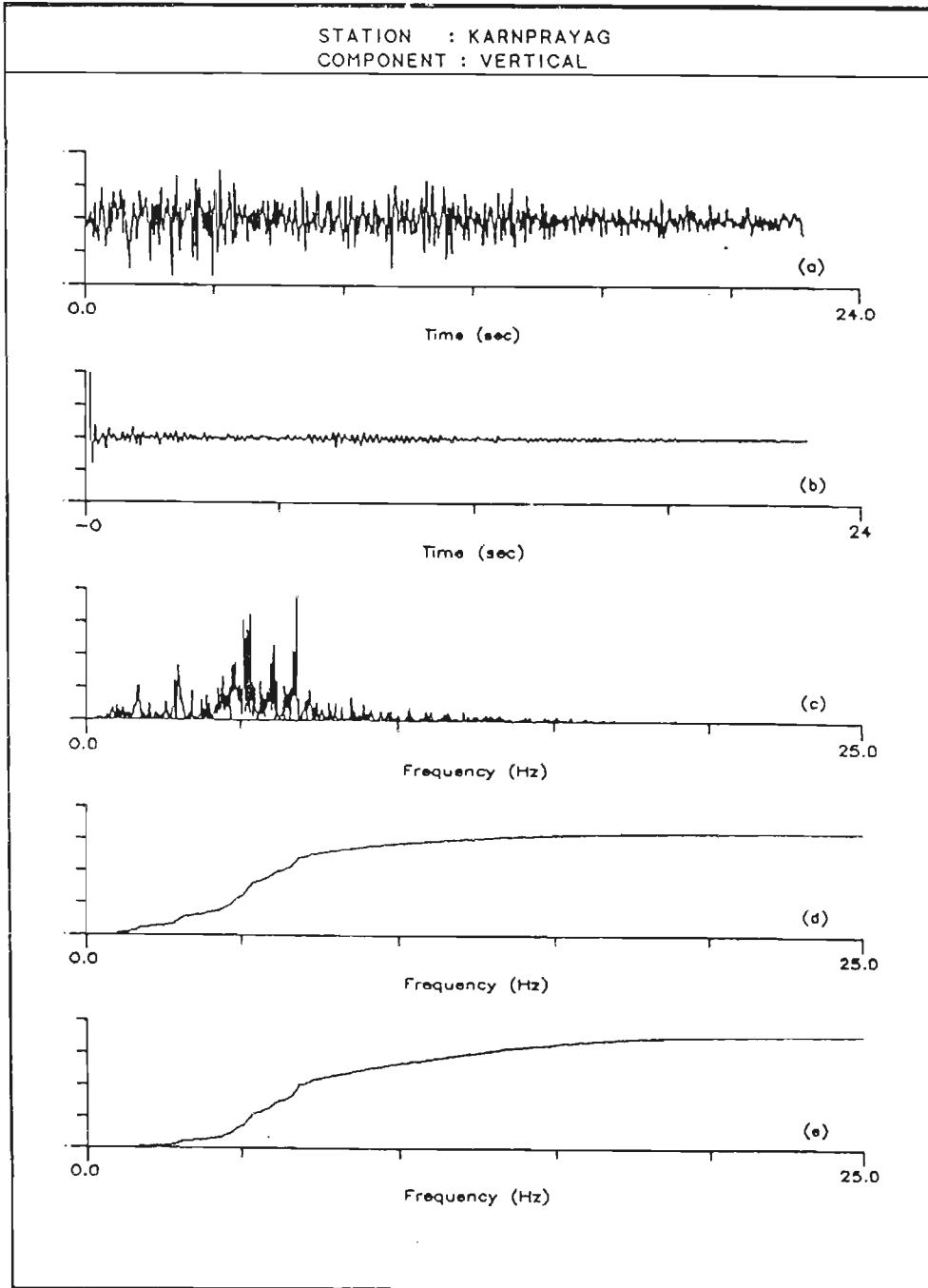


Fig 7.21 Uttarkashi earthquake of 20th Oct, 1991, vertical component recorded at Karnprayag station. Y axis shows normalised value of (a) acceleration record, (b) its autocorrelation function, (c) its power spectrum, (d) its cumulative power spectrum and (e) its frequency weighted cumulative power spectrum. X axis for (a) and (b) shows time and for (c), (d) and (e) shows frequency. Feature extracted from field records at this station is given in Table 7.7.

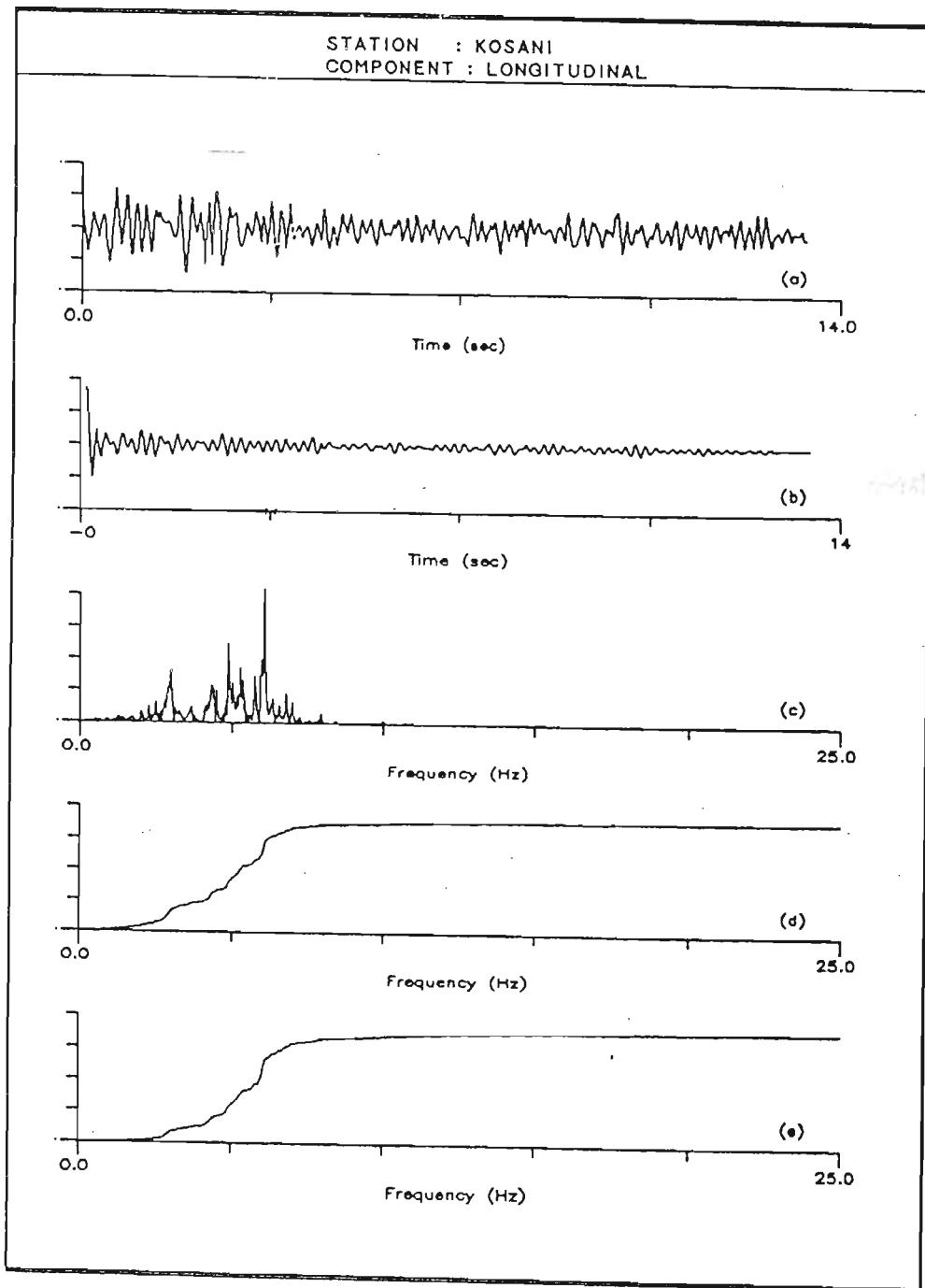


Fig 7.22 Uttarkashi earthquake of 20th Oct, 1991, longitudinal component recorded at Kosani station. Y axis shows normalised value of (a) acceleration record, (b) its autocorrelation function, (c) its power spectrum, (d) its cumulative power spectrum and (e) its frequency weighted cumulative power spectrum. X axis for (a) and (b) shows time and for (c), (d) and (e) shows frequency. Feature extracted from field records at this station is given in Table 7.7.

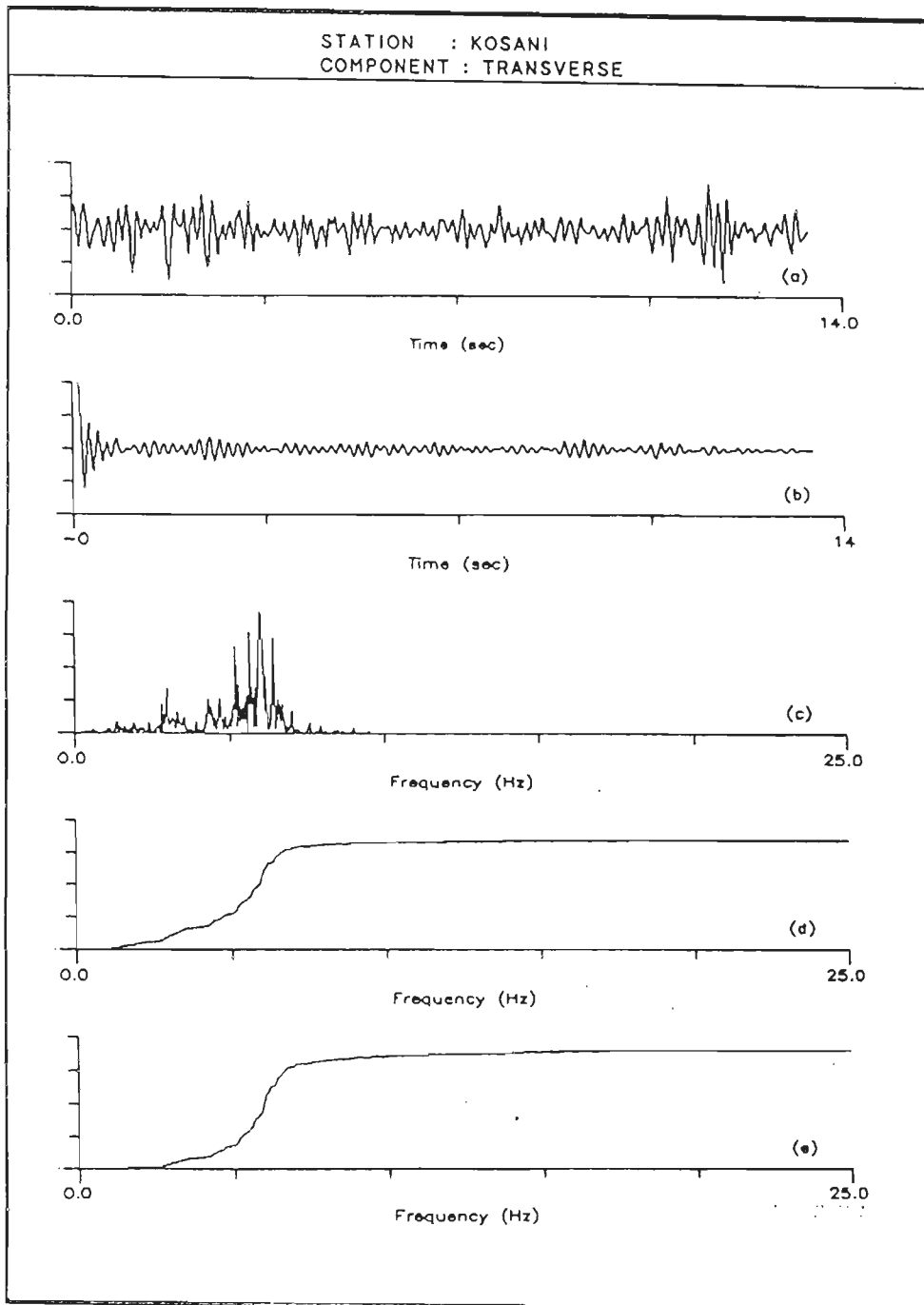


Fig 7.23 Uttarkashi earthquake of 20th Oct, 1991, transverse component recorded at Kosani station. Y axis shows normalised value of (a) acceleration record, (b) its autocorrelation function, (c) its power spectrum, (d) its cumulative power spectrum and (e) its frequency weighted cumulative power spectrum. X axis for (a) and (b) shows time and for (c), (d) and (e) shows frequency. Feature extracted from field records at this station is given in Table 7.7.

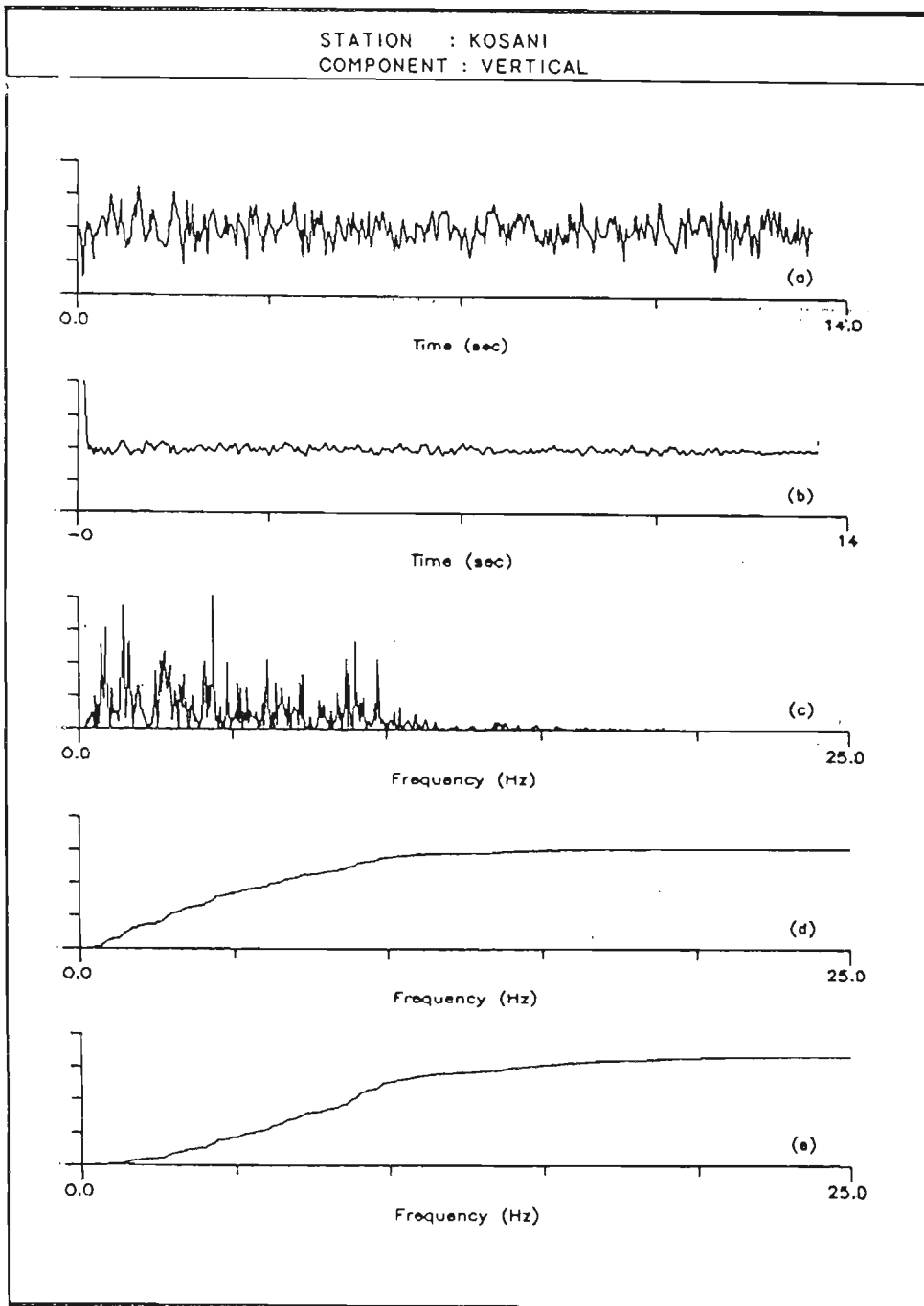


Fig 7.24 Uttarkashi earthquake of 20th Oct, 1991, vertical component recorded at Kosani station. Y axis shows normalised value of (a) acceleration record, (b) its autocorrelation function, (c) its power spectrum, (d) its cumulative power spectrum and (e) its frequency weighted cumulative power spectrum. X axis for (a) and (b) shows time and for (c), (d) and (e) shows frequency. Feature extracted from field records at this station is given in Table 7.7.

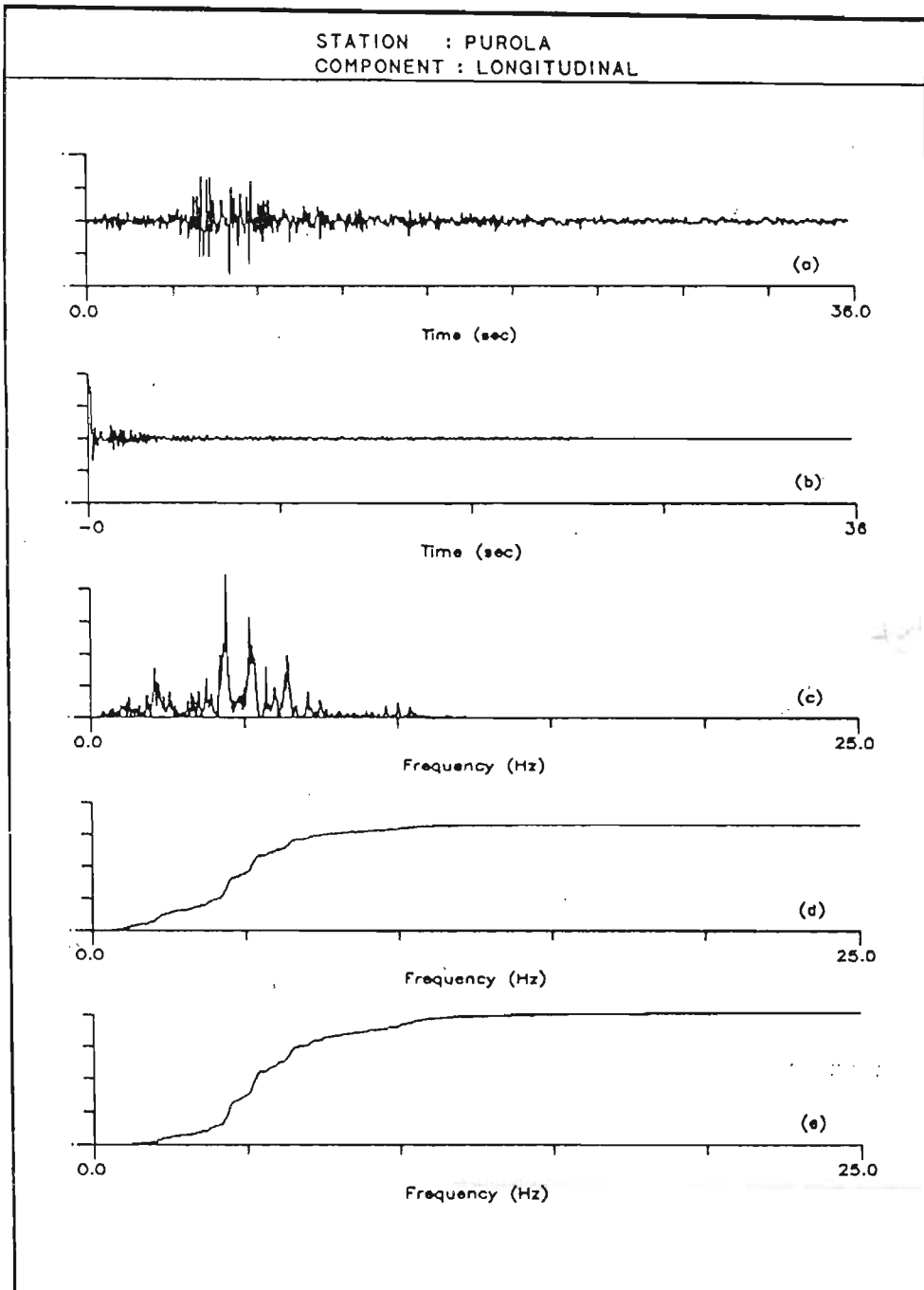


Fig 7.25 Uttarkashi earthquake of 20th Oct, 1991, longitudinal component recorded at Purola station. Y axis shows normalised value of (a) acceleration record, (b) its autocorrelation function, (c) its power spectrum, (d) its cumulative power spectrum and (e) its frequency weighted cumulative power spectrum. X axis for (a) and (b) shows time and for (c), (d) and (e) shows frequency. Feature extracted from field records at this station is given in Table 7.8.

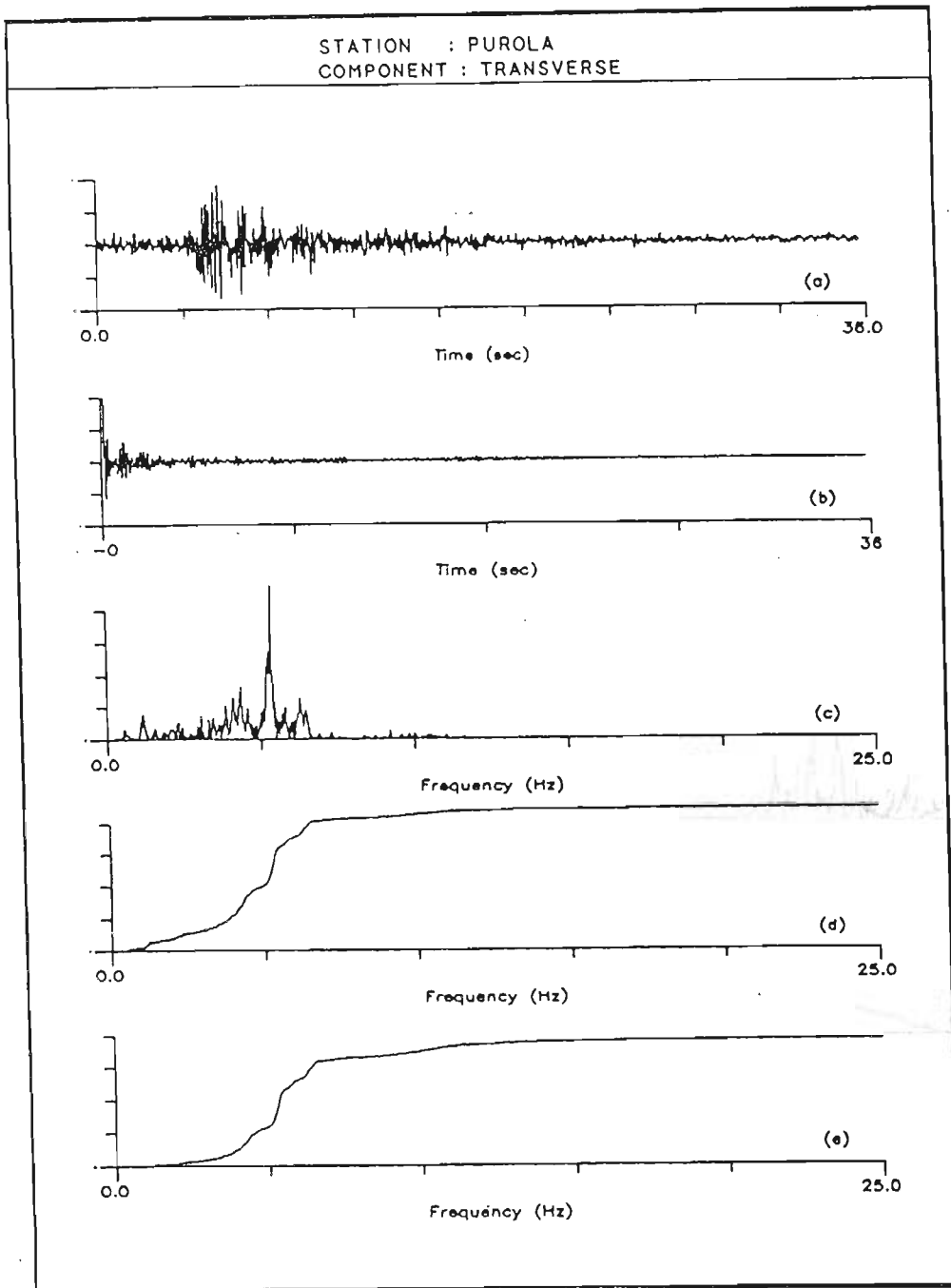


Fig 7.26 Uttarkashi earthquake of 20th Oct, 1991, transverse component recorded at Purola station. Y axis shows normalised value of (a) acceleration record, (b) its autocorrelation function, (c) its power spectrum, (d) its cumulative power spectrum and (e) its frequency weighted cumulative power spectrum. X axis for (a) and (b) shows time and for (c), (d) and (e) shows frequency. Feature extracted from field records at this station is given in Table 7.8.

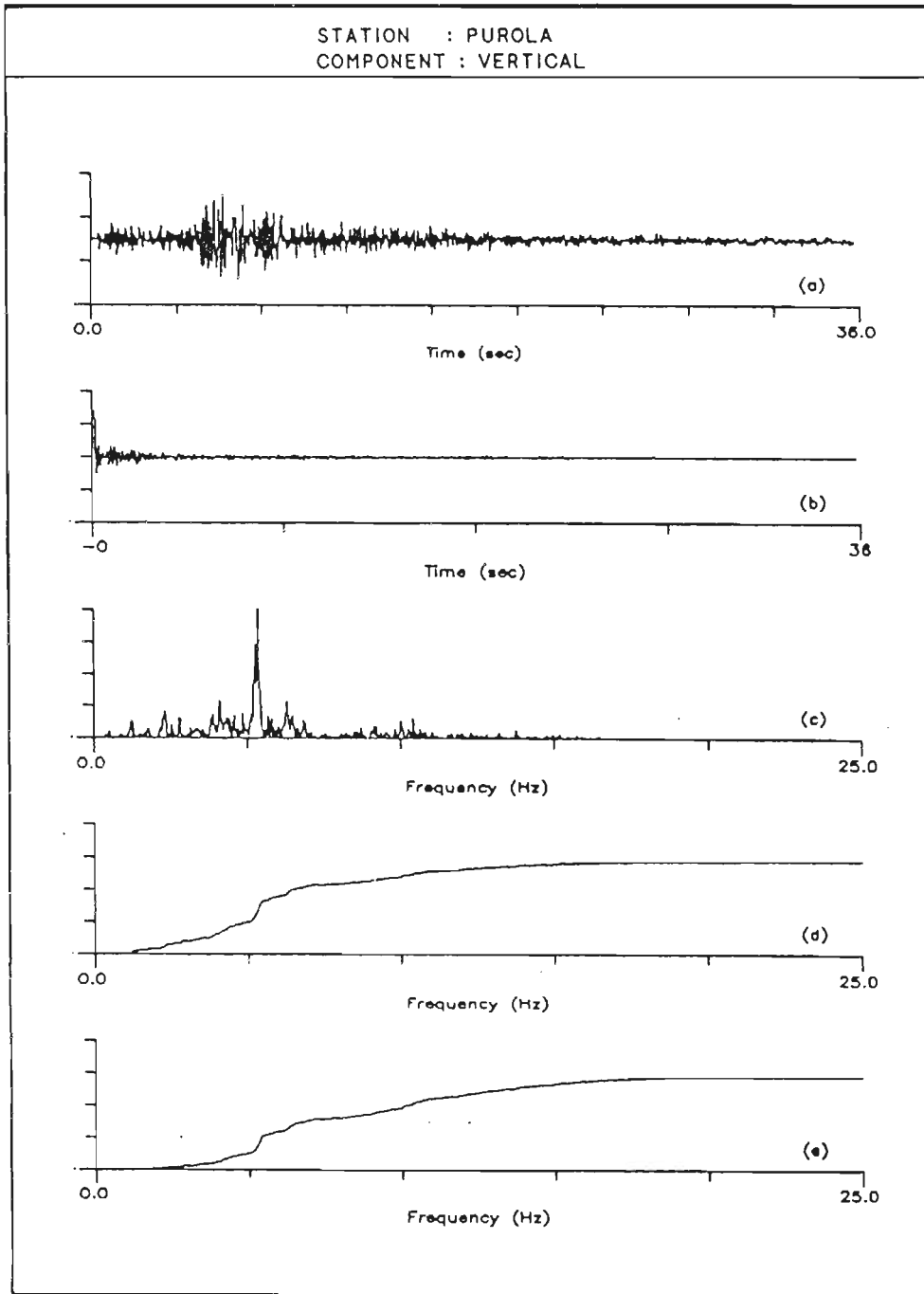


Fig 7.27 Uttarkashi earthquake of 20th Oct, 1991, vertical component recorded at Purola station. Y axis shows normalised value of (a) acceleration record, (b) its autocorrelation function, (c) its power spectrum, (d) its cumulative power spectrum and (e) its frequency weighted cumulative power spectrum. X axis for (a) and (b) shows time and for (c), (d) and (e) shows frequency. Feature extracted from field records at this station is given in Table 7.8.

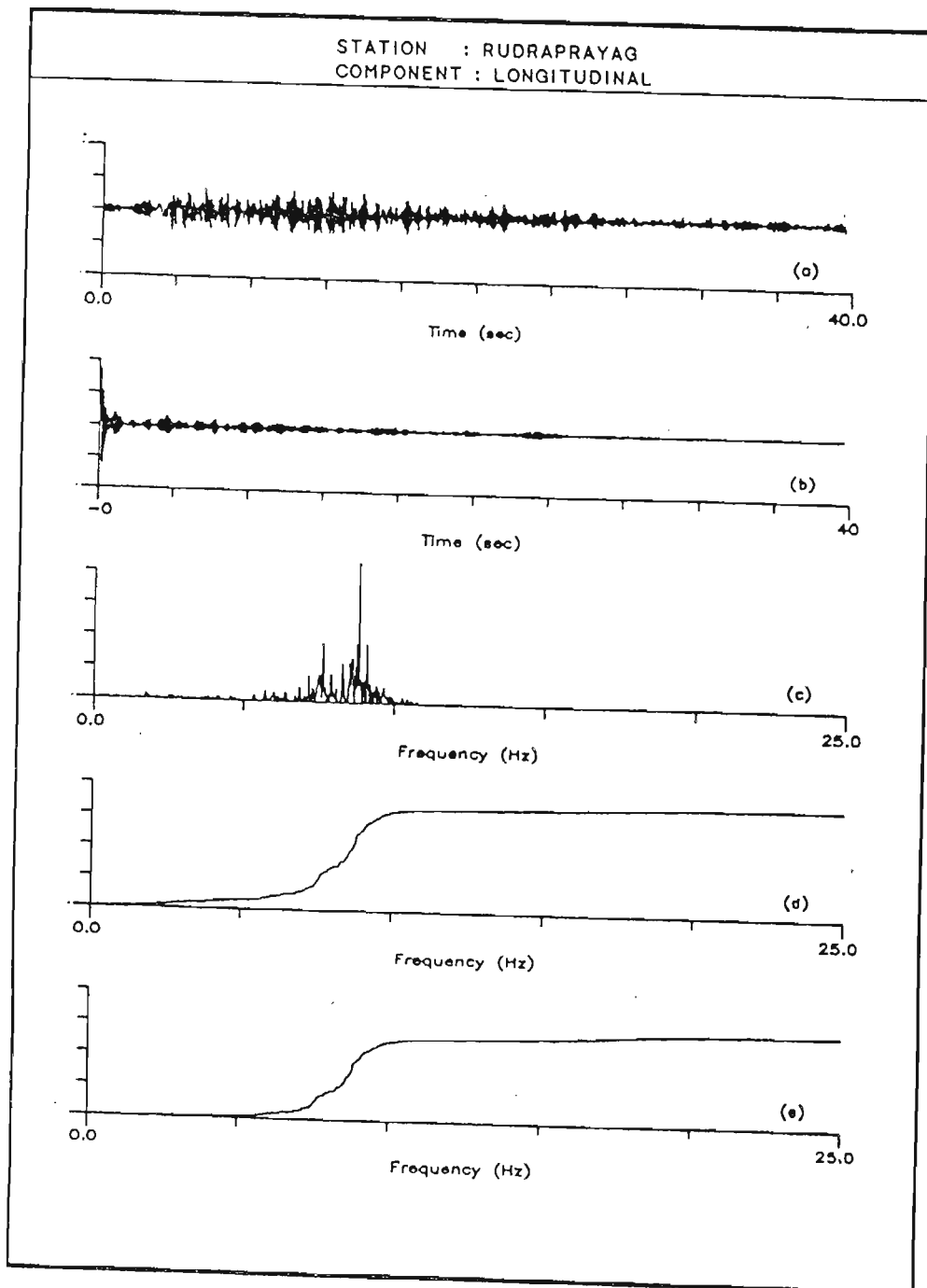


Fig 7.28 Uttarkashi earthquake of 20th Oct, 1991, longitudinal component recorded at Rudraprayag station. Y axis shows normalised value of (a) acceleration record, (b) its autocorrelation function, (c) its power spectrum, (d) its cumulative power spectrum and (e) its frequency weighted cumulative power spectrum. X axis for (a) and (b) shows time and for (c), (d) and (e) shows frequency. Feature extracted from field records at this station is given in Table 7.8.

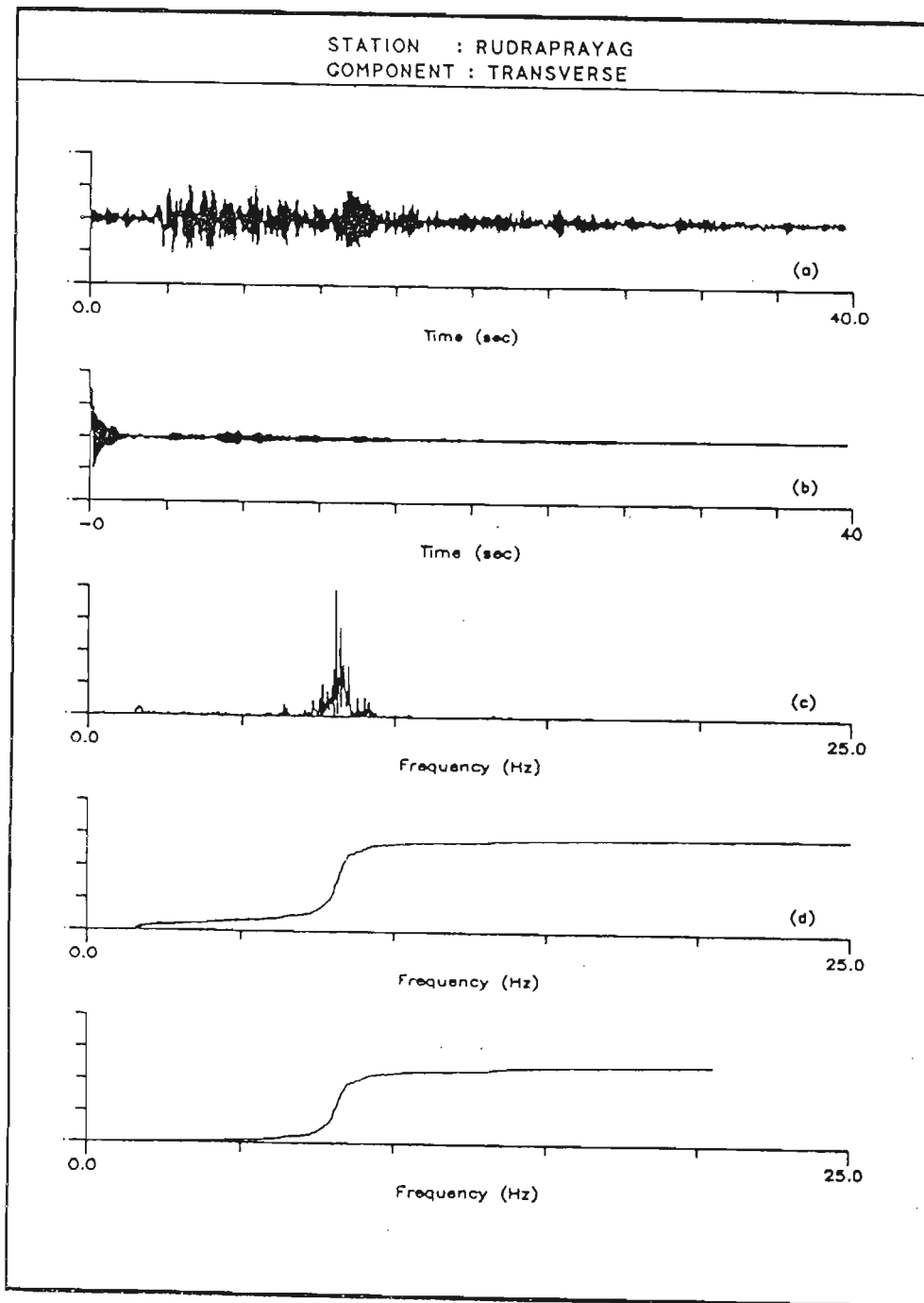


Fig 7.29 Uttarkashi earthquake of 20th Oct, 1991, transverse component recorded at Rudraprayag station. Y axis shows normalised value of (a) acceleration record, (b) its autocorrelation function, (c) its power spectrum, (d) its cumulative power spectrum and (e) its frequency weighted cumulative power spectrum. X axis for (a) and (b) shows time and for (c), (d) and (e) shows frequency. Feature extracted from field records at this station is given in Table 7.8.

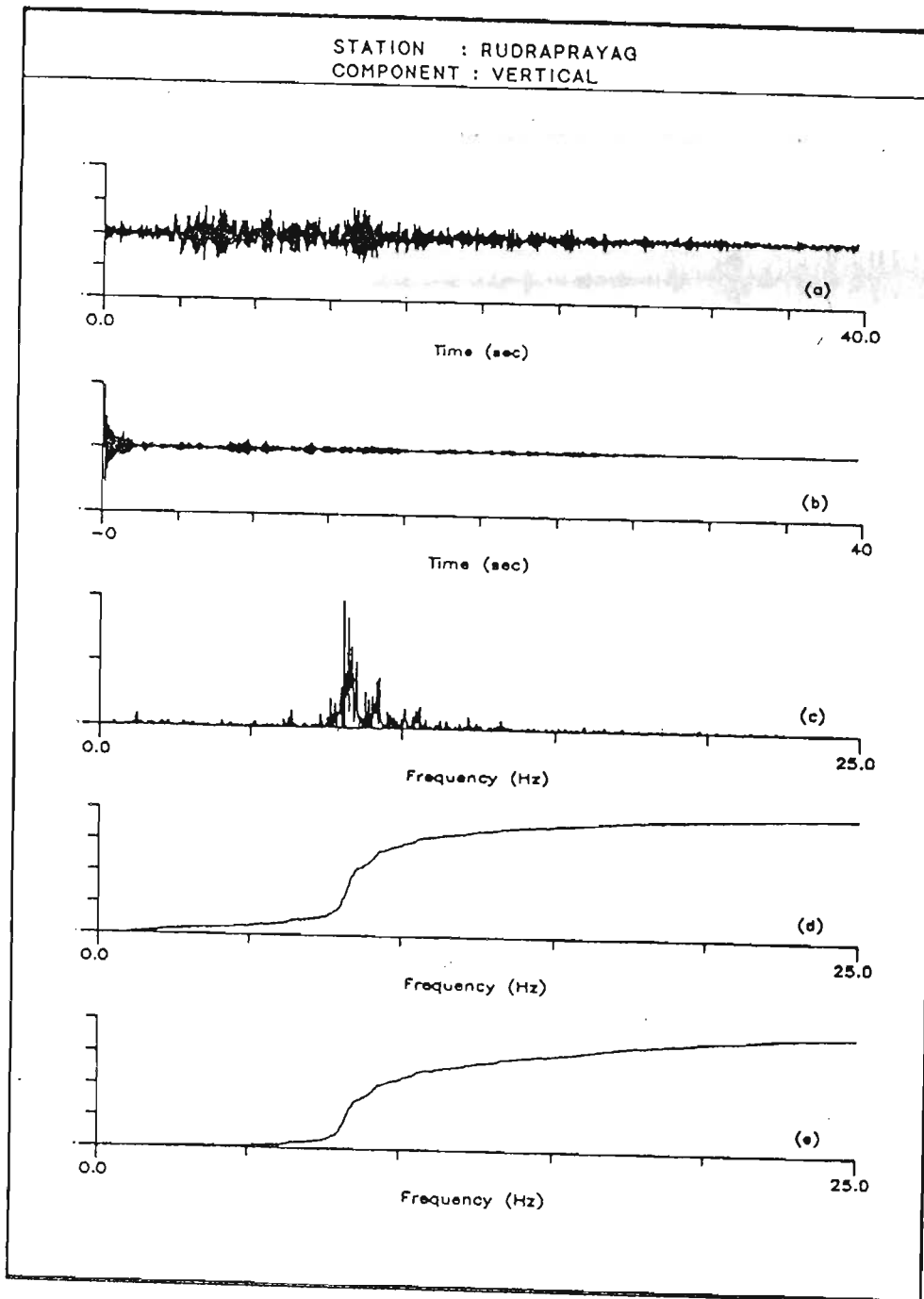


Fig 7.30 Uttarkashi earthquake of 20th Oct, 1991, vertical component recorded at Rudraprayag station. Y axis shows normalised value of (a) acceleration record, (b) its autocorrelation function, (c) its power spectrum, (d) its cumulative power spectrum and (e) its frequency weighted cumulative power spectrum. X axis for (a) and (b) shows time and for (c), (d) and (e) shows frequency. Feature extracted from field records at this station is given in Table 7.8.

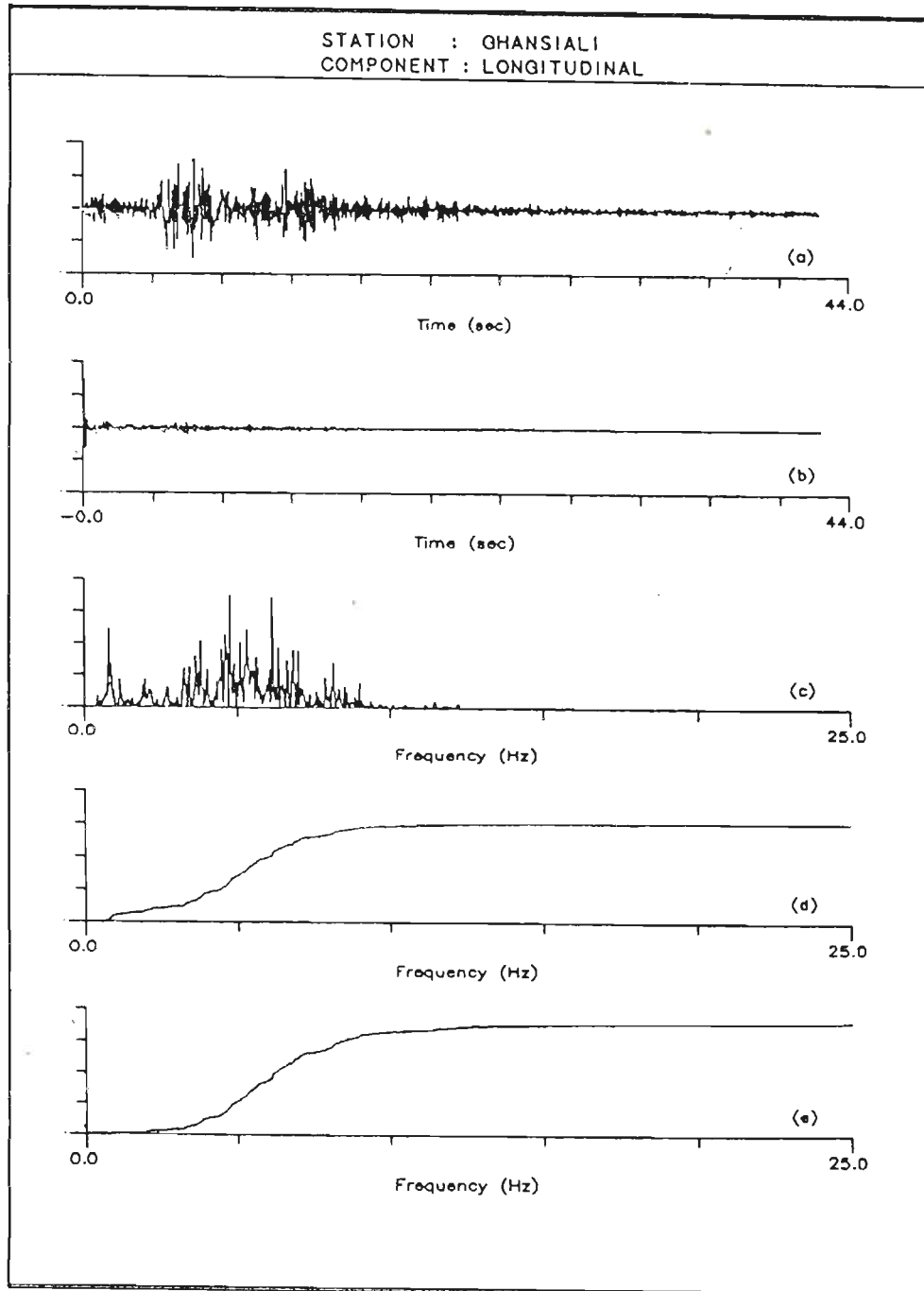


Fig 7.31 Uttarkashi earthquake of 20th Oct, 1991, longitudinal component recorded at Ghansiali station. Y axis shows normalised value of (a) acceleration record, (b) its autocorrelation function, (c) its power spectrum, (d) its cumulative power spectrum and (e) its frequency weighted cumulative power spectrum. X axis for (a) and (b) shows time and for (c), (d) and (e) shows frequency. Feature extracted from field records at this station is given in Table 7.9.

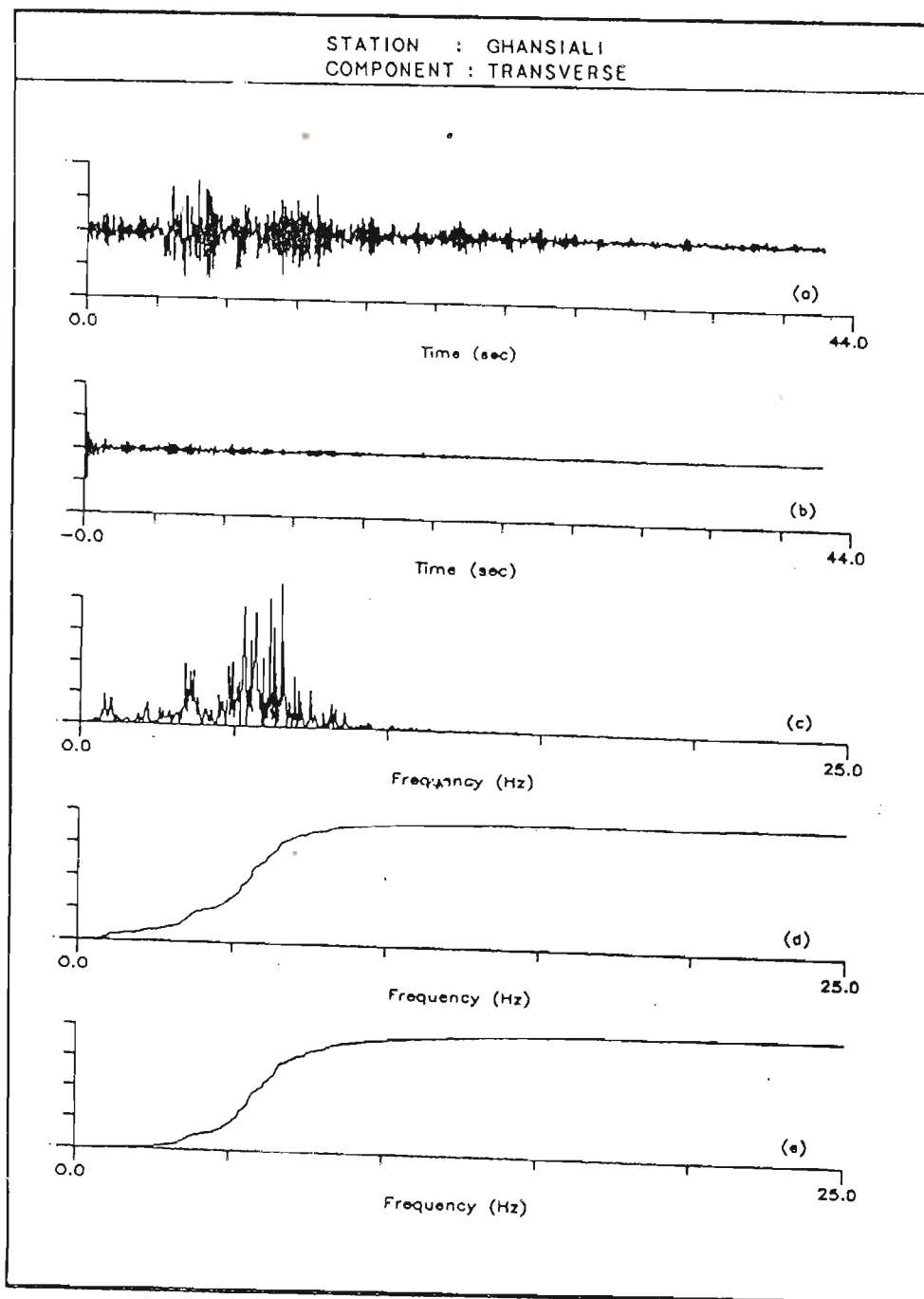


Fig 7.32 Uttarkashi earthquake of 20th Oct, 1991, transverse component recorded at Ghansiali station. Y axis shows normalised value of (a) acceleration record, (b) its autocorrelation function, (c) its power spectrum, (d) its cumulative power spectrum and (e) its frequency weighted cumulative power spectrum. X axis for (a) and (b) shows time and for (c), (d) and (e) shows frequency. Feature extracted from field records at this station is given in Table 7.9.

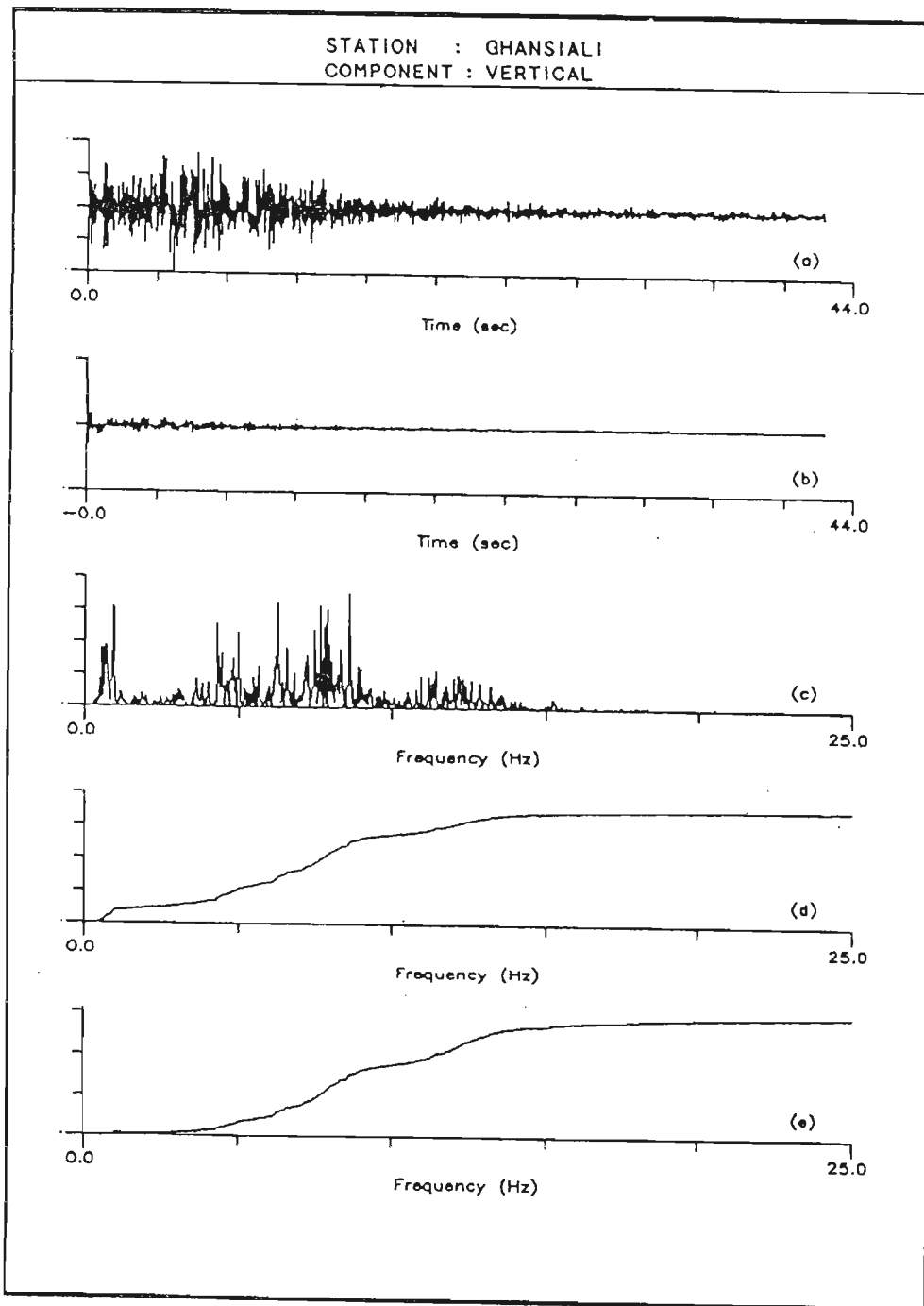


Fig 7.33 Uttarkashi earthquake of 20th Oct, 1991, vertical component recorded at Ghansiali station. Y axis shows normalised value of (a) acceleration record, (b) its autocorrelation function, (c) its power spectrum, (d) its cumulative power spectrum and (e) its frequency weighted cumulative power spectrum. X axis for (a) and (b) shows time and for (c), (d) and (e) shows frequency. Feature extracted from field records at this station is given in Table 7.9.

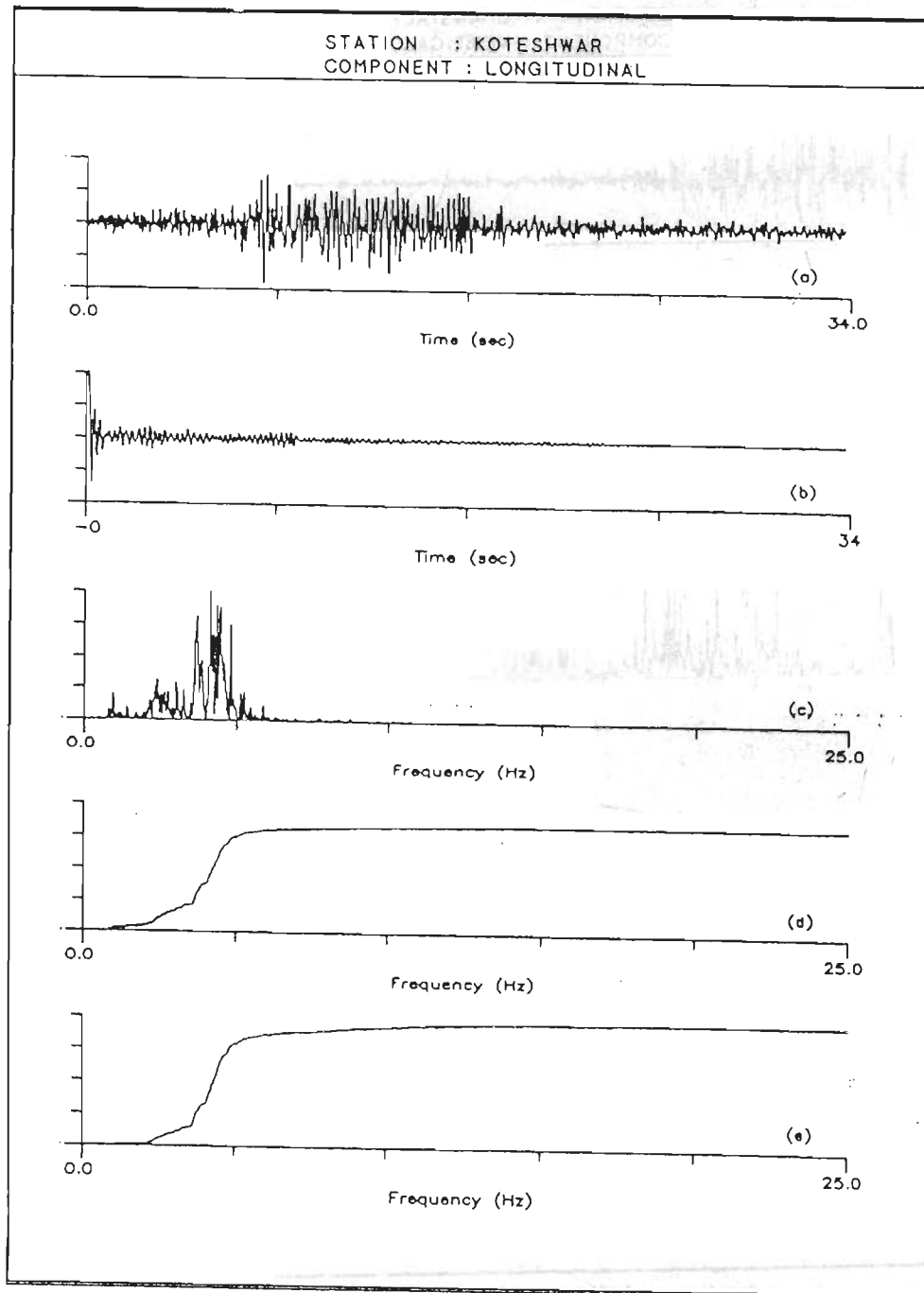


Fig 7.34 Uttarkashi earthquake of 20th Oct, 1991, longitudinal component recorded at Koteswar station. Y axis shows normalised value of (a) acceleration record, (b) its autocorrelation function, (c) its power spectrum, (d) its cumulative power spectrum and (e) its frequency weighted cumulative power spectrum. X axis for (a) and (b) shows time and for (c), (d) and (e) shows frequency. Feature extracted from field records at this station is given in Table 7.9.

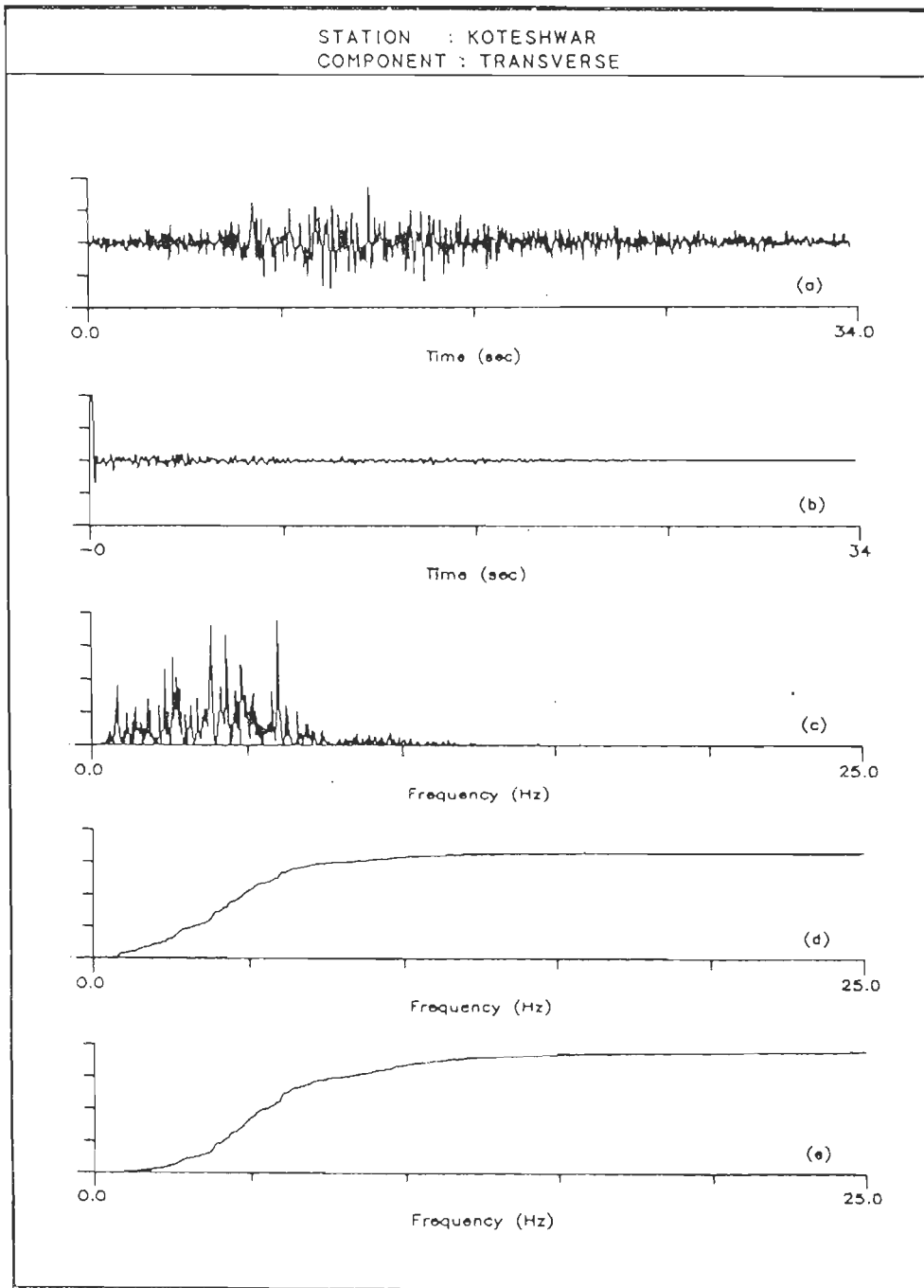


Fig 7.35 Uttarkashi earthquake of 20th Oct, 1991, transverse component recorded at Koteswar station. Y axis shows normalised value of (a) acceleration record, (b) its autocorrelation function, (c) its power spectrum, (d) its cumulative power spectrum and (e) its frequency weighted cumulative power spectrum. X axis for (a) and (b) shows time and for (c), (d) and (e) shows frequency. Feature extracted from field records at this station is given in Table 7.9.

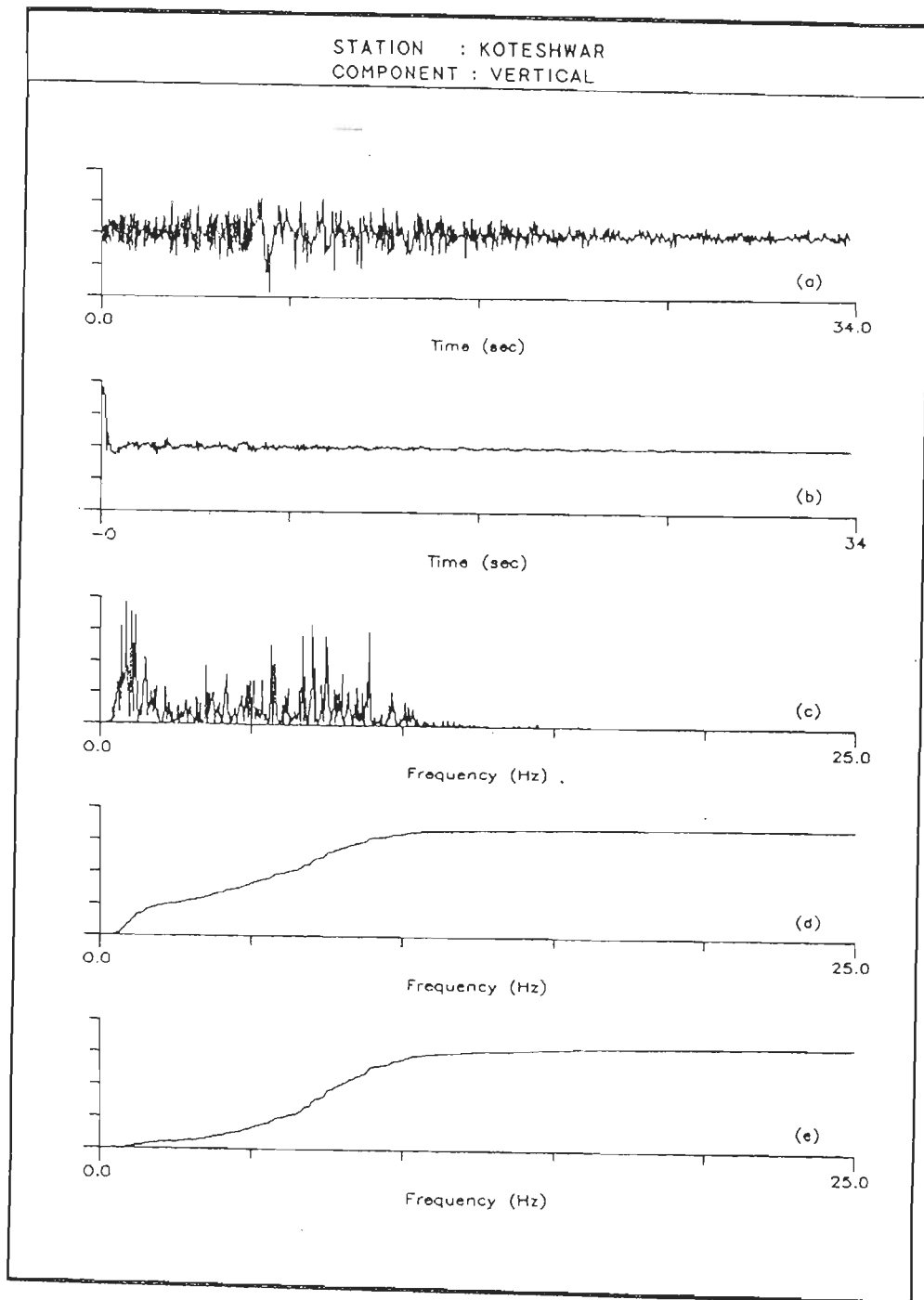


Fig 7.36 Uttarkashi earthquake of 20th Oct, 1991, vertical component recorded at Koteswar station. Y axis shows normalised value of (a) acceleration record, (b) its autocorrelation function, (c) its power spectrum, (d) its cumulative power spectrum and (e) its frequency weighted cumulative power spectrum. X axis for (a) and (b) shows time and for (c), (d) and (e) shows frequency. Feature extracted from field records at this station is given in Table 7.9.

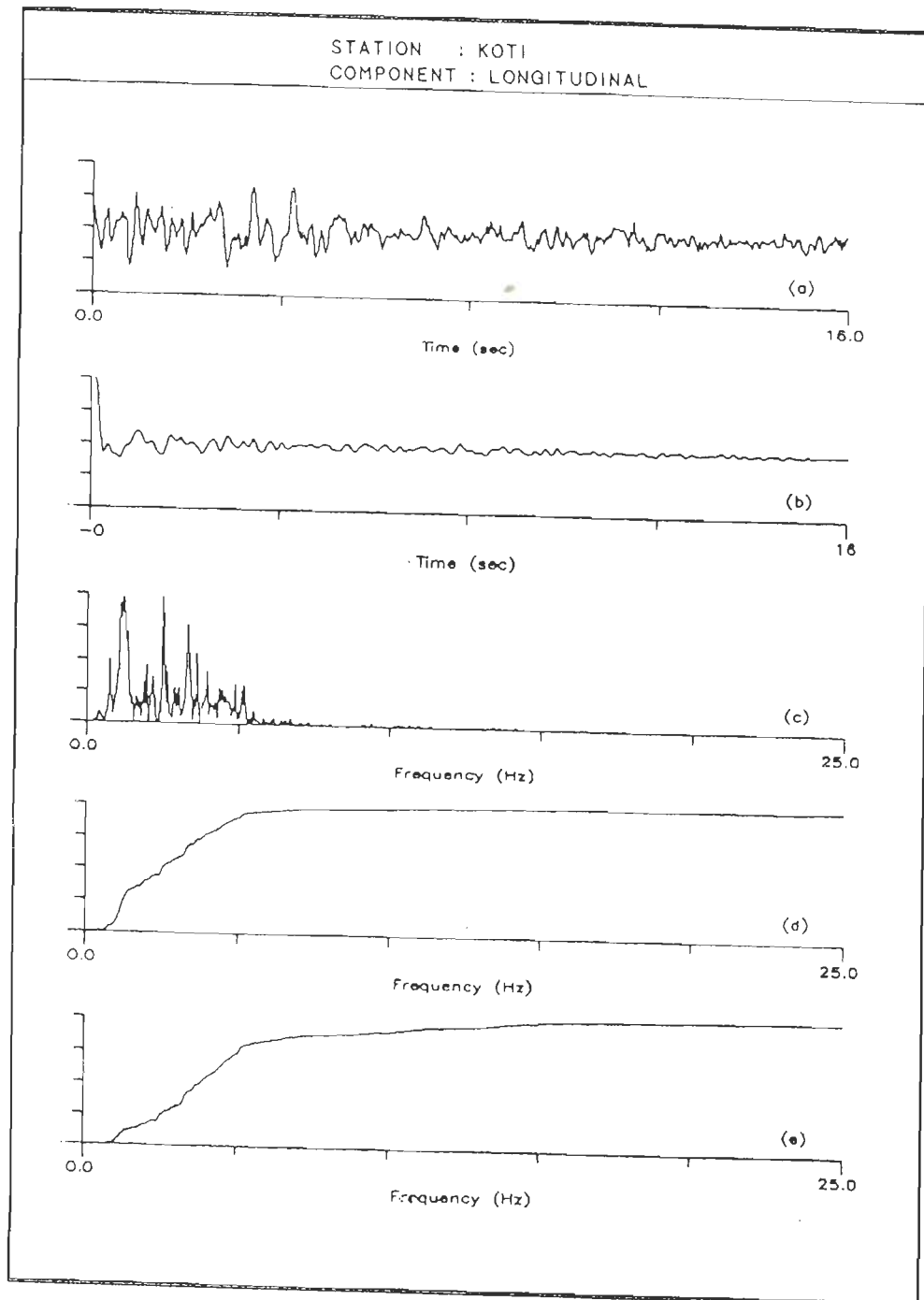


Fig 7.37 Uttarkashi earthquake of 20th Oct, 1991, longitudinal component recorded at Koti station. Y axis shows normalised value of (a) acceleration record, (b) its autocorrelation function, (c) its power spectrum, (d) its cumulative power spectrum and (e) its frequency weighted cumulative power spectrum. X axis for (a) and (b) shows time and for (c), (d) and (e) shows frequency. Feature extracted from field records at this station is given in Table 7.10.

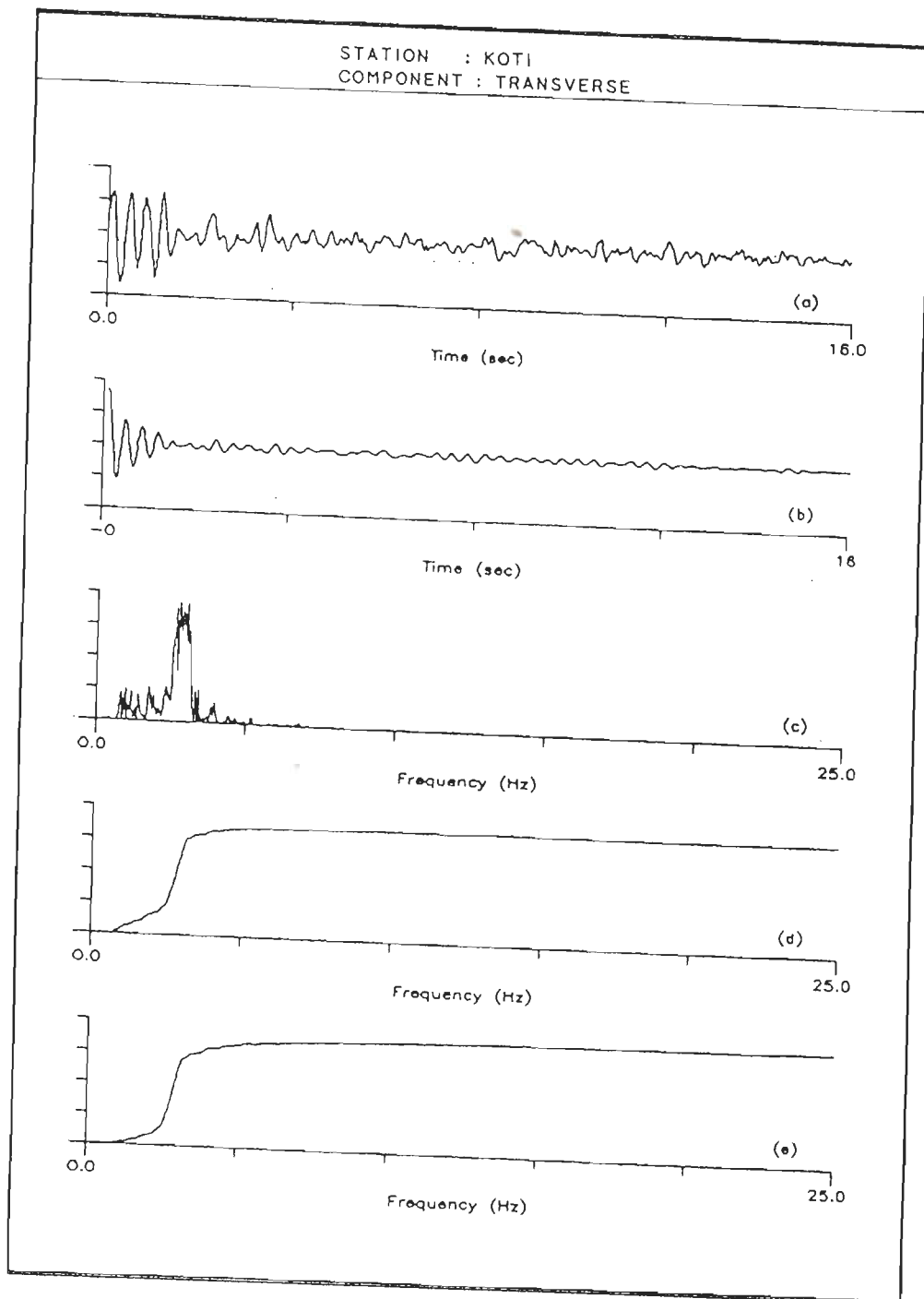


Fig 7.38 Uttarkashi earthquake of 20th Oct, 1991, transverse component recorded at Koti station. Y axis shows normalised value of (a) acceleration record, (b) its autocorrelation function, (c) its power spectrum, (d) its cumulative power spectrum and (e) its frequency weighted cumulative power spectrum. X axis for (a) and (b) shows time and for (c), (d) and (e) shows frequency. Feature extracted from field records at this station is given in Table 7.10.

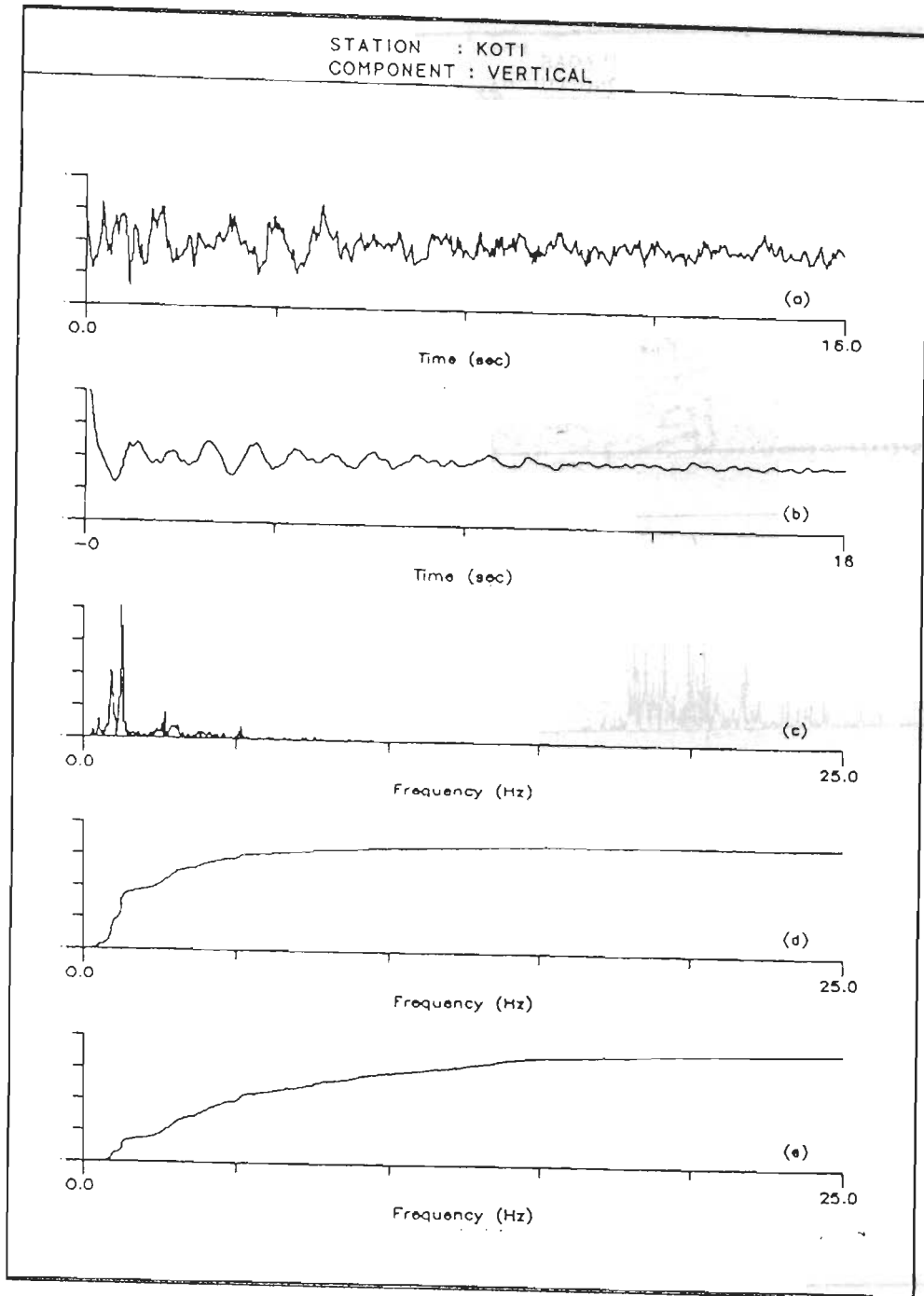


Fig 7.39 Uttarkashi earthquake of 20th Oct, 1991, vertical component recorded at Koti station. Y axis shows normalised value of (a) acceleration record, (b) its autocorrelation function, (c) its power spectrum, (d) its cumulative power spectrum and (e) its frequency weighted cumulative power spectrum. X axis for (a) and (b) shows time and for (c), (d) and (e) shows frequency. Feature extracted from field records at this station is given in Table 7.10.

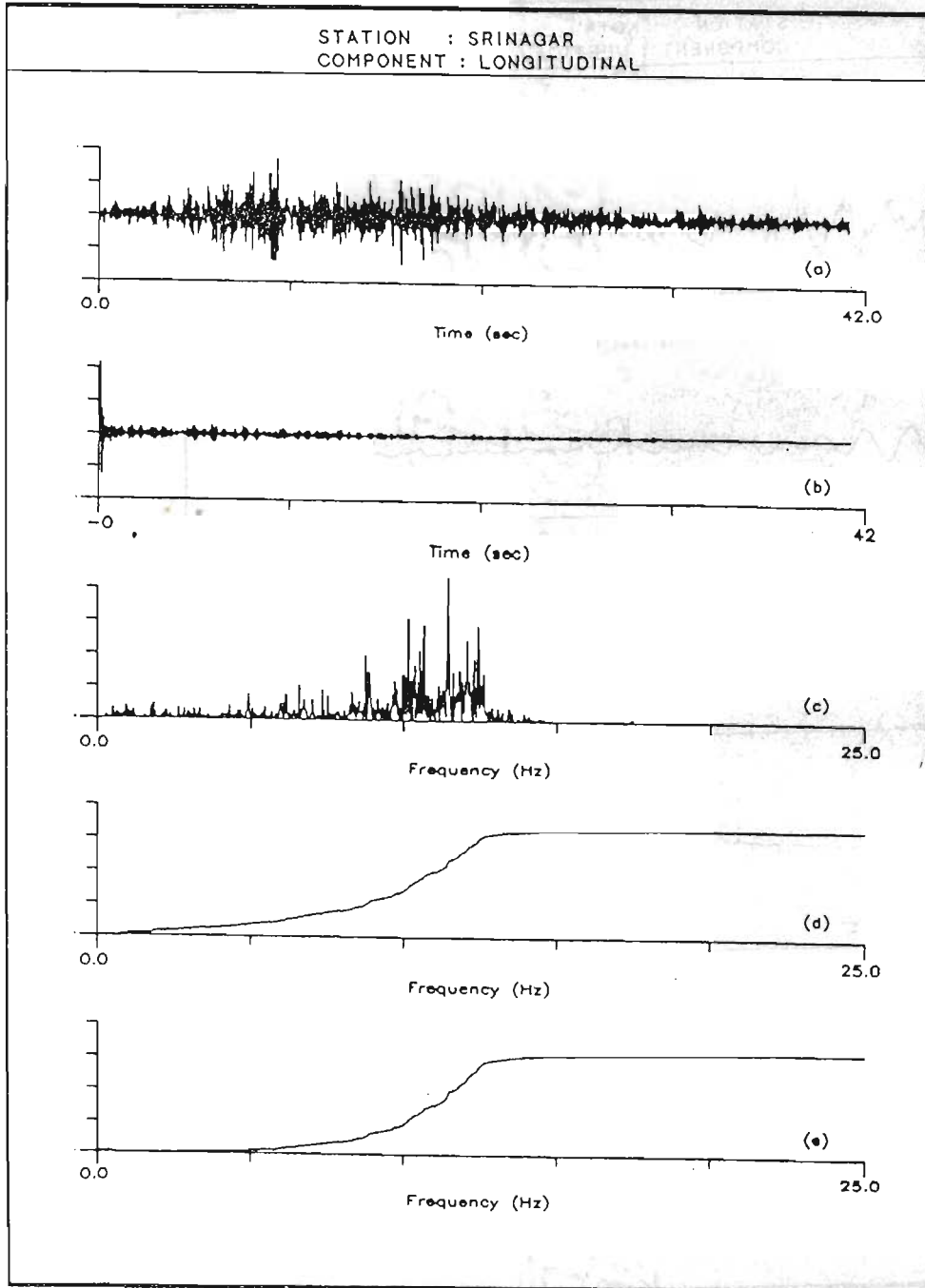


Fig 7.40 Uttarkashi earthquake of 20th Oct, 1991, longitudinal component recorded at Srinagar station. Y axis shows normalised value of (a) acceleration record, (b) its autocorrelation function, (c) its power spectrum, (d) its cumulative power spectrum and (e) its frequency weighted cumulative power spectrum. X axis for (a) and (b) shows time and for (c), (d) and (e) shows frequency. Feature extracted from field records at this station is given in Table 7.10.

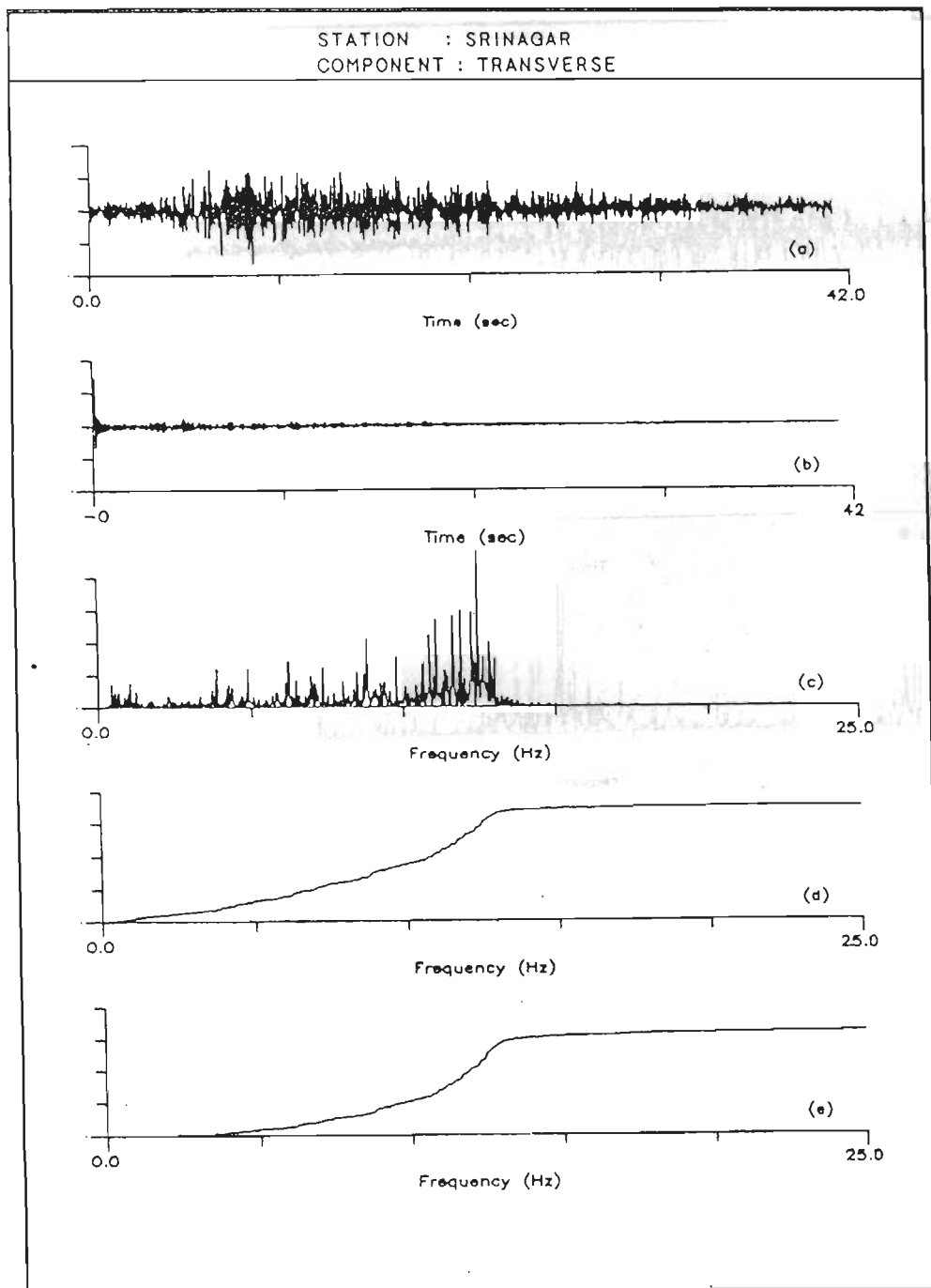


Fig 7.41 Uttarkashi earthquake of 20th Oct, 1991, transverse component recorded at Srinagar station. Y axis shows normalised value of (a) acceleration record, (b) its autocorrelation function, (c) its power spectrum, (d) its cumulative power spectrum and (e) its frequency weighted cumulative power spectrum. X axis for (a) and (b) shows time and for (c), (d) and (e) shows frequency. Feature extracted from field records at this station is given in Table 7.10.

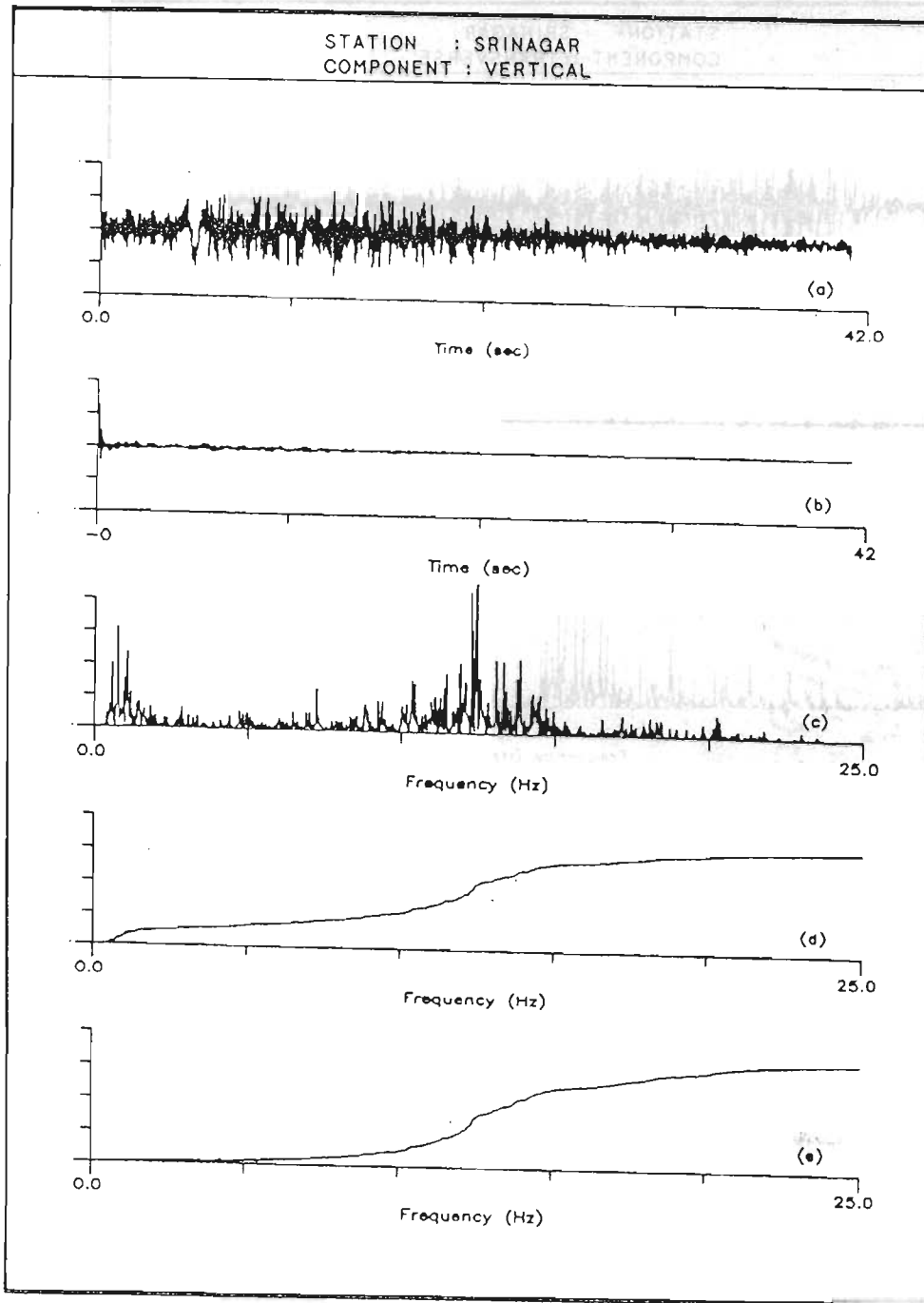


Fig 7.42 Uttarkashi earthquake of 20th Oct, 1991, vertical component recorded at Srinagar station. Y axis shows normalised value of (a) acceleration record, (b) its autocorrelation function, (c) its power spectrum, (d) its cumulative power spectrum and (e) its frequency weighted cumulative power spectrum. X axis for (a) and (b) shows time and for (c), (d) and (e) shows frequency. Feature extracted from field records at this station is given in Table 7.10.

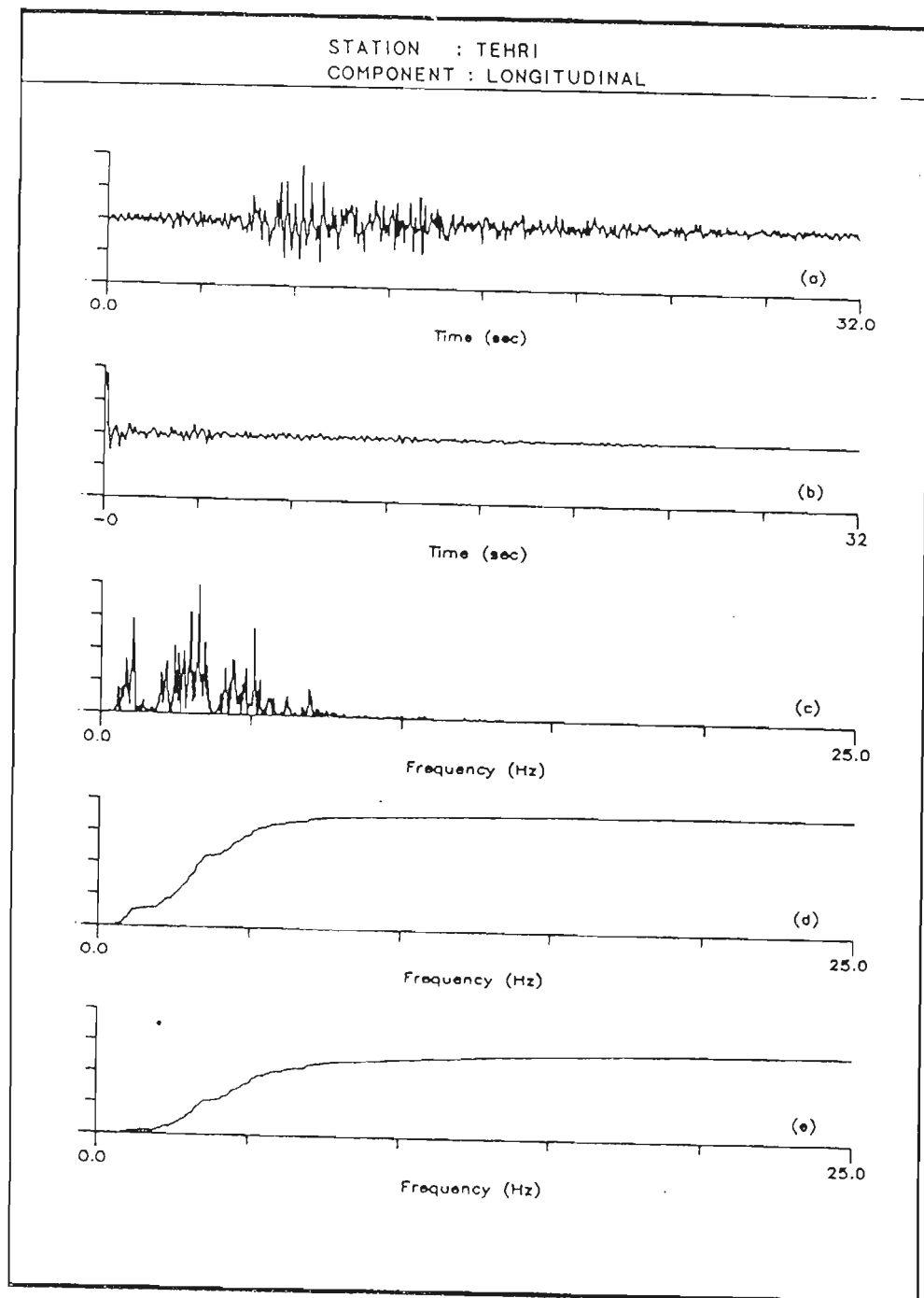


Fig 7.43 Uttarkashi earthquake of 20th Oct, 1991, longitudinal component recorded at Tehri station. Y axis shows normalised value of (a) acceleration record, (b) its autocorrelation function, (c) its power spectrum, (d) its cumulative power spectrum and (e) its frequency weighted cumulative power spectrum. X axis for (a) and (b) shows time and for (c), (d) and (e) shows frequency. Feature extracted from field records at this station is given in Table 7.11.

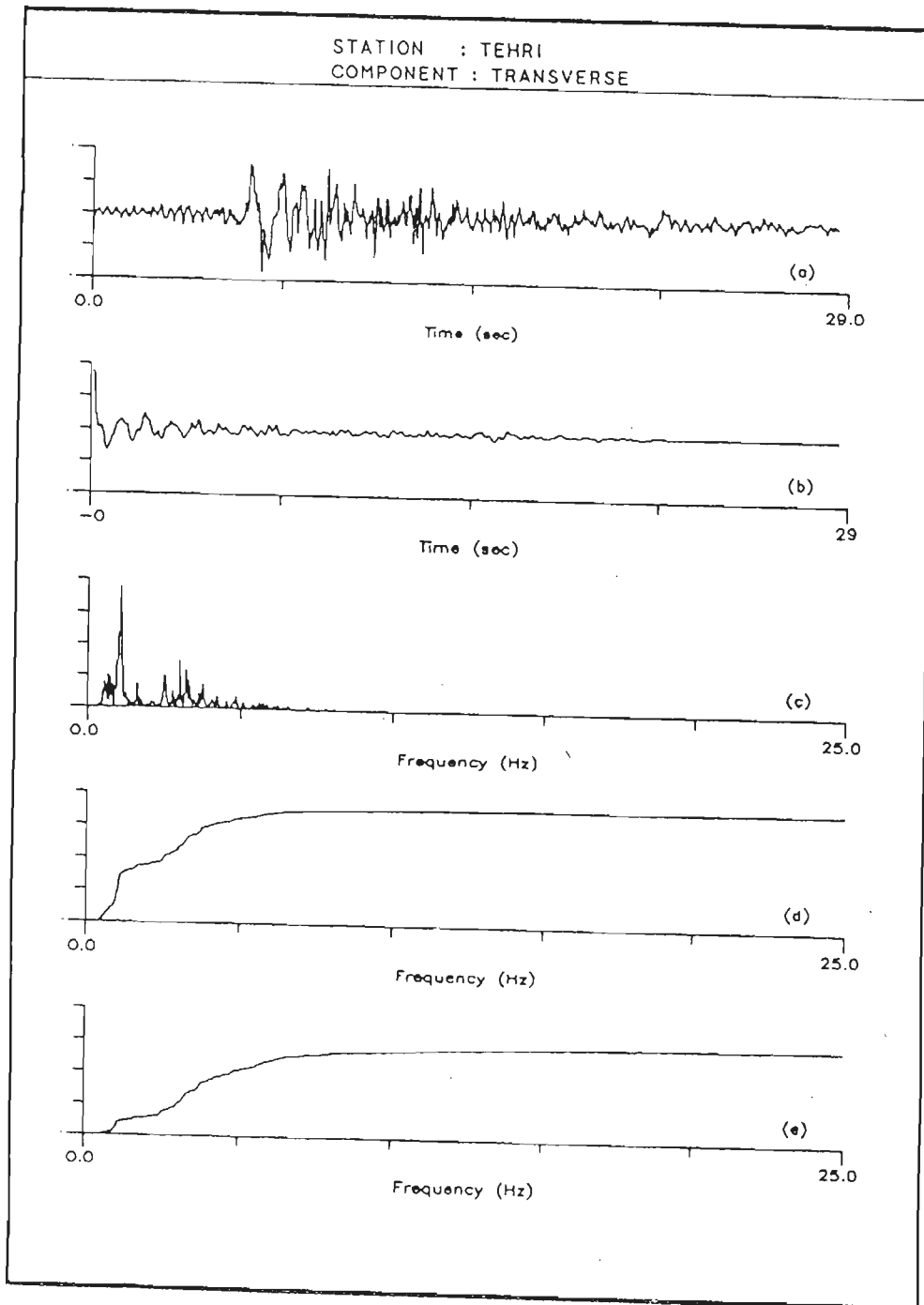


Fig 7.44 Uttarkashi earthquake of 20th Oct, 1991, transverse component recorded at Tehri station. Y axis shows normalised value of (a) acceleration record, (b) its autocorrelation function, (c) its power spectrum, (d) its cumulative power spectrum and (e) its frequency weighted cumulative power spectrum. X axis for (a) and (b) shows time and for (c), (d) and (e) shows frequency. Feature extracted from field records at this station is given in Table 7.11.

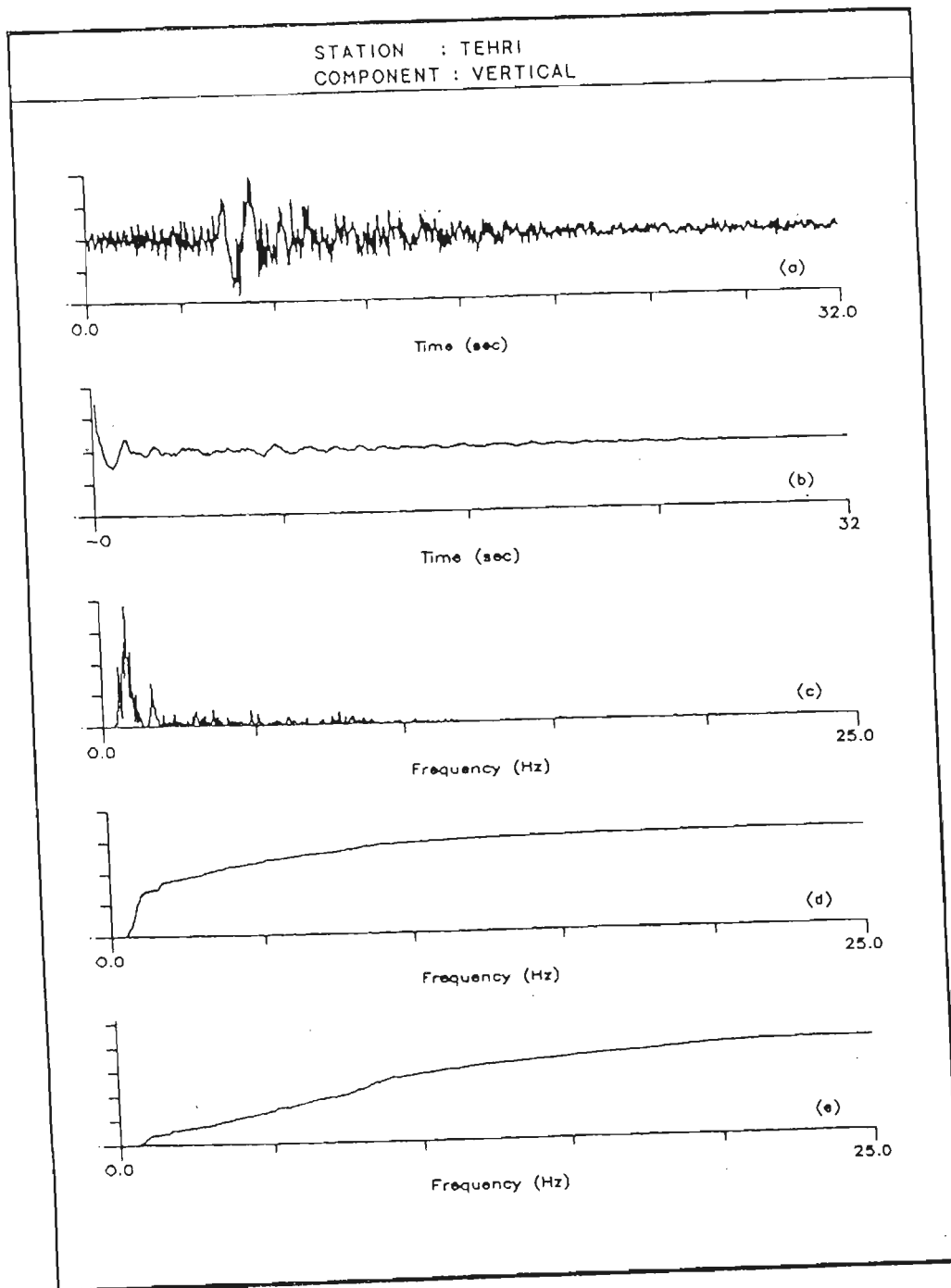


Fig 7.45 Uttarkashi earthquake of 20th Oct, 1991, vertical component recorded at Tehri station. Y axis shows normalised value of (a) acceleration record, (b) its autocorrelation function, (c) its power spectrum, (d) its cumulative power spectrum and (e) its frequency weighted cumulative power spectrum. X axis for (a) and (b) shows time and for (c), (d) and (e) shows frequency. Feature extracted from field records at this station is given in Table 7.11.

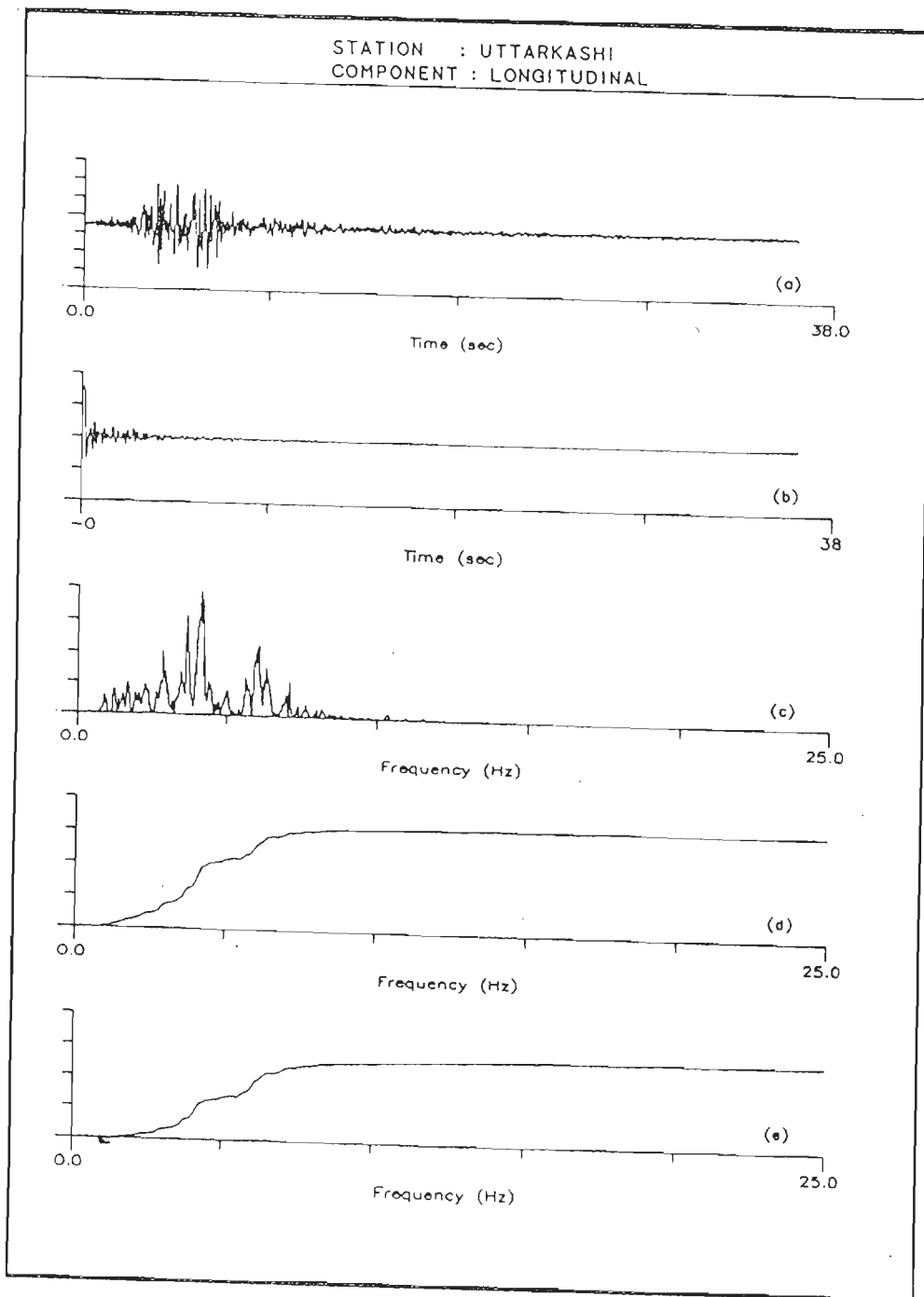


Fig 7.46 Uttarkashi earthquake of 20th Oct, 1991, longitudinal component recorded at Uttarkashi station. Y axis shows normalised value of (a) acceleration record, (b) its autocorrelation function, (c) its power spectrum, (d) its cumulative power spectrum and (e) its frequency weighted cumulative power spectrum. X axis for (a) and (b) shows time and for (c), (d) and (e) shows frequency. Feature extracted from field records at this station is given in Table 7.12.

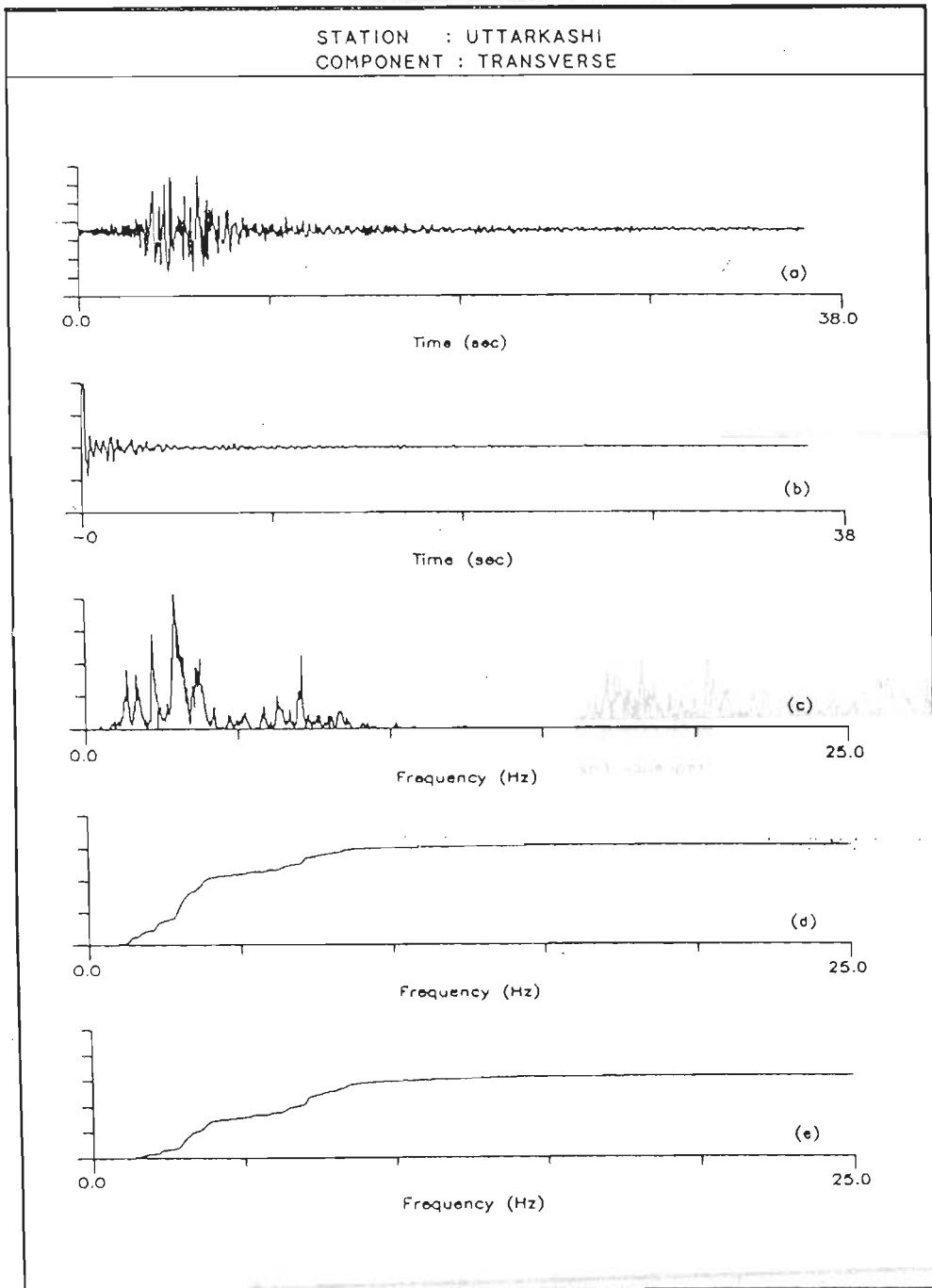


Fig 7.47 Uttarkashi earthquake of 20th Oct, 1991, transverse component recorded at Uttarkashi station. Y axis shows normalised value of (a) acceleration record, (b) its autocorrelation function, (c) its power spectrum, (d) its cumulative power spectrum and (e) its frequency weighted cumulative power spectrum. X axis for (a) and (b) shows time and for (c), (d) and (e) shows frequency. Feature extracted from field records at this station is given in Table 7.12.

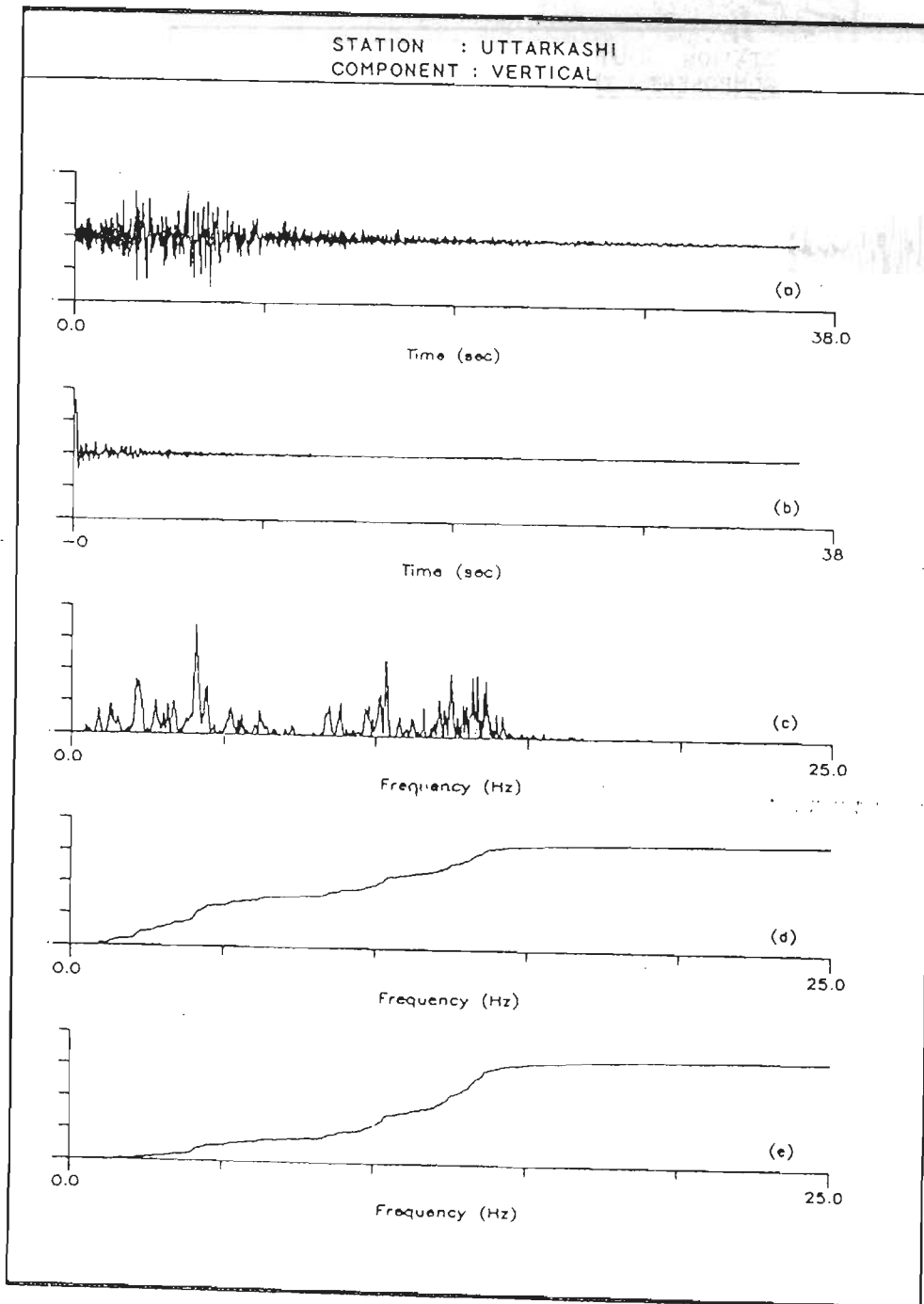


Fig 7.48 Uttarkashi earthquake of 20th Oct, 1991, vertical component recorded at Uttarkashi station. Y axis shows normalised value of (a) acceleration record, (b) its autocorrelation function, (c) its power spectrum, (d) its cumulative power spectrum and (e) its frequency weighted cumulative power spectrum. X axis for (a) and (b) shows time and for (c), (d) and (e) shows frequency. Feature extracted from field records at this station is given in Table 7.12.

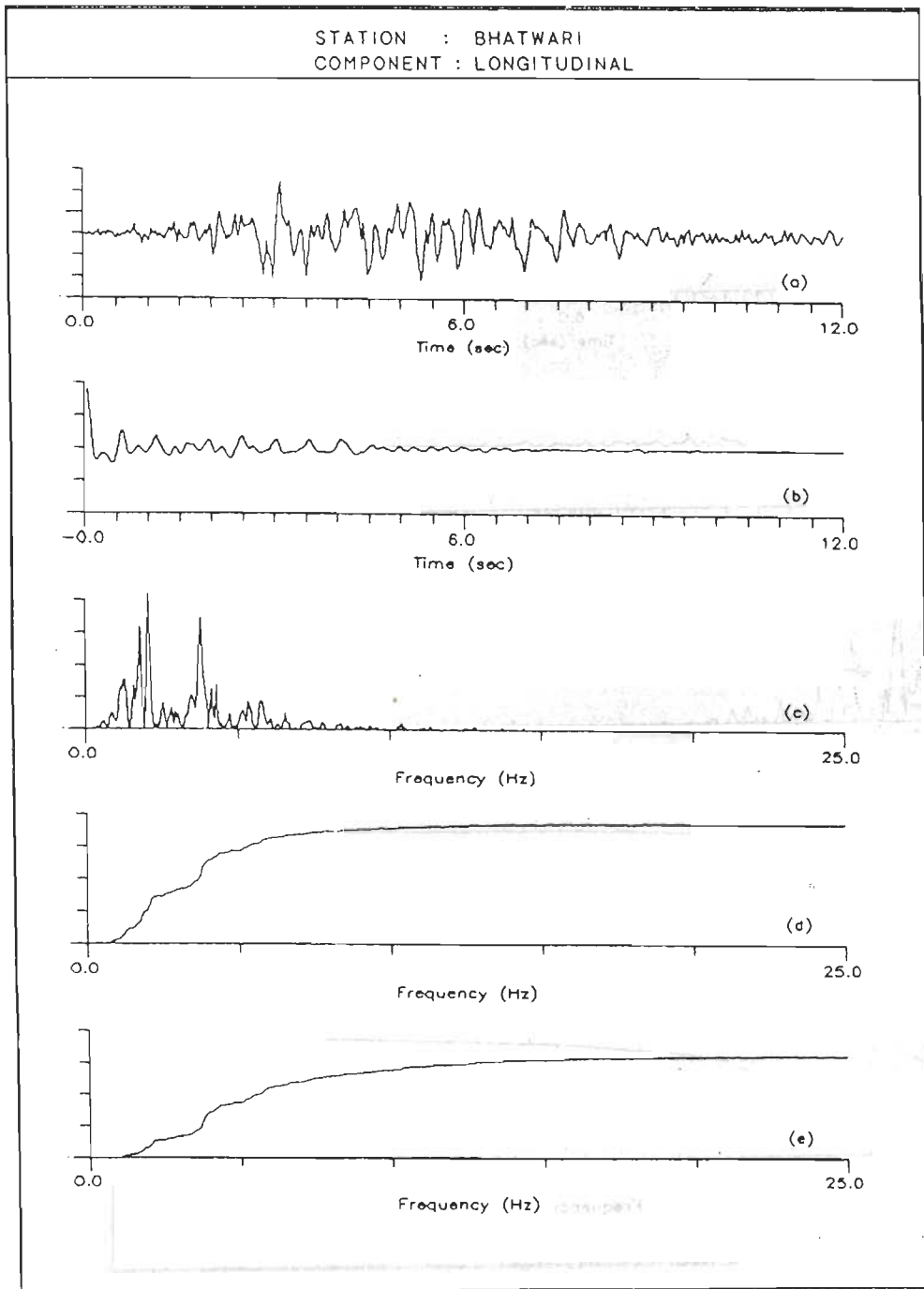


Fig 7.49 Uttarkashi earthquake of 20th Oct, 1991, longitudinal component recorded at Bhatwari station. Y axis shows normalised value of (a) acceleration record, (b) its autocorrelation function, (c) its power spectrum, (d) its cumulative power spectrum and (e) its frequency weighted cumulative power spectrum. X axis for (a) and (b) shows time and for (c), (d) and (e) shows frequency. Feature extracted from field records at this station is given in Table 7.12.

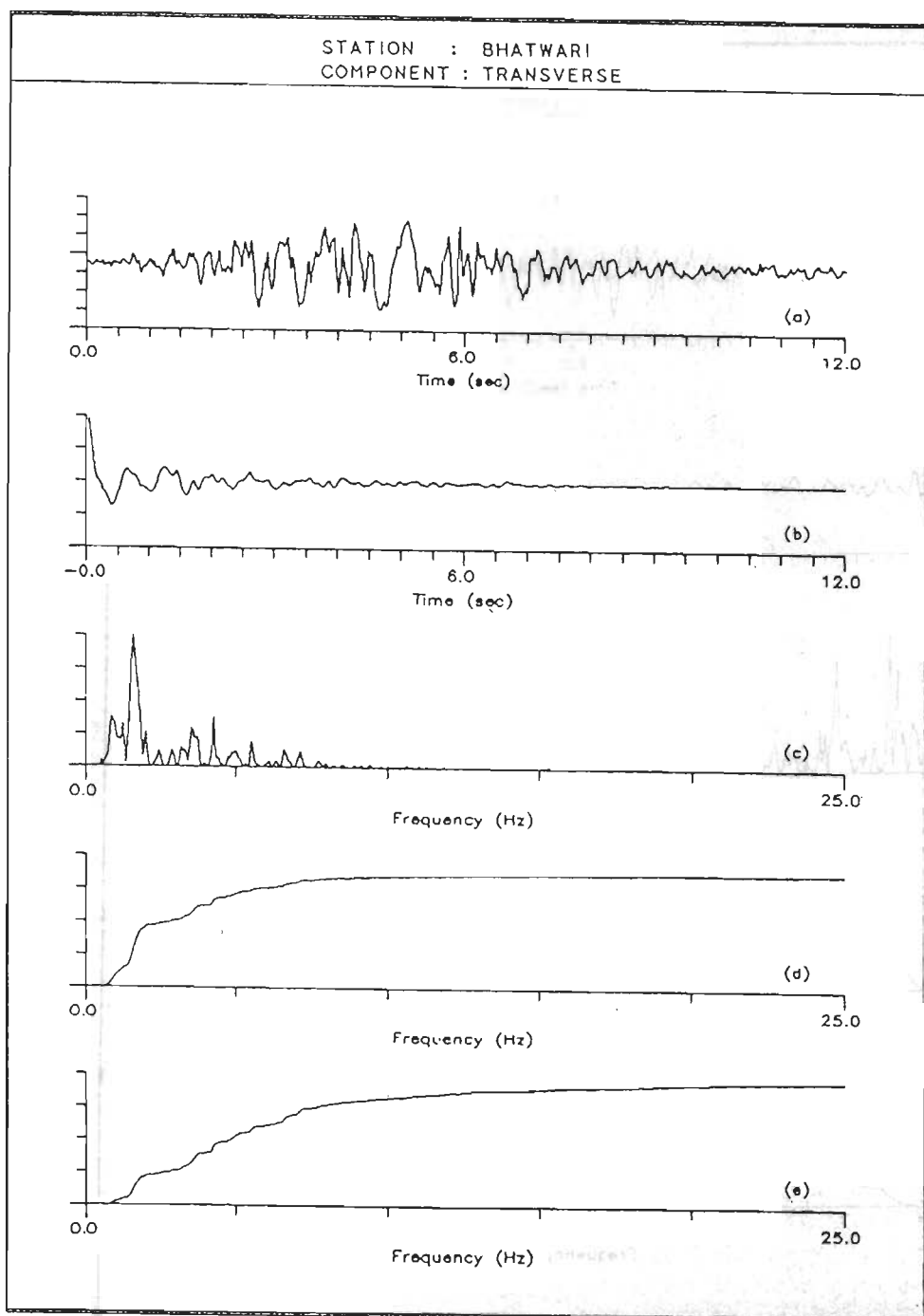


Fig 7.50 Uttarkashi earthquake of 20th Oct, 1991, transverse component recorded at Bhatwari station. Y axis shows normalised value of (a) acceleration record, (b) its autocorrelation function, (c) its power spectrum, (d) its cumulative power spectrum and (e) its frequency weighted cumulative power spectrum. X axis for (a) and (b) shows time and for (c), (d) and (e) shows frequency. Feature extracted from field records at this station is given in Table 7.12.

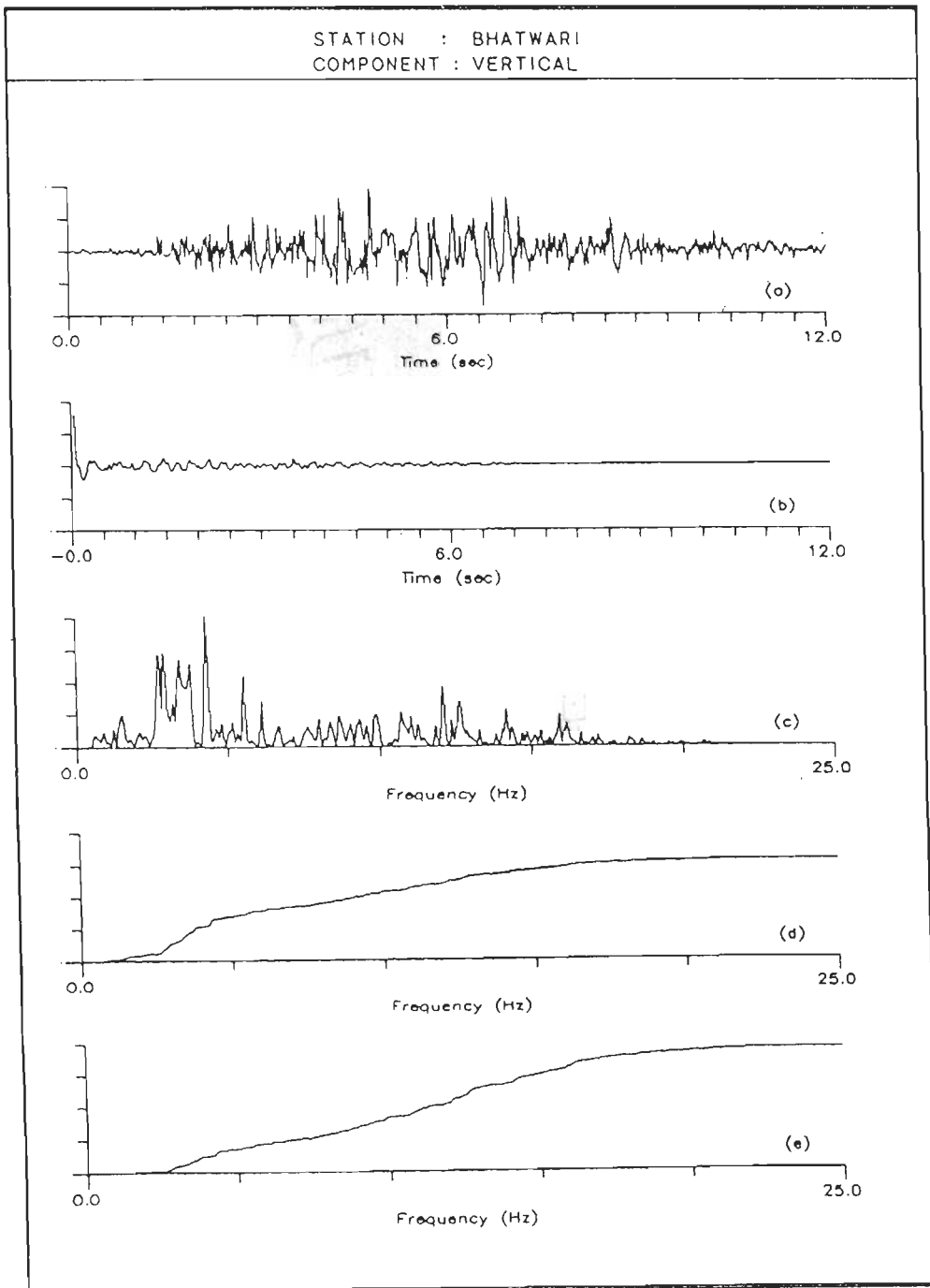


Fig 7.51 Uttarkashi earthquake of 20th Oct, 1991, vertical component recorded at Bhatwari station. Y axis shows normalised value of (a) acceleration record, (b) its autocorrelation function, (c) its power spectrum, (d) its cumulative power spectrum and (e) its frequency weighted cumulative power spectrum. X axis for (a) and (b) shows time and for (c), (d) and (e) shows frequency. Feature extracted from field records at this station is given in Table 7.12.

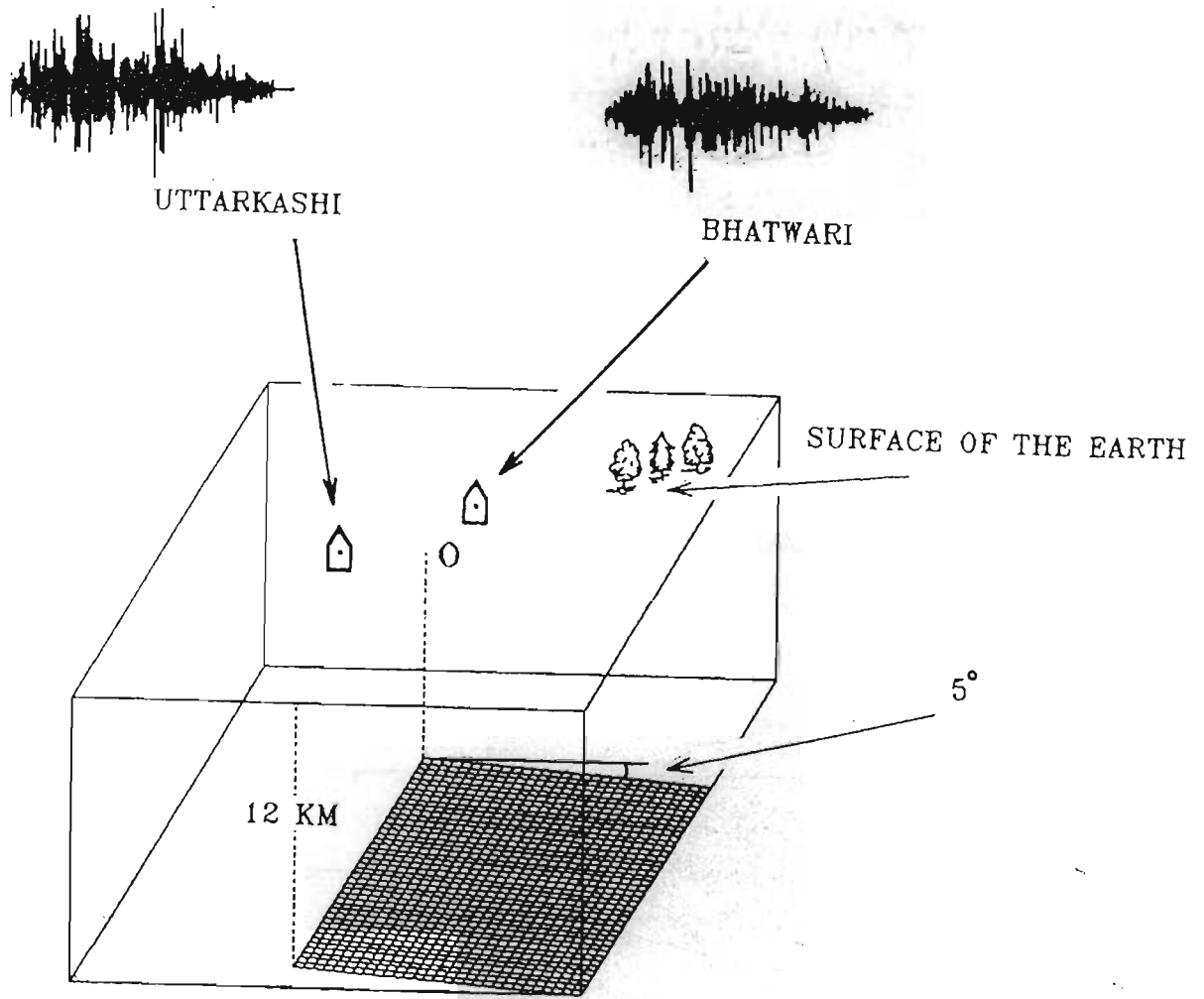


Fig 7.52 Model MU_{d1} for the Uttarkashi earthquake having dip and strike as 5° and 296° , respectively. Simulated acceleration records at Bhatwari and Uttarkashi are shown with the model MU_{d1} of the rupture plane. Parameters extracted from these records are given in Table 7.13.

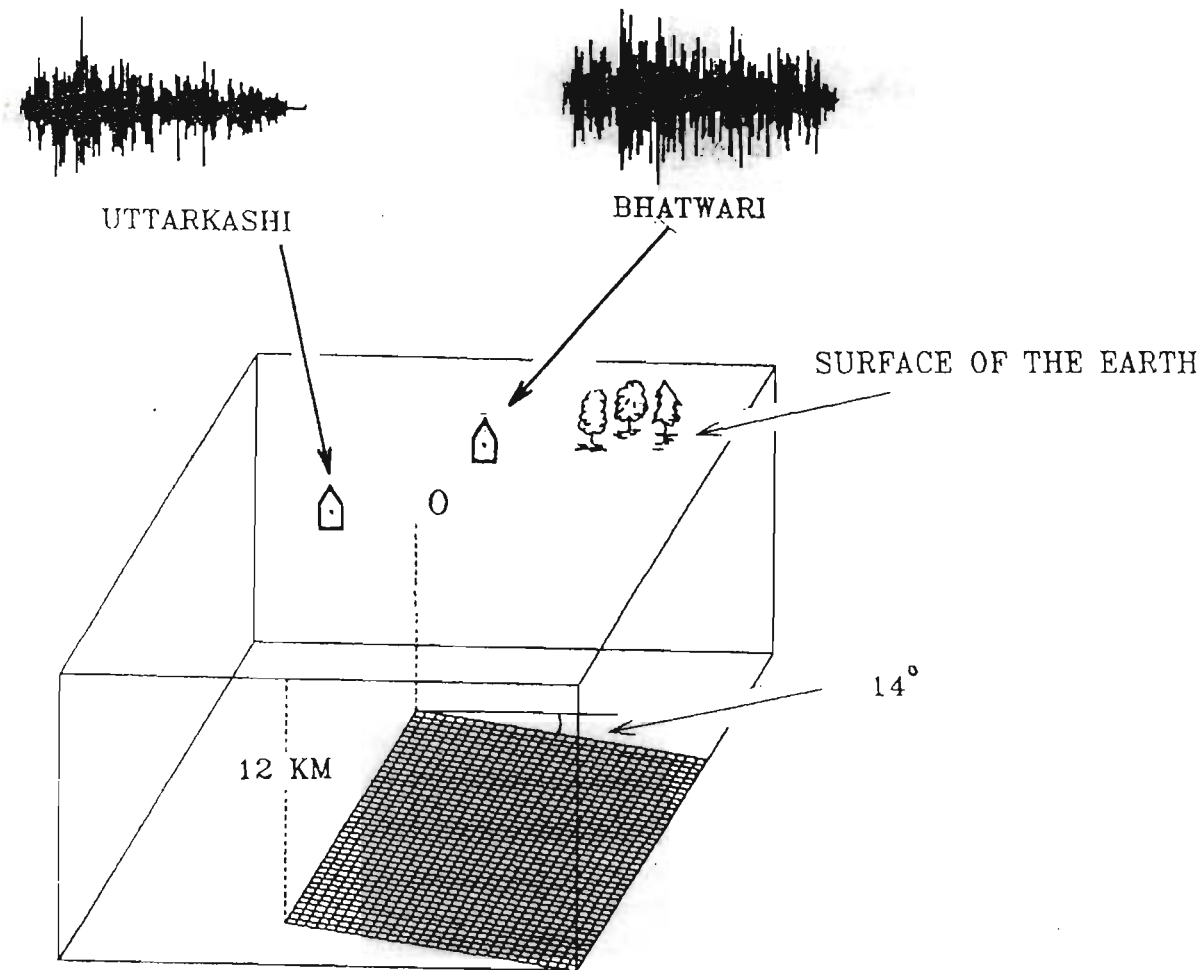


Fig 7.53 Model MU_{d2} for the Uttarkashi earthquake having dip and strike as 14° and 317° , respectively. Simulated acceleration records at Bhatwari and Uttarkashi are shown with the model MU_{d2} of the rupture plane. Parameters extracted from these records are given in Table 7.13.

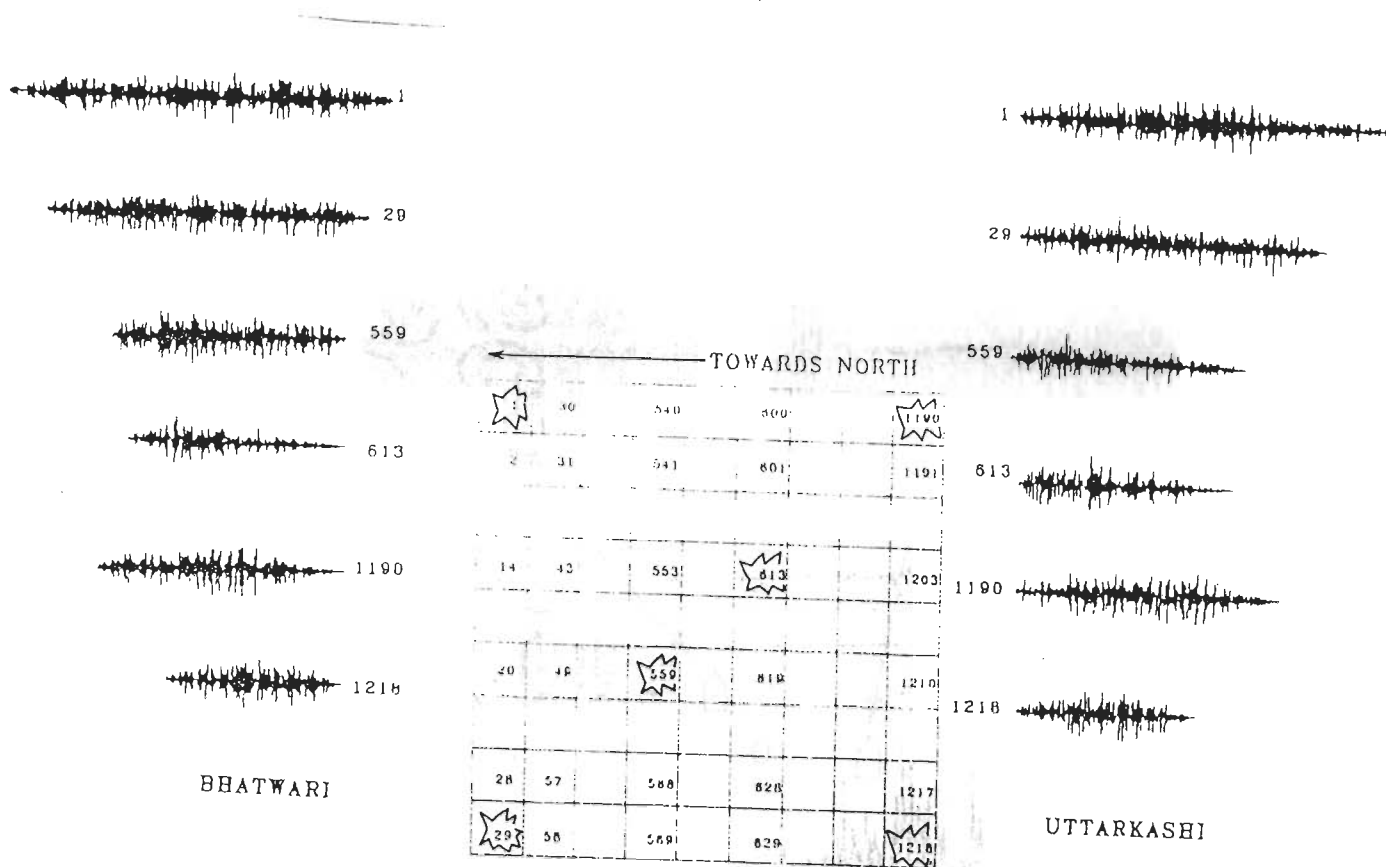


Fig 7.54 Model of rupture plane showing method of numbering elements within the rupture plane. Acceleration records are simulated at Bhatwari and Uttarkashi stations by assuming different elements within rupture plane as starting point of rupture. Number corresponding to each simulated record shows the element number which is assumed as nucleation point. Features extracted from these simulated records at Bhatwari and Uttarkashi are shown in Table 7.15 and 7.16, respectively. The center of element numbered as '1' is the origin of three dimensional coordinate system.

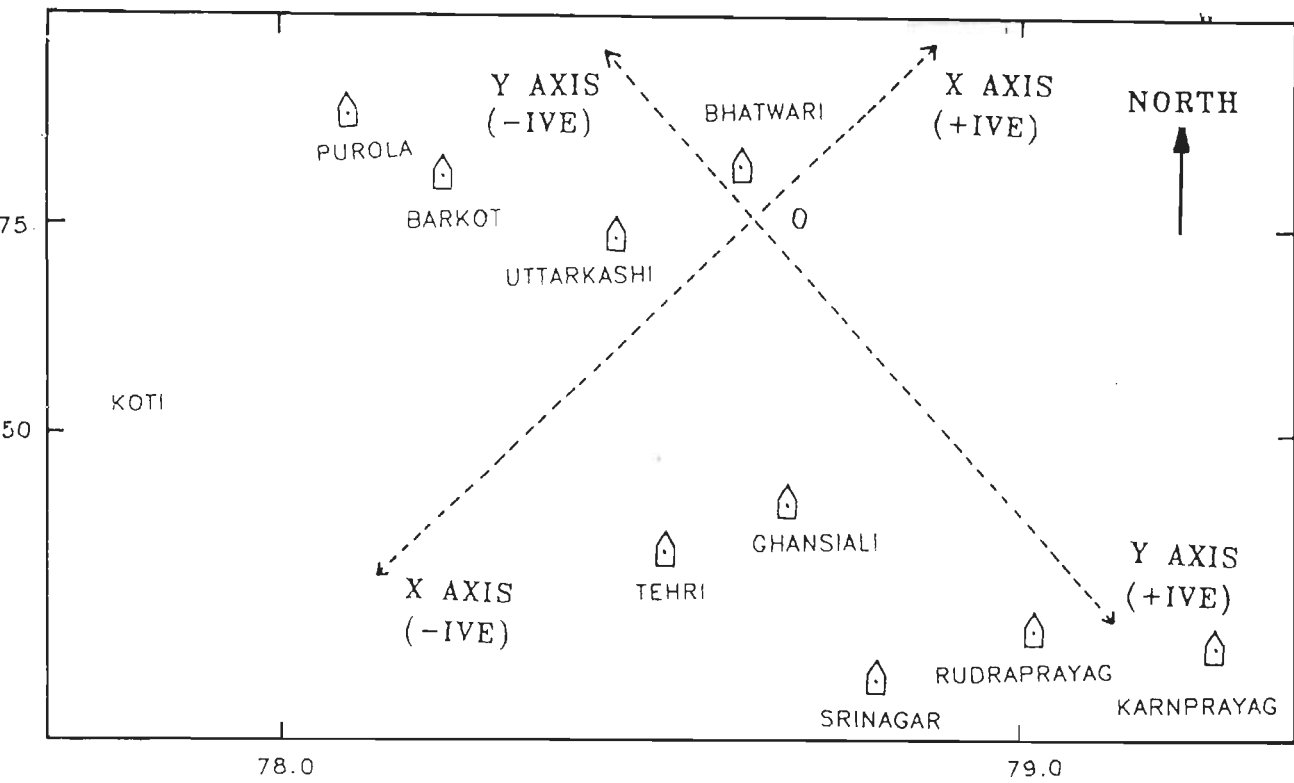


Fig 7.55 Location of points at which acceleration records are simulated. The origin of the assumed coordinate system is placed at a depth of 12 km below point O marked in Fig 7.11. Coordinates of selected stations in rectangular coordinate system is given in Table 7.18.

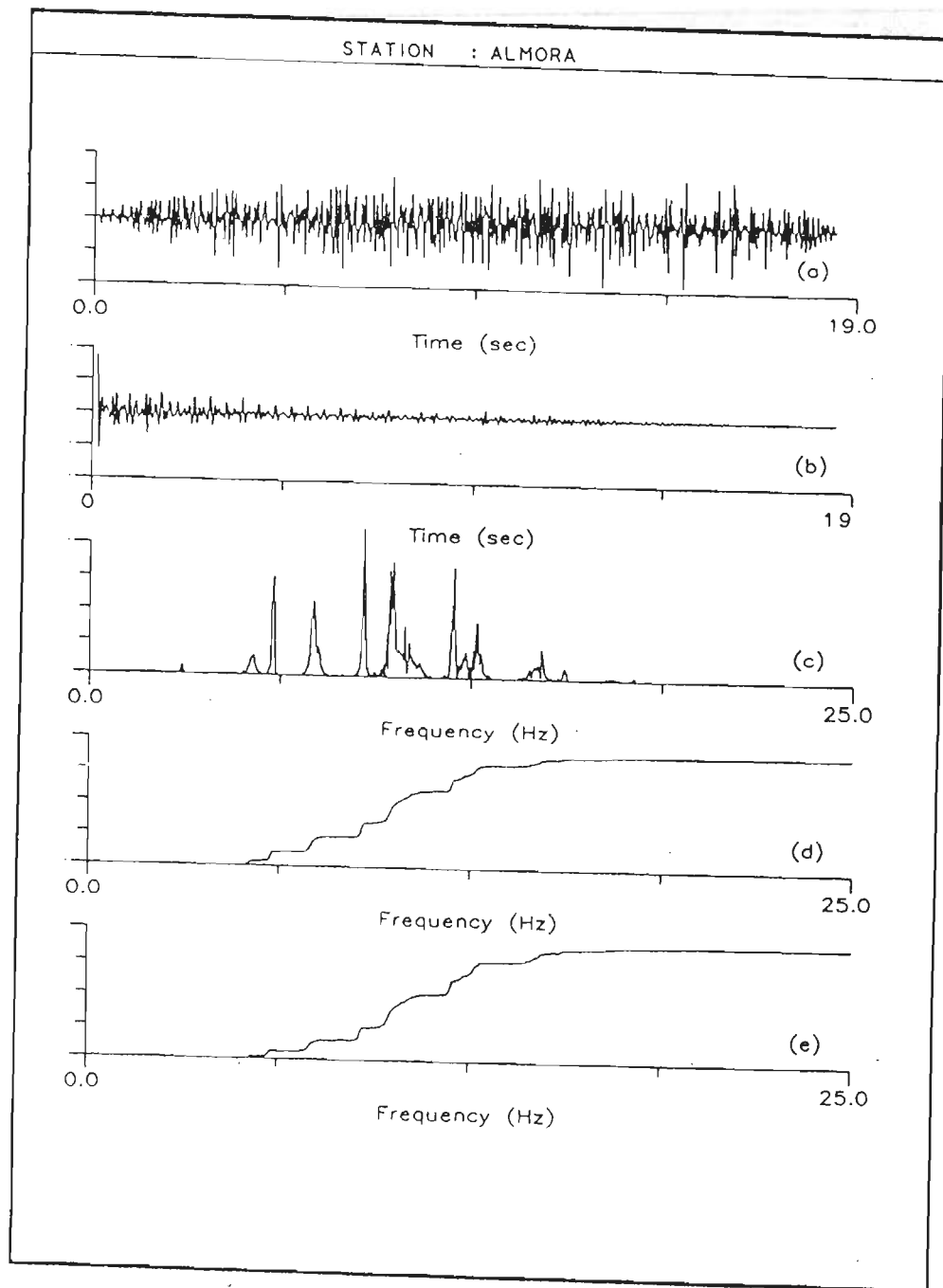


Fig 7.56 Uttarkashi earthquake of 20th Oct, 1991, simulated acceleration record at Almora station. Y axis shows normalised value of (a) acceleration record, (b) its autocorrelation function, (c) its power spectrum, (d) its cumulative power spectrum and (e) its frequency weighted cumulative power spectrum. X axis for (a) and (b) shows time and for (c), (d) and (e) shows frequency. Features extracted from simulated records at this station are given in Table 7.19, 7.20 and 7.21.

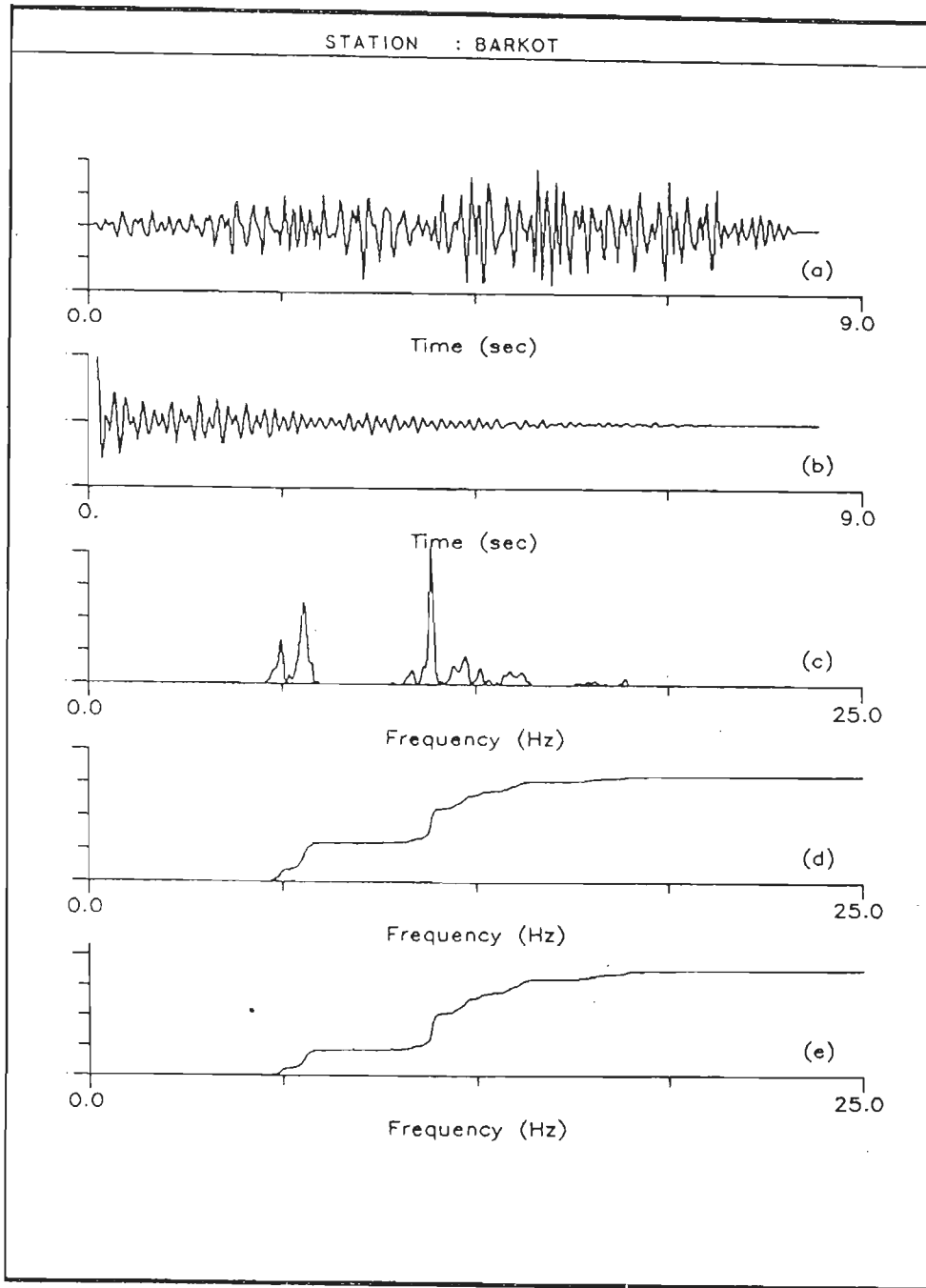


Fig 7.57 Uttarkashi earthquake of 20th Oct, 1991, simulated acceleration record at Barkot station. Y axis shows normalised value of (a) acceleration record, (b) its autocorrelation function, (c) its power spectrum, (d) its cumulative power spectrum and (e) its frequency weighted cumulative power spectrum. X axis for (a) and (b) shows time and for (c), (d) and (e) shows frequency. Features extracted from records at this station are given in Table 7.19, 7.20 and 7.21.

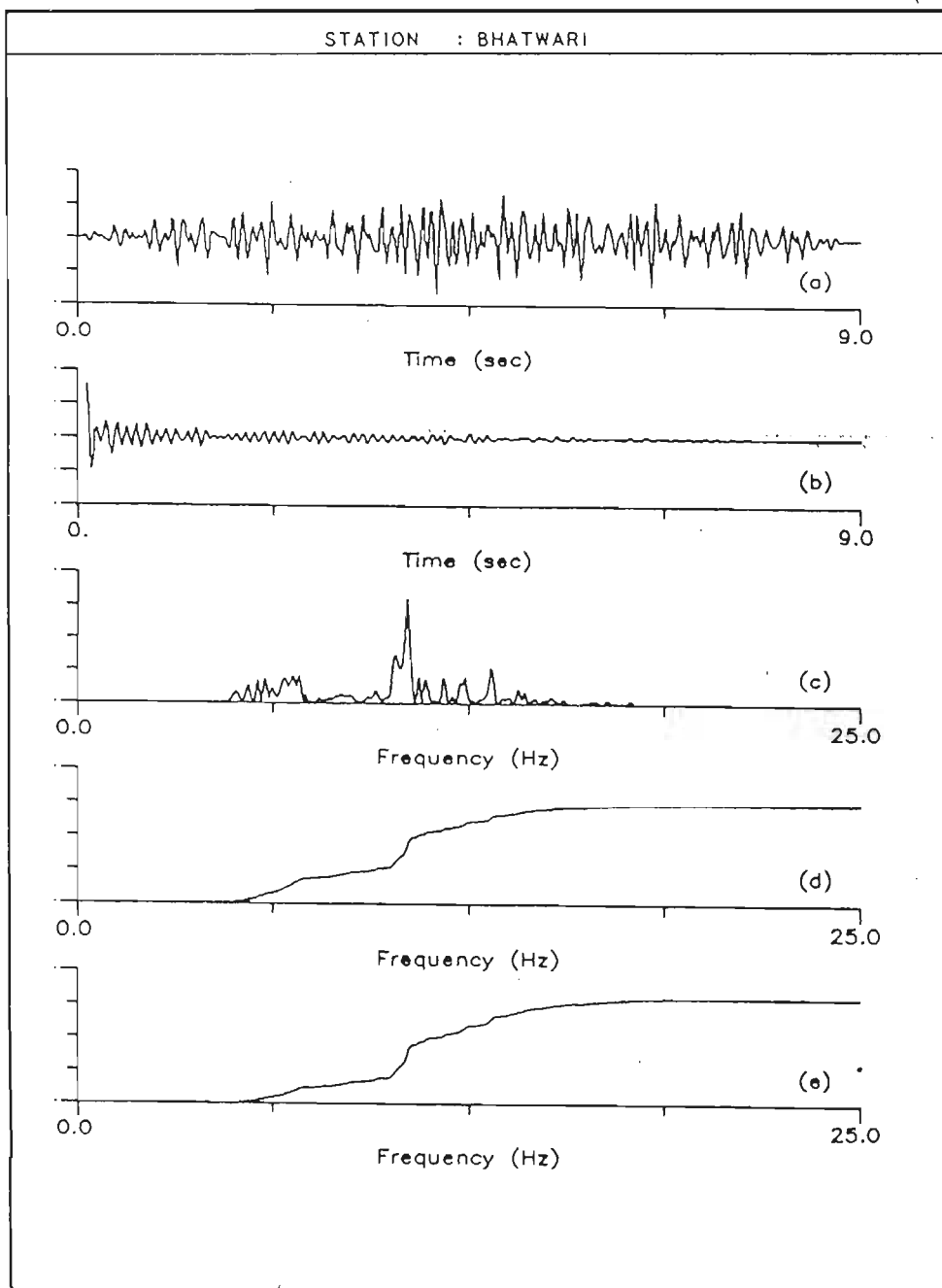


Fig 7.58 Uttarkashi earthquake of 20th Oct, 1991, simulated acceleration record at Bhatwari station. Y axis shows normalised value of (a) acceleration record, (b) its autocorrelation function, (c) its power spectrum, (d) its cumulative power spectrum and (e) its frequency weighted cumulative power spectrum. X axis for (a) and (b) shows time and for (c), (d) and (e) shows frequency. Feature extracted from simulated records at this station are given in Table 7.19, 7.20 and 7.21.

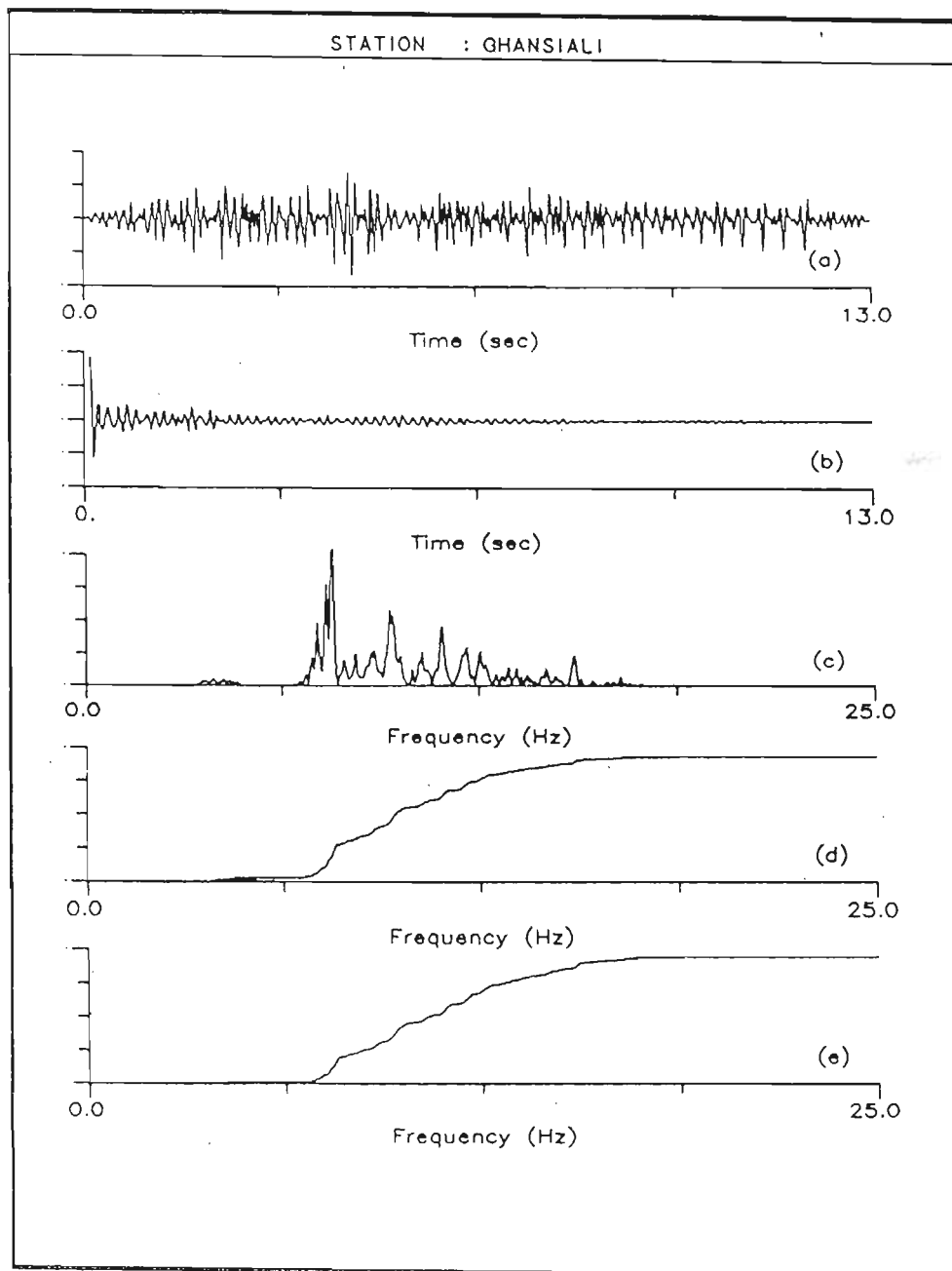


Fig 7.59 Uttarkashi earthquake of 20th Oct, 1991, simulated acceleration record at Ghansiali station. Y axis shows normalised value of (a) acceleration record, (b) its autocorrelation function, (c) its power spectrum, (d) its cumulative power spectrum and (e) its frequency weighted cumulative power spectrum. X axis for (a) and (b) shows time and for (c), (d) and (e) shows frequency. Features extracted from simulated records at this station are given in Table 7.19, 7.20 and 7.21.

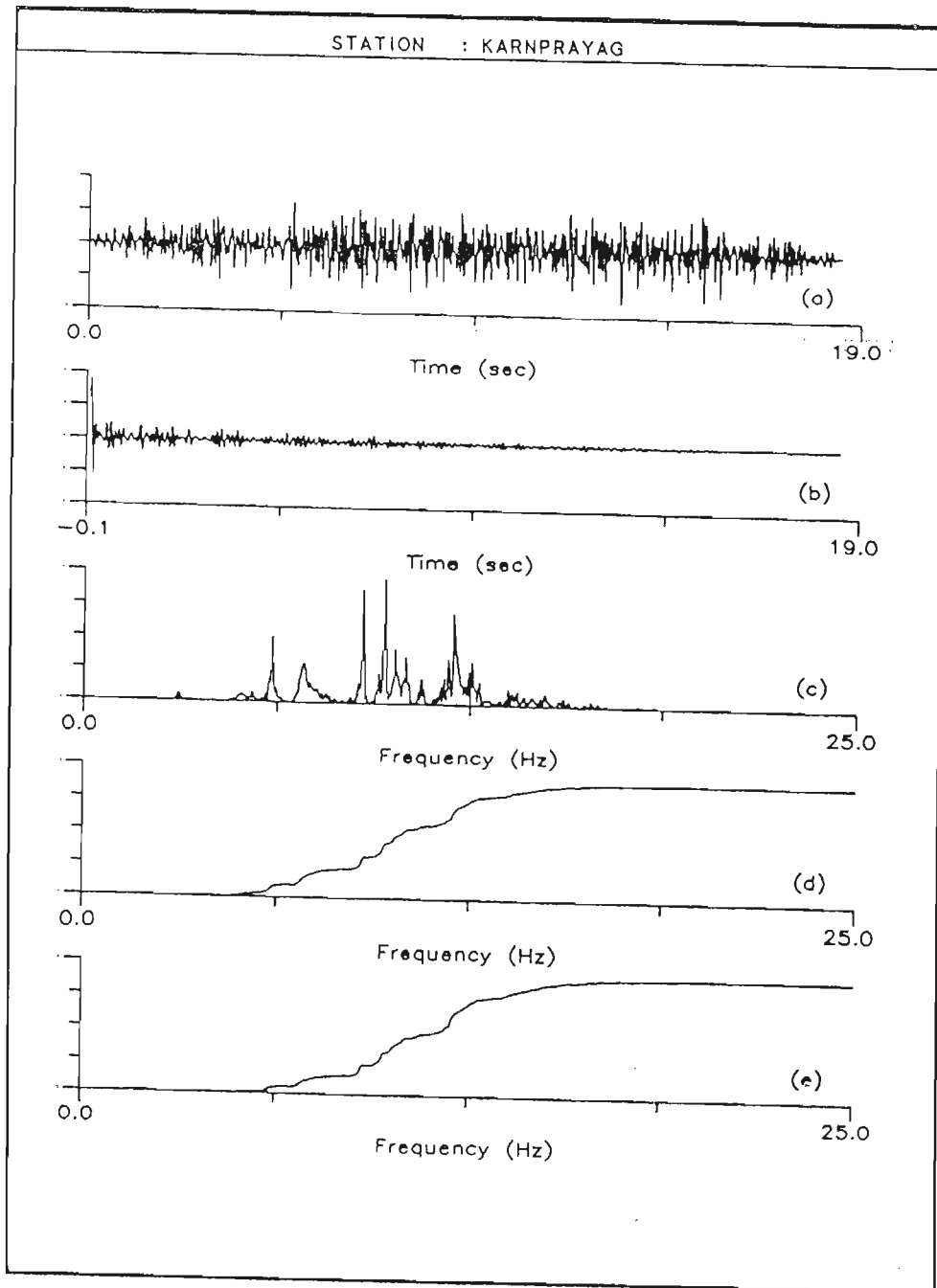


Fig 7.60 Uttarkashi earthquake of 20th Oct, 1991, simulated acceleration record at Karnprayag station. Y axis shows normalised value of (a) acceleration record, (b) its autocorrelation function, (c) its power spectrum, (d) its cumulative power spectrum and (e) its frequency weighted cumulative power spectrum. X axis for (a) and (b) shows time and for (c), (d) and (e) shows frequency. Features extracted from simulated records at this station are given in Table 7.19, 7.20 and 7.21.

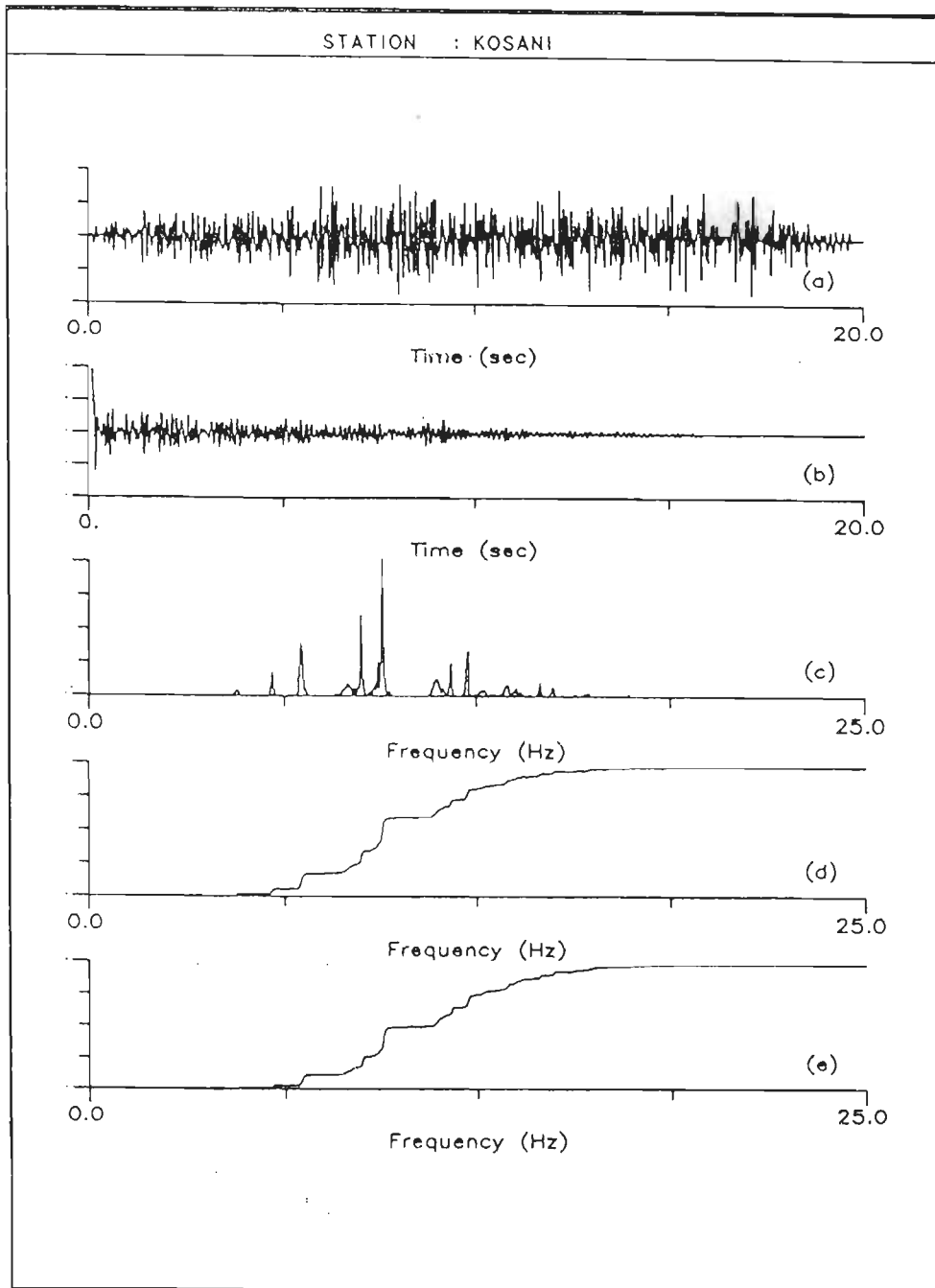


Fig 7.61 Uttarkashi earthquake of 20th Oct, 1991, simulated acceleration record at Kosani station. Y axis shows normalised value of (a) acceleration record, (b) its autocorrelation function, (c) its power spectrum, (d) its cumulative power spectrum and (e) its frequency weighted cumulative power spectrum. X axis for (a) and (b) shows time and for (c), (d) and (e) shows frequency. Features extracted from simulated records at this station are given in Table 7.19, 7.20 and 7.21.

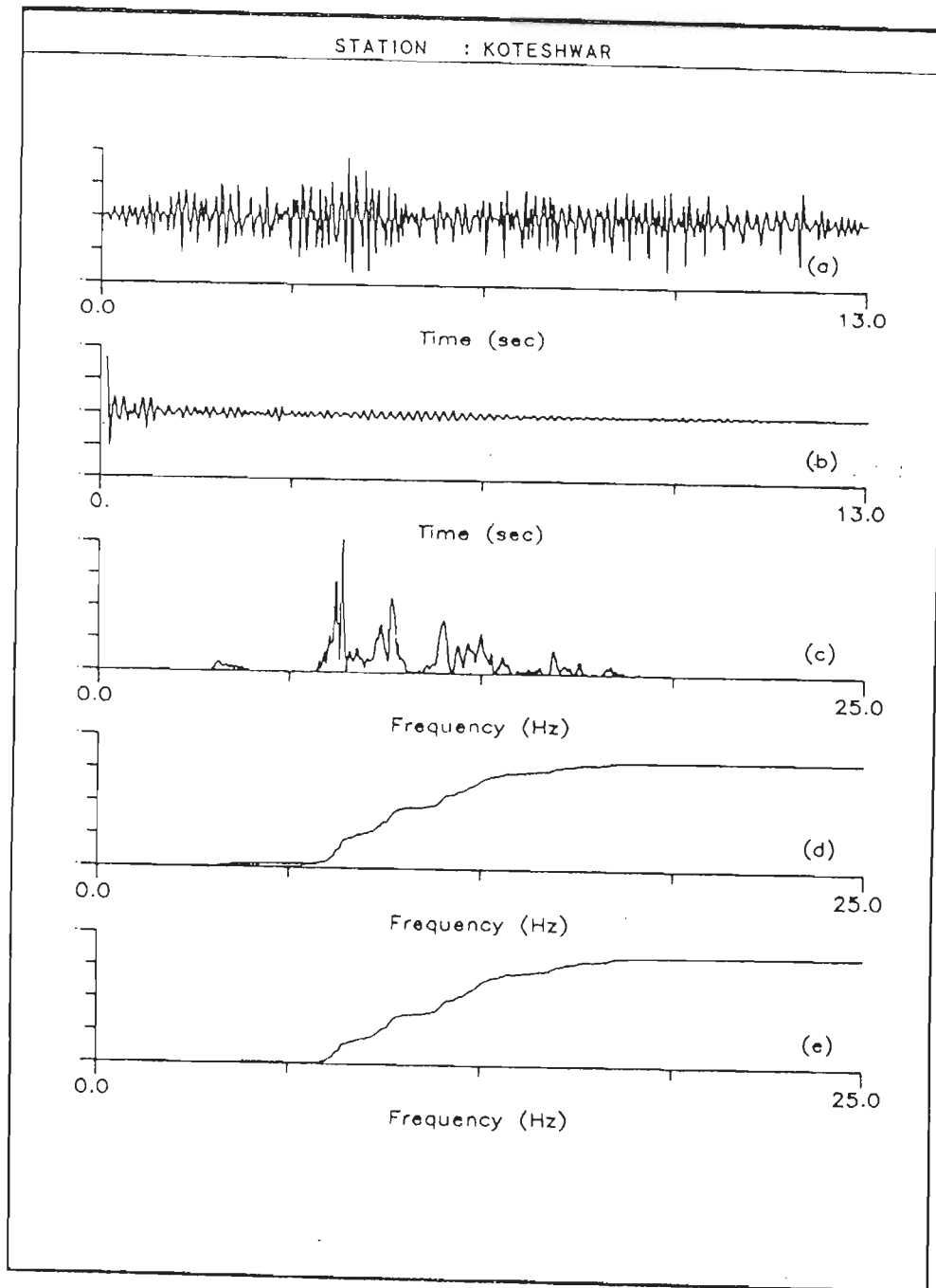


Fig 7.62 Uttarkashi earthquake of 20th Oct, 1991, simulated acceleration record at Koteswar station. Y axis shows normalised value of (a) acceleration record, (b) its autocorrelation function, (c) its power spectrum, (d) its cumulative power spectrum and (e) its frequency weighted cumulative power spectrum. X axis for (a) and (b) shows time and for (c), (d) and (e) shows frequency. Features extracted from simulated records at this station are given in Table 7.19, 7.20 and 7.21.

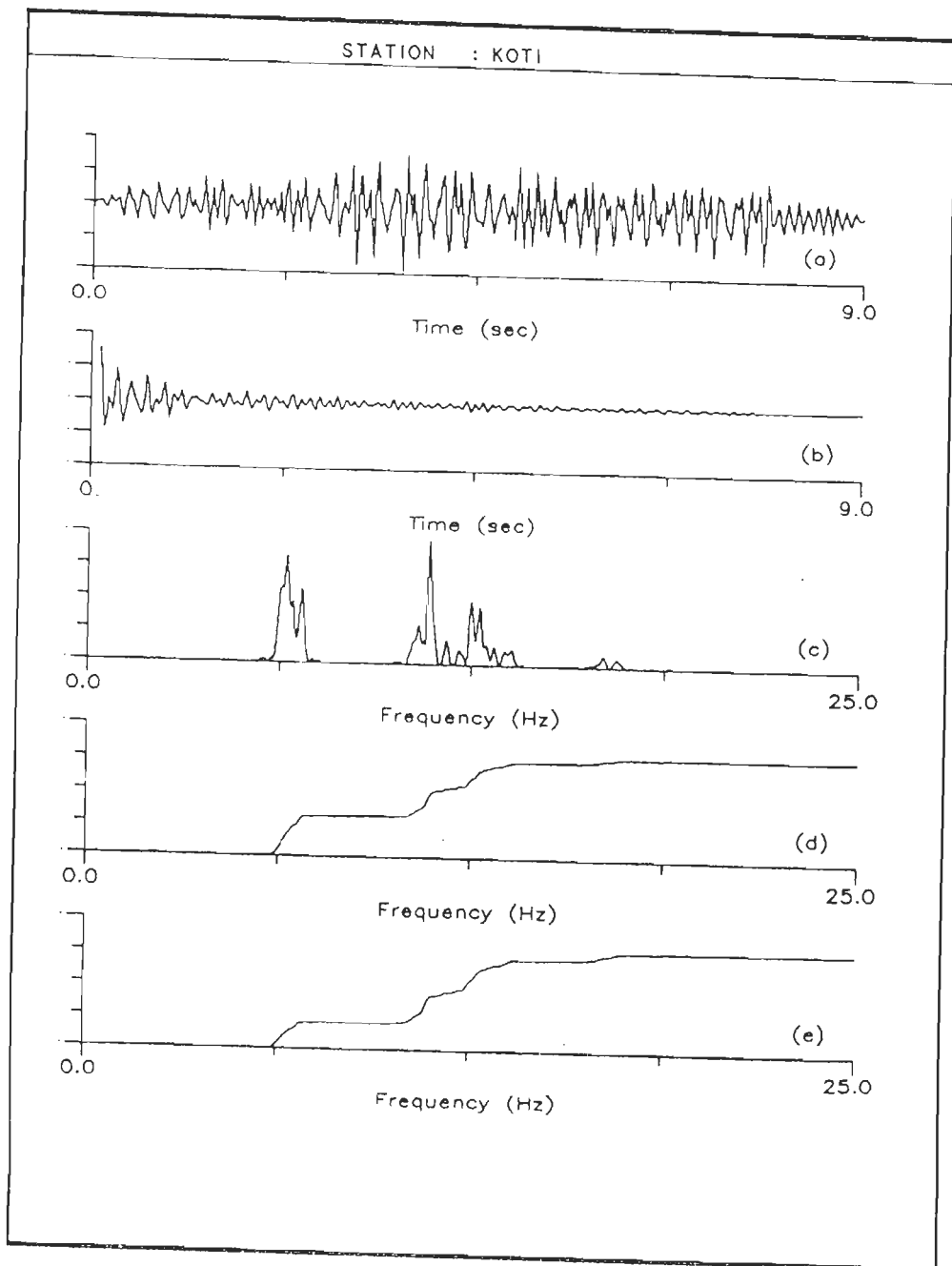


Fig 7.63 Uttarkashi earthquake of 20th Oct, 1991, simulated acceleration record at Koti station. Y axis shows normalised value of (a) acceleration record, (b) its autocorrelation function, (c) its power spectrum, (d) its cumulative power spectrum and (e) its frequency weighted cumulative power spectrum. X axis for (a) and (b) shows time and for (c), (d) and (e) shows frequency. Features extracted from simulated records at this station are given in Table 7.19, 7.20 and 7.21.

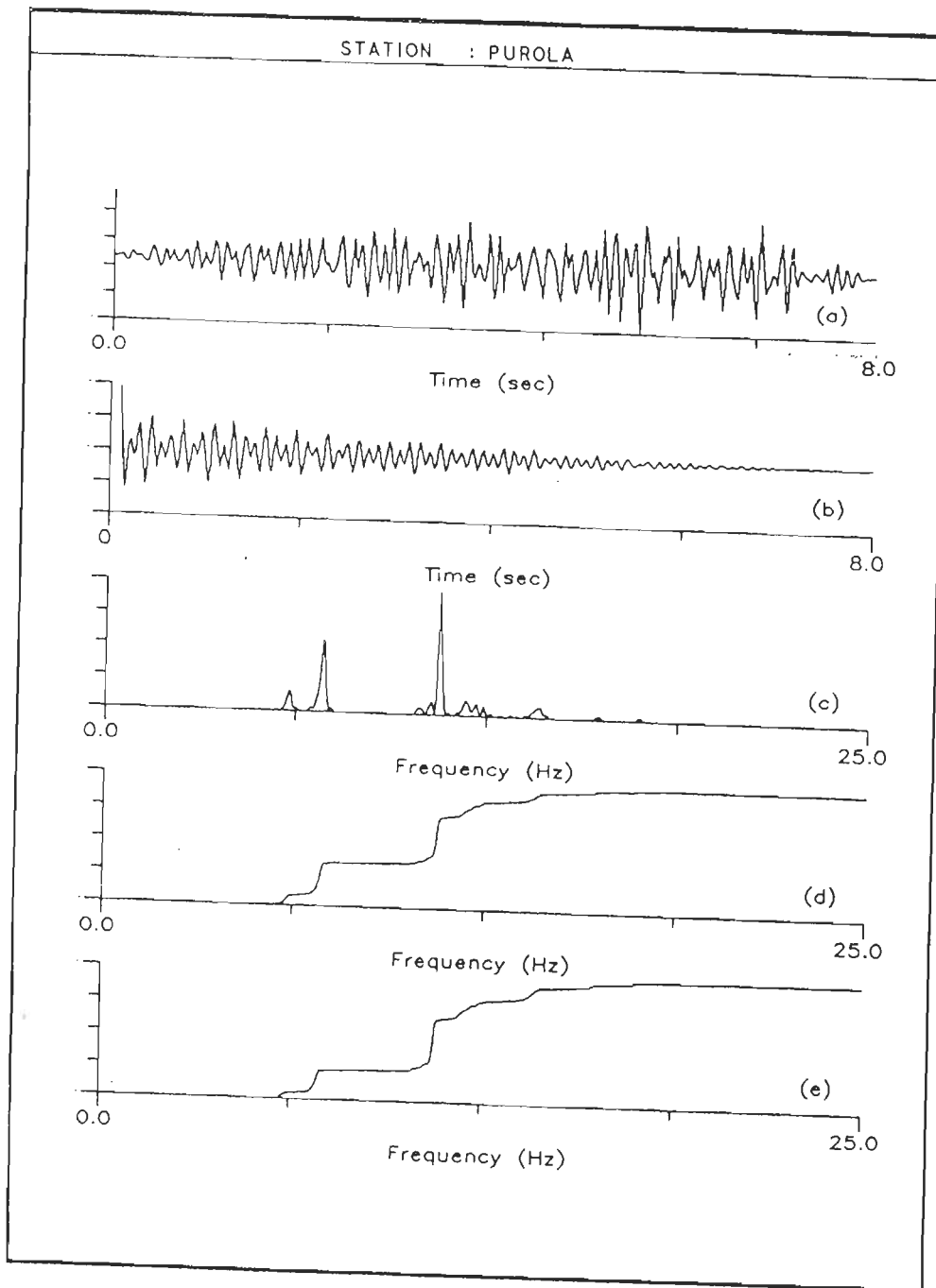


Fig 7.64 Uttarkashi earthquake of 20th Oct, 1991, simulated acceleration record at Purola station. Y axis shows normalised value of (a) acceleration record, (b) its autocorrelation function, (c) its power spectrum, (d) its cumulative power spectrum and (e) its frequency weighted cumulative power spectrum. X axis for (a) and (b) shows time and for (c), (d) and (e) shows frequency. Features extracted from simulated records at this station are given in Table 7.19, 7.20 and 7.21.

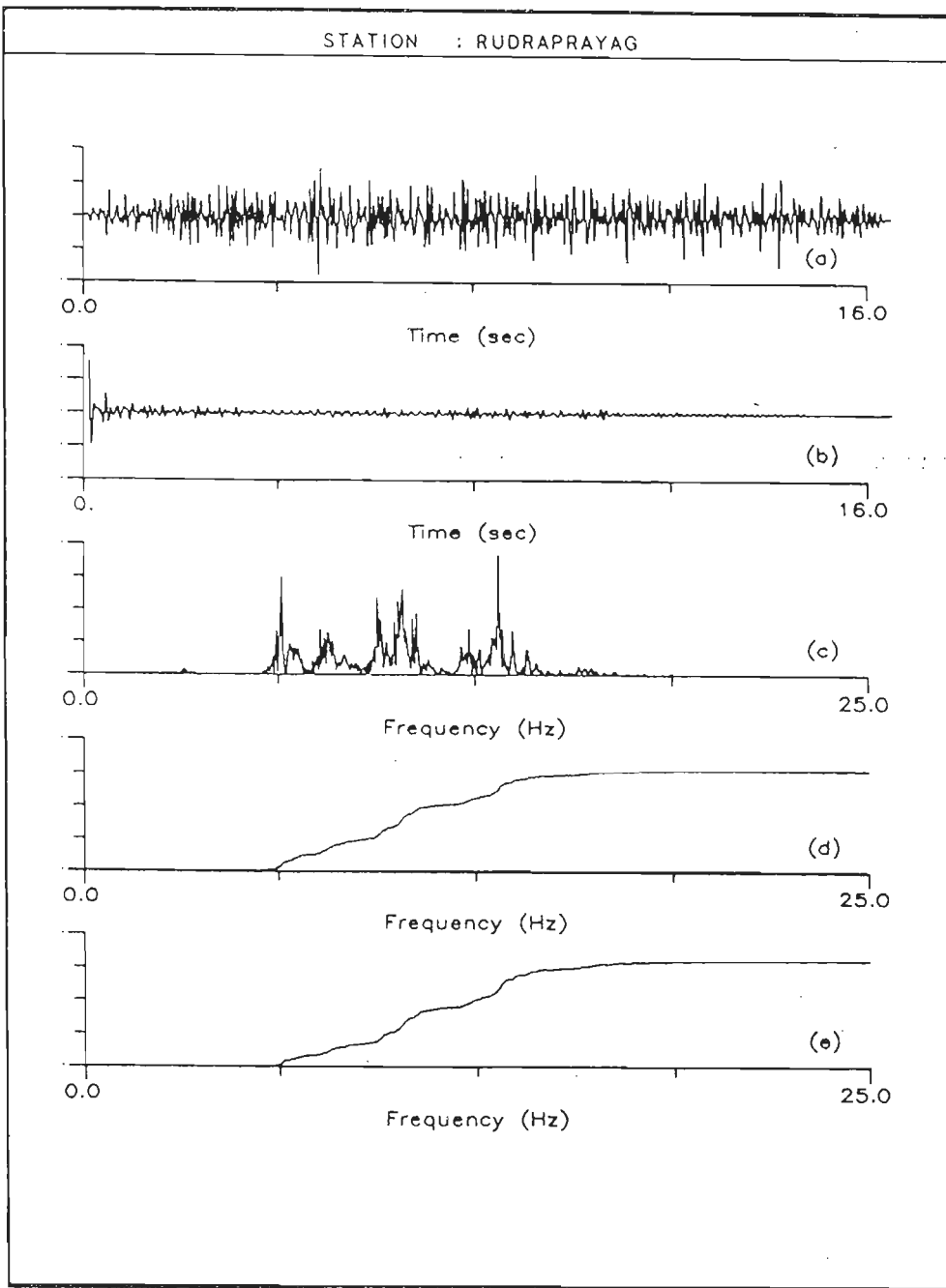


Fig 7.65 Uttarkashi earthquake of 20th Oct, 1991, simulated acceleration record at Rudraprayag station. Y axis shows normalised value of (a) acceleration record, (b) its autocorrelation function, (c) its power spectrum, (d) its cumulative power spectrum and (e) its frequency weighted cumulative power spectrum. X axis for (a) and (b) shows time and for (c), (d) and (e) shows frequency. Features extracted from simulated records at this station are given in Table 7.19, 7.20 and 7.21.

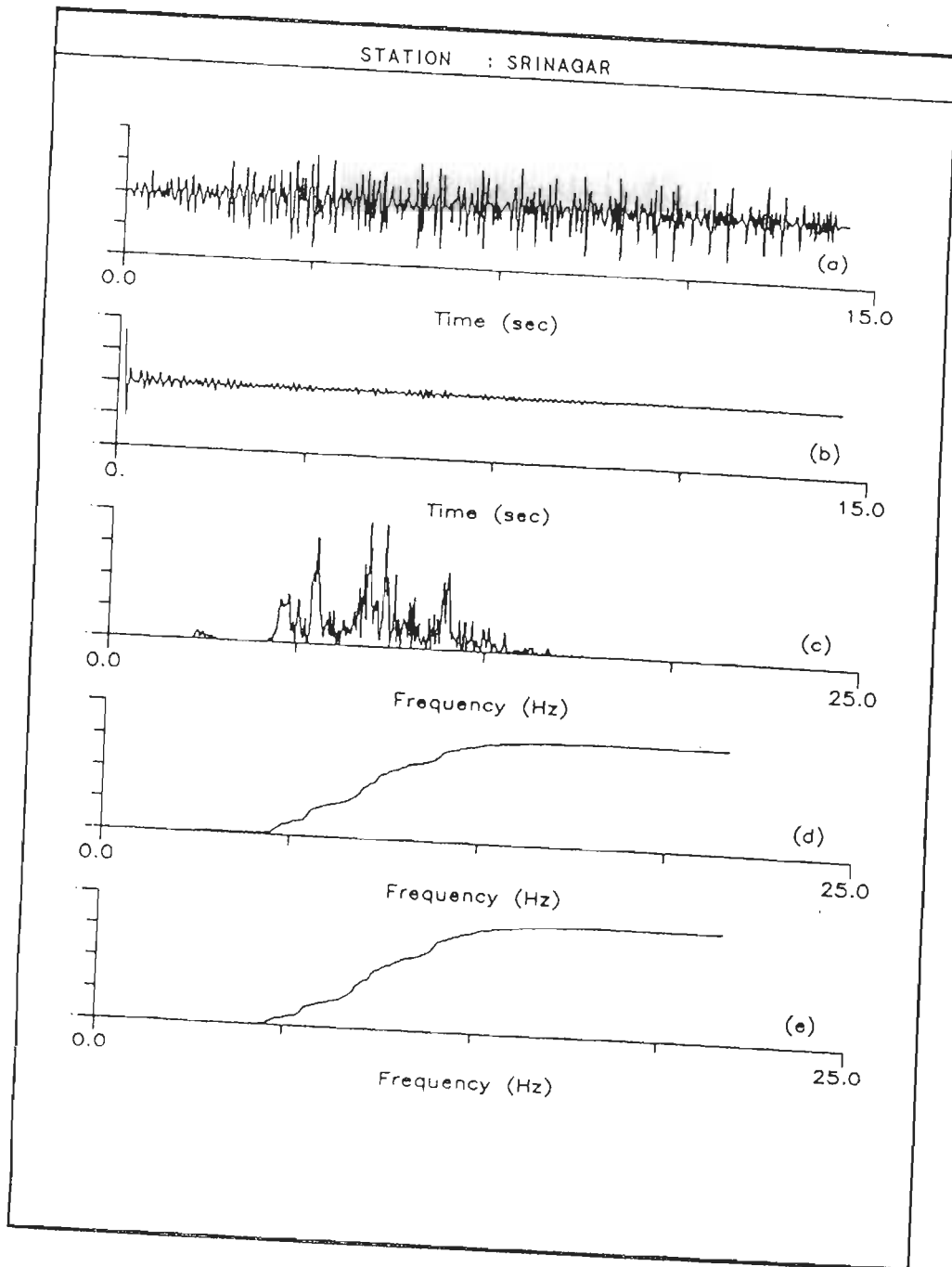


Fig 7.66 Uttarkashi earthquake of 20th Oct, 1991, simulated acceleration record at Srinagar station. Y axis shows normalised value of (a) acceleration record, (b) its autocorrelation function, (c) its power spectrum, (d) its cumulative power spectrum and (e) its frequency weighted cumulative power spectrum. X axis for (a) and (b) shows time and for (c), (d) and (e) shows frequency. Features extracted from simulated records at this station are given in Table 7.19, 7.20 and 7.21.

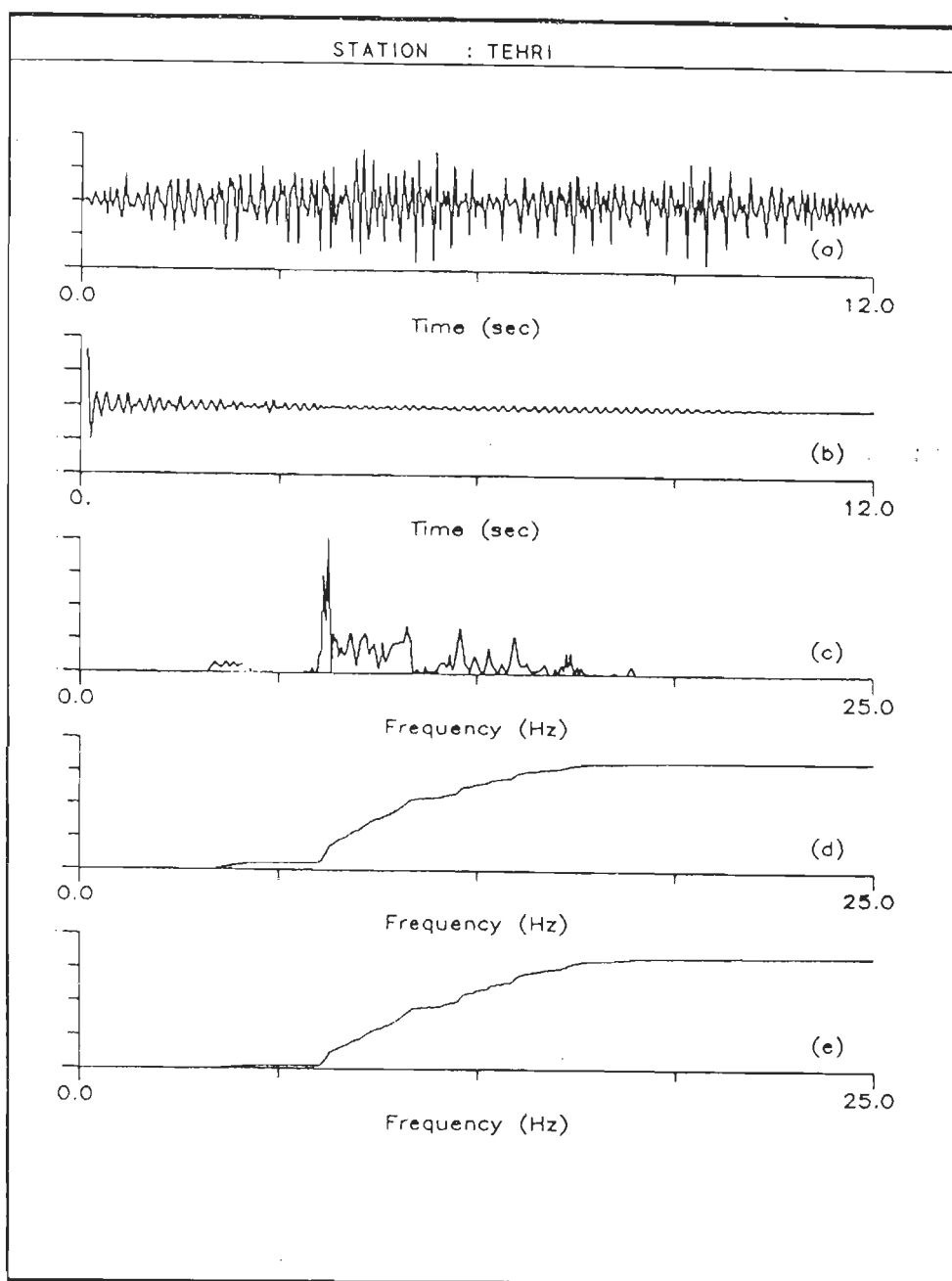


Fig 7.67 Uttarkashi earthquake of 20th Oct, 1991, simulated acceleration record at Tehri station. Y axis shows normalised value of (a) acceleration record, (b) its autocorrelation function, (c) its power spectrum, (d) its cumulative power spectrum and (e) its frequency weighted cumulative power spectrum. X axis for (a) and (b) shows time and for (c), (d) and (e) shows frequency. Features extracted from simulated records at this station are given in Table 7.19, 7.20 and 7.21.



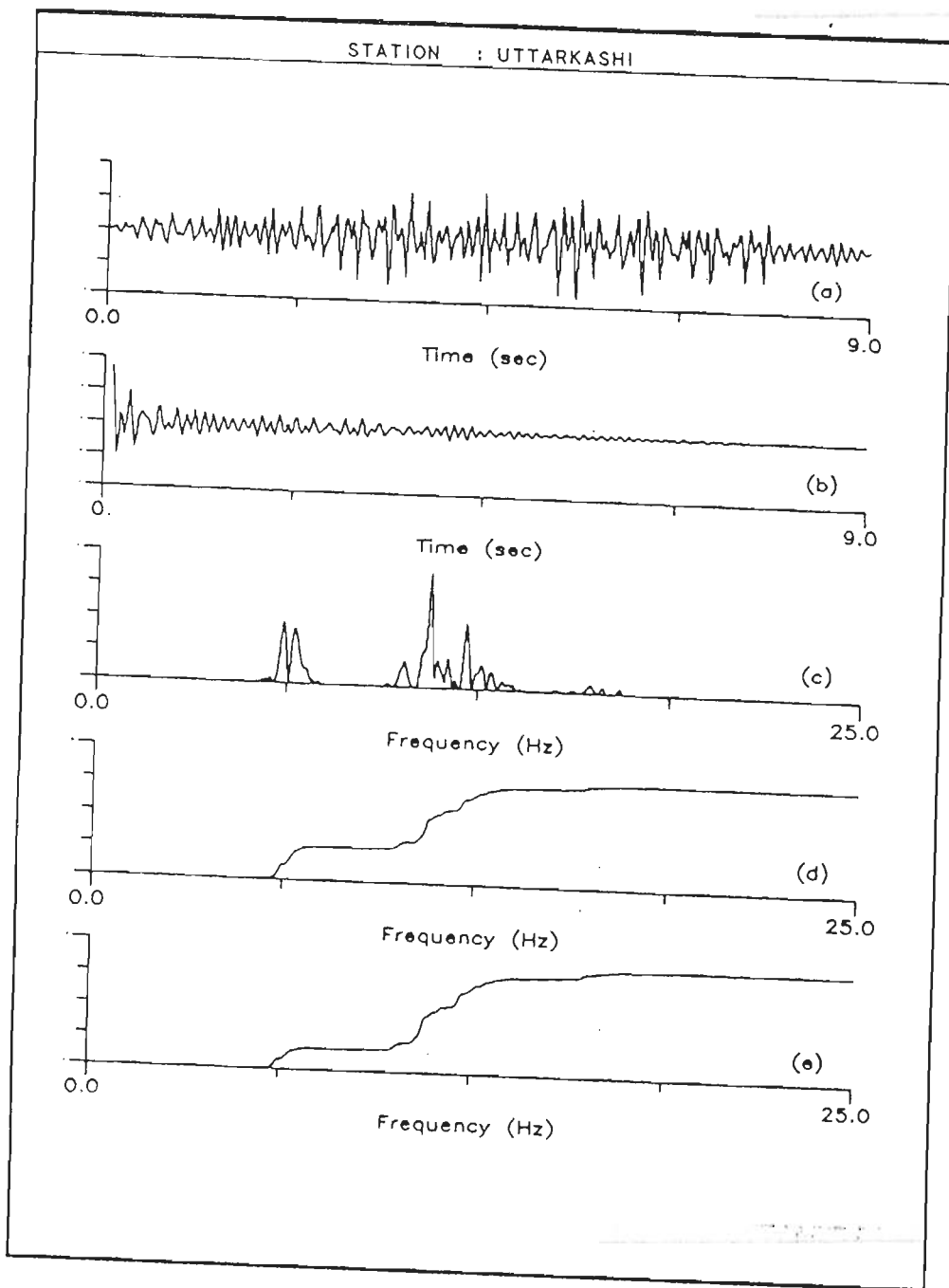


Fig 7.68 Uttarkashi earthquake of 20th Oct, 1991, simulated acceleration record at Uttarkashi station. Y axis shows normalised value of (a) acceleration record, (b) its autocorrelation function, (c) its power spectrum, (d) its cumulative power spectrum and (e) its frequency weighted cumulative power spectrum. X axis for (a) and (b) shows time and for (c), (d) and (e) shows frequency. Features extracted from simulated records at this station are given in Table 7.19, 7.20 and 7.21.

S.N.	Date			Origin time		S	Epicenter		Depth of focus (km)	Magnitude
	Y	M	D	H	M		°N Lat	°E Long		
1	1911	10	14	23	24	-	31.00	80.50	-	-
2	1913	3	6	2	9	-	30.00	83.00	-	-
3	1913	3	6	11	4	-	30.00	83.00	-	-
4	1918	4	28	11	12	-	30.50	82.00	-	-
5	1924	5	27	14	32	-	30.00	85.00	-	-
6	1925	11	6	19	20	-	26.50	81.50	-	-
7	1925	12	15	7	44	-	30.00	85.00	-	-
8	1926	7	27	7	23	-	30.50	80.50	-	-
9	1926	12	31	16	53	-	25.00	77.50	-	-
10	1927	6	2	16	37	-	23.50	81.00	-	-
11	1927	10	8	10	34	-	30.50	80.50	-	-
12	1927	11	29	11	34	-	30.00	83.00	-	-
13	1929	4	10	23	53	-	25.00	77.50	-	-
14	1930	6	25	-	49	-	25.00	77.50	-	-
15	1931	6	18	12	58	-	30.50	84.00	-	-
16	1933	5	18	10	24	-	29.50	80.00	-	-
17	1935	3	5	22	15	-	29.75	80.25	-	-
18	1935	3	15	10	33	-	29.60	80.40	-	-
19	1936	5	27	6	19	-	28.50	83.50	-	-
20	1937	4	30	19	32	-	30.00	81.50	-	-
21	1937	4	30	20	3	-	30.00	81.50	-	-
22	1937	5	31	5	34	-	29.30	81.00	-	-
23	1937	10	20	1	23	-	31.00	78.00	-	-
24	1937	12	20	4	59	-	29.30	81.00	-	-
25	1940	4	10	8	17	-	30.00	81.50	-	-
26	1945	6	4	12	9	-	30.00	80.00	60	-
27	1952	11	8	7	6	-	28.50	83.20	-	-
28	1952	11	8	10	41	-	27.90	82.20	-	-
29	1953	2	16	1	2	-	29.50	81.00	-	-
30	1953	2	23	-	46	-	29.50	81.30	-	-
31	1953	5	27	22	41	-	30.50	80.00	-	-
32	1953	6	29	23	26	-	30.75	80.50	-	-
33	1953	8	29	1	58	-	27.90	82.20	-	-
34	1954	9	4	6	43	-	28.30	83.80	-	-
35	1954	9	4	6	45	-	28.00	83.50	-	-
36	1954	11	20	13	9	-	30.50	82.00	-	-
37	1954	11	20	19	6	-	27.50	82.50	-	-
38	1956	1	19	19	50	-	30.00	81.00	-	-
39	1956	7	3	10	17	-	28.00	84.50	-	-
40	1956	10	10	15	31	-	28.50	78.00	-	-
41	1957	3	1	15	40	-	29.50	79.75	-	-
42	1957	4	14	7	11	-	30.64	84.21	-	-
43	1957	4	14	16	36	-	31.00	84.50	-	-

Continued on next page...

Continued from previous page...

S.N.	Date			Origin time			Epicenter		Depth of focus		Magnitude
	Y	M	D	H	M	S	°N Lat	°E Long	(km)		
44	1957	4	22	-	18	-	30.50	84.50	-	-	
45	1957	4	22	1	42	-	30.50	84.50	-	-	
46	1957	12	9	21	17	-	30.00	79.75	-	-	
47	1958	1	23	5	30	-	30.77	84.16	-	-	
48	1958	3	31	3	42	-	29.50	82.00	-	-	
49	1958	4	30	9	33	-	28.50	82.00	-	-	
50	1958	8	12	12	23	-	30.50	81.50	-	-	
51	1958	8	12	12	40	-	30.50	81.50	-	-	
52	1958	8	15	16	-	0	29.75	81.25	-	-	
53	1958	10	28	10	46	-	30.61	84.47	-	-	
54	1958	11	3	14	31	-	30.51	84.50	-	-	
55	1958	12	28	5	34	-	29.50	80.00	-	-	
56	1958	12	31	3	45	-	30.09	79.86	-	-	
57	1959	10	28	0	0	-	28.50	82.50	-	-	
58	1959	11	3	16	29	-	31.00	81.00	-	-	
59	1959	12	9	18	24	-	31.00	84.00	-	-	
60	1960	3	5	11	25	-	29.00	81.00	-	-	
61	1960	3	5	23	50	-	29.00	81.00	-	-	
62	1960	8	27	15	58	-	28.60	76.70	58	-	
63	1961	2	13	16	10	-	29.90	81.00	35	-	
64	1961	2	15	11	28	-	30.80	84.40	25	-	
65	1961	3	26	23	11	-	30.60	84.40	24	-	
66	1961	7	11	17	23	-	27.10	81.00	25	-	
67	1961	12	24	7	13	-	29.50	80.80	-	-	
68	1962	1	11	3	1	-	27.90	84.90	39	-	
69	1962	1	22	20	22	-	30.70	80.60	25	-	
70	1962	7	7	3	0	-	30.70	84.40	25	-	
71	1962	7	13	5	1	-	30.50	79.60	25	-	
72	1962	7	14	15	58	-	30.40	79.50	40	-	
73	1962	8	29	11	30	-	30.90	78.40	36	-	
74	1963	1	30	10	33	-	29.70	80.60	59	-	
75	1963	3	5	2	35	-	29.20	81.20	-	-	
76	1963	7	14	14	48	-	30.30	78.50	-	4.80	
77	1963	11	27	21	10	-	30.80	79.10	-	5.10	
78	1964	2	8	11	54	-	29.00	82.20	-	-	
79	1964	5	24	0	0	-	30.10	82.10	-	5.10	
80	1964	9	26	0	46	-	30.10	80.70	50	6.20	
81	1964	10	6	20	19	-	29.30	80.90	27	5.10	
82	1964	12	2	8	21	-	29.50	81.30	23	5.10	
83	1964	12	20	3	31	-	29.50	81.00	-	5.20	

Continued on next page...

Continued from previous page...

S.N.	Date			Origin time			Epicenter		Depth of focus Magnitude	
	Y	M	D	H	M	S	°N Lat	°E Long	(km)	
84	1965	3	18	2	41	-	29.90	80.30	-	5.20
85	1965	5	13	10	51	-	29.80	80.50	-	5.10
86	1965	6	1	7	52	-	28.50	83.20	20	5.30
87	1966	6	20	13	42	-	28.70	76.90	34	4.70
88	1966	6	25	12	5	-	30.50	82.30	46	5.10
89	1966	6	27	10	41	-	29.60	80.90	-	6.00
90	1966	6	27	10	47	-	29.50	80.90	43	5.30
91	1966	6	27	10	49	-	29.60	80.90	16	5.90
92	1966	6	27	10	59	-	29.70	81.00	13	6.00
93	1966	6	27	11	21	-	29.70	80.90	-	5.30
94	1966	6	27	13	55	-	29.70	80.90	19	5.40
95	1966	6	28	15	43	-	29.60	80.90	48	5.20
96	1966	6	29	0	42	-	29.80	81.00	15	5.30
97	1966	8	15	2	15	-	28.70	78.90	53	5.60
98	1966	10	5	7	57	-	29.20	81.10	-	-
99	1966	11	5	18	53	-	28.20	84.00	-	5.10
100	1966	12	16	20	52	-	29.70	80.90	15	5.80
101	1966	12	16	22	12	-	29.60	80.90	7	5.10
102	1966	12	18	22	42	-	29.50	80.90	-	4.90
103	1966	12	21	22	10	-	29.70	80.80	21	5.40
104	1967	1	2	22	17	-	30.64	79.28	25	4.80
105	1967	3	11	18	45	-	29.32	81.41	-	4.80
106	1967	3	16	17	38	-	29.85	85.00	15	3.90
107	1967	12	18	10	51	-	29.10	81.90	42	5.20
108	1968	1	5	6	42	-	30.40	79.10	7	5.40
109	1968	5	27	18	35	-	29.67	80.44	27	5.10
110	1968	5	31	3	1	-	29.91	79.95	-	5.10
111	1969	3	3	6	20	-	30.17	79.92	20	5.30
112	1969	3	5	11	15	-	29.25	81.05	63	5.20
113	1969	6	22	1	33	-	30.63	79.37	19	5.40
114	1969	12	5	18	45	-	29.66	80.77	-	4.90
115	1970	2	12	1	51	-	29.36	81.64	44	5.40
116	1970	7	21	15	37	-	27.87	84.81	40	4.70
117	1971	1	30	20	15	-	30.49	79.06	56	4.60
118	1971	5	3	0	33	-	30.78	84.47	16	5.40
119	1972	2	4	14	8	-	30.38	84.61	18	5.20
120	1972	3	15	6	0	0	30.43	84.50	-	5.30
121	1973	4	4	17	53	-	30.49	83.68	48	4.80
122	1973	10	16	9	50	-	28.22	82.95	-	5.20
123	1974	2	24	21	32	-	30.94	78.05	45	4.70
124	1974	3	13	6	47	-	29.25	81.56	65	4.50
125	1974	5	6	1	7	-	29.32	81.65	33	4.50

Continued on next page...

Continued from previous page...

S.N.	Date			Origin time		S	Epicenter		Depth of focus (km)	Magnitude
	Y	M	D	H	M		°N Lat	°E Long		
126	1974	7	7	20	56	-	30.63	78.69	33	4.90
127	1974	12	23	9	45	-	29.41	81.39	45	5.20
128	1975	1	31	12	38	-	28.10	84.72	33	5.40
129	1975	4	9	3	28	-	30.41	84.88	33	4.90
130	1975	8	23	3	8	-	30.61	79.45	33	4.00
131	1975	9	6	4	44	-	29.28	82.16	33	5.10
132	1975	11	6	0	11	-	29.49	78.08	33	4.90
133	1976	5	10	18	43	-	29.28	81.46	33	5.20
134	1976	9	29	2	51	-	29.81	81.39	33	5.00
135	1976	11	24	3	58	-	30.43	79.62	62	-
136	1977	4	20	4	21	-	30.51	79.35	33	4.80
137	1977	5	16	22	37	-	29.72	81.64	33	-
138	1977	9	20	5	51	-	29.51	81.09	23	5.00
139	1977	10	21	12	16	-	30.01	79.92	125	-
140	1977	11	4	23	54	-	29.59	81.27	15	4.90
141	1978	1	7	7	23	-	30.56	79.38	33	4.70
142	1978	2	10	17	29	-	28.07	84.64	33	5.20
143	1978	2	19	4	52	-	29.29	84.99	16	4.70
144	1978	3	7	10	21	-	29.27	81.05	33	4.20
145	1978	3	21	0	5	-	30.00	81.13	76	-
146	1978	12	12	10	0	-	29.04	81.23	56	4.30
147	1978	12	25	20	0	-	28.11	83.91	33	4.50
148	1979	3	5	23	54	-	30.47	79.72	33	4.30
149	1979	5	20	22	59	-	30.02	80.31	33	5.80
150	1979	7	3	16	56	-	27.97	84.47	33	4.20
151	1979	12	28	1	59	-	30.62	78.44	33	5.00
152	1980	4	27	17	-	-	28.60	77.64	33	4.70
153	1980	6	22	14	38	-	30.10	81.76	33	5.10
154	1980	7	29	12	23	-	29.33	81.25	34	5.70
155	1980	7	29	14	58	-	29.59	81.09	18	6.10
156	1980	7	29	18	44	-	29.44	80.71	33	4.40
157	1980	7	29	21	57	-	29.11	81.00	33	4.60
158	1980	7	30	1	0	-	29.59	80.74	33	4.80
159	1980	7	30	5	30	-	29.43	80.82	33	4.50
160	1980	7	31	14	22	-	29.43	80.85	33	4.50
161	1980	8	4	16	52	-	29.41	80.77	33	4.50
162	1980	8	20	1	5	-	29.51	81.18	33	4.30
163	1980	9	8	7	42	-	29.99	80.43	33	4.50
164	1980	10	10	14	2	-	29.17	81.20	33	5.00
165	1981	3	6	5	58	-	29.80	80.65	43	4.90
166	1981	4	9	17	19	-	28.00	84.40	33	4.50

Continued on next page...

S.N.	Y	Date				Origin time M S	Epicenter		Depth of focus (km)	Magnitude
		M	D	H	M		°N Lat	°E Long		
167	1981	5	15	17	22	-	29.50	81.94	33	5.10
168	1981	6	19	10	41	-	30.54	79.21	64	4.40
169	1981	9	10	3	47	-	29.32	81.12	33	4.60
170	1982	7	16	4	15	-	30.71	77.03	103	4.20
171	1982	9	9	12	5	-	28.63	81.10	33	4.40
172	1982	10	16	2	22	-	30.32	79.12	71	4.50
173	1982	11	22	13	57	-	27.75	84.91	64	4.20
174	1982	12	21	12	8	-	29.19	81.37	33	4.70
175	1982	12	21	13	13	-	29.29	81.37	32	4.30
176	1982	12	29	0	9	-	30.27	79.80	33	4.80
177	1983	1	27	4	45	-	29.05	81.39	33	4.80
178	1983	7	5	17	26	-	29.49	80.69	33	4.60
179	1983	8	23	22	43	-	27.96	84.96	61	4.30
180	1983	11	23	5	5	-	30.35	83.10	33	4.60
181	1984	1	6	23	48	-	27.77	84.74	33	4.50
182	1984	2	19	15	46	-	29.86	80.54	21	5.00
183	1984	3	14	1	32	-	29.10	81.11	40	4.90
184	1984	3	23	0	34	-	29.99	78.87	33	5.10
185	1984	4	22	20	22	-	30.64	84.15	33	4.80
186	1984	5	3	13	17	-	30.50	78.40	33	4.50
187	1984	5	18	4	28	-	29.57	81.86	33	5.60
188	1984	5	19	6	36	-	29.29	81.88	45	4.70
189	1984	5	30	22	27	-	28.82	83.93	33	4.50
190	1984	7	21	20	2	-	28.68	82.15	64	4.30
191	1984	7	29	16	37	-	29.41	81.79	44	4.50
192	1984	9	15	10	15	-	29.21	81.52	33	4.60
193	1984	10	24	8	19	-	29.70	80.05	56	4.20
194	1984	11	18	22	4	-	28.79	84.07	33	5.30
195	1984	11	23	6	14	-	29.38	81.57	33	4.40
196	1984	11	26	3	35	-	30.48	79.25	33	4.50
197	1984	12	5	14	14	-	27.20	81.72	33	4.70
198	1984	12	18	22	46	-	29.42	80.86	33	4.70
199	1985	2	15	4	54	-	30.12	81.60	33	4.40
200	1985	5	6	20	59	-	28.32	82.30	47	4.50
201	1985	6	14	17	19	-	29.80	79.31	33	3.90
202	1985	9	13	5	33	-	29.82	84.05	33	4.50
203	1985	10	3	20	23	-	29.21	83.89	14	4.10
204	1985	10	21	8	57	-	28.84	83.97	33	4.50
205	1986	2	27	21	6	-	29.05	81.12	33	-
206	1986	2	28	20	51	-	29.10	81.90	63	4.60
207	1986	3	28	18	5	-	30.80	79.16	33	4.20
208	1986	11	2	6	16	-	26.52	76.89	33	-

Continued on next page...

S.N.	Date			Origin time			Epicenter		Depth of focus (km)	Magnitude
	Y	M	D	H	M	S	°N Lat	°E Long		
209	1987	1	19	7	46	-	28.38	83.68	33	5.20
210	1987	1	19	8	12	-	28.24	83.57	33	4.90
211	1987	2	24	22	17	-	29.05	81.85	112	4.40
212	1987	6	6	3	14	-	30.55	79.26	33	4.70
213	1987	6	6	11	2	-	30.47	79.20	44	4.90
214	1987	7	23	21	1	-	29.90	80.87	33	4.00
215	1987	8	9	21	15	-	29.50	83.71	48	5.60
216	1987	10	19	19	38	-	29.50	80.73	33	-
217	1987	12	16	13	56	-	29.21	82.27	33	-
218	1988	1	23	15	37	-	29.48	81.61	33	4.70
219	1988	2	12	1	41	-	30.51	82.89	33	4.60
220	1988	3	13	11	13	-	28.90	81.36	90	4.30
221	1988	3	19	11	24	-	29.15	81.62	90	4.30
222	1988	5	2	13	26	-	26.98	84.38	95	3.80
223	1988	5	15	20	23	-	29.86	80.48	26	4.80
224	1988	6	9	12	11	-	30.65	79.22	25	4.80
225	1988	6	12	10	15	-	28.48	82.35	33	4.80
226	1988	11	14	9	3	-	30.16	82.14	101	4.50
227	1988	11	24	14	26	-	29.73	80.68	33	-
228	1988	12	2	16	59	-	29.55	81.16	33	4.50
229	1988	12	15	23	14	-	29.12	81.64	112	4.50
230	1988	12	24	10	51	-	29.72	83.72	31	-
231	1988	12	26	11	11	-	30.61	77.98	33	4.20
232	1989	1	13	23	9	-	30.19	83.05	33	-
233	1989	1	19	13	37	-	28.50	84.17	29	-
234	1989	1	27	11	3	-	30.98	78.65	33	3.70
235	1989	3	1	22	52	-	28.19	83.95	33	4.20
236	1989	3	8	7	21	-	28.00	84.02	33	4.50
237	1989	5	25	9	34	-	29.76	83.77	33	-
238	1989	8	28	19	8	-	29.16	80.78	33	3.90
239	1990	2	9	15	51	-	29.92	80.73	33	4.60
240	1990	2	21	7	21	-	28.08	82.43	33	4.80
241	1990	2	23	17	51	-	28.24	84.58	33	-
242	1990	5	15	17	19	-	29.17	76.73	33	4.10
243	1990	5	20	9	10	-	28.45	83.34	33	4.80
244	1990	5	20	18	1	-	28.26	83.19	62	4.50
245	1990	8	21	17	52	-	30.39	83.11	33	-
246	1990	8	21	20	13	-	30.46	82.75	33	-
247	1990	8	23	15	57	-	30.19	83.13	33	-
248	1990	8	30	5	5	-	29.04	84.37	33	-
249	1990	9	21	16	8	-	29.74	79.79	33	5.10
250	1990	10	14	16	13	-	28.76	81.95	143	4.30
251	1990	10	21	16	44	-	30.48	82.15	33	-
252	1990	10	27	15	9	-	29.27	83.61	33	-
253	1990	10	28	17	14	-	30.68	81.55	33	4.50

Table 7.1 Epicenters of important earthquakes in U.P. and surrounding region
Data taken from USGS- NEIC (1990). This epicentral data is plotted in Fig 7.1.

MAGNITUDE	DATE	ORIGIN TIME H:M:S	EPICE- NTER	FOCA- L DEPTH (KM)	REF.	NAME OF EPICE- NTER ON MAP
$M_b = 6.5$ $M_s = 7.1$	20.8.1991	02 20 15.5 (IST)	30.74°N 78.79°E	19.0	PDE	E_{U1}
$M_b = 6.5$ $M_s = 7.1$	19.8.1991	21 23 14.3 (GMT)	30.78°N 78.77°E	10.3	EDR (USGS)	E_{U2}
$M_b = 6.6$	20.8.1991	02 53 16.4 (IST)	30.75°N 78.86°E	12.0	Kam	E_{U3}

Kam Kamble (1992a)

PDE PDE (1991)

Table 7.2 Epicentral parameters of Uttarkashi earthquake of 20th Oct, 1991 reported by different agencies. Epicenters E_{U1} , E_{U2} and E_{U3} given in this table are plotted in Fig 7.6.

DATE	NP1		NP2		REFERENCE
	DIP	STRIKE	DIP	STRIKE	
20.08.1991	85°	116°	5°	296°	USGS
20.08.1991	78°	112°	14°	317°	D

D Dziewonski et al. (1992)

Table 7.3 Fault plane solutions for the Uttarkashi earthquake of 20th Oct, 1991 reported by different agencies.

DATE Y M D	ORIGIN (G.M.T.)	LAT N	LONG E	DEPTH (Km.)	MAG (Md)	NO
911019	22 04 17.74	30-46.27	78-41.60	4.28	*3.4	16
911019	22 08 17.27	30-37.84	78-38.03	12.51	*2.4	14
911019	22 29 20.59	30-37.38	78-42.90	0.71	*4.0	23
911019	22 41 18.26	30-40.23	78-40.70	15.00	*4.7	19
911019	22 56 21.56	30-41.90	78-44.05	1.29	*4.0	11
911019	23 10 06.94	30-43.03	78-40.93	12.08	-	15
911019	23 39 30.35	30-42.26	78-41.26	12.03	*3.5	18
911020	01 04 26.77	30-41.59	78-48.25	11.79	-	15
911020	01 13 13.35	30-50.60	78-47.36	2.07	*2.4	16
911020	01 21 02.04	30-44.53	78-36.32	8.64	*2.3	21
911020	01 24 59.83	30-39.86	78-47.78	6.89	*4.2	20
911020	03 34 29.21	30-46.00	78-53.23	1.10	*2.9	22
911020	04 20 27.87	30-43.57	78-37.85	5.56	*3.0	27
911020	04 31 30.28	30-40.87	78-43.72	8.82	*3.5	15
911020	05 32 27.58	30-43.93	78-37.85	2.01	*5.2	34
911020	05 54 42.83	30-52.21	78-45.27	3.14	-	8
911020	05 57 30.38	30-52.26	78-39.39	3.55	-	8
911020	06 48 07.67	30-45.05	78-31.57	2.62	3.1	24
911020	07 25 49.58	30-35.82	78-36.70	15.00	2.9	15
911020	07 56 31.54	30-39.90	78-45.65	11.45	3.5	29
911020	09 01 05.95	30-32.85	78-35.07	20.95	2.7	11

911020	09	54	05.10	30-45.78	78-37.24	1.91	2.7	9
911020	10	17	56.61	30-44.65	78-37.58	1.57	2.7	12
911020	10	39	22.07	30-44.35	78-30.90	6.74	2.6	8
911020	11	10	29.15	30-43.50	78-38.53	9.47	2.7	11
911020	21	48	47.65	30-44.20	78-42.82	1.79	2.4	9
911020	23	58	37.90	30-46.40	78-34.88	1.52	2.7	7
911021	14	02	44.32	30-45.47	78-48.21	1.82	*3.6	19
911021	14	28	12.17	30-47.84	78-33.48	3.28	2.6	10
911021	14	36	03.08	30-47.26	78-27.23	3.83	2.6	13
911021	18	44	11.54	30-47.93	78-37.98	0.25	2.5	8
911021	22	32	04.55	30-43.89	78-41.41	4.05	2.8	8
911022	06	39	26.60	30-49.23	78-34.23	0.43	2.7	15
911022	11	15	32.75	30-48.61	78-34.01	5.21	*3.4	12
911024	00	04	46.60	30-48.46	78-33.73	4.39	2.5	13
911024	08	11	21.45	30-44.11	78-37.25	0.03	*3.2	10
911024	19	21	00.00	30-43.40	78-35.50	2.92	*3.5	19
911024	20	40	04.00	30-43.73	78-26.93	11.78	2.5	8
911025	15	22	43.44	30-46.24	78-38.28	1.57	2.9	9
911025	19	09	22.53	30-50.19	78-33.29	0.12	2.7	8
911027	00	40	24.15	30-44.57	78-46.64	3.72	*4.1	13
911027	13	19	40.54	30-44.36	78-42.43	3.27	*4.0	12
911027	19	29	38.31	30-46.74	78-47.17	15.00	2.7	7
911111	19	43	44.71	30-51.10	78-22.64	26.48	2.38	6
911111	20	43	47.83	30-43.98	78-34.30	7.48	2.11	6
911111	21	01	24.62	30-43.42	78-08.01	0.86	1.85	5

911111	21	35	13.66	30-63.21	78-21.10	1.94	2.05	6
911112	05	03	01.71	30-44.59	78-38.01	0.88	1.89	5
911112	20	28	52.69	30-38.72	78-38.56	1.60	1.97	5
911112	23	50	12.26	30-43.03	78-37.13	0.59	2.66	6
911113	00	31	34.27	30-41.58	78-38.32	7.82	2.76	6
911113	01	06	13.81	30-42.39	78-39.86	1.10	2.55	5
911113	12	11	13.87	30-45.10	78-32.43	1.34	2.86	5
911113	18	35	00.76	30-42.13	78-36.15	0.31	2.73	6
911114	00	04	27.94	30-36.65	78-49.21	0.50	3.16	6
911114	07	44	38.03	30-42.25	78-35.13	6.11	1.99	6
911114	10	32	09.89	30-43.47	78-36.09	1.17	2.32	6
911114	17	31	57.33	30-33.78	78-38.73	11.27	2.61	6
911114	17	35	38.85	30-44.36	78-33.58	1.07	2.02	6
911114	18	26	14.09	30-40.47	78-41.02	2.16	2.29	6
911114	19	52	28.48	30-40.81	78-36.62	1.41	1.49	6
911114	20	36	01.94	30-43.46	78-38.20	1.15	1.44	6
911114	22	53	16.77	30-43.41	78-35.20	1.17	1.55	6
911115	03	44	42.51	30-40.07	78-45.56	0.99	2.58	6
911115	12	11	21.84	30-41.59	78-39.99	1.41	1.88	6
911115	13	09	16.33	30-45.15	78-36.58	10.37	2.43	5
911115	15	39	14.39	30-41.89	78-37.08	5.58	3.19	6
911115	18	30	57.92	30-41.74	78-35.42	2.45	1.04	6
911115	20	43	39.22	30-30.75	78-29.22	15.90	1.50	5
911116	01	04	46.45	30-34.46	78-39.39	1.37	2.95	6
911117	13	32	07.78	30-44.55	78-35.98	1.39	1.76	6

911117	18	44	50.59	30-45.00	78-37.43	7.84	2.79	5
911118	00	19	17.79	30-44.05	78-33.48	0.37	2.10	5
911118	03	22	22.62	30-43.14	78-37.97	1.08	2.35	6
911118	15	18	14.82	30-42.37	78-35.48	1.08	3.01	5
911118	16	09	55.20	30-55.65	78-17.31	0.89	2.17	6
911119	12	03	17.47	30-45.94	78-33.87	2.12	3.05	5
911119	14	38	06.66	30-43.20	78-35.62	10.46	2.90	6
911119	15	11	58.67	30-45.93	78-36.67	11.61	1.55	6
911119	19	43	33.40	30-46.07	78-34.93	2.91	2.57	6
911119	21	50	06.81	30-50.59	78-24.40	1.16	2.14	5
911120	03	02	26.79	30-44.18	78-33.98	0.93	1.95	6
911120	15	47	28.89	30-42.42	78-36.81	8.55	2.08	6
911120	16	14	56.45	30-29.11	78-33.10	1.34	3.06	6
911120	19	50	06.97	30-41.76	78-44.59	0.85	2.06	6
911121	01	03	03.27	30-40.41	78-36.15	0.97	2.28	6
911121	07	52	35.72	30-46.19	78-29.88	7.01	0.04	6
911121	15	48	35.37	30-42.09	78-36.85	0.08	1.55	6
911121	19	54	03.62	30-49.49	78-38.48	9.27	2.14	6
911122	15	52	24.21	30-43.55	78-37.79	15.13	2.98	8
911122	20	48	29.95	30-39.72	78-40.16	1.04	1.14	6
911123	04	52	07.47	30-42.73	78-36.63	6.14	3.13	7
911123	18	45	26.28	30-44.78	78-28.92	0.28	1.98	6
911123	18	46	02.44	30-44.14	78-28.77	1.32	1.45	6
911123	18	53	39.20	30-39.09	78-45.51	1.19	2.25	6
911123	19	18	30.12	30-41.05	78-40.51	12.14	1.19	6

911123	19	52	44.44	30-42.57	78-32.08	1.06	1.32	6
911123	20	35	03.83	30-45.74	78-36.56	0.31	1.55	6
911123	21	22	07.49	30-42.45	78-36.71	1.53	1.59	6
911124	01	02	47.15	30-40.68	78-38.75	9.60	2.62	6
911124	06	18	40.24	30-43.27	78-39.65	5.51	-	6
911124	13	19	40.31	30-45.59	78-28.77	0.86	2.81	6
911124	23	31	09.48	30-40.06	78-38.34	0.23	1.36	6
911125	14	29	49.89	30-41.76	78-37.68	0.34	3.72	8
911125	18	59	47.40	30-43.64	78-35.05	2.69	3.49	6
911125	19	36	13.80	30-51.41	78-29.64	1.19	2.42	6
911125	21	31	01.96	30-43.48	78-36.73	2.02	1.18	6
911126	07	02	16.33	30-40.55	78-41.49	14.95	2.35	8
911126	08	21	44.42	30-43.05	78-37.95	10.44	1.80	6
911126	10	32	25.37	30-46.84	78-39.26	9.18	2.47	8
911126	18	01	17.46	30-45.06	78-24.07	1.13	0.48	6
911128	05	01	28.12	30-50.23	78-25.92	7.68	2.78	8
911128	22	13	26.68	30-45.68	78-34.51	0.60	3.28	8
911129	01	53	04.70	30-47.25	78-33.27	10.46	1.40	6
911129	23	47	46.01	30-39.72	78-35.76	0.30	2.61	6
911130	00	09	20.27	30-47.56	78-34.50	0.70	1.78	6
911130	12	20	26.34	30-44.56	78-32.45	10.12	2.24	8
911130	13	01	50.54	30-43.51	78-33.89	0.72	2.39	6
911130	21	22	32.38	30-39.32	78-30.66	1.36	2.03	6
911130	21	29	16.68	30-43.65	78-39.64	1.24	1.38	6
911201	15	18	07.44	30-47.04	78-40.24	12.81	1.65	6

911201	16	02	36.31	30-39.69	78-53.10	5.43	2.04	5
911201	16	19	11.27	30-43.46	78-37.75	1.20	1.46	6
911203	01	36	27.74	30-48.43	78-36.44	7.62	2.46	8
911203	03	04	51.47	30-46.50	78-35.26	6.24	2.25	6
911203	06	04	32.19	30-37.01	78-27.10	8.87	2.20	6
911203	18	54	33.17	30-40.95	78-58.15	3.30	1.95	7
911205	00	01	06.39	30-40.60	78-43.82	9.46	1.96	6
911205	03	12	46.56	30-39.38	78-43.26	10.95	2.19	6
911206	11	31	43.29	30-48.70	78-34.07	8.54	2.42	8
911207	00	13	38.12	30-42.87	78-37.90	3.96	1.76	6
911207	01	08	04.33	30-47.07	78-33.46	6.01	1.81	6
911207	17	16	18.68	30-41.70	78-39.44	15.00	2.14	7
911208	15	46	31.79	30-42.64	78-36.70	10.25	3.17	13

MD - Duration Magnitude
 R - Richter magnitude

Note : Duration magnitude calculated by IMD for the month of October is based on the USGS formula:

$$M_d = - 0.87 + 2 \log (T) + 0.035 R$$

Where T is single duration and R is the epicentral distance. Duration magnitude determined by the formula mentioned in the text is less by about .5 unit as compared to the USGS formula for magnitude upto 3.0.

Table 7.4 Location of aftershocks of Uttarkashi earthquake of 20th October, 1991 (Kayal et al., 1992). This data is plotted in Fig 7.7.

STATION	LONGITUDINAL COMPONENT IN CM/SEC ²	TRANSVERSE COMPONENT IN CM/SEC ²	RESULTANT HORIZONTAL ACCELERATION IN CM/SEC ²
Almora	17.4	21.0	22.2
Barkot	93.1	80.4	103.8
Bhatwari	248.4	241.8	271.6
Ghansiali	115.6	114.9	141.9
Karnprayag	60.9	77.3	84.7
Kosani	28.3	31.4	31.5
Koteshwar	98.8	65.2	99.0
Koti	20.6	40.9	41.0
Purola	73.9	91.6	96.1
Rudrprayag	52.2	50.7	65.2
Srinagar	65.4	49.4	65.7
Tehri	71.4	61.2	73.6
Uttarkashi	237.2	304.0	313.0

Table 7.5 Resultant peak ground acceleration of two horizontal components recorded at different stations for Uttarkashi earthquake of 20th Oct, 1991 (After Chandrasekaran and Das, 1991 and 1992c). Isoacceleration contour map of resultant peak acceleration is given in Fig 7.8.

PARAMETER	ALMO LONG	ALMO TRANS	ALMO VERT	BARK LONG	BARK TRANS	BARK VERT
P_A	17.4	21.0	18.4	93.1	80.4	43.6
T_{at}	2.44	.48	.02	1.84	1.58	4.3
T_D	16.28	17.44	18.00	15.1	14.0	18.6
P_v	1.33	1.26	1.54	5.7	4.4	2.7
P_d	.34	.45	.39	1.09	.69	.56
T_{area}	3542	3562	3257	16292	14563	11072
R_{at}	.985	.991	.981	.980	.993	.999
ACF_1	.076	.08	.071	.039	.045	.032
ACF_2	.260	.261	.217	.091	.235	.077
ACF_3	.358	.370	.500	.141	.306	.126
ACF_4	.140	.160	.140	.06	.08	.06
ACF_5	.877	.869	.811	.627	.678	.459
ACF_6	.587	.571	.430	-.051	.086	-.329
ACF_7	.250	.256	.117	-.363	-.273	-.378
ACF_8	-.420	-.351	-.436	-.363	-.297	-.378
ACF_9	1.308	1.303	1.203	2.753	1.355	2.062
ACF_{10}	1.029	1.027	1.028	1.036	1.037	1.038
F_p	3.2	2.3	4.1	8.7	6.8	10.1
F_1	3.1	2.9	3.5	6.8	5.9	8.2
F_2	4.0	4.0	4.7	8.5	7.4	9.9
F_3	5.5	6.4	8.5	9.7	9.3	11.5
F_4	2.4	2.4	2.7	3.3	3.2	5.6
F_5	3.2	3.1	3.8	7.2	6.2	9.0
F_6	4.3	4.3	4.8	8.7	7.9	10.4

Table 7.6 Extracted features from three components of field records of the Uttarkashi earthquake of 20th October, 1991 at **Almora (Almo)** and **Barkot (Bark)** stations. Field records at these stations are shown in Fig 7.13 to 7.18.

PARAMETER	KARN LONG	KARN TRANS	KARN VERT	KOSA LONG	KOSA TRANS	KOSA VERT
P_a	60.99	77.3	25.9	28.3	31.5	11.0
T_{at}	.599	2.02	1.82	1.42	11.24	.002
T_D	12.88	14.02	16.80	11.20	11.44	12.26
P_v	3.69	3.73	1.49	1.8	1.5	.91
P_d	.59	.402	.21	.37	.28	.24
T_{area}	11089	10041	4978	3664	3848	1608
R_{at}	1.00	1.00	1.00	1.025	1.029	1.00
ACF_1	.082	.079	.047	.052	.049	.060
ACF_2	.254	.265	.139	.146	.136	.098
ACF_3	.427	.449	.219	.216	.215	.126
ACF_4	.160	.160	.080	.100	.080	.160
ACF_5	.899	.885	.672	.788	.769	.713
ACF_6	.654	.618	.122	.302	.239	.249
ACF_7	.346	.302	-.239	-.204	-.301	-.002
ACF_8	-.775	-.651	-.404	-.579	-.623	-.123
ACF_9	.686	.748	1.445	1.177	1.084	38.9
ACF_{10}	1.016	1.020	1.034	1.031	1.030	1.044
F_p	2.9	2.9	6.8	6.1	5.9	4.4
F_1	2.8	2.8	5.2	4.8	5.2	4.8
F_2	3.0	3.4	6.7	5.8	5.9	7.9
F_3	3.7	4.9	10.1	6.3	6.4	9.8
F_4	2.8	2.7	4.4	3.7	4.4	2.5
F_5	2.9	2.9	5.4	5.2	5.6	4.4
F_6	3.4	3.7	6.9	6.1	6.1	7.9

Table 7.7 Extracted features from three components of field records of the Uttarkashi earthquake of 20th October, 1991 at Karnprayag (Karn) and Kosani (Kosa) stations. Field records at these stations are shown in Fig 7.19 to 7.24.

PARAMETER	PURO LONG	PURO TRANS	PURO VERT	RUDR LONG	RUDR TRANS	RUDR VERT
P_a	73	91	51	52	50	44
T_{at}	1.9	1.0	3.5	6.5	1.3	1.6
T_D	13.5	11.6	17.8	23.7	21.7	22.6
P_v	4.8	4.5	2.5	2.0	2.7	1.7
P_d	.84	.92	.44	.78	.40	.38
T_{area}	9589	12810	8832	18728	16048	13646
R_{at}	1.03	.982	.976	.99	.99	.99
ACF_1	.054	.053	.046	.031	.033	.029
ACF_2	.158	.151	.153	.091	.092	.088
ACF_3	.242	.240	.231	.148	.153	.148
ACF_4	.10	.10	.10	.060	.060	.060
ACF_5	.785	.789	.65	.482	.525	.358
ACF_6	.312	.315	.092	-.371	-.304	-.416
ACF_7	-.130	-.150	-.190	-.728	-.711	-.580
ACF_8	-.440	-.550	-.370	-.728	-.711	-.580
ACF_9	1.14	1.17	1.32	1.008	1.068	1.128
ACF_{10}	1.035	1.029	1.032	1.017	1.016	1.022
F_p	4.4	5.3	5.3	8.8	8.0	8.0
F_1	4.3	4.5	5.2	7.7	7.9	8.2
F_2	5.2	5.3	6.6	8.7	8.2	9.1
F_3	7.0	6.3	10.8	9.3	8.6	12.9
F_4	3.7	3.9	4.2	7.4	7.5	8.0
F_5	4.7	5.2	5.3	8.5	8.1	8.4
F_6	5.9	5.7	7.6	9.0	8.4	10.2

Table 7.8 Extracted features from three components of field records of the Uttarkashi earthquake of 20th October, 1991 at **Purola (Puro)** and **Rudrprayag (Rudr)** stations. Field records at these stations are shown in Fig 7.25 to 7.30.

PARAMETER	GHAN LONG	GHAN TRANS	GHAN VERT	KOTE LONG	KOTE TRANS	KOTE VERT
P_a	114	115	99	98	65	74
T_{at}	1.9	2.3	4.0	1.00	6.34	6.00
T_D	17.6	16.2	17.7	14.1	18.3	19.4
P_v	7.82	8.0	9.59	5.20	3.92	8.52
P_d	1.33	1.35	2.59	1.11	.07	2.04
T_{area}	27663	24083	20207	22282	14049	14179
R_{at}	1.00	.99	1.02	1.00	1.01	1.00
ACF_1	.048	.051	.037	.065	.060	.054
ACF_2	.135	.140	.100	.188	.177	.092
ACF_3	.218	.255	.183	.298	.241	.198
ACF_4	.08	.08	.06	.120	.100	.480
ACF_5	.750	.759	.546	.859	.803	.739
ACF_6	.204	.243	-.102	.510	.388	.237
ACF_7	-.296	-.212	-.276	.089	.003	-.094
ACF_8	-.537	-.425	-.276	-.674	-.343	-.161
ACF_9	1.280	1.642	3.065	.934	1.738	9.933
ACF_{10}	1.026	1.030	1.036	1.023	1.033	1.032
F_p	6.5	4.8	8.6	4.1	5.9	.8
F_1	5.2	4.7	7.1	3.7	4.0	5.6
F_2	6.0	6.1	8.6	4.3	5.2	7.3
F_3	7.1	7.7	12.2	4.8	7.0	8.8
F_4	4.0	3.8	4.6	3.4	2.7	1.6
F_5	5.5	5.1	7.3	4.1	4.2	5.1
F_6	6.5	6.4	9.3	4.5	5.7	7.4

Table 7.9 Extracted features from three components of field records of the Uttarkashi earthquake of 20th October, 1991 at **Ghansiali (Ghan)** and **Koteshwar (Kote)** stations. Field records at these stations are shown in Fig 7.31 to 7.36.

PARAMETER	KOTI LONG	KOTI TRANS	KOTI VERT	SRI LONG	SRI TRANS	SRI VERT
P_a	20	40	14	65	49	44
T_{at}	3.6	.16	.58	4.6	3.7	10.3
T_D	11.14	11.12	13.06	25.3	25.5	27.8
P_v	2.34	2.86	1.76	1.94	2.02	3.52
P_d	.42	.34	.50	.58	.50	.76
T_{area}	2815	3882	2116	16520	13642	11657
R_{at}	1.024	.998	1.007	.989	1.00	1.01
ACF_1	.101	.096	.238	.027	.029	.027
ACF_2	.727	.277	.711	.071	.071	.056
ACF_3	1.047	.446	1.165	.114	.108	.110
ACF_4	.500	.500	.500	.04	.04	.04
ACF_5	.895	.930	.886	.325	.370	.187
ACF_6	.677	.753	.695	-.575	-.441	-.350
ACF_7	.442	.508	.545	-.401	-.291	.086
ACF_8	-.245	-.660	-.416	-.575	-.441	-.350
ACF_9	.841	.901	.782	1.358	1.871	3.90
ACF_{10}	1.036	1.028	1.020	1.026	1.027	1.032
F_p	2.5	3.0	1.2	11.4	12.4	12.4
F_1	2.6	2.6	2.5	9.6	8.8	11.3
F_2	3.9	2.8	4.4	11.1	11.4	12.7
F_3	5.2	3.1	8.7	12.0	12.4	15.4
F_4	1.2	2.4	1.0	8.2	6.2	6.9
F_5	2.5	2.7	1.2	10.3	10.0	11.8
F_6	3.9	3.0	3.5	11.7	12.0	13.7

Table 7.10 Extracted features from three components of field records of the Uttarkashi earthquake of 20th October, 1991 at **Koti** and **Srinagar (Sri)** stations. Field records at these stations are shown in Fig 7.37 to 7.42.

PARAMETER	TEHR LONG	TEHR TRANS	TEHR VERT
P_a	71	61	57
T_{at}	2.0	.44	3.3
T_D	14.1	13.5	14.2
P_v	4.21	9.23	8.84
P_d	.81	1.98	2.36
T_{area}	10700	11124	9961
R_{at}	.99	.99	1.00
ACF_1	.077	.325	.289
ACF_2	.244	.796	1.014
ACF_3	.429	1.298	1.495
ACF_4	.120	.460	.720
ACF_5	.857	.917	.827
ACF_6	.553	.731	.592
ACF_7	.235	.522	.459
ACF_8	-.314	-.381	-.331
ACF_9	1.788	.798	.682
ACF_{10}	1.031	1.028	1.023
F_p	3.2	1.0	.78
F_1	3.2	2.5	3.6
F_2	4.4	3.6	7.5
F_3	6.2	5.6	11.1
F_4	2.4	1.0	.8
F_5	3.2	2.0	1.6
F_6	4.7	3.5	4.8

Table 7.11 Extracted features from three components of field records of the Uttarkashi earthquake of 20th October, 1991 at Tehri (Tehr) station. Field records at these stations are shown in Fig 7.43 to 7.45.

PARAMETER	UKT LONG	UKT TRANS	UKT VERT	BHT LONG	BHT TRANS	BHT VERT
P_a	237	303	192	248	241	288
T_{at}	3.0	2.4	5.3	.7	2.2	2.2
T_D	6.84	6.84	11.52	7.82	5.46	7.64
P_v	16.9	19.4	14.1	17.8	29.7	13.3
P_d	2.1	1.9	2.2	3.7	5.3	2.3
T_{area}	30928	35605	30367	32665	36945	33530
R_{at}	1.01	1.00	.98	1.01	.98	.99
ACF_1	.059	.072	.035	.086	.152	.046
ACF_2	.233	.237	.067	.470	.522	.048
ACF_3	.340	.377	.095	.618	.779	.070
ACF_4	.100	.180	.120	.400	.360	.140
ACF_5	.819	.837	.470	.846	.869	.499
ACF_6	.402	.474	-.171	.543	.626	-.011
ACF_7	-.031	.125	-.033	.261	.394	.017
ACF_8	-.499	-.433	-.322	-.243	-.401	-.258
ACF_9	1.289	1.021	7.23	.887	.858	.901
ACF_{10}	1.038	1.035	1.044	1.033	1.038	1.055
F_p	4.1	2.9	4.1	2.0	1.5	4.3
F_1	4.0	3.1	8.5	3.5	2.3	6.6
F_2	5.3	5.1	11.4	4.6	4.8	11.1
F_3	6.3	7.1	13.1	7.3	7.1	14.3
F_4	3.3	2.6	4.0	1.8	1.5	3.4
F_5	4.1	3.2	8.4	3.5	1.9	6.0
F_6	5.9	5.8	12.2	4.7	4.3	11.3

Table 7.12 Extracted features from three components of field records of the Uttarkashi earthquake of 20th October, 1991 at **Uttarkashi (Ukt)** and **Bhatwari (Bht)** stations. Field records at these stations are shown in Fig 7.46 to 7.51.

MODEL NAME	MD _{d1}	MU _{d2}	MD _{d1}	MD _{d2}
STATION	UKT	UKT	BHT	BHT
P _a	483	425	352	550
T _{st}	2.4	7.1	1.9	3.16
T _D	11.8	10.2	13.0	10.2
P _v	12.2	13.8	10.5	15.95
P _d	.362	.449	.299	.503
T _{area}	39737	39780	39256	39289
R _{st}	.999	.999	.999	1.00
ACF ₁	.032	.031	.031	.027
ACF ₂	.093	.091	.091	.083
ACF ₃	.161	.143	.156	.101
ACF ₄	.048	.048	.048	.040
ACF ₅	.290	.277	.261	.316
ACF ₆	-.628	-.658	-.663	-.591
ACF ₇	-.484	-.472	-.451	-.513
ACF ₈	-.628	-.658	-.663	-.591
ACF ₉	1.160	1.129	1.132	1.166
ACF ₁₀	1.043	1.047	1.049	1.053
F _p	8.8	10.1	8.1	5.4
F ₁	7.7	7.5	7.8	7.1
F ₂	8.8	8.9	8.8	8.9
F ₃	10.5	10.4	10.6	10.4
F ₄	6.5	6.8	6.2	6.2
F ₅	8.6	8.7	8.4	7.8
F ₆	9.9	10.1	10.3	9.8

Table 7.13 Extracted features from simulated records at Uttarkashi (Ukt) and Bhatwari (Bht) stations for models MU_{d1} and MU_{d2} of rupture planes. The models of these rupture planes and the simulated records are shown in Fig 7.52 and 7.53.

PARAMETER	MODEL GIVING LEAST DIFFERENCE IN THE VALUE OF EXTRACTED PARAMETER FROM SIMULATED AND FIELD RECORD AT UTTARKASHI	MODEL GIVING LEAST DIFFERENCE IN THE VALUE OF EXTRACTED PARAMETER FROM SIMULATED AND FIELD RECORD AT BHATWARI
P_a	MU ₄₂	MU ₄₁
T_{at}	MU ₄₁	MU ₄₁
T_D	MU ₄₂	MD ₄₂
P_v	MU ₄₂	MU ₄₂
P_d	MU ₄₂	MU ₄₂
T_{area}	MD ₄₁	MD ₄₁
R_{at}	MU ₄₁ , MU ₄₂	MU ₄₁
ACF ₁	MU ₄₁	MU ₄₁
ACF ₂	MU ₄₁	MU ₄₁
ACF ₃	MU ₄₁	MU ₄₁
ACF ₄	MU ₄₁ , MU ₄₂	MU ₄₁
ACF ₅	MU ₄₁	MU ₄₂
ACF ₆	MU ₄₁	MD ₄₂
ACF ₇	MU ₄₂	MD ₄₁
ACF ₈	MU ₄₁	MU ₄₂
ACF ₉	MU ₄₂	MU ₄₁
ACF ₁₀	MU ₄₁	MU ₄₁
F_p	MU ₄₁	MU ₄₂
F_1	MU ₄₂	MU ₄₂
F_2	MU ₄₁	MU ₄₁
F_3	MU ₄₂	MU ₄₂
F_4	MU ₄₁	MU ₄₂
F_5	MU ₄₁	MU ₄₂
F_6	MU ₄₁	MU ₄₂

Table 7.14 Selection of dip and strike of rupture plane by comparison of extracted features of field records with that of simulated records obtained after modelling two different models MU₄₁ and MU₄₂ at Uttarkashi and Bhatwari stations.

PARAMETERS	MU _{n1}	MU _{n2}	MU _{n3}	MU _{n4}	MU _{n5}	MU _{n6}
P _n	291	299	368	430	591	352
T _n	11.8	7.7	8.8	3.6	1.6	1.9
T _p	19.5	17.0	10.6	8.3	9.0	13.0
P _v	8.5	9.2	10.7	12.1	15.1	10.5
P _d	.237	.258	.312	.320	.320	.299
T _{area}	47612	48561	35879	31605	39383	39256
R _n	.99	.99	.99	.99	.99	.99
ACF ₁	.031	.031	.031	.032	.031	.031
ACF ₂	.091	.093	.092	.092	.091	.091
ACF ₃	.160	.163	.201	.138	.153	.156
ACF ₄	.048	.048	.048	.048	.048	.048
ACF ₅	.260	.290	.246	.285	.291	.261
ACF ₆	-.670	-.643	-.644	-.621	-.659	-.663
ACF ₇	-.463	-.513	-.395	-.448	-.513	-.451
ACF ₈	-.670	-.643	-.644	-.621	-.656	-.663
ACF ₉	1.11	1.11	1.20	1.21	1.10	1.132
ACF ₁₀	1.03	1.04	1.06	1.05	1.05	1.049
F _p	7.8	8.3	9.2	8.8	8.2	8.1
F ₁	7.8	7.7	7.4	8.3	7.7	7.8
F ₂	8.9	8.6	9.3	8.8	8.5	8.8
F ₃	10.6	10.5	11.1	10.7	10.4	10.6
F ₄	7.4	6.7	6.7	6.1	7.3	6.2
F ₅	7.9	8.3	8.8	8.7	8.3	8.4
F ₆	10.2	10.0	10.6	9.8	10.1	10.3

Table 7.15 Features extracted from simulated records at Bhatwari station for six different locations of nucleation point or starting point of rupture within the rupture plane. The rupture model differs only in the location of nucleation point. These models are named as MU_{n1}, MU_{n2}, MU_{n3}, MU_{n4}, MU_{n5} and MU_{n6}. Simulated acceleration records due to these models are shown in Fig 7.54.

PARAMETERS	MU _{n1}	MU _{n2}	MU _{n3}	MU _{n4}	MU _{n5}	MU _{n6}
P ₀	314	316	344	455	487	483
T _{at}	4.5	15.2	7.5	5.4	3.8	2.4
T _D	18.4	15.8	11.8	8.1	9.7	11.8
P _v	8.8	8.4	9.45	13.3	11.5	12.2
P _d	.29	.22	.31	.41	.42	.36
T _{area}	53075	41731	39730	32535	37574	39737
R _{at}	1.00	1.04	.99	.99	1.00	.99
ACF ₁	.031	.031	.031	.032	.032	.032
ACF ₂	.092	.093	.091	.090	.097	.093
ACF ₃	.161	.181	.144	.127	.144	.161
ACF ₄	.048	.048	.048	.048	.048	.048
ACF ₅	.275	.263	.261	.283	.317	.290
ACF ₆	-.650	-.644	-.644	-.617	-.580	-.628
ACF ₇	-.428	-.445	-.421	-.413	-.484	-.484
ACF ₈	-.650	-.644	-.644	-.617	-.580	-.628
ACF ₉	1.127	1.160	1.184	1.245	1.232	1.160
ACF ₁₀	1.016	1.043	1.054	1.045	1.040	1.043
F _p	8.8	8.6	9.5	9.1	5.5	8.8
F ₁	7.7	7.6	7.2	8.4	6.9	7.7
F ₂	8.8	8.8	9.4	9.1	8.8	8.8
F ₃	10.8	11.3	11.0	10.4	10.7	10.5
F ₄	6.9	6.8	6.5	5.4	5.5	6.5
F ₅	8.7	8.5	8.7	9.0	8.7	8.6
F ₆	10.1	10.6	10.4	10.0	9.6	9.9

Table 7.16 Features -extracted from simulated records at Uttarkashi station for six different locations of nucleation point or starting point of rupture within the rupture plane. The rupture model differs only in the location of nucleation point. These models are named as MU_{n1}, MU_{n2}, MU_{n3}, MU_{n4}, MU_{n5} and MU_{n6}. Simulated acceleration records due to these models are shown in Fig 7.54.

PARAMETERS	MODEL GIVING LEAST DIFFERENCE IN THE VALUE OF EXTRACTED PARAMETER FROM SIMULATED AND FIELD RECORDS AT UTTARKASHI	MODEL GIVING LEAST DIFFERENCE IN THE VALUE OF EXTRACTED PARAMETER FROM SIMULATED AND FIELD RECORDS AT BHATWARI
P_e	MU_{n1}	MU_{n1}
T_{at}	MU_{n6}	MU_{n4}
T_d	MU_{n4}	MU_{n4}
P_v	MU_{n4}	MU_{n4}
P_d	MU_{n4}	MU_{n4}
T_{area}	MU_{n4}	MU_{n4}
R_{at}	MU_{n6}, MU_{n4}	$MU_{n1}, MU_{n2}, MU_{n3}, MU_{n4}, MU_{n5}, MU_{n6}$
ACF_1	MU_{n4}	MU_{n4}
ACF_2	MU_{n2}, MU_{n6}	MU_{n2}
ACF_3	MU_{n2}	MU_{n2}
ACF_4	$MU_{n1}, MU_{n2}, MU_{n3}, MU_{n4}, MU_{n5}, MU_{n6}$	$MU_{n1}, MU_{n2}, MU_{n3}, MU_{n4}, MU_{n5}, MU_{n6}$
ACF_5	MU_{n4}	MU_{n2}
ACF_6	MU_{n4}	MU_{n4}
ACF_7	MU_{n4}	MU_{n4}
ACF_8	MU_{n4}	MU_{n4}
ACF_9	MU_{n1}	MU_{n1}
ACF_{10}	MU_{n2}	MU_{n1}
F_p	MU_{n2}	MU_{n1}
F_1	MU_{n2}	MU_{n2}
F_2	$MU_{n1}, MU_{n2}, MU_{n6}$	MU_{n2}
F_3	MU_{n4}	MU_{n2}
F_4	MU_{n4}	MU_{n4}
F_5	MU_{n2}	MU_{n1}
F_6	MU_{n4}	MU_{n4}

Table 7.17 Selection of possible location of nucleation point within the rupture plane by comparison of extracted parameters of field records with that of simulated records due to models MU_{n1} , MU_{n2} , MU_{n3} , MU_{n4} , MU_{n5} and MU_{n6} of rupture plane at Uttarkashi and Bhatwari stations.

STATION	X, Y AND Z COORDINATES OF STATION IN THE RECTANGULAR COORDINATE SYSTEM
Almora	(180,-30,-12)
Barkot	(-32,-23,-11.5)
Bhatwari	(-5.5,2.7,11.5)
Ghansiali	(32,-28,-12.0)
Karnprayag	(80,1,-12.0)
Kosani	(174,19,-12.0)
Koteshwar	(36,-45,-11.1)
Koti	(-44,-68.7,12.0)
Purola	(-47,-27,-12.0)
Rudrprayag	(62,-13,-12.0)
Srinagar	(51,-32,-10.6)
Tehri	(21.0,-40.0,-10.7)
Uttarkashi	(-11.2,-14,-11.1)

Table 7.18 Selected observation points with coordinates in rectangular coordinate system. The origin of the coordinate system lies at a depth of 12 km from the point O denoted in Fig 7.10.

PARAMETERS	BHATWARI	UTTARKASHI	PUROLA	BARKOT
P_a	430	455	469	421
T_{at}	3.6	5.4	5.3	3.8
T_D	8.3	8.1	7.3	7.3
P_v	12.1	13.3	14.0	11.7
P_d	.320	.417	.320	.350
T_{area}	31605	32535	32653	30355
R_{at}	.99	.99	1.02	1.02
ACF_1	.032	.032	.031	.032
ACF_2	.092	.090	.092	.092
ACF_3	.138	.127	.134	.125
ACF_4	.048	.048	.048	.048
ACF_5	.285	.283	.284	.283
ACF_6	-.621	-.617	-.633	-.603
ACF_7	-.448	-.413	-.459	-.411
ACF_8	-.621	-.617	-.633	-.603
ACF_9	1.202	1.245	1.175	1.265
ACF_{10}	1.058	1.045	1.028	1.040
F_p	8.8	9.1	10.9	11.0
F_1	8.3	8.4	10.2	10.1
F_2	8.8	9.1	10.9	11.0
F_3	10.7	10.4	12.1	12.5
F_4	6.1	5.4	7.2	6.9
F_5	8.7	9.0	10.9	10.9
F_6	9.8	10.0	11.5	12.0

Table 7.19 Extracted features from simulated records at various stations for Uttarkashi earthquake of 20th October, 1991. Simulated records at these stations is shown in Fig 7.56 to 7.68.

PARAMETERS	TEHRI	KOTESHWAR	SRINAGAR	KOTI
P_a	333	372	299	383
T_{at}	3.5	3.7	10.3	2.1
T_D	11.8	13.4	14.4	8.5
P_v	9.24	10.4	8.2	11.1
P_d	.230	.222	.240	.330
T_{area}	38189	38704	40893	31932
R_{at}	.99	1.00	1.09	.99
ACF_1	.032	.031	.030	.032
ACF_2	.095	.093	.088	.094
ACF_3	.176	.171	.166	.104
ACF_4	.048	.048	.048	.048
ACF_5	.288	.269	.225	.291
ACF_6	-.617	-.651	-.699	-.570
ACF_7	-.479	-.481	-.406	-.382
ACF_8	-.617	-.651	-.699	-.570
ACF_9	1.175	1.122	1.109	1.375
ACF_{10}	1.053	1.048	1.055	1.049
F_p	7.7	7.9	8.6	11.1
F_1	8.5	8.9	8.1	7.0
F_2	10.3	11.1	9.1	11.2
F_3	13.0	12.5	11.1	12.7
F_4	7.9	8.0	6.9	6.6
F_5	9.6	9.6	8.7	10.9
F_6	12.0	12.1	10.6	12.5

Table 7.20 Extracted features from simulated records at various stations for Uttarkashi earthquake of 20th October, 1991. Simulated records at these stations is shown in Fig 7.56 to 7.68.

PARAMETERS	RUDRP- RAYAG	KARNPR- AYAG	GHANSIALI	ALMORA	KOSANI
P_a	330	321	418	292	273
T_{at}	3.8	13.9	4.1	13.4	7.1
T_D	16.7	17.7	13.4	18.8	19.3
P_v	9.7	8.6	11.4	8.6	9.53
P_d	.240	.260	.365	.258	.272
T_{area}	43807	50275	41013	49885	52489
R_{at}	1.02	.99	.980	1.00	1.01
ACF_1	.031	.031	.032	.032	.032
ACF_2	.092	.091	.095	.092	.094
ACF_3	.204	.143	.178	.153	.175
ACF_4	.048	.048	.048	.048	.048
ACF_5	.260	.276	.287	.295	.295
ACF_6	-.642	-.648	-.632	-.629	-.633
ACF_7	-.427	-.456	-.508	-.490	-.516
ACF_8	-.642	-.648	-.632	-.629	-.633
ACF_9	1.178	1.156	1.129	1.157	1.127
ACF_{10}	1.041	1.037	1.052	1.029	1.020
F_p	13.2	9.7	7.9	8.9	9.4
F_1	9.4	9.1	8.5	8.9	8.8
F_2	10.6	10.8	10.5	10.3	10.4
F_3	13.2	12.5	10.6	12.5	12.3
F_4	7.9	8.5	7.8	7.6	8.6
F_5	10.1	10.5	9.7	9.9	9.4
F_6	12.8	12.1	11.9	11.9	12.1

Table 7.21 Extracted features from simulated records at various stations for Uttarkashi earthquake of 20th October, 1991. Simulated records at these stations is shown in Fig 7.56 to 7.68.

CHAPTER 8

MEGHALAYA EARTHQUAKE OF 10TH SEPTEMBER, 1986

The state of Meghalaya in north eastern part of India lies in highly seismic region of the country and has experienced many damaging earthquakes in the recent past. The epicenters of recent earthquakes in the region are shown in Fig 8.1 and the earthquake parameters are given in Table 8.1 (USGS-NEIC, 1990). This region was also the locale for the great Assam earthquake of 1897 which is considered as one of the most devastating earthquakes ever.

Meghalaya earthquake of 10th Sept, 1986 (hereafter referred to as the Meghalaya earthquake) is among the few earthquakes which have been recorded at several stations of the strong motion array installed in this region. The identification of the most probable causative fault and modelling of the rupture plane along the identified fault for the Meghalaya earthquake has been attempted in this work. The approach adopted is similar to that adopted for the Dharamsala and the Uttarkashi earthquakes as discussed in Chapters 6 and 7. The identification of most probable causative fault is based on very limited set of observational and field data. A simple model of the rupture plane is modelled to simulate strong motion records at the selected observation points which contain field records of this earthquake. The parameter extracted from simulated records are compared with that of field records, to establish the efficacy of the model.

8.1 STRONG MOTION ARRAY

The strong motion instrumentation array in this region consist of forty five three component instrument of SMA-1 type with Time Code Generator (TCG) card manufactured by M/S Kinematics, U.S.A. Location of stations of array is given in Table 8.2 and is shown in Fig 8.2. The instrument spacing in this array is large due to paucity of instruments and very difficult site conditions and terrain (Chandrasekaran et al., 1988).

Twelve elements of the strong motion array registered the Meghalaya earthquake. Other elements of the array were not triggered by this event as the intensity of ground motion at the respective sites was lower than trigger level of the starting device. The maximum recorded peak horizontal acceleration was 142.0 cm/sec^2 on N32°E component at station Saitsama, while the maximum recorded peak vertical acceleration was also at Saitsama and was 63.3 cm/sec^2 .

8.2 SALIENT FEATURES OF MEGHALAYA EARTHQUAKE OF 10TH SEPTEMBER, 1986

A moderate earthquake of magnitude 5.2 (M_b) occurred in the Meghalaya region on 10th Sept, 1986. This was the first time, that instrumental records of strong ground motion had been obtained from northeastern part of India. Strong motion records from this earthquakes have been analysed by Chandrasekaran and Das (1990a, 1990b, 1992a and 1992b) and Chandrasekaran et al. (1988). Epicenter of this earthquake using strong motion data was computed by Das and Chandrasekaran (1993). Various parameters of this earthquakes are given as :

ORIGIN TIME	7 hr, 50 min, 0 sec
MAGNITUDE M_b M_s	5.2 4.5
EPICENTER	25.385° N, 91.6° E
DEPTH OF HYPOCENTER	43 km

Parameters of this earthquake as given by other agencies are shown in Table 8.3.

8.3 IDENTIFICATION OF MOST PROBABLE CAUSATIVE FAULT FOR MEGHALAYA EARTHQUAKE OF 10TH SEPT, 1986

The most probable causative fault for the Meghalaya earthquake is identified on the basis of following maps :

- (i) Tectonic map of the region (Tilak et al. 1983) and
- (ii) Isoacceleration map of resultant peak horizontal acceleration

8.3.1. TECTONIC MAP OF THE REGION (TILAK ET AL., 1983)

Tectonic map (Tilak et al. 1983) of the region is shown in Fig 8.3. The tectonic lineaments in the region have a general NW strike trend. Prominent feature in the region which is striking EW is Dauki fault. Many lineaments are marked in this region which are close to the epicenter of the Meghalaya earthquake. Epicenter of the Meghalaya earthquake lies at a perpendicular distance of 10 km from a lineament named as lineament-1.

8.3.2. ISOACCELERATION MAP

Acceleration records are available for the Meghalaya earthquake for twelve stations which cover the entire epicentral area. Resultant peak acceleration data at these stations is taken from Chandrasekaran et al. (1988) and is reproduced in Table 8.4. Contours of resultant peak acceleration are made from this data. A contour interval of 50 cm/sec^2 is used with maximum contour value 150 cm/sec^2 and minimum contour value 50 cm/sec^2 . Isoacceleration contour map for this earthquake is shown in Fig 8.4. From this map it is seen that the trend of elongated axis of peak acceleration contour is in $N45^\circ E$ direction. Epicenter of the Meghalaya earthquake (After USGS) lies within area covered by contour value 100 cm/sec^2 .

8.3.3. COMPOSITE ISOACCELERATION AND TECTONIC MAP OF THE REGION

Isoacceleration map and Tectonic map of Meghalaya (Tilak et al., 1983) are superimposed to get a composite map of isoacceleration contours and tectonic map of the region shown in Fig 8.5.

8.3.4 IDENTIFIED MOST PROBABLE CAUSATIVE FAULT FOR MEGHALAYA EARTHQUAKE OF 10TH SEPT, 1986

A perusal of the composite map indicates that :

- (i) Direction of the elongated axis of isoacceleration contours of the Meghalaya earthquake is in $N45^\circ E$ direction. Strike of lineament- 1 is computed as $N52^\circ E$ from Fig 8.5.

- (ii) The point O_M which is the point of intersection of lineament -1 with other lineament can be assumed as a possible corner of rupture plane. The distance of epicenter is 8 km from this point.

The above observations suggests lineament-1 with strike $N52^\circ E$ (Fig 8.5) can be assumed as the most probable causative fault for the Meghalaya earthquake with the rupture plane located at point O_M .

8.4 SELECTION OF OBSERVATION POINTS

The Meghalaya earthquake was recorded on twelve strong motion recording stations. Fig 8.6 to 8.17 shows the field acceleration records, their autocorrelation function, power spectrum, cumulative power spectrum and frequency weighted power spectrum. Table 8.5 to 8.10 gives the values of extracted features from three components of acceleration records at twelve different stations.

The component of field acceleration record at a station which gives maximum value of parameter T_{area} has been used for comparison with the simulated record at the same station. Table below shows the component of acceleration record selected for comparison with the simulated record at the same station.

S.NO.	STATION NAME	COMPONENT OF ACCELERATION RECORD
1.	Baithalangso	Longitudinal
2.	Dauki	Longitudinal
3.	Khliehriat	Transverse

S.NO.	STATION NAME	COMPONENT OF ACCELERATION RECORD
4.	Nongkhlaw	Transverse
5.	Nongpoh	Longitudinal
6.	Nonstoin	Transverse
7.	Panimur	Transverse
8.	Pynursla	Longitudinal
9.	Saitsama	Transverse
10.	Ummulong	Longitudinal
11.	Umrongso	Longitudinal
12.	Umsning	Longitudinal

8.5 MODELLING PARAMETERS OF RUPTURE PLANE

The rupture plane for the Meghalaya earthquake has been modelled by specifying various parameters and adopting the methodology given in previous chapters. Data for this earthquake is less as compared to the other earthquakes which have been studied in the present work. It is for this reason that the geometry of the rupture plane is assumed to be simple. However, the comparison of the simulated and field records shows marked similarities which make the model acceptable.

8.5.1 LENGTH OF RUPTURE PLANE (L)

The length of the rupture plane for the Meghalaya earthquake ($M_b = 5.2$ and $M_s = 4.5$) calculated using different empirical relations is given in the following table:

Station	Component	Length (L)
Duki	Longitudinal	5
Khirsitri	Transverse	4

S.NO.	RUPTURE LENGTH (KM)	RUPTURE LENGTH CALCULATED USING EMPIRICAL RELATION GIVEN BY
1.	6.0 km	Otsuka (1965)
2.	1 km	Araya and Kiureghian (1988)
2.	5 -10 km	Naeim (1989)

The rupture length for this earthquake is assumed as 6 km (calculated using Otsuka (1965) relation) as this value lies between the limit defined by Naeim (1989).

8.5.2. DOWNWARD EXTENSION OF RUPTURE PLANE (D)

Downward extension of the rupture plane is assumed as 6 km which is equal to the length of the rupture plane as discussed in Chapter 2.

8.5.3. LENGTH OF ELEMENT (L)

The entire rupture plane is divided into square elements of 1 km side. As there are 6 elements each along the length and the downward extension of the rupture plane, the total number of elements within the entire rupture plane are 6 x 6 i.e., 36.

8.5.4. THREE DIMENSIONAL COORDINATE SYSTEM

The point O_M is the point of intersection of two lineaments, hence this point is assumed as a possible corner of the rupture plane along the identified probable causative fault. Strike of identified lineament-1 is $N52^\circ E$, and epicenter is lying on the southern side of O_M hence using the earlier convention of coordinate system, the line

from O_M along the strike of lineament-1 towards southern direction is assumed as X axis (positive), while Y axis is assumed to be positive on eastern side. Direction of X axis and Y axis with respect to geographic grid are $N52^\circ E$ and $N38^\circ W$, respectively. Z axis is assumed positive in vertically downward direction. Station elevations are taken from Chandrasekaran et al. (1988) and are included as third axis coordinate in the three dimensional coordinate system.

8.5.5 SOURCE WAVELET

The form of source wavelet used for the Meghalaya earthquake is the same as that used for modelling of rupture plane for the Uttarkashi and the Dharamsala earthquakes. The normalised value of the source wavelet of frequency 5 Hz is scaled by a factor of .13 cm/sec as explained in detail in Section 3.1.

8.5.6 VELOCITY OF THE MEDIUM (V)

Velocity of body wave in the medium around the epicentral area is taken from Saha et al. (1981). This velocity structure is computed from microearthquake survey in and around the region of Shillong. Following velocity structure has been given by Saha et al. (1981) :

LAYER	VELOCITY KM/SEC	DEPTH IN KM	THICKNESS IN KM
1	4.0	0.0	1.0
2	6.0	1.0	24.0
3	6.7	25.0	20.00
4	8.1	45.0	1000.0

The rupture plane lies at a depth of 28 km from the surface of the earth and at this depth velocity of P wave is 6.7 km/sec. Hence for modelling the rupture plane for simulating strong motion records velocity of the medium is taken as 6.7 km/sec. The velocity of S wave is taken as 3.8 km/sec which is equal to $V_p/(3)^{1/2}$.

8.5.7 RUPTURE VELOCITY (V_r)

The rupture velocity is taken as 80% of S wave velocity in the medium. For S wave velocity of 3.8 km/sec the rupture velocity is computed as 3.0 km/sec.

The parameters used for modelling of the rupture plane along the identified causative fault for the Meghalaya earthquake of 20th September, 1986 are :

S.No	Parameter	Value.	S.No.	Parameter	Value
1.	L (Length of rupture plane)	6 km	7.	Coordinate of nucleation point	(2,0,2)
2.	D (Downward extension of rupture plane)	6 km	8.	Depth of rupture plane	28 km
3.	L_e (Length of element)	1 km	9.	V (Velocity of the medium)	6.7 km/sec
4.	N (Total number of elements)	36	10.	V_r (Rupture velocity)	3.0 km/sec
5.	ϕ (Strike of rupture plane)	N52°E			
6.	δ (Dip of rupture plane)	90°			

These are initial parameters of rupture plane. The dip (δ) and coordinates of nucleation point are deduced by iteratively modelling the rupture plane and comparison of parameters of simulated and field records at Saitsama and Ummulong stations.

8.5.8 SELECTION OF DIP OF (δ) OF THE RUPTURE PLANE

The vertical, horizontal and dipping rupture planes named as MM_{d1} , MM_{d2} and MM_{d3} (shown in Fig 8.18, 8.19 and 8.20) are assumed for simulating strong motion records at Saitsama and Ummulong stations for the Meghalaya earthquake. The dip and strike for these models are given in following table :

MODEL NAME	STRIKE (ϕ)	DIP (δ)
MM_{d1}	N52°E	90°
MM_{d2}	N52°E	0°
MM_{d3}	N52°E	45°

Rupture plane is placed at a depth of 28 km from point O_M and the parameters of these three models of rupture plane are taken as :

MODELLING PARAMETER	MM_{d1}	MM_{d2}	MM_{d3}
L (Length of rupture plane in km)	6	6	6
D (Downward extension of rupture plane in km)	6	6	6
δ (Dip in degree)	90°	0°	45°
ϕ (Strike in degree)	N52°E	N52°E	N52°E
L_e (Length of element in km)	1	1	1
Coordinates of nucleation point in km	(0,0,0)	(0,0,0)	(0,0,0)
V (Velocity of medium in km/sec)	6.7	6.7	6.7
V_r (Rupture velocity in km/sec)	3.00	3.00	3.00

Coordinates of Saitsama and Ummulong stations are given in the following table shown in next page.

STATION	COORDINATES
Saitsama	(23.5,9.2,-28.4)
Ummulong	(-5.5,13.7,-28.8)

Features extracted from the simulated records shown in Fig 8.18, 8.19 and 8.20 are presented in Table 8.11. It is seen that for both Saitsama and Ummulong stations model MM_{d1} shows least difference between the extracted parameters of simulated and field records (Table 8.12). It is for this reason that model MM_{d1} with a dip of 90° is selected for final modelling purposes.

8.5.9 SELECTION OF STARTING POINT OF RUPTURE (OR NUCLEATION POINT) WITHIN THE RUPTURE PLANE

There is possibility that starting point of rupture can be any element within the rupture plane and this possibility is checked out by assuming different elements within the rupture plane as nucleation point. The modelling parameters of the rupture plane are:

PARAMETER	VALUE
L (Length of rupture plane in km)	6
D (Downward extension of rupture plane in km)	6
δ (Dip in degree)	90°
ϕ (Dip in degree)	$N52^\circ E$
L_e (Length of element in km)	1
V (Velocity of the medium in km/sec)	6.7
V_r (Rupture velocity in km/sec)	3.0

Five different elements within rupture plane are assumed as the nucleation point. The assumed nucleation points for different models lie at the four different corners of rupture plane and at the center. X,Y and Z coordinates of nucleation point and the name of models are given in the following table :

X,Y AND Z COORDINATES OF NUCLEATION POINT	MODEL NAME
(0,0,0)	MM _{n1}
(0,0,5)	MM _{n2}
(5,0,0)	MM _{n3}
(5,0,5)	MM _{n4}
(2,0,2)	MM _{n5}

Coordinates of Saitsama and Ummulong obtained by placing the origin of the rectangular coordinate system at O_M are :

STATION NAME	COORDINATES IN ASSUMED RECTANGULAR COORDINATE SYSTEM
Saitsama	(23.5,9.2,-28.4)
Ummulong	(-5.5,13.7,-28.8)

Simulated records at these two stations for five models i.e., MM_{n1}, MM_{n2}, MM_{n3}, MM_{n4} and MM_{n5} are shown in Fig 8.21. The features extracted from the strong motion records simulated at these stations for the five models are given in Table 8.13 and 8.14.

It is seen that for both Saitsama and Ummulong stations models MM_{n4} and MM_{n5} gives least difference between the extracted parameters of simulated and field records

(Table 8.15). The peak acceleration obtained at Ummulong station from the simulated record due to model MM_{nd} is higher as compared to its value at Saitsama. However, reverse of this is observed in the field records. Hence model MM_{ns} is selected for final modelling purposes with the depth of nucleation point at 31 km from the surface of the earth.

8.6 SIMULATION OF STRONG MOTION RECORDS AT SELECTED OBSERVATION POINTS

The parameters finally selected for modelling the rupture plane along the identified probable causative fault are :

S.NO	PARAMETER	VALUE.	S.NO.	PARAMETER	VALUE
1.	L (Length of rupture plane)	6 km	7.	Coordinate of nucleation point	(2,0,2)
2.	D (Downward extension of rupture plane)	6 km	8.	Depth of rupture plane	28 km
3.	L_e (Length of element)	1 km	9.	V (Velocity of the medium)	6.7 km/sec
4.	N (Total number of elements)	36	10.	V_r (Rupture velocity)	3.0 km/sec
5.	ϕ (Dip)	N52°E			
6.	δ (Strike)	90°			

The model of rupture plane for the Meghalaya earthquake is shown in Fig 8.22. The coordinates of selected stations on the rectangular coordinate system and the location of recording stations are shown in Table 8.16 and Fig 8.23, respectively.

Extracted parameters from simulated records at these stations are shown in Table 8.17 and 8.18.

Plots of simulated acceleration records, their autocorrelation function, power spectrum, cumulative power spectrum and frequency weighted cumulative power spectrum at different stations are shown in Fig 8.24 to 8.27.

8.7 COMPARISON OF FIELD AND SIMULATED RECORDS

At Saitsama and Ummulong stations the trend of peak acceleration from simulated record matches with that of field records as given in the table below :

STATION	HYPOCENTRAL DISTANCE (KM)	PEAK ACCELERATION IN SIMULATED RECORD	PEAK ACCELERATION IN FIELD RECORD
Saitsama	36	100 cm/sec ²	142 cm/sec ²
Ummulong	32	80 cm/sec ²	116 cm/sec ²

This may be due to the source directivity effect which has already been discussed in Chapter 6.

The minimum and maximum value of parameters extracted from field and simulated strong motion records and the corresponding stations are given in the following table :

PARAMETER	FIELD	RECORD	SIMULATED	RECORD
	MAXIMUM VALUE AND STATION	MINIMUM VALUE AND STATION	MAXIMUM VALUE AND STATION	MINIMUM VALUE AND STATION
P_a	142 cm/sec ² Saitsama	14.1 cm/sec ² Nongstoin	122 cm/sec ² Khliehriat	63 cm/sec ² Nongpoh, Nongstoin
T_{at}	1.2 sec/ Dauki	.06 sec Nongstoin	1.4 sec Dauki	.2 sec Pynursla, Saitsama
T_d	7.4 sec Nongstoin	1.6 sec Nongpoh	2.0 sec Umsning	1.3 sec Baithalangso, Panimur
P_v	5.7 cm/sec Nongkhwai	1.0 cm/sec Nongstoin	2.6 cm/sec Umrongso	1.4 cm/sec Nongpoh, Nongstoin
P_d	5.3 cm Nongkhwai	.6 Panimur	.23 Umrongso	.1 Dauki, Nongkhlaw
T_{area}	85840 Saitsama	1112 Umrongso	3291 Khliehriat	1912 Nongkhwai
R_{at}	1.259 Umrongso	.95 Baithalangso	.99 Baithalangso	.90 Panimur, Pynursla

This table shows that in field as well as simulated records minimum value of extracted parameters P_a and P_v is obtained at the same stations. The maximum value of parameters T_{at} from simulated and field records is also obtained at the same stations.

Following table presents the minimum and maximum values of parameters extracted from autocorrelation function of field and simulated acceleration records and the corresponding stations.

PARAMETERS	FIELD	RECORD	SIMULATED	RECORD
	MAXIMUM VALUE AND STATION	MINIMUM VALUE AND STATION	MAXIMUM VALUE AND STATION	MINIMUM VALUE AND STATION
ACF ₁	.071 sec Nongkhlaw	.030 sec Ummulong	.031 sec Nongkhlaw	.026 sec Baithalangso
ACF ₂	.264 sec Baithalangso	.095 sec Umrongso	.094 sec Nongkhlaw, Umsning	.073 sec Baithalangso
ACF ₃	.366 sec Nongkhlaw	.152 sec Umrongso	.180 sec Dauki	.113 sec Baithalangso
ACF ₄	.140 sec Nongkhlaw	.06 sec Ummulong, Umrongso	.06 at all station except Baithalangso	.04 sec Baithalangso
ACF ₅	.831 Nongkhlaw	.158 Nongpoh	.460 Umsning	.363 Baithalangso
ACF ₆	.543 Nongkhlaw	-.377 Ummulong	-.404 Nongkhlaw	-.694 Baithalangso
ACF ₇	.192 Nongkhlaw	-.569 Pynursla	-.555 Baithalangso	-.841 Khliehriat
ACF ₈	.192 Nongkhlaw	-.687 Pynursla	-.603 Nongkhlaw	-.841 Khliehriat
ACF ₉	1.58 Panimur	.694 Nongkhlaw	1.18 Nongkhlaw	.873 Khliehriat
ACF ₁₀	1.12 Umrongso	1.04 Saitsama	1.10 Nongkhlaw	1.00 Khliehriat

This table shows that the maximum value of parameters ACF₁, ACF₄, ACF₆ and ACF₈ is observed at same stations for both simulated and field records.

The minimum and maximum value of parameters extracted from the power spectrum of field and simulated acceleration record and the corresponding stations, are given in the following table.

PARAMETER	FIELD	RECORD	SIMULATED	RECORD
	MAXIMUM VALUE AND STATION	MINIMUM VALUE AND STATION	MAXIMUM VALUE AND STATION	MINIMUM VALUE AND STATION
F_p	7.9 Umrongso	2.1 Khliehriat	10.2 Pynursla, Ummulong	7.4 Umsning
F_1	7.9 Umrongso	3.4 Nongkhlaw	9.9 Baithalangso	7.4 Umsning
F_2	11.5 Umsning	3.6 Nongkhlaw	11.2 Baithalangso	8.5 Khliehriat
F_3	17.9 Baithalangso	6.4 Nongkhlaw	11.4 Baithalangso	9.8 Khliehriat
F_4	6.8 Ummulong	3.2 Baithalangso	8.3 Baithalangso, Nongstoin, Panimur	7.1 Umrongso
F_5	8.2 Umrongso	3.5 Nongkhlaw	11.1 Baithalangso	8.2 Nongkhlaw
F_6	11.8 Umsning	3.5 Nongkhlaw	11.4 Baithalangso	9.3 Khliehriat

The comparison shows that maximum value of parameter F_3 occur at same station for both simulated and field records. Minimum value of parameter F_5 occur at same station for both simulated and field records.

Following table present the parameters extracted from the simulated records and the number of stations at which their value varies less than twenty percent with that of field records.

PARAMETER	NUMBER OF STATIONS HAVING A DIFFERENCE OF LESS THAN 20% IN THE VALUE OF EXTRACTED PARAMETER FROM SIMULATED AND FIELD RECORDS.
P_a	4
T_{at}	4
T_D	1
R_{at}	11
T_{area}	2
ACF_1	4
ACF_2	2
ACF_3	1
ACF_4	2
ACF_5	4
ACF_8	1
ACF_9	6
ACF_{10}	11
F_p	1
F_1	3
F_2	6
F_3	8
F_4	2
F_5	3
F_6	6

The difference in the values of extracted parameters from simulated and field records at different stations can be due to various factors which are not taken into account in the present study as discussed in Chapter 10.

8.8 SUMMARY

Lineament 1 has been identified as the most probable causative fault for the Meghalaya earthquake (Fig 8.5). The rupture plane is placed at a vertical depth of 28 km from the surface of the earth and is modelled to simulate strong motion records at twelve selected observation points for which field records are available for the Meghalaya earthquake. The final modelling parameters of rupture plane are :

S.NO	PARAMETER	VALUE.	S.NO.	PARAMETER	VALUE
1.	L (Length of rupture plane)	6 km	7.	Coordinate of nucleation point	(2,0,2)
2.	D (Downward extension of rupture plane)	6 km	8.	Depth of rupture plane	28 km
3.	L_e (Length of element)	1 km	9.	V (Velocity of the medium)	6.7 km/sec
4.	N (Total number of elements)	36	10.	V_r (Rupture velocity)	3.0 km/sec
5.	ϕ (Dip)	N52°E			
6.	δ (Strike)	90°			

From the simulated and field strong motion records at twelve stations twenty four parameters were extracted for comparison and it is seen that parameters P_a , T_{at} , T_D , R_{at} , ACF_1 , ACF_2 , ACF_3 , ACF_4 , ACF_5 , ACF_8 , ACF_9 , ACF_{10} , F_p , F_1 , F_2 , F_3 , F_4 , F_5 and F_6 differ less than 20% at various stations thereby establishing that the model chosen is acceptable.

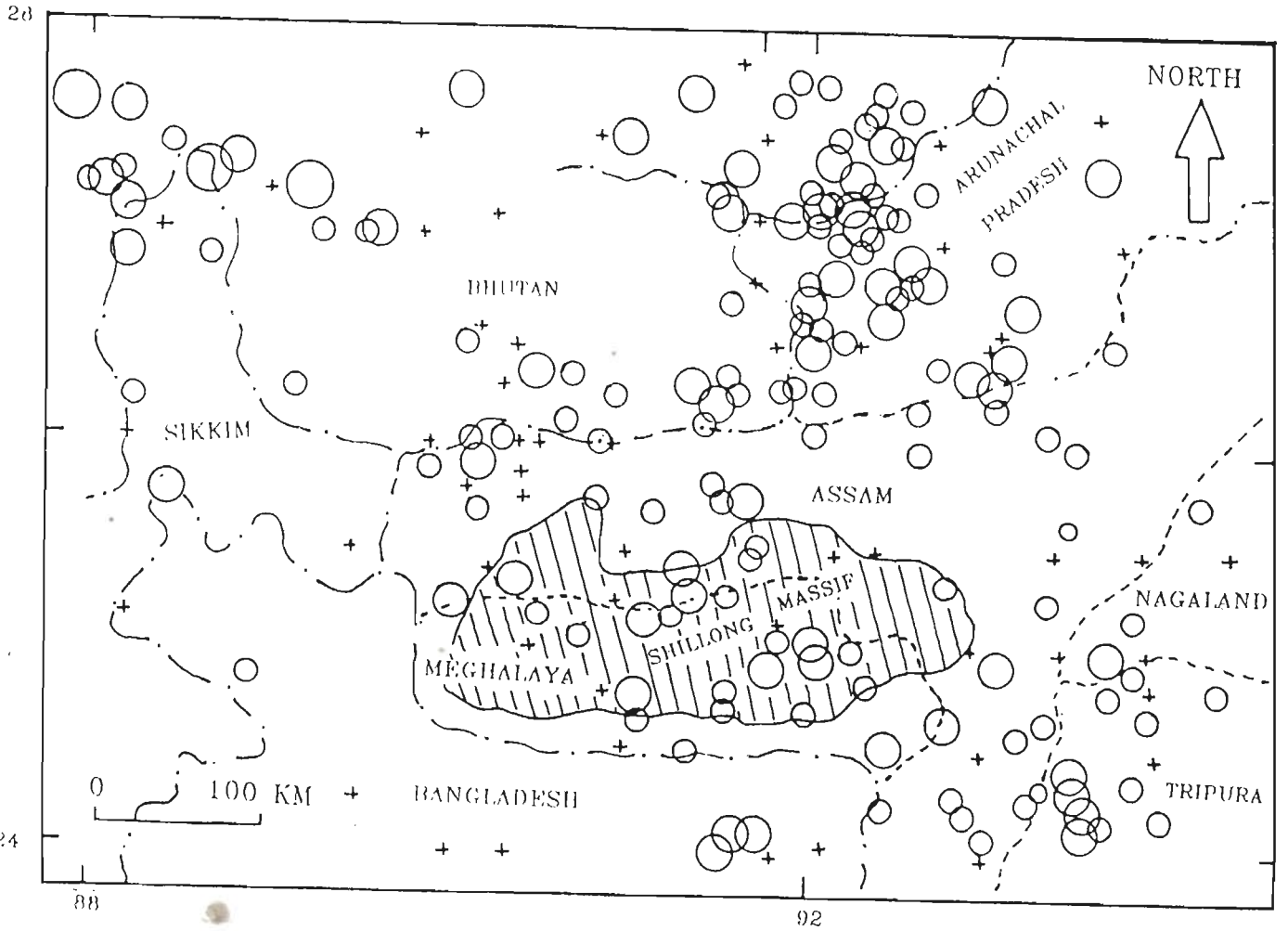


Fig 8.1 Locations of epicenters in Meghalaya and surrounding region. Epicentral data is taken from USGS-NEIC (1990) and reproduced in Table 8.1. The tectonics of the region is taken from Eremenko and Negi (1968).

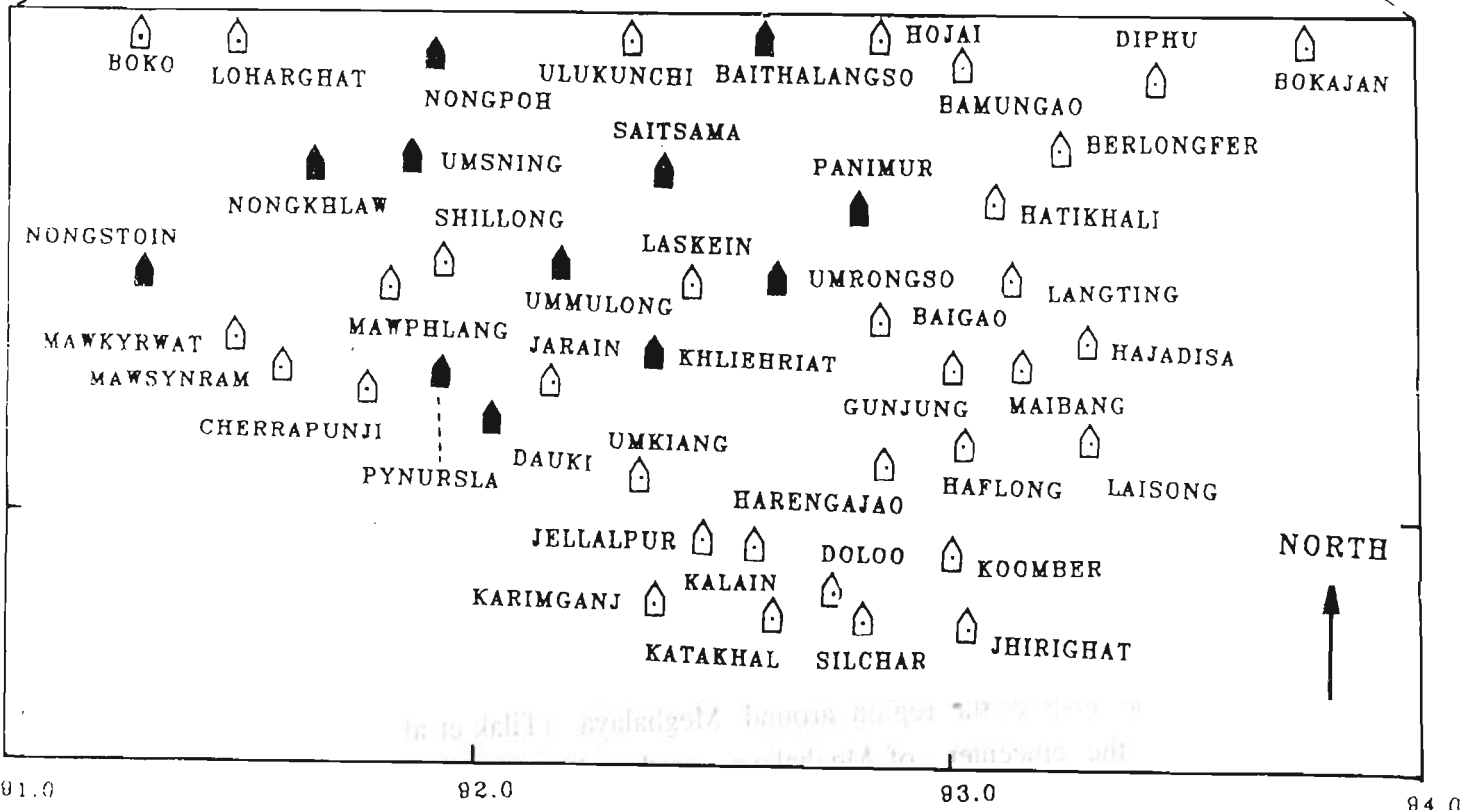
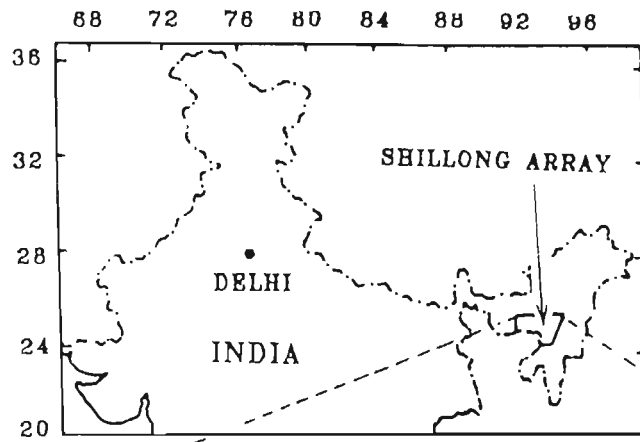


Fig 8.2 Location of recording stations of strong motion Shillong array. Geographical coordinates of recording stations is taken from Chandrasekaran and Das (1992b) and reproduced in Table 8.2. The stations marked with black colour represent those which had recorded the Meghalaya earthquake of 10th Sept, 1986.

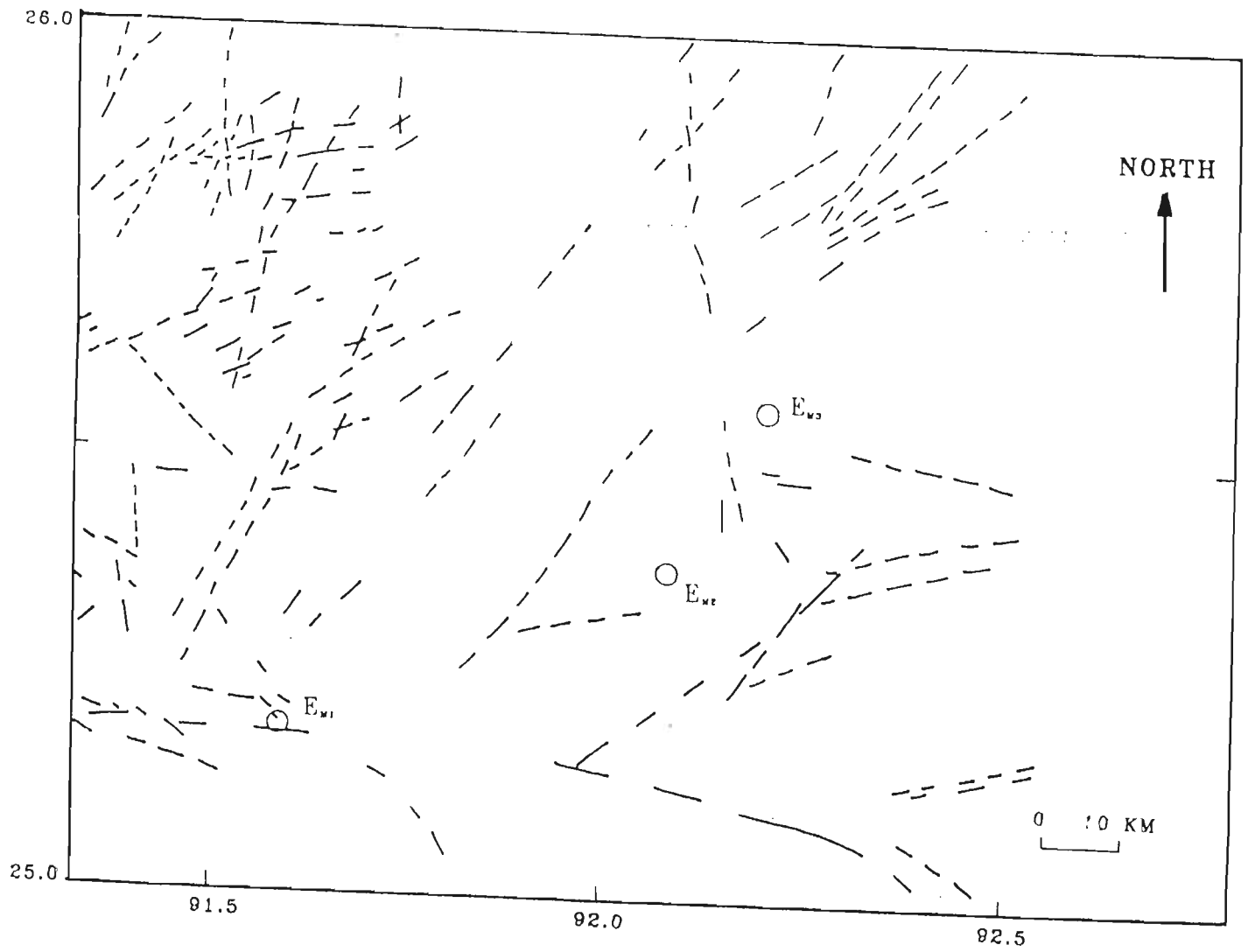


Fig 8.3 Tectonic map of the region around Meghalaya (Tilak et al. 1983). E_{m1} , E_{m2} , and E_{m3} are the epicenter of Meghalaya earthquake of 10th Sept, 1986 given by different agencies and reproduced in Table 8.3.

8.2.4 Location of recording stations of strong motion Shillong and Jorhat. Coordinates of recording stations is taken from Chandrasekaran and Das (1980) and reproduced in Table 8.2. The stations marked with black colour square those which had recorded the Meghalaya earthquake of 10th Sept, 1986.

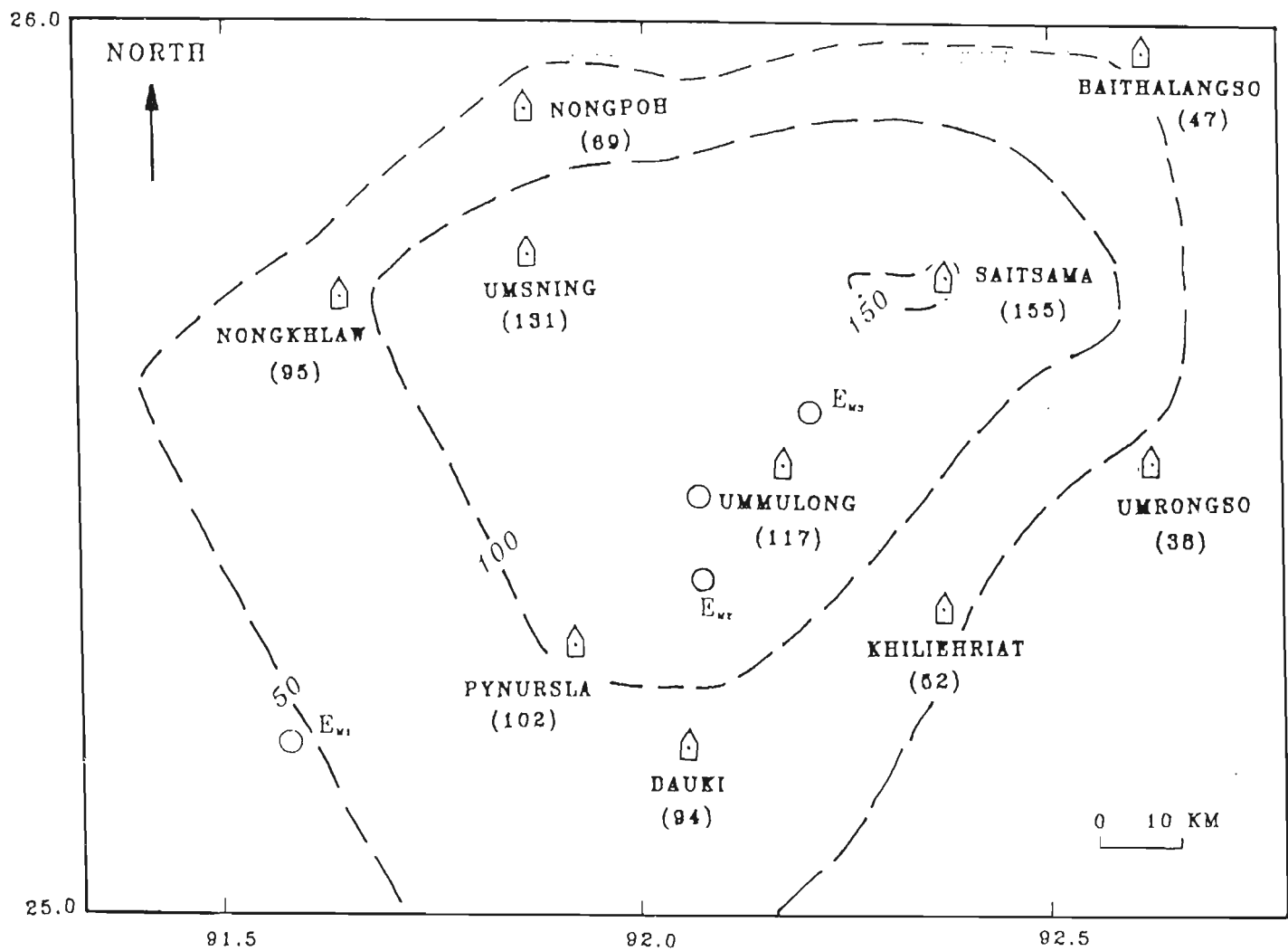


Fig 8.4 Isoacceleration map for Meghalaya earthquake of 10th Sept, 1986 prepared from resultant peak acceleration given by Chandrasekaran et al. (1988) and reproduced in Table 8.4.

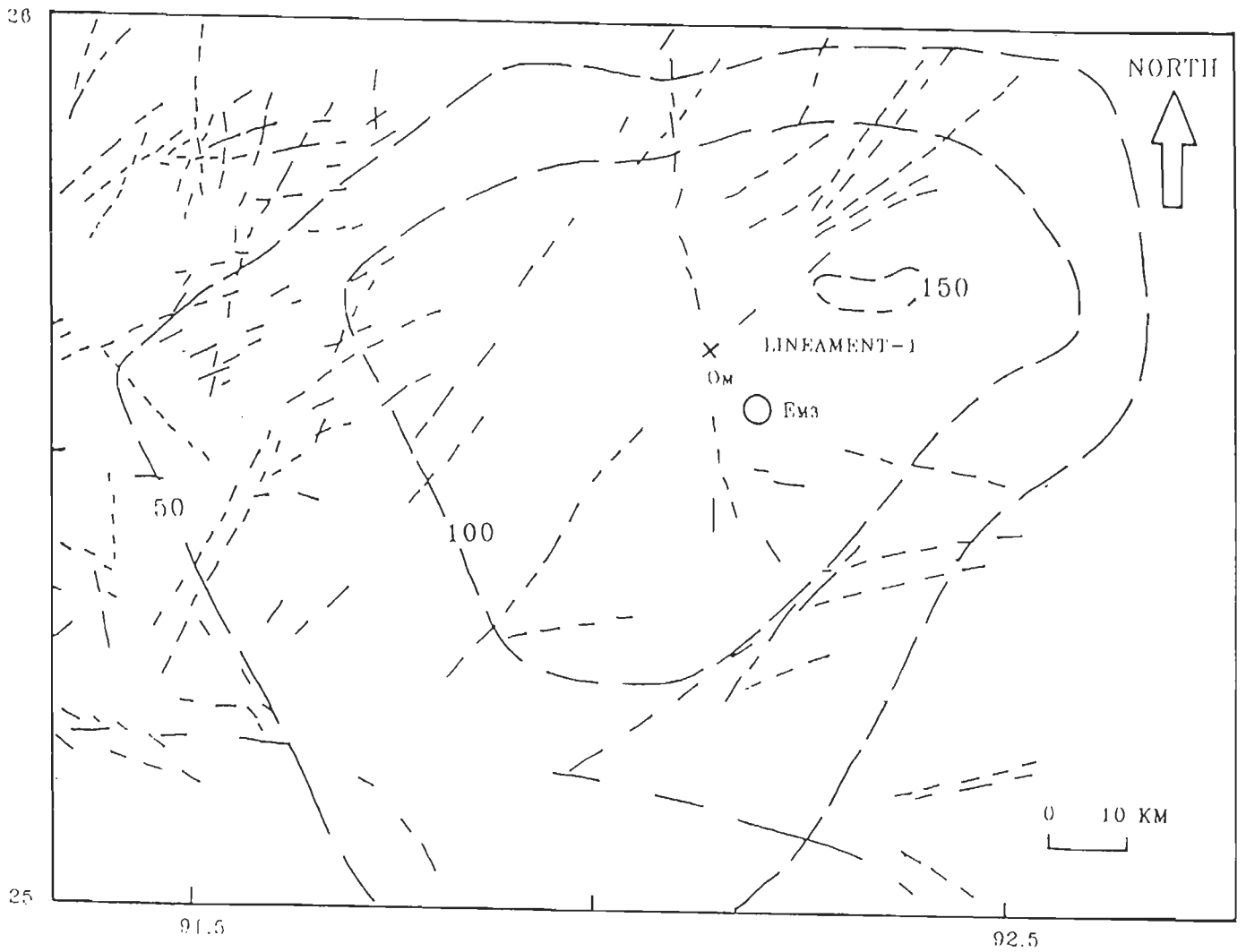


Fig 8.5 Superimposed isoacceleration and tectonic map (Tilak et al, 1983) in the epicentral region of Meghalaya earthquake of 10th, Sept, 1986.

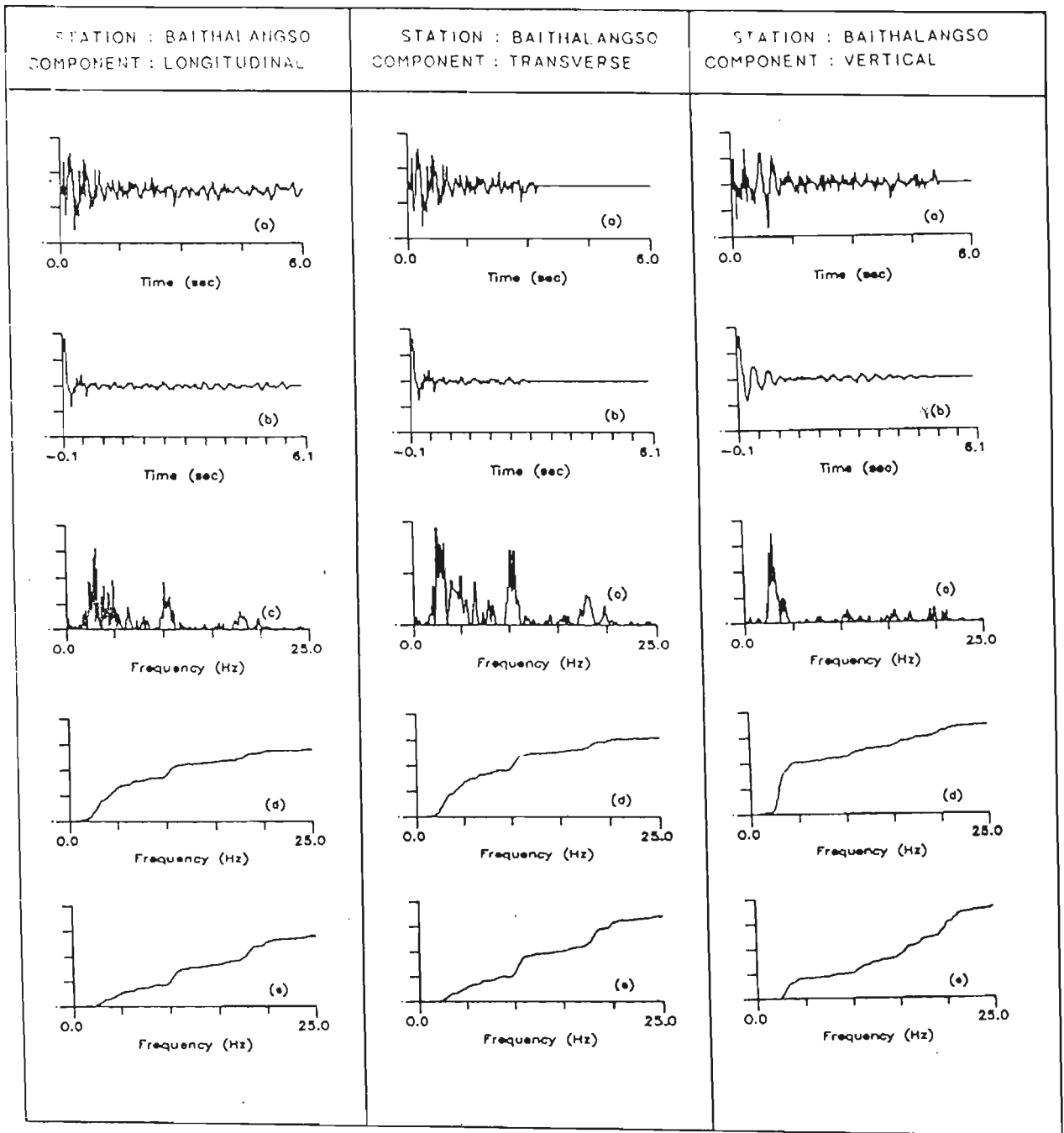


Fig 8.6 Meghalaya earthquake of 10th Sept, 1986, longitudinal, transverse and vertical components of acceleration record at Baithalangso station. Y axis shows normalised value of (a) acceleration record, (b) its autocorrelation function, (c) its power spectrum, (d) its cumulative power spectrum and (e) its frequency weighted cumulative power spectrum. X axis for (a) and (b) shows time and for (c), (d) and (e) shows frequency. Features extracted from field records at this station are given in Table 8.5.

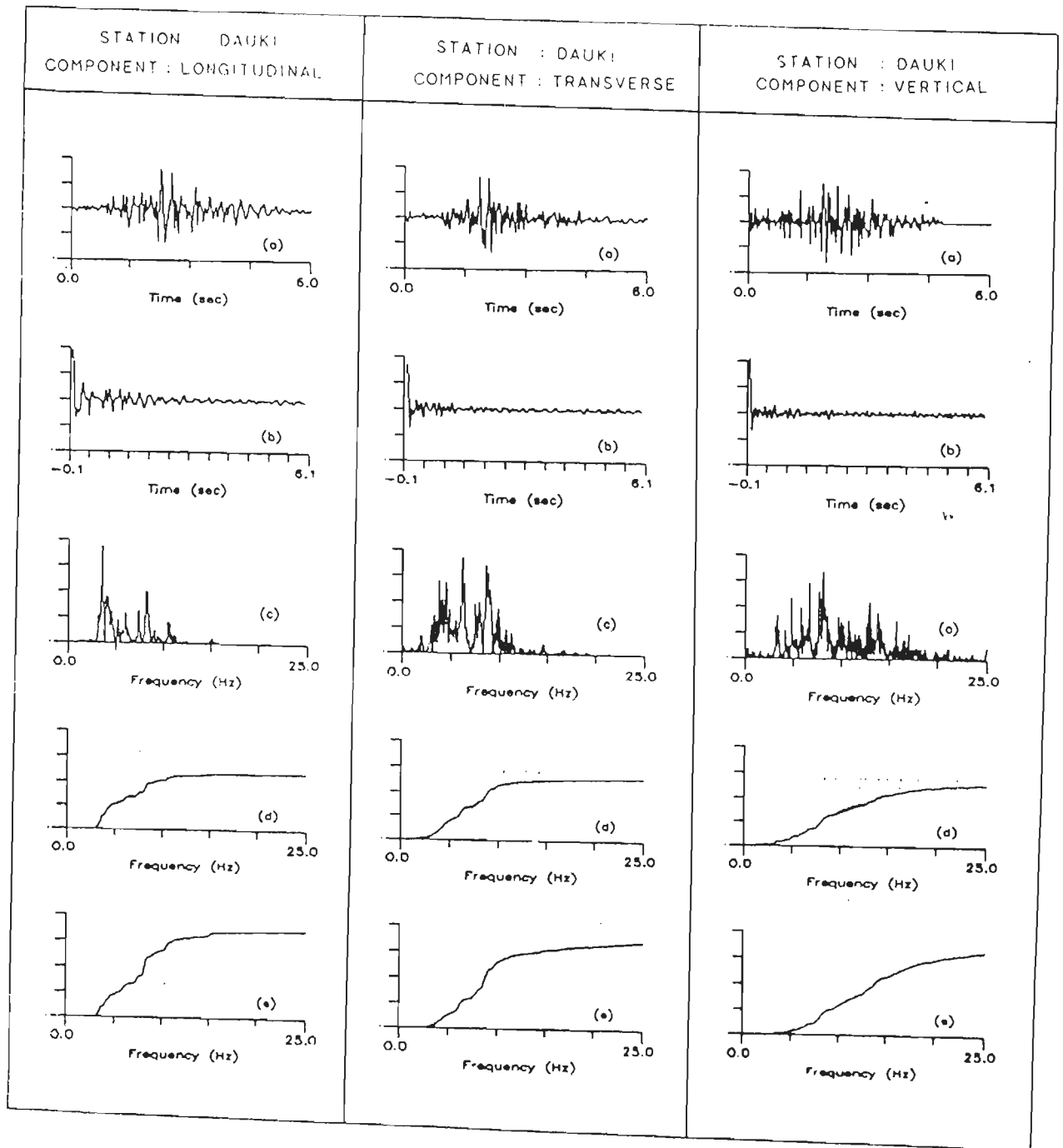


Fig 8.7 Meghalaya earthquake of 10th Sept, 1986, longitudinal, transverse and vertical components of acceleration record at Dauki station. Y axis shows normalised value of (a) acceleration record, (b) its autocorrelation function, (c) its power spectrum, (d) its cumulative power spectrum and (e) its frequency weighted cumulative power spectrum. X axis for (a) and (b) shows time and for (c), (d) and (e) shows frequency. Features extracted from field records at this station are given in Table 8.5.

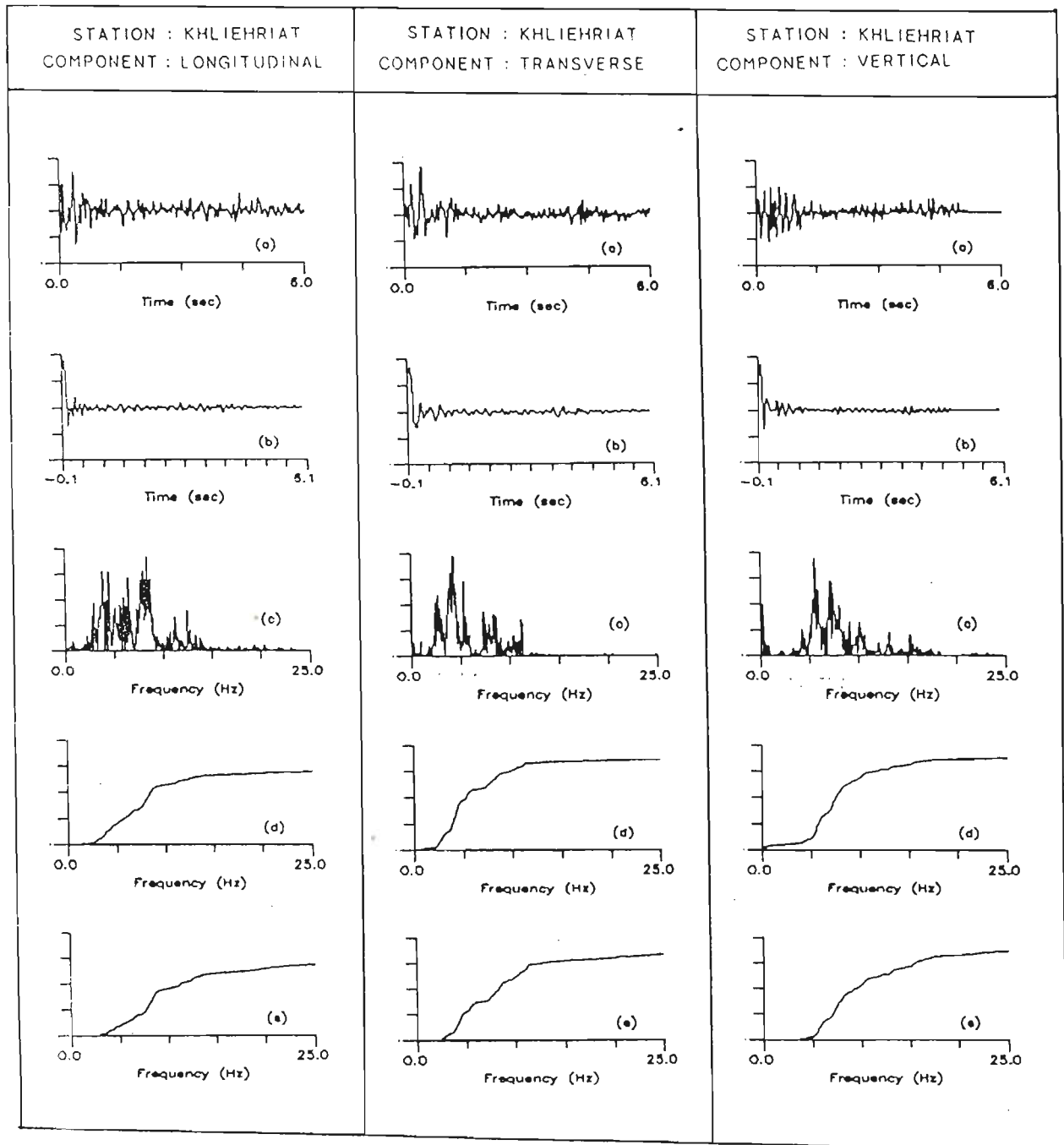


Fig 8.8 Meghalaya earthquake of 10th Sept, 1986, longitudinal, transverse and vertical components of acceleration record at Khliehriat station. Y axis shows normalised value of (a) acceleration record, (b) its autocorrelation function, (c) its power spectrum, (d) its cumulative power spectrum and (e) its frequency weighted cumulative power spectrum. X axis for (a) and (b) shows time and for (c), (d) and (e) shows frequency. Features extracted from field records at this station are given in Table 8.6.

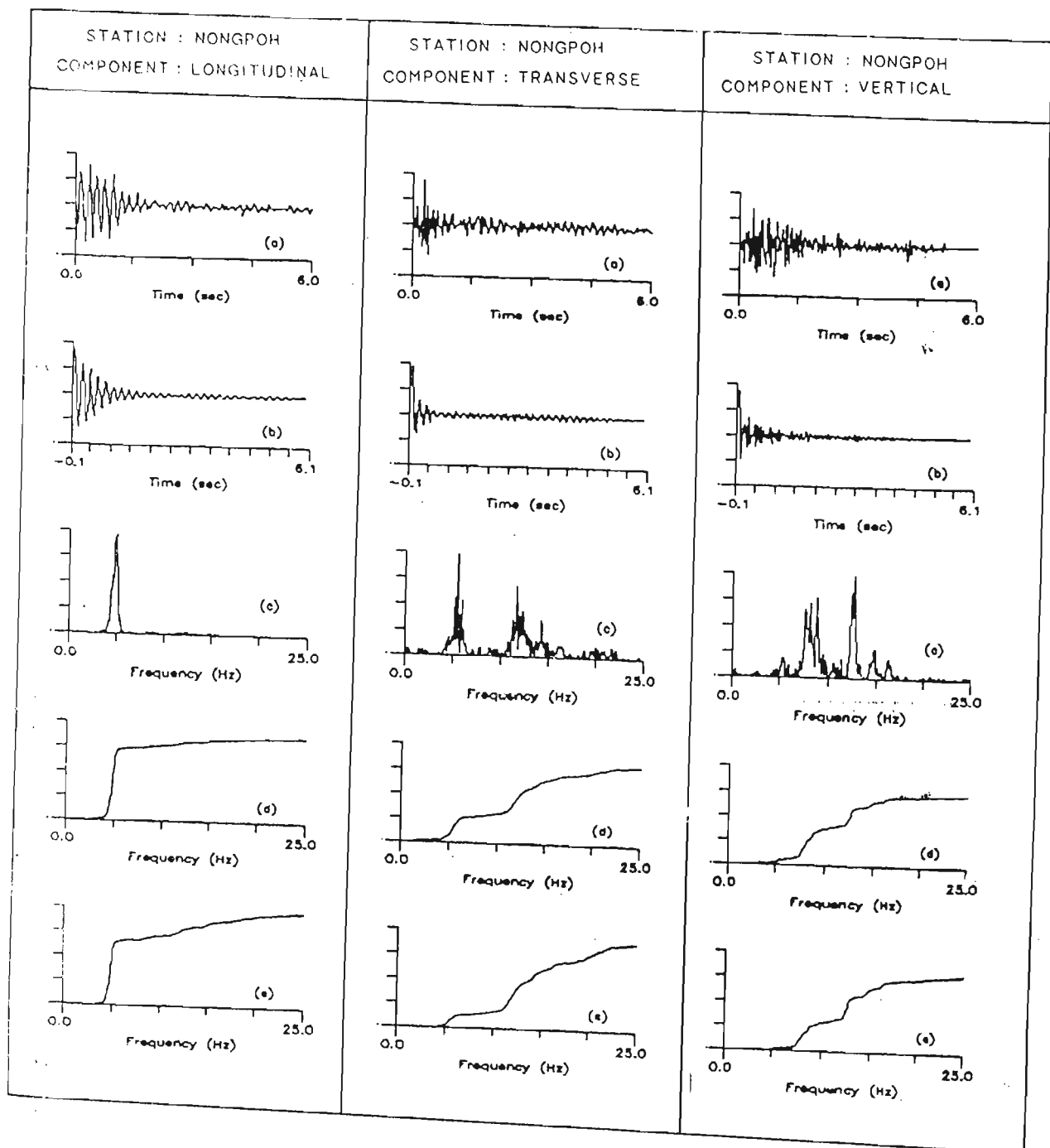


Fig 8.9 Meghalaya earthquake of 10th Sept, 1986, longitudinal, transverse and vertical components of acceleration record at Nongpoh station. Y axis shows normalised value of (a) acceleration record, (b) its autocorrelation function, (c) its power spectrum, (d) its cumulative power spectrum and (e) its frequency weighted cumulative power spectrum. X axis for (a) and (b) shows time and for (c), (d) and (e) shows frequency. Features extracted from field records at this station are given in Table 8.6.

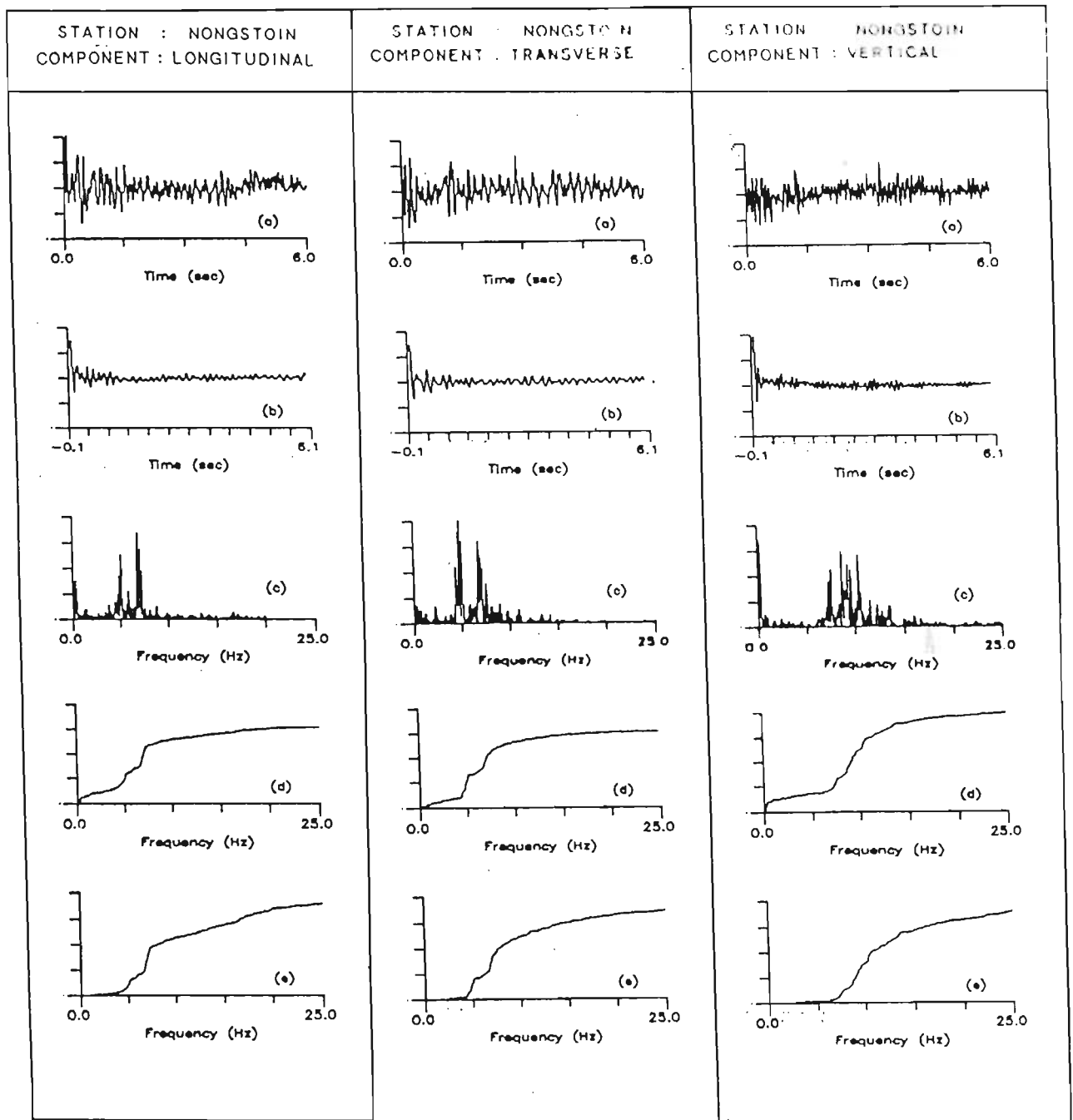


Fig 8.10 Meghalaya earthquake of 10th Sept, 1986, longitudinal, transverse and vertical components of acceleration record at Nongstoin station. Yaxis shows normalised value of (a) acceleration record, (b) its autocorrelation function, (c) its power spectrum, (d) its cumulative power spectrum and (e) its frequency weighted cumulative power spectrum. X axis for (a) and (b) shows time and for (c), (d) and (e) shows frequency. Features extracted from field records at this station are given in Table 8.7.

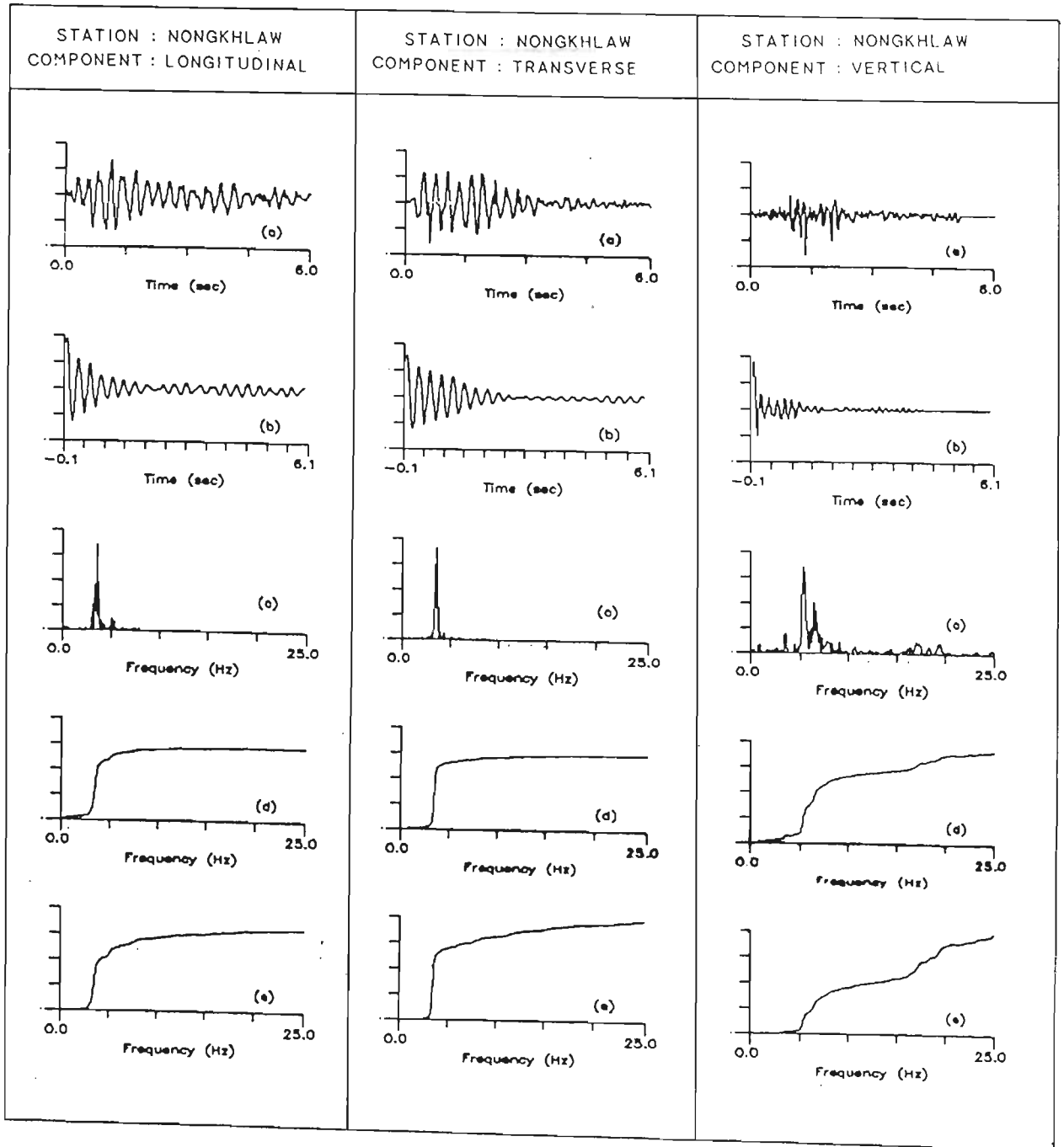


Fig 8.11 Meghalaya earthquake of 10th Sept, 1986, longitudinal, transverse and vertical components of acceleration record at Nongkhlaw station. Y axis shows normalised value of (a) acceleration record, (b) its autocorrelation function, (c) its power spectrum, (d) its cumulative power spectrum and (e) its frequency weighted cumulative power spectrum. X axis for (a) and (b) shows time and for (c), (d) and (e) shows frequency. Features extracted from field records at this station are given in Table 8.7.

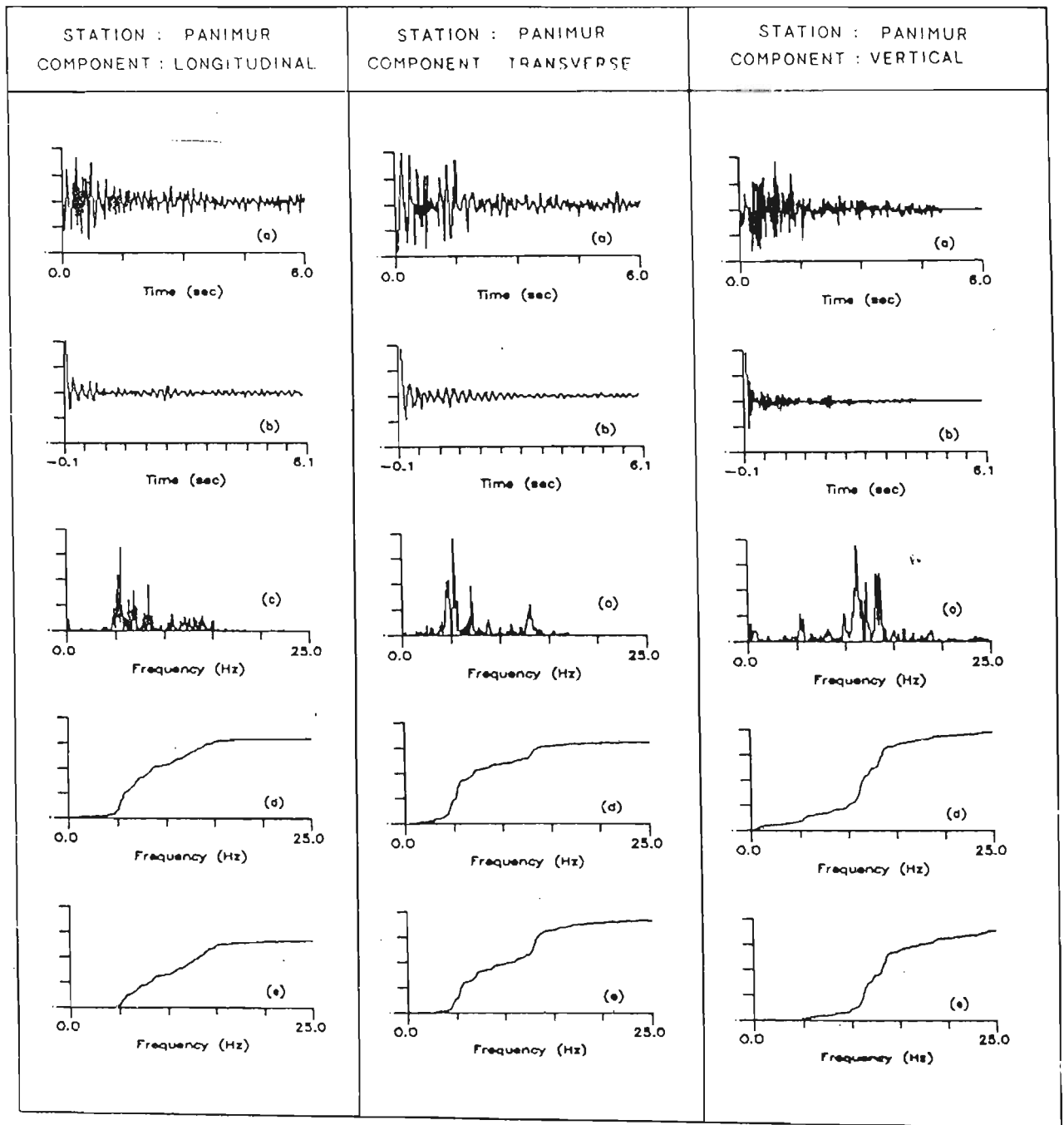


Fig 8.12 Meghalaya earthquake of 10th Sept, 1986, longitudinal, transverse and vertical components of acceleration record at Panimur station. Y axis shows normalised value of (a) acceleration record, (b) its autocorrelation function, (c) its power spectrum, (d) its cumulative power spectrum and (e) its frequency weighted cumulative power spectrum. X axis for (a) and (b) shows time and for (c), (d) and (e) shows frequency. Features extracted from field records at this station are given in Table 8.8.

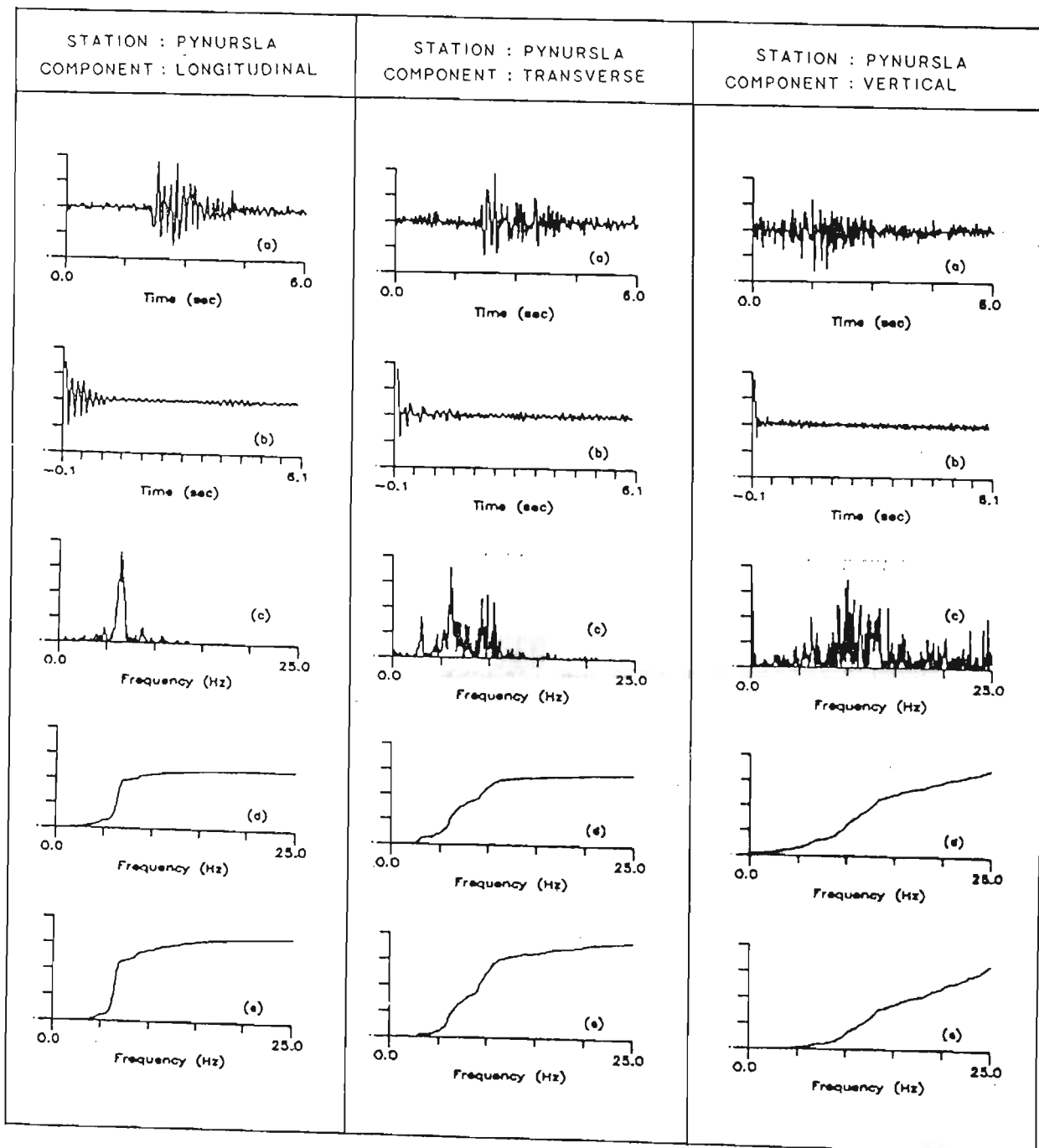


Fig 8.13 Meghalaya earthquake of 10th Sept, 1986, longitudinal, transverse and vertical components of acceleration record at Pynursla station. Y axis shows normalised value of (a) acceleration record, (b) its autocorrelation function, (c) its power spectrum, (d) its cumulative power spectrum and (e) its frequency weighted cumulative power spectrum. X axis for (a) and (b) shows time and for (c), (d) and (e) shows frequency. Features extracted from field records at this station are given in Table 8.8.

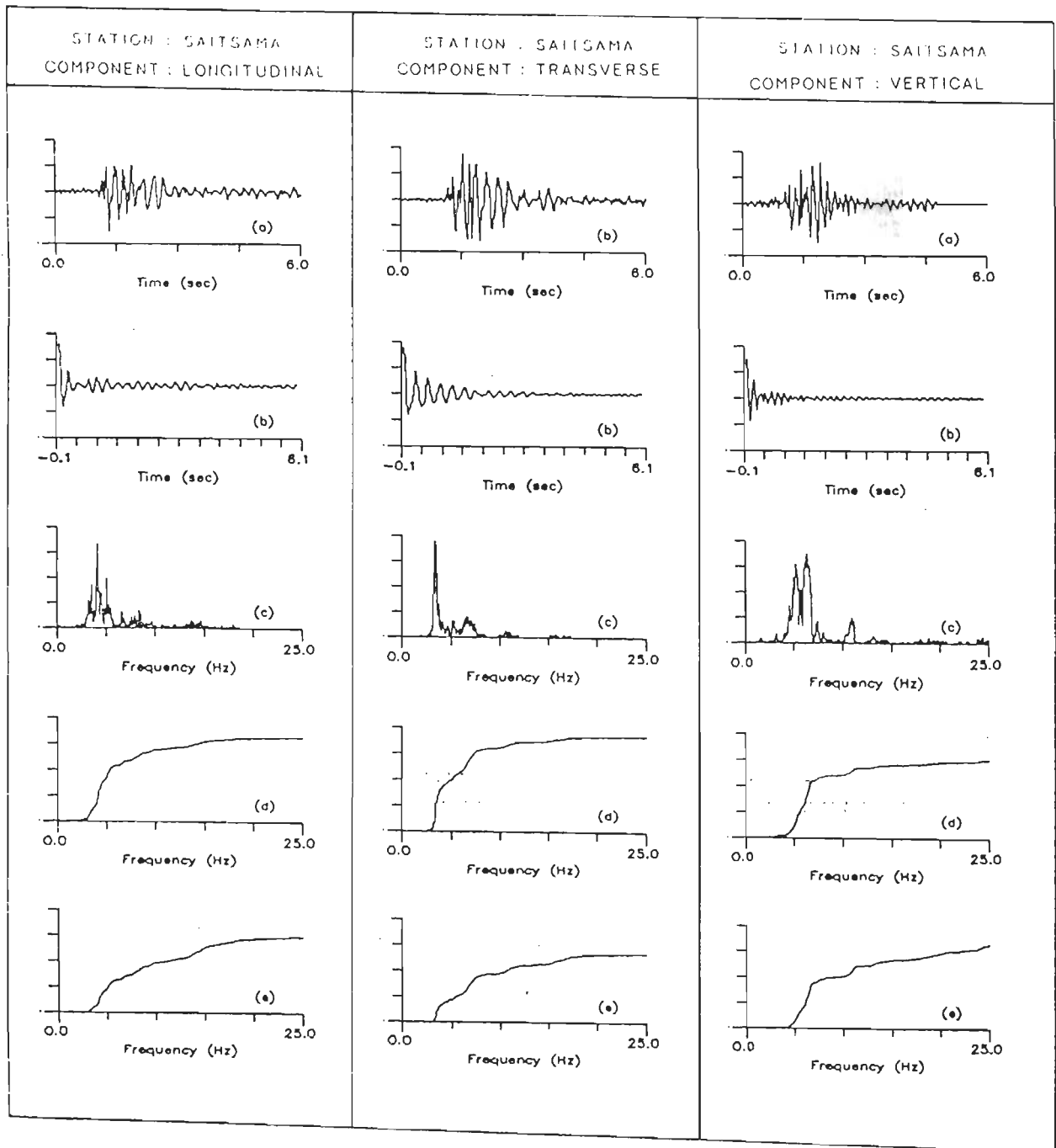


Fig 8.14 Meghalaya earthquake of 10th Sept, 1986, longitudinal, transverse and vertical components of acceleration record at Saitsama station. Y axis shows normalised value of (a) acceleration record, (b) its autocorrelation function, (c) its power spectrum, (d) its cumulative power spectrum and (e) its frequency weighted cumulative power spectrum. X axis for (a) and (b) shows time and for (c), (d) and (e) shows frequency. Features extracted from field records at this station are given in Table 8.9.

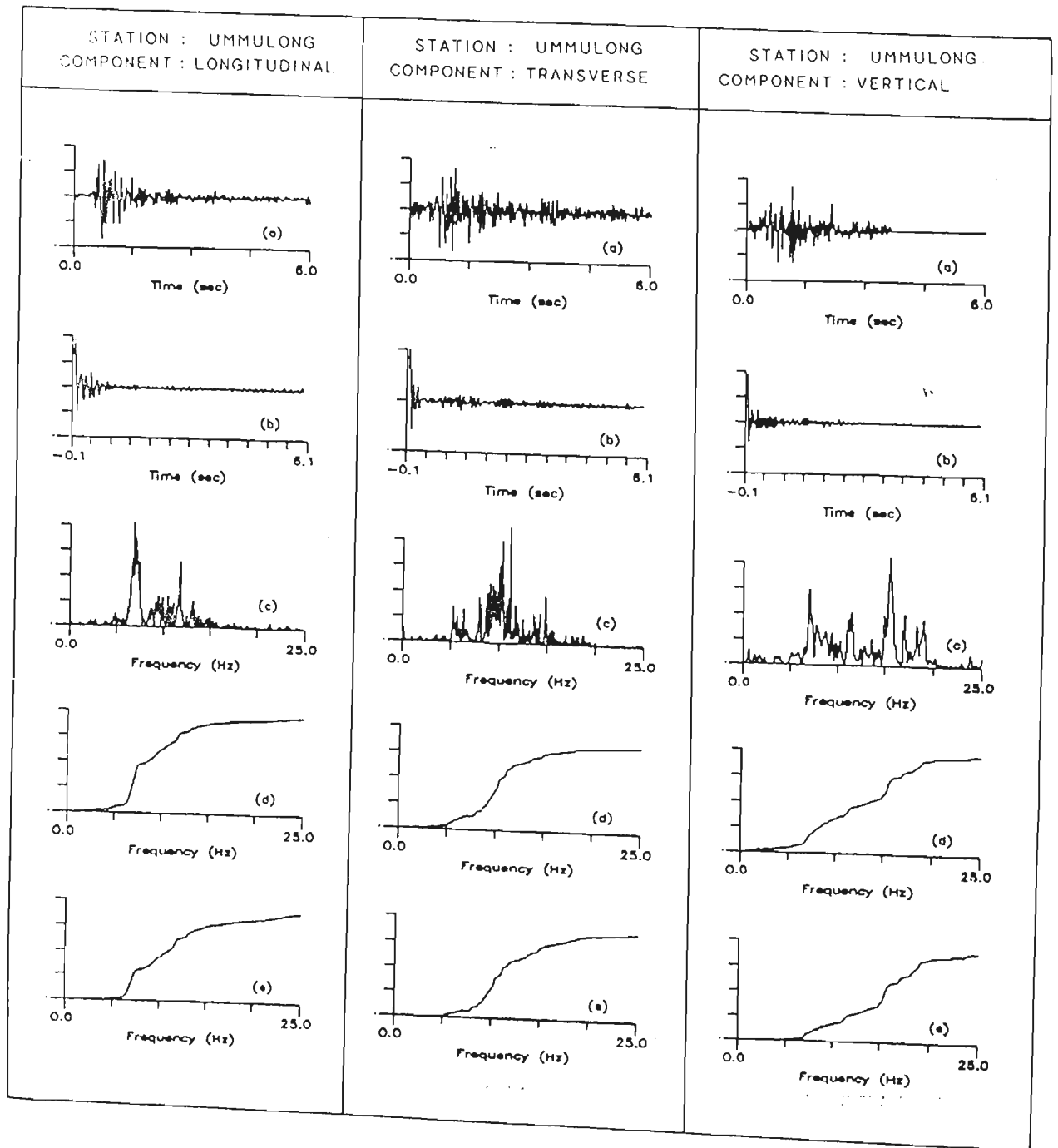


Fig 8.15 Meghalaya earthquake of 10th Sept, 1986, longitudinal, transverse and vertical components of acceleration record at Ummulong station. Y axis shows normalised value of (a) acceleration record, (b) its autocorrelation function, (c) its power spectrum, (d) its cumulative power spectrum and (e) its frequency weighted cumulative power spectrum. X axis for (a) and (b) shows time and for (c), (d) and (e) shows frequency. Features extracted from field records at this station are given in Table 8.9.

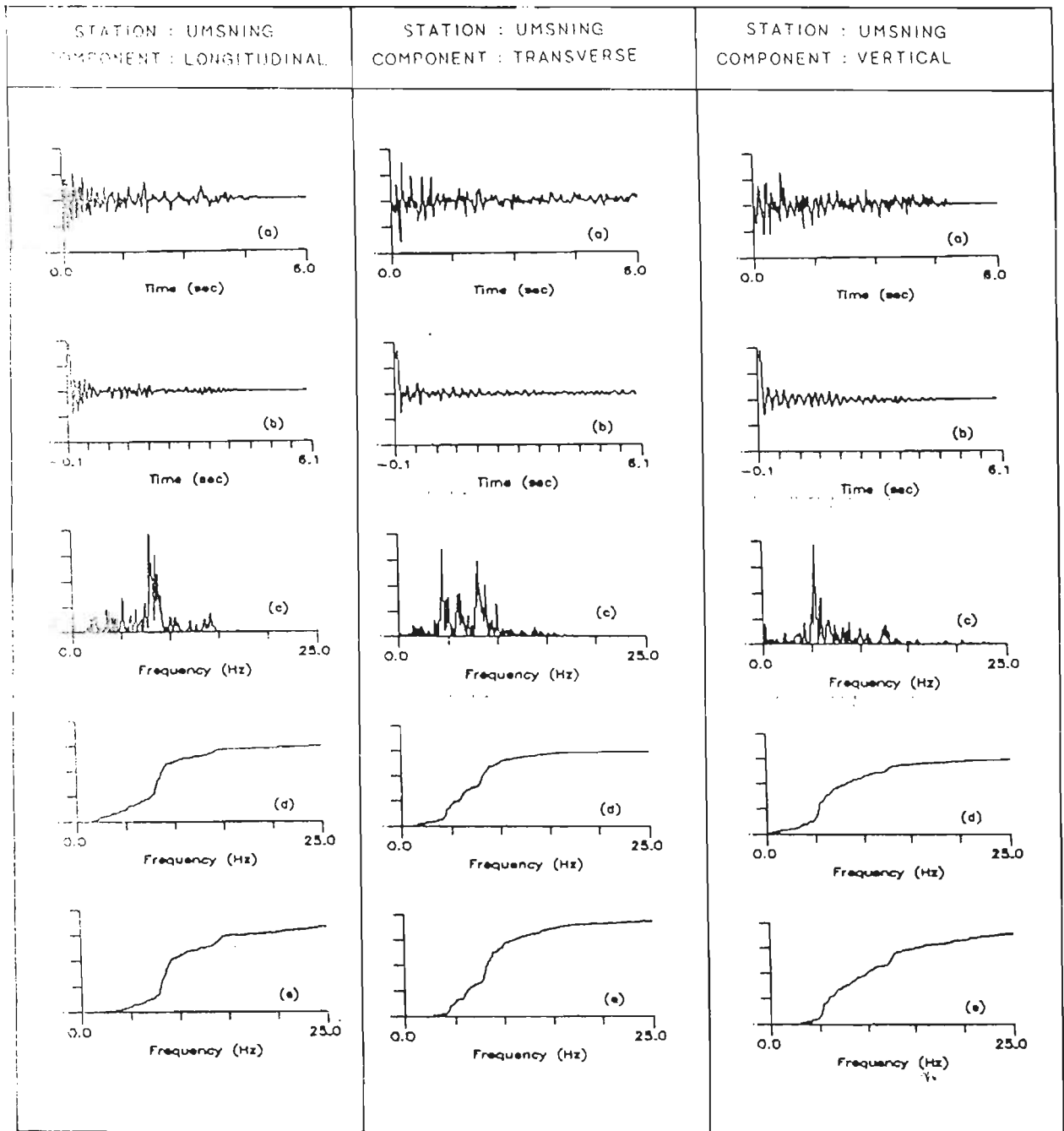


Fig 8.16 Meghalaya earthquake of 10th Sept, 1986, longitudinal, transverse and vertical components of acceleration record at Umsning station. Y axis shows normalised value of (a) acceleration record, (b) its autocorrelation function, (c) its power spectrum, (d) its cumulative power spectrum and (e) its frequency weighted cumulative power spectrum. X axis for (a) and (b) shows time and for (c), (d) and (e) shows frequency. Features extracted from field records at this station are given in Table 8.10.

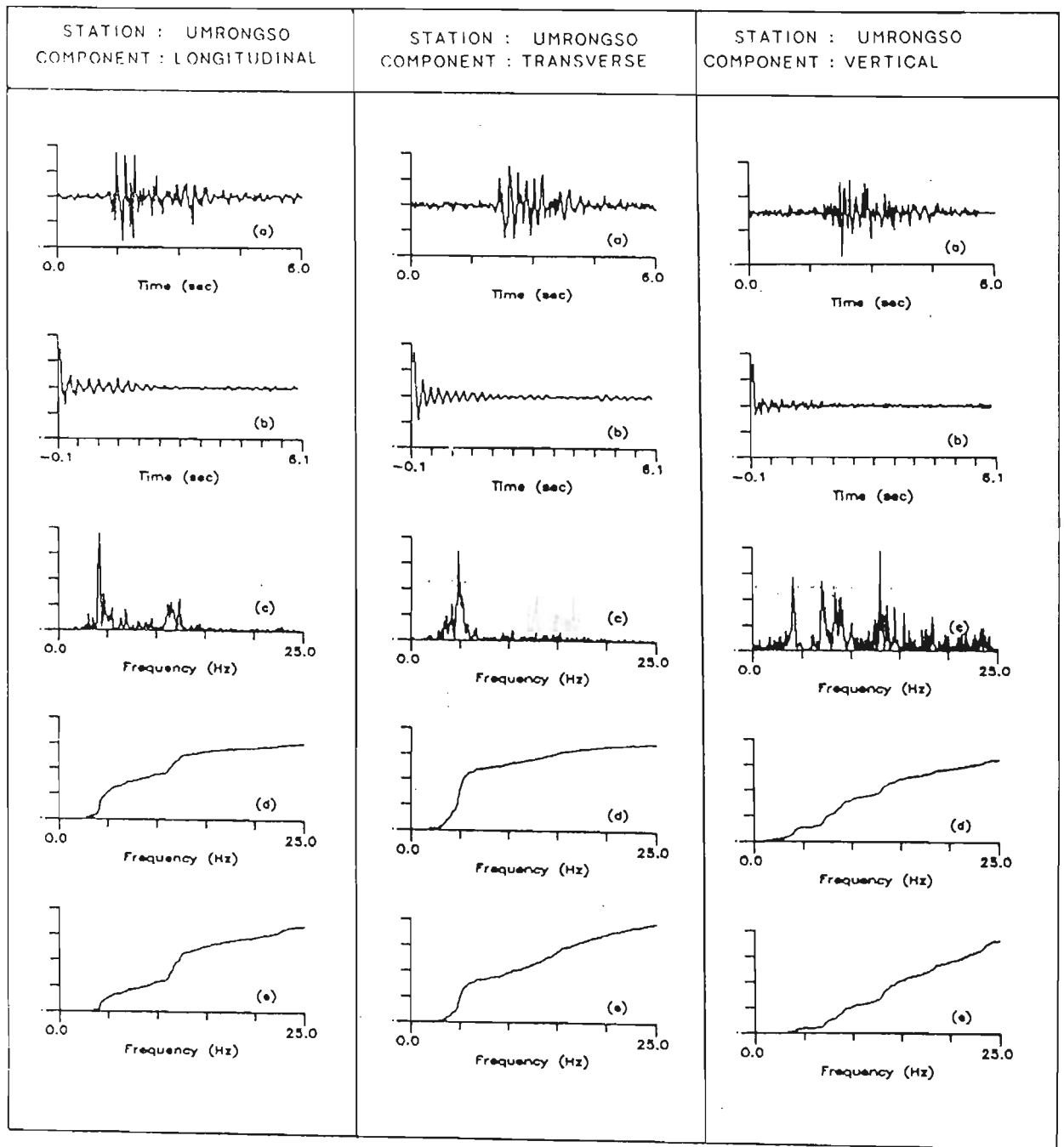


Fig 8.17 Meghalaya earthquake of 10th Sept, 1986, longitudinal, transverse and vertical component of acceleration record at Umrongso station. Y axis shows normalised value of (a) acceleration record, (b) its autocorrelation function, (c) its power spectrum, (d) its cumulative power spectrum and (e) its frequency weighted cumulative power spectrum. X axis for (a) and (b) shows time and for (c), (d) and (e) shows frequency. Features extracted from field records at this station are given in Table 8.10.

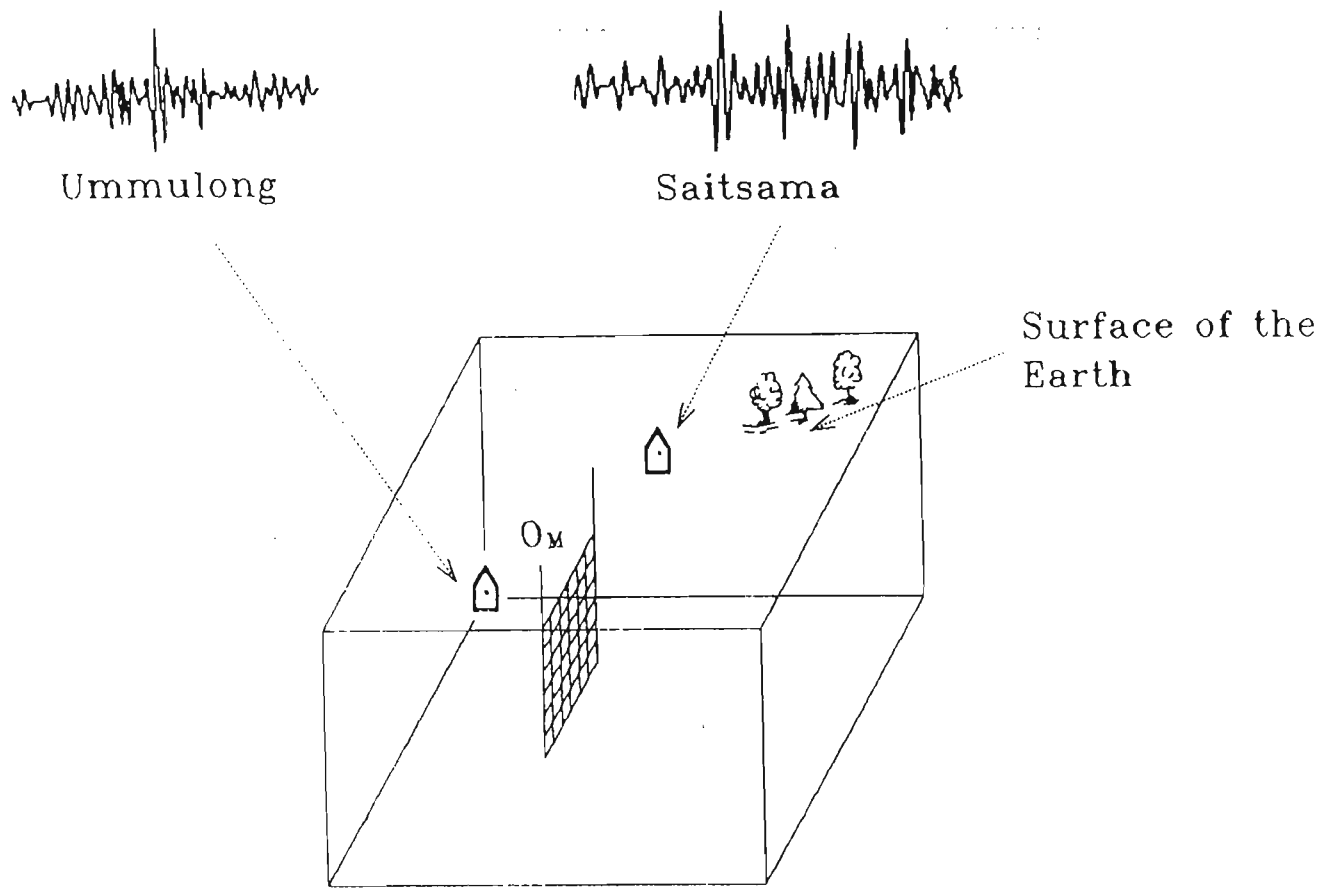


Fig 8.18 Rupture model MM_{d1} for Meghalaya earthquake of 10th Sept, 1986 having 90° dip. Parameters extracted from simulated acceleration records shown in this figure at Saitsama and Ummulong stations due to this model are given in Table 8.11.

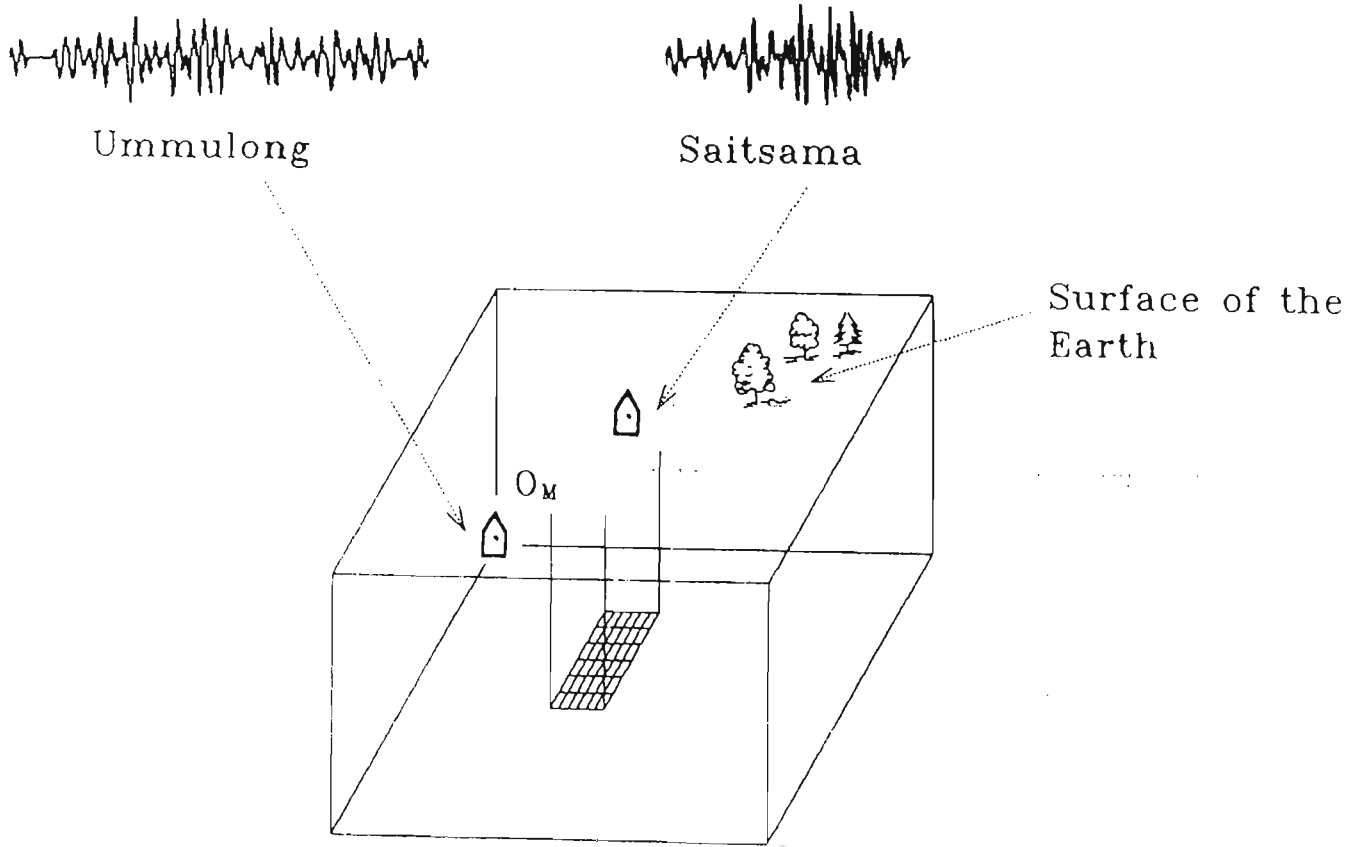


Fig 8.19 Rupture model MM_{d2} for Meghalaya earthquake of 10th Sept, 1986 having 0° dip. Parameters extracted from simulated acceleration records shown in this figure at Saitsama and Ummulong stations due to this model are given in Table 8.11.

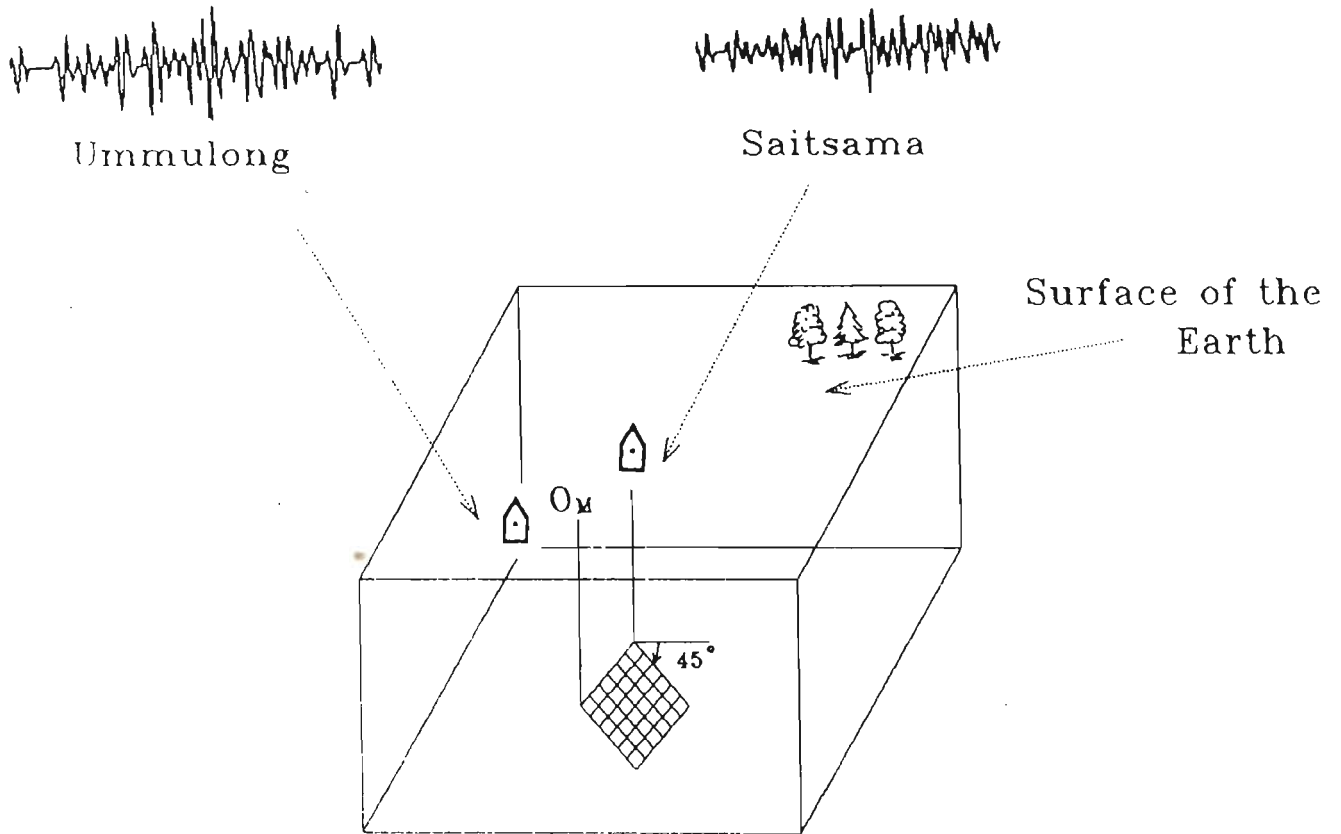


Fig 8.20 Rupture model MM_{d3} for Meghalaya earthquake of 10th Sept, 1986 having 45° dip. Parameters extracted from simulated acceleration records shown in this figure at Saitsama and Ummulong stations due to this model are given in Table 8.11.

UMMULONG

SAITSAMA



TOWARDS NORTH →

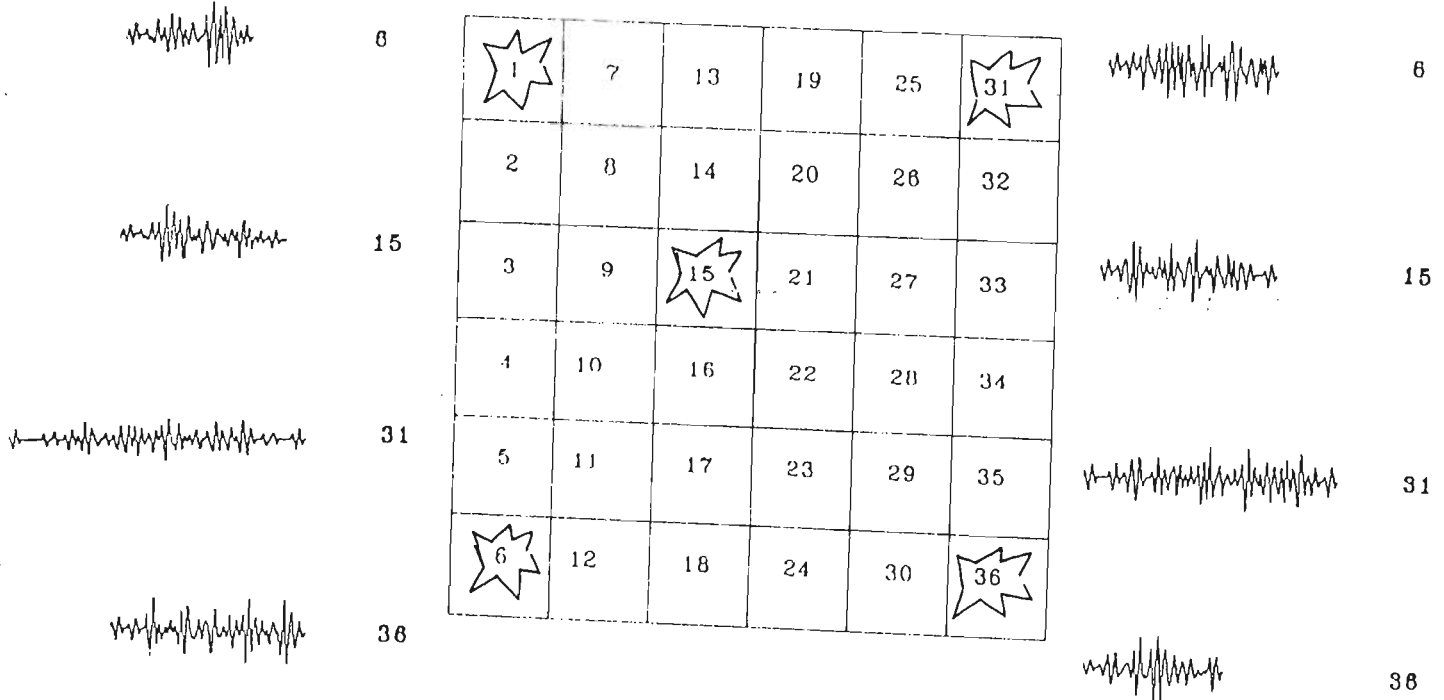


Fig 8.21 Model of rupture plane showing method of numbering elements within the rupture plane. Acceleration records are simulated at Saitsama and Ummulong stations by assuming different elements within rupture plane as starting point of rupture. Number corresponding to each simulated record shows the element number which is assumed as nucleation point. Feature extracted from these simulated records at Saitsama and Ummulong stations are shown in Table 8.13 and 8.14, respectively. The center of element numbered as '1' is the origin of three dimensional coordinate system.

Ummulong

Saitsama

Surface of the Earth

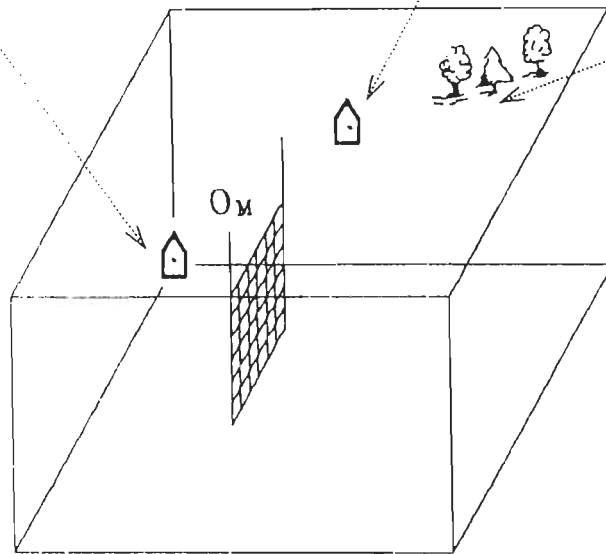


Fig 8.22 Model of rupture plane for Meghalaya earthquake of 10th Sept, 1986.

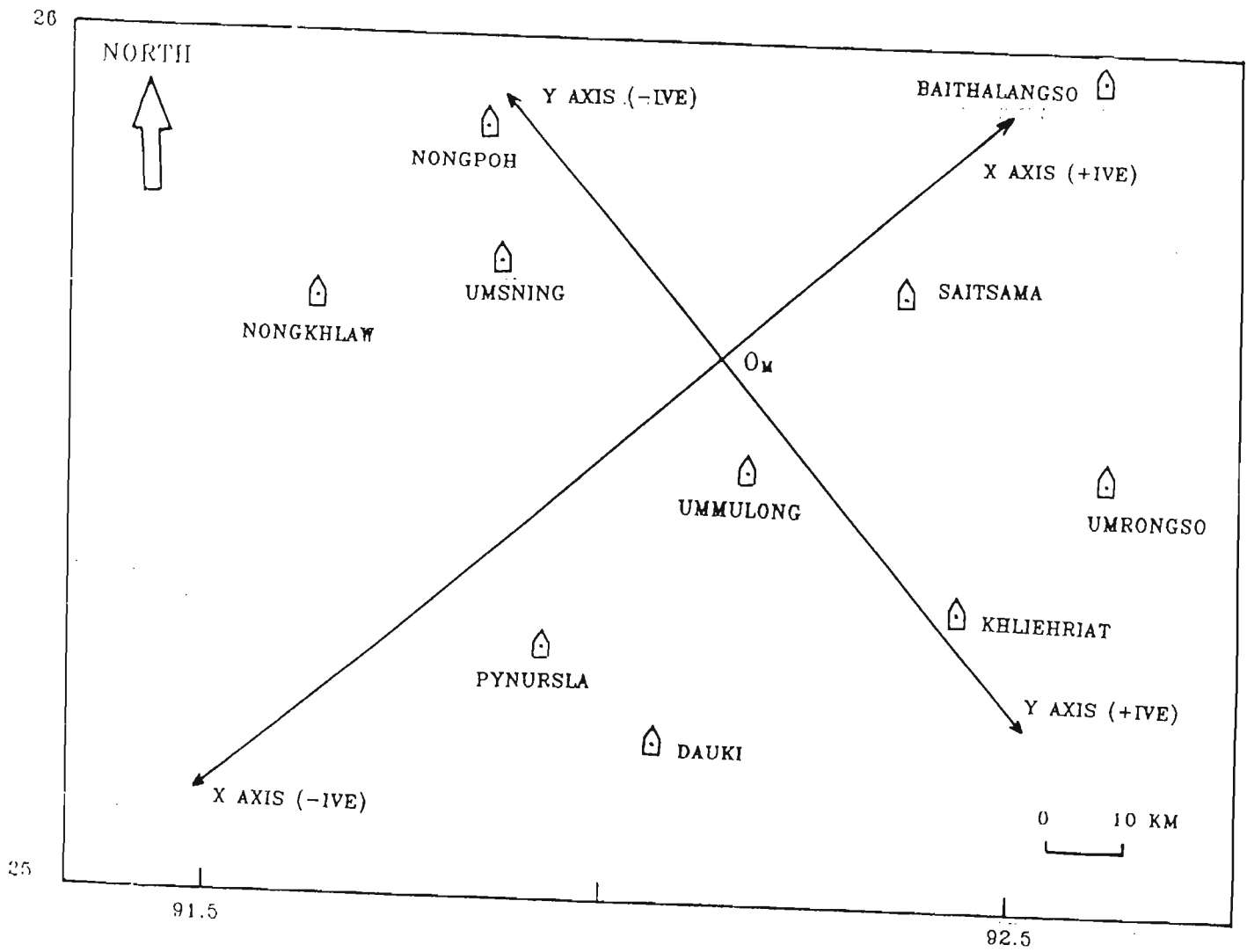


Fig 8.23 Location of selected observation points at which strong motion records are synthesised. The origin point of the coordinate system is placed at a depth of 28 km below point O_M marked in Fig 8.6. The coordinates of selected observation points in rectangular coordinate system is given in Table 8.16.

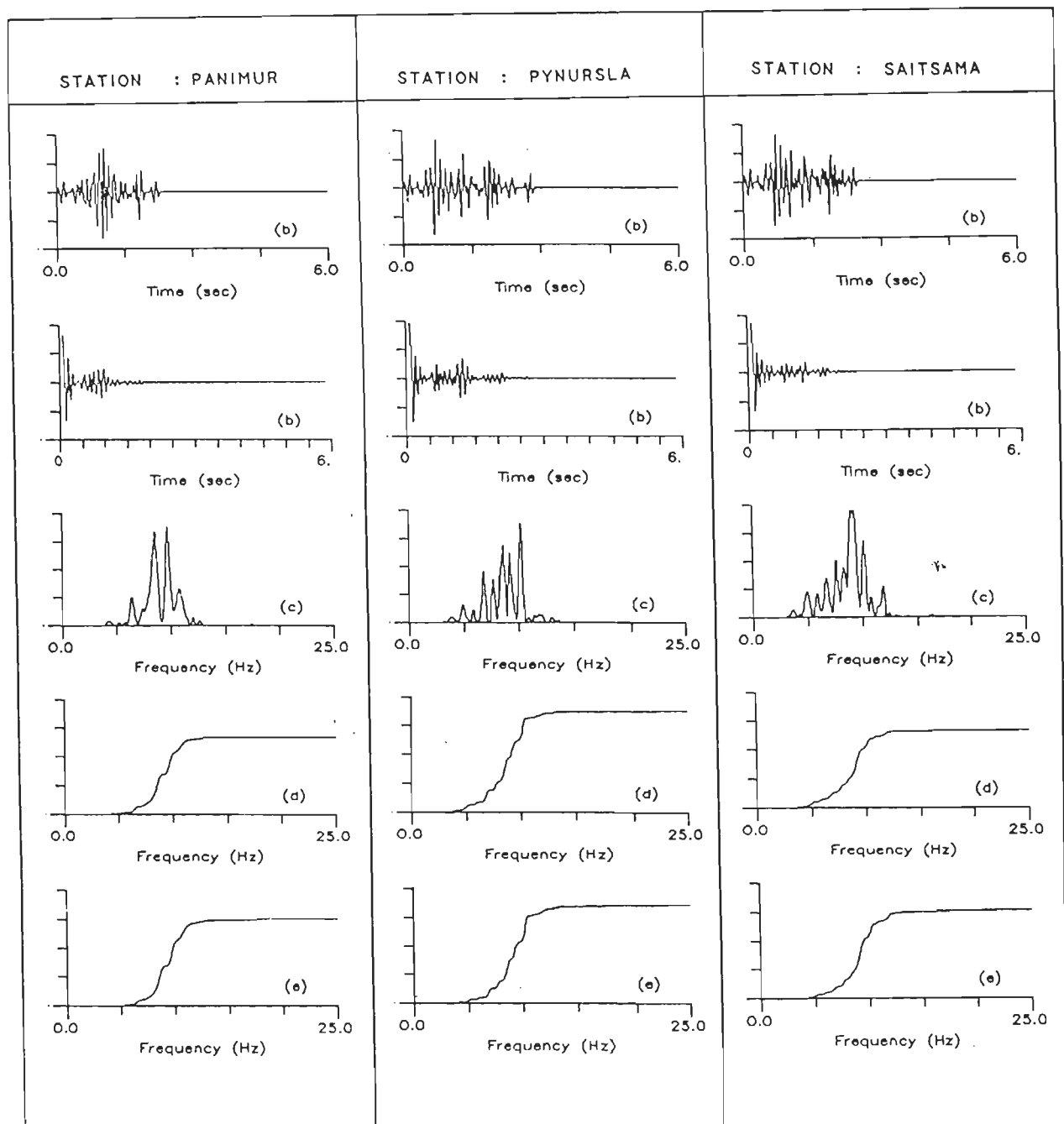


Fig 8.24 Meghalaya earthquake of 10th Sept, 1986, simulated records at stations. Y axis shows normalised value of (a) acceleration record, (b) its autocorrelation function, (c) its power spectrum, (d) its cumulative power spectrum and (e) its frequency weighted cumulative power spectrum. X axis for (a) and (b) shows time and for (c), (d) and (e) shows frequency. Feature extracted from these records at these station are given in Table 8.17 and 8.18.

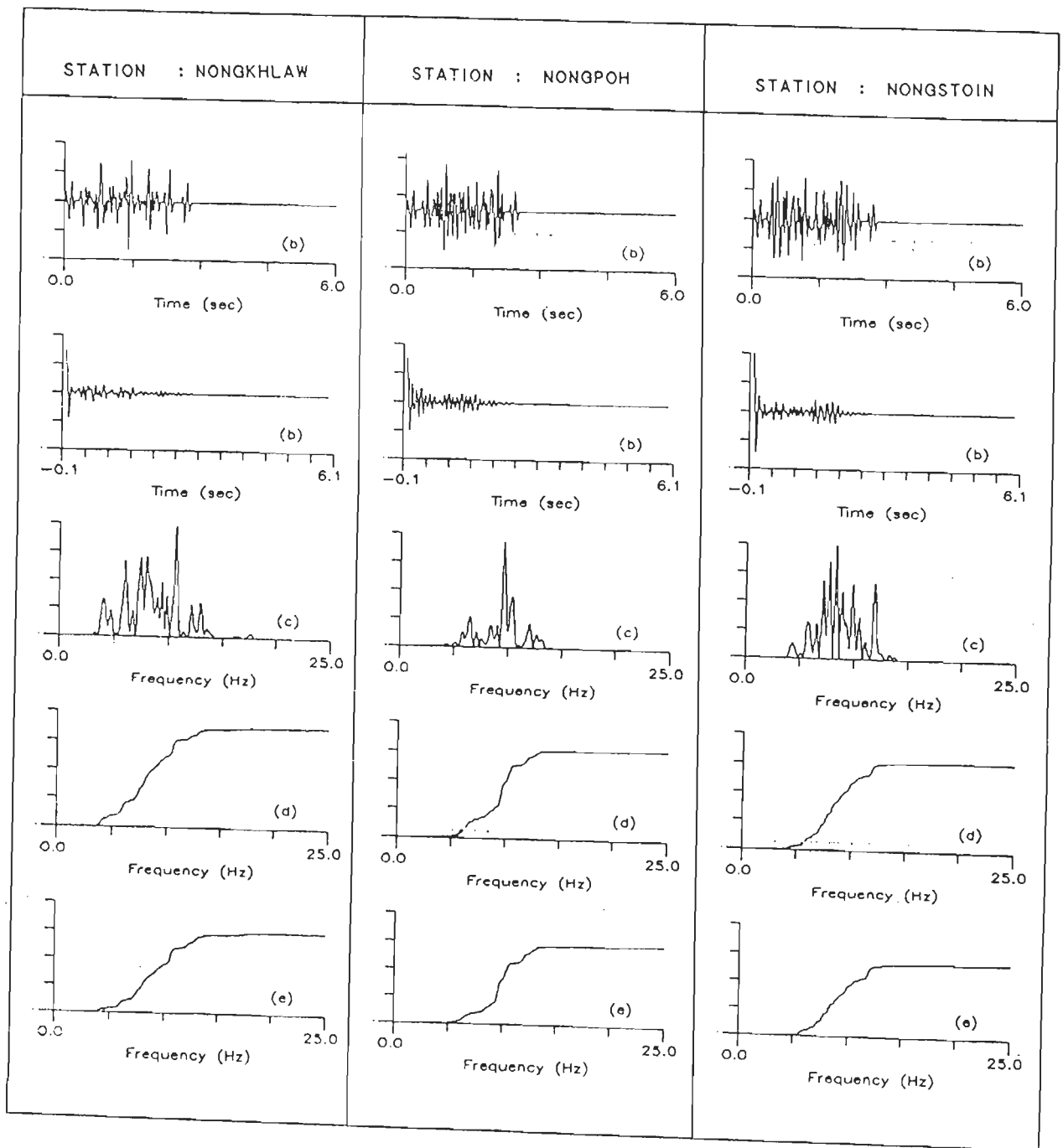


Fig 8.25 Meghalaya earthquake of 10th Sept, 1986, simulated records at stations. Y axis shows normalised value of (a) acceleration record, (b) its autocorrelation function, (c) its power spectrum, (d) its cumulative power spectrum and (e) its frequency weighted cumulative power spectrum. X axis for (a) and (b) shows time and for (c), (d) and (e) shows frequency. Feature extracted from these records at these stations are given in Table 8.17 and 8.18.

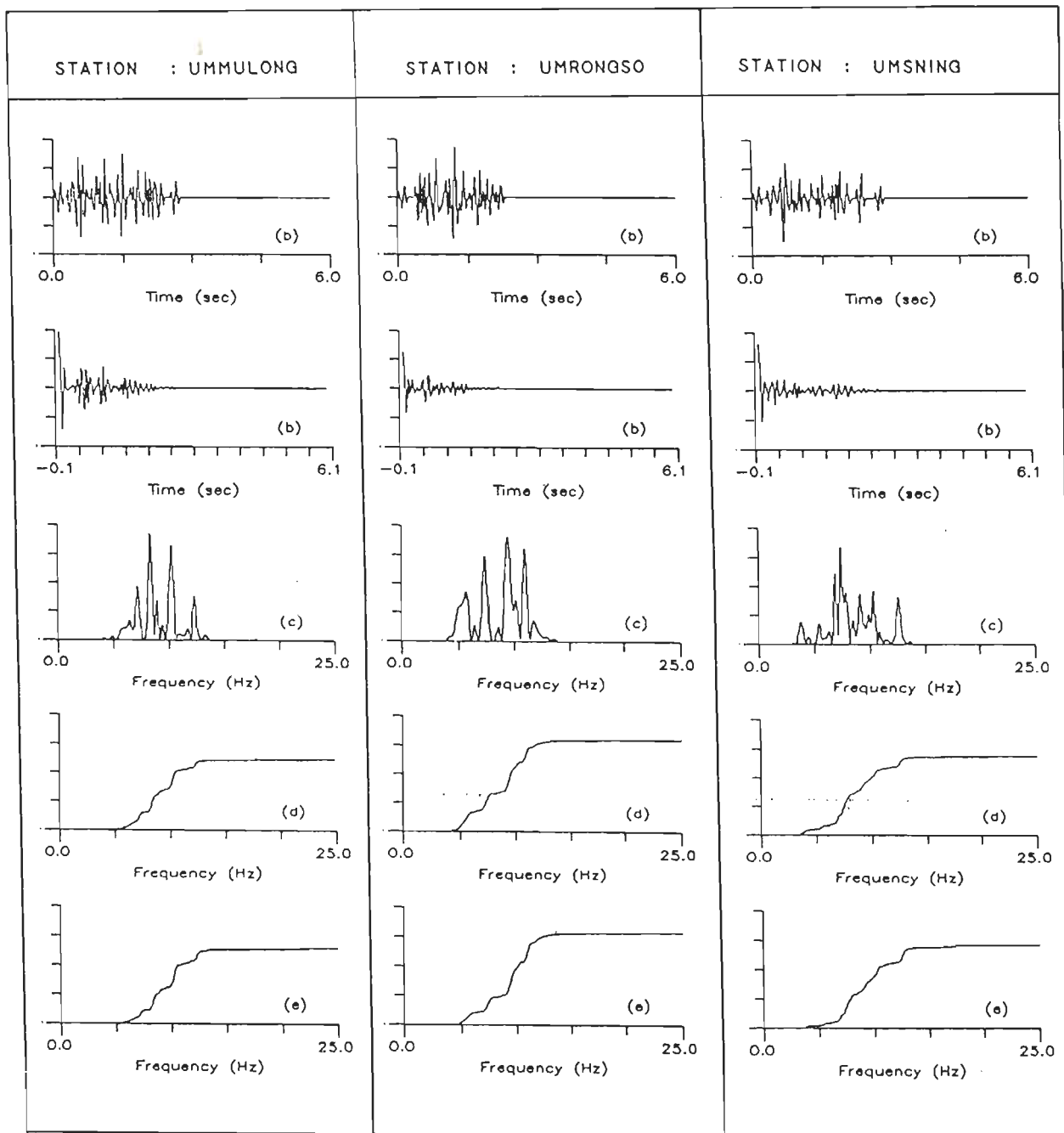


Fig 8.26 Meghalaya earthquake of 10th Sept, 1986, simulated records at stations. Y axis shows normalised value of (a) acceleration record, (b) its autocorrelation function, (c) its power spectrum, (d) its cumulative power spectrum and (e) its frequency weighted cumulative power spectrum. X axis for (a) and (b) shows time and for (c), (d) and (e) shows frequency. Feature extracted from these records at these stations are given in Table 8.17 and 8.18.

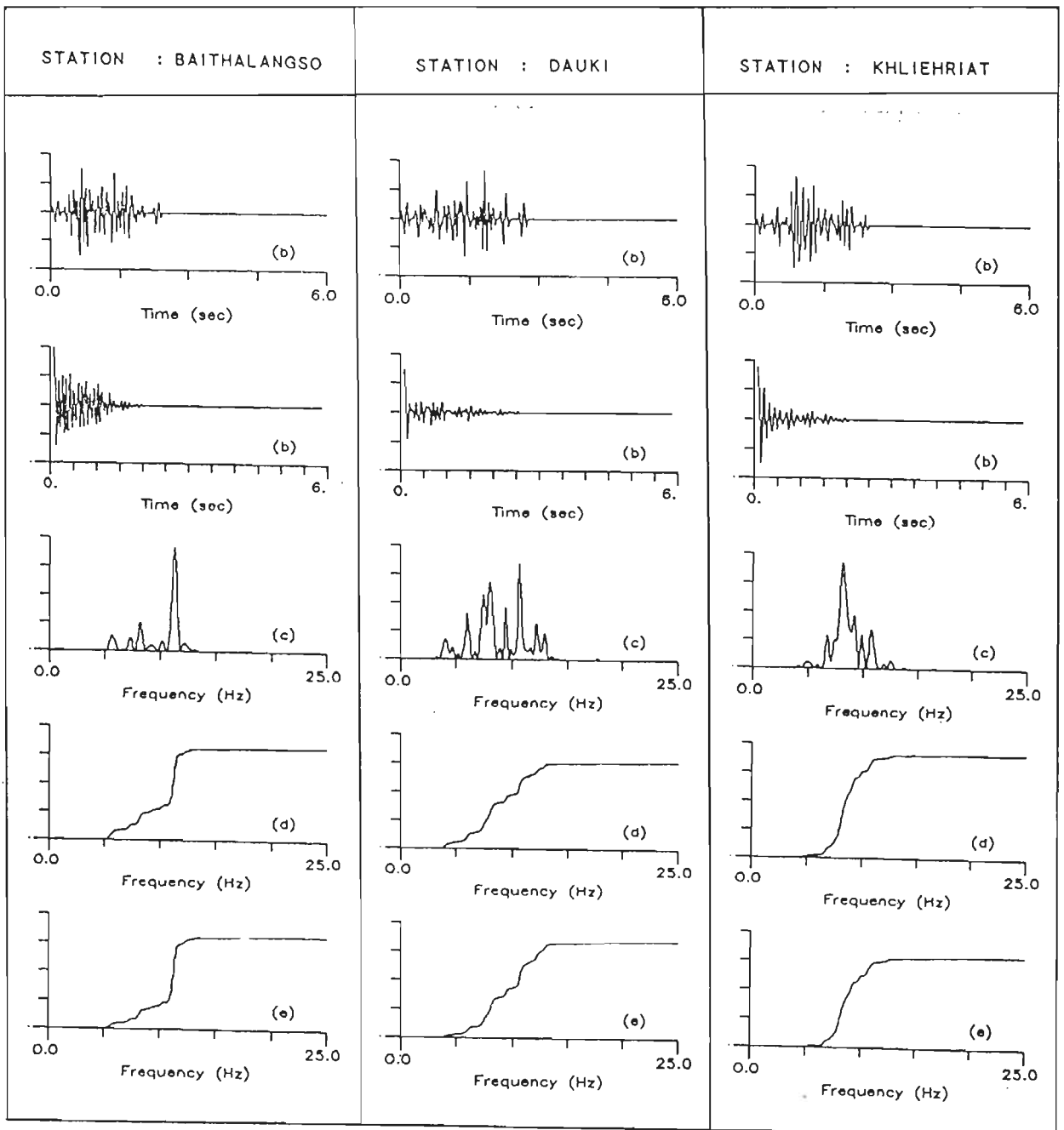


Fig 8.27 Meghalaya earthquake of 10th Sept, 1986, simulated records at stations. Y axis shows normalised value of (a) acceleration record, (b) its autocorrelation function, (c) its power spectrum, (d) its cumulative power spectrum and (e) its frequency weighted cumulative power spectrum. X axis for (a) and (b) shows time and for (c), (d) and (e) shows frequency. Feature extracted from these records at these stations are given in Table 8.17 and 8.18.

S.NO.	DATE		ORIGIN TIME			EPICENTER		DEPTH OF FOCUS	MAGNITUDE
	YEAR	M D	H M S	LAT	LONG	KM			
1	1918	7 8	10 22	- 24.50	91.00	- 7.60			
2	1923	9 9	22 3	- 25.25	91.00	- 7.10			
3	1924	1 30	0 5	- 25.00	93.00	- -			
4	1926	10 23	14 30	- 25.00	93.00	- -			
5	1927	2 13	3 33	- 25.50	93.50	- -			
6	1928	2 6	0 23	- 28.00	91.00	- -			
7	1928	11 15	15 34	- 25.50	93.50	- -			
8	1930	7 2	21 3	- 25.50	90.00	- 7.10			
9	1930	7 3	0 19	- 25.80	90.20	- -			
10	1930	7 3	6 1	- 25.80	90.20	- -			
11	1930	7 4	18 54	- 25.80	90.20	- -			
12	1930	7 4	21 34	- 25.80	90.20	- -			
13	1930	7 8	4 32	- 25.80	90.20	- -			
14	1930	7 8	9 43	- 25.80	90.20	- -			
15	1930	7 11	7 6	- 25.00	93.50	- -			
16	1930	7 13	14 0	- 25.80	90.20	- -			
17	1930	9 22	14 19	- 25.00	94.00	- 6.30			
18	1931	2 7	15 3	- 25.80	90.20	- -			
19	1932	3 6	0 17	- 25.50	92.50	- 5.60			
20	1932	3 24	16 8	- 25.00	90.00	- 5.60			
21	1932	3 27	8 44	- 24.50	92.00	- 5.60			
22	1932	11 9	18 30	- 26.50	92.00	- 5.60			
23	1933	3 6	13 5	- 26.00	90.50	- 5.60			
24	1935	3 21	0 4	- 24.25	89.50	80 6.30			
25	1936	2 11	20 7	- 26.50	92.00	- -			
26	1936	5 30	7 8	- 25.70	90.50	- -			
27	1936	6 18	14 56	- 26.60	90.30	- -			
28	1937	3 9	20 19	- 27.00	92.00	- -			
29	1937	3 21	16 12	- 25.50	94.00	- -			
30	1937	3 31	10 36	- 28.00	90.50	- -			
31	1938	2 26	12 10	- 28.00	90.50	- -			
32	1938	4 13	1 10	- 26.00	91.00	- -			
33	1939	5 27	3 45	- 24.50	94.00	75 6.80			
34	1940	2 13	11 46	- 27.00	92.00	- -			
35	1940	8 2	3 3	- 28.00	90.50	- -			
36	1941	1 21	12 41	- 27.00	92.00	100 6.80			
37	1941	1 27	2 30	- 26.50	92.50	180 6.50			
38	1941	5 22	1 0	- 27.50	93.00	- 5.60			
39	1941	9 6	3 17	- 27.00	92.00	- -			
40	1942	2 21	21 46	- 24.00	90.30	- -			
41	1942	5 15	14 8	- 24.00	90.30	- -			
42	1943	10 23	17 23	- 26.00	93.00	- 7.20			
43	1950	2 26	3 35	- 28.00	91.00	- -			
44	1950	8 15	21 42	- 25.00	93.00	- -			
45	1950	8 16	12 38	- 27.90	91.90	- -			
46	1950	8 16	17 51	- 27.90	91.90	- -			
47	1950	8 17	23 56	- 27.90	91.90	- -			

Continued on next page...

Continued from previous page...

S.NO.	YEAR	DATE			ORIGIN TIME			EPICENTER		DEPTH OF FOCUS KM	MAGNITUDE
		M	D	H	M	S	LAT °N	LONG °E			
48	1950	9	25	12	25	-	24.00	93.00	-	-	
49	1950	12	29	22	35	-	24.00	91.80	-	-	
50	1951	4	7	20	29	-	25.90	90.50	-	-	
51	1952	8	25	1	44	-	28.00	94.00	-	-	
52	1952	11	7	4	33	-	25.50	94.00	-	-	
53	1954	2	23	6	40	-	27.50	91.00	-	5.60	
54	1954	12	13	20	38	-	27.00	93.00	-	-	
55	1955	1	14	7	44	-	24.90	94.00	100	-	
56	1955	4	17	3	49	-	26.50	90.00	-	4.50	
57	1955	8	29	16	4	-	26.00	90.50	-	4.30	
58	1955	9	20	20	21	-	27.50	90.00	-	5.70	
59	1955	11	23	2	33	-	26.50	90.00	-	5.00	
60	1956	6	12	3	12	-	24.80	90.90	-	5.30	
61	1957	7	1	19	30	-	25.00	94.00	-	-	
62	1957	11	29	21	34	-	25.50	92.25	-	-	
63	1957	12	12	20	5	-	24.50	93.00	-	-	
64	1957	12	16	13	11	-	24.00	90.00	-	-	
65	1958	1	4	8	27	-	27.00	92.00	-	-	
66	1958	2	9	9	31	-	25.00	90.50	-	5.00	
67	1958	2	13	0	11	-	27.50	92.00	-	5.50	
68	1958	7	13	15	28	-	24.50	94.00	-	-	
69	1959	5	24	11	28	-	25.99	90.34	-	-	
70	1959	5	25	19	20	-	27.00	94.00	-	-	
71	1959	9	22	6	3	-	28.00	91.00	-	-	
72	1959	12	3	14	0	-	25.00	94.00	-	-	
73	1959	12	15	7	9	-	27.00	88.00	-	-	
74	1960	1	4	3	57	-	26.00	90.00	-	-	
75	1960	5	9	14	36	-	25.50	89.50	-	-	
76	1960	5	26	20	5	-	27.00	93.00	-	5.00	
77	1960	7	29	10	42	-	26.50	90.50	-	5.50	
78	1960	8	21	3	29	-	27.00	88.50	29	5.50	
79	1960	8	27	12	31	-	27.00	90.00	-	-	
80	1961	11	6	7	59	-	26.70	91.90	37	-	
81	1961	12	25	11	19	-	27.10	90.40	-	-	
82	1962	5	19	21	28	-	26.70	92.20	15	-	
83	1962	10	30	16	13	-	26.60	93.30	-	-	
84	1963	3	16	3	35	-	26.00	92.80	39	4.50	
85	1963	6	19	10	47	-	25.00	92.10	51	5.90	
86	1963	6	21	15	26	-	24.90	92.10	53	5.70	
87	1963	7	5	7	19	-	27.70	92.10	0	4.20	
88	1963	9	2	22	25	-	26.20	90.00	220	-	
89	1963	11	10	4	58	-	26.50	93.20	66	-	
90	1964	2	18	3	48	-	27.50	91.10	30	5.60	
91	1964	3	27	23	3	-	27.20	89.30	32	6.30	
92	1964	4	13	3	20	-	27.60	90.20	52	5.40	
93	1964	8	17	14	42	-	24.20	94.00	184	4.70	
94	1964	8	30	2	35	-	27.60	88.30	21	5.20	

Continued on next page...

S.NO.	YEAR	DATE				ORIGIN TIME		EPICENTER °N °E		DEPTH OF FOCUS	MAGNITUDE
		M	D	H	M	S	LAT	LONG	KM		
95	1964	9	1	13	22	-	27.20	92.30	0	5.70	
96	1965	1	12	13	32	-	27.60	88.00	23	6.10	
97	1965	4	11	22	33	-	26.70	92.30	70	5.10	
98	1965	6	18	8	17	-	25.00	93.70	66	5.80	
99	1965	11	6	16	4	-	27.10	91.70	40	4.30	
100	1965	12	9	20	26	-	27.40	92.50	29	5.30	
101	1966	2	24	0	16	-	26.30	91.50	51	5.10	
102	1966	3	23	22	52	-	25.90	90.00	20	4.40	
103	1966	4	23	4	17	-	26.00	90.40	25	4.70	
104	1966	6	5	8	29	-	24.60	93.40	45	4.10	
105	1966	6	26	10	56	-	26.20	92.80	49	4.80	
106	1966	7	5	10	1	-	27.80	92.70	0	4.80	
107	1966	9	26	5	10	-	27.50	92.60	19	5.50	
108	1966	9	26	6	3	-	27.50	92.70	0	4.20	
109	1967	1	30	7	9	-	25.39	90.47	46	5.00	
110	1967	2	25	11	56	-	27.41	92.43	0	5.10	
111	1967	7	7	22	56	-	27.80	92.20	0	4.90	
112	1967	9	6	1	43	-	24.10	91.70	18	5.00	
113	1967	9	15	10	32	-	27.40	91.80	57	5.80	
114	1967	11	10	6	4	-	25.50	91.70	59	4.40	
115	1967	11	14	0	4	-	24.00	91.50	0	5.10	
116	1968	1	18	19	57	-	24.30	93.20	100	4.70	
117	1968	5	2	0	26	-	26.25	92.25	53	4.80	
118	1968	6	12	4	29	-	24.87	91.93	44	5.30	
119	1968	8	18	14	18	-	26.44	90.57	31	5.20	
120	1968	11	18	8	49	-	26.78	92.26	72	4.00	
121	1968	12	27	14	38	-	24.13	91.60	26	5.20	
122	1969	2	7	9	25	-	27.58	93.97	-	-	
123	1969	2	22	20	37	-	26.58	92.36	52	4.80	
124	1969	6	1	8	35	-	25.76	91.76	20	5.00	
125	1969	6	30	8	51	-	26.89	92.63	64	5.10	
126	1969	11	5	20	25	-	27.70	90.22	13	5.00	
127	1969	11	11	5	49	-	26.26	91.72	0	4.50	
128	1969	12	19	14	41	-	24.41	93.64	57	4.70	
129	1970	2	19	7	10	-	27.40	93.99	18	5.50	
130	1970	3	13	18	24	-	24.90	93.94	62	4.90	
131	1970	7	25	1	35	-	25.71	88.50	0	5.20	
132	1970	8	13	7	0	-	24.70	93.92	40	4.70	
133	1970	8	28	1	24	-	24.66	91.67	17	4.90	
134	1971	4	21	9	15	-	26.57	92.17	0	4.30	
135	1971	7	17	15	0	-	26.47	93.23	49	5.30	
136	1971	10	31	15	54	-	26.17	90.73	0	4.60	
137	1972	3	26	6	10	-	25.87	93.89	0	4.50	
138	1972	8	21	18	55	-	27.23	88.02	0	5.10	
139	1972	11	6	10	56	-	26.96	88.71	0	4.80	

Continued on next page...

Continued from previous page...

S.NO.	DATE		ORIGIN TIME			EPICENTER °N °E		DEPTH OF FOCUS		MAGNITUDE
	YEAR	M D	H M S	LAT	LONG	KM				
140	1973	5 31	23 39	- 24.28	93.55	30	5.90			
141	1973	7 4	16 44	- 27.24	92.47	26	5.20			
142	1973	9 11	15 55	- 27.00	92.53	54	4.80			
143	1973	10 9	4 1	- 27.75	93.35	0	4.80			
144	1973	11 2	12 9	- 25.72	91.60	20	4.80			
145	1974	1 28	14 17	- 25.68	93.60	42	3.80			
146	1974	5 15	3 51	- 25.54	91.79	32	4.50			
147	1974	7 9	7 17	- 27.36	92.33	53	4.60			
148	1974	9 21	6 27	- 25.68	90.90	27	4.70			
149	1975	1 23	1 37	- 27.31	88.25	33	4.80			
150	1975	3 3	19 24	- 24.13	93.54	42	5.00			
151	1976	2 1	15 38	- 24.41	93.50	59	4.00			
152	1976	3 16	4 55	- 24.44	93.25	59	3.80			
153	1976	12 17	10 21	- 27.74	92.44	33	4.70			
154	1977	1 17	16 14	- 26.21	90.48	33	-			
155	1977	2 6	16 53	- 24.30	92.88	42	4.70			
156	1977	6 5	19 21	- 26.22	88.31	33	4.80			
157	1977	11 13	21 2	- 26.47	93.11	33	5.00			
158	1978	3 18	18 40	- 24.28	92.86	39	4.60			
159	1978	4 19	17 1	- 27.66	92.68	51	4.90			
160	1978	4 19	18 58	- 27.65	92.59	33	4.60			
161	1978	10 10	18 14	- 24.31	93.66	33	4.70			
162	1978	11 18	13 24	- 26.24	92.09	55	4.40			
163	1978	12 30	23 33	- 24.45	93.91	33	4.60			
164	1979	1 9	2 39	- 25.41	92.86	18	4.40			
165	1979	1 13	3 27	- 27.16	91.86	33	4.50			
166	1979	1 28	6 6	- 24.61	91.16	33	4.90			
167	1979	2 26	6 54	- 26.27	91.20	33	4.20			
168	1979	3 4	17 40	- 24.64	93.39	33	4.60			
169	1979	4 11	16 8	- 25.97	88.82	33	4.80			
170	1979	7 29	14 15	- 26.75	91.73	66	4.60			
171	1979	11 16	19 17	- 27.24	88.15	33	4.60			
172	1980	6 11	5 25	- 25.75	90.21	33	4.80			
173	1980	11 19	19 0	- 27.39	88.75	17	6.00			
174	1980	12 22	4 36	- 26.33	89.31	33	4.50			
175	1981	2 9	15 49	- 27.03	89.75	33	5.10			
176	1981	2 28	1 58	- 26.03	93.63	33	4.70			
177	1981	12 9	10 52	- 27.46	92.45	33	4.50			
178	1982	1 11	20 52	- 24.69	92.06	33	4.70			
179	1982	1 28	7 18	- 25.17	90.66	33	4.20			
180	1982	2 26	0 5	- 25.56	90.74	64	4.70			
181	1982	2 26	8 14	- 26.19	92.17	33	4.60			
182	1982	4 5	2 19	- 27.41	88.86	33	5.10			
183	1982	6 20	15 29	- 26.49	90.20	33	4.50			
184	1982	7 5	6 13	- 25.96	90.56	33	-			
185	1982	7 6	6 13	- 25.91	90.31	33	5.10			

Continued on next page...

S.NO.	DATE		ORIGIN TIME			EPICENTER		DEPTH OF FOCUS KM	MAGNITUDE
	YEAR	M D	H M S	LAT	LONG	°N	°E		
186	1982	8 18	18 1	-	27.08	89.49	58	4.60	
187	1982	8 21	4 26	-	25.05	92.33	33	4.70	
188	1982	8 31	10 42	-	25.38	91.47	33	5.00	
189	1982	9 21	12 38	-	25.14	91.39	33	4.60	
190	1982	11 18	6 2	-	26.10	91.56	33	4.80	
191	1982	12 30	8 37	-	26.15	91.64	41	5.00	
192	1982	12 30	12 29	-	26.32	92.05	33	4.60	
193	1983	1 19	12 9	-	25.63	91.28	10	4.90	
194	1983	2 2	20 44	-	26.89	92.89	33	5.20	
195	1984	3 21	23 6	-	26.57	93.36	33	4.90	
196	1984	5 6	15 19	-	24.25	93.54	33	5.70	
197	1984	6 9	23 7	-	27.04	92.42	33	4.40	
198	1984	9 16	1 26	-	24.72	93.59	41	4.70	
199	1984	9 22	9 10	-	26.52	92.18	33	5.20	
200	1984	9 30	21 35	-	25.36	91.46	33	5.10	
201	1984	10 3	21 45	-	25.38	93.44	33	4.70	
202	1984	11 15	21 9	-	26.69	92.71	74	4.70	
203	1984	12 30	23 33	-	24.64	92.89	23	5.60	
204	1985	1 7	16 13	-	27.15	91.98	12	5.60	
205	1985	1 7	20 14	-	27.82	92.69	33	-	
206	1985	6 17	21 52	-	25.59	90.22	22	4.70	
207	1985	10 2	16 33	-	27.08	89.74	46	4.40	
208	1985	10 12	18 22	-	27.13	92.53	9	5.30	
209	1985	10 12	19 35	-	27.13	92.58	10	4.60	
210	1985	10 25	19 59	-	27.10	92.59	33	4.70	
211	1985	10 31	15 26	-	27.12	92.50	18	4.90	
212	1985	12 22	21 35	-	24.13	93.20	49	4.50	
213	1985	12 26	18 4	-	27.13	92.07	13	5.00	
214	1986	1 7	20 20	-	26.93	88.32	70	5.00	
215	1986	2 19	17 34	-	25.13	91.18	18	5.30	
216	1986	9 10	7 50	-	25.38	92.07	43	5.20	
217	1986	10 14	14 3	-	25.03	91.97	33	4.70	
218	1986	10 25	21 25	-	26.06	88.24	33	-	
219	1986	11 8	18 24	-	27.17	92.32	33	4.50	
220	1986	12 31	15 49	-	26.47	92.93	49	4.80	
221	1987	1 24	10 34	-	27.65	92.68	27	4.90	
222	1987	6 11	17 29	-	26.17	93.52	33	4.40	
223	1987	7 17	21 12	-	27.69	92.88	33	4.80	
224	1987	9 6	23 38	-	26.68	93.41	44	5.10	
225	1987	10 15	16 22	-	27.33	92.94	50	4.70	
226	1987	10 22	21 23	-	27.29	89.15	33	-	
227	1987	11 15	15 13	-	26.56	93.43	33	4.10	
228	1987	12 1	8 50	-	26.32	93.25	49	4.90	
229	1987	12 11	6 39	-	26.02	90.94	55	4.60	
230	1988	2 6	14 50	-	24.69	91.57	33	5.80	

Continued on next page...

S.NO.	DATE		ORIGIN TIME			EPICENTER		DEPTH OF FOCUS KM	MAGNITUDE
	YEAR	M D	H M S	°N	°E	LAT	LONG		
231	1988	2 12	5 51	-	25.12	93.86	33	4.30	
232	1988	2 17	1 2	-	24.52	91.43	39	4.50	
233	1988	2 17	6 30	-	27.14	92.22	44	4.80	
234	1988	2 28	5 55	-	24.70	91.57	29	4.60	
235	1988	4 18	5 18	-	24.83	93.85	71	4.30	
236	1988	4 30	3 27	-	25.91	91.57	33	4.20	
237	1988	5 10	7 16	-	25.10	88.25	33	-	
238	1988	5 26	16 30	-	27.42	88.56	43	4.70	
239	1988	9 4	8 1	-	26.28	91.77	33	4.00	
240	1988	9 27	19 10	-	27.17	88.29	33	5.00	
241	1988	12 20	9 45	-	27.62	91.15	34	5.00	
242	1989	1 6	13 31	-	25.10	91.59	10	-	
243	1989	1 10	19 21	-	24.10	92.46	33	4.30	
244	1989	1 16	10 49	-	24.05	92.10	33	-	
245	1989	2 28	0 26	-	27.13	92.64	44	4.60	
246	1989	3 8	20 2	-	26.98	92.75	33	5.10	
247	1989	4 13	7 25	-	24.47	92.50	33	5.10	
248	1989	4 29	12 55	-	25.24	91.60	33	4.30	
249	1989	6 11	13 42	-	26.41	90.76	33	4.60	
250	1989	9 19	17 7	-	26.79	92.79	67	4.60	
251	1990	2 5	2 6	-	24.87	92.42	33	4.10	
252	1990	2 22	22 7	-	24.94	93.10	52	5.10	
253	1990	4 30	1 55	-	26.43	93.31	33	5.30	
254	1990	5 19	2 18	-	25.51	91.06	33	-	
255	1990	8 29	2 41	-	27.18	92.75	33	4.80	
256	1990	9 2	6 29	-	26.64	92.67	46	5.20	
257	1990	10 29	11 32	-	26.52	92.40	33	4.90	

Table 8.1 Epicenters of important earthquakes in Meghalaya and surrounding region. Data taken from USGS-NEIS (1990). This epicentral data is plotted in Fig 8.1.

S.NO.	STATION NAME	LATITUDE	LONGITUDE	ELEVATION METER
1.	Baigao	25 4	92 51	650
2.	Baitha Langso	25 58	92 36	70
3.	Bamungao	25 53	93 00	100
4.	Berlongfer	25 46	93 15	160
5.	Bokajan	26 00	93 46	120
6.	Boko	25 58	91 14	50
7.	Cherrapunji	25 16	91 44	1140
8.	Dauki	25 11	92 01	40
9.	Diphu	25 55	93 26	160
10.	Doloo	24 55	92 47	100
11.	Gunjung	25 18	93 00	540
12.	Haflong	25 10	93 01	540
13.	Hajadisa	25 22	93 18	280
14.	Hareggajao	25 06	92 51	160
15.	Hatikhali	25 39	93 06	140
16.	Hojai	25 59	92 51	70
17.	Jarain	25 19	92 07	360
18.	Jellalpur	25 00	92 27	500
19.	Jhirighat	24 48	93 06	40
20.	Kalain	24 58	92 34	20
21.	Katakhal	24 49	92 38	20
22.	Karimganj	24 51	92 21	20
23.	Khliehriat	25 21	92 22	1180
24.	Koomber	24 57	93 00	60
25.	Laisong	25 12	93 18	800
26.	Langting	25 29	93 07	160
27.	Laskein	25 30	92 24	1200
28.	Loharghat	25 58	91 28	60
29.	Maibang	25 18	93 08	150
30.	Mawkyrwat	25 22	91 28	1000
31.	Mawphlang	25 27	91 46	1700
32.	Mawsynram	25 17	91 35	1360
33.	Nongkhlaw	25 41	91 38	900

S.NO.	STATION NAME	LATITUDE		LONGITUDE		ELEVATION (METERS)
		D	M	D	M	
34.	Nongpoh	25	54	91	52	560
35.	Nongstoin	25	30	91	16	1400
36.	Panimur	25	39	92	48	150
37.	Pynursla	25	18	91	54	1300
38.	Saitsama	25	43	92	23	900
39.	Shillong	25	33	91	54	1540
40.	Silchar	24	49	92	48	20
41.	Ulukunchi	25	58	92	18	500
42.	Umkiang	25	08	92	20	800
43.	Ummulong	25	30	92	09	1300
44.	Umrongso	25	30	92	37	720
45.	Umsning	25	44	91	53	800

Table 8.2 List of stations of Shillong array. Geographical coordinates and elevation of recording stations is taken from Chandrasekaran and Das (1992b). Location of stations of array is shown in Fig 8.2.

Date	Mag	Origin Time (h:m:s)	Epicenter	Focal Depth	Ref	Symbo -l for epicent -er
10.09.86	$M_L = 5.5$ $M_b = 5.7$	-	25.2°N 91.6°E	Shallow	IMD (Priliminary)	E_{M1}
10.09.86	$M_b = 5.2$	7:50:25.5	25.385°N 92.077°E	43 km	USGS	EM_2
10.09.86	-	7:50:28.5	25.428°N 92.083°E	28 km	D,C	E_{M3}

D,C Das and Chandrasekaran (1993)

Table 8.3 Epicentral parameters of Meghalaya earthquake of 10th September, 1986 reported by different agencies. . . The epicenters E_{M1} , E_{M2} and E_{M3} given in this Table are plotted in Fig 8.3.

S.No.	Station Name	Longitudinal cm/sec ²	Transverse cm/sec ²	Resultant cm/sec ²
1.	Baithalangso	46.4	42.4	47.6
2.	Dauki	88.7	90.9	94.9
3.	Khliehriat	30.7	46.7	52.3
4.	Nongkhlaw	54.3	94.0	95.3
5.	Nongpoh	54.1	61.9	69.7
6.	Nonstoin	20.5	14.0	22.0
7.	Panimur	41.0	49.4	62.2
8.	Pynursla	92.3	76.5	102.8
9.	Saitsama	114.3	142.0	155.4
10.	Ummmulong	116.5	66.0	117.7
11.	Umrongso	27.7	32.0	38.3
12.	Umsning	105.9	78.4	131.0

Table 8.4 Resultant peak ground acceleration of two horizontal components recorded at different stations for Meghalaya earthquake of 10th Sept, 1986 (After Chandrasekaran et al., 1988). Isoacceleration contour map of resultant peak acceleration is shown in Fig 8.4.

STATION NAME	BAIT	BAIT	BAIT	DAUK	DAUK	DAUK
COMP	LONG	TRAN	VERT	LONG	TRAN	VERT
P _z	46.4	42.4	25.3	88.7	90.9	33.9
T _{at}	.2	.2	.8	1.2	2.7	.02
T _D	4.8	2.3	3.9	3.3	4.5	7.0
P _v	2.6	1.4	1.1	3.5	4.3	3.0
P _d	1.8	.7	.8	1.2	2.5	2.4
T _{area}	1882	1356	828	4649	3996	2620
R _{at}	.95	1.067	1.00	1.00	1.098	1.08
ACF ₁	.065	.061	.08	.042	.038	.029
ACF ₂	.264	.266	.248	.202	.118	.110
ACF ₃	.320	.319	.422	.312	.124	.164
ACF ₄	.140	.140	.160	.08	.06	.04
ACF ₅	.454	.430	.445	.657	.581	.262
ACF ₆	.101	.068	.286	.042	-.076	-.324
ACF ₇	.035	.006	.269	-.321	-.441	-.254
ACF ₈	-.439	-.447	-.491	-.359	-.441	-.324
ACF ₉	1.215	1.072	.818	.949	3.59	1.653
ACF ₁₀	1.089	1.132	1.068	1.056	1.11	1.111
F _p	3.2	2.5	2.9	3.5	6.2	8.1
F ₁	6.6	7.4	7.5	4.7	6.2	8.3
F ₂	10.7	10.7	15.2	8.1	8.5	12.5
F ₃	17.9	18.1	19.5	9.6	9.9	15.8
F ₄	3.2	3.3	2.9	4.0	4.5	6.6
F ₅	5.5	6.4	3.8	5.8	6.5	8.9
F ₆	10.6	10.7	12.9	8.3	8.8	13.5

Table 8.5 Extracted features from three components of field records of Meghalaya earthquake of 10th Sept, 1986 recorded at Baithalango (Bait) and Dauki (Dauk) stations. Field records at these stations are shown in Fig 8.6 and 8.7, respectively.

STATION NAME	KHIL			NON		
COMP	LONG	TRAN	VERT	LONG	TRAN	VERT
P _a	30.7	46.8	17.2	54.1	61.1	35.4
T _u	.3	.2	.1	.3	.2	.1
T _D	5.2	4.4	4.2	1.6	4.4	3.1
P _v	1.2	3.3	2.1	2.3	1.8	1.2
P _d	1.1	2.1	2.1	.9	1.3	1.2
T _{area}	1257	1370	734	2112	1497	1342
R _u	.976	1.09	1.26	.984	1.02	.933
ACF ₁	.038	.051	.035	.051	.026	.026
ACF ₂	.134	.196	.111	.157	.074	.078
ACF ₃	.145	.295	.218	.262	.084	.165
ACF ₄	.06	.14	.06	.100	.120	.04
ACF ₅	.552	.669	.502	.158	.458	.217
ACF ₆	-.076	.193	-.163	-.337	-.258	-.543
ACF ₇	-.381	-.158	-.419	-.095	-.351	-.329
ACF ₈	-.381	-.348	-.419	-.392	-.351	-.543
ACF ₉	3.670	1.230	1.326	-.392	-.351	1.394
ACF ₁₀	1.082	1.091	1.223	4.233	1.696	1.094
F _p	3.1	2.1	5.6	5.0	5.4	12.7
F ₁	6.4	4.3	6.9	4.8	11.3	8.7
F ₂	8.3	7.5	8.3	5.0	12.7	12.5
F ₃	11.8	10.3	12.9	11.4	16.6	14.5
F ₄	4.5	3.7	5.6	4.7	5.9	7.9
F ₅	7.3	4.5	7.2	4.9	11.7	9.7
F ₆	8.6	7.8	9.5	5.1	14.2	12.7

Table 8.6 Extracted features from three components of field records of Meghalaya earthquake of 10th Sept, 1986 recorded at Khliehriat (Khil) and Nongpoh (Non) stations. Field records these stations are shown in Fig 8.8 and 8.9, respectively.

STATION NAME	NOGS	NOGS	NOGS	NONK	NONK	NONK
COMP	LONG	TRAN	VERT	LONG	TRAN	VERT
P _z	20.5	14.1	9.4	54	94	35
T _{at}	.02	.06	.2	6.0	.3	.2
T _D	7.7	7.4	5.3	15.5	6.6	5.3
P _y	1.6	1.0	1.7	7.3	5.7	4.3
P _d	1.1	.8	.7	7.7	5.3	4.3
T _{area}	1174	1206	554	7171	8629	1465
R _{at}	.986	1.06	1.252	1.085	1.019	.880
ACF ₁	.045	.042	.031	.069	.071	.041
ACF ₂	.115	.125	.075	.212	.218	.129
ACF ₃	.207	.292	.154	.367	.366	.218
ACF ₄	.08	.08	.06	.140	.140	.08
ACF ₅	.579	.616	.367	.843	.831	.387
ACF ₆	.074	.036	-.305	.524	.543	.015
ACF ₇	-.218	-.331	-.321	.156	.192	-.239
ACF ₈	-.373	-.429	-.321	.156	.192	-.239
ACF ₉	2.039	1.503	2.18	.823	.694	1.138
ACF ₁₀	1.043	1.056	1.195	1.033	1.018	1.111
F _p	6.8	4.8	.2	3.6	3.6	5.4
F ₁	6.5	5.8	8.7	3.5	3.4	6.3
F ₂	7.3	7.1	10.4	3.7	3.6	12.2
F ₃	14.1	10.9	13.5	5.5	6.4	18.3
F ₄	4.7	4.8	7.2	3.4	3.4	5.3
F ₅	6.8	6.4	9.0	3.6	3.5	6.4
F ₆	7.4	7.7	10.8	4.0	3.6	12.0

Table 8.7 Extracted features from three components of field records of Meghalaya earthquake of 10th Sept, 1986 recorded at Nongstoin (Nongs) and Nongkhlaw (Nonk) stations. Field records at these stations are shown in Fig 8.10 and 8.11, respectively.

STATION NAME	PANI	PANI	PANI	PYN	PYN	PYN
COMP	LONG	TRAN	VERT	LONG	TRAN	VERT
P ₁	41.0	49.4	23.8	92.3	76.5	32.6
T ₁	.3	.1	.7	.1	2.6	5.4
T _D	9.4	5.5	2.8	2.8	7.2	7.8
P _v	2.8	3.0	1.4	3.1	2.2	2.2
P _d	2.0	.6	1.3	2.6	2.5	2.7
T _{area}	2655	2868	903	4183	3969	2241
R ₁	1.01	1.03	.997	.999	1.065	.972
ACF ₁	.023	.038	.024	.038	.035	.021
ACF ₂	.129	.141	.064	.118	.111	.070
ACF ₃	.235	.251	.106	.196	.214	.115
ACF ₄	.06	.100	.04	.08	.06	.04
ACF ₅	.458	.533	.127	.630	.523	.015
ACF ₆	-.258	-.074	-.547	-.055	-.176	-.298
ACF ₇	-.351	-.227	-.090	-.569	-.494	-.171
ACF ₈	-.351	-.481	-.547	-.687	-.494	-.298
ACF ₉	1.696	1.58	1.769	.939	1.396	2.162
ACF ₁₀	1.048	1.05	1.089	1.053	1.077	1.082
F _p	5.5	5.2	11.2	6.4	5.9	10.0
F ₁	6.7	5.6	11.1	6.3	6.3	10.9
F ₂	10.2	8.9	12.5	6.6	9.2	14.3
F ₃	13.1	13.1	14.1	8.5	10.6	20.2
F ₄	5.5	4.7	9.9	6.1	5.8	9.0
F ₅	7.1	5.6	11.4	6.4	6.9	11.9
F ₆	11.3	10.8	13.4	6.8	9.6	16.2

Table 8.8 Extracted features from three components of field records of Meghalaya earthquake of 10th Sept, 1986 recorded at Panimur (Pani) and Pynursla (Pyn) stations. Field records at these stations are shown in Fig 8.12 and 8.13, respectively.

STATION NAME	SAIT			UMU		
COMP	LONG	TRAN	VERT	LONG	TRAN	VERT
P _s	114	142	63.3	116	66	52
T _{st}	2.1	.2	1.4	.1	2.5	.6
T _d	6.6	2.4	2.2	6.3	9.6	2.2
P _v	4.2	5.5	2.4	2.8	2.3	2.0
P _d	1.1	1.7	2.1	2.7	2.2	2.3
T _{area}	64793	85840	2714	5477	5225	1372
R _{st}	1.025	1.014	1.026	1.07	1.03	1.072
ACF ₁	.051	.034	.040	.030	.026	.02
ACF ₂	.185	.213	.132	.101	.077	.058
ACF ₃	.297	.329	.214	.185	.126	.065
ACF ₄	.100	.080	.08	.06	.040	.04
ACF ₅	.633	.699	.554	.367	.242	-.001
ACF ₆	.143	.229	-.006	-.377	-.563	-.412
ACF ₇	-.114	-.107	-.459	-.525	-.407	.045
ACF ₈	-.509	-.441	-.596	-.525	-.563	-.412
ACF ₉	.95	.913	.876	1.201	1.218	2.427
ACF ₁₀	1.049	1.045	1.076	1.077	1.059	1.149
F _p	4.2	3.4	6.3	6.8	11.1	15.5
F ₁	4.5	3.9	5.8	7.2	9.5	11.2
F ₂	7.6	6.6	6.6	10.2	10.8	15.4
F ₃	13.6	10.6	12.6	13.1	13.9	17.8
F ₄	4.1	3.4	5.3	6.8	8.7	8.2
F ₅	4.9	4.4	6.2	7.9	10.2	12.8
F ₆	7.9	6.9	7.3	11.5	11.7	15.8

Table 8.9 Extracted features from three components of field records of Meghalaya earthquake of 10th Sept, 1986 recorded at Saitsama (Sait) and Ummulong (Umu) stations. Field records at these stations is shown in Fig 8.14 and 8.15.

STATION NAME	UMSG	UMSG	UMSG	UMSO	UMSO	UMSO
COMP	LONG	TRAN	VERT	LONG	TRAN	VERT
P ₂	105.9	78.4	52.0	27.7	32.0	13.0
T ₂₁	.2	4.4	6.1	.6	.4	.6
T ₀	2.6	6.2	7.9	3.4	5.0	3.7
P _v	3.6	2.9	2.9	1.3	1.2	1.7
P _d	1.3	1.5	2.5	1.1	.9	1.7
T _{area}	5089	4229	2357	1112	1096	509
R ₂₁	.980	1.037	1.123	1.259	1.056	1.18
ACF ₁	.035	.051	.028	.033	.037	.039
ACF ₂	.160	.162	.114	.095	.115	.136
ACF ₃	.285	.262	.155	.152	.152	.243
ACF ₄	.120	.100	.180	.06	.06	.08
ACF ₅	.396	.536	.140	.463	.579	.534
ACF ₆	-.139	.118	-.212	-.251	-.107	-.037
ACF ₇	-.195	-.103	-.188	-.496	-.448	-.284
ACF ₈	-.456	-.548	-.213	-.496	-.448	-.308
ACF ₉	.998	.917	2.181	1.466	1.440	1.403
ACF ₁₀	1.058	1.064	1.137	1.120	1.074	1.124
F _p	4.2	4.8	12.9	7.9	4.4	5.3
F ₁	7.0	4.9	9.1	7.9	6.2	5.8
F ₂	11.5	10.0	13.8	8.7	8.2	8.8
F ₃	14.5	15.5	19.5	12.1	9.9	12.7
F ₄	4.3	4.6	7.1	6.4	4.8	5.1
F ₅	7.6	5.1	9.9	8.2	6.9	6.0
F ₆	11.8	9.7	14.8	9.1	8.6	9.8

Table 8.10 Extracted features from three components of field records of Meghalaya earthquake of 10th Sept, 1986 recorded at Umrongso (Umsso) and Umsning (Umsg) stations. Field records at these stations is shown in Fig 8.16 and 8.17.

STATION NAME	SAIT	SAIT	SAIT	UMMU	UMMU	UMMU
MODEL NAME	MM _{d1}	MM _{d2}	MM _{d3}	MM _{d1}	MM _{d2}	MM _{d3}
P _s	89.1	73.4	60.7	57.1	127.0	66.1
T _{st}	.60	1.27	1.42	1.4	1.02	1.56
T _D	2.4	1.77	2.51	3.3	2.22	2.91
P _v	1.81	1.58	1.23	1.33	2.43	1.28
P _d	.172	.137	.116	.126	.233	.104
T _{area}	3402	2488	2471	3444	3334	2722
R _{st}	.994	.999	.992	.994	.994	.993
ACF ₁	.029	.027	.029	.030	.028	.029
ACF ₂	.086	.075	.085	.089	.083	.086
ACF ₃	.138	.118	.133	.150	.136	.138
ACF ₄	.06	.04	.06	.06	.06	.06
ACF ₅	.43	.318	.42	.452	.404	.424
ACF ₆	-.525	-.648	-.522	-.489	-.590	-.519
ACF ₇	-.744	-.549	-.695	-.756	-.773	-.722
ACF ₈	-.744	-.648	-.695	-.756	-.773	-.722
ACF ₉	.995	1.101	1.067	.970	.963	1.016
ACF ₁₀	1.074	1.094	1.074	1.061	1.069	1.064
F _p	9.4	9.5	9.9	8.3	8.4	7.8
F ₁	7.7	9.4	8.5	7.9	8.3	7.8
F ₂	9.4	10.1	9.7	8.8	9.3	9.8
F ₃	10.5	12.4	10.7	10.1	10.5	10.2
F ₄	7.5	8.7	7.3	7.3	8.3	7.7
F ₅	9.2	9.7	9.9	8.4	8.7	9.2
F ₆	10.1	11.8	10.1	9.9	10.4	10.1

Table 8.11 Extracted features from simulated records at Saitama and Ummulong stations due to three different models MM_{d1}, MM_{d2} and MM_{d3} of rupture planes. The model of these rupture planes and the simulated records are shown in Fig 8.18, 8.19 and 8.20.

PARAMETERS	MODEL GIVING LEAST DIFFERENCE IN THE VALUE OF THE EXTRACTED PARAMETER FROM SIMULATED AND FIELD RECORDS AT SAITSAMA	MODEL GIVING LEAST DIFFERENCE IN THE VALUE OF THE EXTRACTED PARAMETER FROM SIMULATED AND FIELD RECORDS AT UMMULONG
P_s	MM_{d1}	MM_{d2}
T_{s1}	MM_{d1}	MM_{d2}
T_D	MM_{d3}	MM_{d1}
P_v	MM_{d1}	MM_{d2}
P_v	MM_{d3}	MM_{d2}
T_{area}	MM_{d1}	MM_{d1}
R_{a1}	MM_{d2}	MM_{d1}, MM_{d2}
ACF_1	MM_{d1}, MM_{d3}	MM_{d1}
ACF_2	MM_{d1}	MM_{d1}
ACF_3	MM_{d1}	MM_{d1}
ACF_4	MM_{d1}, MM_{d3}	$MM_{d1}, MM_{d2}, MM_{d3}$
ACF_5	MM_{d1}	MM_{d2}
ACF_6	MM_{d3}	MM_{d1}
ACF_7	MM_{d2}	MM_{d1}
ACF_8	MM_{d2}	MM_{d1}
ACF_9	MM_{d1}	MM_{d3}
ACF_{10}	MM_{d1}, MM_{d3}	MM_{d2}
F_p	MM_{d1}	MM_{d3}
F_1	MM_{d1}	MM_{d3}
F_2	MM_{d1}	MM_{d2}
F_3	MM_{d1}	MM_{d2}
F_4	MM_{d3}	MM_{d1}
F_5	MM_{d3}	MM_{d1}
F_6	MM_{d3}	MM_{d1}

Table 8.12 Selection of dip of the rupture plane by comparing extracted parameters of simulated records at Saitsama and Ummulong stations for three different models of rupture plane having different dip.

MODEL NAME	MM _{n1}	MM _{n2}	MM _{n3}	MM _{n4}	MM _{n5}
P _s	89.1	73.3	56.6	32.3	100.1
T _v	.60	.88	1.73	1.54	.22
T _D	2.4	1.2	3.3	2.2	1.5
P _v	1.81	1.52	1.33	1.91	2.30
P _d	.172	.139	.070	.175	.208
T _{area}	3402	2037	2961	3272	2612
R _v	.994	.991	.993	.994	.993
ACF ₁	.029	.029	.030	.029	.030
ACF ₂	.086	.085	.090	.087	.088
ACF ₃	.138	.135	.146	.140	.139
ACF ₄	.06	.06	.06	.06	.06
ACF ₅	.43	.423	.442	.432	.455
ACF ₆	-.525	-.548	-.477	-.523	-.487
ACF ₇	-.744	-.780	-.710	-.746	-.764
ACF ₈	-.744	-.780	-.710	-.746	-.764
ACF ₉	.995	.958	1.021	.991	.983
ACF ₁₀	1.074	1.069	1.059	1.063	1.098
F _p	9.4	9.3	9.4	7.5	9.2
F ₁	7.7	9.0	7.4	7.5	8.2
F ₂	9.4	9.3	9.3	9.4	9.1
F ₃	10.5	9.8	10.4	10.7	10.0
F ₄	7.5	8.2	6.9	7.4	7.5
F ₅	9.2	9.3	9.0	89.1	8.3
F ₆	10.1	9.6	9.7	10.5	9.5

Table 8.13 Feature extracted from simulated records at Saitsama station for five different locations of nucleation point or starting point of rupture within the rupture plane. The rupture model differ with other only in the location of nucleation point. These models are named as MM_{n1}, MM_{n2}, MM_{n3}, MM_{n4} and MM_{n5}. Simulated records due to these models at Saitsama station are shown in Fig 8.21.

MODEL NAME	MM _{n1}	MM _{n2}	MM _{n3}	MM _{n4}	MM _{n5}
P ₂	57.1	70.0	66.0	118.1	80.1
T _{n1}	1.4	.96	2.00	.74	1.1
T _D	3.3	1.96	3.03	1.58	1.86
P _v	1.33	1.67	1.41	2.38	1.58
P _d	.126	.161	.094	.208	.147
T _{area}	3444	3030	3256	3043	2769
R _{at}	.994	.994	.995	.994	.993
ACF ₁	.030	.029	.028	.030	.028
ACF ₂	.089	.088	.082	.090	.085
ACF ₃	.150	.191	.136	.158	.142
ACF ₄	.06	.06	.06	.06	.06
ACF ₅	.452	.424	.399	.464	.381
ACF ₆	-.489	-.502	-.583	-.489	-.566
ACF ₇	-.756	-.668	-.696	-.814	-.727
ACF ₈	-.756	-.688	-.696	-.814	-.727
ACF ₉	.970	1.077	1.035	.889	.997
ACF ₁₀	1.061	1.094	1.067	1.055	1.076
F _p	8.3	6.3	9.6	7.7	10.2
F ₁	7.9	7.9	8.4	7.7	8.2
F ₂	8.8	9.2	9.7	8.0	9.9
F ₃	10.1	10.8	10.4	10.4	10.9
F ₄	7.3	6.7	8.0	7.6	7.9
F ₅	8.4	8.6	8.9	7.9	9.4
F ₆	9.9	10.5	10.3	10.1	10.6

Table 8.14 Feature extracted from simulated records at Ummulong station for five different locations of nucleation point or starting point of rupture within the rupture plane. The rupture model differ with other only in the location of nucleation point. These models are named as MM_{n1}, MM_{n2}, MM_{n3}, MM_{n4} and MM_{n5}. Simulated records due to these models at Ummulong station are shown Fig 8.21.

PARAMETERS	MODEL GIVING LEAST DIFFERENCE IN THE VALUE OF THE EXTRACTED PARAMETER FROM SIMULATED AND FIELD RECORDS AT SAITSAMA	MODEL GIVING LEAST DIFFERENCE IN THE VALUE OF THE EXTRACTED PARAMETER FROM SIMULATED AND FIELD RECORDS AT UMMULONG
P_a	MM_{n5}	MM_{n4}
T_{at}	MM_{n5}	MM_{n4}
T_d	MM_{n1}	MM_{n4}
P_v	MM_{n5}	MM_{n4}
P_d	MM_{n5}	MM_{n4}
T_{area}	MM_{n1}	MM_{n4}
R_{sl}	MM_{n1}, MM_{n4}	$MM_{n1}, MM_{n2}, MM_{n3}, MM_{n4}$
ACF_1	MM_{n3}, MM_{n5}	MM_{n1}, MM_{n4}
ACF_2	MM_{n5}	MM_{n4}
ACF_3	MM_{n5}	MM_{n2}
ACF_4	$MM_{n1}, MM_{n2}, MM_{n3}, MM_{n4}, MM_{n5}$	$MM_{n1}, MM_{n2}, MM_{n3}, MM_{n4}, MM_{n5}$
ACF_5	MM_{n5}	MM_{n5}
ACF_6	MM_{n3}	MM_{n1}, MM_{n4}
ACF_7	MM_{n3}	MM_{n2}
ACF_8	MM_{n3}	MM_{n2}
ACF_9	MM_{n2}	MM_{n2}
ACF_{10}	MM_{n3}	MM_{n5}
F_p	MM_{n4}	MM_{n2}
F_1	MM_{n3}	MM_{n4}
F_2	MM_{n5}	MM_{n5}
F_3	MM_{n1}	MM_{n5}
F_4	MM_{n1}	MM_{n2}
F_5	MM_{n5}	MM_{n4}
F_6	MM_{n5}	MM_{n5}

Table 8.15 Selection of possible location of nucleation point within the rupture plane by comparing extracted parameters of simulated records at Saitsama and Ummulong stations for five different models of rupture plane having different positions of nucleation point within the rupture plane.

S.NO.	STATION NAME	GEOGRAPHICAL COORDINATE		ELEVATION (M)	COORDINATE IN RECTANGULAR THREE DIMENSIONAL SYSTEM (IN KM)
		LAT D M	LONG D M		
1.	Baithalangso	25°58'	92°36'	70	(59.2, .25, -27.5)
2.	Dauki	25°12'	92°02'	40	(-36.5, 34.0, 27.5)
3.	Khliehriat	25°21'	92°22'	1180	(.7, 40.5, -28.6)
4.	Nongkhlaw	25°41'	92°38'	900	(-36.2, -33.7, -28.4)
5.	Nongpoh	25°55'	91°53'	560	(-3.0, -40.0, -28.0)
6.	Nonstoin	25°31'	91°16'	1400	(-78.0, -43.7, -28.9)
7.	Panimur	25°40'	92°48'	150	(46.7, 48.1, -28.3)
8.	Pynursla	25°18'	95°55'	1300	(-41.2, 16.7, -28.8)
9.	Saitsama	25°43'	92°23'	900	(23.5, 9.2, -28.4)
10.	Ummmulong	25°31'	92°10'	1300	(-5.5, 13.7, -28.8)
11.	Umrongso	25°31'	92°38'	720	(30.2, 41.5, -28.2)
12.	Umsning	25°44'	91°53'	800	(-24.2, -15.2, -28.3)

Table 8.16 Selected observation points with geographical coordinates, elevation and coordinates in assumed rectangular three dimensional rectangular coordinate system. Geographical coordinates and elevation of stations had been taken from Chandrasekaran and Das (1992b). The origin of the assumed coordinate system is defined by O_M on map. Fig 8.23 shows location of these selected observation points and the assumed three dimensional coordinate system on map.

STATION NAME	BAITH	DAUKI	KHILIKH	NONGKHL	NONGP	NONGST
P_s	121	76	122	66	63	63
T_{s1}	.22	1.4	.36	1.2	.43	.60
T_{s2}	1.3	1.9	1.5	2.3	1.7	1.9
P_v	2.4	1.4	2.5	1.5	1.4	1.4
P_{v1}	.2	.1	.2	.1	.12	.12
T_{area}	3234	2080	3291	1912	2193	2720
R_{s1}	.994	.99	.994	.990	.991	.993
ACF_1	.026	.029	.029	.031	.028	.030
ACF_2	.073	.088	.089	.094	.079	.090
ACF_3	.113	.180	.150	.162	.128	.160
ACF_4	.04	.06	.06	.06	.06	.06
ACF_5	.363	.421	.456	.458	.366	.447
ACF_6	-.694	-.481	-.513	-.404	-.608	-.479
ACF_7	-.555	-.615	-.841	-.603	-.666	-.711
ACF_8	-.694	-.615	-.841	-.603	-.666	-.711
ACF_9	1.044	1.165	.873	1.180	1.072	1.020
ACF_{10}	1.059	1.091	1.00	1.107	1.076	1.094
F_p	9.9	7.8	8.0	7.5	9.1	7.7
F_1	9.9	7.8	8.0	7.5	9.1	7.7
F_2	11.2	9.6	8.5	9.3	9.8	9.0
F_3	11.4	11.2	9.8	10.7	10.7	10.6
F_4	8.3	7.4	7.9	6.6	8.3	7.3
F_5	11.1	8.3	8.3	8.2	9.7	8.4
F_6	11.4	10.7	9.3	10.5	10.4	10.0

Table 8.17 Extracted features from simulated records of Meghalaya earthquake of 10th September, 1986 at various stations. Simulated records at these stations is shown in Fig 8.24 to 8.27.

STATION NAME	PANI	PYNUR	SAIT	UMRAN	UMMUL	UMSING
P _s	114	96	100	116	80	100
T _{st}	.3	.2	.2	.8	1.1	.3
T _d	1.3	1.7	1.5	1.5	1.9	2.0
P _v	2.1	2.3	2.3	2.6	1.5	2.4
P _d	.19	.22	.208	.234	.147	.222
T _{area}	2661	2577	2612	2827	2769	2398
R _{st}	.90	.90	.93	.93	.93	.99
ACF ₁	.028	.030	.030	.030	.028	.030
ACF ₂	.084	.087	.088	.088	.085	.094
ACF ₃	.137	.139	.139	.127	.142	.165
ACF ₄	.06	.06	.06	.06	.06	.06
ACF ₅	.414	.451	.455	.451	.381	.460
ACF ₆	-.580	-.493	-.487	-.466	-.566	-.423
ACF ₇	-.805	-.771	-.764	-.669	-.727	-.645
ACF ₈	-.805	-.771	-.764	-.669	-.727	-.645
ACF ₉	.927	.975	.983	1.124	.997	1.105
ACF ₁₀	1.091	1.080	1.098	1.099	1.076	1.095
F _p	9.7	10.2	9.2	9.5	10.2	7.4
F ₁	8.4	8.3	8.2	7.5	8.3	7.4
F ₂	9.5	9.2	9.1	9.5	9.9	9.1
F ₃	10.2	10.2	10.1	10.9	10.9	10.7
F ₄	8.3	7.6	7.6	7.1	7.9	7.0
F ₅	8.8	8.7	8.9	9.3	9.5	7.9
F ₆	9.9	10.1	9.6	10.3	10.5	10.1

Table 8.18 Extracted features from simulated records of Meghalaya earthquake of 10th September, 1986 at various stations. Simulated records at these stations is shown in Fig 8.24 to 8.27.

CHAPTER 9

APPLICATION OF THE MODELLING TECHNIQUE TO A HYPOTHETICAL EVENT

An application of the modelling technique evolved in the present study is to estimate the likely scenario in terms of strong ground motion for any given site for a future hypothetical earthquake event. This in turn can be used for deciding the possible earthquake resistant design criteria for a given site.

As a case study Tehri region of Uttar Pradesh has been chosen. The reason for choosing this particular area are :

- (a) Tehri (30.4°N , 78.5°E) is 34 km from the epicenter (30.78°N , 78.79°E) of the Uttarkashi earthquake, and lies within the same tectonic regime (MBT, MCT etc.). Tehri lies at an approximate distance of 30 and 20 km from Krol and Main Boundary thrusts, respectively,
- (b) Since Tehri is the site for a large proposed dam it will be interesting to visualise a future hypothetical earthquake scenario in this region and
- (c) Tehri lies within seismic microzone D2 identified on the seismic microzonation map of Tehri Gharhwal region (Joshi, 1989, Sinvhal et al., 1990, 1991). It has part of two major lineaments : the North Almora and Tons Nayar Thrusts within this zone.

9.1 MODELLING OF RUPTURE PLANE ALONG THE NORTH ALMORA THRUST

A hypothetical earthquake of magnitude 6.6 (M_b) i.e., same magnitude as the Uttarkashi earthquake, is assumed to nucleate on the North Almora Thrust. The tectonic map of the Tehri region is shown in Fig 9.1 (Jain, 1987). On this map point 'A' is at a distance of about 19 km southeast of Tehri township where the North Almora Thrust is intersected by two other tectonic lineaments. Point 'A' is assumed to be the surface manifestation of one of the corners of rupture plane for this hypothetical earthquake. Following assumptions are also made for modelling the rupture plane to simulate strong motion records at Tehri :

- (1) Magnitude of hypothetical earthquake is assumed as 6.6 (M_b).
- (2) North Almora Thrust is assumed to be the causative fault for the hypothetical earthquake.
- (3) Point 'A' on this fault is selected as the most likely point at which rupture is initiated. The point A is 19 km southeast of Tehri (Fig 9.1).
- (4) The fault is buried 12 km below point A. Therefore the modelled rupture plane will lie at a depth of 12 km below point A. The Uttarkashi earthquake was also modelled for this depth of burial.
- (5) The rupture is assumed to extend 42 km southwest of point A on the North Almora Thrust. This length is same as was taken for the Uttarkashi earthquake.
- (6) Downward extension of the rupture plane is 29 km. The dip and strike used for this rupture model are 14° and 317° , respectively.
- (7) Five models with this kind of a setup were considered.
- (8) The depths of nucleation points for two models each are 12 and 19 km, while for

one model this depth is equal to 15 km.

- (9) Hypocentral distances for these nucleation points are 19, 33, 57, 63 and 38 km.
- (10) For two models the rupture propagates towards Tehri whereas for other two it is away from Tehri and for one model it propagates uniformly.
- (11) Parameters of modelled rupture plane for five models are :

	Model 1	Model 2	Model 3	Model 4	Model 5
Depth of nucleation point	12 km	19 km	12 km	19 km	15 km
Hypocentral distance	19 km	33 km	57 km	63 km	38 km
Epicentral distance	15 km	28 km	56 km	60 km	36 km
Direction of rupture propagation (w.r.t. Tehri)	Away	Away	Towards	Towards	Center

Using the method discussed in Section 2.2.5, coordinates of Tehri are computed as (-15.0,3.0,-11.2). The various modelling parameters of the rupture plane for this hypothetical earthquake are given in the Table below and the model of the rupture plane is shown in Fig 9.2.

SN	Parameter	Value	S N	Parameter	Value
1	L (Length of the rupture plane)	42 km	5	Depth of rupture plane from surface	12 km
2	D (Downward extension)	29 km	6	V_r (Rupture velocity)	2.6 km/sec
3	δ (Dip)	14°	7	V (velocity of the medium)	5.7 km/sec
4	ϕ (Strike)	317°	8	Total number of elements	1218

9.1.1 SIMULATION OF STRONG MOTION RECORDS AT TEHRI

By assuming five nucleation points within the rupture plane five records are simulated at Tehri, Fig 9.3. Table 9.1 gives the values of twenty four extracted parameters for the five simulated records. The peak acceleration for these five simulated records are given in the following table :

Coordinates of the nucleation point within the rupture plane in km	Peak acceleration from simulated record (cm/sec ²)
(0.0,0.0,0.0)	273
(0.0,27.0,6.7)	341
(41.0,0.0,0.0)	360
(41.0,27.1,6.7)	446
(20.0,12.6,3.1)	405

Peak acceleration obtained for the five simulated records at Tehri varies between 273 and 446 cm/sec². This strongly suggests that the peak acceleration at Tehri will be atleast 273 cm/sec² and can go upto as much as 446 cm/sec², depending upon: the position of nucleation point, and the direction of propagation of rupture within the rupture plane. The maximum peak acceleration of 446 cm/sec² is observed when the nucleation point lies at the southernmost lower corner of the rupture plane i.e., of all five nucleation points this lies farthest from Tehri. This could be due to directivity, whereby maximum ground motion at any observation point is observed when rupture front moves towards it. The value of peak acceleration obtained from simulated record depends on the position of the nucleation point within the rupture plane and is observed to be the highest when the rupture propagates towards Tehri. The minimum peak acceleration obtained from the five simulated records is 273 cm/sec² and is observed

when nucleation point lies at the closest northern corner of rupture plane. For this model the direction of propagation of rupture is away from Tehri. Therefore hypocentral distance cannot be taken as a diagnostic feature in computing peak accelerations, as it depends strongly on the direction of propagation of rupture.

The validity of simulated records at Tehri can be checked only by comparison of its twenty four extracted parameters shown in Table 9.1 with strong motion records. However, field records for Tehri are not available for the present study and hence this comparison could not be attempted.

9.2 PEAK ACCELERATION BY ATTENUATION RELATIONS

Peak acceleration at any given site is usually computed by using attenuation relations where hypocentral distance plays a very important role, and has been given by various workers such as Abrahamson and Litehiser (1989) and Mcguire (1977). The relation given by Abrahamson and Litehiser (1989) for computing horizontal peak acceleration is :

$$\text{Log}_{10} a_H(g) = -.62 + 0.177M - 0.982 \log_{10}(R + e^{284M}) + .132F - .0008ER \quad (9.1)$$

Where,

M = Magnitude of the earthquake

R = Hypocentral distance

$a_H(g)$ = Horizontal peak acceleration

E is 1 for interplate event and 0 for intraplate event. F is 1 for reverse or reverse oblique events and 0 otherwise. For Tehri region, the local conditions favour using the

values $E = 1$ and $F = 1$ and hence the same are used for calculating the accelerations by this expression.

The attenuation relation given by McGuire (1977) is given as:

$$P_a = (472) 10^{-.278M} (R + 25)^{-1.301} \quad (9.2)$$

Where, M is the magnitude of the earthquake and R is the hypocentral distance.

The following table gives peak accelerations computed from attenuation relations given in expression 9.1 and 9.2 for different positions of nucleation point within the rupture plane.

COORDINATES OF NUCLEATION POINT WITHIN THE RUPTURE PLANE IN KM	HYPOCENTRAL DISTANCE (KM)	PEAK ACCELERATION (P_a) CALCULATED BY EXPRESSION 9.1 IN (CM/SEC ²)	PEAK ACCELERATION (P_a) CALCULATED BY EXPRESSION 9.2 IN (CM/SEC ²)
(0.0,0.0,0.0)	19.0	188	235
(0.0,27.1,6.7)	33.0	119	164
(41.0,0.0,0.0)	57.0	71	104
(41.0,27.1,6.7)	63.0	64	95
(20.0,12.6,3.1)	38.0	105	147

The peak acceleration obtained by expression 9.1 varies between 64 and 188 cm/sec², while for expression 9.2 it varies between 95 and 235 cm/sec². Maximum peak acceleration of 188 and 235 cm/sec² is obtained by expressions 9.1 and 9.2,

respectively. Minimum peak acceleration of 64 and 95 cm/sec^2 is obtained by expression 9.1 and 9.2, respectively. Value of peak acceleration obtained by these expressions (9.1 and 9.2) is inversely proportional to the hypocentral distance and is minimum when the hypocentral distance is maximum, i.e., 63 km. These attenuation relations do not take into account the direction of propagation of rupture. Hence peak acceleration computed from such formulae should be used with caution where propagation of rupture plays an important role.

9.3 PEAK ACCELERATION BY SHIFTING ISOACCELERATION CONTOURS

A preliminary estimation of peak acceleration at Tehri can also be made by using acceleration contours of an earthquake which has occurred in a similar tectonic setting. For an earthquake in Tehri region with the same magnitude as the Uttarkashi earthquake of 20th Oct, 1991, the source dimension can also be assumed to be the same. Since the two regions are separated by a distance of 34 km and are associated with the Main Central Thrust and Main Boundary Thrust, therefore Tehri can be assumed to have a similar tectonic setup as Uttarkashi region. For this reason the point O (Fig 7.8) on the isoacceleration map prepared for the Uttarkashi earthquake of 20th Oct, 1991 is superposed at point A on the tectonic map of Tehri (Fig 9.4). At point A the North Almora Thrust is intersected by two other lineaments. By interpolation of the isoacceleration contours the peak acceleration at Tehri is computed as 278 cm/sec^2 . This value is obtained at an epicentral distance of 19 km. If point O is coincided with Tehri then the peak acceleration at Tehri will be maximum and larger than 300 cm/sec^2 .

9.4 SUMMARY

This study indicates that peak acceleration is a very sensitive parameter and depends on the direction of propagation of rupture within the causative fault. For this reason the strong motion records obtained during an earthquake need to be quantified in terms of robust and consistent parameters for earthquake resistant design of structures. The methodology evolved for the modelling of rupture plane along an identified fault can be used for estimating the scenario in the event of a future hypothetical earthquake in any area, and thus can help in estimation of maximum possible peak acceleration and in drawing mitigation plans for an area.

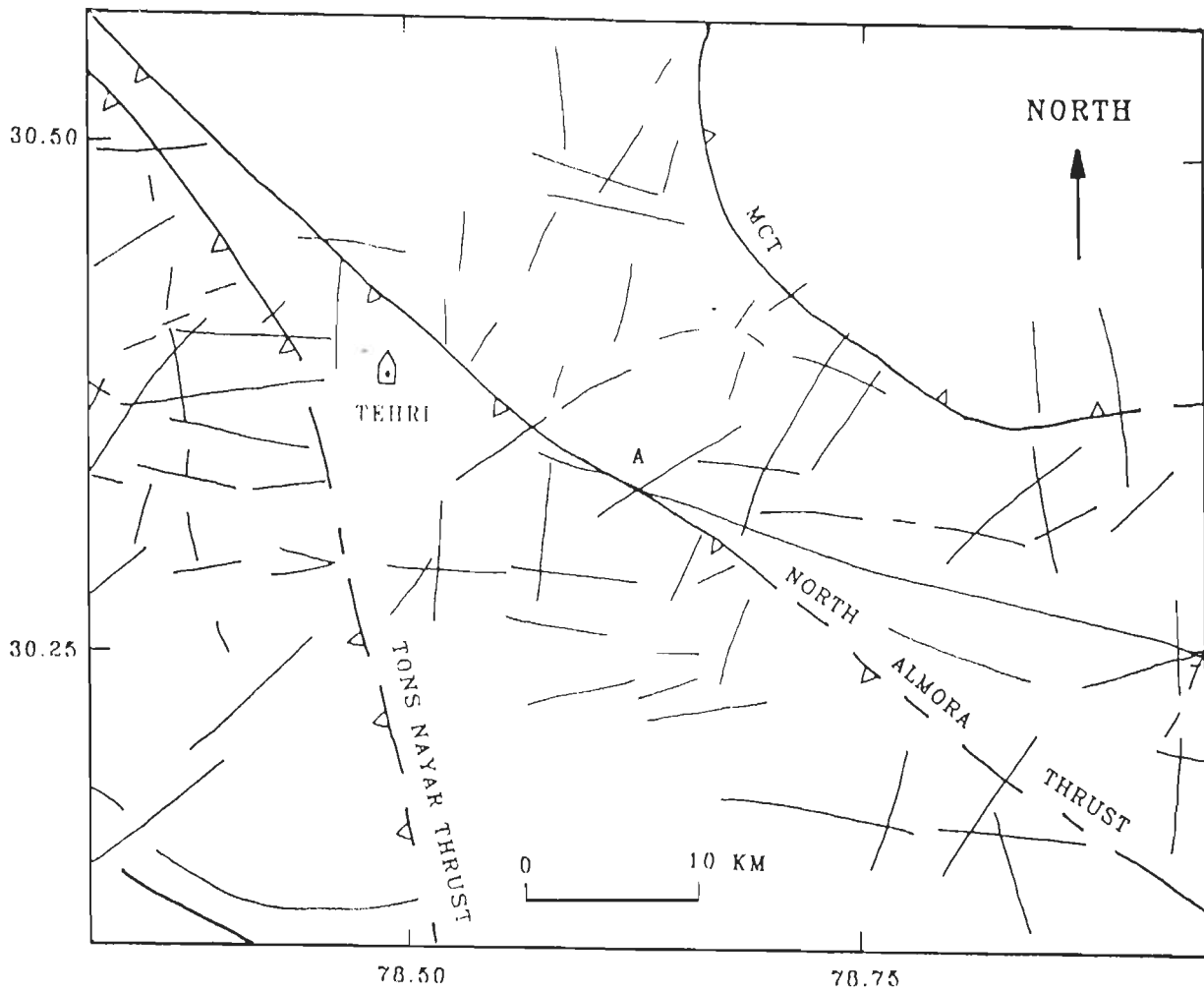


Fig 9.1 Tectonics of the region around Tehri (Jain, 1987) and the location of identified most probable causative fault on map.

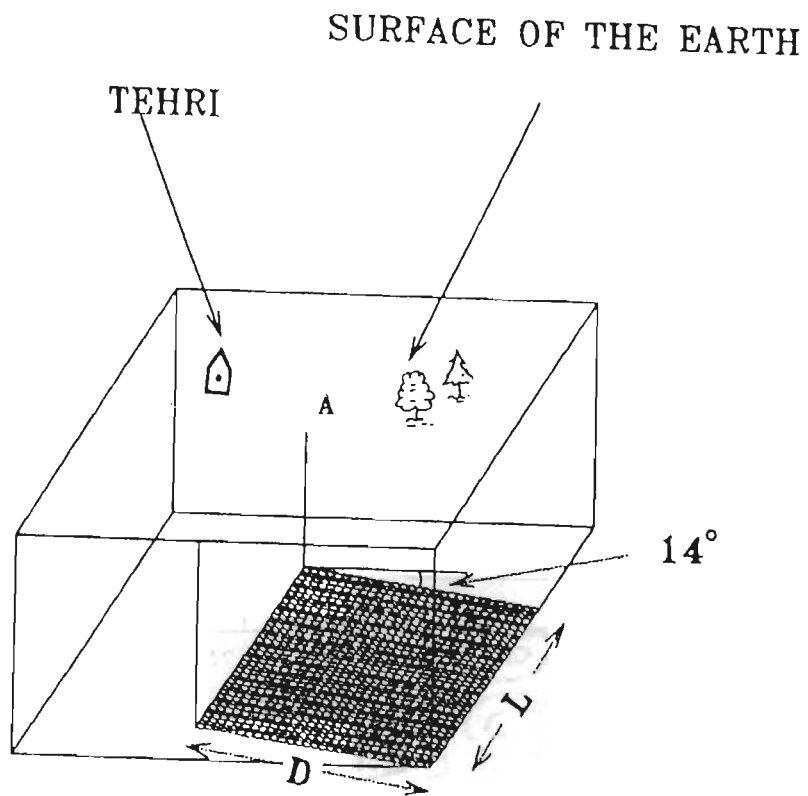


Fig 9.2 Model of rupture plane used for simulating acceleration records at Tehri.

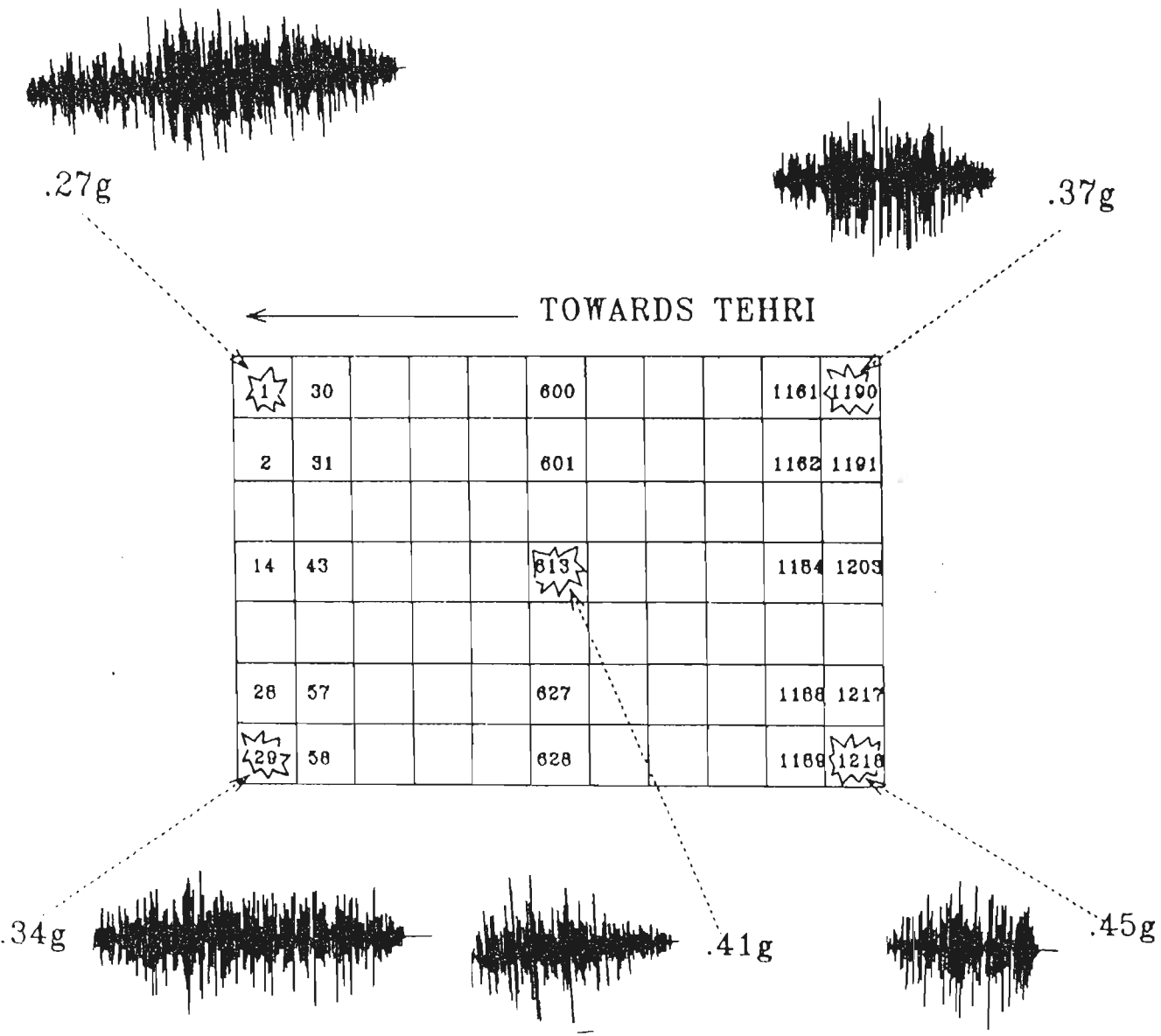


Fig 9.3 Rupture model and obtained peak acceleration from simulated acceleration records. The peak acceleration is obtained from simulated records after assuming various elements within the rupture plane as starting point of rupture. The center of element numbered as '1' is the origin of assumed coordinate system.

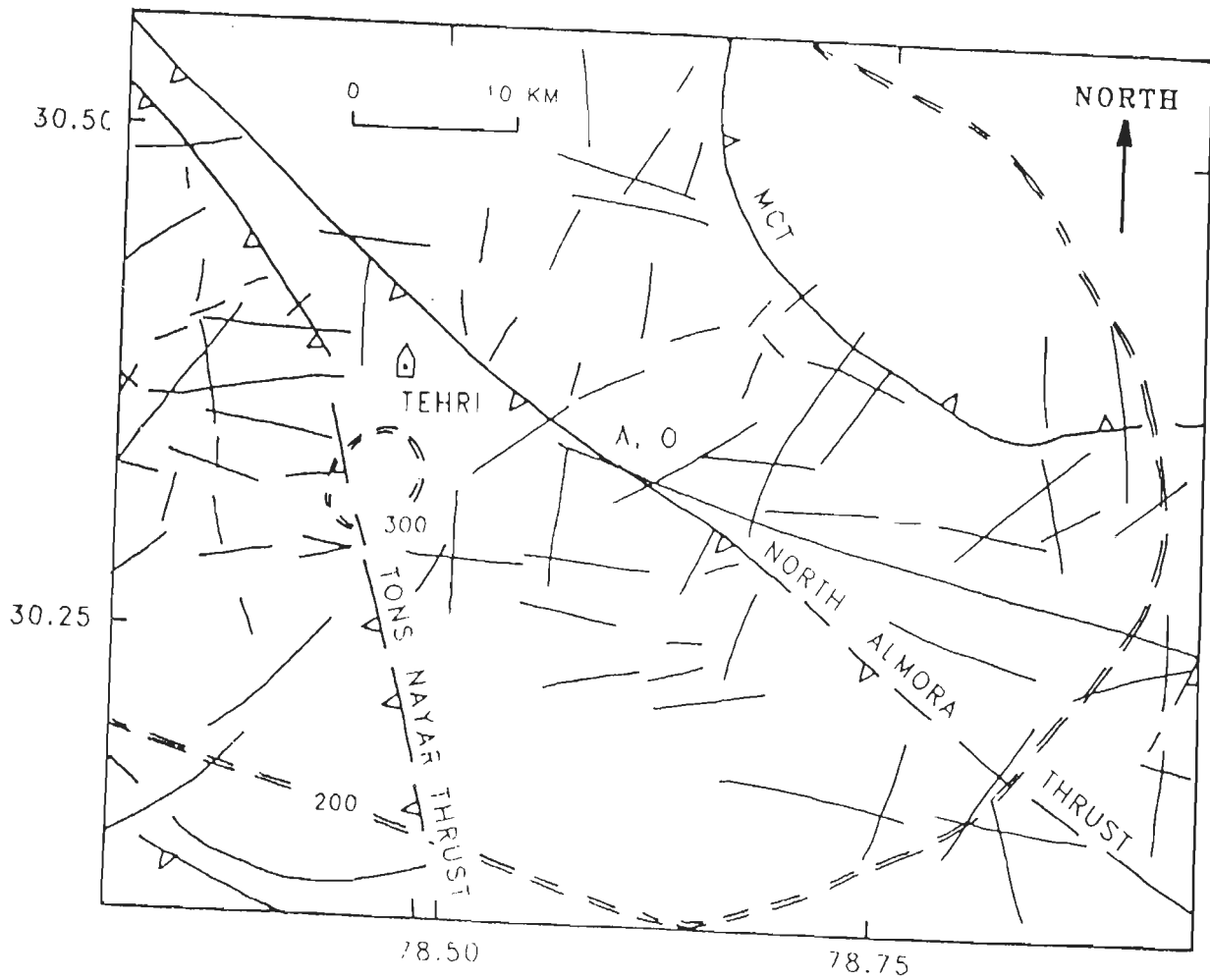


Fig 9.4 Isoacceleration contours of Uttarkashi earthquake of 20th Oct, 1991 shifted at Tehri. The tectonics of the region is taken after Jain (1987) shown in Fig 7.4. The isoacceleration contour map for the Uttarkashi earthquake is shown in Fig 7.8. The point of intersection of two or more faults or lineaments in the epicentral region of Uttarkashi is O and is shown in Fig 7.9.

Coordinates of nucleation point	(0,0,0)	(0,27.1,6.7)	(41,0,0)	(41,27.1,6.7)	(20,12.6,3.1)
Parameter					
P_a	273	341	360	446	405
T_a	19.8	16.8	9.8	8.3	9.7
T_b	8.8	4.0	4.8	5.8	3.3
P_v	8.5	9.6	9.8	12.0	13.0
P_d	.266	.267	.29	.36	.42
T_{max}	52373	48583	38103	31162	33426
R_a	1.00	1.00	.99	.98	1.00
ACF_1	.031	.032	.027	.026	.026
ACF_2	.092	.093	.085	.077	.076
ACF_3	.159	.246	.159	.116	.132
ACF_4	.048	.048	.040	.040	.040
ACF_5	.288	.289	.294	.275	.261
ACF_6	-.649	-.633	-.608	-.621	-.646
ACF_7	-.512	-.491	-.502	-.431	-.435
ACF_8	-.644	-.633	-.608	-.621	-.646
ACF_9	1.109	1.147	1.111	1.212	1.167
ACF_{10}	1.00	1.046	1.067	1.053	1.057
F_p	9.2	9.9	8.2	10.6	10.3
F_1	9.2	9.2	8.2	9.9	9.3
F_2	10.5	10.4	10.5	10.7	10.5
F_3	12.4	12.6	13.3	13.0	13.2
F_4	8.3	7.7	7.8	7.1	8.3
F_5	10.2	9.9	9.1	10.6	10.2
F_6	12.0	12.2	12.0	11.4	12.2

Table 9.1 Features extracted from simulated strong motion records at Tehri station for a hypothetical earthquake. Records are simulated for five different positions of nucleation point within the rupture plane.

CHAPTER 10

CONCLUSIONS

In the present work three earthquakes viz., the Dharamsala earthquake of 26th April, 1986, the Uttarkashi earthquake of 20th Oct, 1991 and the Meghalaya earthquake of 10th Sept, 1986 were studied. The most probable causative faults for these three earthquakes were identified using the available data and rupture plane for these earthquakes were modelled to simulate strong ground motion data at few selected observation points where actual field records for these earthquakes were available. Simulated records were compared with field records to check the efficacy of the model and the approach. The match between the extracted parameters of the simulated and observed records suggests that the approach is valid and the models are acceptable. The various outcomes of the present study are summarised below :

(1) IDENTIFICATION OF THE MOST PROBABLE CAUSATIVE FAULT FOR MODELLING OF RUPTURE PLANE

The identification of the most probable causative fault plays a significant role in locating the rupture plane. In the present study the most probable causative faults were identified for three earthquakes. The data used include tectonic map, acceleration data from strong motion records, isoseismal map, fault plane solution, depth section and the location of aftershocks map. A fault was assumed to be relatively weak where it was intersected by another tectonic lineament or fault and the rupture plane was assumed

to be associated with the intersection. For modelling the rupture along the identified probable causative fault the computer software developed models a rupture that propagates radially outwards from an assumed nucleation point.

(2) SIMULATION OF STRONG MOTION RECORDS

Seven models were conceptualised for each of the Uttarkashi and the Meghalaya earthquakes and nine for the Dharamsala earthquake. Strong motion records were simulated through a computer program developed on PC AT (486). This software can simulate strong motion records at any observation point for a given geometry of rupture propagation. Strong motion records were simulated at two stations which were on different sides and closest to the surface manifestation of the identified fault. A visual study of the simulated records shows that peak acceleration is a very sensitive parameter and is vulnerable to : propagation of the rupture within the identified fault, dip, strike and location of the fault on the map. Since peak acceleration is a very important criterion which is taken for design of earthquake resistant structures therefore, these source conditions become vital when this parameter is to be assigned. Therefore, this sensitive and single parameter is not enough to be considered on its own for design purposes. For this reason strong motion records need to be quantified and more robust and consistent parameters are needed for design.

(3) COMPARISON OF EXTRACTED PARAMETERS FROM STRONG MOTION RECORDS

It is easier to select or reject any adopted model of the rupture plane by comparing the value of extracted features for simulated and field records. Twenty four

different parameters were identified for this purpose. Among these 17 are in time domain and 7 in frequency domain and these were extracted via two different computer programs developed. Out of these twenty four variables three hold promise. These variables are (i) R_{at} : Ratio of the area covered by acceleration record on both side of time axis; (ii) ACF_{10} : Ratio of area covered by the autocorrelation function of acceleration record on both side of abscissa and (iii) F_3 : Frequency at which 75th percentile of power occurs. Value of parameter R_{at} extracted from the synthetic record is more than 80% of its value extracted from field record at all stations for Dharamsala and Uttarkashi earthquakes, while the same is true for the Meghalaya earthquake at eleven stations out of twelve. Value of parameter ACF_{10} extracted from the synthetic record is more than 80% of its value extracted from field record at all stations for Dharamsala and Uttarkashi earthquakes, while for the Meghalaya earthquake this statement holds good at eleven stations out of twelve. Value of parameter F_3 extracted from the synthetic record is more than 80% of its value extracted from field record at two stations for Dharamsala and Uttarkashi earthquakes, while for the Meghalaya earthquake this is the case at eight stations out of twelve. This analysis brings out that three variables R_{at} , ACF_{10} and F_3 should also be considered in future for evolving strategies for earthquake resistant design of structures, instead of only the peak ground acceleration.

The study is applied for estimating a likely scenario in term of strong ground motion for techno economically important Tehri region for a hypothetical earthquake equivalent to the Uttarkashi earthquake of 20th Oct, 1991, i.e, magnitude 6.6 (M_b). Five models were used for simulating strong ground motion records and twenty four features were extracted from these records. This study indicates that peak acceleration (P_a) is a very sensitive parameter and should not be used as a sole criteria for design of

earthquake resistant structures. Application of present work brings out that the approach hold promise and there is immense scope for evolving better strategies for simulating strong ground motion data.

10.1 FUTURE WORK

As it is not possible to predict an earthquake hence it is difficult to install strong motion instruments in the vicinity of a future causative fault. However, wherever strong motion arrays are in operation it will be worthwhile to have a micro earthquake network as well. Also, an attempt should be made to gather as much data as possible of aftershock activities by installing an array of sensitive portable seismographs just after each major seismic event so that the aftershock zone is properly identified and delineated. This will help in an improved estimation of the ruptured area and the possible direction of rupture of the main event. Detailed tectonic maps should be made for such regions. Such maps will help in the identification of areas where future shocks can be expected. Higher density of instrumental coverage will lead to a better determination of source parameters. In modelling the rupture plane for simulating strong motion records following factors, if included, will give an improved quality of synthetic data : multiple nucleation points, non uniform release of energy by each element, layering of the earth, site effects including topography, attenuation, diffraction, divergence, complex transmission paths, noise, instrumental characteristics, effects of local geology of the region and source wavelet. This will obviously lead to a better understanding of the rupture at the source.

REFERENCES

- Abe, M., Kikuchi, T. and Sato, T., 1992,** Computer Simulation of Wave Propagation Characteristics Near a Source Using a Framework, Proceedings of Tenth World Conference on Earthquake Engineering, 19-24 July, 1992, Madrid, Spain, A.A. Balkema, pp. 663-668.
- Abrahamson, N.A., 1985,** Estimation of Seismic Wave Coherency and Rupture Velocity Using the SMART-1 Strong Motion Array Recordings, UCB/EERC-85/02, 127p.
- Abrahamson, N. A., and Litehiser, J.J., 1989,** Attenuation of Vertical Peak Acceleration, BSSA, No. 3, Vol. 79, pp. 549 - 580.
- Abrahamson, N.A., Somerville, P.G., and Cornell, C.A., 1990,** Goodness of Fit for Numerical Strong Motion Simulations and Uncertainty in Numerical Strong Motion Predictions, Proc. 4th US National Conference on Earthquake Engineering, Palm Springs, 1, pp. 317-326.
- Agarwal, N.C. and Kumar, G., 1973,** Geology of Upper Bhagirathi and Yamuna Valleys, Uttarkashi District, Kumaun Himalaya, Himalayan Geology, Vol. 3, Ed. A.G. Jhingaran and K.S. Valdiya, WIHG, pp. 1-23.

- Araya, R. and Kiureghian, A.D., 1988, Seismic Hazard Analysis: Improved Models, Uncertainties and Sensitivities, UCB/EERC- 90/11, 155p.**
- Arya, A. S., Lavania, B.V.K., Gupta, S.P. and Kumar, A., 1986, Dharamsala Earthquake of 26th April, 1986, Proceedings of 8th Symposium on Earthquake Engineering, pp. 73-91.**
- Balakrishnan, T.S. and S.K. Choudhury, 1976, Geophysical studies of Himalayan Foothills of Punjab and Himachal Pradesh and Their Geological Correlation With Adjoining Punjab Plains, Himalayan Geology Seminar, Geological Survey of India Miscellaneous Publications No. 41, pp. 175-183.**
- Bath, M., 1974, Spectral Analysis in Geophysics, Elsevier Scientific Publication Co., New York, 362p.**
- Bolt, B.A., C.H.Loh, J.Penzien, Y.B. Tsai, Y.T. Yeh, 1982, Preliminary Report on the SMART-1 Strong Motion Array in Taiwan, UCB/EERC-82/13, Earthquake Engineering Research Center, University of California, 200p.**
- Brune, J.N., 1970, Tectonic Stress and the Spectra of Seismic Shear Waves from Earthquakes, J. Geophys. Res., V. 75, pp. 4997-5009.**
- Chandra, U., 1977, Earthquakes of Peninsular India - A seismotectonic study, BSSA, Vol. 67, No. 5, pp. 1387 - 1414.**

Chandra, U., 1978, Seismicity, Earthquake Mechanism and Tectonics along the Himalayan Mountain Range and Vicinity, *Phy. Earth and Planet. Inter.*, V.16, pp. 109 -131.

Chandra, B., Kumar, A., and Bansal, M.K., 1992, A Study of Strong Motion Data Obtained During Uttarkashi Earthquake of 20th October, 1991 From INSMIN Network, 1992, (Abstract Published) Synthesis of the Uttarkashi Earthquake Data, 20th Oct, 1991, and Seismotectonics of Garhwal - Kumaon Himalaya, 12-13 Nov, 1992, New Delhi, pp. 29-30.

Chadha, R.K., 1992, The Causative Fault of the Uttarkashi Earthquake of October 20, 1991, Synthesis of the Uttarkashi Earthquake Data, 20th October, 1991, and Seismotectonics of Garhwal-Kumaon Himalaya, 12-13, November, 1992, New Delhi (Abstract Published), pp. 20 -22.

Chandrasekaran, A. R., 1988a, Strong Motion Array in Himachal Pradesh, India, *Earthquake Engineering Studies*, EQ 88-09, 26p.

Chandrasekaran, A. R. , 1988b, Analysis of Strong Motion Accelerogram of Dharamsala Earthquake of 26th April, 1986, *Earthquake Engineering Studies*, EQ 88-10, 90p.

Chandrasekaran, A. R., Prakash, V. and Das, J.D., 1988, Analysis of Strong Motion Accelerograms of Meghalaya Earthquake of 10th Sept, 1986, India, EQ 88-12, Department of Earthquake Engineering, University of Roorkee, India, 119p.

- Chandrasekaran, A.R. and Das, J.D., 1990a**, Characteristics of Strong Motion Records of N.E. India, Proceedings Ninth Symposium on Earthquake Engineering, Vol. 1, pp. 2-23 to 2-32.
- Chandrasekaran, A.R. and Das, J.D., 1990b**, Characteristics of Recent Recorded Events, BISET, Vol. 27, No.1, pp. 1-66.
- Chandrasekaran, A.R. and Das, J.D., 1991**, Analysis of Strong Ground Motion Accelerograms of Uttarkashi Earthquake of October 20, 1991, EQ 91-10, Department of earthquake Engineering, University of Roorkee, India.
- Chandrasekaran, A.R., and Das, J.D., 1992a**, Strong Motion Array in India and Analysis of Data from Shillong Array, Current Science, Vol. 62, No. 1 and 2, pp. 233-251.
- Chandrasekaran, A.R. and Das, J.D., 1992b**, Strong Motion Array in Indian and Characteristics of Recent Recorded Events, Himalayan Seismicity, G.D. Gupta (Ed.), Geological Society of India, pp. 81-122.
- Chandrasekaran, A.R. and Das, J.D., 1992c**, Analysis of Strong Ground Motion Accelerograms of Uttarkashi Earthquake of October 20, 1991, B.I.S.E.T., No.315, Vol.29, pp. 35-55.
- Chaudhury, H.M. and Srivastava, H.N., 1977**, The Kinnaur Earthquake of January 19, 1975 and its Aftershocks, 6WCEE, Vol.1, pp. 242-248.

- Claerbout, J. F., 1976, Fundamentals of geophysical data processing - with applications to Petroleum Prospecting, McGraw - Hill International Series in the Earth and Planetary Science, 274p.**
- Dan, K., Watanabe, T., Tanaka, T. and Sato, R., 1990, Stability of Earthquake Ground Motion Synthesised by Using Different Small Records as Empirical Green's Function, BSSA, V. 80, No. 6, pp. 1433-1455.**
- Das, J.D. and Chandrasekaran, A.R., 1993, Determination of Epicenter and Comparison of Some Formulae with Observed Data of Acceleration from Two Events in Himalaya, Journal Geological Society of India, Vol. 41, pp. 417-430.**
- Dasgupta, S., Mukhopadhyay, M. and Nandy, D.R., 1987, Active Transverse Features in The Central Portion of the Himalaya, Tectonophysics, Vol. 136, No.2. pp. 255 - 264.**
- Daut, C.R., Braile, L.W., Nowack, R.L. and Chiang, C.S., 1989, A Comparison of Finite Difference and Fourier Method of Calculations of Synthetic Seismogram, BSSA, Vol. 70, No. 4, pp. 1210-1230.**
- DHA NEWS, 1993, Why Earthquakes ?, pp. 42, Jan/Feb issue.**
- Dziewonski, A.M., Ekstrom, G. and Salganik, M.P., 1992, Centroid Moment Tensor Solution for October Dec 1991, Physics of Earth and Planetary Interiors, Vol. 74, Nos. 3-4, pp. 89-100.**

- Eremenko, N.A., and Negi, B.S., 1968, Tectonic Map of India, Oil and Natural Gas Commission, Dehradun, 1:2,000,000 scale.
- Fujiwara, T., Sato, T., Kubo, T., Murakami, H.O., 1989, Reconnaissance Report on The Nepal India Border Region, No. B- 63-4, Research Report on Natural Disasters, Supported by the Japanese Ministry of Education, Science and Culture (Grant no. 63115047) Japanese Group for the study of Natural Disaster Science, 121p.
- Fukuyama, E. and Irikura, K., 1986, Rupture Process of the 1983 Japan Sea (Akita-Oki) Earthquake using a waveform inversion method, BSSA, Vol. 76, No.6, pp. 1623-1640.
- Gupta, S.K., Kumar, S., Jalote., P.M., Sharan, R.B. and Relan, A.K., 1986, A Macroseismic study of Dharamsala earthquake of 26th April, 1986, 8th Symposium on Earthquake Engineering. Roorkee, December 29-31, 1986. Vol.1, pp. 31-38.
- Gupta, R.P, Saraf, A.K., Saxena, P. and Chander, R., 1994, IRS Detection of Surface Effects of the Uttarkashi Earthquake of 20th October, 1991, Himalaya, Int. J. Remote Sensing (Submitted for Publication).
- Gutenberg, B. and C.F. Richter, 1956, Magnitude and Energy of Earthquakes. Ann. Geofis. V.9, pp. 1-15.

Hadley, D.M. and Helmberger, D.V., 1980, Simulation of Strong Ground Motion, BSSA, Vol. 70, pp. 617-630.

Hartzell, S., 1978, Earthquake Aftershocks as Green's Function, Geophys. Res. Letters, V 5, pp. 1-24.

Hartzell, S.H., and Helmberger, D. V., 1982. Strong Motion Modelling of Imperial Valley Earthquake of 1979, BSSA, v 72, pp. 571-796.

Haskell, N.A., 1964, Total Energy and Energy Spectral Density of Elastic Wave Radiation From Propagating Fault, BSSA, 54, pp. 1811-41.

Housner, G.W., 1970, Strong Ground Motion, Earthquake Engineering, Englewood Cliff: Prentice Hall, 518p.

Housner, G.W. and Jennings, P.C., 1964, Generation of Artificial Earthquakes, J. Engineering Mechanics Div., Proceedings of the American Society of Civil Engineers, pp. 113 - 149.

Howell, JR., B. F., 1959, Introduction to Geophysics, McGraw - Hill Book Company, Inc., New York, 399p.

Irikura, K., 1983, Semi Empirical Estimation of Strong Ground Motions During Large Earthquakes, Disaster Prev. Res. Inst. Kyoto Univ. Bull., 33, pp. 63-104.

- Irikura, K., 1986**, Prediction of Strong Acceleration Motions Using Empirical Green's Function, Proc. 7th Japan Earthquake Engineering Symp., pp. 151-156.
- Irikura, K. and Muramatsu, I., 1982**, Synthesis of Strong Ground Motions from Large Earthquakes Using Observed Seismogram of Small Events, Proc. 3rd Inter. Earthq. Microzonation Conf., Seattle, pp. 447-458.
- Jain, A.K., 1987**, Kinematics of Transverse Regional Tectonics and Holocene Stress Field in the Garhwal Himalayas, Journal of Geological Society of India, Vol. 30, No.3, pp. 160-186.
- Jain, S.K., Singh, V.N. and Chander, R., 1992**, On Estimation of Local Magnitude (M_L) of the Dharamsala Earthquake of 1986 Using Strong Motion Data, BISET, Vol. 29, No. 2, pp. 29-36.
- Joshi, A., 1990**, Strong Motion Modelling of Earthquake Source, M.Tech Dissertation (Unpublished), University of Roorkee, Roorkee, 114p.
- Joshi, G., 1989**, A Pattern Recognition Technique for Earthquake Prediction Using Computer Aided Cartography, M.Tech Dissertation (Unpublished), University of Roorkee, Roorkee, 60p.
- Kamble, V.P., 1992a**, Parameters of Uttarkashi earthquake of October 20th, 1991, (Abstract) "Synthesis of the Uttarkashi Earthquake Data, 20th October, 1991, and Seismotectonics of Garhwal-Kumaon Himalaya", 12-13 Nov, 1992, New Delhi, pp. 25.

- Kamble, V.P., 1992b**, Aftershock Sequence of Uttarkashi Earthquake of October 20th, 1991, (Abstract Published) Synthesis of the Uttarkashi Earthquake Data, 20th Oct, 1991, and Scismotectonics of Garhwal - Kumaon Himalaya, 12-13 Nov, 1992, New Delhi, pp. 14.
- Kamiyama, M., 1988**, Prediction of Strong Ground Motions by a Simplified Synthesis Method of Accelerograms, Proceedings of Ninth World Conference on Earthquake Engineering, August 2/9, Tokyo-Kyoto, Japan (Vol.II).
- Kanamori, H. and Anderson, D.L., 1975**, Theoretical Basis of Some Empirical Relations in Seismology, BSSA, Vol. 65, pp. 1073- 1095.
- Kanamori, H., 1979**, A Semi Empirical Approach to Prediction of Long Period Ground Motion From Great Earthquakes, BSSA, Vol. 69, pp. 1654-1670.
- Kasahara, K., 1981**, Earthquake Mechanics, Cambridge University Press, Cambridge Earth Science Series, 248p.
- Kayal, J.R., 1994**, Long Term Seismicity, Foreshocks and Aftershocks of the Uttarkashi Earthquake - October 20, 1991 at Garhwal Himalaya, Group discussion on 'Geological Hazards in the Himalayan Region : Assessment and Mitigation, 10-12 March, 1994, Dehra Dun, pp. 17-18.
- Kayal, J.R., Kamble, V.P. and Rastogi, B.K., 1992**, Aftershock Sequence of Uttarkashi Earthquake of October 20, 1991, Uttarkashi Earthquake October 20, 1991, Geological Survey of India Special Publication (No. 30), pp. 203-217.

- Kayal, J.R., Gosh, B., Chakraborty, P. and De, Reena, 1993,** Aftershock study of the October 20, 1991 Earthquake at Garhwal Himalaya by a Temporary MEQ network, Jour. Geol. Soc. India (Submitted).
- Kawase, H. and Aki, K., 1989,** A Study on the Response of a Soft Basin For Incident S, P and Rayleigh Waves with Special Reference to the Long Duration Observed in Mexico City, BSSA, Vol. 79, No. 5, pp. 1361-1382.
- Khattri, K. N., 1994,** Numerical Simulation of Earthquake Strong Ground Motion : Implications for Seismic Hazard Assessment, Group discussion on 'Geological Hazards in the Himalayan Region : Assessment and Mitigation, 10-12 March, 1994, Dehra Dun, pp. 19 -21.
- Knopoff, L. and Gilbert, F., 1959,** Radiation from a Strike Slip Fault, BSSA, Vol. 49, pp. 163-78.
- Kumar, S. and Mahajan, A.K., 1990,** Study of Intensities of 26th April 1986 Dharamsala Earthquake (Himachal Pradesh) and Associated Tectonics, Journ Geol Soci of India , V. 5, no.2, pp. 213-219.
- Kumar, S. and Mahajan, A.K., 1991,** Dharamsala Seismotectonic Zone - Neotectonics and State of Stress in Area, Journal of Himalayan Geology, Vol. 2(1), 1991, pp. 53-57.
- Kumar, S. and Mahajan, A.K., 1994,** The Uttarkashi Earthquake of 20th October, 1991 : Field Observations, Terra Nova, 6, pp. 95 - 99.

- Li, X., Bielak, J. and Ghattas, O., 1992,** Three Dimensional Earthquake Site Response on a CM-2, Proceedings of Tenth World Conference on Earthquake Engineering, 19-24 July, 1992, Madrid, Spain, A.A. Balkema, pp. 959-964.
- Lipschutz, S., and Poe, A., 1982,** Theory and Problems of Programming with Fortran Including Structured Fortran, Schaum's Outline Series, McGraw - Hill Book Company, Singapore, pp. 314.
- Makaris, D.I., Stavrakakis, G.N. and Drakopoulos, J.C., 1992,** Expected Ground Motion at a Site Based on Hypothetical Fault Models, Earthquake Engineering, Tenth World Conference, Vol 2, Balkema, Rotterdam, pp. 703 - 708.
- Mcguire, R.K., 1977,** Seismic Design Spectra and mapping Procedures Using Hazard Analysis Based Directly on Oscillator Response, Earthquake Engineering and Structural Dynamics, Vol.5, pp. 211 - 234.
- Menahem, A. B. and Singh, S.J., 1981,** Seismic Waves and Sources, Springer Verlag New York Inc., 1108p.
- Mendoza, C. and Hartzell, S., 1988,** Inversion for Slip Distribution Using Teleseismic P waveforms, North Palm Springs, Borah Peak, and Michoacan Earthquakes, BSSA, Vol. 78, No. 3, pp. 1092 - 1111.
- Middlemiss, C. S., 1910 (reprint 1981),** The Kangra Earthquake of 4th April 1905, Memoirs of G.S.I., Vol. XXXVIII, 409p.

- Midorikawa, S., 1993**, Semi Empirical Estimation of Peak Ground Acceleration From Large Earthquakes, *Tectonophysics*, V 218, pp. 287-295.
- Midorikawa, S. and Kobayashi, H., 1980**, Isoseismal map in near field With Regard to Fault Rupture and Site Geological Conditions, *7WCEE*, Vol. 2, Instabul, Turkey, pp. 259 - 262.
- Mikumo, T. and Miyatake, T., 1978**, Dynamical Rupture Process on a Three Dimensional Fault With Non Uniform Frictions and Near Field Seismic Waves, *Geophys. J. R. Astr. Soc.*, 54, pp. 417-438.
- Minami, T. and Ohori, M., 1992**, Relatively Long Period Ground Motion Expected in Tokyo Bay Region, *Proceedings of Tenth World Conference on Earthquake Engineering*, 19-24 July, 1992, Madrid, Spain, A.A. Balkema, pp. 599-601.
- Molnar, P., 1990**, A Review of the Seismicity and Rates of Active Underthrusting, *Journal of Himalayan Geology*, Vol. 1, No. 2, pp. 131-154.
- Molnar, P. and Tapponier, P., 1975**, Cenozoic Tectonics of Asia Effects of a Continental Collision, *Science*, v. 489, pp. 419 - 426.
- Naeim, F., 1989**, *The Seismic Design Handbook*, Van Nostrand Reinhold, 450p.
- Narula, P. L., and Shome, S.K., 1992**, Macro seismic Studies of Recent Earthquakes in North-West Himalaya- A Review, *Current Science*, Vol.62, pp. 24-34.

- Narula, P.L., Shome, S.K., Kumar, S. and Pande, P., 1992,** Damage Patterns and Delineation of Isoseismals of Uttarkashi Earthquake of 20th October, 1991, (Abstract Published) Synthesis of the Uttarkashi Earthquake Data, 20th Oct, 1991, and Seismotectonics of Garhwal - Kumaon Himalaya, Sponsored by D.S.T., 12-13 Nov, 1992, New Delhi, pp. 25-26.
- Newmark, N.M. and Rosenblueth, E., 1971,** Fundamentals of Earthquake Engineering, Prentice Hall Inc. Englewood Cliffs, N.J., 640p.
- Ni, J. and Barazangi, M., 1984,** Seismotectonics of the Himalayan Collision Zone : Geometry of the Underthrusting Indian Plate beneath the Himalaya, J. Geophys. Res., V. 89, pp. 1147-1163.
- Oliveira, C. S., 1978,** Seismic Risk Studies for San Francisco and for Greater San Francisco Bay Area, UCB/EERC-78/16, Earthquake Engineering Research Center, College of Engineering, University of California, Berkeley, California.
- Oppenheim, A.V., and Schafer, R.W., 1988,** Digital Signal Processing, Prentice Hall International, Inc. Englewood Cliffs, p 585.
- Otsuka, M., 1965,** Earthquake Magnitude and Surface Fault Formation, Zisin. J. Seismol. Soc. Japan, 2nd Series, 18, 1-8 (In Japanese with english abstract).
- Papageorgiou, A.S. and Kim, J., 1991,** Study of the Propagation and Amplification of Seismic Waves in Caracas Valley with Reference to the 29 July 1967 Earthquake : SH Waves, BSSA, Vol. 81, No. 6, pp. 2214-2233.

- PDE, 1991**, Preliminary Determination of Epicenters, No. 42-91, U.S. Department of the Interior, Geological Survey.
- Purohit, K.K., Islam, R. and Thakur, V.C., 1990**, Metamorphism of Psammo-Pelitic Rocks of Bhagirahi Valley, Garhwal Himalaya, *Journal of Himalayan Geology*, Vol. 1, No.2, pp. 167-174.
- Raiverman, V., Ganju, J.L. and Misra, V.N., 1979**, A New Look into the Stratigraphy of Cenozoic Sediments of the Himalayan Foot- Hills Between Ravi and Yamuna Rivers, Himalayan Geology Seminar, Geological Survey of India Miscellaneous Publication, No.41, Pt.V, pp. 233-246.
- Rastogi, B.K., 1992a**, Seismotectonics inferred from earthquakes and earthquake sequences in India during 1980's, *Current Science*, Vol 62, No. 1 and 2, pp. 101-109.
- Rastogi, B.K., 1992b**, Source Parameters of Uttarkashi earthquake, (Abstract) "Synthesis of the Uttarkashi Earthquake Data, 20th October, 1991, and Seismotectonics of Garwal-Kumaon Himalaya", Sponsored by D.S.T., 12-13 Nov, 1992, New Delhi, pp. 25.
- Reiter, L., 1990**, Earthquake Hazard Analysis - Issues and Insights, Columbia University Press, New York, 254p.
- Ricker, N., 1940**, The Form and Nature of Seismic Waves and Structure of Seismograms, *Geophysics*, Vol. 5, pp. 348-366.

Ricker, N. H., 1977, Transient Waves in Viscoelastic Media, Developments in Solid Earth Geophysics 10, Elsevier Scientific Publishing Company, 278p.

Saha, S.N., Gaur, V.K., Bansal, V., Wyss, M. and Khattri, K.N., 1981, Microearthquakes in North East India, Earthquake Disaster Mitigation, Vol.2, Sarita Prakashan, 154p.

Saklani, P.S., 1992, Geological Characteristics of the Uttarkashi Earthquake, (Abstract Published) Synthesis of the Uttarkashi Earthquake Data, 20th Oct, 1991, and Seismotectonics of Garhwal - Kumaon Himalaya, Sponsored by D.S.T., 12-13 Nov, 1992, New Delhi, pp. 11.

Sato, R., 1979, Theoretical Basis on Relation Between Focal Parameters and Earthquake Magnitude, J. Phys. Earth., Vol. 27, pp. 353- 372.

Sato, T. and Kiyono, J., 1986, Attenuation Peak Ground Motion Taking into Account the Fault Extent, Proc. of the 7th Japan Earthquake Engineering Symposium, pp. 541-546.

Seeber, L., Armbruster, J. and Quittmeyer, R., 1981, Seismicity and Continental Subduction in the Himalayan Arc, In : Gupta, H.K. and Delany, F.M. (eds) Zagros, Hindu Kush, Himalaya, Geodynamics evolution : Geodynamic series, American Geophysical Union, Washington 3, pp. 215-242.

Singh, R.P, and Prasad, Y.I.J., 1992, Attenuation Relation and Strong Ground Motion Data For Uttarkashi Earthquake, 1992, (Abstract Published) Synthesis of

the Uttarkashi Earthquake Data, 20th Oct, 1991, and Seismotectonics of Garhwal - Kumaon Himalaya, Sponsored by D.S.T., 12-13 Nov, 1992, New Delhi, pp. 39.

Singh, S., P. Sinha, A.K. Jain, V.N. Singh and L.S. Srivastava, 1975, Preliminary report on January 19, 1975, Kinnaur earthquake in Himachal Pradesh, BISET, V. 12, pp. 1 - 57.

Singh, S., Jain, A.K., Singh, V.N. and Srivastava, L.S., 1977, Damage During Kinnaur Earthquake of January 19, 1975 in Himachal Pradesh, India, 6WCEE, Vol. 1, pp. 184-190.

Sinvhal, A., 1976, A stochastic Study of the Properties of the Synthetic Seismograms Characterising Sub Surface Lithology, M.Tech. Dissertation, University of Roorkee, Roorkee, 85p.

Sinvhal, A., 1979, Application of Seismic reflection Data to Discriminate Subsurface Lithostratigraphy, Ph.D. Thesis, University of Roorkee, Roorkee, 218p.

Sinvhal, A., Joshi, G., Sinvhal, H. and Singh, V.N., 1990, A Pattern Recognition Technique for Microzonation, Proceedings of 9th Symposium on Earthquake Engineering, University of Roorkee, Roorkee, p 24 - 30.

Sinvhal, A., Sinvhal, H., Joshi, G., 1991, A Valid Pattern of Microzonation, Proceedings of 4th Conference on Seismic Microzonation, Stanford University, USA, V 3, p 641-648.

Sinvhal, A. and Srivastava, L.S., 1986, A Note on Simulation of Ground Motion Due to Quarry Blasts, Proceedings of 8th Symposium on Earthquake Engineering, Vol. 2, pp. 45 -53.

Sinvhal, A. and Sinvhal, H., 1992, Seismic Modelling and Pattern Recognition in Oil Exploration, Kluwer Academic Publishers, 178p.

Sinvhal, A., Sinvhal, H. and Joshi, A., 1990, Strong Motion Modelling of a Fault Plane, Sixteenth Annual Convention and Seminar on Exploration Geophysics (Abstract Published), pp. A12- 13.

Sinvhal, A., Joshi, A. and Sinvhal, H., 1993, Predicting Strong Ground Motion by Modelling Rupture at Source, Paper published in the Proceedings of the 28th Annual Convention and the Seminar on " Geophysics for Rural Development" Held during 17th to 19th December, 1991, Indian Geophysical Union, Hyderabad, India, pp. 68 - 74.

Sinvhal, A., Sinvhal, H., Jain, A.K., Manickavasagam, Rm., Joshi, A. and Joshi, G., 1992, Modelling of Uttarkashi Earthquake of October 20, 1991, in Terms of Seismic Microzonation and Causative Fault, (Abstract Published) Synthesis of the Uttarkashi Earthquake Data, 20th Oct, 1991, and Seismotectonics of Garhwal - Kumaon Himalaya 12-13 Nov, 1992, pp. 42-43.

Somerville, P., Sen, M. and Cohee, B., 1991, Simulation of Strong Ground Motions recording during the 1985 Michocan Mexico, and Valpazaiso Chile Earthquake, BSSA, Vol. 81, No.1, pp. 1-27.

- Srivastava, H.N., 1989**, Application of Strong Motion Data for Epicentral Determination of Earthquakes, *BISET*, V. 26, no. 1, pp. 221 - 235.
- Srivastava, H.N. and Chatterjee, S. N., 1986**, Seismic Activity Over India During 1983 - 1986, Eight Symposium on Earthquake Engineering, Vol. 2, Dec 29-31, University of Roorkee, Roorkee, pp. 53 - 66.
- Takemiya, H. and Tomono, T., 1992**, Topographical Site Response for Harmonic and Pseudo-Earthquake Motion, Proceedings of Tenth World Conference on Earthquake Engineering, 19-24 July, 1992, Madrid, Spain, A.A. Balkema, pp. 929-934.
- Takemura, M. and Ikeura, T., 1988**, A Semi-Empirical Method Using a Hybrid of Stochastic and Deterministic Fault Models: Simulation of Strong Ground Motions During Large Earthquakes, *J. Phys. Earth*, 36, pp. 89-106.
- Tanaka, T., Yoshizawa, S., Sakaue, M. and Osawa, Y., 1982**, Estimation of Acceleration Characteristics of Strong Ground Motion by Synthesis of Accelerogram obtained during a small earthquake, *Bull. Earthquake Res. Inst. Tokyo Univ.*, V 57, pp. 561-579.
- Tandon, A.N., 1992**, Seismology in India - An overview upto 1970, *Current Science*, Vol 62, No. 1 and 2, pp. 9-17.
- Telford, W.M., Geldart, L.P., Sheriff, R.E. and Keys, D.A., 1976**, *Applied Geophysics*, Cambridge University Press, 860p.

Thakur, V.C. and Kumar, Sushil., 1994, Seismotectonics of the 20 October, 1991, Uttarkashi Earthquake in Garhwal Himalaya, North India, Terra Nova, 6, pp.90-94.

Tilak, N.B.G., Mukhopadhyay, U.S. and Sharda, Y.P., 1983, Seismo Tectonic Map of North Eastern India, G.S.I.

Tocher, D., 1958, Earthquake Energy and Ground Breakage, BSSA, V. 48, 147.

Trifunac, M. D., and Brady, A. G., 1975, A Study of Duration of Strong Earthquake Ground Motion, BSSA, V. 65, pp. 581-626.

USGS - NEIC, 1990, Preliminary Determination of Earthquakes, Jan 1991 - Aug 1991, World Hypocentral Data file 1900 - 1991, USA

UNDRO, 1990, Mitigating Natural Disasters Phenomena, Effects and Options - A manual for Policy Makers and Planners, United Nation Publication, pp. 164.

Vygodsky, 1975, Mathematical Handbook, Higher Mathematics, Mir Publishers, Moscow, 872p.

APPENDIX I

ENERGY RELEASED IN AN EARTHQUAKE

Following paragraphs are taken from Kasahara (1981, p 14 -16) and have been used in Chapter 3. Seismic energy released during an earthquake and its relation to the radiated waves have been discussed in the following paragraphs.

The magnitude scale measures earthquake size in a relative manner. In other words, it compares large and small earthquakes quantitatively, but indicates little about the physical properties of their source. For a precise discussion of a seismic source property, therefore, relation of the scale to a basic physical parameter such as energy is needed.

let us introduce a point source radiating a wave train uniformly in all directions (Fig 3.2). Suppose a seismic wave reaching a station at the epicenter is given in terms of the ground displacement as :

$$X = A_0 \cos (2\pi t/T_0),$$

Then the velocity of ground motion there is

$$v = - (2\pi A_0/T_0) \sin (2\pi t/T_0)$$

Where A_o and T_o denotes the amplitude and period of wave respectively. hence the density of the kinetic energy of the ground motion e (per unit volume) is:

$$e = (\rho/2T_o) \int_0^{T_o} v^2 dt = (\rho/2T_o) (2\pi A_o/T_o)^2 \int_0^{T_o} \sin^2 (2\pi t/T_o) dt$$

$$= (\rho/4) (2\pi A_o/T_o)^2$$

Where, ρ is the density of the medium. If the wave train, of duration t_{no} , has n wave periods in it ($t_{no} = nT_o$) and is propagated with velocity c ; than the energy flow per unit area at the station is $ct_{no}e$ (ignoring the effect of surface reflection). Therefore, integration over a spherical surface with radius h (where h is the depth of origin), gives the total kinetic energy from the origin of the earthquake

$$E_k = 4\pi h^2 c t_{no} e = 4\pi^3 h^2 c t_{no} \rho (A_o/T_o)^2$$

The following factors must be considered to calculate the total seismic energy 'E':

- (a) Since the mean potential and kinetic energy are equal, we may take $E = 2E_k$.
- (b) Due to doubling of amplitude at the epicenter (free surface), $A_o = 2A_o$, where A_o denotes the amplitude recorded at the free surface.
- (c) The calculation above dealt with the waves of maximum energy, which at short distance are S - waves. The energy of P - waves must be added, which is provisionally assumed to be half that of the S waves (Gutenberg and Richter, 1956). Accordingly following expression is obtained :

$$E = 3\pi^3 h^2 c t_{no} \rho (A_o/T_o)^2$$

APPENDIX II

LIST OF FIGURES

Fig 1.1 Location of epicenters of (i) Dharamsala earthquake of 26th April 1986, (ii) Uttarkashi earthquake of 20th October, 1991 and (iii) Meghalaya earthquake of 10th Sept 1986.

Fig 1.2 Model of a vertical rupture plane within an identified most probable causative fault.

Fig 2.1 Two dimensional coordinate system used for modelling the rupture plane. Origin of coordinate system is at the center of (topmost element) extreme corner of the rupture plane. In this case origin lies at the topmost element at extreme left corner of rupture plane.

Fig 2.2 Three dimensional coordinate system used for modelling the rupture plane. Origin of coordinate system is at the center of (topmost element) extreme corner of the rupture plane. In this case origin lies at the topmost element at extreme left corner of rupture plane.

Fig 2.3 Method of computing the location of the nucleation point within the rupture plane. 'E' is the epicenter and 'h' is the hypocentral depth of the earthquake and ' δ ' is dip of the rupture plane. The distance OH gives the location of nucleation point within the rupture plane.

Fig 2.4 Normalised (a) Displacement form, (b) Velocity form and (c) Acceleration form of source wavelet of frequency 5 Hz at sampling interval of 4 ms. Acceleration and displacement form of source wavelet is computed by differentiation and integration of velocity form, respectively. The data is given in Table 2.2.

Fig 2.5 Velocity type source wavelet of frequencies (a) 2.5 Hz, (b) 5.0 Hz, (c) 7.5 Hz and (d) 10.0 Hz. The normalised values of source wavelets at sampling interval of 4 ms is given in Table 2.3.

Fig 2.6 Radial type of rupture propagation from nucleation element, within rupture plane. Number 1,2,3,4,... represent 1st, 2nd, 3rd, 4th etc. group of elements within rupture plane effected by the propagation of rupture from nucleation point.

Fig 2.7 Time of arrival of released source wavelet from the center of element 'C' within the rupture plane to the observation point. This time is the sum of (a) time taken by rupture to reach the center of the element 'C' within the rupture plane from the nucleation point and the time taken by released wavelet from the center 'C' of the element to reach the observation point.

Fig 3.1 Block diagram showing various steps involved for scaling the amplitude of the source wavelet released by an element.

Fig 3.2 Schematic diagram of part of a wave train from point source approaching a station at the epicenter (After Kasahara, 1981).

iii

Fig 3.3 Normalised form of velocity type sinusoidal wavelet with peak amplitude A_v .

Fig 3.4 Normalised form of velocity type wavelet with peak amplitude A_v , assumed for present study.

Fig 3.5 (a) Model of rupture plane with various elements represented by different numbers. Element numbered as 15 is the starting point of rupture in the assumed model. This model is same as used for the Meghalaya earthquake of 10th Sept, 1986. (b) Impulse response due to the rupture model shown in Fig 3.5(a) at Saitsama station. Time of arrival of spikes at station is arrival time of source wavelet from the center of the element to reach the observation point. Time of arrival of spikes at station is shown in Fig 2.7. (c) Source wavelets released by different element with appropriate arrival time at Saitsama. Arrival time at the station takes into consideration time taken by rupture to reach a particular element and the time taken by source wavelet from same element to reach observation point. The number in this figure corresponds to the element number shown in (a). and (d) addition of delayed source wavelets shown in Fig 3.5(b) to obtain velocity record at the observation point.

Fig 3.6 Normalised value of (a) Simulated velocity record at 4 msec (.004 sec) sampling interval, at Saitsama station due to the rupture model shown in Fig 3.5 (a), (b) acceleration record at 4 msec sampling interval obtained after differentiation of simulated velocity record, (c) acceleration record at 20 msec (.02 sec) sampling interval and (d) displacement record obtained from integration of simulated velocity record at sampling interval of 100 ms (.1 sec).

Fig 4.1 Method of extraction of parameter P_a from acceleration record. Acceleration record shown in this figure is a simulated record at Saitsama station for

Meghalaya earthquake of 10th Sept, 1986.

Fig 4.2 Method of extraction of parameter P_v from velocity record. Velocity record shown in this figure is a simulated record at Saitsama station for Meghalaya earthquake of 10th Sept, 1986.

Fig 4.3 Method of extraction of parameter P_d from displacement record. Displacement record shown in this figure is a simulated record at Saitsama station for Meghalaya earthquake of 10th Sept, 1986.

Fig 4.4 Extraction of variable T_D , duration of record as per Trifunac and Brady criteria (1975). This is computed from the cumulative addition of the square of the acceleration values shown in this figure. T_{d1} and T_{d95} are defined as the time at which the value becomes 5% and 95% of maximum value, respectively. The acceleration record used for this purpose is the simulated acceleration record at Saitsama station for Meghalaya earthquake of 10th Sept, 1986.

Fig 4.5 Method of extraction of variable T_{at} from the acceleration record. Acceleration record shown in this figure is a simulated record at Saitsama station for the Meghalaya earthquake of 10th Sept, 1986.

Fig 4.6 Normalised value of autocorrelation function of simulated acceleration record at Saitsama station for Meghalaya earthquake of 10th Sept, 1986. Autocorrelation function till .24 sec is shown in detail in Fig 4.7 from which various parameters of autocorrelation function are taken.

Fig 4.7 Normalised value of a portion of autocorrelation function (ACF) for acceleration record at Saitsama station for Meghalaya earthquake of 10th Sept, 1986, shown in Fig 4.6, showing variables $A_0, A_1, A_2, A_3, A_4, A_m, T_1, T_2, T_3$ and T_m . A_i ($i=1,4$) is the value of ACF at subscripted lag, A_m is value of global minima in ACF, T_i ($i=1,2,3$) represent i th zero crossing in the ACF and T_m is the time of arrival of global minima in ACF.

Fig 4.8 Method of computing T_1 (i.e. first zero crossing) in the autocorrelation function (ACF) of the simulated acceleration record at Saitsama station for Meghalaya earthquake of 10th Sept, 1986. A_1 and A_2 are value of the ACF at lag 1 and 2, respectively and also shown in Fig 4.7. The time between first zero crossing and time of ACF at 1 lag is shown by t_1 . This method has also been used for computing parameter T_2 and T_3 , respectively.

Fig 4.9 Method of computing parameter F_p from the power spectrum of the acceleration record. Acceleration record used here is the simulated record at Saitsama station for Meghalaya earthquake of 10th Sept, 1986.

Fig 4.10 Method of computing parameters F_1, F_2 and F_3 from the cumulative power spectrum of acceleration record. Acceleration record used here is the simulated record at Saitsama station for Meghalaya earthquake of 10th Sept, 1986. For this case $F_1 = 8.3$ Hz, $F_2 = 9.9$ Hz and $F_3 = 10.9$ Hz.

Fig 4.11 Method of computing parameters F_4, F_5 and F_6 from the frequency weighted power spectrum of acceleration record. Acceleration record used here is the simulated record at Saitsama station for Meghalaya earthquake of 10th Sept,

1986. For this case $F_4 = 7.9$ Hz, $F_5 = 9.5$ Hz and $F_6 = 10.5$ Hz.

Fig 5.1 Various symbols used for preparation of flow charts.

Fig 5.2 Flow chart of subroutine **RRG**.

Fig 5.3 Flow chart of subroutine **TIME**.

Fig 5.4 Flow chart of subroutine **SCALE**.

Fig 5.5 Flow chart of subroutine **VEL**.

Fig 5.6 Flow chart of subroutine **DELAY**.

Fig 5.7 Flow chart of subroutine **SHIFT**

Fig 5.8 Flow chart of subroutine **DIF**.

Fig 5.9 Flow chart of subroutine **DATA**.

Fig 5.10a Function divided into numbers of trapezoids. This rule has been used for integration of a given function.

Fig 5.10b Flow chart of subroutine **INTEG**.

Fig 5.11 Flow chart of subroutine **SWAVE**.

Fig 5.12 Flow chart of subroutine **VELR**.

Fig 5.13 Flow chart of subroutine **PTD**.

Fig 5.14 Flow chart of subroutine **PICK**.

Fig 5.15 Flow chart of subroutine **DURA**.

Fig 5.16 Flow chart of subroutine **AREAT**.

Fig 5.17 Flow chart of subroutine **AUTO**.

Fig 5.18 Flow chart of subroutine **ACAM**.

Fig 5.19 Flow chart of subroutine **RATIO**.

Fig 5.20 Flow chart of subroutine **INTERPL**.

Fig 5.21 Flow chart of program **AREA**.

Fig 5.22 Flow chart of subroutine **COMPLEX**.

Fig 5.23 Flow chart of the decimation in time decomposition of N point DFT computations into $N/2$ point DFT computations ($N=8$) (Oppenheim and Schaffer, 1988).

Fig 5.24 Flow chart of subroutine **POLAR**.

Fig 5.25 Flow chart of subroutine **POWER**.

Fig 5.26 Flow chart of subroutine **VPOW**.

Fig 5.27 Flow chart of subroutine **PICKF**.

Fig 6.1 Location of epicenters in H.P. and surrounding region. Epicentral data is taken from Singh et al. (1975) and USGS - NEIC (1990) and reproduced in Table 6.1. The tectonics of the region is taken from Eremenko and Negi (1968).

Fig 6.2 Location of elements of strong motion Kangra array. Geographical coordinates of recording stations is taken from Chandrasekaran and Das (1992b) and reproduced in Table 6.3. Station is represented by a number given in Table 6.3. The station marked by black colour represent those which had recorded the Dharamsala earthquake of 26th April, 1986.

Fig 6.3 Isoseismal map of Dharamsala earthquake of 26th April, 1986 (After Kumar and Mahajan, 1990, 1991).

Fig 6.4a Tectonic map of region around Dharamsala (After Kumar and Mahajan, 1991) showing location of Drini thrust. Legend given in Fig 6.4b.

Fig 6.4b Geological section showing Drini thrust. (After Kumar and Mahajan, 1990, 1991) along the section line shown in Fig 6.4a.

Fig 6.5 Tectonic map of region around Dharamsala (Raiverman et al. 1979). Epicentral coordinates for the epicenter E_{D1} , E_{D2} , E_{D3} and E_{D4} are shown in Table 6.4.

Fig 6.6 Isoacceleration contours of resultant horizontal peak acceleration for the Dharamsala earthquake of 26th April, 1986. Data for resultant peak acceleration is taken from Chandrasekaran (1988b) and reproduced in Table 6.6.

Fig 6.7 Composite tectonic map (Raiverman et al. 1979) and isoseismal map (Kumar and Mahajan, 1990, 1991) for the Dharamsala earthquake of 26th April, 1986.

Fig 6.8 Composite Tectonic (Raiverman et al., 1979) and isoacceleration map for Dharamsala earthquake of 26th April, 1986.

Fig 6.9 Superimposed composite map of tectonics (After Raiverman et al., 1979), isoseismal (After Kumar and Mahajan, 1990, 1991) and isoacceleration contour for Dharamsala earthquake of 26th April, 1986. Details of rectangle is shown in Fig 6.10.

Fig 6.10 Detailed portion of the rectangular block shown in Fig 6.9 giving the Location of identified causative fault for the Dharamsala earthquake of 26th April, 1986.

Fig 6.11 Dharamsala earthquake of 26th April, 1986, longitudinal, transverse and vertical components recorded at Dharamsala station. Y axis shows normalised value of (a) acceleration record, (b) its autocorrelation function, (c) its power spectrum, (d) its cumulative power spectrum and (e) its frequency weighted cumulative power spectrum. X axis for (a) and (b) shows time and for (c), (d) and

(e) shows frequency. Features extracted from these records are given in Table 6.7.

Fig 6.12 Dharamsala earthquake of 26th April, 1986, longitudinal, transverse and vertical components recorded at Shahpur station. Y axis shows normalised value of (a) acceleration record, (b) its autocorrelation function, (c) its power spectrum, (d) its cumulative power spectrum and (e) its frequency weighted cumulative power spectrum. X axis for (a) and (b) shows time and for (c), (d) and (e) shows frequency. Feature extracted from these records are given in Table 6.7.

Fig 6.13 Dharamsala earthquake of 26th April, 1986, longitudinal, transverse and vertical components recorded at Kangra station. Y axis shows normalised value of (a) acceleration record, (b) its autocorrelation function, (c) its power spectrum, (d) its cumulative power spectrum and (e) its frequency weighted cumulative power spectrum. X axis for (a) and (b) shows time and for (c), (d) and (e) shows frequency. Feature extracted from these records are given in Table 6.8.

Fig 6.14 Dharamsala earthquake of 26th April, 1986, longitudinal, transverse and vertical components recorded at Nagrota Bagwan station. Y axis shows normalised value of (a) acceleration record, (b) its autocorrelation function, (c) its power spectrum, (d) its cumulative power spectrum and (e) its frequency weighted cumulative power spectrum. X axis for (a) and (b) shows time and for (c), (d) and (e) shows frequency. Feature extracted from these records are given in Table 6.8.

Fig 6.15 Dharamsala earthquake of 26th April, 1986, longitudinal, transverse and vertical components recorded at Baroh station. Y axis shows normalised value of (a) acceleration record, (b) its autocorrelation function, (c) its power spectrum, (d) its cumulative power spectrum and (e) its frequency weighted cumulative power spectrum. X axis for (a) and (b) shows time and for (c), (d) and (e) shows frequency. Feature extracted from these records are given in Table 6.9.

Fig 6.16 Dharamsala earthquake of 26th April, 1986, longitudinal, transverse and vertical components recorded at Bhawarana station. Y axis shows normalised value of (a) acceleration record, (b) its autocorrelation function, (c) its power spectrum, (d) its cumulative power spectrum and (e) its frequency weighted cumulative power spectrum. X axis for (a) and (b) shows time and for (c), (d) and (e) shows frequency. Feature extracted from these records are given in Table 6.9.

Fig 6.17 Dharamsala earthquake of 26th April, 1986, longitudinal, transverse and vertical components recorded at Bandlakhas station. Y axis shows normalised value of (a) acceleration record, (b) its autocorrelation function, (c) its power spectrum, (d) its cumulative power spectrum and (e) its frequency weighted cumulative power spectrum. X axis for (a) and (b) shows time and for (c), (d) and (e) shows frequency. Feature extracted from these records are given in Table 6.10.

Fig 6.18 Dharamsala earthquake of 26th April, 1986, longitudinal, transverse and vertical components recorded at Sihunta station. Y axis shows normalised value of (a) acceleration record, (b) its autocorrelation function, (c) its power spectrum,

(d) its cumulative power spectrum and (e) its frequency weighted cumulative power spectrum. X axis for (a) and (b) shows time and for (c), (d) and (e) shows frequency. Feature extracted from these records are given in Table 6.10.

Fig 6.19 Dharamsala earthquake of 26th April, 1986, longitudinal, transverse and vertical components recorded at Jawali station. Y axis shows normalised value of (a) acceleration record, (b) its autocorrelation function, (c) its power spectrum, (d) its cumulative power spectrum and (e) its frequency weighted cumulative power spectrum. X axis for (a) and (b) shows time and for (c), (d) and (e) shows frequency. Feature extracted from these records are given in Table 6.11.

Fig 6.20 Locations at which micro earthquake studies were carried out for estimating velocity structure (After Srivastava and Chatterjee, 1986).

Fig 6.21 Model of the rupture plane for Dharamsala earthquake of 26th April, 1986. Minimum distance between the fault and Dharamsala station is 2 km and Shahpur is 7 km from the edge of the modelled fault.

Fig 6.22 Model MD_u of rupture plane for Dharamsala earthquake of 26th April, 1986. Dip and strike of this model are 74° and 153° , respectively. Simulated acceleration records at Dharamsala and Shahpur stations are shown with the model of rupture plane. The parameters extracted from these records are given in Table 6.12.

Fig 6.23 Model MD_k of rupture plane for Dharamsala earthquake of 26th April, 1986. Dip and strike of this model are 69° and 131° , respectively. Simulated

acceleration records at Dharamsala and Shahpur stations are shown with the model of rupture plane. The parameters extracted from these records are given in Table 6.12.

Fig 6.24 Drini thrust has been identified as the causative fault at which rupture could have possibly started. O_1A , O_2B and O_3C are three portions along this fault which have been modelled for simulation. Feature extracted from the simulated acceleration records shown in this figure are given in Table 6.14.

Fig 6.25 Model of rupture plane showing method of numbering elements within the rupture plane. Acceleration records are simulated at Dharamsala and Shahpur stations by assuming different elements within rupture plane as starting point of rupture. Number corresponding to each simulated record shows the element number which is assumed as nucleation point. Feature extracted from these simulated records are given in Table 6.16 and 6.17. The center of the element numbered as '1' is the origin of three dimensional rectangular coordinate system.

Fig 6.26 Location of observation points at which acceleration records are synthesised. The origin point of the coordinate system is placed at O_3 also shown in Fig 6.10. The coordinates of observation points in rectangular coordinate system are given in Table 6.19.

Fig 6.27 Dharamsala earthquake of 26th April, 1986, simulated records at Shahpur, Dharamsala, and Kangra stations. Y axis shows normalised value of (a) acceleration record, (b) its autocorrelation function, (c) its power spectrum, (d) its cumulative power spectrum and (e) its frequency weighted cumulative power

spectrum. X axis for (a) and (b) shows time and for (c), (d) and (e) shows frequency. Feature extracted from simulated records at these stations are given in Table 6.20.

Fig 6.28 Dharamsala earthquake of 26th April, 1986, simulated records at Nagrota Bagwan, Sihunta and Bhawarna stations. Y axis shows normalised value of (a) acceleration record, (b) its autocorrelation function, (c) its power spectrum, (d) its cumulative power spectrum and (e) its frequency weighted cumulative power spectrum. X axis for (a) and (b) shows time and for (c), (d) and (e) shows frequency. Feature extracted from simulated records at these stations are given in Table 6.20 and 6.21.

Fig 6.29 Dharamsala earthquake of 26th April, 1986, simulated records at Baroh, Bandlakhas and Jawali stations. Y axis shows normalised value of (a) acceleration record, (b) its autocorrelation function, (c) its power spectrum, (d) its cumulative power spectrum and (e) its frequency weighted cumulative power spectrum. X axis for (a) and (b) shows time and for (c), (d) and (e) shows frequency. Feature extracted from simulated records at these stations are given in Table 6.20 and 6.21.

Fig 6.30 Elevations of different recording stations with respect to Mean Sea Level (MSL) that have recorded Dharamsala earthquake of 26th April, 1986. Elevation data for each station is taken from Chandrasekaran and Das (1988) and reproduced in Table 6.19. The diagram shows the relative height of the stations with respect to each other. The maximum elevation of the recording station is at 1800 m at Bandlakhas and the minimum elevation of recording station is 500 m

at Bhawarana.

Fig 7.1 Location of epicenters in Uttarkashi and surrounding region. Epicentral data is taken from USGS-NEIC (1990) and reproduced in Table 7.1. The tectonics of the region is taken from Eremenko and Negi (1968).

Fig 7.2 Location of recording stations of strong motion array in Uttarkashi region. The stations marked with black colour represent those which had recorded the Uttarkashi earthquake of 20th Oct, 1991.

Fig 7.3 Isoseismal map of Uttarkashi earthquake of 20th October, 1991 (Sinvhal et al. 1992).

Fig 7.4 Lineament map from satellite imagery of Garhwal Himalaya (After Jain, 1987). Study area shown by dashed rectangle is enlarged in Fig 7.5.

Fig 7.5 Tectonics of the region around Uttarkashi taken from map shown in Fig 7.4. E_{U1} , E_{U2} and E_{U3} are the epicenter of Uttarkashi earthquake of 20th October, 1991 given by different agencies and this data is given in Table 7.2.

Fig 7.6 Tectonic map of Uttarkashi region (After Purohit et al., 1990).

Fig 7.7 Location of aftershocks of Uttarkashi earthquake of 20th October, 1991. Data plotted in this figure is reproduced in Table 7.4 and the tectonics of the region is taken after Jain (1987). Epicentral parameter of main shock is reproduced in Table 7.4.

Fig 7.8 Isoacceleration contour map for Uttarkashi earthquake of 20th October, 1991. Acceleration data is taken from Chandrasekaran and Das (1991, 1992c) and reproduced in Table 7.5.

Fig 7.9 Composite map of isoacceleration contours, aftershock location, meizoseismal area of Uttarkashi earthquake of 20th October, 1991 and tectonics of the region. (Data taken from Chandrasekaran and Das, 1991, 1992c, Kayal et al. 1992 and Jain, 1987).

Fig 7.10 Location of identified most probable causative fault from the composite map shown in Fig 7.9. Tectonics of the region is after Jain (1987).

Fig 7.11 Location of MCT-1 from the tectonic map of Purohit et al. (1990).

Fig 7.12 Geological section in the dip direction of the MCT showing the downward extension D of the rupture plane (Modified after Kayal, 1994). Shaded zone indicates the MEQ aftershocks area (After Kayal et al., 1993). The plane of detachment and Basement thrust are taken from Seeber et al. (1981). Solid arrows indicate relative movement of the plates. F_1 , F_2 and F_3 represent foreshocks of the Uttarkashi earthquake of 20th October, 1991 that occurred 49 hours before the main shocks (M.S.). Largest foreshock F_2 has magnitude 4.7 (M_L). A_1 and A_2 represent aftershocks that occurred 24 hours of main shock. Largest aftershock A_2 has magnitude 5.2 (M_L). Point O marked in this figure is also shown in Fig 7.11.

Fig 7.13 Uttarkashi earthquake of 20th Oct, 1991 longitudinal component recorded at

Almora station. Y axis shows normalised value of (a) acceleration record, (b) its autocorrelation function, (c) its power spectrum, (d) its cumulative power spectrum and (e) its frequency weighted cumulative power spectrum. X axis for (a) and (b) shows time and for (c), (d) and (e) shows frequency. Feature extracted from field records at this station is given in Table 7.6.

Fig 7.14 Uttarkashi earthquake of 20th Oct, 1991 transverse component recorded at Almora station. Y axis shows normalised value of (a) acceleration record, (b) its autocorrelation function, (c) its power spectrum, (d) its cumulative power spectrum and (e) its frequency weighted cumulative power spectrum. X axis for (a) and (b) shows time and for (c), (d) and (e) shows frequency. Feature extracted from field records at this station is given in Table 7.6.

Fig 7.15 Uttarkashi earthquake of 20th Oct, 1991 vertical component recorded at Almora station. Y axis shows normalised value of (a) acceleration record, (b) its autocorrelation function, (c) its power spectrum, (d) its cumulative power spectrum and (e) its frequency weighted cumulative power spectrum. X axis for (a) and (b) shows time and for (c), (d) and (e) shows frequency. Feature extracted from field records at this station is given in Table 7.6.

Fig 7.16 Uttarkashi earthquake of 20th Oct, 1991, longitudinal component recorded at Barkot station. Y axis shows normalised value of (a) acceleration record, (b) its autocorrelation function, (c) its power spectrum, (d) its cumulative power spectrum and (e) its frequency weighted cumulative power spectrum. X axis for (a) and (b) shows time and for (c), (d) and (e) shows frequency. Feature extracted from field records at this station is given in Table 7.6.

Fig 7.17 Uttarkashi earthquake of 20th Oct, 1991, transverse component recorded at Barkot station. Y axis shows normalised value of (a) acceleration record, (b) its autocorrelation function, (c) its power spectrum, (d) its cumulative power spectrum and (e) its frequency weighted cumulative power spectrum. X axis for (a) and (b) shows time and for (c), (d) and (e) shows frequency. Feature extracted from field records at this station is given in Table 7.6.

Fig 7.18 Uttarkashi earthquake of 20th Oct, 1991, vertical component recorded at Barkot station. Y axis shows normalised value of (a) acceleration record, (b) its autocorrelation function, (c) its power spectrum, (d) its cumulative power spectrum and (e) its frequency weighted cumulative power spectrum. X axis for (a) and (b) shows time and for (c), (d) and (e) shows frequency. Feature extracted from field records at this station is given in Table 7.6.

Fig 7.19 Uttarkashi earthquake of 20th Oct, 1991, longitudinal component recorded at Karnprayag station. Y axis shows normalised value of (a) acceleration record, (b) its autocorrelation function, (c) its power spectrum, (d) its cumulative power spectrum and (e) its frequency weighted cumulative power spectrum. X axis for (a) and (b) shows time and for (c), (d) and (e) shows frequency. Feature extracted from field records at this station is given in Table 7.7.

Fig 7.20 Uttarkashi earthquake of 20th Oct, 1991, transverse component recorded at Karnprayag station. Y axis shows normalised value of (a) acceleration record, (b) its autocorrelation function, (c) its power spectrum, (d) its cumulative power spectrum and (e) its frequency weighted cumulative power spectrum. X axis for (a) and (b) shows time and for (c), (d) and (e) shows frequency. Feature

extracted from field records at this station is given in Table 7.7.

Fig 7.21 Uttarkashi earthquake of 20th Oct, 1991, vertical component recorded at Karnprayag station. Y axis shows normalised value of (a) acceleration record, (b) its autocorrelation function, (c) its power spectrum, (d) its cumulative power spectrum and (e) its frequency weighted cumulative power spectrum. X axis for (a) and (b) shows time and for (c), (d) and (e) shows frequency. Feature extracted from field records at this station is given in Table 7.7.

Fig 7.22 Uttarkashi earthquake of 20th Oct, 1991, longitudinal component recorded at Kosani station. Y axis shows normalised value of (a) acceleration record, (b) its autocorrelation function, (c) its power spectrum, (d) its cumulative power spectrum and (e) its frequency weighted cumulative power spectrum. X axis for (a) and (b) shows time and for (c), (d) and (e) shows frequency. Feature extracted from field records at this station is given in Table 7.7.

Fig 7.23 Uttarkashi earthquake of 20th Oct, 1991, transverse component recorded at Kosani station. Y axis shows normalised value of (a) acceleration record, (b) its autocorrelation function, (c) its power spectrum, (d) its cumulative power spectrum and (e) its frequency weighted cumulative power spectrum. X axis for (a) and (b) shows time and for (c), (d) and (e) shows frequency. Feature extracted from field records at this station is given in Table 7.7.

Fig 7.24 Uttarkashi earthquake of 20th Oct, 1991, vertical component recorded at Kosani station. Y axis shows normalised value of (a) acceleration record, (b) its autocorrelation function, (c) its power spectrum, (d) its cumulative power

spectrum and (e) its frequency weighted cumulative power spectrum. X axis for (a) and (b) shows time and for (c), (d) and (e) shows frequency. Feature extracted from field records at this station is given in Table 7.7.

Fig 7.25 Uttarkashi earthquake of 20th Oct, 1991, longitudinal component recorded at Purola station. Y axis shows normalised value of (a) acceleration record, (b) its autocorrelation function, (c) its power spectrum, (d) its cumulative power spectrum and (e) its frequency weighted cumulative power spectrum. X axis for (a) and (b) shows time and for (c), (d) and (e) shows frequency. Feature extracted from field records at this station is given in Table 7.8.

Fig 7.26 Uttarkashi earthquake of 20th Oct, 1991, transverse component recorded at Purola station. Y axis shows normalised value of (a) acceleration record, (b) its autocorrelation function, (c) its power spectrum, (d) its cumulative power spectrum and (e) its frequency weighted cumulative power spectrum. X axis for (a) and (b) shows time and for (c), (d) and (e) shows frequency. Feature extracted from field records at this station is given in Table 7.8.

Fig 7.27 Uttarkashi earthquake of 20th Oct, 1991, vertical component recorded at Purola station. Y axis shows normalised value of (a) acceleration record, (b) its autocorrelation function, (c) its power spectrum, (d) its cumulative power spectrum and (e) its frequency weighted cumulative power spectrum. X axis for (a) and (b) shows time and for (c), (d) and (e) shows frequency. Feature extracted from field records at this station is given in Table 7.8.

Fig 7.28 Uttarkashi earthquake of 20th Oct, 1991, longitudinal component recorded at

Rudraprayag station. Y axis shows normalised value of (a) acceleration record, (b) its autocorrelation function, (c) its power spectrum, (d) its cumulative power spectrum and (e) its frequency weighted cumulative power spectrum. X axis for (a) and (b) shows time and for (c), (d) and (e) shows frequency. Feature extracted from field records at this station is given in Table 7.8.

Fig 7.29 Uttarkashi earthquake of 20th Oct, 1991, transverse component recorded at Rudraprayag station. Y axis shows normalised value of (a) acceleration record, (b) its autocorrelation function, (c) its power spectrum, (d) its cumulative power spectrum and (e) its frequency weighted cumulative power spectrum. X axis for (a) and (b) shows time and for (c), (d) and (e) shows frequency. Feature extracted from field records at this station is given in Table 7.8.

Fig 7.30 Uttarkashi earthquake of 20th Oct, 1991, vertical component recorded at Rudraprayag station. Y axis shows normalised value of (a) acceleration record, (b) its autocorrelation function, (c) its power spectrum, (d) its cumulative power spectrum and (e) its frequency weighted cumulative power spectrum. X axis for (a) and (b) shows time and for (c), (d) and (e) shows frequency. Feature extracted from field records at this station is given in Table 7.8.

Fig 7.31 Uttarkashi earthquake of 20th Oct, 1991, longitudinal component recorded at Ghansiali station. Y axis shows normalised value of (a) acceleration record, (b) its autocorrelation function, (c) its power spectrum, (d) its cumulative power spectrum and (e) its frequency weighted cumulative power spectrum. X axis for (a) and (b) shows time and for (c), (d) and (e) shows frequency. Feature extracted from field records at this station is given in Table 7.9.

Fig 7.32 Uttarkashi earthquake of 20th Oct, 1991, transverse component recorded at Ghansiali station. Y axis shows normalised value of (a) acceleration record, (b) its autocorrelation function, (c) its power spectrum, (d) its cumulative power spectrum and (e) its frequency weighted cumulative power spectrum. X axis for (a) and (b) shows time and for (c), (d) and (e) shows frequency. Feature extracted from field records at this station is given in Table 7.9.

Fig 7.33 Uttarkashi earthquake of 20th Oct, 1991, vertical component recorded at Ghansiali station. Y axis shows normalised value of (a) acceleration record, (b) its autocorrelation function, (c) its power spectrum, (d) its cumulative power spectrum and (e) its frequency weighted cumulative power spectrum. X axis for (a) and (b) shows time and for (c), (d) and (e) shows frequency. Feature extracted from field records at this station is given in Table 7.9.

Fig 7.34 Uttarkashi earthquake of 20th Oct, 1991, longitudinal component recorded at Koteswar station. Y axis shows normalised value of (a) acceleration record, (b) its autocorrelation function, (c) its power spectrum, (d) its cumulative power spectrum and (e) its frequency weighted cumulative power spectrum. X axis for (a) and (b) shows time and for (c), (d) and (e) shows frequency. Feature extracted from field records at this station is given in Table 7.9.

Fig 7.35 Uttarkashi earthquake of 20th Oct, 1991, transverse component recorded at Koteswar station. Y axis shows normalised value of (a) acceleration record, (b) its autocorrelation function, (c) its power spectrum, (d) its cumulative power spectrum and (e) its frequency weighted cumulative power spectrum. X axis for (a) and (b) shows time and for (c), (d) and (e) shows frequency. Feature

extracted from field records at this station is given in Table 7.9.

Fig 7.36 Uttarkashi earthquake of 20th Oct, 1991, vertical component recorded at Koteswar station. Y axis shows normalised value of (a) acceleration record, (b) its autocorrelation function, (c) its power spectrum, (d) its cumulative power spectrum and (e) its frequency weighted cumulative power spectrum. X axis for (a) and (b) shows time and for (c), (d) and (e) shows frequency. Feature extracted from field records at this station is given in Table 7.9.

Fig 7.37 Uttarkashi earthquake of 20th Oct, 1991, longitudinal component recorded at Koti station. Y axis shows normalised value of (a) acceleration record, (b) its autocorrelation function, (c) its power spectrum, (d) its cumulative power spectrum and (e) its frequency weighted cumulative power spectrum. X axis for (a) and (b) shows time and for (c), (d) and (e) shows frequency. Feature extracted from field records at this station is given in Table 7.10.

Fig 7.38 Uttarkashi earthquake of 20th Oct, 1991, transverse component recorded at Koti station. Y axis shows normalised value of (a) acceleration record, (b) its autocorrelation function, (c) its power spectrum, (d) its cumulative power spectrum and (e) its frequency weighted cumulative power spectrum. X axis for (a) and (b) shows time and for (c), (d) and (e) shows frequency. Feature extracted from field records at this station is given in Table 7.10.

Fig 7.39 Uttarkashi earthquake of 20th Oct, 1991, vertical component recorded at Koti station. Y axis shows normalised value of (a) acceleration record, (b) its autocorrelation function, (c) its power spectrum, (d) its cumulative power

spectrum and (e) its frequency weighted cumulative power spectrum. X axis for (a) and (b) shows time and for (c), (d) and (e) shows frequency. Feature extracted from field records at this station is given in Table 7.10.

Fig 7.40 Uttarkashi earthquake of 20th Oct, 1991, longitudinal component recorded at Srinagar station. Y axis shows normalised value of (a) acceleration record, (b) its autocorrelation function, (c) its power spectrum, (d) its cumulative power spectrum and (e) its frequency weighted cumulative power spectrum. X axis for (a) and (b) shows time and for (c), (d) and (e) shows frequency. Feature extracted from field records at this station is given in Table 7.10.

Fig 7.41 Uttarkashi earthquake of 20th Oct, 1991, transverse component recorded at Srinagar station. Y axis shows normalised value of (a) acceleration record, (b) its autocorrelation function, (c) its power spectrum, (d) its cumulative power spectrum and (e) its frequency weighted cumulative power spectrum. X axis for (a) and (b) shows time and for (c), (d) and (e) shows frequency. Feature extracted from field records at this station is given in Table 7.10.

Fig 7.42 Uttarkashi earthquake of 20th Oct, 1991, vertical component recorded at Srinagar station. Y axis shows normalised value of (a) acceleration record, (b) its autocorrelation function, (c) its power spectrum, (d) its cumulative power spectrum and (e) its frequency weighted cumulative power spectrum. X axis for (a) and (b) shows time and for (c), (d) and (e) shows frequency. Feature extracted from field records at this station is given in Table 7.10.

Fig 7.43 Uttarkashi earthquake of 20th Oct, 1991, longitudinal component recorded at

Tehri station. Y axis shows normalised value of (a) acceleration record, (b) its autocorrelation function, (c) its power spectrum, (d) its cumulative power spectrum and (e) its frequency weighted cumulative power spectrum. X axis for (a) and (b) shows time and for (c), (d) and (e) shows frequency. Feature extracted from field records at this station is given in Table 7.11.

Fig 7.44 Uttarkashi earthquake of 20th Oct, 1991, transverse component recorded at Tehri station. Y axis shows normalised value of (a) acceleration record, (b) its autocorrelation function, (c) its power spectrum, (d) its cumulative power spectrum and (e) its frequency weighted cumulative power spectrum. X axis for (a) and (b) shows time and for (c), (d) and (e) shows frequency. Feature extracted from field records at this station is given in Table 7.11.

Fig 7.45 Uttarkashi earthquake of 20th Oct, 1991, vertical component recorded at Tehri station. Y axis shows normalised value of (a) acceleration record, (b) its autocorrelation function, (c) its power spectrum, (d) its cumulative power spectrum and (e) its frequency weighted cumulative power spectrum. X axis for (a) and (b) shows time and for (c), (d) and (e) shows frequency. Feature extracted from field records at this station is given in Table 7.11.

Fig 7.46 Uttarkashi earthquake of 20th Oct, 1991, longitudinal component recorded at Uttarkashi station. Y axis shows normalised value of (a) acceleration record, (b) its autocorrelation function, (c) its power spectrum, (d) its cumulative power spectrum and (e) its frequency weighted cumulative power spectrum. X axis for (a) and (b) shows time and for (c), (d) and (e) shows frequency. Feature extracted from field records at this station is given in Table 7.12.

Fig 7.47 Uttarkashi earthquake of 20th Oct, 1991, transverse component recorded at Uttarkashi station. Y axis shows normalised value of (a) acceleration record, (b) its autocorrelation function, (c) its power spectrum, (d) its cumulative power spectrum and (e) its frequency weighted cumulative power spectrum. X axis for (a) and (b) shows time and for (c), (d) and (e) shows frequency. Feature extracted from field records at this station is given in Table 7.12.

Fig 7.48 Uttarkashi earthquake of 20th Oct, 1991, vertical component recorded at Uttarkashi station. Y axis shows normalised value of (a) acceleration record, (b) its autocorrelation function, (c) its power spectrum, (d) its cumulative power spectrum and (e) its frequency weighted cumulative power spectrum. X axis for (a) and (b) shows time and for (c), (d) and (e) shows frequency. Feature extracted from field records at this station is given in Table 7.12.

Fig 7.49 Uttarkashi earthquake of 20th Oct, 1991, longitudinal component recorded at Bhatwari station. Y axis shows normalised value of (a) acceleration record, (b) its autocorrelation function, (c) its power spectrum, (d) its cumulative power spectrum and (e) its frequency weighted cumulative power spectrum. X axis for (a) and (b) shows time and for (c), (d) and (e) shows frequency. Feature extracted from field records at this station is given in Table 7.12.

Fig 7.50 Uttarkashi earthquake of 20th Oct, 1991, transverse component recorded at Bhatwari station. Y axis shows normalised value of (a) acceleration record, (b) its autocorrelation function, (c) its power spectrum, (d) its cumulative power spectrum and (e) its frequency weighted cumulative power spectrum. X axis for (a) and (b) shows time and for (c), (d) and (e) shows frequency. Feature

extracted from field records at this station is given in Table 7.12.

Fig 7.51 Uttarkashi earthquake of 20th Oct, 1991, vertical component recorded at Bhatwari station. Y axis shows normalised value of (a) acceleration record, (b) its autocorrelation function, (c) its power spectrum, (d) its cumulative power spectrum and (e) its frequency weighted cumulative power spectrum. X axis for (a) and (b) shows time and for (c), (d) and (e) shows frequency. Feature extracted from field records at this station is given in Table 7.12.

Fig 7.52 Model MU_{d1} for the Uttarkashi earthquake having dip and strike as 5° and 296° , respectively. Simulated acceleration records at Bhatwari and Uttarkashi are shown with the model MU_{d1} of the rupture plane. Parameters extracted from these records are given in Table 7.13.

Fig 7.53 Model MU_{d2} for the Uttarkashi earthquake having dip and strike as 14° and 317° , respectively. Simulated acceleration records at Bhatwari and Uttarkashi are shown with the model MU_{d2} of the rupture plane. Parameters extracted from these records are given in Table 7.13.

Fig 7.54 Model of rupture plane showing method of numbering elements within the rupture plane. Acceleration records are simulated at Bhatwari and Uttarkashi stations by assuming different elements within rupture plane as starting point of rupture. Number corresponding to each simulated record shows the element number which is assumed as nucleation point. Features extracted from these simulated records at Bhatwari and Uttarkashi are shown in Table 7.15 and 7.16, respectively. The center of element numbered as '1' is the origin of three

7.21.

Fig 7.62 Uttarkashi earthquake of 20th Oct, 1991, simulated acceleration record at Koteshwar station. Y axis shows normalised value of (a) acceleration record, (b) its autocorrelation function, (c) its power spectrum, (d) its cumulative power spectrum and (e) its frequency weighted cumulative power spectrum. X axis for (a) and (b) shows time and for (c), (d) and (e) shows frequency. Features extracted from simulated records at this station are given in Table 7.19, 7.20 and 7.21.

Fig 7.63 Uttarkashi earthquake of 20th Oct, 1991, simulated acceleration record at Koti station. Y axis shows normalised value of (a) acceleration record, (b) its autocorrelation function, (c) its power spectrum, (d) its cumulative power spectrum and (e) its frequency weighted cumulative power spectrum. X axis for (a) and (b) shows time and for (c), (d) and (e) shows frequency. Features extracted from simulated records at this station are given in Table 7.19, 7.20 and 7.21.

Fig 7.64 Uttarkashi earthquake of 20th Oct, 1991, simulated acceleration record at Purola station. Y axis shows normalised value of (a) acceleration record, (b) its autocorrelation function, (c) its power spectrum, (d) its cumulative power spectrum and (e) its frequency weighted cumulative power spectrum. X axis for (a) and (b) shows time and for (c), (d) and (e) shows frequency. Features extracted from simulated records at this station are given in Table 7.19, 7.20 and 7.21.

Fig 7.65 Uttarkashi earthquake of 20th Oct, 1991, simulated acceleration record at Rudrprayag station. Y axis shows normalised value of (a) acceleration record, (b) its autocorrelation function, (c) its power spectrum, (d) its cumulative power spectrum and (e) its frequency weighted cumulative power spectrum. X axis for (a) and (b) shows time and for (c), (d) and (e) shows frequency. Features extracted from simulated records at this station are given in Table 7.19, 7.20 and 7.21.

Fig 7.66 Uttarkashi earthquake of 20th Oct, 1991, simulated acceleration record at Srinagar station. Y axis shows normalised value of (a) acceleration record, (b) its autocorrelation function, (c) its power spectrum, (d) its cumulative power spectrum and (e) its frequency weighted cumulative power spectrum. X axis for (a) and (b) shows time and for (c), (d) and (e) shows frequency. Features extracted from simulated records at this station are given in Table 7.19, 7.20 and 7.21.

Fig 7.67 Uttarkashi earthquake of 20th Oct, 1991, simulated acceleration record at Tehri station. Y axis shows normalised value of (a) acceleration record, (b) its autocorrelation function, (c) its power spectrum, (d) its cumulative power spectrum and (e) its frequency weighted cumulative power spectrum. X axis for (a) and (b) shows time and for (c), (d) and (e) shows frequency. Features extracted from simulated records at this station are given in Table 7.19, 7.20 and 7.21.

Fig 7.68 Uttarkashi earthquake of 20th Oct, 1991, simulated acceleration record at Uttarkashi station. Y axis shows normalised value of (a) acceleration record, (b) its autocorrelation function, (c) its power spectrum, (d) its cumulative power spectrum and (e) its frequency weighted cumulative power spectrum. X axis for (a) and (b) shows time and for (c), (d) and (e) shows frequency. Features extracted from simulated records at this station are given in Table 7.19, 7.20 and 7.21.

Fig 8.1 Locations of epicenters in Meghalaya and surrounding region. Epicentral data is taken from USGS-NEIC (1990) and reproduced in Table 8.1. The tectonics of the region is taken from Eremenko and Negi (1968).

Fig 8.2 Location of recording stations of strong motion Shillong array. Geographical coordinates of recording stations is taken from Chandrasekaran and Das (1992b) and reproduced in Table 8.2. The stations marked with black colour represent those which had recorded the Meghalaya earthquake of 10th Sept, 1986.

Fig 8.3 Tectonic map of the region around Meghalaya (Tilak et al. 1983). E_{m1} , E_{m2} , and E_{m3} are the epicenter of Meghalaya earthquake of 10th Sept, 1986 given by different agencies and reproduced in Table 8.3.

Fig 8.4 Isoacceleration map for Meghalaya earthquake of 10th Sept, 1986 prepared from resultant peak acceleration given by Chandrasekaran et al. (1988) and reproduced in Table 8.4.

Fig 8.5 Superimposed isoacceleration and tectonic map (Tilak et al, 1983) in the

epicentral region of Meghalaya earthquake of 10th, Sept, 1986.

Fig 8.6 Meghalaya earthquake of 10th Sept, 1986, longitudinal, transverse and vertical components of acceleration record at Baithalangso station. Y axis shows normalised value of (a) acceleration record, (b) its autocorrelation function, (c) its power spectrum, (d) its cumulative power spectrum and (e) its frequency weighted cumulative power spectrum. X axis for (a) and (b) shows time and for (c), (d) and (e) shows frequency. Features extracted from field records at this station are given in Table 8.5.

Fig 8.7 Meghalaya earthquake of 10th Sept, 1986, longitudinal, transverse and vertical components of acceleration record at Dauki station. Y axis shows normalised value of (a) acceleration record, (b) its autocorrelation function, (c) its power spectrum, (d) its cumulative power spectrum and (e) its frequency weighted cumulative power spectrum. X axis for (a) and (b) shows time and for (c), (d) and (e) shows frequency. Features extracted from field records at this station are given in Table 8.5.

Fig 8.8 Meghalaya earthquake of 10th Sept, 1986, longitudinal, transverse and vertical components of acceleration record at Khliehriat station. Y axis shows normalised value of (a) acceleration record, (b) its autocorrelation function, (c) its power spectrum, (d) its cumulative power spectrum and (e) its frequency weighted cumulative power spectrum. X axis for (a) and (b) shows time and for (c), (d) and (e) shows frequency. Features extracted from field records at this station are given in Table 8.6.

Fig 8.9 Meghalaya earthquake of 10th Sept, 1986, longitudinal, transverse and vertical components of acceleration record at Nongpoh station. Y axis shows normalised value of (a) acceleration record, (b) its autocorrelation function, (c) its power spectrum, (d) its cumulative power spectrum and (e) its frequency weighted cumulative power spectrum. X axis for (a) and (b) shows time and for (c), (d) and (e) shows frequency. Features extracted from field records at this station are given in Table 8.6.

Fig 8.10 Meghalaya earthquake of 10th Sept, 1986, longitudinal, transverse and vertical components of acceleration record at Nongstoin station. Y axis shows normalised value of (a) acceleration record, (b) its autocorrelation function, (c) its power spectrum, (d) its cumulative power spectrum and (e) its frequency weighted cumulative power spectrum. X axis for (a) and (b) shows time and for (c), (d) and (e) shows frequency. Features extracted from field records at this station are given in Table 8.7.

Fig 8.11 Meghalaya earthquake of 10th Sept, 1986, longitudinal, transverse and vertical components of acceleration record at Nongkhlaw station. Y axis shows normalised value of (a) acceleration record, (b) its autocorrelation function, (c) its power spectrum, (d) its cumulative power spectrum and (e) its frequency weighted cumulative power spectrum. X axis for (a) and (b) shows time and for (c), (d) and (e) shows frequency. Features extracted from field records at this station are given in Table 8.7.

Fig 8.12 Meghalaya earthquake of 10th Sept, 1986, longitudinal, transverse and vertical components of acceleration record at Panimur station. Y axis shows normalised

value of (a) acceleration record, (b) its autocorrelation function, (c) its power spectrum, (d) its cumulative power spectrum and (e) its frequency weighted cumulative power spectrum. X axis for (a) and (b) shows time and for (c), (d) and (e) shows frequency. Features extracted from field records at this station are given in Table 8.8.

Fig 8.13 Meghalaya earthquake of 10th Sept, 1986, longitudinal, transverse and vertical components of acceleration record at Pynursla station. Y axis shows normalised value of (a) acceleration record, (b) its autocorrelation function, (c) its power spectrum, (d) its cumulative power spectrum and (e) its frequency weighted cumulative power spectrum. X axis for (a) and (b) shows time and for (c), (d) and (e) shows frequency. Features extracted from field records at this station are given in Table 8.8.

Fig 8.14 Meghalaya earthquake of 10th Sept, 1986, longitudinal, transverse and vertical components of acceleration record at Saitsama station. Y axis shows normalised value of (a) acceleration record, (b) its autocorrelation function, (c) its power spectrum, (d) its cumulative power spectrum and (e) its frequency weighted cumulative power spectrum. X axis for (a) and (b) shows time and for (c), (d) and (e) shows frequency. Features extracted from field records at this station are given in Table 8.9.

Fig 8.15 Meghalaya earthquake of 10th Sept, 1986, longitudinal, transverse and vertical components of acceleration record at Ummulong station. Y axis shows normalised value of (a) acceleration record, (b) its autocorrelation function, (c) its power spectrum, (d) its cumulative power spectrum and (e) its frequency

weighted cumulative power spectrum. X axis for (a) and (b) shows time and for (c), (d) and (e) shows frequency. Features extracted from field records at this station are given in Table 8.9.

Fig 8.16 Meghalaya earthquake of 10th Sept, 1986, longitudinal, transverse and vertical components of acceleration record at Umsning station. Y axis shows normalised value of (a) acceleration record, (b) its autocorrelation function, (c) its power spectrum, (d) its cumulative power spectrum and (e) its frequency weighted cumulative power spectrum. X axis for (a) and (b) shows time and for (c), (d) and (e) shows frequency. Features extracted from field records at this station are given in Table 8.10.

Fig 8.17 Meghalaya earthquake of 10th Sept, 1986, longitudinal, transverse and vertical component of acceleration record at Umrongso station. Y axis shows normalised value of (a) acceleration record, (b) its autocorrelation function, (c) its power spectrum, (d) its cumulative power spectrum and (e) its frequency weighted cumulative power spectrum. X axis for (a) and (b) shows time and for (c), (d) and (e) shows frequency. Features extracted from field records at this station are given in Table 8.10.

Fig 8.18 Rupture model MM_{d1} for Meghalaya earthquake of 10th Sept, 1986 having 90° dip. Parameters extracted from simulated acceleration records shown in this figure at Saitsama and Ummulong stations due to this model are given in Table 8.11.

Fig 8.19 Rupture model MM_{d2} for Meghalaya earthquake of 10th Sept, 1986 having 0°

dip. Parameters extracted from simulated acceleration records shown in this figure at Saitsama and Ummulong stations due to this model are given in Table 8.11.

Fig 8.20 Rupture model MM_{d3} for Meghalaya earthquake of 10th Sept, 1986 having 45° dip. Parameters extracted from simulated acceleration records shown in this figure at Saitsama and Ummulong stations due to this model are given in Table 8.11.

Fig 8.21 Model of rupture plane showing method of numbering elements within the rupture plane. Acceleration records are simulated at Saitsama and Ummulong stations by assuming different elements within rupture plane as starting point of rupture. Number corresponding to each simulated record shows the element number which is assumed as nucleation point. Feature extracted from these simulated records at Saitsama and Ummulong stations are shown in Table 8.13 and 8.14, respectively. The center of element numbered as '1' is the origin of three dimensional coordinate system.

Fig 8.22 Model of rupture plane for Meghalaya earthquake of 10th Sept, 1986.

Fig 8.23 Location of selected observation points at which strong motion records are synthesised. The origin point of the coordinate system is placed at a depth of 28 km below point O_M marked in Fig 8.6. The coordinates of selected observation points in rectangular coordinate system is given in Table 8.16.

Fig 8.24 Meghalaya earthquake of 10th Sept, 1986, simulated records at stations. Y axis shows normalised value of (a) acceleration record, (b) its autocorrelation function, (c) its power spectrum, (d) its cumulative power spectrum and (e) its frequency weighted cumulative power spectrum. X axis for (a) and (b) shows time and for (c), (d) and (e) shows frequency. Feature extracted from these records at these station are given in Table 8.17 and 8.18.

Fig 8.25 Meghalaya earthquake of 10th Sept, 1986, simulated records at stations. Y axis shows normalised value of (a) acceleration record, (b) its autocorrelation function, (c) its power spectrum, (d) its cumulative power spectrum and (e) its frequency weighted cumulative power spectrum. X axis for (a) and (b) shows time and for (c), (d) and (e) shows frequency. Feature extracted from these records at these stations are given in Table 8.17 and 8.18.

Fig 8.26 Meghalaya earthquake of 10th Sept, 1986, simulated records at stations. Y axis shows normalised value of (a) acceleration record, (b) its autocorrelation function, (c) its power spectrum, (d) its cumulative power spectrum and (e) its frequency weighted cumulative power spectrum. X axis for (a) and (b) shows time and for (c), (d) and (e) shows frequency. Feature extracted from these records at these stations are given in Table 8.17 and 8.18.

Fig 8.27 Meghalaya earthquake of 10th Sept, 1986, simulated records at stations. Y axis shows normalised value of (a) acceleration record, (b) its autocorrelation function, (c) its power spectrum, (d) its cumulative power spectrum and (e) its frequency weighted cumulative power spectrum. X axis for (a) and (b) shows time and for (c), (d) and (e) shows frequency. Feature extracted from these

records at these stations are given in Table 8.17 and 8.18.

Fig 9.1 Tectonics of the region around Tehri (Jain, 1987) and the location of identified most probable causative fault on map.

Fig 9.2 Model of rupture plane used for simulating acceleration records at Tehri.

Fig 9.3 Rupture model and obtained peak acceleration from simulated acceleration records. The peak acceleration is obtained from simulated records after assuming various elements within the rupture plane as starting point of rupture. The center of element numbered as '1' is the origin of assumed coordinate system.

Fig 9.4 Isoacceleration contours of Uttarkashi earthquake of 20th Oct, 1991 shifted at Tehri. The tectonics of the region is taken after Jain (1987) shown in Fig 7.4. The isoacceleration contour map for the Uttarkashi earthquake is shown in Fig 7.8. The point of intersection of two or more faults or lineaments in the epicentral region of Uttarkashi is O and is shown in Fig 7.9.

APPENDIX III

LIST OF TABLES

Table 2.1 Rupture length for the Dharamsala earthquake of 26th April, 1986 calculated from different empirical relations. The rupture length calculated by relation of Otsuka (1965) and Naeim (1989) gives the maximum rupture length and the upper and lower limits of the rupture length, respectively.

Table 2.2 Sampled values of (a) displacement, (b) velocity and (c) acceleration form of source wavelet of frequency 5 Hz at a sampling interval of 4 ms. Displacement and acceleration form of the source wavelet is obtained after the integration and the differentiation of velocity form of source wavelet, respectively. Fig 2.4 shows the plot of displacement, velocity and acceleration form of source wavelet using data from this table.

Table 2.3 Normalised value of velocity form of source wavelets of 2.5, 5.0, 7.5 and 10.0 Hz frequency. This data has been used in figure 2.5.

Table 6.1 Epicenters of important earthquakes in H.P. and surrounding regions. Data taken from Singh et al., (1975) and USGS-NEIC (1990). This epicentral data is plotted in Fig 6.1.

Table 6.2 Estimated acceleration at various places for Kangra earthquake of 4th April, 1905. (Middlemiss, 1910, reprint 1981).

Table 6.3 List of stations of Kangra array. Geographical coordinates and elevation of station is taken from Chandrasekaran and Das (1992b). Location of stations of array is shown in Fig 6.2. Station name in the Fig 6.2 is represented by number given in bracket for each station.

Table 6.4 Epicentral parameters of Dharamsala earthquake of 26th April 1986 reported by different agencies. The epicenter E_{D1} , E_{D2} , E_{D3} and E_{D4} given in this Table are plotted in Fig 6.5.

Table 6.5 Dip and strike of two nodal planes of fault plane solutions for Dharamsala earthquake of 26th April, 1986 given by different agencies.

Table 6.6 Resultant peak ground acceleration of two horizontal components recorded at different stations for Dharamsala earthquake of 26th April, 1986 (Chandrasekaran, 1988b). Isoacceleration contour map of resultant peak acceleration for this earthquake is shown in Fig 6.6.

Table 6.7 Extracted features from three components of field records of Dharamsala earthquake of 26th April, 1986 recorded at Dharamsala and Shahpur stations. Field records at Dharamsala and Shahpur stations are shown in Fig 6.11 and 6.12, respectively.

Table 6.8 Extracted features from three components of field records of Dharamsala earthquake of 26th April, 1986 recorded at Kangra and Nagrota Bagwan (Nagrota) stations. Field records at Kangra and Nagrota Bagwan stations are shown in Fig 6.13 and 6.14, respectively.

Table 6.9 Extracted features from three components of field records of Dharamsala earthquake of 26th April, 1986 recorded at Baroh and Bhawarna (Bhawar) stations. Field records at Baroh and Bhawarna stations are shown in Fig 6.15 and 6.16, respectively.

Table 6.10 Extracted features from three components of field records of Dharamsala earthquake of 26th April, 1986 recorded at Sihunta and Bandlakhas (Bandl) stations. Field records at Bandlakhas and Sihunta stations are shown in Fig 6.17 and 6.18, respectively.

Table 6.11 Extracted features from three components of field records of Dharamsala earthquake of 26th April, 1986 recorded at Jawali station. Field records at Jawali station is shown in Fig 6.19.

Table 6.12 Extracted features from simulated records at Dharamsala and Shahpur stations for two different models. MD_u and MD_k of rupture planes. The model of these two rupture planes and the simulated records are shown in Fig 6.22 and 6.23.

Table 6.13 Selection of dip and strike of rupture plane by comparing extracted parameters of simulated records at Dharamsala and Shahpur stations due to two different models MD_u and MD_k of rupture planes shown in Fig 6.22 and 6.23, respectively.

Table 6.14 Feature extracted from simulated records at Shahpur and Dharamsala

stations for three different models MD_1 , MD_2 and MD_3 of rupture planes along Drini thrust shown in Fig 6.24.

Table 6.15 Selection of possible location of rupture plane along identified causative fault on map by comparing the extracted parameters of field records at Dharamsala and Shahpur stations with that of simulated records at these stations due to models MD_1 , MD_2 and MD_3 . Rupture plane is located at three different locations shown in Fig 6.24.

Table 6.16 Feature extracted from simulated records at Dharamsala station for six different locations of nucleation point or starting point of rupture within the rupture plane. The rupture model differ from each other only in the location of nucleation point. These models are named as MD_{n1} , MD_{n2} , MD_{n3} , MD_{n4} , MD_{n5} and MD_{n6} . Location of nucleation points and simulated acceleration records at Dharamsala station are shown in Fig 6.25.

Table 6.17 Feature extracted from simulated records at Shahpur station for six different locations of nucleation point or starting point of rupture within the rupture plane. The rupture model differ from each other only in the location of nucleation point. These models are named as MD_{n1} , MD_{n2} , MD_{n3} , MD_{n4} , MD_{n5} and MD_{n6} . Location of nucleation points and simulated acceleration records at Shahpur station are shown in Fig 6.25.

Table 6.18 Selection of possible location of nucleation point within the rupture plane by comparing extracted parameters of simulated records at Dharamsala and

Shahpur stations for six different models of rupture plane having different positions of nucleation point within the rupture plane.

Table 6.19 Selected observation points with geographical coordinates, elevation and coordinates in assumed rectangular three dimensional coordinate system. Geographical coordinates and elevation of stations had been taken from Chandrasekaran and Das (1992b). The origin of the assumed coordinate system is defined by O_3 on map. Fig 6.26 shows location of these selected observation points and the assumed three dimensional coordinate system on map.

Table 6.20 Features extracted from simulated records at different stations for Dharamsala earthquake of 26th April, 1986. Simulated records are shown in Fig 6.27, 6.28 and 6.29.

Table 6.21 Features extracted from simulated records at different stations for Dharamsala earthquake of 26th April, 1986. Simulated records are shown in Fig 6.27, 6.28 and 6.29.

Table 7.1 Epicenters of important earthquakes in Uttarkashi and surrounding region. Data taken from USGS-NEIC (1990). This epicentral data is plotted in Fig 7.1.

Table 7.2 Epicentral parameters of Uttarkashi earthquake of 20th October, 1991 reported by different agencies. The epicenter E_{U1} , E_{U2} and E_{U3} given in this table are plotted in Fig 7.5.

Table 7.3 Fault plane solutions Uttarkashi earthquake of 20th October, 1991 given by different agencies.

Table 7.4 Location of aftershocks of Uttarkashi earthquake of 20th October, 1991 (Kayal et al., 1992). This data is plotted in Fig 7.7.

Table 7.5 Resultant peak ground acceleration of two horizontal components recorded at different stations for Uttarkashi earthquake of 20th Oct, 1991 (After Chandrasekaran and Das, 1991 and 1992c). Isoacceleration contour map of resultant peak acceleration is shown in Fig 7.8.

Table 7.6 Extracted features from three components of field records of Uttarkashi earthquake of 20th October, 1991 recorded at Almora (Almo) and Barkot (Bark) stations. Field records at Almora and Barkot stations are shown in Fig 7.13 to 7.18, respectively.

Table 7.7 Extracted features from three components of field records of Uttarkashi earthquake of 20th October, 1991 recorded at Karnprayag (Karn) and Kosani (Kosa) stations. Field records at these stations are shown in Fig 7.19 to 7.24, respectively.

Table 7.8 Extracted features from three components of field records of Uttarkashi earthquake of 20th October, 1991 recorded at Purola (Puro) and Rudrprayag (Rudr) stations. Field records at these stations is shown in Fig 7.25 to 7.30, respectively.

Table 7.9 Extracted features from three components of field records of Uttarkashi earthquake of 20th October, 1991 recorded at Ghansiali (Ghan) and Koteswar (Kote) stations. Field records these stations are shown in Fig 7.31 to 7.36, respectively.

Table 7.10 Extracted features from three components of field records of Uttarkashi earthquake of 20th October, 1991 recorded at Koti and Srinagar (Sri) stations. Field records at these stations are shown in Fig 7.37 to 7.42, respectively.

Table 7.11 Extracted features from three components of field records of Uttarkashi earthquake of 20th October, 1991 recorded at Tehri (Tehr) station. Field records at these stations is shown in Fig 7.43 to 7.45, respectively.

Table 7.12 Extracted features from three components of field records of Uttarkashi earthquake of 20th October, 1991 recorded at Uttarkashi (Ukt) and Bhatwari (Bhat) stations. Field records at these stations is shown in Fig 7.46 to 7.51, respectively.

Table 7.13 Extracted features from simulated records at Uttarkashi (Ukt) and Bhatwari (Bhat) stations for models MU_{d1} and MU_{d2} of rupture planes. The models of these two rupture planes and the simulated records are shown in Fig 7.52 and 7.53.

Table 7.14 Selection of dip and strike of rupture plane by comparison of extracted parameters of field records with that of simulated records obtained after modelling two different models MU_{d1} and MU_{d2} at Uttarkashi and Bhatwari stations.

Table 7.15 Feature extracted from simulated records at Bhatwari station for six different locations of nucleation point or starting point of rupture within the rupture plane. The rupture model differ only in the location of nucleation point. These models are named as MU_{n1} , MU_{n2} , MU_{n3} , MU_{n4} , MU_{n5} and MU_{n6} . Simulated acceleration records due to these models are shown in Fig 7.54.

Table 7.16 Feature extracted from simulated records at Uttarkashi station for six different locations of nucleation point or starting point of rupture within the rupture plane. The rupture model differ only in the location of nucleation point. These models are named as MU_{n1} , MU_{n2} , MU_{n3} , MU_{n4} , MU_{n5} and MU_{n6} . Simulated acceleration records due to these models are shown in Fig 7.54.

Table 7.17 Selection of possible location of nucleation point within the rupture plane by comparison of extracted parameters of field records with that of simulated records due to models MU_{n1} , MU_{n2} , MU_{n3} , MU_{n4} , MU_{n5} and MU_{n6} of rupture planes at Uttarkashi and Bhatwari stations.

Table 7.18 Selected observation points with coordinates in rectangular coordinate system. The origin of the assumed coordinate system lies at a depth of 12 km from the point O denoted in Fig 7.10.

Table 7.19 Extracted features from simulated records of Uttarkashi earthquake of 20th October, 1991 at various stations. Simulated records at these stations is shown in Fig 7.56 to 7.68.

Table 7.20 Extracted features from simulated records of Uttarkashi earthquake of 20th October, 1991 at various stations. Simulated records at these stations is shown in Fig 7.56 to 7.68.

Table 7.21 Extracted features from simulated records of Uttarkashi earthquake of 20th October, 1991 at various stations. Simulated records at these stations is shown in Fig 7.56 to 7.68.

Table 8.1 Epicenters of important earthquakes in Meghalaya and surrounding region. Data taken from USGS-NEIC (1990). This epicentral data is plotted in Fig 8.1.

Table 8.2 List of stations of Shillong array. Geographical coordinates and elevation of station is taken from Chandrasekaran and Das (1992b). Location of stations of array is shown in Fig 8.2.

Table 8.3 Epicentral parameters of Meghalaya earthquake of 10th September, 1986 reported by different agencies. The epicenter E_{M1} , E_{M2} and E_{M3} given in this Table are plotted in Fig 8.3.

Table 8.4 Resultant peak ground acceleration of two horizontal components recorded at different stations for Meghalaya earthquake of 10th Sept, 1986 (After Chandrasekaran et al., 1988). Isoacceleration contour map of resultant peak acceleration is shown in Fig 8.4.

Table 8.5 Extracted features from three components of field records of Meghalaya earthquake of 10th Sept, 1986 recorded at Baithalangso (Bait) and Dauki (Dauk)

stations. Field records at these stations are shown in Fig 8.6 and 8.7, respectively.

Table 8.6 Extracted features from three components of field records of Meghalaya earthquake of 10th Sept, 1986 recorded at Khliehriat (Khil) and Nongpoh (Non) stations. Field records these stations are shown in Fig 8.8 and 8.9, respectively.

Table 8.7 Extracted features from three components of field records of Meghalaya earthquake of 10th Sept, 1986 recorded at Nongstoin (Nogs) and Nongkhlaw (Nonk) stations. Field records at these stations are shown in Fig 8.10 and 8.11, respectively.

Table 8.8 Extracted features from three components of field records of Meghalaya earthquake of 10th Sept, 1986 recorded at Panimur (Pani) and Pynursla (Pyn) stations. Field records at these stations are shown in Fig 8.12 and 8.13, respectively.

Table 8.9 Extracted features from three components of field records of Meghalaya earthquake of 10th Sept, 1986 recorded at Saitsama (Sait) and Ummulong (Umu) stations. Field records at these stations is shown in Fig 8.14 and 8.15.

Table 8.10 Extracted features from three components of field records of Meghalaya earthquake of 10th Sept, 1986 recorded at Umsning (Umsg) and Umrongso (Umso) stations. Field records at these stations is shown in Fig 8.16 and 8.17.

Table 8.11 Extracted features from simulated records at Saitsama and Ummulong stations due to three different models MM_{d1} , MM_{d2} and MM_{d3} of rupture planes. The model of these rupture planes and the simulated records are shown in Fig 8.18, 8.19 and 8.20.

Table 8.12 Selection of dip of the rupture plane by comparing extracted parameters of simulated records at Saitsama and Ummulong stations due to three different models of rupture plane having different dip.

Table 8.13 Feature extracted from simulated records at Saitsama station for five different locations of nucleation point or starting point of rupture within the rupture plane. The rupture model differ with other only in the location of nucleation point. These models are named as MM_{n1} , MM_{n2} , MM_{n3} , MM_{n4} and MM_{n5} . Simulated records due to these models at Saitsama station are shown in Fig 8.21.

Table 8.14 Feature extracted from simulated records at Ummulong station for five different locations of nucleation point or starting point of rupture within the rupture plane. The rupture model differ with other only in the location of nucleation point. These models are named as MM_{n1} , MM_{n2} , MM_{n3} , MM_{n4} and MM_{n5} . Simulated records due to these models at Ummulong station are shown Fig 8.21.

Table 8.15 Selection of possible location of nucleation point within the rupture plane by comparing extracted parameters of simulated records at Saitsama and Ummulong stations due to five different models of rupture plane having different positions of nucleation point.

Table 8.16 Selected observation points with geographical coordinates, elevation and coordinates in assumed rectangular three dimensional rectangular coordinate system. Geographical coordinates and elevation of stations had been taken from Chandrasekaran and Das (1992b). The origin of the assumed coordinate system is defined by O_M on map. Fig 8.23 shows location of these selected observation points and the assumed three dimensional coordinate system on map.

Table 8.17 Extracted features from simulated records of Meghalaya earthquake of 10th September, 1986 at various stations. Simulated records at these stations is shown in Fig 8.24 and 8.27.

Table 8.18 Extracted features from simulated records of Meghalaya earthquake of 10th September, 1986 at various stations. Simulated records at these stations is shown in Fig 8.24 and 8.27.

Table 9.1 Features extracted from simulated strong motion records at Tehri station for a hypothetical earthquake. Records are simulated for five different positions of nucleation point within the rupture plane.

APPENDIX IV

LIST OF SYMBOLS

A	Area of the rupture plane
A_d	Amplitude of displacement form of sinusoidal wavelet
A_v	Amplitude of velocity form of sinusoidal wavelet
A_{vr}	Amplitude of velocity form of source wavelet assumed for present study
A_i	($i=0,1,2$ and 3) Autocorrelation function at subscripted lag 'i'
A_m	Autocorrelation function when it has minimum global value
AI(t)	Function representing cumulative addition of the square of acceleration value in the acceleration record a(t)
ACF	Autocorrelation function of the acceleration record
ACF ₁	Time of first zero crossing
ACF ₂	Time of second zero crossing
ACF ₃	Time of third zero crossing
ACF ₄	Time of arrival of global minima
ACF ₅	A_1/A_0
ACF ₆	A_2/A_0
ACF ₇	A_3/A_0
ACF ₈	A_m/A_0
ACF ₉	Ratio of area under ACF time $T=0$ to time $T=T_1$ and area under ACF from time $T=T_1$ and $T=T_2$
ACF ₁₀	Ratio of area under ACF above the abscissa and area under ACF below the abscissa






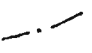
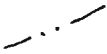




$a(t)$	Acceleration record, t is variable used for denoting time
$a_H(t)$	Peak horizontal acceleration computed using attenuation relation
C	Velocity of Ricker wavelet travelling in the medium
D	Downward extension of rupture plane
D_r	Distance between starting point of rupture and center of the element
E	Energy released in an earthquake
E_e	Energy released by a single element
F_p	Frequency at which maximum power occurs
F_1, F_2, F_3	Frequency at which 25th, 50th and 75th percentile of power occurs
F_4, F_5, F_6	Frequency at which 25th, 50th and 75th percentile value of frequency weighted power occurs
f_c	Frequency of Ricker wavelet
H	Hypocenter of the earthquake
h	Hypocentral depth
L	Length of rupture plane
L_e	Length of unit element
L_m	Maximum length of rupture
N	Total number of elements within rupture plane
M	Richter magnitude of the earthquake
M_b	Body wave magnitude of the earthquake
M_L	Local magnitude of the earthquake
M_o	Seismic moment of the earthquake
M_s	Surface wave magnitude of an earthquake
P_a	Peak acceleration of acceleration record of an earthquake
P_v	Peak velocity in the velocity record of an earthquake
P_d	Peak displacement in the displacement record of an earthquake

R	Distance between center of element and the observation point
$s(t)$	Source wavelet
T	Total time taken by source wavelet to reach an observation point just after initiation of rupture
T_a	Time at which peak acceleration occurs in acceleration record of an earthquake
T_i	($i=1,2$ and 3) Time of i th zero crossing in the autocorrelation function of acceleration record
T_m	Time of global minima in autocorrelation function of acceleration record
T_D	Duration of acceleration record
T_{at}	Arrival time of peak in acceleration record (i.e. time difference of the arrival of strong motion signal and peak acceleration)
T_{dl}	Time at which 5% of maximum value of function $AI(t)$ occurs
T_{dh}	Time at which 95% of maximum value of function $AI(t)$ occurs
T_o	Period of sinusoidal wavelet
t_o	Time of activation of nucleation element. At this time source wavelet from nucleation element starts travelling towards observation point.
t_{no}	Total duration of wave train radiated by point source
V	Velocity of the medium
V_r	Rupture velocity
$U(t)$	Function used for generating source wavelet
$X(t)$	Displacement form of sinusoidal wavelet as a function of time
$v(t)$	Velocity form of sinusoidal wavelet as a function of time
$v_s(t)$	Form of velocity type source wavelet released by point source
$Vl(i)$	i th Sample of velocity record

APPENDIX V

LIST OF SYMBOL USED IN FIGURES

A_d	Amplitude of displacement form of sinusoidal wavelet
A_i	($i=0,1,2$ and 3) Autocorrelation function at subscripted lag 'i'
A_m	Autocorrelation function when it has global minimum value
A_v	Amplitude of velocity form of sinusoidal wavelet
A_{vr}	Amplitude of velocity form of source wavelet assumed for present study
c	Center of an element within rupture plane
D	Downward extension of the rupture plane
E	Epicenter of the earthquake
F_p	Frequency at which maximum power occurs
F_1, F_2, F_3	Frequency at which 25th, 50th and 75th percentile of power occurs
F_4, F_5, F_6	Frequency at which 25th, 50th and 75th percentile value of frequency weighted power occurs
H	Hypocenter of the earthquake
h	Hypocentral depth
L	Length of rupture plane
L_e	Length of unit element
P_a	Peak acceleration of acceleration record of an earthquake
P_v	Peak velocity in the velocity record of an earthquake
P_d	Peak displacement in the displacement record of an earthquake
si	Sampling interval of strong motion record

T_a	Time at which peak acceleration occurs in acceleration record of an earthquake
T_i	($i=1,2$ and 3) Time of i th zero crossing in the autocorrelation function of acceleration record
T_d	Duration of acceleration record
T_{at}	Arrival time of peak in acceleration record (i.e. time difference of the arrival of strong motion signal and peak acceleration)
T_{d1}	Time at which 5% of maximum value of function $AC(I)$ occurs
T_{d95}	Time at which 95% of maximum value of function $AC(I)$ occurs
T_m	Time of global minima in autocorrelation function of acceleration record
t_1	Time of zero crossing from the arrival time of last positive value of autocorrelation function of acceleration record
t_2	Time of zero crossing from the arrival time of last negative value of autocorrelation function of acceleration record
	Isoseismal of intensity V on MMI scale
	Isoacceleration contours
	Epicenter of an earthquake
	Thrust
	Lineament
	Anticline
	Syncline
	River
	Rupture plane
	Recording station
	Place

δ

Dip of the rupture plane

Distance travelled by rupture within the rupture plane

- . - . - .

Distance travelled by source wavelet within the medium

.

Center of element within the rupture plane

*

Starting point of rupture or nucleation point

▭

For start or stop statement in the flow chart of the computer program

▭

For calculation or process other than decision in the flow chart of the computer program

◇

For a decision in the flow chart of the computer program

▭

For input or output statement in the flow chart of computer program

○

For a connection in the flow chart of the computer program



...the ...
...by ...
...by ...
...with ...

...

